Nuclear Energy Research Initiative
Project 2002-196

FINAL TECHNICAL REPORT FOR THE PERIOD SEPTEMBER 2002 THROUGH SEPTEMBER 2005

April 2006

Contents

1. H2-MHR Pre-Conceptual Design Report: SI-Based Plant, General Atomics Report GA-A25401, April 2006.

2. H2-MHR Pre-Conceptual Design Report: HTE-Based Plant, General Atomics Report GA-A25402, April 2006.

3. Milestone Status and Budget Summary.

Part 1

H2-MHR Pre-Conceptual Design Report: SI-Based Plant, General Atomics Report GA-A25401, April 2006.

H2-MHR

GA-A25401

Hydrogen
Production
Modular Helium
Reactor

H2-MHR Pre-Conceptual Design Report: SI-Based Plant

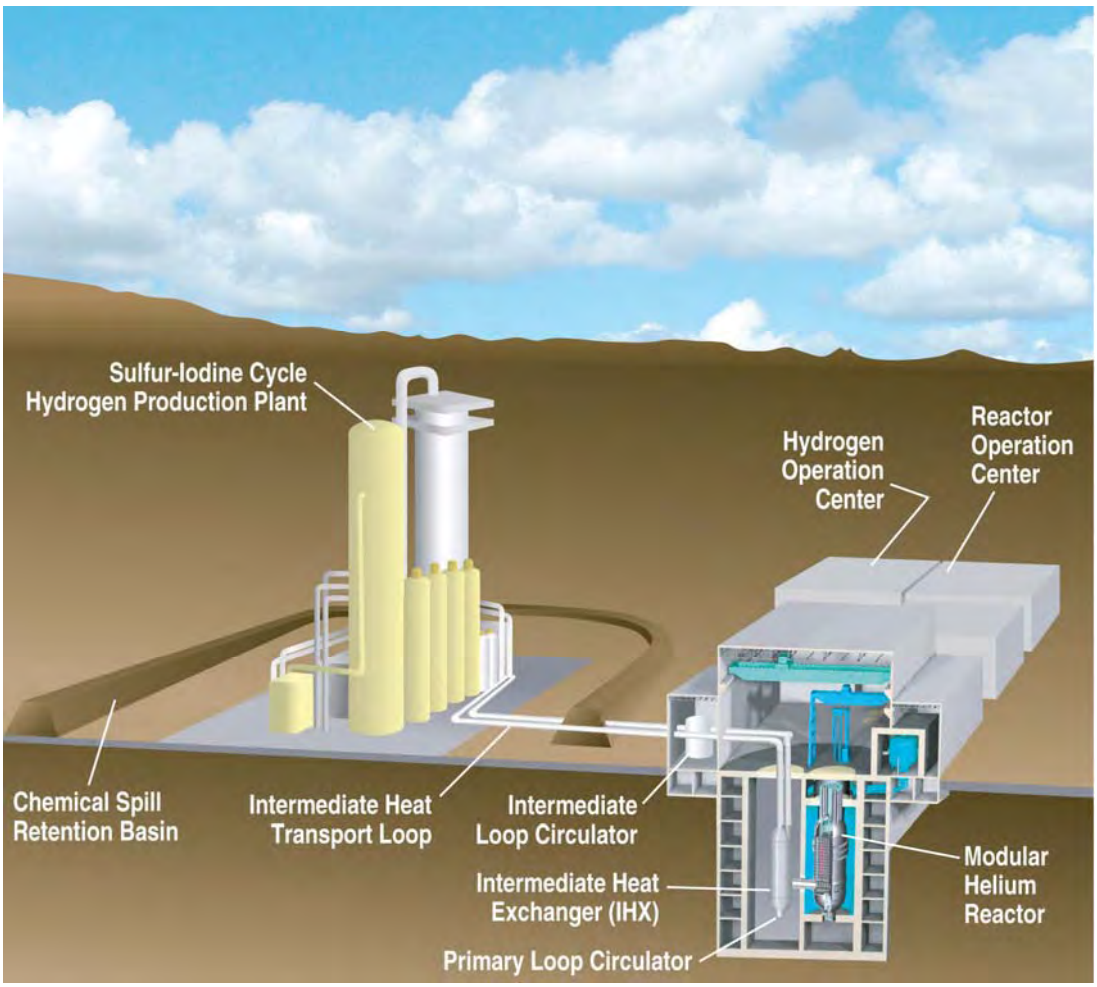

GENERAL ATOMICS

Idaho National Laboratory
Texas A&M University

US DOE Contract No. DE-FG03-02SF22609/A000
Nuclear Energy Research Initiative

April 2006

DISCLAIMER

H2-MHR PRE-CONCEPTUAL DESIGN REPORT: SI-BASED PLANT

FINAL TECHNICAL REPORT FOR THE PERIOD SEPTEMBER 2002 THROUGH SEPTEMBER 2005

by

M.B. Richards, A.S. Shenoy, L.C. Brown, R.T. Buckingham, E.A. Harvego,[†] K.L. Peddicord,[‡] S.M.M. Reza,[‡] and J.P. Coupey[‡]

[†]Idaho National Laboratory, Idaho Falls, ID
[‡]Texas A&M University, College Station, TX

US DOE Contract No. DE-FG03-02SF22609/A000
Nuclear Energy Research Initiative
Project 2002-196

General Atomics Project 30165

GA-A25401

April 2006

GENERAL ATOMICS

EXECUTIVE SUMMARY

Hydrogen and electricity are expected to dominate the world energy system in the long term. The world currently consumes about 50 million metric tons of hydrogen per year, with the bulk of it being consumed by the chemical and refining industries. The demand for hydrogen is expected to increase, especially if the U.S. and other countries shift their energy usage towards a hydrogen economy, with hydrogen consumed as an energy commodity by the transportation, residential, and commercial sectors. However, there is strong motivation to not use fossil fuels in the future as a feedstock for hydrogen production, because the greenhouse gas carbon dioxide is a byproduct and fossil fuel prices are expected to increase significantly.

For electricity and hydrogen production, an advanced reactor technology receiving considerable international interest is a modular, passively-safe version of the high-temperature, gas-cooled reactor (HTGR), known in the U.S. as the Modular Helium Reactor (MHR), which operates at a power level of 600 MW(t). For electricity production, the MHR operates with an outlet helium temperature of 850°C to drive a direct, Brayton-cycle power-conversion system (PCS) with a thermal-to-electrical conversion efficiency of 48 percent. This concept is referred to as the Gas Turbine MHR (GT-MHR). For hydrogen production, the process heat from the MHR is used to produce hydrogen. This concept is referred to as the H2-MHR.

The growing international interest in the MHR concept is the direct result of MHR design features, which include:

(1) Passive Safety, Competitive Economics, and Siting Flexibility. The MHR does not require active safety systems to ensure public and worker safety. The high-energy conversion efficiency of the MHR, combined with the elimination of active safety systems, result in a design that is passively safe and economically competitive with other non-passively safe reactor concepts. Because of its high efficiency, the MHR rejects less waste heat than other reactor concepts. This design feature, combined with passive safety, allows for more flexible siting options for the MHR.

(2) High Temperature Capability and Flexible Energy Outputs. The MHR is capable of producing process-heat temperatures of 950°C and higher. This high-temperature capability translates into a high-energy conversion efficiency for a variety of energy outputs, including electricity, hydrogen production, and synthetic fuel production.

(3) Flexible Fuel Cycles. The MHR can operate efficiently and economically with several different fuel cycles. MHR designs have been developed utilizing low-enriched (LEU) uranium fuels, high-enriched uranium (HEU) fuels, mixed uranium/thorium and plutonium/thorium fuels, and surplus weapons-grade plutonium fuels. The thermal neutron spectrum of the MHR, combined with robust, ceramic-coated particle fuel, allow for very high burnup in a single pass through the reactor. More recently, an MHR design has been developed to deeply burn plutonium and other transuranic (TRU) actinides recovered from light-water reactor (LWR) spent fuel. The flexible fuel cycle capability of the MHR, combined with its flexible energy output capability (see Fig. E-1), result in a design concept that is very well suited for a wide variety of energy-growth scenarios.

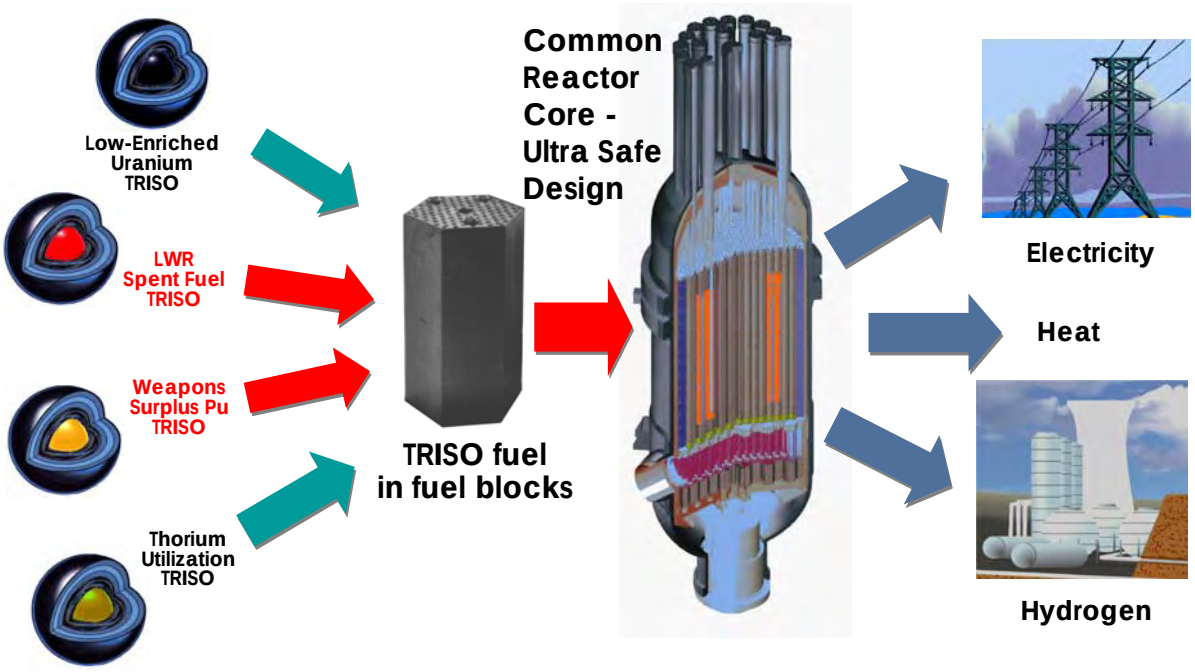

Fig. E-1. MHR Fuel Cycle and Energy Output Options

Nuclear Hydrogen Production

In principle, nuclear electricity can be used to split water using conventional low-temperature electrolyzers. For a conventional LWR that produces electricity with approximately 33% thermal efficiency and current generation electrolyzers operating with an efficiency of about 75% to convert electricity to high-pressure hydrogen, the overall efficiency for hydrogen production is approximately 25%. If a GT-MHR is used to produce the electricity with 48% thermal efficiency, the overall efficiency for hydrogen production improves to 36%. However, even with high-efficiency electricity production, economic evaluations of coupling nuclear energy to low-temperature electrolysis have generally not been favorable when compared to steam-methane reforming (SMR). For these reasons, two concepts that make direct use of the MHR high-temperature process heat are being investigated in order to improve the efficiency and economics of hydrogen production. The first concept involves coupling the MHR to the Sulfur-Iodine (SI) thermochemical water splitting process and is referred to as the SI-Based H2-MHR. The second concept involves coupling the MHR to high-temperature electrolysis (HTE) and is referred to as the HTE-Based H2-MHR. Both processes have the potential to produce hydrogen with high efficiency and have been proven to work at the laboratory scale. This report provides a pre-conceptual design description of a full-scale, n^{th}-of-a-kind SI-Based H2-MHR plant, as illustrated in Fig. E-2. The HTE-Based H2-MHR is described in a separate report.

Overall Plant Design

As shown in Fig. E-3, the heat required to drive the SI process is supplied by Modular Helium Reactors (MHRs). The plant consists of four 600 MW(t) MHR modules, with each module coupled to an Intermediate Heat Exchanger (IHX) to transfer the heat to a secondary helium loop. The heat is then transferred to the SI-based Hydrogen Production System. Waste heat is rejected using cooling towers in a manner similar to that for electricity-producing plants. In

addition to the heat required to drive the SI process, the plant requires approximately 800 MW(e). Most of this electricity is needed to power pumps and compressors that are part of the Hydrogen Production System design. For this study, it is assumed that the H2-MHR plant is part of an energy park that also includes GT-MHRs that provide the necessary electricity. Nominal plant design parameters are given in Table E-1. At a 90% capacity factor, the plant produces 3.68×10^5 metric tons of hydrogen per year at an efficiency of 45.0% (based on the higher heating value of hydrogen) with a product gas pressure of 4.0 MPa.

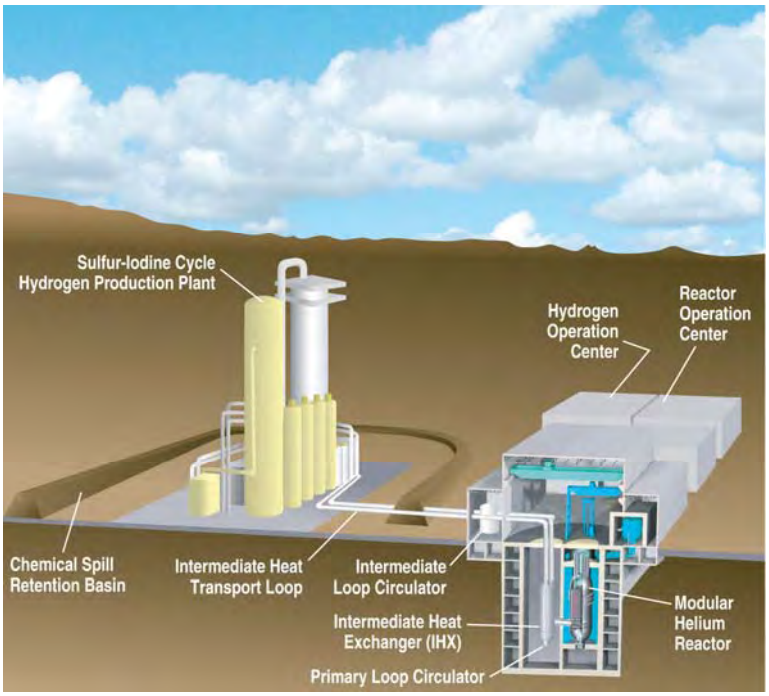

Figure E-2. SI-Based H2-MHR Concept

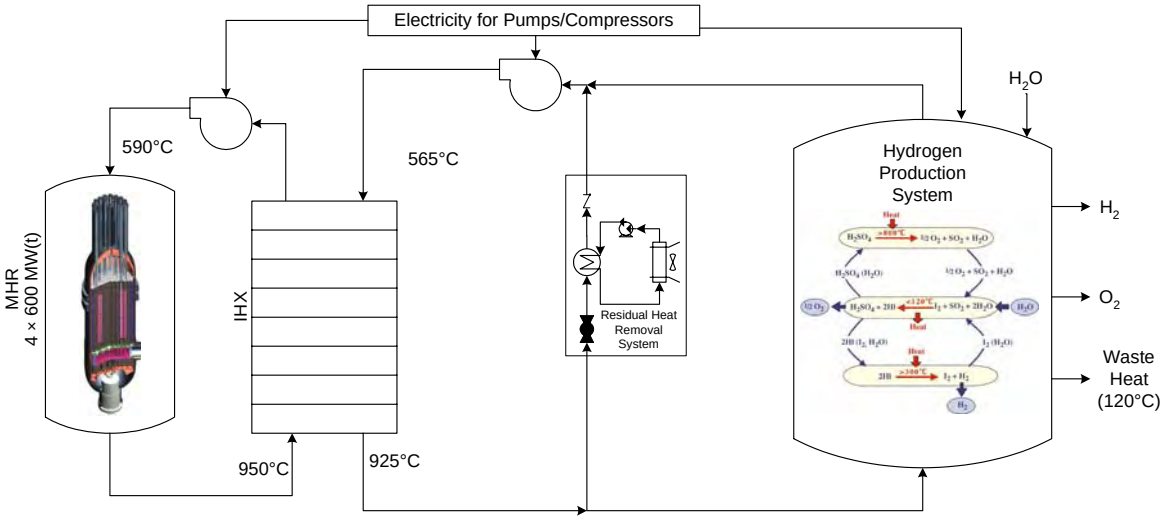

Figure E-3. SI-Based H2-MHR Process Schematic

Table E-1. H2-MHR Nominal Plant Design Parameters

MHR System	
Number of modules	4
Module power rating	600 MW(t)
Core inlet/outlet temperatures	590°C / 950°C
Peak fuel temperature – normal operation	1250°C - 1350°C
Peak fuel temperature – accident conditions	< 1600°C
Heat Transport System	
Primary coolant fluid	helium
Primary coolant pressure	7.0 MPa
Primary coolant flow rate	320 kg/s
Total pressure drop – primary circuit	100 kPa
Secondary coolant fluid	helium
Secondary coolant pressure	7.1 MPa
Secondary coolant flow rate	320 kg/s
Secondary coolant cold leg/hot leg temperatures	565°C / 925°C
Total pressure drop – secondary circuit	146 kPa
Hydrogen Production System	
Peak process temperature	900°C
Peak process pressure	7.0 MPa
Product hydrogen pressure	4.0 MPa
Annual hydrogen production*	3.68×10^5 metric tons
Plant hydrogen production efficiency**	45.0%

* Based on an overall plant capacity factor of 90%.
** Based on the higher heating value of hydrogen (141.9 MJ/kg)

MHR Design and Passive Safety Features

The MHR design is shown in Fig. E-4. Passive safety features of the MHR include the (1) ceramic, coated-particle fuel that maintains its integrity at high temperatures during normal operation and loss of coolant accidents (LOCAs); (2) an annular graphite core with high heat capacity that limits the temperature rise during a LOCA; (3) a relatively low power density that helps to maintain acceptable temperatures during normal operation and accidents; (4) an inert helium coolant, which reduces circulating and plateout activity; and (5) a negative temperature coefficient of reactivity that ensures control of the reactor for all credible reactivity insertion events. The fuel, the graphite, the primary coolant pressure boundary, and the low-pressure vented containment building provide multiple barriers to the release of fission products.

The MHR fuel element and its components are shown in Fig. E-5. The fuel for the H2-MHR consists of microspheres of uranium oxycarbide that are coated with multiple layers of pyrocarbon and silicon carbide. The H2-MHR core is designed to use a blend of two different particle types; a fissile particle that is enriched to 19.8% U-235 and fertile particle with natural uranium (0.7% U-235). The fissile/fertile loading ratio is varied with location in the core, in order to optimize reactivity control, minimize power peaking, and maximize fuel cycle length. The

buffer, inner pyrolytic carbon (IPyC), silicon carbide (SiC), and outer pyrolytic carbon (OPyC) layers are referred to collectively as a TRISO coating. The coating system can be viewed as a miniature pressure vessel that provides containment of radionuclides and gases. This coating system is also an excellent engineered barrier for long-term retention of radionuclides in a repository environment.

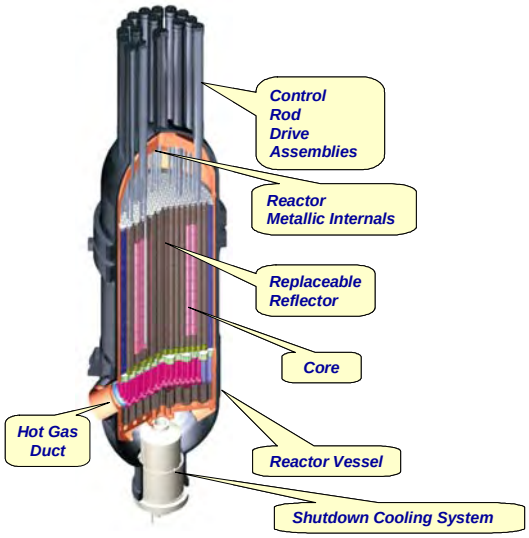

Figure E-4. MHR Design

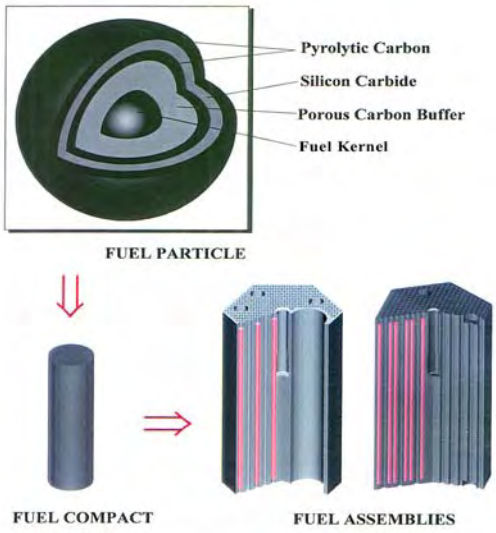

Figure E-5. MHR Fuel Element Components

The H2-MHR is not expected to present any significant licensing challenges relative to the GT-MHR or other reactor concepts. However, a key consideration for safety and licensing of the H2-MHR is co-location of the MHR modules with a hydrogen production plant. As illustrated in Fig. E-2, it is proposed to locate the two facilities as close as possible (within 100 m or less) in order to minimize the distance over which high-temperature heat is transferred. Idaho National Laboratory (INL) has recently performed an engineering evaluation for these separation requirements and has concluded separation distances in the range of 60 m to 120 m should be adequate in terms of safety.

Economic Evaluation

An economic evaluation was performed assuming the plant could be constructed in 36 months with an annual interest rate of 7% and a fixed charge rate of 12.6% (corresponding to a regulated utility). The capital costs of the MHR System and Hydrogen Production System were estimated to be $1.44 billion and $1.07 billion, respectively, for a total H2-MHR plant capital cost of $2.51 billion. The installed capital costs are approximately $1,360/kW-$H_2$ using the higher heating value of hydrogen (141.9 MJ/kg). The total operations and maintenance (O&M) costs are estimated to be $340 million per year, of which about two-thirds are electricity costs. The hydrogen production costs are estimated to be $1.97/kg. As shown in Fig. E-6, electricity costs contribute to about 30% of the hydrogen production costs. If the pumping power required by the SI process could be reduced by 50%, the hydrogen production costs could be reduced to about $1.62/kg and the overall efficiency of the process would increase from 45% to 55%.

Figure E-7 shows a comparison of nuclear hydrogen production costs with the costs for producing hydrogen using SMR. In December 2005 the wellhead price for natural gas was $10.02 per 1000 cubic feet, which corresponds to $9.72/MMBtu. At this price, nuclear hydrogen production is economically competitive with SMR. Nuclear hydrogen production is economically competitive with SMR for natural gas prices in the range $6 to $8/MMBtu, if a CO_2 sequestration/disposal cost for SMR and an O_2 credit for nuclear hydrogen production are assumed.

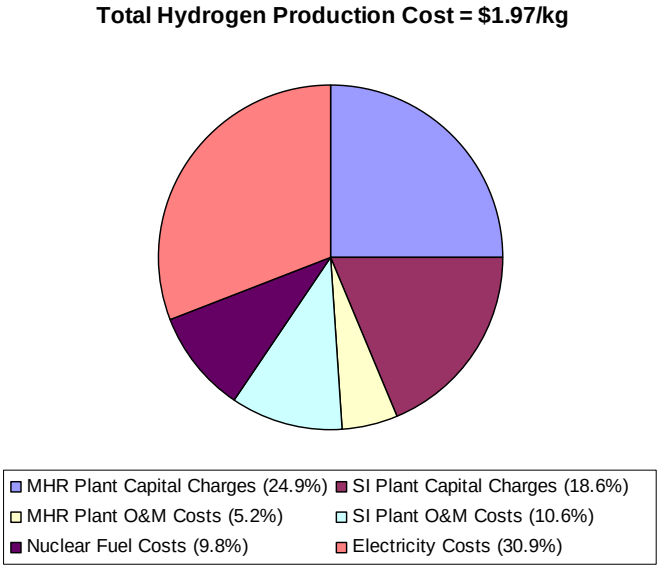

Figure E-6. Hydrogen Production Costs (Baseline Estimate)

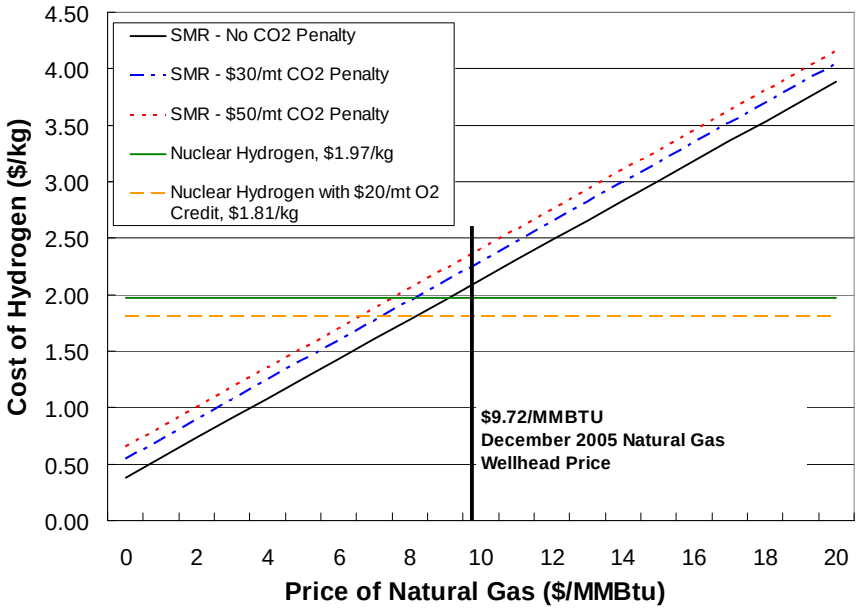

Figure E-7. Comparison of Nuclear and SMR Hydrogen Production Costs

Recommendations

Based on this pre-conceptual design study, the H2-MHR is capable of producing hydrogen economically, safely, and with minimal environmental impact. It is recommended that the H2-MHR design development be continued through the conceptual, preliminary, and final design phases. Also, it is recommended that future H2-MHR design work be closely coupled with ongoing and planned technology-development programs, in order to ensure that the data obtained by these programs satisfies specific needs of the H2-MHR design. This model for integration of design with technology development is illustrated in Fig. E-8 and is based on successful Engineering Development and Demonstration (ED&D) programs conducted and managed by General Atomics for Department of Energy projects, including Accelerator Production of Tritium, the Salt Waste Processing Facility, the commercial GT-MHR, and the New Production Reactor.

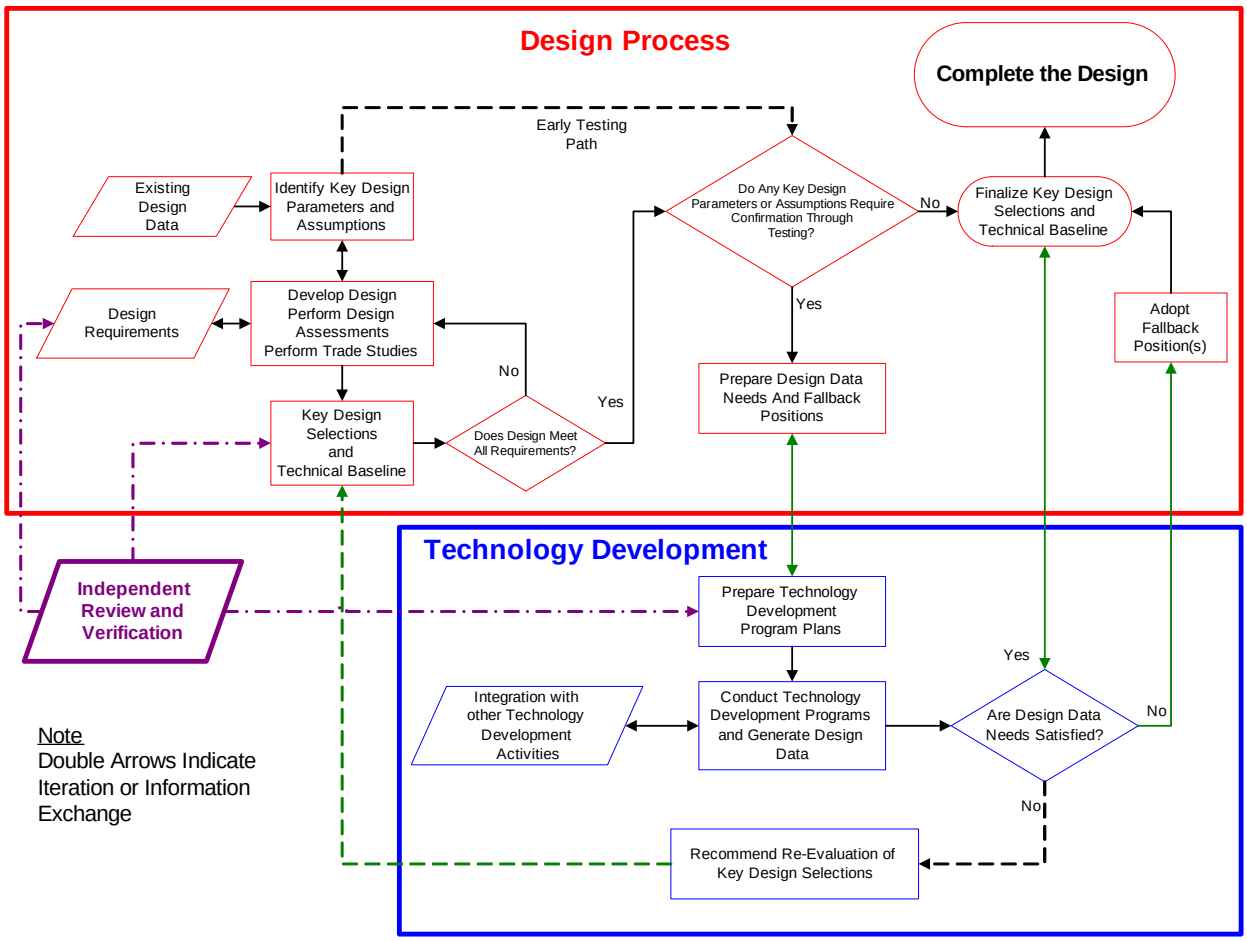

Figure E-8. Integration of Design with Technology Development

ACKNOWLEDGEMENTS

This work was funded by the U.S. Department of Energy Nuclear Energy Research Initiative (NERI), under grant DE-FG03-02SF22609/A000.

The authors would also like to acknowledge the contributions and assistance provided by Toshiba Corporation of Yokohama, Japan, Fuji Electric Systems of Kawasaki city, Japan, and the Japan Atomic Energy Agency (JAEA) of Oarai, Japan. From Toshiba Corporation, thanks are extended to Norihiko Handa, Ryoma Kato, and Masaru Fukuie for sharing their concepts for Intermediate Heat Exchanger design. From Fuji Electric Systems, thanks are extended to Futoshi Okamoto, Yoshihiro Kiso, and Nobumasa Tsuji for their help with optimizing the Modular Helium Reactor thermal hydraulic design for higher temperature operation. In 2004 and 2005, JAEA conducted very successful and very informative workshops on nuclear hydrogen production, which provided information that was very useful for this NERI project. The primary author would especially like to thank Dr. Kazuhiko Kunitomi and Dr. Tetsuaki Takeda of JAEA for their assistance and hospitality.

This NERI project also benefited greatly from a close working relationship with Savannah River National Laboratory (SRNL) on a related NERI project titled Centralized Hydrogen Production from Nuclear Power: Infrastructure Analysis and Test-Case Design Study (NERI Project 2002-160). Special thanks are extended to Dr. William Summers, Dr. Maximilian Gorensek, Dr. Melvin Buckner, and Mr. Edward Danko of SRNL, and to Professor Francis A. Gadala-Maria of the University of South Carolina.

TABLE OF CONTENTS

Executive Summary iii
Acronyms and Abbreviations xvi

1. Introduction and Background 1-1
1.1 Modular Helium Reactor Design Status 1-2
1.2 Hydrogen Production Using the Sulfur-Iodine Process 1-4
2. Overall Plant Description 2-1
2.1 Plant Level Functions and Performance Requirements 2-1
2.2 Work Breakdown Structure and Responsibility Assignment Matrix 2-5
2.3 Overall Plant Arrangement 2-7
2.4 Nominal Plant Design Parameters 2-7
2.5 Plant Operation 2-9
3. Plant Technical Description 3-1
3.1 MHR System Design 3-1
3.1.1 Reactor System 3-1
3.1.1.1 Fuel Design 3-3
3.1.1.2 Reactor Core and Internals 3-9
3.1.1.3 Neutron Control System 3-11
3.1.2 Cross Vessel and Hot Duct Assembly 3-15
3.1.3 Reactor Vessel 3-15
3.1.4 Design Modifications for Higher Temperature Operation 3-18
3.1.4.1 Inlet Flow Configuration Modifications 3-18
3.1.4.2 Vessel Cooling 3-24
3.1.4.3 Power and Flow Distribution Optimization 3-25
3.1.5 Shutdown Cooling System 3-29
3.1.6 Reactor Cavity Cooling System 3-33
3.1.6.1 RCCS Cooling Panels 3-34
3.1.6.2 RCCS Operation 3-35
3.1.7 Fuel Performance and Radionuclide Control 3-36
3.1.7.1 Radionuclide Containment System 3-37
3.1.7.2 Fuel Failure Mechanisms 3-39
3.1.7.3 Performance Capability of High-Quality TRISO Fuel 3-45
3.1.7.4 Radionuclide Transport Mechanisms 3-47
3.1.7.5 Fuel Quality and Performance Requirements 3-50
3.2 Heat Transport Systems 3-53
3.2.1 Primary Heat Transport System 3-54
3.2.1.1 IHX Design 3-54
3.2.1.2 Primary Coolant Circulator 3-57
3.2.2 Secondary Heat Transport System 3-58
3.2.2.1 Piping Configuration 3-58
3.2.2.2 High-Temperature Isolation Valves 3-60
3.2.3 Residual Heat Removal System 3-61
3.3 Helium Services Systems 3-61

3.3.1 Primary Coolant Helium Purification System....3-61
3.3.2 Secondary Coolant Helium Purification System....3-64
3.3.3 Helium Transfer and Storage Systems....3-64
3.3.4 Tritium Control....3-64
3.4 Hydrogen Production System....3-69
3.4.1 Sulfur-Iodine Process Description....3-69
3.4.1.1 Section 1 (Bunsen Reaction)....3-69
3.4.1.2 Section 2 (Sulfuric Acid Decomposition)....3-73
3.4.1.3 Section 3 (Hydrogen Iodide Decomposition)....3-77
3.4.2 Major Equipment Description....3-82
3.4.3 Overall Plant Efficiency....3-85
3.5 Plant Protection and Monitoring Systems....3-85
3.5.1 Reactor Protection System....3-85
3.5.2 Investment Protection System....3-85
3.5.3 Plant Monitoring System....3-86
3.6 Balance of Plant and Auxiliary Systems....3-87
3.6.1 Fuel Handling and Storage System....3-87
3.6.2 Spent Fuel Storage System....3-89
3.6.3 Radioactive Waste Management and Decontamination System....3-89
3.6.4 Heating, Ventilation, and Air Conditioning Systems....3-89
3.6.5 Hydrogen Production Water Supply System....3-89
3.6.6 Waste Heat Rejection System....3-90
3.7 Buildings and Structures....3-90
3.7.1 Reactor Building and Vented Low-Pressure Containment....3-90
3.7.2 Other Major Buildings....3-92
4. Plant Assessments....4-1
4.1 Safety Assessment....4-1
4.1.1 Passive Safety Features....4-1
4.1.2 Safety-Related Systems, Structures, and Components....4-1
4.1.3 Accident Analysis....4-1
4.2 Availability Assessment....4-3
4.2.1 Scheduled Outages....4-4
4.2.2 Forced Outages – MHR Nuclear Island....4-4
4.2.3 Forced Outages – Hydrogen Production Plant....4-5
4.3 Licensing Assessment....4-7
4.4 Economic Assessment....4-7
4.4.1 Capital Costs....4-8
4.4.2 Operations and Maintenance Costs....4-10
4.4.3 Hydrogen Production Costs....4-10
4.4.4 Parametric Studies....4-12
4.4.5 Comparison with Steam-Methane Reforming....4-13
5. Technology Development and Risk Reduction....5-1
6. References....6-1
Appendix A – Advanced Fuels....A-1
Appendix B – Publications....B-1

List of Figures

Figure 1-1. SI-Based H2-MHR Concept 1-1
Figure 1-2. SI-Based H2-MHR Process Schematic 1-2
Figure 1-3. The Gas-Turbine Modular Helium Reactor 1-3
Figure 1-4. The SI Thermochemical Water Splitting Process 1-4
Figure 1-5. Simplified SI Process Flow Schematic 1-5
Figure 2-1. H2-MHR High-Level Function Flow Block Diagram 2-2
Figure 2-2. H2-MHR Plant Arrangement 2-10
Figure 3-1. Modular Helium Reactor System 3-1
Figure 3-2. MHR Fuel Element Components 3-3
Figure 3-3. MHR Standard Fuel Element 3-7
Figure 3-4. MHR Core Design 3-10
Figure 3-5. MHR Core Arrangement 3-11
Figure 3-6. Outer Neutron Control Assembly Design 3-12
Figure 3-7. Neutron Control Assembly Installation 3-13
Figure 3-8. Control Rod Design 3-14
Figure 3-9. Hot Duct Assembly 3-16
Figure 3-10. Reactor Vessel 3-17
Figure 3-11. GT-MHR Cross Section at Vessel Midplane 3-19
Figure 3-12. Reactor Vessel Configured with Alternative Inlet Flow Paths 3-20
Figure 3-13. MHR Configured with PSR Inlet Flow 3-21
Figure 3-14. ATHENA Model for the MHR Vessel and Internals 3-22
Figure 3-15. ATHENA Model for the RCCS 3-23
Figure 3-16. Predicted Failure of the SiC Layer by Fission Product Corrosion 3-26
Figure 3-17. Axial Temperature Distribution in the H2-MHR Hot Coolant Channel 3-26
Figure 3-18. Column-Average Power Factors 3-27
Figure 3-19. MHR FLOWNET Coolant Flow Distribution Model 3-28
Figure 3-20. Shutdown Cooling System General Arrangement 3-29
Figure 3-21. SCS Circulator and Heat Exchanger 3-31
Figure 3-22. SCS Circulator Sectional View 3-32
Figure 3-23. Passive Air-Cooled RCCS 3-33
Figure 3-24. RCCS Panel Layout 3-35
Figure 3-25. H2-MHR Radionuclide Containment System 3-37
Figure 3-26. TRISO Particle Failure Mechanisms 3-39
Figure 3-27. Calculated Tangential Stresses at the Middle of the SiC Layer 3-41
Figure 3-28. Irradiation-Induced Strain in Pyrocarbon as a Function of BAF 3-42
Figure 3-29. OPyC Performance Predictions 3-42
Figure 3-30. Localized Fission-Product Attack of the SiC Layer 3-44
Figure 3-31. Breakthrough Time for Ag Diffusing Through a 35-μm SiC Layer 3-45
Figure 3-32. Irradiation Conditions During Testing of High-Quality German Fuel 3-47
Figure 3-33. Principal Steps in Radionuclide Release from the H2-MHR Core 3-48
Figure 3-34. Postirradiation Heating of Japanese LEU UO_2 Fuel 3-49
Figure 3-35. Logic for Derivation of Fuel Quality Requirements 3-51
Figure 3-36. PCHE Design Technology 3-54
Figure 3-37. Preliminary IHX Design Concept 3-56
Figure 3-38. Primary Circulator Design Concept 3-57
Figure 3-39. Parallel and Concentric Piping Concepts for Secondary HTS 3-58
Figure 3-40. High-Temperature Isolation Valve Design Concept 3-60

Figure 3-41. Helium Purification Train Block Diagram 3-62
Figure 3-42. Helium Transfer and Storage System Block Diagram 3-65
Figure 3-43. Tritium Release from TRISO-Coated Fuel Particles 3-66
Figure 3-44. Measured Tritium Concentration in Fort St. Vrain Primary Coolant 3-67
Figure 3-45. Tritium Migration Pathways in the SI Cycle 3-68
Figure 3-46. SI Process Section 1 Flowsheet 3-71
Figure 3-47. SI Process Section 2 Flowsheet 3-75
Figure 3-48. Extractive Distillation Process Schematic 3-77
Figure 3-49. Reactive Distillation Process Schematic 3-78
Figure 3-50. SI Process Section 3 Flowsheet 3-80
Figure 3-51. Fuel Handling and Storage System Layout 3-87
Figure 3-52. Fuel Handling Equipment Arrangement 3-88
Figure 4-1. Passive Heat Removal to the RCCS During HPCC and LPCC Events 4-2
Figure 4-1. Peak Fuel Temperatures During HPCC and LPCC Events 4-3
Figure 4-3. Peak Vessel Temperatures During HPCC and LPCC Events 4-4
Figure 4-4. Master Fault Tree Model for Hydrogen Production Processes 4-6
Figure 4-5. Concept for Co-Location of the MHR with Hydrogen Production 4-8
Figure 4-6. SI-Based H2-MHR Plant Hydrogen Production Costs (Baseline Estimate) 4-11
Figure 4-7. Comparison of Nuclear and SMR Hydrogen Production Costs 4-14
Figure 5-1. Integration of Design Process with Technology Development 5-2
Figure A-1. Neutron Total Absorption Cross Sections for Silicon and Zirconium A-1
Figure A-2. Core Reactivity as a Function of Irradiation Time A-2
Figure A-3. Cross Section of an Irradiated ZrC-gettered, SiC-TRISO Particle A-3

List of Tables

Table 2-1. Work Breakdown Structure and Responsibility Assignment Matrix 2-7
Table 2-2. H2-MHR Nominal Plant Design Parameters 2-9
Table 3-1. H2-MHR Core Design Parameters 3-2
Table 3-2. Coated Particle Design Parameters 3-4
Table 3-3. Fuel Compact Design Parameters 3-6
Table 3-4. H2-MHR Standard Fuel Element Design Parameters 3-8
Table 3-5. Reactor Vessel Design Parameters 3-18
Table 3-6. Impact of Higher Coolant Temperatures 3-23
Table 3-7. Optimized PSR Inlet Flow Configuration 3-24
Table 3-8. Reactor Vessel and Fuel Temperatures as a Function of Vessel Cooling Flow Rate 3-25
Table 3-9. Shutdown Cooling System Design Parameters 3-30
Table 3-10. RCCS Steady State Performance at 100% Reactor Power 3-36
Table 3-11. Summary of Performance Data for High-Quality TRISO Fuel Manufactured in Germany 3-46
Table 3-12. Service Conditions for Fissile and Fertile Fuel 3-52
Table 3-13. As-Manufactured Quality Requirements for Fissile and Fertile Fuel 3-52
Table 3-14. In-Service Performance Requirements for Fissile and Fertile Fuel 3-53
Table 3-15. 600-MW(t) IHX Design Parameters 3-55
Table 3-16. Secondary Heat Transport System Design Parameters 3-59
Table 3-17. Comparison of Parallel and Concentric Piping Configurations 3-59
Table 3-18. Primary Helium Purification System Description 3-63

Table 3-19. SI Process Section 1 Flow Stream Description 3-72
Table 3-20. SI Process Section 2 Flow Stream Description 3-76
Table 3-21. SI Process Section 3 Flow Stream Description 3-81
Table 3-22. Description of Major Equipment – Section 1 3-82
Table 3-23. Description of Major Equipment – Section 2 3-83
Table 3-24. Description of Major Equipment – Section 3 3-84
Table 4-1. EFOH for MHR Nuclear Island System 4-5
Table 4-2. Summary of SI-Based H2-MHR Capital Costs 4-9
Table 4-3. Summary of SI-Based H2-MHR O&M Costs 4-10
Table 4-4. Summary of SI-Based H2-MHR Plant Hydrogen Production Costs 4-11
Table 4-5. Results of H2-MHR Plant Economic Parametric Studies 4-12

Acronyms and Abbreviations

AOO	Anticipated Operational Occurrence
ASME	American Society of Mechanical Engineers
ATHENA	Advanced Thermal Energy Network Analysis
BAF	Bacon Anisotropy Factor
CAA	Clean Air Act
C-C	Carbon-Fiber Reinforced Carbon
CCPS	Center for Chemical Process Safety
CFR	Code of Federal Regulations
CWA	Clean Water Act
DDN	Design Data Need
EAB	Exclusion Area Boundary
ED&D	Engineering Development and Demonstration
EFOH	Effective Forced Outage Hours
EFPD	Effective Full Power Days
EIReDA	European Industry Reliability Data Bank
EPRI	Electric Power Research Institute
ESH&Q	Environmental, Safety, Health, and Quality
FDDM	Fuel Design Data Manual
FHSS	Fuel Handling and Storage System
FIMA	Fissions per Initial Metal Atom
FFBD	Function Flow Block Diagram
GA	General Atomics
GT-MHR	Gas Turbine MHR
H2-MHR	Hydrogen Production MHR
HEU	High-Enriched Uranium
HM	Heavy Metal
HPCC	High Pressure Conduction Cooldown
HPS	Helium Purification System
HTE	High Temperature Electrolysis
HTGR	High Temperature Gas-Cooled Reactor

Acronyms and Abbreviations

HTIV	High Temperature Isolation Valve
HTS	Heat Transport System
HTTR	High Temperature Test Reactor
HVAC	Heating, Ventilation, and Air Conditioning
IAEA	International Atomic Energy Agency
IHX	Intermediate Heat Exchanger
INL	Idaho National Laboratory
IPS	Investment Protection System
IPyC	Inner Pyrocarbon
JAEA	Japan Atomic Energy Agency
LBP	Lumped Burnable Poison
LOCA	Loss of Coolant Accident
LPCC	Low Pressure Conduction Cooldown
LEU	Low-Enriched Uranium
LWR	Light Water Reactor
MHR	Modular Helium Reactor
MMBtu	million (thousand-thousand) Btu
NERI	Nuclear Energy Research Initiative
NESHAP	National Emissions Standards for Hazardous Air Pollutants
O&M	Operations & Maintenance
OSHA	Occupational, Safety, and Health Administration
OPyC	Outer Pyrocarbon
OREDA	Offshore Reliability Data
PCS	Power Conversion System
PSR	Permanent Side Reflector
PyC	Pyrocarbon
R/B	Release Rate to Birth Rate
RHRS	Residual Heat Removal System
RSC	Reserve Shutdown Control
RCCS	Reactor Cavity Cooling System
RPS	Reactor Protection System
SAPHIRE	Systems Analysis Programs for Hands-on Integrated Reliability

Acronyms and Abbreviations

	Evaluations
SI	Sulfur-Iodine
SiC	Silicon Carbide
SCS	Shutdown Cooling System
SFSS	Spent Fuel Storage System
SNL	Sandia National Laboratories
SMR	Steam-Methane Reforming
SSC	Systems, Structures, and Components
TBD	To Be Determined
TRISO	TRI-material, ISOtropic
TRU	Transuranic
VLPC	Vented Low Pressure Containment
WBS	Work Breakdown Structure

1. Introduction and Background

This report provides a pre-conceptual design description of a full-scale, n^{th}-of-a-kind nuclear hydrogen production plant that is based on coupling the Modular Helium Reactor (MHR) to the Sulfur Iodine (SI) thermochemical water splitting process. This concept is illustrated in Fig. 1-1. As shown in Fig. 1-2, the heat required to drive the SI process is supplied by Modular Helium Reactors (MHRs). The plant consists of four 600 MW(t) MHR modules, with each module coupled to an Intermediate Heat Exchanger (IHX) to transfer the heat to a secondary helium loop. The heat is then transferred to the SI-based Hydrogen Production System. Waste heat is rejected using cooling towers in a manner similar to that for electricity-producing plants. In addition to the heat required to drive the SI process, the plant requires approximately 800 MW(e). Most of this electricity is needed to power pumps and compressors that are part of the Hydrogen Production System design. For this study, it is assumed that the H2-MHR plant is part of an energy park that also includes GT-MHRs that provide the necessary electricity.

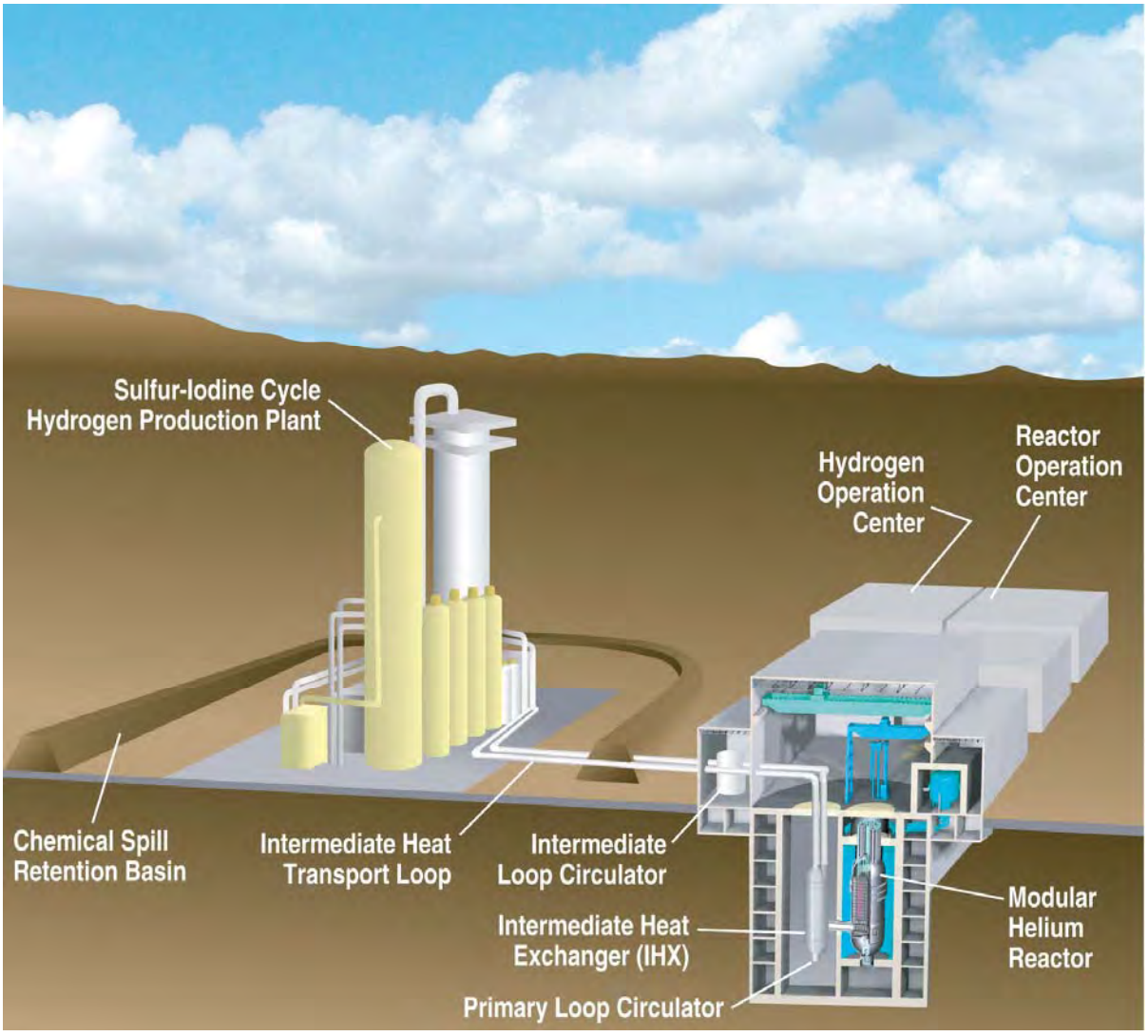

Figure 1-1. SI-Based H2-MHR Concept

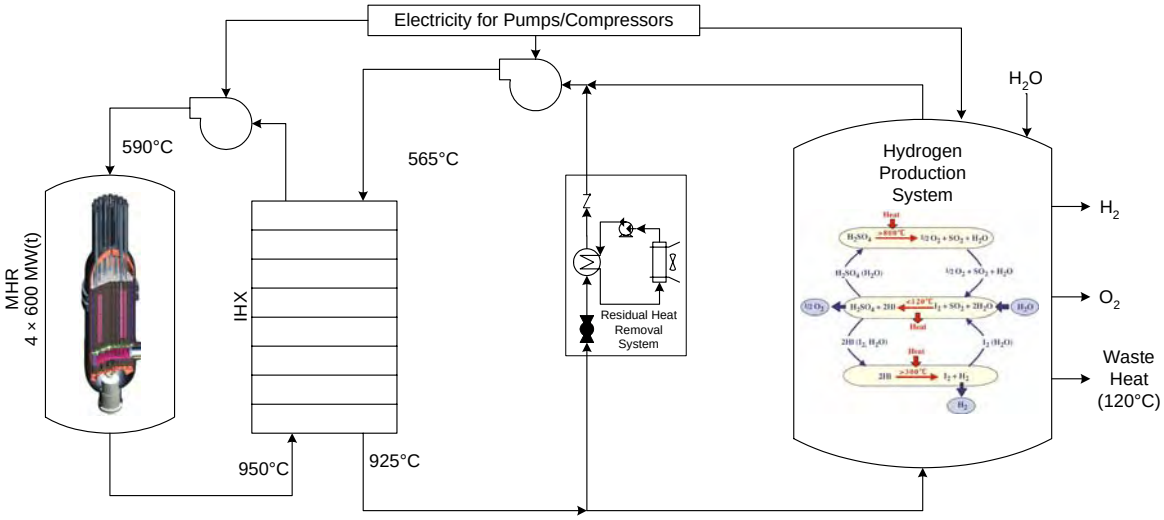

Figure 1-2. SI-Based H2-MHR Process Schematic

1.1 Modular Helium Reactor Design Status

The Modular Helium Reactor Design is based on high-temperature, gas-cooled reactor technology that has been under development since the middle 1960s for electricity production and a variety of process-heat applications, including the production of hydrogen. In more recent years, General Atomics (GA) has been developing a passively safe, modular-sized design referred to as the Modular Helium Reactor (MHR). For electricity production, this concept operates with a thermal power level of 600 MW and an outlet helium temperature of 850°C to drive a direct, Brayton cycle power-conversion system (PCS) with a thermal-to-electrical conversion efficiency of 48 percent (see Fig. 1-3). This concept is referred to as the Gas Turbine MHR (GT-MHR) and is described in [Shenoy, 1996].

Development of the GT-MHR has continued under the International GT-MHR Project, which was started in 1995 by GA and Minatom (currently Rosatom) of Russia for the mission of disposition of surplus weapons-grade plutonium. The project is currently being funded on a parity basis by the U.S. and Russian governments under the "Agreement Between the Government of the United States of America and the Government of the Russian Federation on Scientific and Technical Cooperation in the Management of Plutonium that has Been Withdrawn from Nuclear Military Programs". Some funding for development of the PCS was obtained from the Electric Power Research Institute (EPRI) in the U.S. and from the European Union and Japan through their membership in the International Science and Technology Center. Under this project the bulk of the design work and technology development is performed in Russia. United States organizations, including GA and Oak Ridge National Laboratory, have assisted the project through oversight and sharing experiences in design and operation of gas-cooled reactors and transferring technologies and computer codes used for design.

The GT-MHR Conceptual Design for plutonium disposition was completed in 1997 and was independently reviewed by a panel of experts representing the U.S., Russia, Japan, Germany and France. The review confirmed the capability of the GT-MHR to deeply burn weapons-grade plutonium in a once-through fuel cycle. The panel concluded the GT-MHR was a viable design

that merited further development and there were no insurmountable obstacles to prevent construction of a GT-MHR on a reasonable schedule. The Preliminary Design Phase was completed in 2002 and reviewed by Minatom. The GT-MHR was approved in Russia as an innovative, next-generation concept for generation of electricity and process heat. Work is currently focused on areas related to technical risks, including coated particle fuel development, demonstration of the PCS with electromagnetic bearings, and verification/validation of computer codes for core design, including core physics, thermal hydraulics, fuel performance, and fission product transport. [LaBar, 2003] provides additional information on the GT-MHR design and its technology background.

For hydrogen production, the reactor design is essentially the same as that for the GT-MHR, but with some minor modifications to allow operation with a higher coolant-outlet temperature of 950°C in order to increase hydrogen-production efficiency. The power conversion system is replaced with an IHX and a helium circulator on the cold leg of the primary helium circuit.

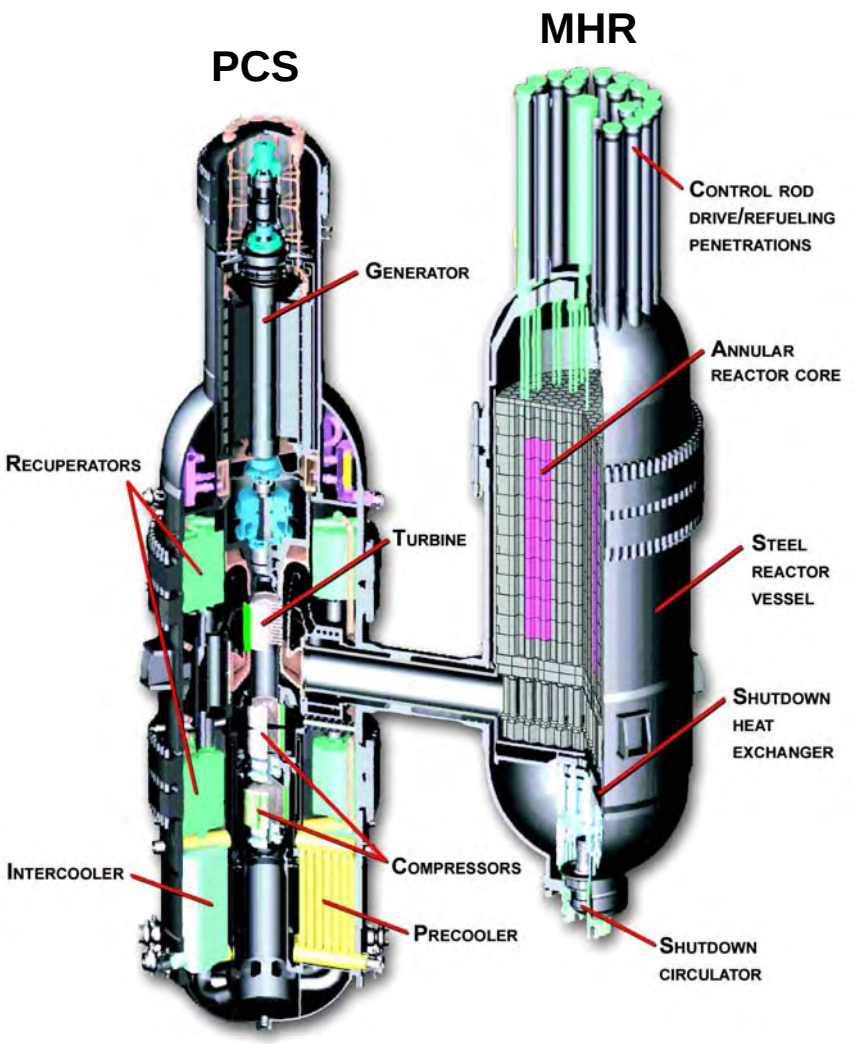

Figure 1-3. The Gas-Turbine Modular Helium Reactor

1.2 Hydrogen Production Using the Sulfur-Iodine Process

As part of an earlier study sponsored by the U.S. Department of Energy Nuclear Energy Research Initiative (NERI), a team headed by GA and supported by Sandia National Laboratories (SNL) and the University of Kentucky evaluated 115 different thermochemical cycles that produce hydrogen [Brown, 2003]. The sulfur-iodine (SI) cycle was determined to be the best cycle for coupling to the MHR because of its high efficiency and potential for further improvement. The Japanese Atomic Energy Agency (JAEA) has also selected the SI process for further development and has successfully completed bench-scale demonstrations of the SI process at atmospheric pressure [Kubo, 2005]. JAEA also plans to proceed with pilot-scale demonstrations of the SI process and eventually plans to couple an SI demonstration plant to its High Temperature Test Reactor (HTTR) ([Terada, 2005], [Iyoku, 2005]). As part of an international NERI project, GA, SNL, and the French Commissariat L'Energie Atomique will perform laboratory–scale demonstrations of the SI process at prototypical temperatures and pressures. This demonstration will be performed at General Atomics in San Diego, CA. Integration of the loop components is expected to start in March 2007.

Water thermally dissociates at significant rates into hydrogen and oxygen at temperatures approaching 4000°C. As indicated in Fig. 1-4, the SI process consists of three primary chemical reactions that accomplish the same result at much lower temperatures. The process involves decomposition of sulfuric acid and hydrogen iodide, and regeneration of these reagents using the Bunsen reaction. Process heat is supplied at temperatures greater than 800°C to concentrate and decompose sulfuric acid. The exothermic Bunsen reaction is performed at temperatures below 120°C and releases waste heat to the environment. Hydrogen is generated during the decomposition of hydrogen iodide, using process heat at temperatures greater than 300°C. Figure 1-5 shows a simplified process flow diagram of the SI cycle. The product hydrogen gas is produced at a pressure of 4.0 MPa.

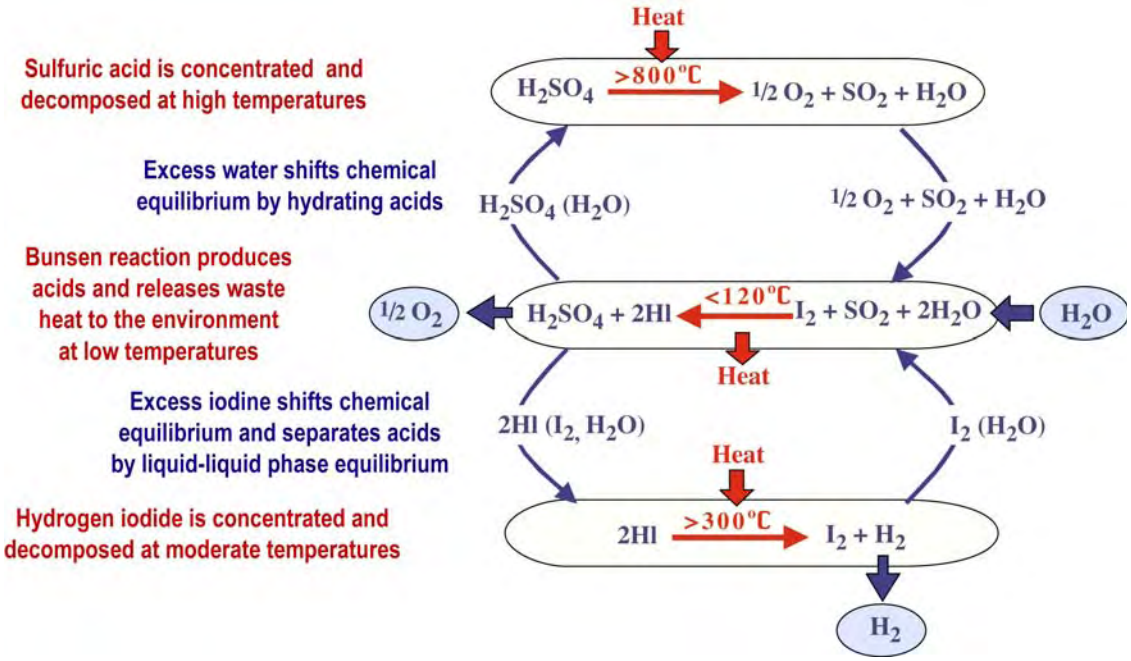

Figure 1-4. The SI Thermochemical Water Splitting Process

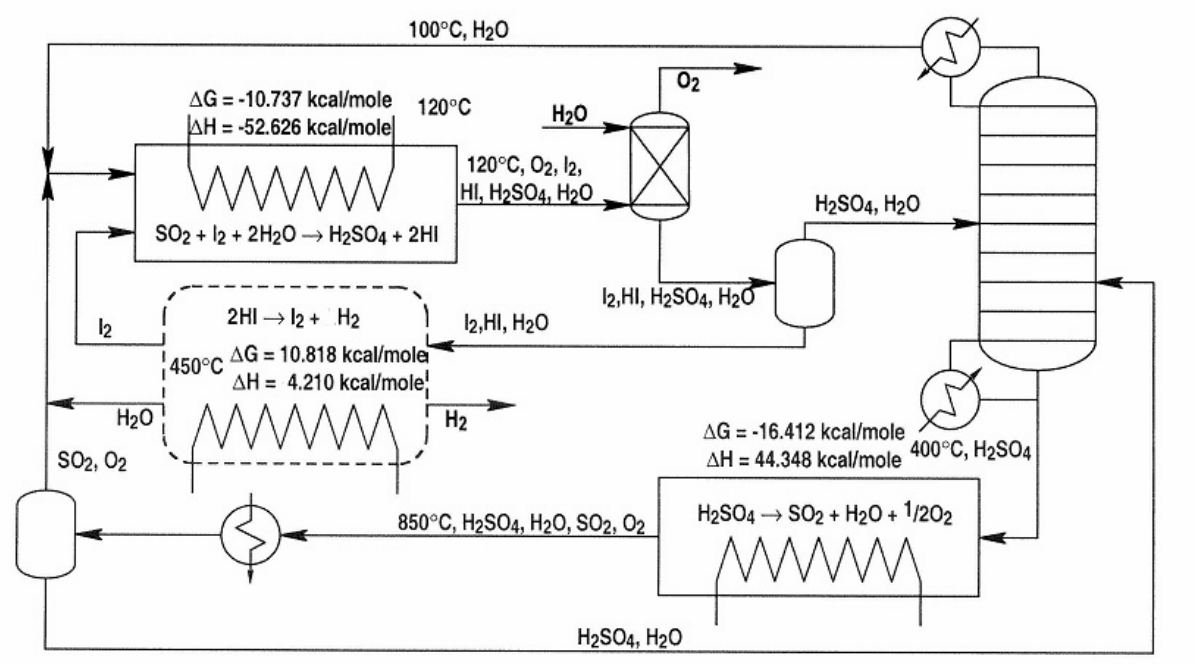

Figure 1-5. Simplified SI Process Flow Schematic

2. Overall Plant Description

2.1 Plant Level Functions and Performance Requirements

As part of this pre-conceptual design study, a systems-engineering approach has been used to develop functions and performance requirements for the H2-MHR at the plant/major system level. A function is a succinct statement that describes the purpose of the plant/system. Each function must have at least one performance requirement. A performance requirement quantifies how well its associated function must be performed. Brackets **[ ]** are used to identify information that is preliminary in nature, results from a design uncertainty, originates from insufficient documentation, or needs verification. **TBD** (To Be Determined) is used when numeric values or descriptive information is not yet available.

The following numbering convention is used to identify functions: F-P-XXXX, where F stands for Function, P stands for Plant/Major System level, and XXXX is a 4-digit number. Similarly, performance requirements are identified according to PR-P-XXXX, where PR stands for Requirement.

The primary function of the H2-MHR is to supply hydrogen gas to end users. This is accomplished using the SI process to thermochemically split water, with the heat supplied from an MHR. As shown in Fig. 2-1, the functional decomposition has been developed using a Function Flow Block Diagram (FFBD). When viewed from left-to-right, the functions flow from higher level to lower level. The lower-level functions describe how higher level functions are performed. Preliminary performance requirements have been prepared for the higher-level functions and are given below.

F-P-0010 Supply Hydrogen Gas

The Performance Requirement(s) associated with this function are:

PR-P-0010 The availability of hydrogen gas supplied from the H2-MHR plant shall be **[**99%**]**.

PR-P-0020 The H2-MHR plant shall supply **[**3.68×10^5**]** mt of hydrogen per year.

PR-P-0020 Chemical impurities in the product hydrogen gas shall be less than **[**0.2**]** %.

PR-P-0025 The moisture content of the product hydrogen gas shall not exceed **TBD** ppm

PR-P-0030 The tritium content in the product hydrogen gas shall not exceed **TBD** picocuries per liter.

PR-P-0040 The concentration of total radioactivity in the hydrogen gas shall not exceed **TBD** Ci/m^3.

PR-P-0050 Hydrogen gas shall be supplied at a pressure of **[**4**]** MPa.

PR-P-0060 Hydrogen gas shall be supplied at a temperature of **[**30**]** °C.

PR-P-0070 The H2-MHR plant shall have a hydrogen storage capacity of **TBD** mt.

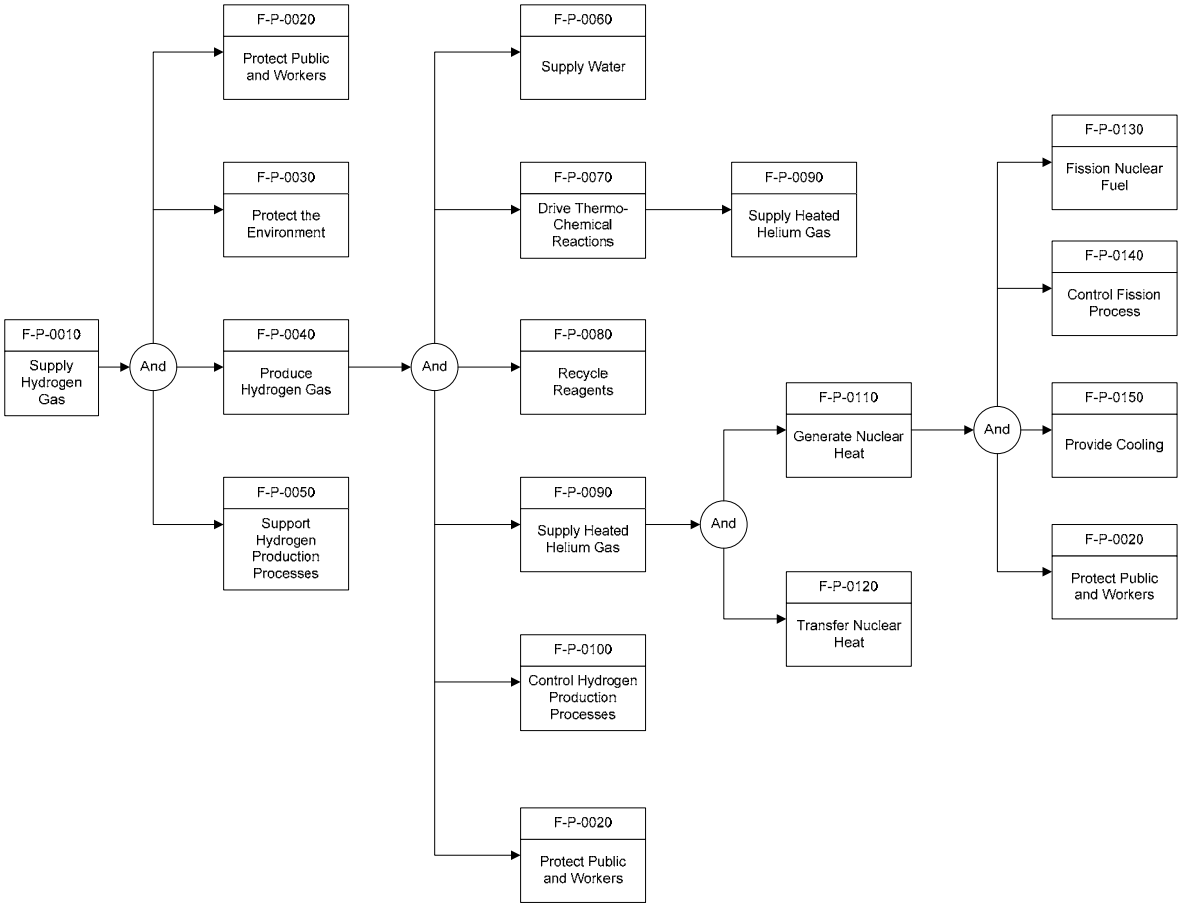

Figure 2-1. H2-MHR High-Level Function Flow Block Diagram

F-P-0020 Protect Public and Workers

The Performance Requirement(s) associated with this function are:

PR-P-0080 Occupational radiation exposures shall be no greater than 10% of the limits specified in 10 CFR 20.

PR-P-0090 During design-basis accidents, offsite radiation doses to the public shall be less than the limits specified in 10 CFR 100.

PR-P-0100 During design-basis accidents, offsite doses at the site Exclusion Area Boundary (EAB) shall be less than those specified in the Manual of Protective

Action Guides and Protective Actions for Nuclear Incidents (EPA-520/1-75-001) for sheltering and evacuation.

PR-P-0110 During normal operation, offsite radiation doses to the public shall be less than the limits specified in Appendix I of 10 CFR 50 and 40 CFR 190.

PR-P-0120 The individual acute and latent fatality risks shall be less than the limits specified on 51 FR 130.

PR-P-0130 The H2-MHR plant shall comply with all applicable OSHA General Industry Standards, including 29 CFR 1910.132 - 133 and 135 - 136, Personal Protective Equipment (including general requirements, eye and face protection) and 29 CFR1910.134, Respiratory Protection for applicable hazardous chemicals including sulfuric acid, hydriodic acid, phosphoric acid, and iodine.

PR-P-0140 Exposures to any given hazardous chemical shall not exceed the maximum acceptable levels found in OSHA 29 CFR1910.1000, Subpart Z; and other OSHA substance-specific standards.

PR-P-0150 Total releases of sulfur dioxide to the atmosphere shall be less than **TBD** for normal operation, and **TBD** during any accident or upset condition.

PR-P-0160 The H2-MHR plant shall comply with OSHA requirements contained in 29 CFR 1910.119 for preventing or minimizing the consequences of catastrophic releases of toxic, reactive, flammable, or explosive chemicals [inventories of hydrogen, sulfur dioxide (liquid), sulfur trioxide, and sulfuric acid in excess of threshold quantities].

F-P-0030 Protect the Environment

The Performance Requirement(s) associated with this function are:

PR-P-0170 Emissions from the H2-MHR plant shall not exceed established EPA limits on the amount of sulfur dioxide and other hazardous air pollutants, all other applicable requirements of the Clean Air Act/Air Programs (CAA), 40 CFR 50-99, and all state and local requirements.

PR-P-0180 Emissions from the H2-MHR plant will comply with all applicable requirements of the Clean Water Act/Water Programs (CWA), 40 CFR 100-149, and all state and local requirements.

PR-P-0190 Emissions from the H2-MHR plant shall comply with the requirements of 40 CFR 61, National Emissions Standards for Hazardous Air Pollutants (NESHAP) and all applicable state and local air permit requirements.

PR-P-0200 The release of gaseous, liquid, and solid radioactive materials to the environment shall not exceed applicable federal, state, and local environmental protection requirements.

F-P-0040 Produce Hydrogen Gas

The Performance Requirement(s) associated with this function are:

PR-P-0210 The overall efficiency for hydrogen production shall be **[**>40%**]**.

F-P-0050 Support Hydrogen Production Processes

The Performance Requirement(s) associated with this function are:

PR-P-0220 **TBD** MW of electricity shall be supplied to the H2-MHR plant.

PR-P-0230 **TBD** MW of electricity shall be available to the H2-MHR plant from a backup power source.

PR-P-0240 A nominal **[**336**]** MW of waste heat shall be removed from the H2-MHR plant systems when all 4 modules are operating at 100% capacity under the following ambient conditions: **[**35.5**]**°C dry-bulb temperature, **[**25**]**°C wet-bulb temperature.

PR-P-0250 Systems and components shall be protected from the effects of the environment, including natural phenomena hazards.

2.2 Work Breakdown Structure and Responsibility Assignment Matrix

A level 2 Work Breakdown Structure (WBS) has been developed for the H2-MHR project and is shown in Table 2-1, along with the Responsibility Assignment Matrix for the Design Organization, Technology Organization, and Owner/Operator. It is expected the Design Organization would be a consortium of companies with experience in designing and building commercial-scale nuclear reactors and large-scale chemical plants. The Technology Organization would include U.S. national laboratories and other organizations qualified to perform the required technology development activities. The Owner/Operator could be a commercial utility, an energy company, the U.S. Department or Energy, or a consortium of these organizations. The H2-MHR project could also include international collaboration in the Design, Technology, and Owner/Operator areas.

Table 2-1. Work Breakdown Structure and Responsibility Assignment Matrix

WBS	Title	Design Organization	Technology Organization	Owner / Operator
1.0	Plant Definition			
1.1	Systems Identification	X		
1.2	Plant and Systems Functions	X		X
1.3	Performance Requirements	X		X
1.4	Design Requirements	X		X
1.5	ESH&Q* Requirements	X		X
1.6	Interface Requirements	X		X
2.0	MHR System Design			
2.1	Core Nuclear / Thermal Hydraulic Design	X		
2.2	Fuel Design	X		
2.3	Reactor Internals Design	X		
2.5	Shutdown Cooling System Design	X		
2.4	RCCS Design	X		
2.5	Fuel Performance / Radionuclide Transport	X		
3.0	MHR System Technology Development			
3.1	Fuel	X	X	
3.2	Graphite	X	X	
3.3	Metals	X	X	
3.4	Radionuclide Transport	X	X	
4.0	Heat Transport System (HTS) Design			
4.1	IHX Design	X		
4.2	Primary and Secondary Coolant Circulators	X		
4.3	Secondary Loop Piping	X		
4.4	High Temperature Isolation Valves	X		
4.5	Residual Heat Removal System Design	X		
5.0	HTS Technology Development		X	
5.1	IHX	X	X	

Table 2-1. Work Breakdown Structure and Responsibility Assignment Matrix

WBS	Title	Design Organization	Technology Organization	Owner / Operator
5.2	High Temperature Helium Circulators	X	X	
5.3	High Temperature Isolation Valves	X	X	
6.0	H_2 Production System Design			
6.1	Sulfur-Iodine H_2 Production Process	X		
6.2	Heat / Mass Balances	X		
6.3	Reaction Vessels / Heat Exchangers Design	X		
6.4	Hydraulics / Pump Design	X		
6.5	Waste Heat Rejection	X		
6.6	Facility Layout	X		
7.0	H_2 Production System Technology Development			
7.1	Pilot-Scale Demonstration	X	X	
7.2	Reaction Vessels / Heat Exchangers	X	X	
7.3	Materials Development	X	X	
8.0	Plant Level Systems Design			
8.1	Plant Site / Arrangement	X		X
8.2	BOP and Auxiliary Systems	X		
8.3	Plant Integration	X		X
8.4	Design Review / Customer Requirements			X
9.0	Plant Assessments			
9.1	Trade Studies and Sensitivity Analysis	X		
9.2	Safety Assessment	X		
9.3	Availability Assessment	X		
9.4	Licensing Assessment	X		X
9.5	Economic Assessment	X		X
9.6	Nominal Plant Performance / Operation	X		
9.7	Transient Operation and Control	X		
9.8	Identification of Design Data Needs	X		
10.0	Project Management			
10.1	Project Planning and Coordination	X		
10.2	Project Monitoring	X		
10.3	Project Review	X	X	X
10.4	Annual / Final Reports	X	X	X

* ESH&Q = Environmental, Safety, Health, and Quality

2.3 Overall Plant Arrangement

The plot plan for the H2-MHR plant is shown on Fig. 2-2. The layout is very similar to the layout for a 4-unit GT-MHR plant [Shenoy, 1996], with the addition of the chemical process equipment for Hydrogen Production Plant. The plant occupies a footprint of approximately 690 m × 503 m. The Hydrogen Production Plant is located outside of the nuclear plant boundary and is classified as a non-nuclear system.

2.4 Nominal Plant Design Parameters

The nominal plant design parameters are given in Table 2-2. On an annual basis, the SI-based H2-MHR plant produces 3.68×10^5 metric tons at a plant capacity factor of 90%. The overall plant efficiency for hydrogen production is 45.0%.

Table 2-2. H2-MHR Nominal Plant Design Parameters

MHR System	
Number of modules	4
Module power rating	600 MW(t)
Core inlet/outlet temperatures	590°C / 950°C
Peak fuel temperature – normal operation	1250°C - 1350°C
Peak fuel temperature – accident conditions	< 1600°C
Heat Transport System	
Primary coolant fluid	helium
Primary coolant pressure	7.0 MPa
Primary coolant flow rate	320 kg/s
Total pressure drop – primary circuit	100 kPa
Secondary coolant fluid	helium
Secondary coolant pressure	7.1 MPa
Secondary coolant flow rate	320 kg/s
Secondary coolant cold leg/hot leg temperatures	565°C / 925°C
Total pressure drop – secondary circuit	146 kPa
Hydrogen Production System	
Peak process temperature	900°C
Peak process pressure	7.0 MPa
Product hydrogen pressure	4.0 MPa
Annual hydrogen production*	3.68×10^5 metric tons
Plant hydrogen production efficiency**	45.0%

* Based on an overall plant capacity factor of 90%.
** Based on the higher heating value of hydrogen (141.9 MJ/kg).

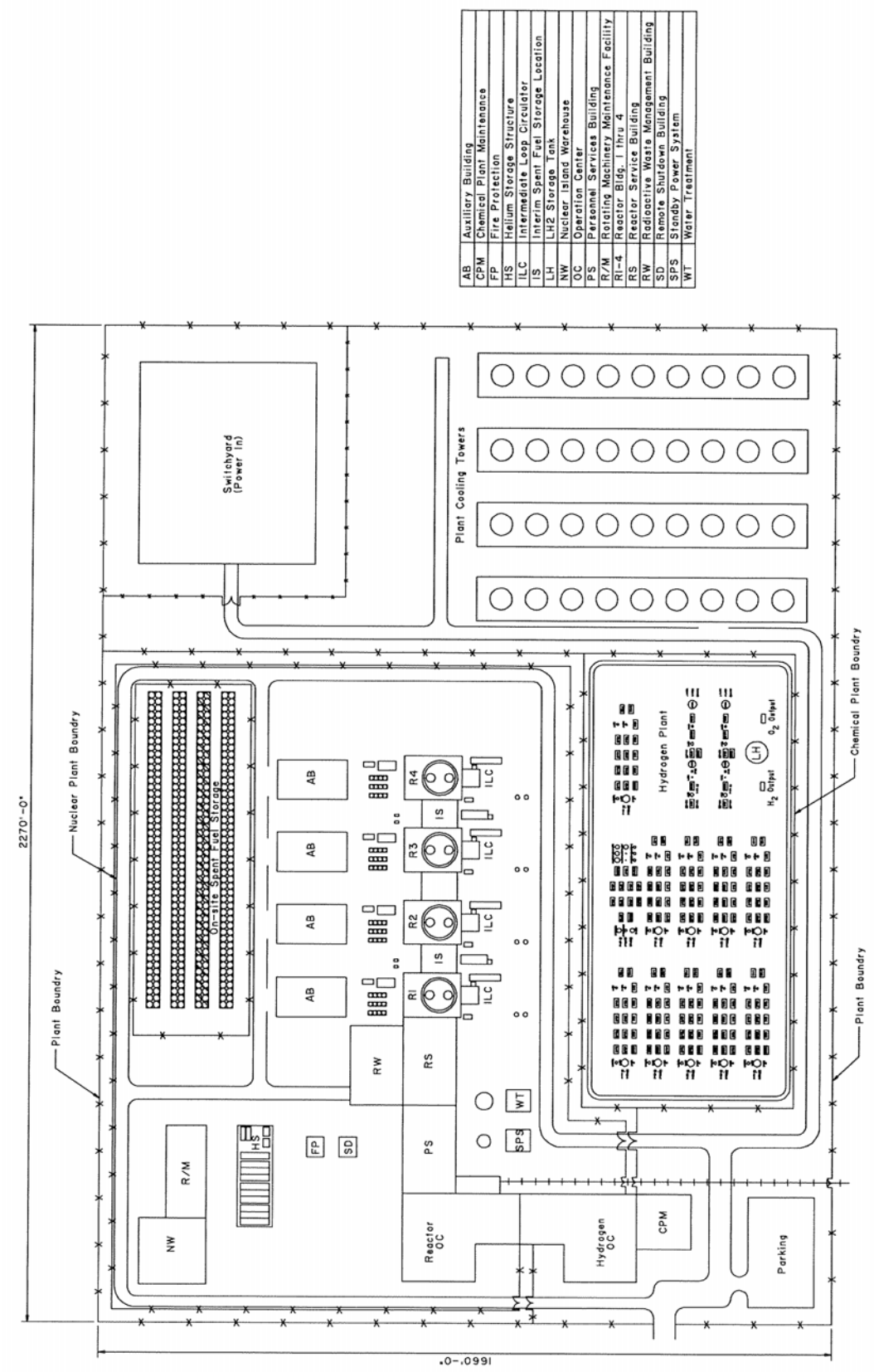

Figure 2-2. H2-MHR Plant Arrangement

2.5 Plant Operation

The H2-MHR is intended to operate at full, base-load power excect during planned outages for refueling and other maintenance. Planned outages for the MHR System will be staggered from module to module to minimize the overall impact on availability. Also, the H2-MHR plant will be part of a network of plants that includes a hydrogen storage system in order to ensure overall hydrogen availability of 99% or greater to the end user. When hydrogen demand is lower, the H2-MHR plants will continue to operate at their base-load capacity, but divert some of the hydrogen to the storage facility for later use when demand is higher. For example, if hydrogen is used primarily by the transportation sector, stored hydrogen would be recovered primarily during peak driving periods.

Procedures for startup/shutdown of the plant and overall plant control will be developed during the preliminary and final design phases. A potential issue is propagation of thermal disturbances in the Hydrogen Production System (e.g., from failure of a pump motor) that impact the MHR primary coolant inlet/outlet temperatures beyond the scram setpoints. As discussed in [Inaba, 2005], the propagation of thermal disturbances in the Hydrogen Production System can be mitigated by ensuring there is sufficient fluid in the Hydrogen Production System that undergoes phase change at constant temperature.

3. Plant Technical Description

3.1 MHR System Design

The MHR system design includes the Reactor System, Cross Vessel and Hot Duct Assembly, Reactor Vessel, Shutdown Cooling System (SCS), and Reactor Cavity Cooling System (RCCS). These systems and design modifications for higher temperature operation are described in the following sections. The MHR design features for fuel performance and radionuclide control are described in Section 3.1.7.

3.1.1 Reactor System

Figure 3-1 shows a cross-sectional view of the Reactor System, which includes the reactor core, the Neutron Control System, and other equipment within the reactor vessel. The H2-MHR core design parameters are summarized in Table 3-1.

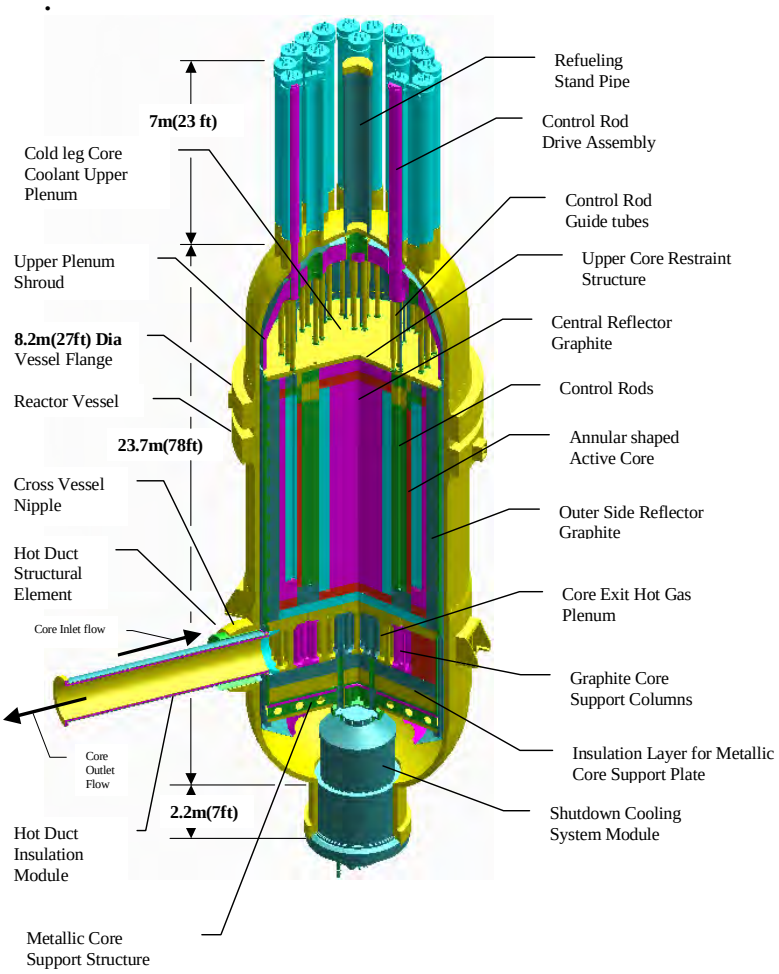

Figure 3-1. Modular Helium Reactor System

Table 3-1. H2-MHR Core Design Parameters

Core thermal power (MW)	600
Number of fuel columns	102
Number of fuel blocks per column	10
Thermal power density (MW/m^3)	6.6
Effective inner diameter of active core (m)	2.96
Effective outer diameter of active core (m)	4.83
Active core height (m)	7.93
Fissile fuel (19.8% enriched in U-235)	$UC_{0.5}O_{1.5}$
Fertile Fuel (natural U)	$UC_{0.5}O_{1.5}$
Equilibrium fuel cycle length (full-power days)	425
Number of columns per refueling segment	51
Mass of heavy metal per refueling segment (kg)	1748 (fissile fuel)
	514 (fertile fuel)
Core inlet temperature (°C)	590
Core outlet temperature (°C)	950
Core upper plenum inlet pressure (MPa)	7.1
Core pressure drop (MPa)	0.058
Coolant flow rate (kg/s)	320

3.1.1.1 Fuel Design

The H2-MHR fuel element and its components are shown in Fig. 3-2. The fuel for the H2-MHR consists of microspheres of uranium oxycarbide that are coated with multiple layers of pyrocarbon and silicon carbide. The H2-MHR core is designed to use a blend of two different particle types; a fissile particle that is enriched to 19.8% U-235 and fertile particle with natural uranium (0.7% U-235). The fissile/fertile loading ratio is varied with location in the core, in order to optimize reactivity control, minimize power peaking, and maximize fuel cycle length. The buffer, inner pyrolytic carbon (IPyC), silicon carbide (SiC), and outer pyrolytic carbon (OPyC) layers are referred to collectively as a TRISO[1] coating. The coating system can be viewed as a miniature pressure vessel that provides containment of radionuclides and gases. This coating system is also an excellent engineered barrier for long-term retention of radionuclides in a repository environment. Coated particle design parameters are given in Table 3-2. The functions of the fuel kernel and coating layers during operation of the H2-MHR are described below.

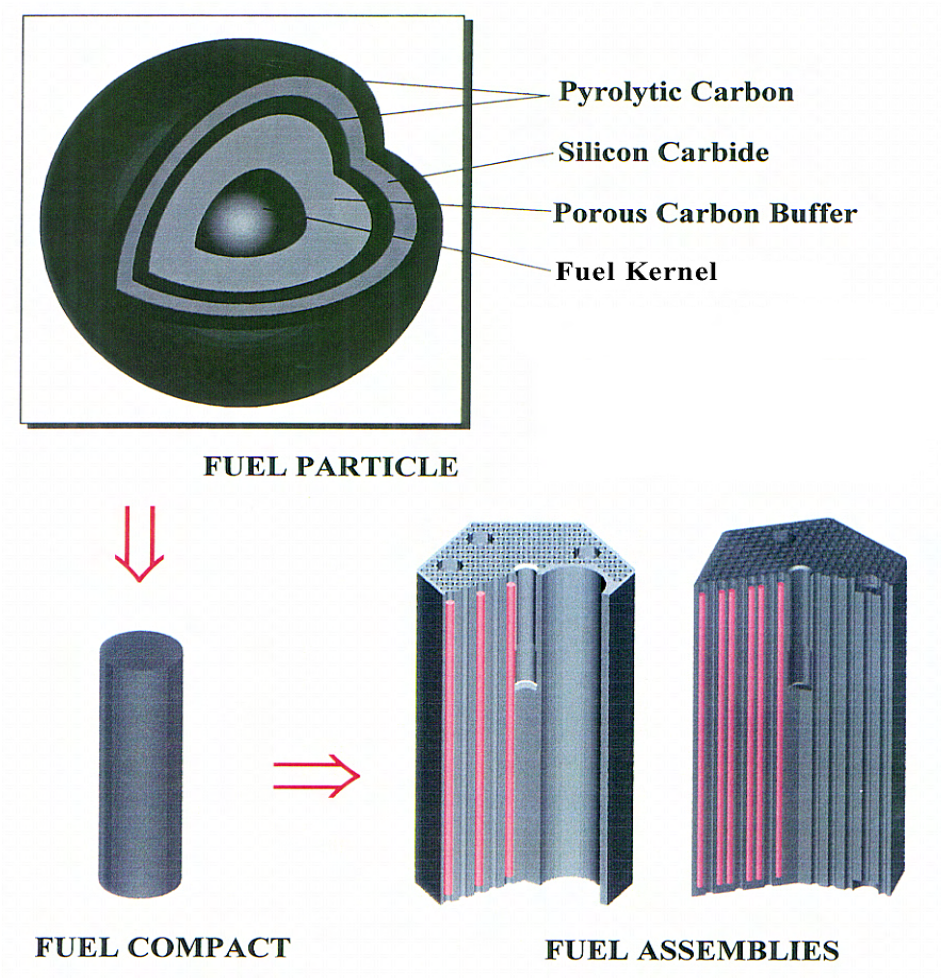

Figure 3-2. MHR Fuel Element Components

[1] TRISO is an acronym for TRI-material, ISOtropic, with the materials being low-density pyrolytic carbon (buffer), high density pyrolytic carbon (IPyC and OPyC), and SiC.

Table 3-2. Coated Particle Design Parameters

	Fissile Particle	Fertile Particle
Composition	$UC_{0.5}O_{1.5}$	$UC_{0.5}O_{1.5}$
Uranium enrichment, %	19.8	0.7 (Natural Uranium)
Dimensions (µm)		
Kernel Diameter	350	500
Buffer thickness	100	65
IPyC thickness	35	35
SiC thickness	35	35
OPyC thickness	40	40
Particle diameter	770	850
Material Densities (g/cm^3)		
Kernel	10.5	10.5
Buffer	1.0	1.0
IPyC	1.87	1.87
SiC	3.2	3.2
OPyC	1.83	1.83
Elemental Content Per Particle (µg)		
Carbon	305.7	379.9
Oxygen	25.7	61.6
Silicon	104.5	133.2
Uranium	254.1	610.2
Total particle mass (µg)	690.0	1184.9
Design burnup (% FIMA)[a]	26	7

Note
a. FIMA is an acronym for Fissions per Initial Metal Atom.

Fuel Kernel

The oxycarbide kernel composition was selected for the H2-MHR primarily because of its ability to perform well at relatively high burnup. The carbide component of the kernel undergoes oxidation to getter excess oxygen released during fission. If the carbide component were not present, excess oxygen would react with carbon in the buffer to form carbon monoxide. High levels of carbon monoxide can lead to failure of the coating system by overpressurization and kernel migration (see Section 3.1.7.2). The oxide component of the kernel is highly effective at retaining many radionuclides that can chemically attack or diffuse through the coating layers (e.g., lanthanides and strontium, respectively).

Buffer

The buffer is deposited over the kernel and consists of low-density, porous pyrocarbon. The buffer attenuates fission fragments that recoil from the kernel and provides sufficient void space to accommodate gases, including gaseous fission products and CO. The buffer also acts as a sacrificial layer to accommodate potential kernel migration and swelling and isolates the kernel from load-bearing layers of the coating system.

IPyC Layer

The high-density IPyC layer serves to protect the kernel and buffer from chemical attack by chlorine compounds, which are generated as byproducts during deposition of the SiC layer. The IPyC layer also provides a smooth surface for deposition of the SiC layer and delays transport of radionuclides to the SiC layer. The IPyC layer shrinks with the accumulation of fast neutron fluence, which helps to maintain the SiC layer in compression, provided the bond between the IPyC and SiC layers remains strong and continuous during irradiation (see Section 3.1.7.2).

SiC Layer

The SiC layer is deposited under conditions to produce a high-density, high-strength coating with a fine-grain microstructure. This layer provides the primary structural support to accommodate stresses generated by internal gas pressure and irradiation-induced dimensional changes of the pyrocarbon layers. The SiC layer provides an impermeable barrier to gaseous, volatile, and most metallic fission products during normal operation and hypothetical accidents. Dimensional changes of the SiC are very small during irradiation, and it is considered to be dimensionally stable.

OPyC Layer

The high-density OPyC layer protects the SiC layer from mechanical damage that may occur during fabrication of fuel compacts and fuel elements, and provides a bonding surface for the compact matrix. The OPyC layer also shrinks during irradiation, which helps to maintain the SiC layer in compression. The OPyC layer prevents the release of gaseous fission products, if both the IPyC and SiC layers are defective or fail in service.

Fuel Compacts

Each fuel compact is a mixture of fissile, fertile, and graphite shim particles bonded together with a carbonaceous matrix into a rod-shaped compact with dimensions 12.45 mm (0.49 in.) in diameter and 49.3 mm (1.94 in.) in length. The fuel compacts are stacked in the blind fuel holes of the graphite fuel element. Graphite plugs are cemented into the tops of the fuel holes to enclose the stacked compacts. Because of sorption mechanisms, the fuel compacts can provide an additional barrier to the release of metallic fission products. Fuel compact design parameters are given in Table 3-3.

Graphite Fuel Element Blocks

The standard GT-MHR fuel-element graphite block and the arrangement of fuel holes, coolant holes, and lumped burnable poison[2] (LBP) holes is shown in Figure 3-3. The graphite blocks are fabricated from high-purity, nuclear-grade graphite. Each block is a right hexagonal prism with dimensions 794 mm (31.2 in.) in length and 360 mm (14.2 in.) across the flats of the hexagonal cross section. Fuel and coolant holes run parallel through the length of the block in a regular triangular pattern of nominally two fuel holes per coolant hole. The pitch of the coolant and fuel-hole array is 18.8 mm (0.74 in.). The minimum web thickness between a coolant hole

[2] B_4C is used as lumped (or fixed) burnable poison to control reactivity. Compacts containing coated B_4C and graphite shim granules are inserted into holes designated for lumped burnable poison, which are located near the corners of the block.

and fuel hole is 4.5 mm (0.18 in.). This web provides an additional barrier to release of metallic fission products. Design parameters for the standard fuel element are given in Table 3-4. A standard fuel element has 210 blind fuel holes, 108 coolant holes, and contains 3126 fuel compacts. In addition to standard fuel elements, the GT-MHR active core contains fuel elements with a single, larger diameter channel (3.75 to 4.0 in.) to allow insertion of additional poison for reserve shutdown capability.

Table 3-3. Fuel Compact Design Parameters

Diameter, mm	12.45
Length, mm	49.3
Volume, cm^3	6.0
Shim particle composition	H-451 or TS-1240 graphite
Shim particle size	99 wt % < 1.19 mm
	95 wt % < 0.59 mm
Shim particle density (g/cm^3)	1.74
Binder type	Petroleum pitch
Filler	Petroleum derived graphite flour
Matrix density (g/cm^3)	0.8 to 1.2
Volume fraction occupied by matrix	0.39
Volume fraction occupied by shim particles in an average compact[a]	0.41
Volume fraction occupied by fissile particles in an average compact[a]	0.17
Volume fraction occupied by fertile particles in an average compact[a]	0.03
Number of fissile particles in an average compact[a]	4310
Number of fertile particles in an average compact[a]	520
Mass of carbon in an average compact,[a,b] g	6.62

Notes
a. Values for an average compact are determined by assuming heavy metal (uranium) is distributed uniformly in the reactor core.
b. This value excludes carbon in the layers of the coated particles. For an average compact, there is an additional 1.32 g of carbon associated with fissile particles and an additional 0.20 g of carbon associated with fertile particles.

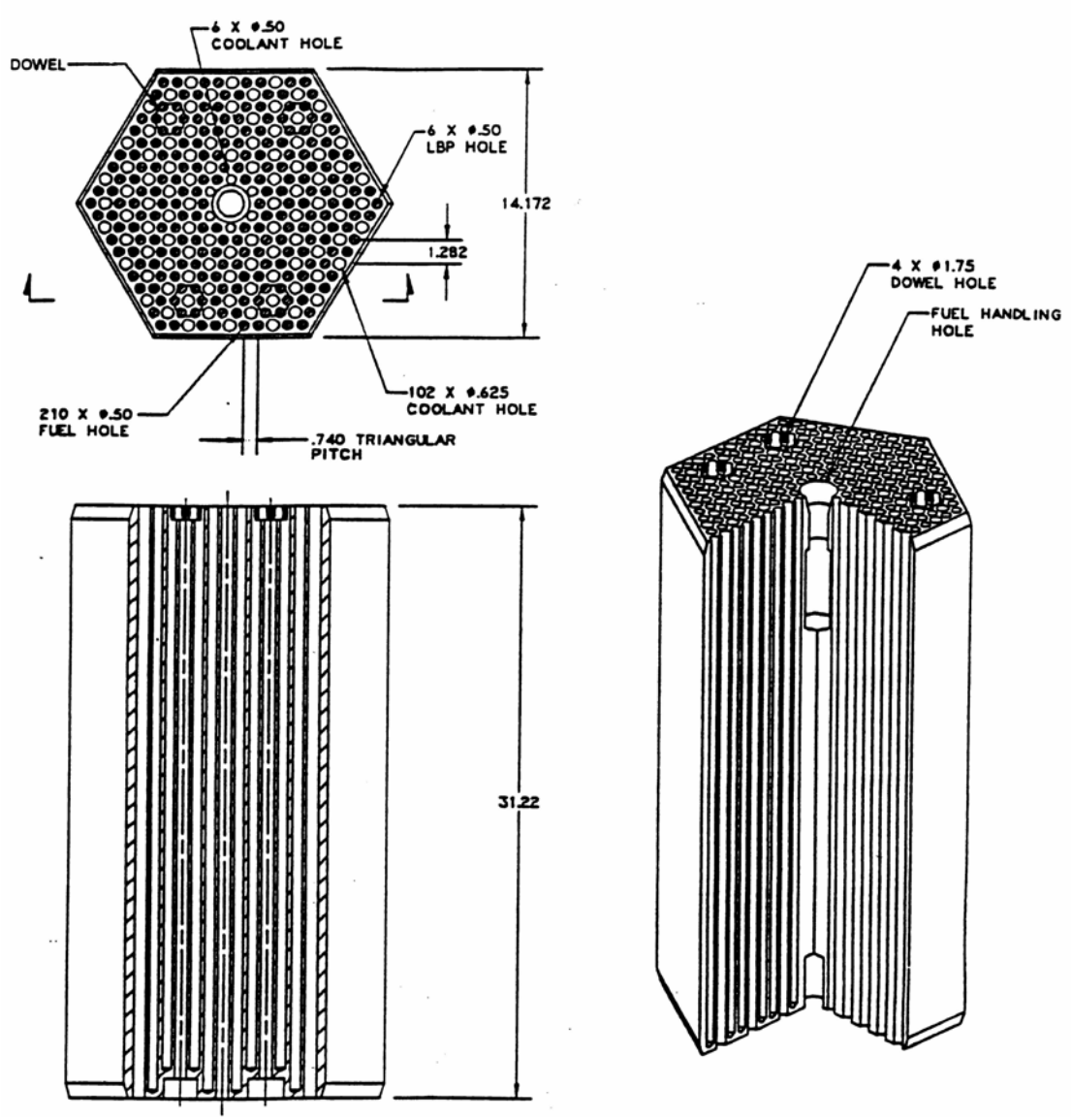

Figure 3-3. MHR Standard Fuel Element (dimensions shown are in inches)

Table 3-4. H2-MHR Standard Fuel Element Design Parameters

Shape	Hexagonal Prism
Type of graphite	Nuclear Grade H-451 or Equivalent
Mass of graphite per element	90 kg
Dimensions	794 mm (31.2 in.) in length
	360 mm (14.2 in.) across flats of hexagon
Volume[a]	0.0889 m^3
Total number of fuel holes	210
Number of fuel holes under dowels	24
Fuel hole diameter	12.7 mm (0.5 in.)
Fuel hole length	752.6 mm (29.63 in.) under dowels
	781.5 mm (30.77 in.) not under dowels
Number of fuel compacts per fuel hole	14 for holes under dowels
	15 for holes not under dowels
Number of fuel compacts per element	3126
LBP holes per element	6
LBP hole diameter	12.7 mm (0.5 in.)
LBP hole length	781.5 mm (30.77 in.)
Total number of coolant holes	108
Coolant hole diameter	15.88 mm (0.625 in.) for larger holes
	12.7 mm (0.5 in.) for the 6 smaller holes near the center of the block
Pitch of coolant/fuel-hole array	18.8 mm (0.74 in.)
Total mass of an average fuel element[b,c]	122 kg
Mass of carbon in an average fuel element[b,d]	110.7 kg
Mass of low-enriched uranium fuel in an average fresh fuel element[b]	3.43 kg
Mass of natural uranium fuel in an average fresh fuel element[b]	0.995 kg
Number of fissile particles in an average fuel element[b]	1.35×10^7
Number of fertile particles in an average fuel element[b]	1.63×10^6
Electrical energy generated by an average fuel element at discharge[b]	0.637 MW_e-yr

Notes
a. Calculated assuming a solid hexagonal prism with all fuel and coolant holes filled, i.e., this is the physical volume a fuel element would occupy.
b. Values for an average fuel element are determined by assuming heavy metal (uranium) is distributed uniformly in the reactor core.
c. This value includes graphite and fuel compacts, but excludes lumped burnable poison.
d. This value excludes carbon in the layers of the coated particles. For an average fuel element, there is an additional 4.13 kg of carbon associated with fissile particles and an additional 0.62 kg of carbon associated with fertile particles.

3.1.1.2 Reactor Core and Internals

Figure 3-4 shows the MHR core design. The MHR active core consists of 102 fuel columns in three annular rings with 10 fuel blocks per fuel column, for a total of 1020 fuel blocks in the active core. As shown in Fig. 3-5, the core is designed with 120-degree symmetry and the control rods are also operated symmetrically. The outer reflector contains 36 control rods, arranged as 12 groups with 3 rods per group. There are 4 control-rod groups in the active core, again with 3 rods per group. The core also contains 18 channels for insertion of reserve shutdown control (RSC) material (in the form of boronated pellets), in the event the control rods become inoperable. During operation, control rods in the active core are completely withdrawn, and only the control rods in the outer reflector are used for control. This control method precludes damage to the in-core control rods during loss-of-coolant accidents. A control rod design using a carbon-carbon composite for the cladding material is being evaluated that would allow the in-core rods (or control rods located in the inner reflector) to be used during normal operation, which will provide greater flexibility for flattening the radial power distribution and provide some additional margin for maintaining fuel temperatures and fuel performance within acceptable limits.

For the equilibrium fuel cycle, one-half of the core (510 fuel elements) is reloaded every 425 full-power days, corresponding to an equilibrium residence time of 850 effective full-power days (EFPD) for each fuel element. Each reload segment contains 1746 kg of low-enriched uranium and 507 kg of natural uranium.

In addition to the fuel elements, other graphite reactor internal components include the side, central, top, and bottom graphite reflector elements and the graphite core support assembly. Fuel and reflector elements are aligned using four dowel/socket connections at each axial element-to-element interface. Metallic reactor internal components include the metallic core support, the upper core restraint, and the upper plenum shroud. These metallic components are manufactured from high-temperature alloys (e.g., Incoloy 800H, Hastelloy-X, or Inconel 617).

From top to bottom, the graphite core support assembly consists of two layers of hexagonal elements, support pedestals for the fuel and reflector columns that form the lower plenum, and the lower plenum floor, which consists of a layer of graphite elements and two layers of ceramic elements that insulate the metallic core support from the hot helium in the lower plenum. The upper core restraint elements have the same hexagonal cross sections as the graphite elements below them and are one-half the height of a standard fuel element. Dowel/socket connections are used to align the core-restraint elements with the graphite blocks. The core restraint elements are also keyed to each other and to the core barrel. The upper core restrain blocks provide stability during refueling and maintain relatively uniform and small gaps between columns during operation. The metallic core support surrounds the core and includes a floor section and a core barrel that are welded together. The metallic core support is supported both vertically and laterally by the reactor vessel. The upper plenum shroud is a welded, continuous dome that rests on top of the core barrel to form the upper plenum. The upper plenum shroud includes penetrations for inserting control rods and reserve shutdown material, for refueling, and for core component replacement.

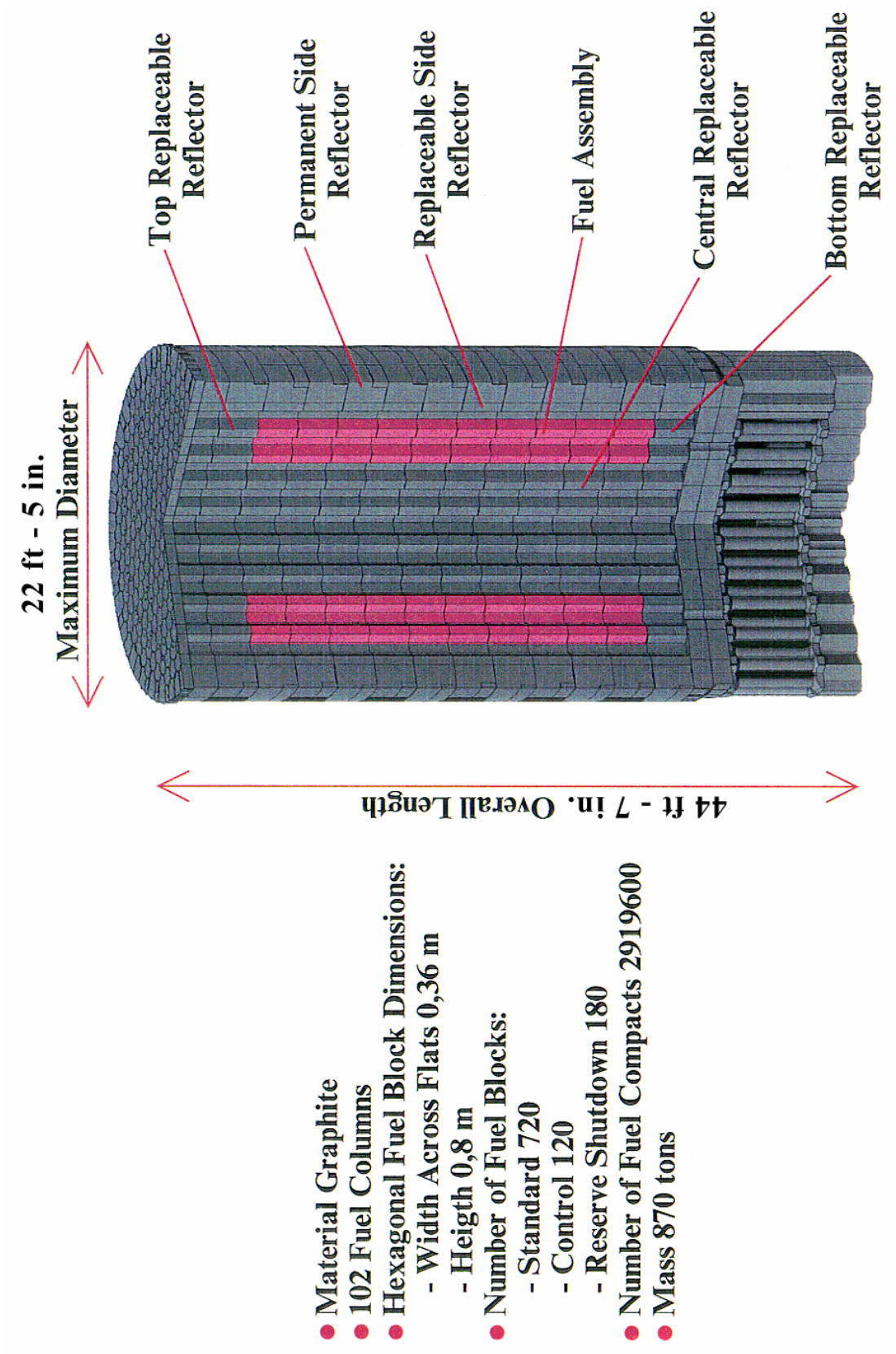

Figure 3-4. MHR Core Design

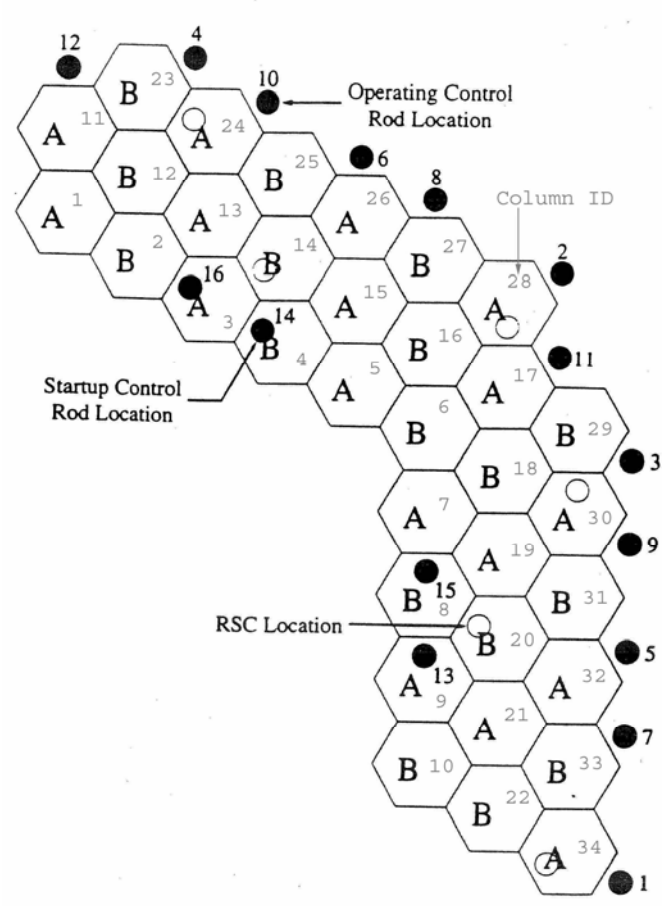

Figure 3-5. MHR Core Arrangement. The letters A and B identify the two fuel segments. The numbered, filled circles identify locations of the control-rod groups. The open circles identify the locations of RSC channels.

3.1.1.3 Neutron Control System

The neutron control system design is the same as that for the GT-MHR (Ref. 1). The system components consist of inner and outer neutron control assemblies, source-range detector assemblies, ex-vessel neutron detector assemblies, and the in-core flux mapping system. The locations of neutron control assemblies and RSC channels are shown in Fig. 3-5.

Figure 3-6 shows the design of an outer neutron control assembly and Fig. 3-7 shows installation of the neutron control assemblies in the top head of the reactor vessel. The structural equipment consists of an upper structural frame, gamma shielding, neutron shielding, thermal barrier, upper and lower guide tubes, and seals. The gamma shielding is a corrosion-resistant plug that protects maintenance crew against gamma radiation from the core and activated control rods. The neutron shielding consists of boronated graphite elements that

prevent activation of the upper portion of the vessel. The control rod guide tubes extend from the gamma shielding downward through the top head of the reactor vessel and upper plenum shroud to the upper core restraint elements. The guide tubes provide a clear passage for the control rods as they are inserted into and withdrawn from the core.

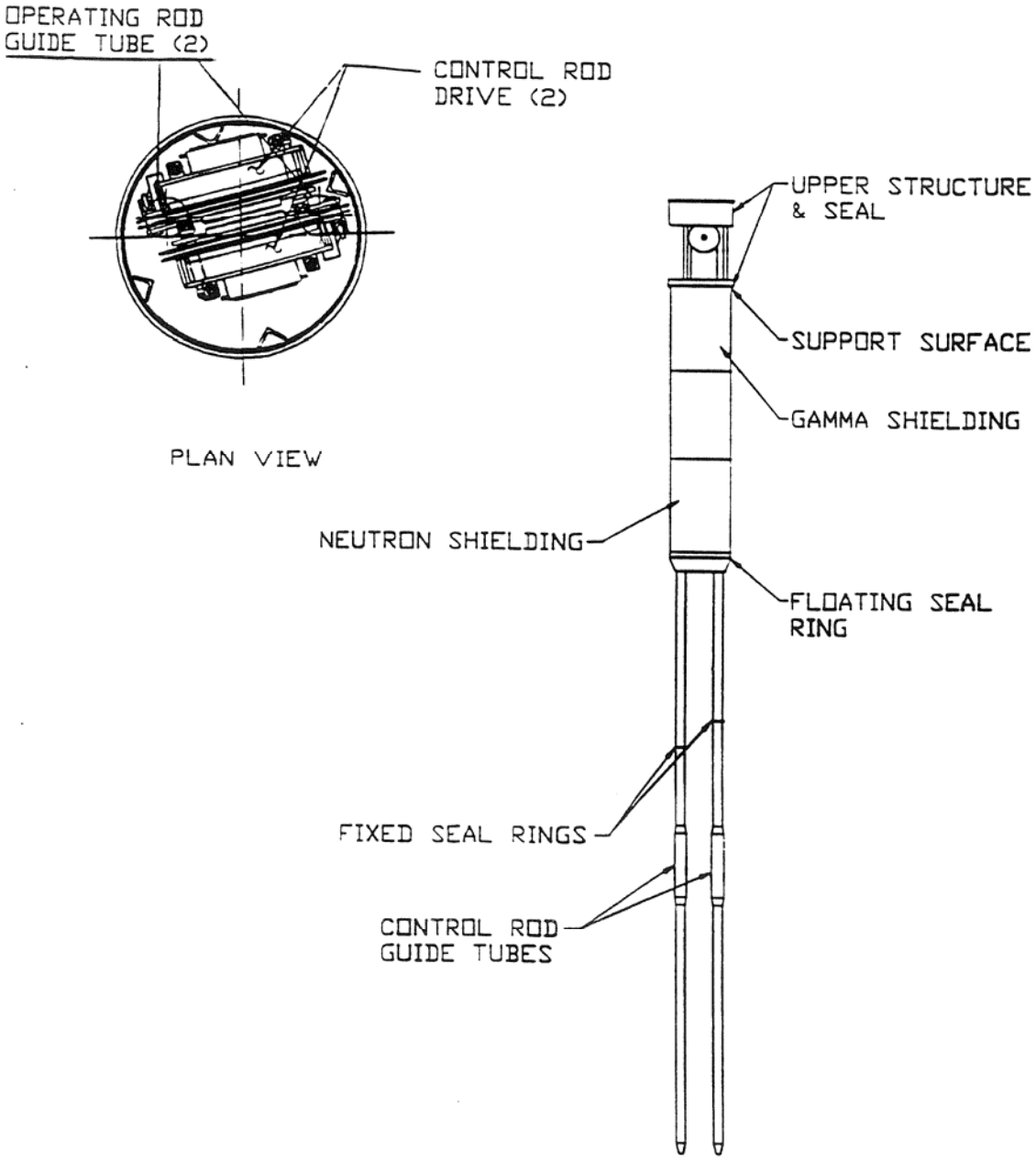

Figure 3-6. Outer Neutron Control Assembly Design

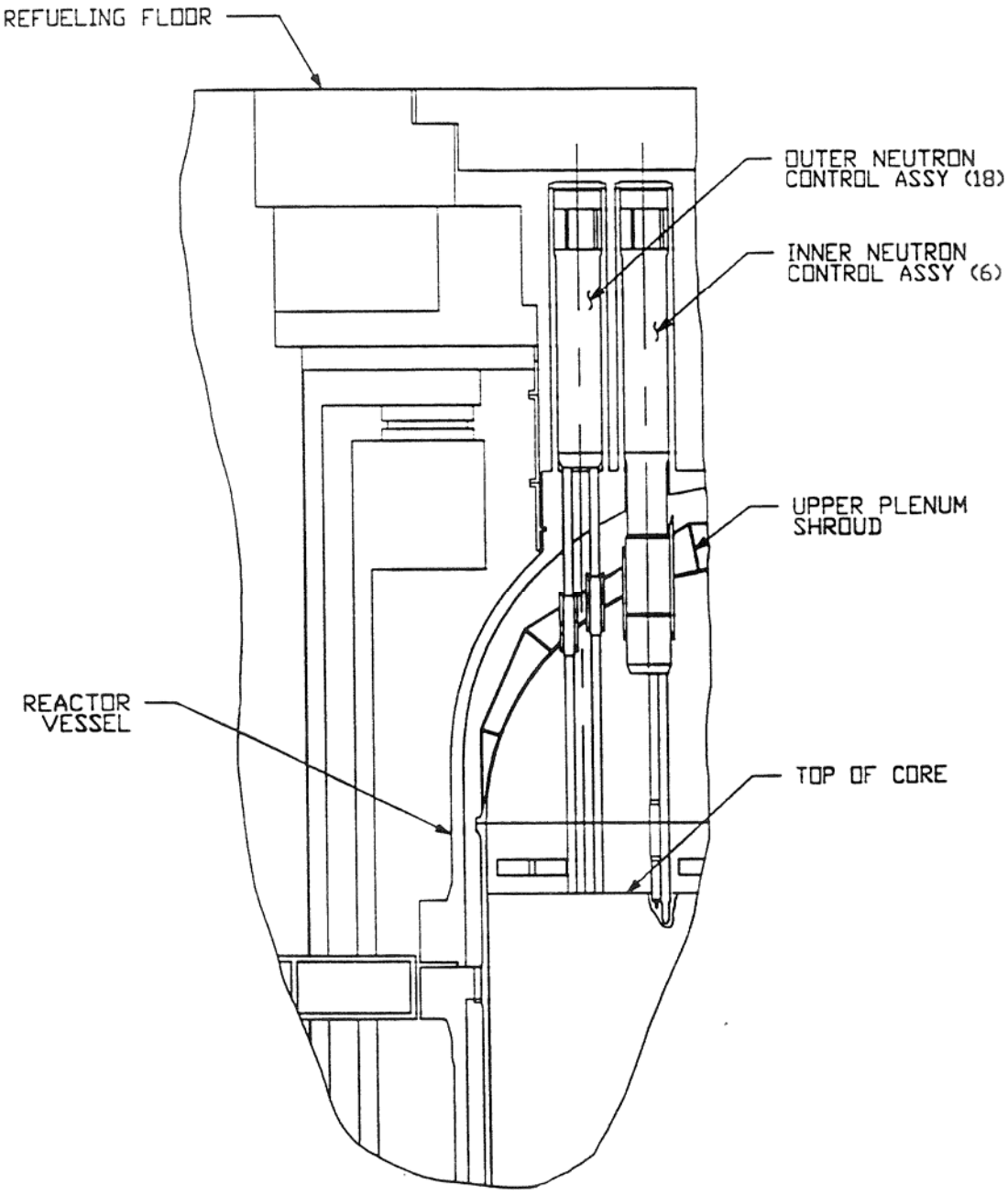

Figure 3-7. Neutron Control Assembly Installation

All neutron control assemblies are equipped with two independent control rod drive units. The control rod drive equipment is located in the upper part of the neutron control assembly. The equipment consists of a DC torque motor, a 60:1 speed reducer, and a cable storage drum, all of which are mounted on a metal frame. The control rod is lowered and raised with a flexible high-nickel alloy cable.

Figure 3-8 shows the control rod design. The neutron absorber material consists of B_4C granules uniformly dispersed in a graphite matrix and formed into annular compacts. The boron is enriched to 90 weight percent B-10 and the compacts contain 40 weight percent B_4C. The compacts have an inner diameter of 52.8 mm and an outer diameter of 82.6 diameter, and are enclosed in Incoloy 800H canisters for structural support. Alternatively, carbon-fiber reinforced carbon (C-C) composite canisters may be used for structural support. The control rod consists of a string of 18 canisters with sufficient mechanical flexibility to accommodate any postulated offset between elements, even during a seismic event.

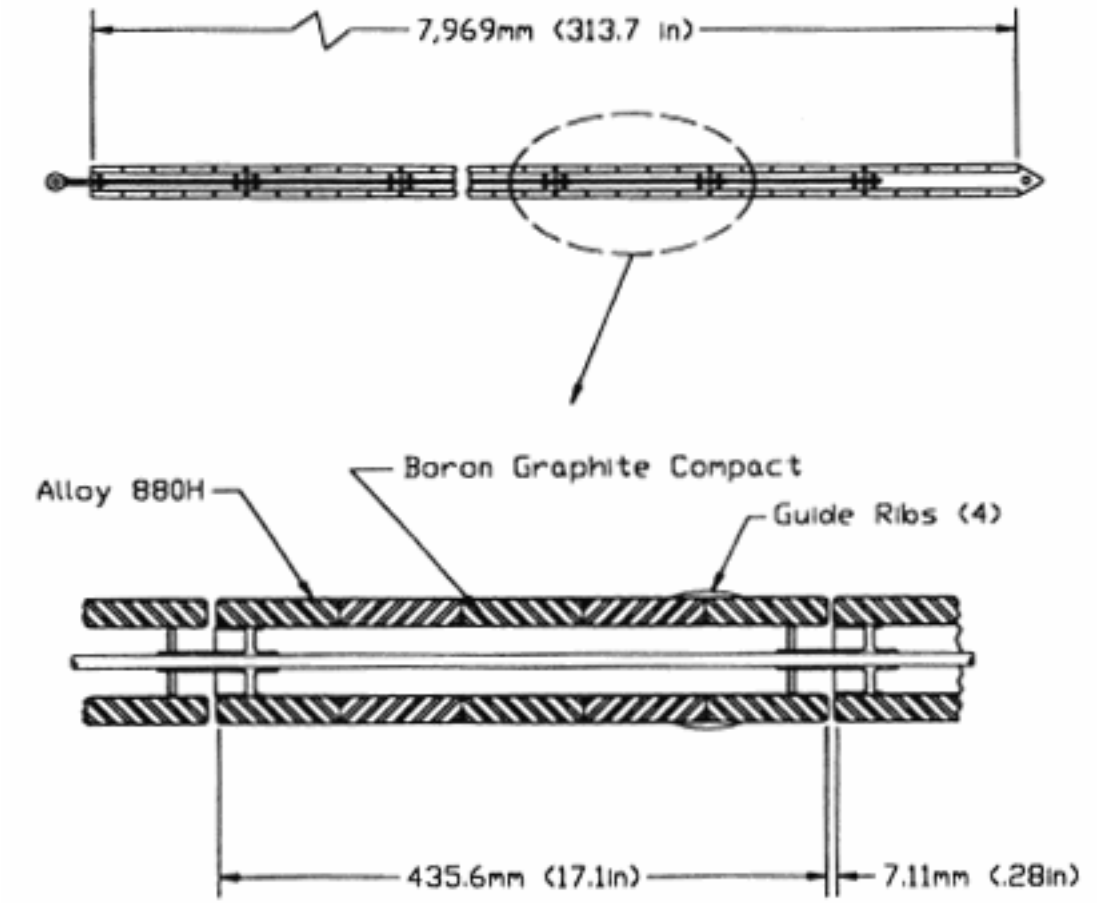

Figure 3-8. Control Rod Design

The reserve shutdown control material is of the same composition as that for the control rods, except the B_4C granules and graphite matrix are formed into cylindrical pellets with rounded ends and a diameter of 14 mm. The B_4C granules are coated with dense PyC to prevent oxidation during off-normal events. The pellets are stored in hoppers located above the reactor core in both the both the inner and outer neutron control assemblies.

During normal operation, the neutron flux levels are monitored by 6, symmetrically-spaced ex-vessel fission chamber thermal neutron detectors. The signals from these detectors interface with the automatic control and protection systems to operate the control rod drives or the reserve shutdown control equipment. Three fission chamber source-range detectors are used

to monitor neutron flux during startup and shutdown. These detectors are symmetrically spaced in reentrant penetrations located in the bottom head of the reactor vessel. These penetrations extend into vertical channels in the reflector elements near the bottom of the core. The in-core flux mapping system consists of movable detectors in the central column of the inner reflector and in the outer permanent reflectors. The system enters from a housing located above the reactor vessel and vertically traverses down through the core to the bottom reflectors. The system contains two independent fission chambers and a single thermocouple.

3.1.2 Cross Vessel and Hot Duct Assembly

As shown in Fig. 3-9, the hot duct is concentrically located within the cross vessel. The hot duct provides the hot-leg primary coolant flow path from the reactor vessel to the IHX vessel. The annular space between the hot duct assembly and cross vessel provides the cold-leg primary coolant flow path from the IHX vessel to the reactor vessel. The hot duct assembly includes a ceramic fiber insulation layer to minimize heat transfer between the hot-leg and cold-leg flow paths. The hot duct material is a high-temperature alloy (e.g., Incoloy 800H, Hastelloy-X, or Inconel 617).

The cross vessel is a one-piece forged cylinder that is designed and fabricated according to Section III of the ASME Code. The cross vessel has an inner diameter of 2.29 m, a wall thickness of 7.62 cm, and is approximately 2.86 m in length. The reference material for the cross vessel is 9Cr-1Mo-V steel. Other candidate materials are 2¼Cr-1Mo steel and 15Cr-2Mo-V steel. As discussed in Section 3.1.4, a design alternative is being considered to incorporate cooling of the reactor vessel, such that proven light water reactor vessel materials (e.g., SA533 steel) could be used for the reactor vessel without causing creep damage. If this alternative is selected, the cross vessel would also likely be manufactured using the same material, which would require using internal insulation to protect the cross vessel from creep damage.

3.1.3 Reactor Vessel

The H2-MHR reactor vessel design is nearly identical to that for the GT-MHR. Modifications to the H2-MHR reactor vessel design for higher temperature operation are described in Section 3.1.4.

As shown in Fig. 3-10, the reactor vessel is composed of a main cylindrical section with hemispherical upper and lower heads. The upper head is bolted to the cylindrical section and includes penetration housings for the neutron control assemblies and the in-vessel flux monitoring unit. These housings are sealed with a blind flange. The lower head is welded to the cylindrical section and includes penetrations for the Shutdown Cooling System (SCS), in-service inspection access, and source-range neutron detectors. The upper portion of the lower head incorporates a ring forging that provides support to the core through the core support structure. Lateral seismic restraint is provided to the core by six lugs welded to the interior surface of the vessel, near the top of the cylindrical section. The cylindrical section also includes a nozzle forging for attachment of the cross vessel, reactor vessel support lugs, and lateral restraint keys. The reference material for the reactor vessel is 9Cr-1Mo-V steel. Other candidate materials are 2¼Cr-1Mo steel and 15Cr-2Mo-V steel. The reactor vessel design parameters are given in Table 3-5.

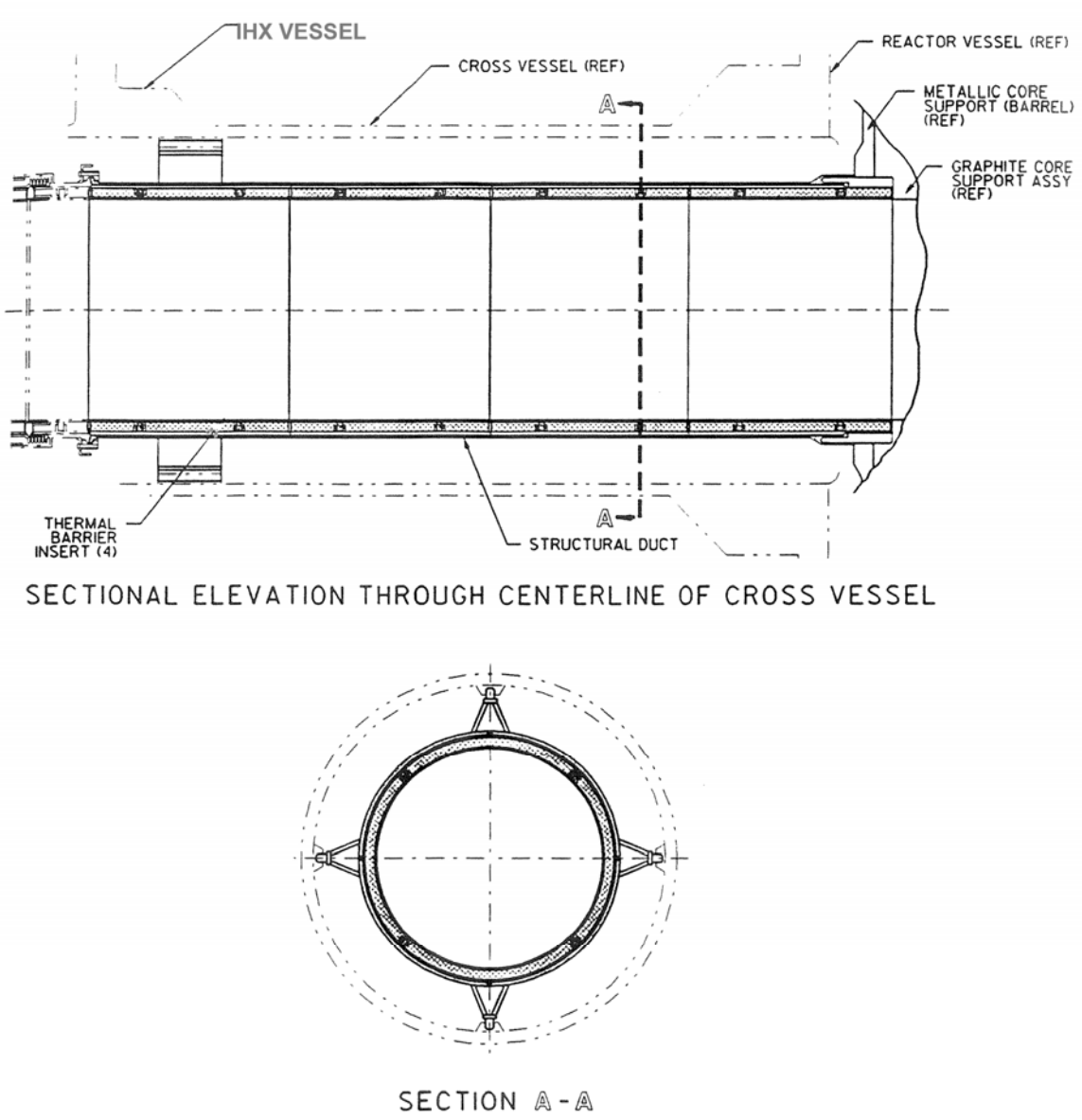

Figure 3-9. Hot Duct Assembly

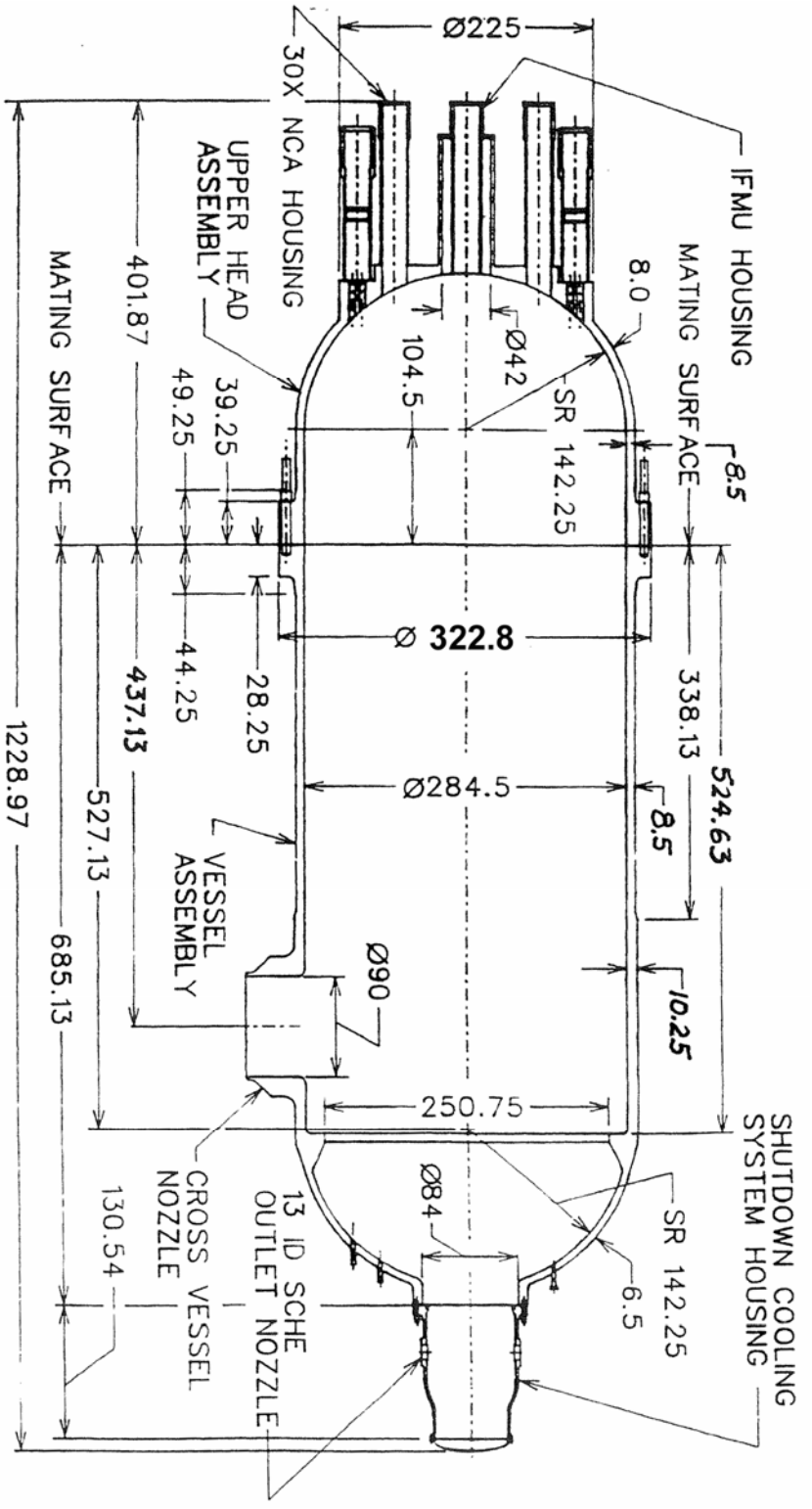

Figure 3-10. Reactor Vessel (dimensions are in Inches)

Table 3-5. Reactor Vessel Design Parameters

Reference Material	9Cr-1Mo-V steel
Height	31.0 m
Vessel Inner Diameter	7.2 m
Vessel Outer Diameter	8.2 m (at flange)
Wall Thicknesses	
Top Head	0.203 m
Shell	0.216 m
Thickened Ring	0.261 m
Bottom Head	0.165 m
Total Vessel Assembly Weight	838 mt
Upper Head Weight	490 mt
Design Lifetime	60 y
Design Temperature	495°C

3.1.4 Design Modifications for Higher Temperature Operation

Modifications to the MHR design for higher temperature operation include routing the inlet flow through holes in the Permanent Side Reflector (PSR) to lower vessel temperatures, optimization of the fuel block loading during refueling to reduce peak power factors, and minor changes to the reactor internal design to reduce bypass flow. An additional modification under consideration is using a slipstream flow of lower temperature helium to provide vessel cooling, such that proven light water vessel materials could be used for the MHR vessel.

3.1.4.1 Inlet Flow Configuration Modifications

The GT-MHR was designed to operate with coolant inlet and outlet helium temperatures of 490°C and 850°C, respectively. For the GT-MHR, the inlet coolant flow is routed through riser channel boxes between the core barrel and vessel (see Fig. 3-11). With this configuration, the design of the reactor vessel (including wall thickness and materials selection) is driven in large measure by the design point selected for the coolant inlet temperature. For the GT-MHR, the inlet temperature also has a significant impact on performance of the PCS. The design point of 490°C ensures high-efficiency operation of the PCS and acceptable operating conditions for a reactor vessel manufactured from a Cr-Mo steel (e.g., 2¼Cr-1Mo, 9Cr-1Mo-V, and 15Cr-2Mo-V). The design point of 850°C for the outlet temperature eliminates the need for turbine blade cooling and ensures acceptable performance of the ceramic coated-particle fuel during normal operation.

For the H2-MHR, it is desirable to increase the coolant outlet temperature in order to improve the efficiency and economics of hydrogen production, and a design point of 950°C has been selected. Scoping calculations have shown a point design with coolant inlet and outlet temperatures of 490°C and 1000°C, respectively may be feasible in terms of acceptable fuel temperatures during normal operation if the coolant flow distribution is optimized to divert more flow to the hotter columns using fixed orifices in the upper and/or lower reflectors of the cooler columns [Richards 2004]. However, confirmation of this design option will require a significant level of design work, including developing a fuel cycle that ensures relatively stable power

distributions over the entire fuel cycle and for all anticipated operating conditions. Also, operating with an outlet temperature above 950°C will have a significant impact on the IHX design and may require a ceramic or super-alloy IHX, which could involve a significant period of development and testing before it is qualified as a nuclear reactor primary coolant boundary.

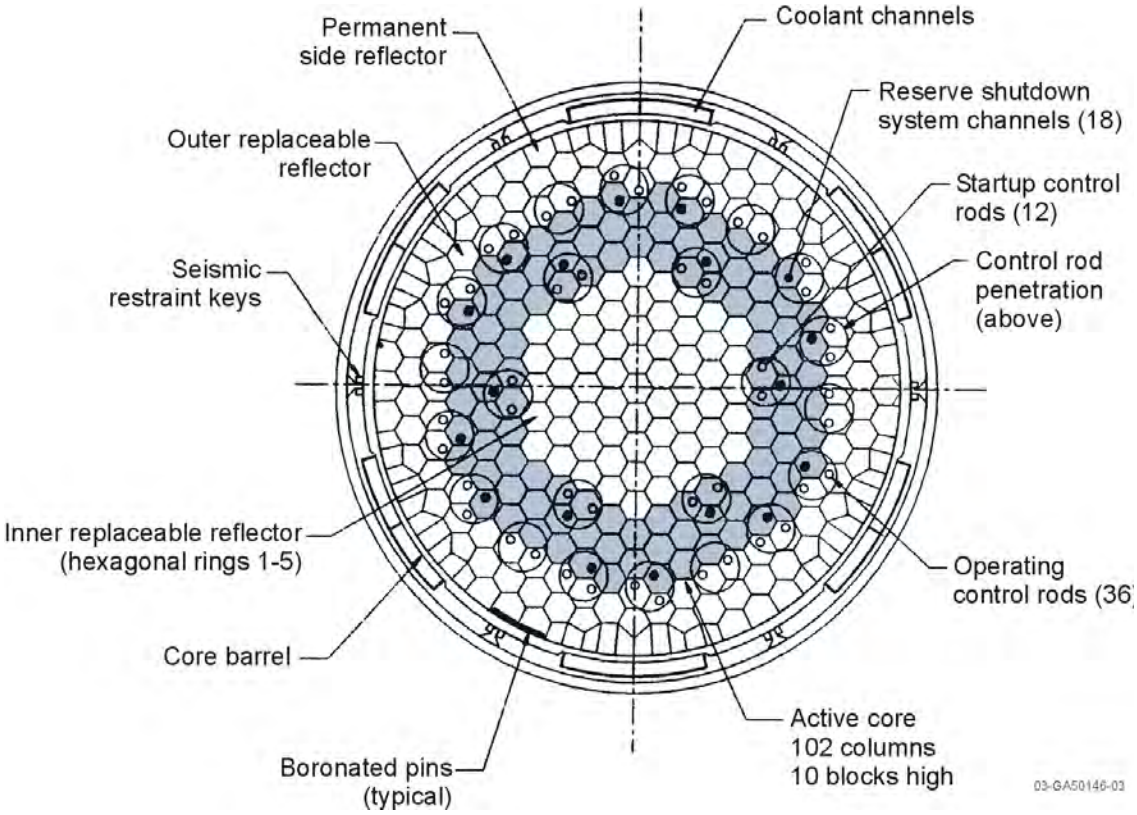

Figure 3-11. GT-MHR Cross Section at Vessel Midplane. Inlet flow is routed through the channel boxes located between the core barrel and reactor vessel.

The coolant inlet temperature was also increased by 100°C to 590°C to provide a sufficiently high coolant flow and convective heat-transfer rate within the MHR core that ensures acceptable fuel performance and limits release of Ag-110m and other noble-metal fission products that can diffuse through intact SiC coatings at high temperatures. However, this higher coolant-inlet temperature will result in reactor vessel temperatures that could exceed the limits for Cr-Mo steels if the current GT-MHR flow configuration was used. Higher vessel temperatures will also result in higher parasitic heat losses to the RCCS during normal operation.

The Advanced Thermal Energy Network Analysis (ATHENA) code [Carlson, 1986] was used to assess the impact of higher coolant temperatures on steady-state vessel temperatures, parasitic RCCS heat losses, and fuel temperatures during normal operation and accident conditions. Both the reference GT-MHR inlet flow configuration and two alternative inlet flow configurations were evaluated. These alternative configurations route the flow through either holes in the inner

reflector [see Fig. 3-12(a)] or holes in the PSR [see Fig. 3-12(b)], in order to increase the thermal resistance between the inlet flow path and the vessel. Preliminary evaluations showed that both configurations had nearly the same effect in terms of reducing vessel temperatures and parasitic heat losses to the RCCS. However, routing the inlet flow through the inner reflector resulted in a greater loss of heat capacity (from removal of graphite to provide the flow paths), which caused peak fuel temperatures to increase by about 40°C during a depressurized loss-of-coolant accident (LOCA). For these reasons, the PSR inlet flow configuration was adopted for the H2-MHR. Figure 3-13 shows a cross-sectional view of the revised configuration with inlet coolant holes in the PSR.

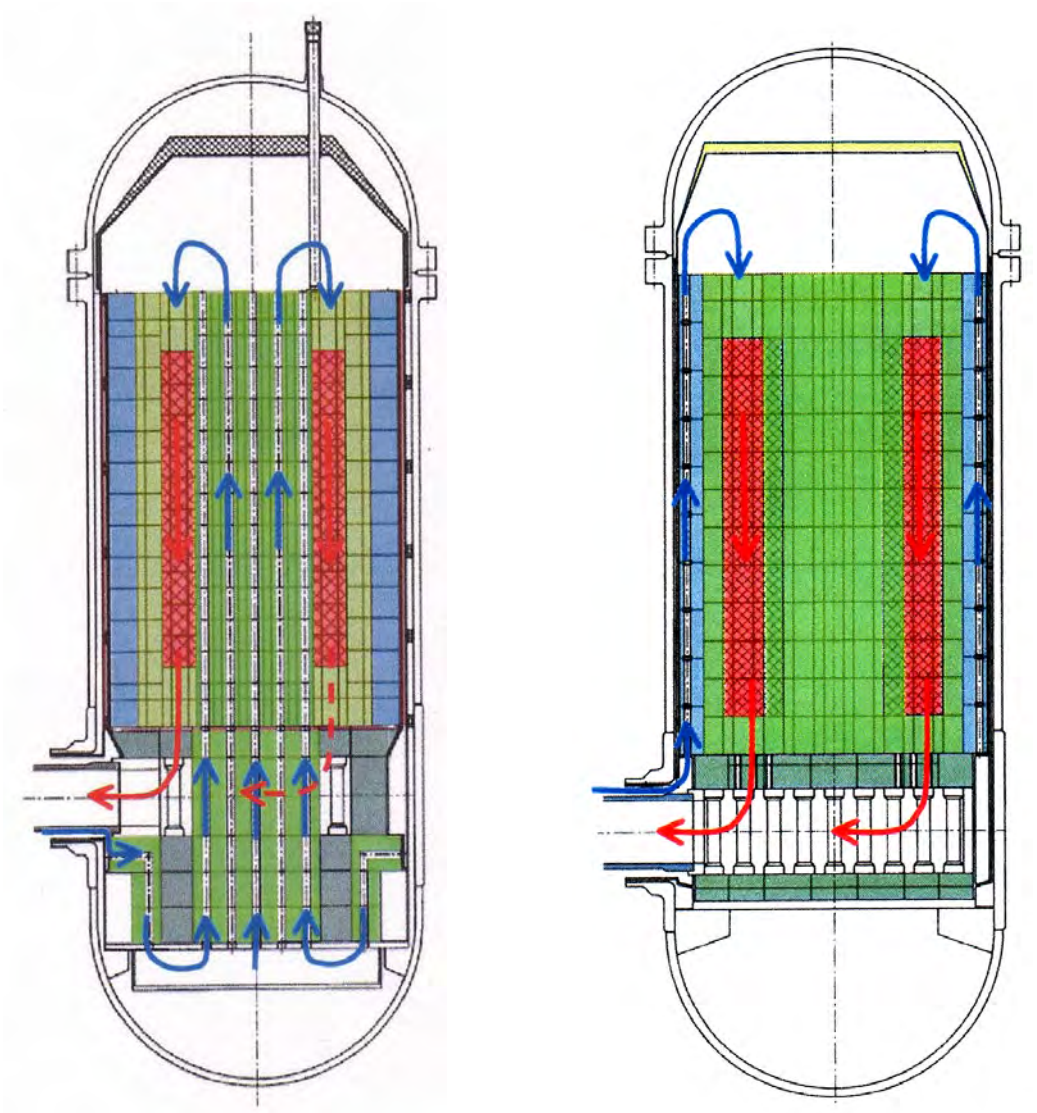

Figure 3-12. Reactor Vessel Configured with Alternative Inlet Flow Paths. (a) Flow routed through inner reflector. (b) Flow routed through PSR. (Figure courtesy of Fuji Electric Systems, Kawasaki-city, Japan)

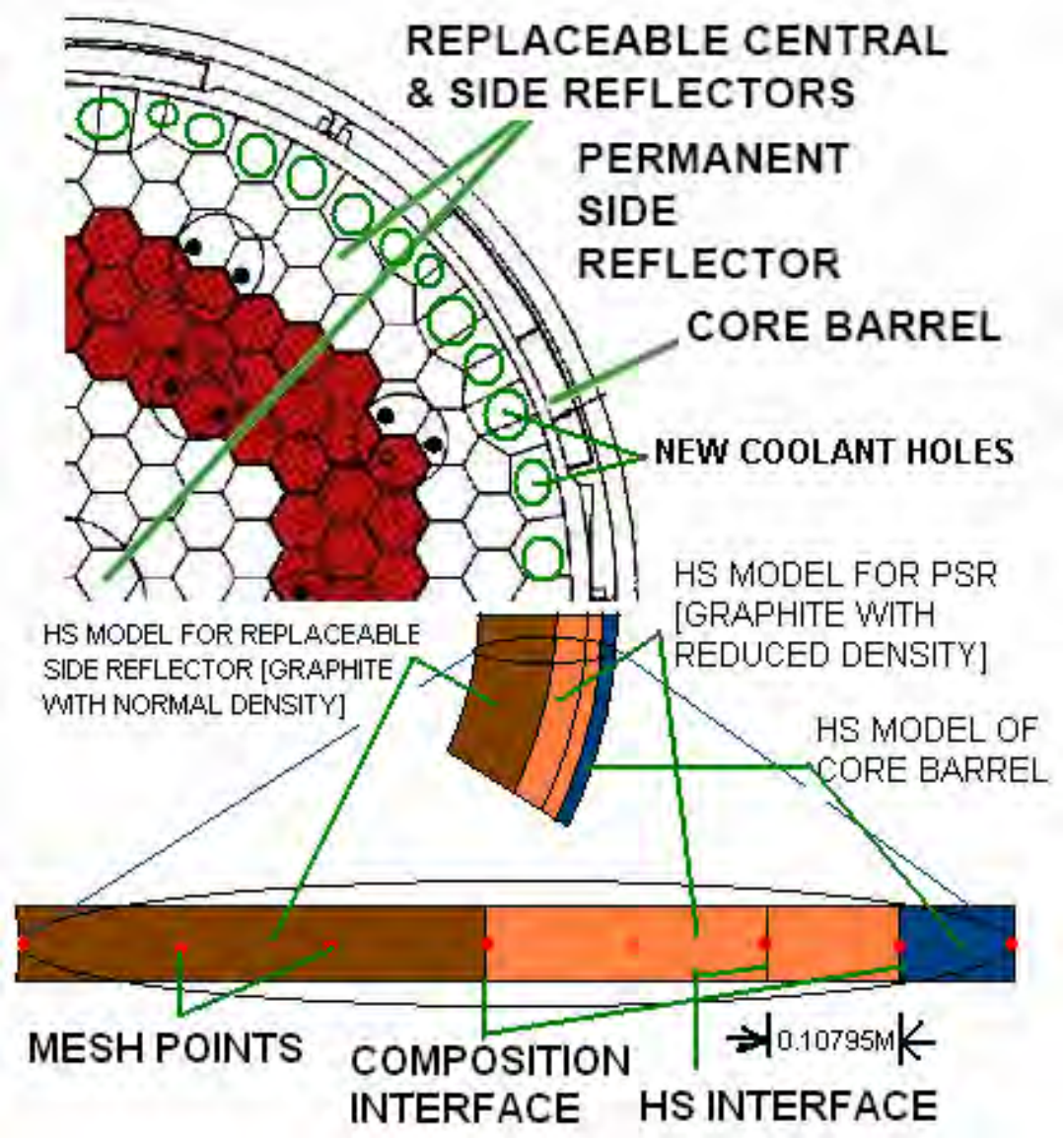

Figure 3-13. MHR Configured with PSR Inlet Flow (HS = ATHENA Heat Structure)

Figure 3-14 shows the ATHENA thermal hydraulic model for the MHR vessel and internals. The active core is modeled as three annular rings with an axial node for each of the ten fuel blocks in the active core. Flow from the upper plenum to the outer plenum is modeled using five parallel channels. Three of these channels provide cooling for the active core (one channel for each fuel ring) and two channels are used to represent bypass flow. Radial and axial conduction are modeled in the active core and reflectors, and radiative heat transfer is modeled between the core barrel and reactor vessel. Heat is conducted through the reactor vessel and radiative heat transfer is modeled between the reactor vessel and RCCS. Figure 3-15 shows the ATHENA thermal hydraulic model for the RCCS. ATHENA heat structures are used to model the RCCS risers and downcomers.

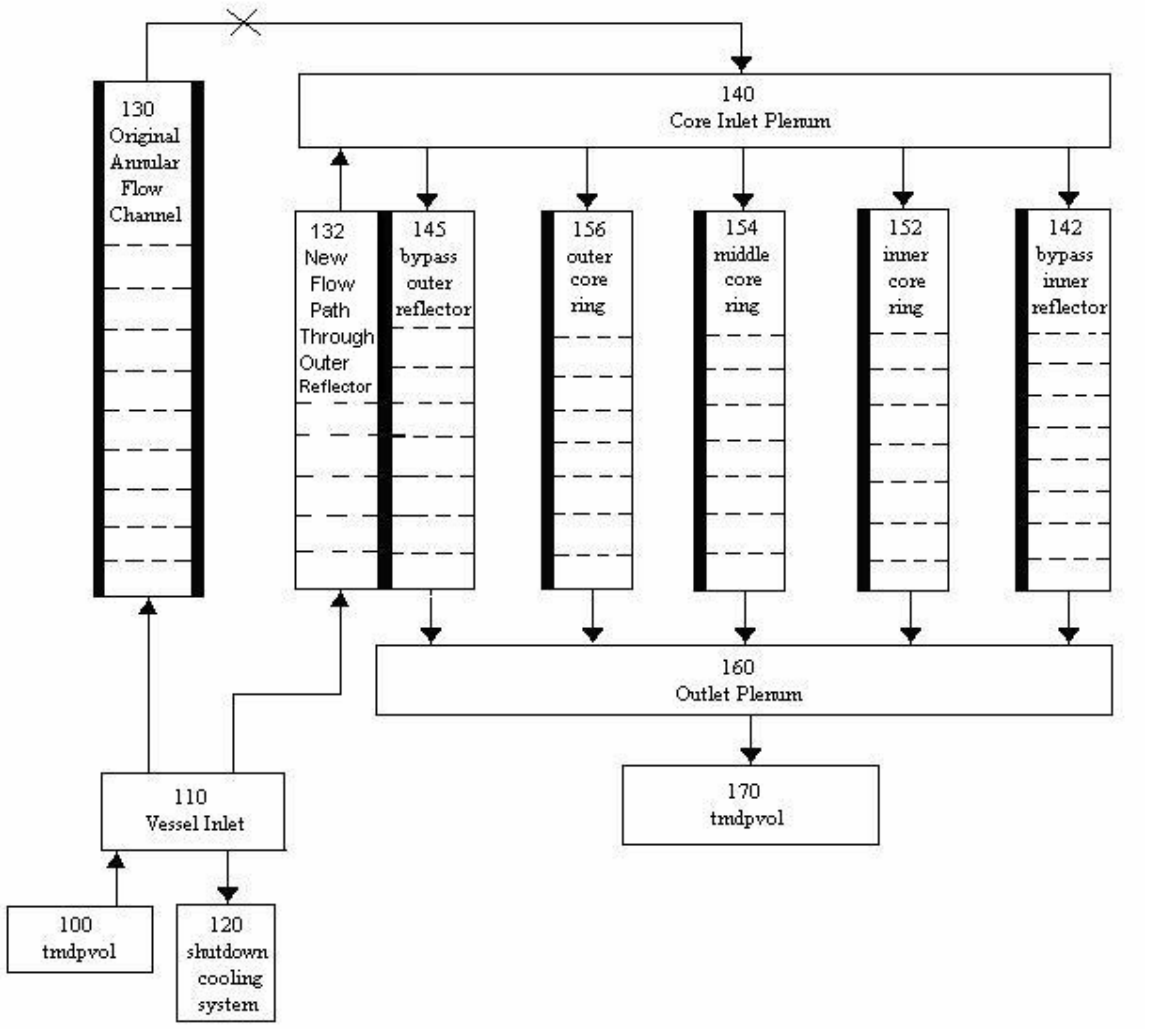

Figure 3-14. ATHENA Model for the MHR Vessel and Internals

Calculations performed using the current GT-MHR flow configuration are given in Table 3-5. Increasing the coolant inlet temperature from 490°C to 590°C causes the peak vessel temperature to increase from 453°C to 541°C, which exceeds the design limit of 495°C specified for 9Cr-1Mo-V steel (see Table 3-6). The parasitic heat loss to the RCCS increases from 3.3 MW to 4.5 MW and the core pressure drop increases by about 10% because of the increase in helium viscosity with temperature.

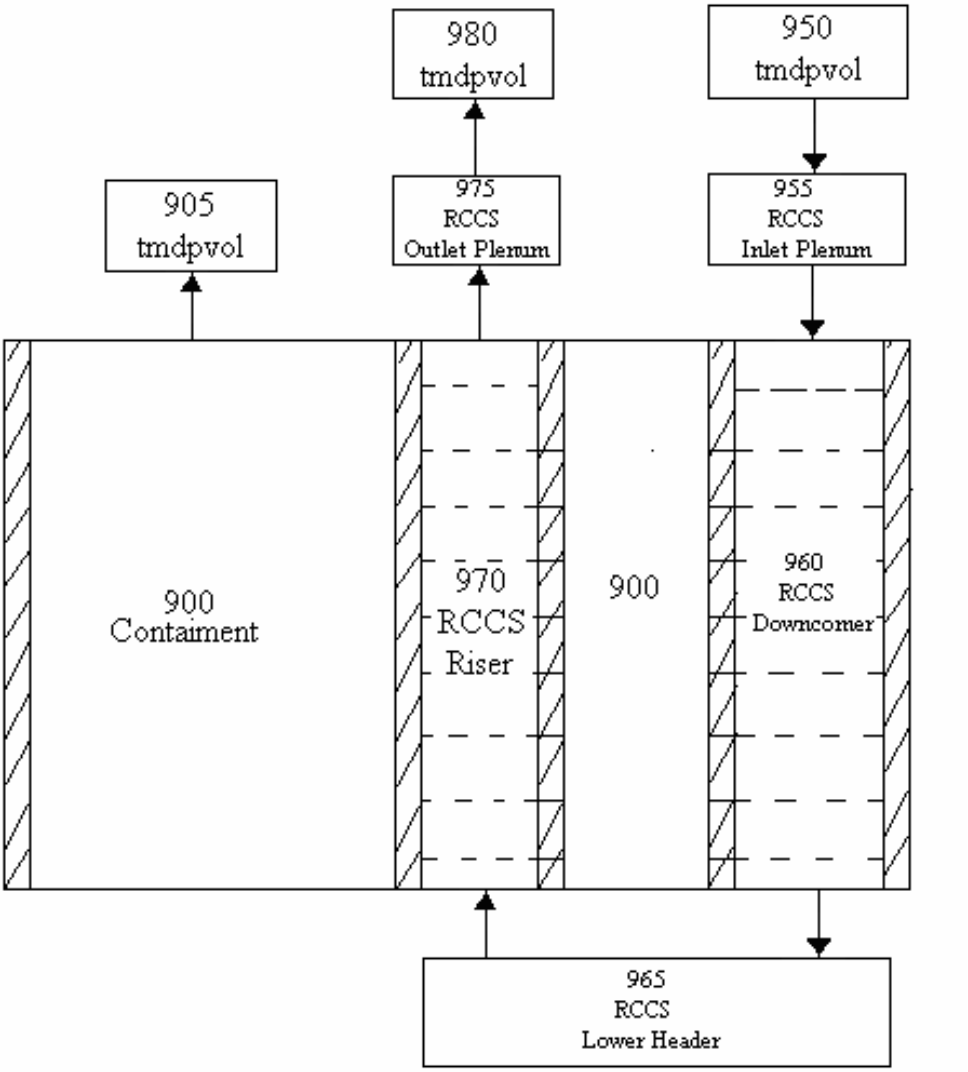

Figure 3-15. ATHENA Model for the RCCS

Table 3-6. Impact of Higher Coolant Temperatures (Reference GT-MHR Flow Configuration)

	Coolant Inlet/Outlet Temperature (°C)	
	490/850	**590/950**
Maximum Vessel Temperature (°C)	453	541
Parasitic Heat Loss to RCCS (MW)	3.3	4.5
Total Core Pressure Drop (kPa)	51	56

Calculations were performed with the ATHENA model to optimize the PSR inlet flow configuration. Considerations included the quantity of graphite (and associated heat capacity) removed to form the coolant holes, total pressure drop through the vessel and its impact on pumping power requirements, and coolant inlet velocity. Inlet coolant hole diameters of 4, 6, and 8 inches were used, depending on the cross-sectional area and shape of the PSR columns. The reconfigured PSR blocks should provide sufficient wall thicknesses to accommodate stresses and, if necessary, provide space to include boronated rods to reduce the accumulated fast neutron fluence to the reactor vessel. Parameters for the optimized PSR inlet flow configuration are given in Table 3-7. The maximum steady-state fuel temperature was predicted to be 1106°C. These calculations were performed using centrally-peaked axial power profiles. The maximum fuel temperature will be approximately 100°C higher under conditions of partial control rod insertion, which shifts the peak axial power factor towards the bottom of the core where coolant temperatures are higher. However, the fuel temperatures should be well within the margins of acceptable performance for SiC-TRISO fuel under all anticipated conditions for normal operation. The maximum steady-state vessel temperature was predicted to be 420°C, which is well within the margin for acceptable performance of 9Cr-1Mo-V steel. Additional analyses are needed to determine the impact on vessel temperatures of any leakage flow from the PSR inlet flow path to the annular space between the core barrel and reactor vessel.

Table 3-7. Optimized PSR Inlet Flow Configuration

PSR Total Inlet Coolant Flow Area	1.64 m^2
Total Graphite Removed from Outer Reflector	10%
Number of Coolant Holes	
4 in.	18
6 in.	18
18 in.	36
Total Vessel Pressure Drop	80 kPa
Maximum Steady State Fuel Temperature	1106°C
Maximum Steady State Vessel Temperature	420°C
Parasitic Heat Loss to RCCS	2.1 MW
Maximum Coolant Velocity in Core	53.2 m/s
Maximum Inlet Coolant Velocity in PSR	45.5 m/s

The primary impact of the PSR inlet flow configuration is an increase in total vessel pressure drop of about 25 kPa, primarily because the inlet flow area is reduced from 4.62 m^2 for the original channel-box flow configuration to 1.64 m^2 for the PSR flow configuration. As shown in Section 4.1, the PSR inlet flow configuration has little impact on fuel and vessel temperatures during accident conditions.

3.1.4.2 Vessel Cooling

Although 2¼Cr-1Mo steel was used to manufacture the reactor vessel for the JAEA 30-MW(t) High Temperature Test Reactor, there is limited experience with using this material, and no

large nuclear reactor vessels have been manufactured using this material or 9Cr-1Mo-V steel. For this reason, it is of interest to pursue design options that would lower the vessel temperature, such that proven light water reactor vessel materials (e.g., SA533 steel) could be used for the MHR vessel. JAEA has adopted a configuration for the GTHTR300 design (which is similar to the GT-MHR) that routes a small fraction of the 140°C flow from the high-pressure compressor to a path between the core barrel and reactor vessel in order to keep the SA533 vessel temperature below the creep-damage limit. For H2-MHR, a potential source of cold helium is the return path from the slipstream flow that is routed through the helium purification system to control chemical impurities and circulating radioactivity (see Section 3.3.1). Table 3-8 shows preliminary ATHENA results for peak fuel and vessel temperatures as a function of the cold helium flow rate used to provide vessel cooling. These results are consistent with the JAEA results, and show that vessel cooling may be a viable design option. However, additional analyses are required, particularly in terms of the impact of this configuration on passive safety and investment protection. If steel with higher-temperature capability is required for the reactor vessel, a viable option is 15Cr-2Mo-V, which has been used in Russia for nuclear pressure vessels.

Table 3-8. Reactor Vessel and Fuel Temperatures as a Function of Vessel Cooling Flow Rate

Vessel cooling flow rate (kg/s)	0	9.6	12.8	16.0
Vessel cooling inlet temperature (°C)	—	140	140	140
Coolant inlet temperature (°C)	590	590	590	590
Peak fuel temperature (°C)	1168	1172	1174	1176
Maximum wall-averaged vessel temperature (°C)	480	378	356	338

3.1.4.3 Power and Flow Distribution Optimization

At sufficiently high temperatures, failure of the SiC layer of the TRISO coating can occur as the result of corrosion by fission products (mainly Pd). Figure 3-16 shows an estimate (using GA design correlations) of the SiC layer failure probability as a function of time and temperature. Based on these calculations, temperatures in the range 1250°C to 1350°C have generally been adopted as a “rule of thumb” peak temperature limit for SiC-TRISO fuel during normal operation. Because the coolant flows downward through the MHR core, the peak fuel temperatures tend to occur toward the bottom of the core (see Fig. 3-17), and an increase in coolant-outlet temperature generally results in a near proportional increase in fuel temperature. However, the increase in coolant outlet temperature can be compensated for by optimizing the core power and flow distributions.

The baseline refueling scheme for the GT-MHR is to replace entire columns, such that at the beginning of an equilibrium cycle one-half of the core consists of fuel columns that contain fresh (“new”) fuel and the other half of the core consists of columns that contain “old” fuel that has been irradiated for one 425-EFPD cycle. Previous studies have shown that power distributions can be flattened if a concept referred to as fuel placement is used. With this concept, each column contains both new and old fuel in alternating layers at the beginning of an equilibrium cycle. In effect, fuel placement reduces the “age” component of power peaking. As shown in Fig. 3-18, the fuel-placement refueling scheme can reduce the peak column-averaged power factor by about 6%. Also, the use of high-temperature, composite-clad control rods will allow the use of control rods in the inner reflector, which could further reduce power peaking factors.

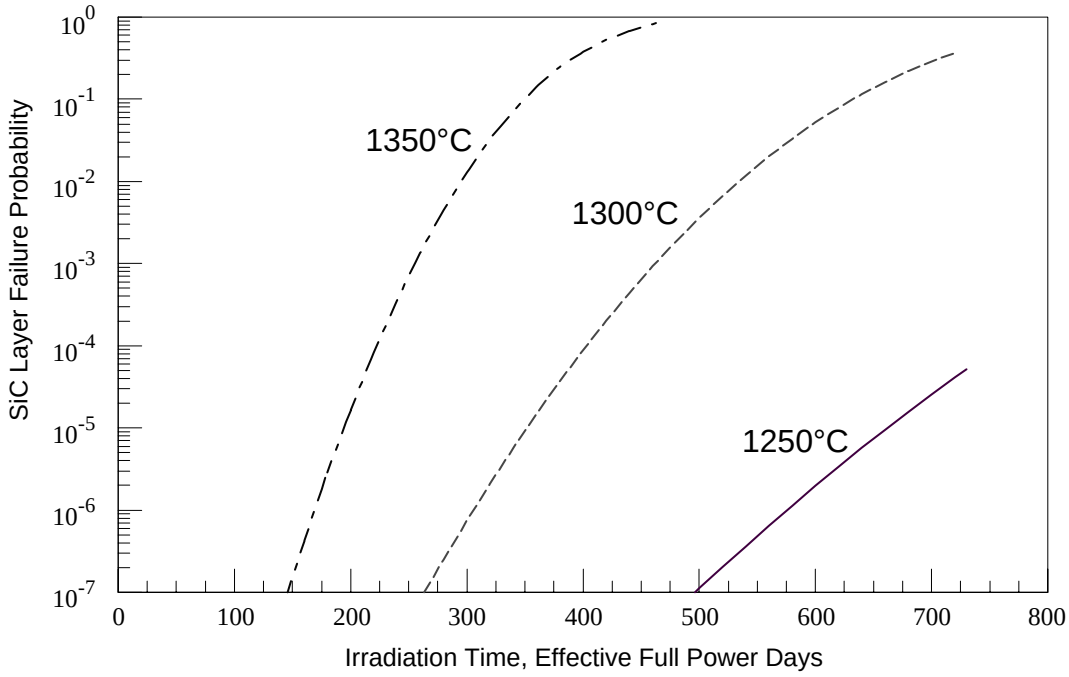

Figure 3-16. Predicted Failure of the SiC Layer by Fission Product Corrosion

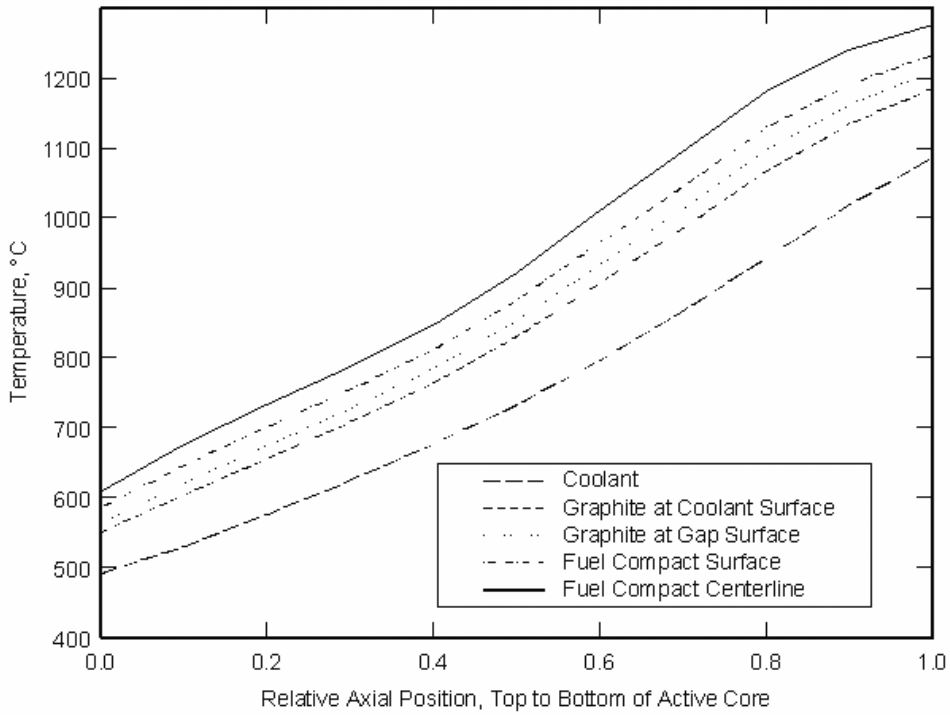

Figure 3-17. Axial Temperature Distribution in the H2-MHR Hot Coolant Channel

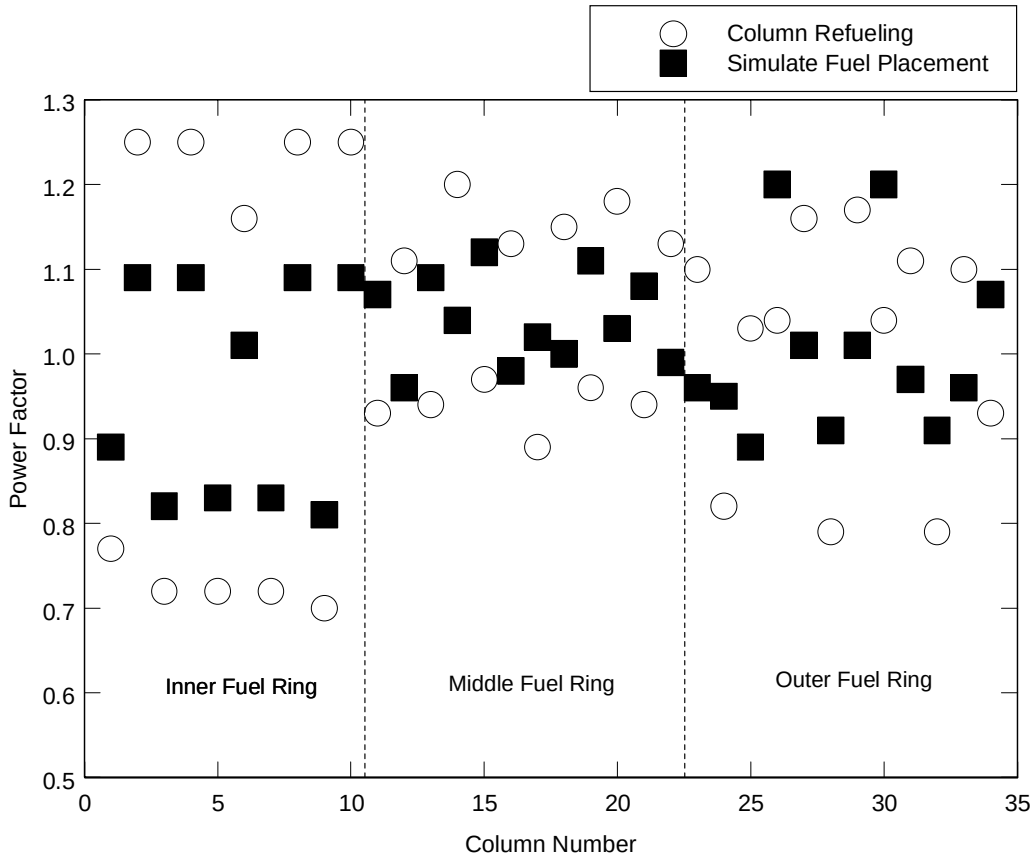

Figure 3-18. Column-Average Power Factors

Fuel temperatures can also be reduced by reducing bypass flow. For the reference GT-MHR core design, a portion of the coolant (~20%) bypasses the coolant holes and flows into gaps between the blocks and into control-rod channels. The control-rod channels have orifices to minimize bypass flow while also maintaining adequate cooling for the control rods. Approximately 3% of the coolant flows into control-rod channels. Composite-clad control rods require little or no cooling, which helps reduce the bypass flow fraction. Bypass flow can also be reduced by using additional lateral restraints and graphite sealing keys below the active core. Figure 3-19 shows a FLOWNET [Maruyama, 1994] model used to estimate the coolant flow distribution in the MHR core. Parametric studies performed with this model show that bypass flow near the bottom of the core (where temperatures are the highest) can be reduced to about 10% of the total flow [Richards, 2004].

Preliminary calculations have shown these measures to optimize the core nuclear and thermal hydraulic design should effectively compensate for the increase in the inlet and outlet coolant temperature design points, in terms of maintaining acceptable fuel temperatures during normal operation. If necessary, using fixed orifices on selected fuel columns can be used as an option to provide additional margin for fuel temperatures.

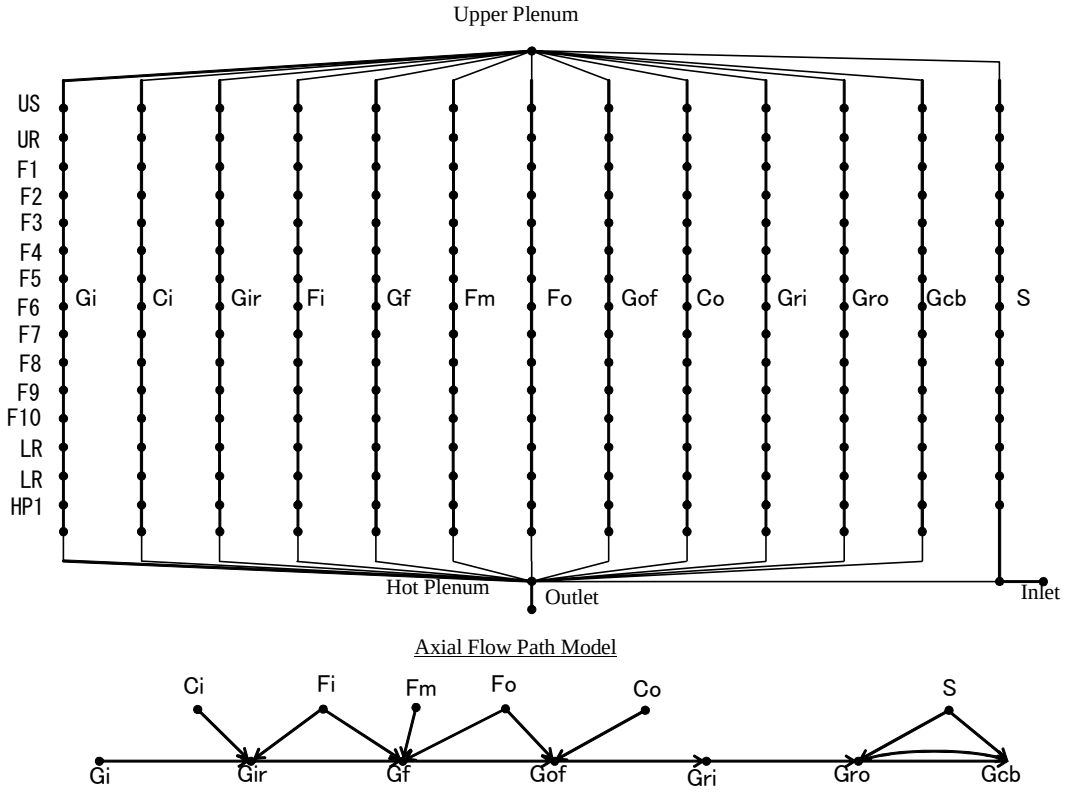

Ci:	Control rod hole in fuel region
Co:	Control rod hole in outer reflector
Fi:	Coolant channel of inner layer fuel column
Fm:	Coolant channel of central layer fuel column
Fo:	Coolant channel of outer layer fuel column
Gi:	Gap flow path in inner reflector region
Gri:	Gap flow path between inner reflector and fuel region
Gf:	Gap flow path in fuel region
Gof:	Gap flow path between fuel and outer reflector column
Gri:	Gap flow path among outer replaceable reflector
Gro:	Gap flow path between outer replaceable reflector and permanent reflector
Gcb:	Gap flow path between permanent reflector and core barrel
S:	Inlet flow path

Figure 3-19. MHR FLOWNET Coolant Flow Distribution Model (Figure courtesy of Fuji Electric Systems, Kawasaki-city, Japan)

3.1.5 Shutdown Cooling System

The Shutdown Cooling System (SCS) provides decay heat removal when the Heat Transport System (HTS) is off line. The SCS consists of a circulator with shutoff valve, a heat exchanger, a control system, a shutdown cooling water system, and equipment for servicing the circulator and heat exchanger. The SCS design is the same as that for the GT-MHR [Shenoy, 1996]. Figure 3-20 shows the SCS cooling loop and the location of the shutdown heat exchanger and shutdown circulator in the reactor vessel.

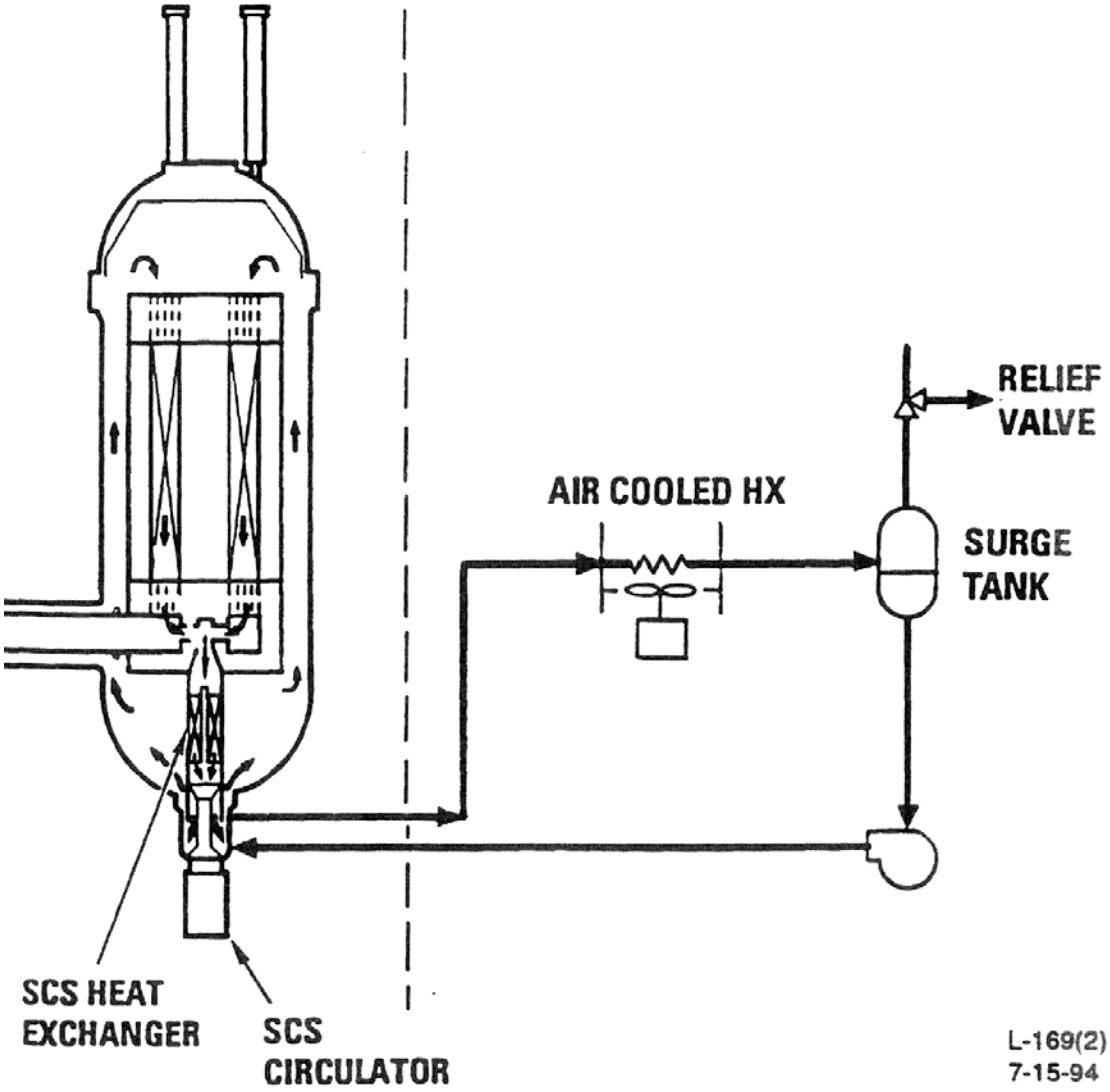

Figure 3-20. Shutdown Cooling System General Arrangement

The SCS consists of a single loop (one per reactor module) with the heat exchanger in series with the circulator and loop shutoff valve assembly. These components are located at the bottom of the reactor vessel. Hot helium from the core outlet plenum flows through multiple

parallel openings (pipes) in the center of the core support structure and into the heat exchanger. Once cooled, the helium continues downward through the loop shutoff valve to the circulator where it is compressed and discharged into the reactor vessel bottom head cavity. The cool helium then flows through the internal passage formed by the core support structure, up through the flow channels in the PSR, and into the core inlet plenum. The loop is completed as the helium flows down through the reactor core. The heat is transferred to a cooling water system that rejects the heat to the atmosphere through an air-cooled heat exchanger.

Because of the pressure drop associated with the IHX and other primary HTS components, there will be some back flow of helium through the IHX vessel. This backflow is factored into the SCS design in order to prevent local flow reversals and ensure adequate core cooling.

The SCS is sized to remove decay heat under both pressurized and depressurized conditions. Under pressurized conditions the SCS is sized to remove up to 40 MW(t) per module. When the reactor system is shutdown and depressurized for maintenance or refueling, the SCS is sized to remove up to 14.1 MW(t). [Typically, maintenance activities are performed at least 24 hr after reactor shutdown, which corresponds to a decay heat load of about 5.8 MW(t).] To ensure high reliability, the SCS can draw electrical power from either normal or standby systems. Table 3-9 provides the design parameters for the SCS heat exchanger and circulator, which are shown in Fig 3-21. Figure 3-22 shows a sectional view of the SCS circulator.

Table 3-9. Shutdown Cooling System Design Parameters

Shutdown Heat Exchanger	**Depressurized**	**Pressurized**
Design Heat duty, MW(t)	14.1	40
Helium inlet temperature, °C (°F)	1032 (1890)	807 (1485)
Helium outlet temperature, °C (°F)	179 (355)	341 (645
Helium flow, kg/sec (lb/hr)	3.21 (25,438)	14.51 (115,200)
Water flow, kg/sec (lb/hr)	57.19 (454,000)	57.19 (454,000)
Water inlet temperature, °C (°F)	60 (140)	60 (140)
Shutdown Circulator		
Motor power, kW (hp)	323 (433)	TBD
Speed, rpm	6000	TBD
Exit pressure, kPa (psia)	84.1 (12.2)	TBD
Inlet temperature, °C (°F)	179 (355)	341 (645)
Helium pressure rise, kPa (psid)	6.14 (0.89)	TBD
Helium flow, kg/sec (lb/hr)	3.21 (25,438)	14.51 (115,200)

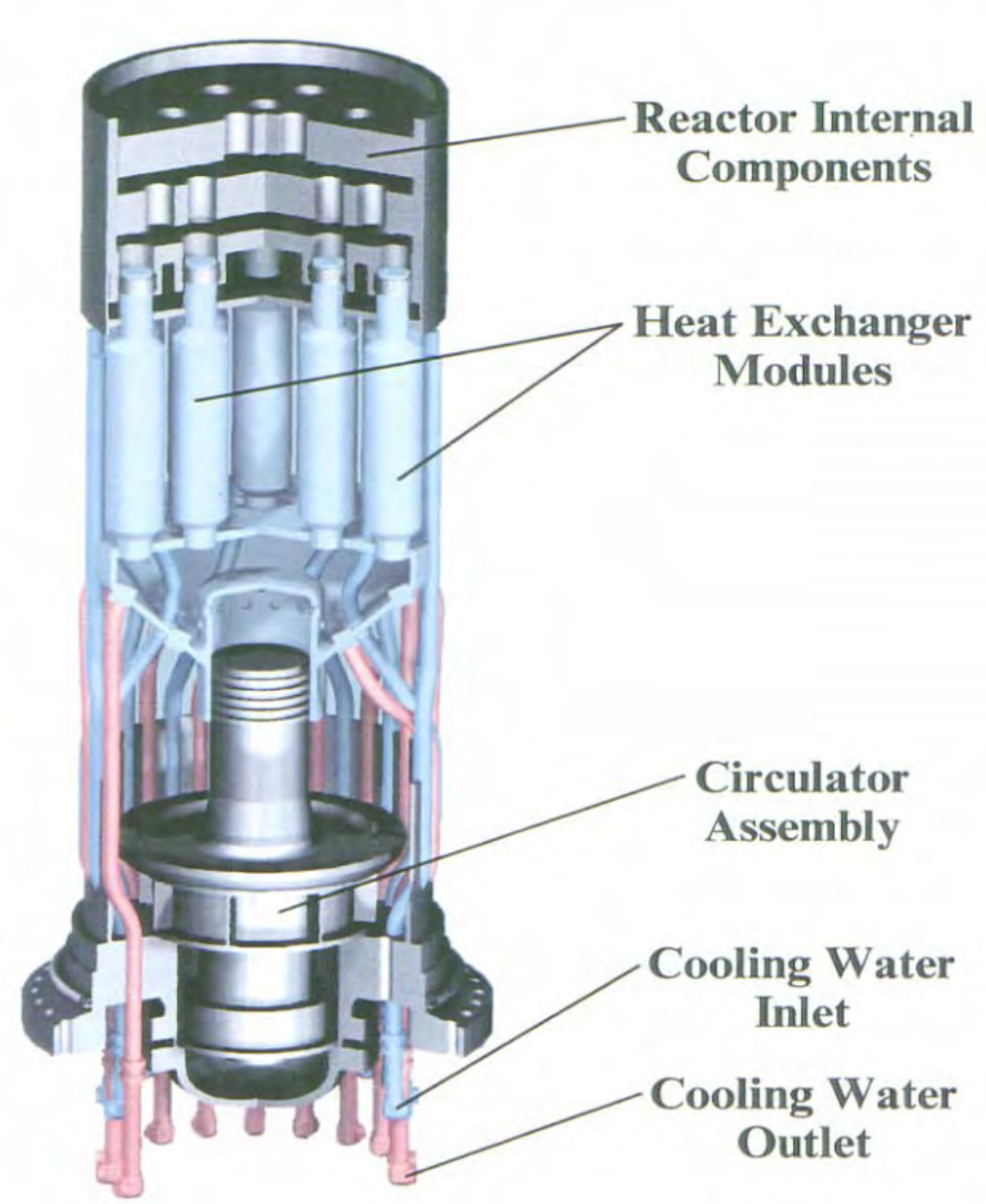

Figure 3-21. SCS Circulator and Heat Exchanger

During normal operation of the reactor system, the SCS operates in a standby mode. During this mode, a small amount of cold leg helium leaks (back flows) through the closed shutdown valve and flows opposite the normal flow direction through the SCS circulator and over the SCS heat exchanger tubes. In this mode the circulator is not operating, but the SCS cooling water system supplies a small amount of water flow to the heat exchanger. This water flow prevents thermal shock when the SCS switches to an active cooling mode, but also results in a parasitic heat loss of up to 1.3 MW(t) during normal operation. Therefore, the standby-mode water flow must be set as low as possible without resulting in one or both of the following adverse conditions: (a) boiling and/or (b) static instability due to the large hydrostatic head in the heat exchanger. During standby mode, the primary coolant helium pressure is higher than the SCS

water pressure, in order to prevent water ingress into the reactor system during normal operation. The SCS is manually switched from standby mode to an active cooling mode at the discretion of an operator.

The SCS control system includes protection features to actuate isolation valves and shutdown the circulator if the following events are detected: heat exchanger leaks, circulator overspeed, low cooling water flow, loss of net positive suction head, and high heat exchanger temperatures.

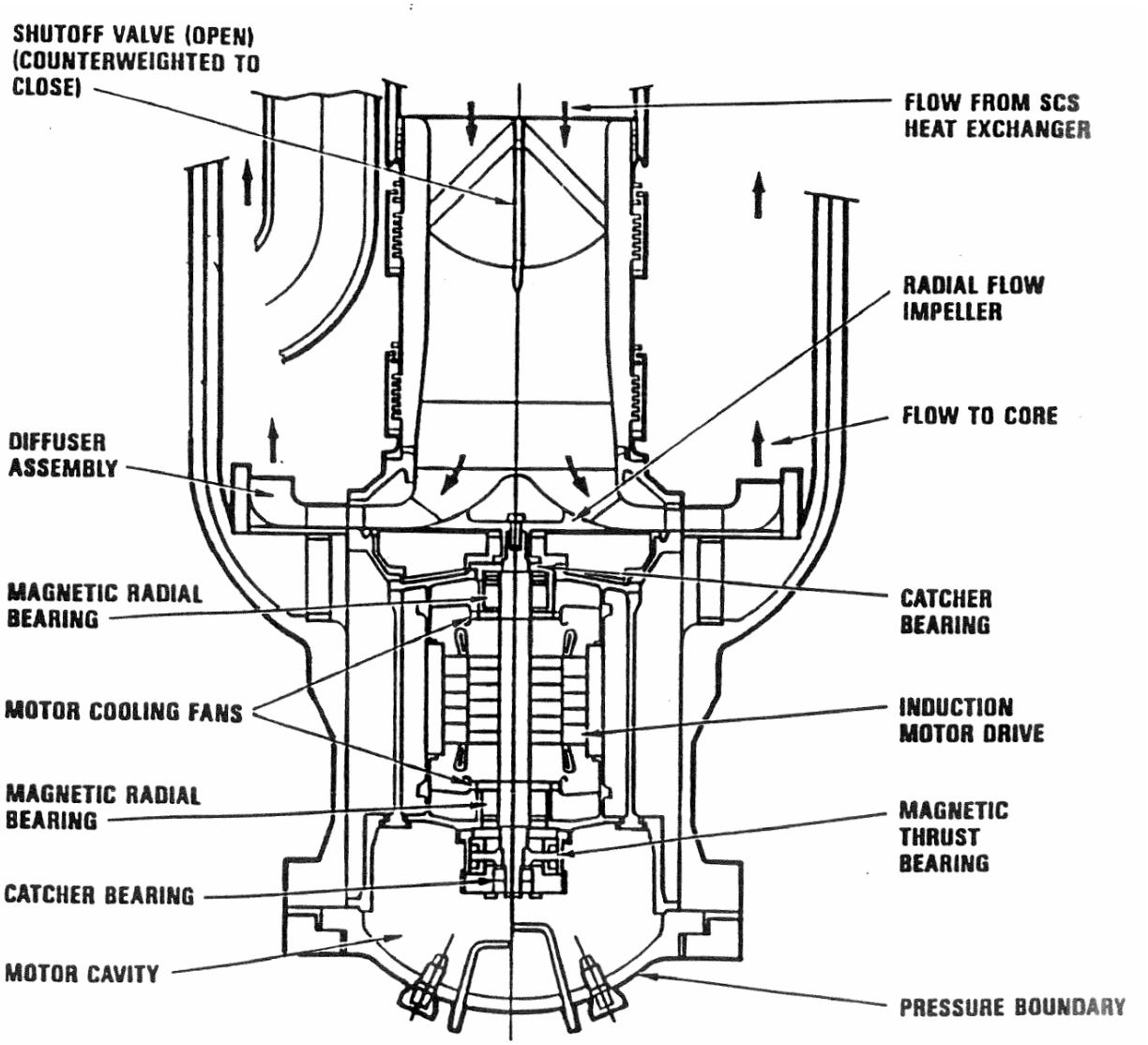

Figure 3-22. SCS Circulator Sectional View

3.1.6 Reactor Cavity Cooling System

The Reactor Cavity Cooling System (RCCS) is a Safety-Related system that provides a passive means of removing core residual heat during accident conditions when neither the HTS nor the SCS is available. The RCCS design is the same as that for the GT-MHR (GA 1996). Shown schematically in Fig. 3-23, the RCCS is a completely passive design that has no pumps, circulators, valves, or other active components. The RCCS receives heat transferred from the uninsulated reactor vessel by thermal radiation and natural convection. RCCS components include cooling panels that surround the reactor vessel, inlet/outlet structures that are located above grade on top of the reactor building, and a concentric duct system with the annular, outer flow path acting as the cold leg and the inner flow path acting as the hot leg. Through a balance of buoyancy and gravitational forces, natural convection airflow is established through the RCCS circuit.

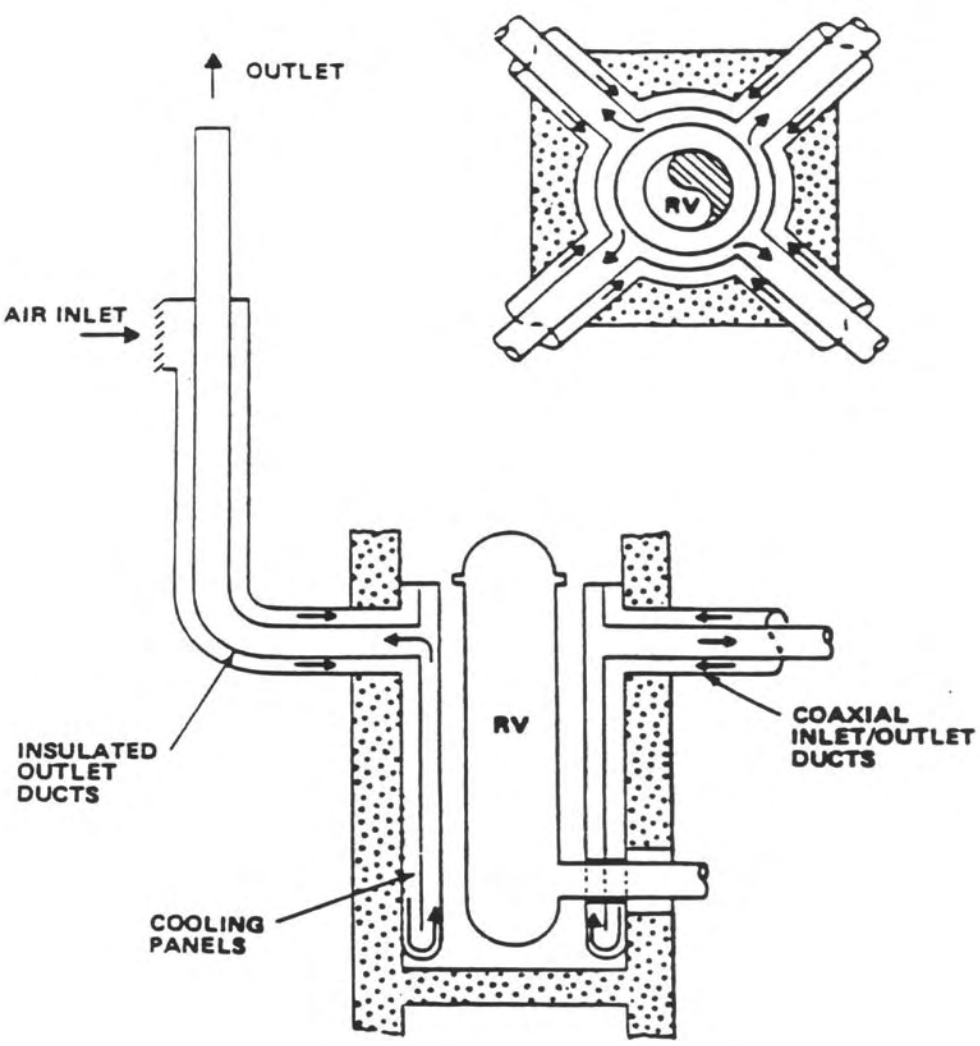

Figure 3-23. Passive Air-Cooled RCCS

The RCCS has multiple inlet/outlet ports and interconnected parallel flow paths to ensure cooling in the event of blockage of any single duct or opening, and is robustly designed to survive all credible accidents scenarios. Nevertheless, if the RCCS were to fail, the MHR is designed to allow heat transfer from the core to the surrounding ground. Under these beyond-design basis accident conditions, damage to the reactor vessel and silo concrete may occur, but peak fuel temperatures remain below 1600°C and 10CFR100 offsite dose limits are not exceeded.

The system is required to operate continuously in all modes of plant operation to support normal operation, and, if forced cooling is lost, it functions to remove decay heat to ensure investment and safety protection. The RCCS consists of a cooling panel which includes cold downcomers and hot risers and is located inside the reactor cavity surrounding the reactor vessel. Connected to the cooling panel are the concentric hot and cold ducts which connect the panel to the inlet/outlet structure.

3.1.6.1 RCCS Cooling Panels

As shown in Fig. 3-24, the RCCS panels follow the internal contour of the reactor cavity and surround the reactor vessel over its full circumference and length. The cold sides of the RCCS panels consists of four parts: upper cold plenum, downcomer, bottom cold plenum, and drain arrangement. The upper cold plenum receives cold air from the ductwork and distributes the cold air over the full circumference and directs the airflow to the downcomers. It also protects the concrete portion of the cavity ceiling from reactor vessel heat and serves as a quiescent/damping chamber which attenuates the effects of any atmospheric disturbance in the incoming cold air.

A reflective surface/insulation with a metal cover is provided as a part of the downcomer. This surface is attached to the inner plate and faces the reactor vessel. It serves to reflect the reactor vessel heat back to the cavity, and also protects the cold incoming air from being prematurely heated as it flows through the downcomer.

The bottom cold plenum, located at the bottom end of the downcomer, is essentially a box-shaped continuous ring header around the reactor vessel along the cavity wall. It permits change in airflow direction with minimal flow resistance and facilitates proper distribution of airflow to the riser part of the cooling panel. Any atmospheric disturbance and maldistribution that may have propagated down to the bottom of the cooling panel is suppressed in the bottom plenum and proper airflow distribution is restored.

Several drain connections are provided in the bottom cold plenum to drain any water that may be collected from the incoming air. Although the input/output structure is designed to prevent rain water from entering the RCCS, potential sources of water are mist entrained in the air, or some condensation on the cooler surfaces. The drain lines do not have any valves or pumps, and the cooling panels drain to the sump by gravity. The drain lines are oversized to provide flow in the event they become partially obstructed.

The hot side of the RCCS cooling panel consists of two parts: the riser and the hot plenum. The riser part consists of vertical rectangular structural steel tubes arranged around the reactor vessel. The tubes rise from the bottom cold plenum and connect to the hot plenum located at the top of the reactor cavity. The hot riser tubes are supported on the bottom plenum which

enables the tubes and the hot plenum to expand as they are heated. The design and configuration of the lateral support plates also accommodate thermal expansion of the tubes. The entire RCCS cooling panel assembly is a stable rigid structure which is designed for all required thermal, seismic, and pressure loading (due to tornado or pipe rupture).

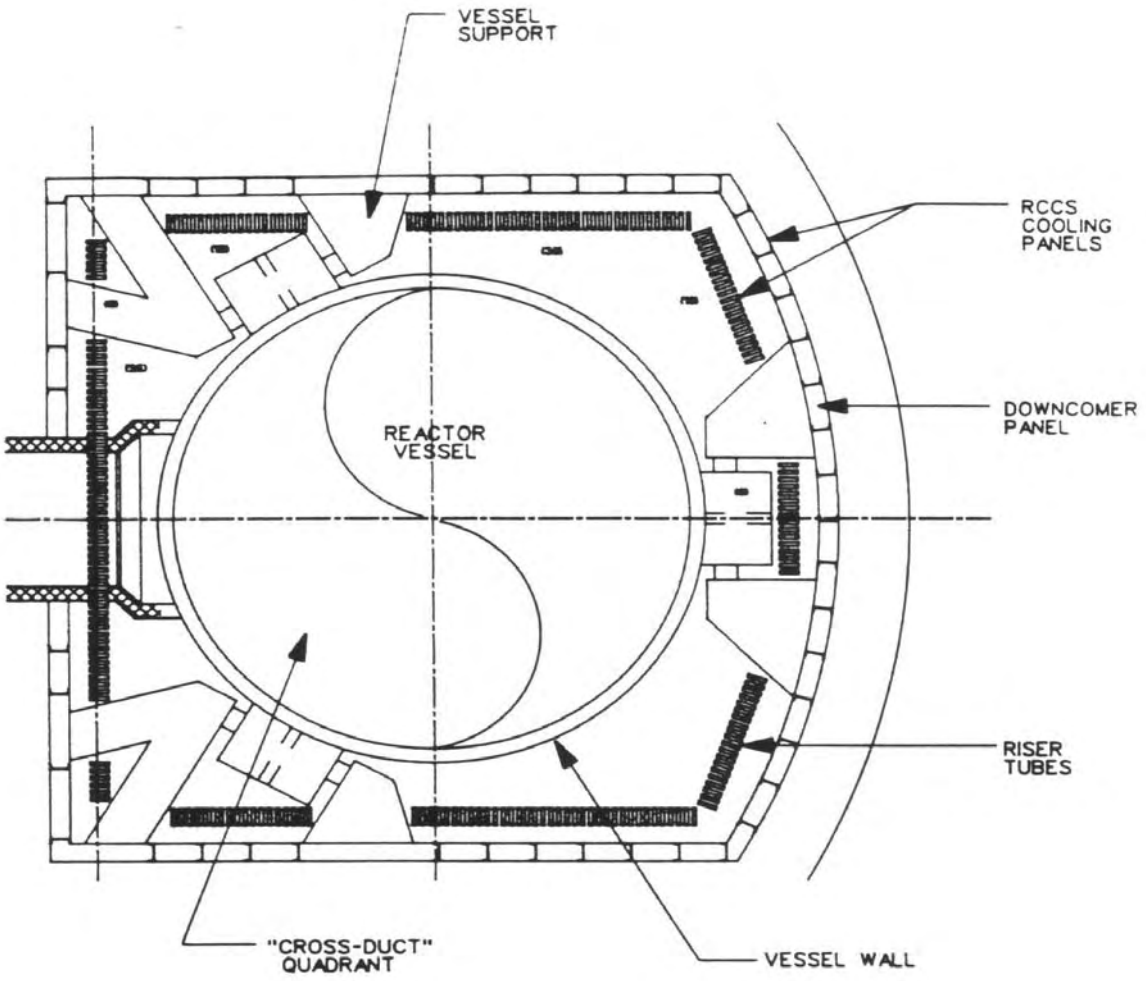

Figure 3-24. RCCS Panel Layout

3.1.6.2 RCCS Operation

The RCCS is designed to remove ~4 MW when the primary cooling circuit is either pressurized or depressurized. The RCCS is not required to remove decay heat during normal operation. However, since the system is passive, the system removes some parasitic heat during normal power operation, and removes some decay heat during normal shutdown because of the difference in the reactor vessel temperature and the outside air temperature.

During normal power operation, forced circulation of the primary coolant results in a near-uniform vessel temperature. The RCCS is designed to accommodate outside air temperatures

over a range of -42°C (-45°F) to 43°C (110°F). The performance of the RCCS at 100% reactor power with 43°C ambient air temperature is summarized in Table 3-10. The H2-MHR is designed to operate with coolant inlet and outlet temperatures that are 100°C than those for the GT-MHR. However, as discussed in Section 3.1.4, design modifications for higher-temperature operation of the H2-MHR should result in vessel temperatures and parasitic heat losses to the RCCS that are within the envelope of the GT-MHR RCCS design.

Table 3-10. RCCS Steady State Performance at 100% Reactor Power

Reactor Vessel	
Heat loss to RCCS, kW	3300
Inside wall temperature, °C (°F)	485 (905)
Average outside wall temperature, °C (°F) (not including flange)	446 (835)
Maximum outside wall temperature, °C (°F)	474 (886)
Cooling Panel (Front)	
Average temperature, °C (°F)	267 (513)
Maximum temperature, °C (°F)	323 (613)
Air inlet temperature, °C (°F)	43 (110)
Air outlet temperature, °C (°F)	274 (515)
Airflow kg/sec (lbm/hr)	14.3 (113,500)
Maximum velocity, m/sec (ft/sec) at exit from panel	11.5 (37.7)
Structure	
Concrete surface temperature, °C (°F)	49 (120)

3.1.7 Fuel Performance and Radionuclide Control

For modular gas-cooled reactor designs, a hallmark philosophy has been adopted since the early 1980s to design the plant such that radionuclides would be retained in the core during normal operation and postulated accidents. The key to achieving this safety goal is the reliance upon ceramic-coated fuel particles for primary fission product containment at their source, along with passive cooling to assure that the integrity of the coated particles is maintained even if the normal active cooling systems were permanently disrupted. This design philosophy has been carried forward for all subsequent MHR designs, including the H2-MHR. Fuel performance and radionuclide control in gas-cooled reactors is discussed in detail in numerous publications, including IAEA 1997, Hanson 2002, and Hanson 2003.

3.1.7.1 Radionuclide Containment System

The radionuclide containment system for the MHR, which reflects a defense-in-depth philosophy, is comprised of multiple barriers to limit radionuclide release from the core to the environment to insignificant levels during normal operation and postulated accidents. As shown schematically in Fig. 3-25, the five principal release barriers are: (1) the fuel kernel; (2) the particle coatings (particularly the SiC coating); (3) the fuel element structural graphite; (4) the primary coolant pressure boundary; and (5) the reactor building/containment structure. The effectiveness of each individual barrier for containing radionuclides depends upon a number of fundamental factors including the chemistry and half-lives of the various radionuclides, the service conditions in terms of burnup, fluence, temperature, and time at temperature, and the specific conditions associated with accident scenarios.

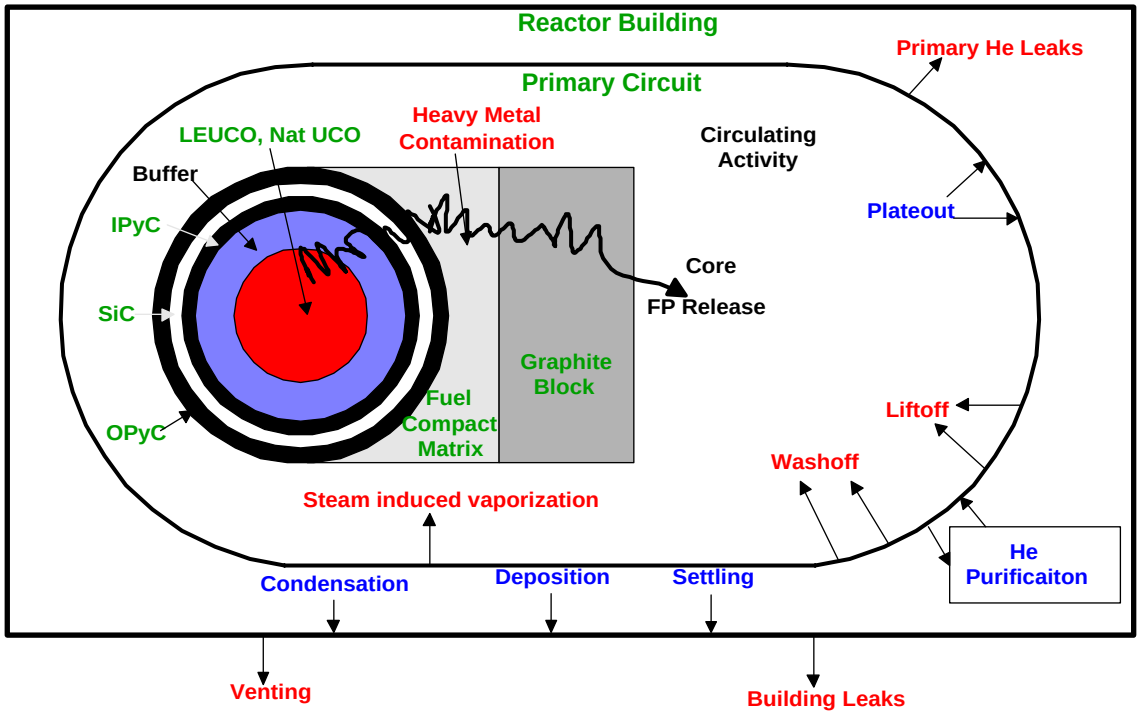

Figure 3-25. H2-MHR Radionuclide Containment System

The first barrier to fission product release is the fuel kernel itself. Under normal operating conditions, the kernel retains >95% of the radiologically important, short-lived fission gases such as Kr-88 and I-131. However, the effectiveness of a UCO kernel for retaining gases can be reduced at elevated temperatures or if an exposed kernel is hydrolyzed by reaction with trace amounts of water vapor which may be present in the helium coolant. The retentiveness of oxidic fuel kernels for long-lived, volatile fission metals such as Cs, Ag, and Sr is strongly dependent upon temperature and burnup.

The second, and most important, barrier to fission product release from the core is the silicon carbide and pyrocarbon coatings of each fuel particle. Both the SiC and PyC coatings provide a barrier to the release of fission gases. The SiC coating acts as the primary barrier to the

release of metallic fission products because of the low solubilities and diffusion coefficients of fission metals in SiC; the PyC coatings are partially retentive of Cs at lower temperatures but provide little holdup of Ag and Sr.

The fuel-compact matrix and the graphite fuel block collectively are the third release barrier. The compact matrix is relatively porous and provides little holdup of the fission gases which are released from the fuel particles. However, the matrix is a composite material which has a high content of amorphous carbon, and this constituent of the matrix is highly sorptive of metallic fission products, especially Sr. While the matrix is highly sorptive of metals, it provides little diffusive resistance to the release of fission metals because of its high interconnected porosity.

The fuel-element graphite, which is denser and has a more ordered structure than the fuel-compact matrix, is somewhat less sorptive of the fission metals than the matrix, but it is much more effective as a diffusion barrier than the latter. The effectiveness of the graphite as a release barrier decreases as the temperature increases. Under typical core conditions, the fuel element graphite attenuates the release of Cs from the core by an order of magnitude, and the Sr is essentially completely retained.

Typically, the two dominant sources of fission product release from the core are as-manufactured, heavy-metal (HM) contamination (i.e., heavy metal outside the coated particles) and particles whose coatings are defective or fail in service. In addition, volatile fission metals (e.g., Cs, Ag, Sr) can diffuse through intact SiC coatings if the fuel is maintained at high temperatures for sufficiently long time periods. However, for the H2-MHR core design, this mechanism should not be a significant contributor to fission-product release during normal operation, except possibly for Ag-110m and other isotopes of Ag.

The fourth release barrier is the primary coolant pressure boundary. Once the fission products have been released from the core into the coolant, they are transported throughout the primary circuit by the helium coolant. The helium purification system (HPS) efficiently removes both gaseous and metallic fission products from the primary coolant at a rate determined by the slipstream flow rate through the purification system. However, for the condensable fission products, the dominant removal mechanism is deposition (“plateout”) on the various helium-wetted surfaces in the primary circuit (i.e., the deposition rate greatly exceeds the purification rate). The plateout rate is determined by the mass transfer rates from the coolant to the fixed surfaces and by the sorptivities of the various materials of construction for the volatile fission products and by their service temperatures. Condensable radionuclides may also be transported throughout the primary circuit sorbed on particulates (“dust”) which may be present in the primary coolant; the plateout distribution of these contaminated particulates may be considerably different than the distribution of radionuclides transported as atomic species.

The circulating and plateout activities in the primary coolant circuit are potential sources of environmental release in the event of primary coolant leaks or as a result of the venting of primary coolant in response to over pressurization of the primary circuit. The fraction of the circulating activity lost during such events is essentially the same as the fraction of the primary coolant that is released, although the radionuclide release can be mitigated by pump down through the HPS if the leak rate is sufficiently slow. A small fraction of the plateout may also be reentrained, or “lifted off,” if the rate of depressurization is sufficiently rapid. The amount of fission product liftoff is expected to be strongly influenced by the amount of dust in the primary

circuit as well as by the presence of friable surface films on primary circuit components which could possibly spall off during a rapid depressurization.

The reactor building/containment structure is the fifth barrier to the release of radionuclides to the environment. Its effectiveness as a release barrier is highly event-specific. The vented low pressure containment (VLPC) may be of limited value as a release barrier during rapid depressurization events; however, it is of major importance during longer-term events during which forced cooling is unavailable. Under such conditions, the natural removal mechanisms occurring in the VLPC, including condensation, fallout, and plateout, serve to attenuate the release of condensable radionuclides, including radiologically important iodines, by at least an order of magnitude.

3.1.7.2 Fuel Failure Mechanisms

A number of failure mechanisms have been observed during irradiation testing and post-irradiation heating of coated-particle fuels, including pressure-vessel failure, kernel migration, and corrosion of the SiC layer by fission products. These failure mechanisms are illustrated in Fig. 3-26 and may be categorized as structural/mechanical or thermochemical in nature. Failure mechanisms in both categories can be affected by the release of excess oxygen during fission and subsequent formation of carbon monoxide. [IAEA, 1997] provides an excellent overview of these mechanisms and an extensive bibliography.

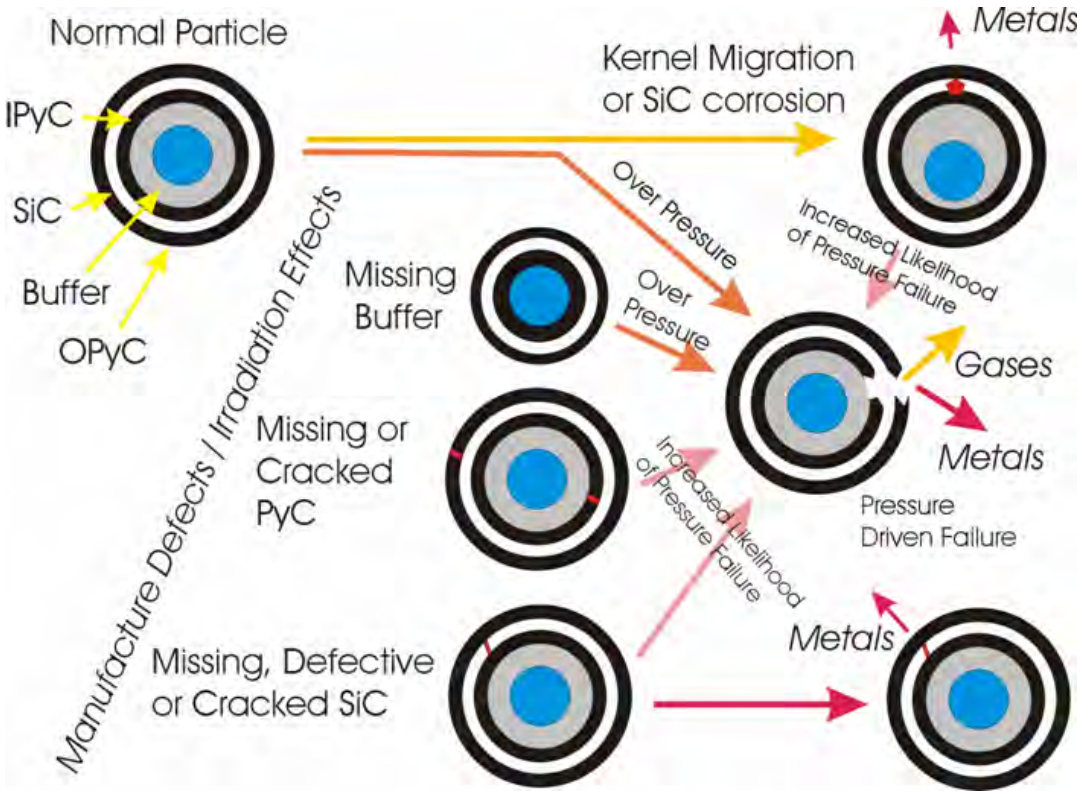

Figure 3-26. TRISO Particle Failure Mechanism

Carbon Monoxide Formation

For a substoichiometric metal oxide kernel (MO_{2-x}) or an oxycarbide (MC_xO_{2-x}), a mass balance for the excess oxygen generated as a function of burnup is given by

$$N_O / N_M = [2 - N_B] [FIMA - x/2] - (N_B) (x/2) \quad ,$$

where N_O = number of excess oxygen atoms, N_M = number of initial heavy metal atoms, and N_B = number of oxygen atoms bound per fission.[3] The burnup $FIMA_{CO}$ at which CO formation begins is given by

$$FIMA_{CO} = x/(2 - N_B) \quad .$$

For uranium fuels at moderate burnups, a reasonable lower bound for N_B is approximately 1.5. For x in the range 0.2 to 0.5, the quantity $FIMA_{CO}$ = 0.4 to 1.0 (40% to 100%), which virtually precludes CO formation during irradiation of H2-MHR fuel.

Structural/Mechanical Mechanisms

During irradiation, long-lived and stable fission gases are released from the kernel into the buffer, which increases the internal gas pressure. For some particle designs, carbon monoxide can also be generated during irradiation, which further increases the gas pressure. Because the SiC layer has a much higher elastic modulus than the pyrocarbon layers,[4] it bears most of the internal pressure force, which produces a tensile stress. However, the pyrocarbon layers undergo shrinkage during irradiation, which produces compressive forces in the SiC layer. As shown in Fig. 3-27, the compressive forces from pyrocarbon shrinkage more than compensate for the tensile stresses from internal pressure, such that the SiC remains in compression provided at least one of the pyrocarbon layers remains intact. From a structural / mechanical perspective, the SiC layer will remain intact provided (a) it remains in compression or (b) the tensile stress in the SiC layer does not exceed its strength.

As discussed above, shrinkage of the pyrocarbon layers during irradiation is a favorable attribute, in terms of the compressive forces applied to the SiC layer. However, pyrocarbon shrinkage produces tensile stresses in the pyrocarbon layers themselves, which can lead to failure of these layers. The strains and stresses generated in the pyrocarbon layers are complex functions of fast neutron fluence, irradiation temperature, and coating material properties. A property that greatly affects pyrocarbon performance is anisotropy, which can be quantified using X-ray or optical diffraction techniques. Anisotropy is usually expressed in terms of the Bacon Anisotropy Factor (BAF). For a perfectly isotropic material, BAF = 1, and for a perfectly oriented medium, BAF = ∞. Figure 3-28 shows irradiation-induced strains of pyrocarbon in the tangential direction for BAF values ranging from 1.02 to 1.05. Pyrocarbon layers are able to perform well out to high fast neutron fluences because the irradiation-induced strains and stresses are relaxed to some extent by irradiation-induced creep. Unfortunately, the

[3] Oxygen atoms are released during the fission process. The parameter N_B is the number of oxygen atoms per fission that are bound as stable oxides. These bound oxygen atoms are not available to react with carbon in the buffer layer to form CO.

[4] In other words, SiC is much stiffer than pyrocarbon. Because of this property, it is reasonable to assume the IPyC and OPyC are isolated from each other when evaluating performance of these layers and overall performance of the TRISO coating system.

measured data for pyrocarbon creep coefficients is widely scattered. Figure 3-29 shows calculations of OPyC performance for a range of creep coefficients (denoted by K_S on Fig. 3-29) that are well within the measured data base. At an irradiation temperature of 1200°C and a fast neutron fluence of 8×10^{25} n/m^2, the predicted OPyC failure fraction can range from 1.0 (K_S = 1.0) to < 2×10^{-3} (K_S = 2.5). Also shown on Fig. 3-29 is the model taken from the General Atomics Fuel Design Data Manual (FDDM) [Myers, 1987]. Although the FDDM model is very simplistic, it is representative of the data base for pyrocarbons that perform well under irradiation.

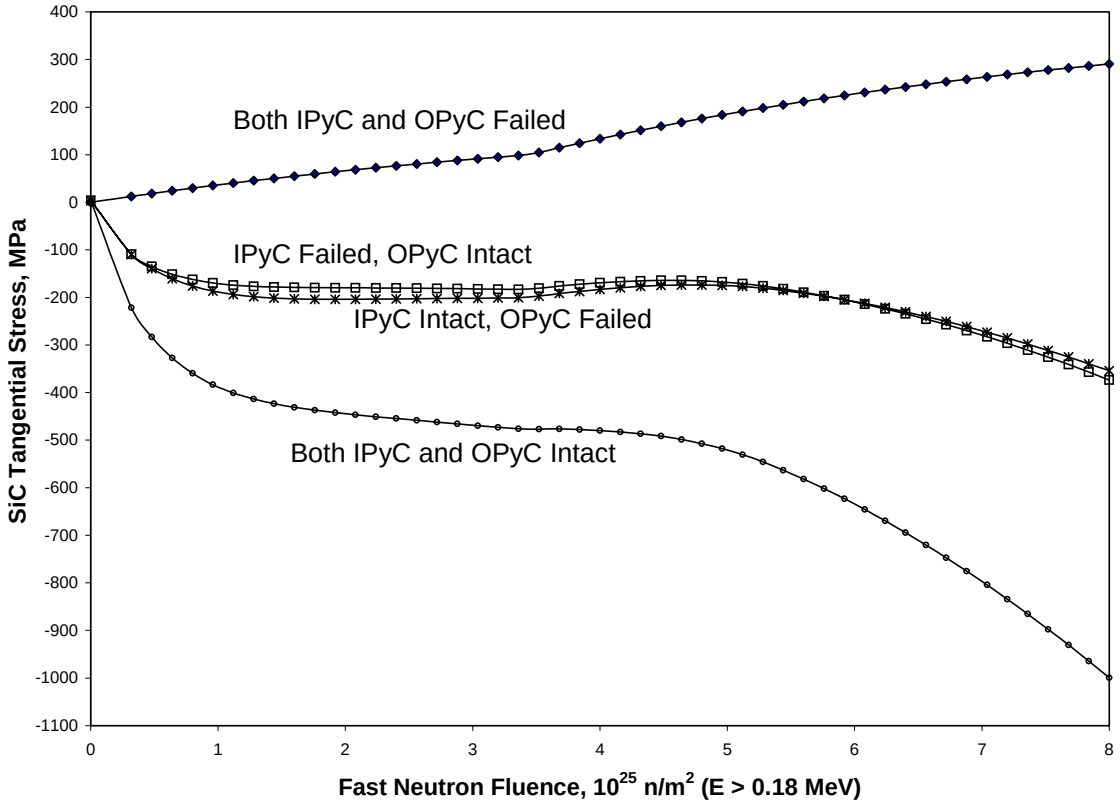

Figure 3-27. Calculated Tangential Stresses at the Middle of the SiC Layer. As indicated in the figure, the SiC layer remains in compression if one or both pyrocarbon layers remains intact.

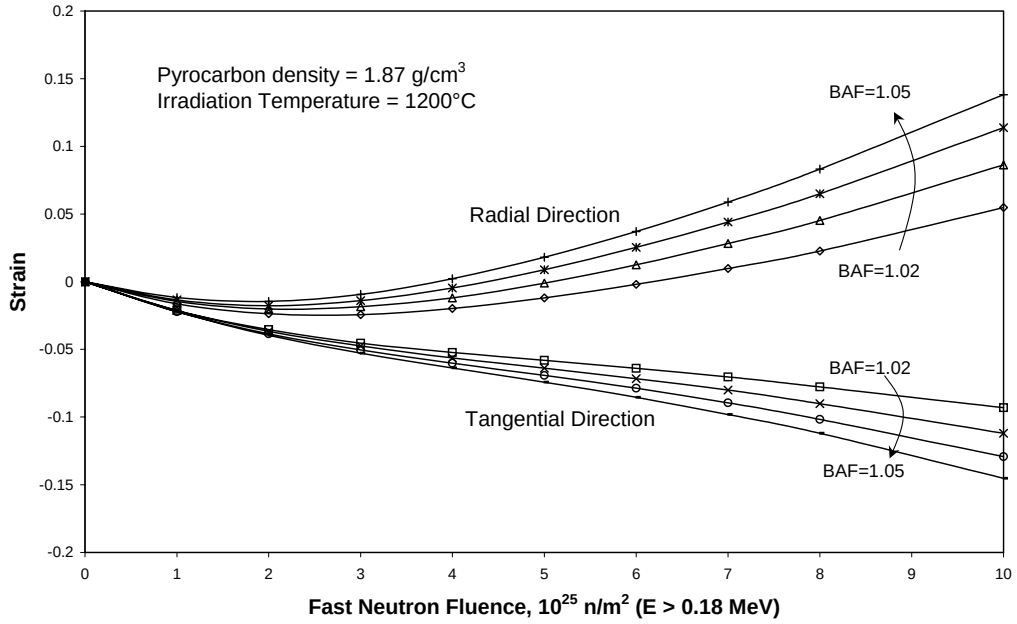

Figure 3-28. Irradiation-Induced Strain in Pyrocarbon as a Function of BAF

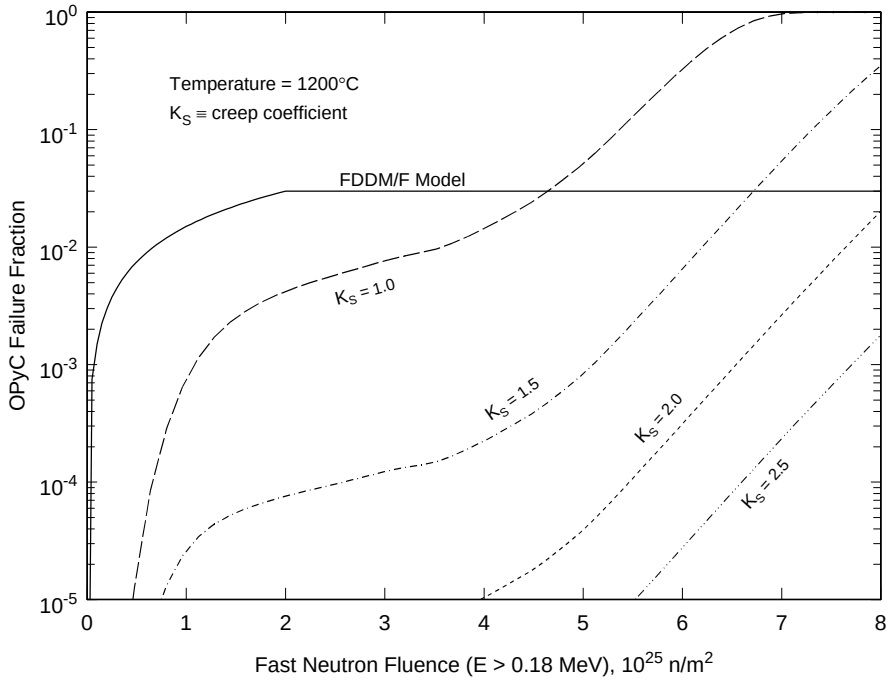

Figure 3-29. OPyC Performance Predictions. Calculations were performed for creep coefficients ranging from 1.0 to 2.5.

In the absence of compressive forces from the pyrocarbon layers, the tensile stress σ_{SiC} in the SiC layer may be calculated with reasonable accuracy using the thin-shell approximation:

$$\sigma_{SiC} = \frac{P r_{SiC}}{2 t_{SiC}} \quad ,$$

where P ≡ internal pressure inside the particle, r_{SiC} ≡ radius to the middle of the SiC layer, and t_{SiC} ≡ thickness of the SiC layer. Pressure vessel failure occurs when σ_{SiC} exceeds the strength of the SiC layer. The SiC layer failure fraction (f_{SiC}) is calculated using a Weibull distribution for the strength of the SiC layer. Assuming volume flaws and a uniform stress distribution in the SiC layer, the quantity failure probability f_{SiC} is determined from:

$$f_{SiC} = 1 - \exp\left[-\left(\frac{\sigma_{SiC}}{\sigma_o} \right)^m V_{SiC} \right] \quad ,$$

where σ_o ≡ Weibull characteristic strength, m ≡ Weibull modulus, and V_{SiC} ≡ volume of the SiC layer. The parameters σ_o and m are derived from experimental data. For the H2-MHR fissile and fertile particle designs, the internal pressure results almost entirely from the release of stable fission gases, because the carbide phase of the kernel getters excess oxygen and precludes formation of CO (see discussion above). For these particle designs, pressure vessel failure occurs only in the small fraction of particles with defective (missing or undersized) buffer layers that do not provide sufficient void space for gas accumulation.

Thermochemical Mechanisms

Under conditions of high temperature and high thermal gradient, oxide and carbide fuel kernels can migrate up the thermal gradient. This phenomenon is often referred to as the “amoeba effect” and can lead to complete failure of the coating system. For carbide kernels, migration is caused by solid-state diffusion of carbon to the cooler side of the kernel. For oxide kernels, migration may be caused by carbon diffusion or gas-phase diffusion of CO or other gaseous carbon compounds. As discussed above, CO generation should be negligible for H2-MHR fuel, and kernel migration should be a negligible contributor to fuel failure.

Noble metals (e.g., Ru, Rh, Pd, and Ag) are produced with relatively high yield during fission of uranium and plutonium fuels. During irradiation, the thermochemical conditions are not conducive for these elements to form stable oxides, and they can readily migrate out of the fuel kernel, regardless of its composition. Reactions of SiC with Pd have been observed during post-irradiation examinations of TRISO fuel. Although the quantity of Pd is small compared with the mass of the SiC layer, the reaction is highly localized, and complete penetration of the SiC layer can occur if high temperatures are maintained for long periods of time (see Fig. 3-30). As discussed in Section 3.1.4.3, corrosion of the SiC layer by fission products is a key factor for determining limitations on fuel temperatures.

At very high temperatures (above about 1800°C for extended periods of time), SiC will decompose into its constituent elements. The silicon vaporizes, leaving a porous carbon structure. For the H2-MHR, this failure mechanism should be a negligible contributor to fuel failure during normal operation and accident conditions.

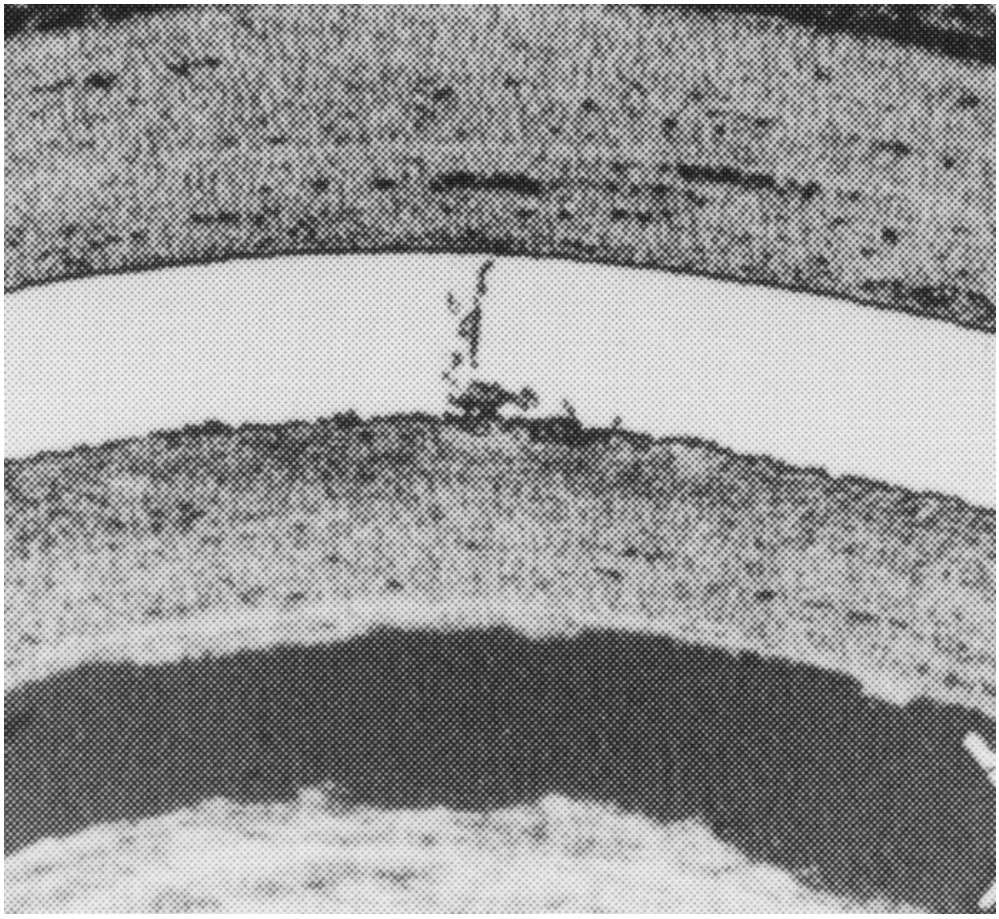

Figure 3-30. Localized Fission-Product Attack of the SiC Layer.

Diffusive Release Through Intact Coatings

Based on previous irradiation testing and post-irradiation heating, SiC is not very retentive of Ag (and possibly other noble metals) at high temperatures. The Ag-110m transports through the primary cooling circuit and deposits on the cooler wetted surfaces, which could impact operations and maintenance activities. The plateout activity is also a potential source of radioactivity release during hypothetical accidents involving a rapid loss of coolant, when the shear forces during depressurization are sufficiently high to remove some of the deposited activity. Figure 3-31 shows the breakthrough time as a function of temperature for Ag diffusing through a 35-µm SiC layer. For temperatures above 1000°C, the breakthrough time is less than 100 days, which is well below the fuel residence time of 850 days. As discussed in Section 3.1.4, limiting the release of Ag to acceptable levels is largely accomplished through optimization of the nuclear and thermal hydraulic design of the reactor core.

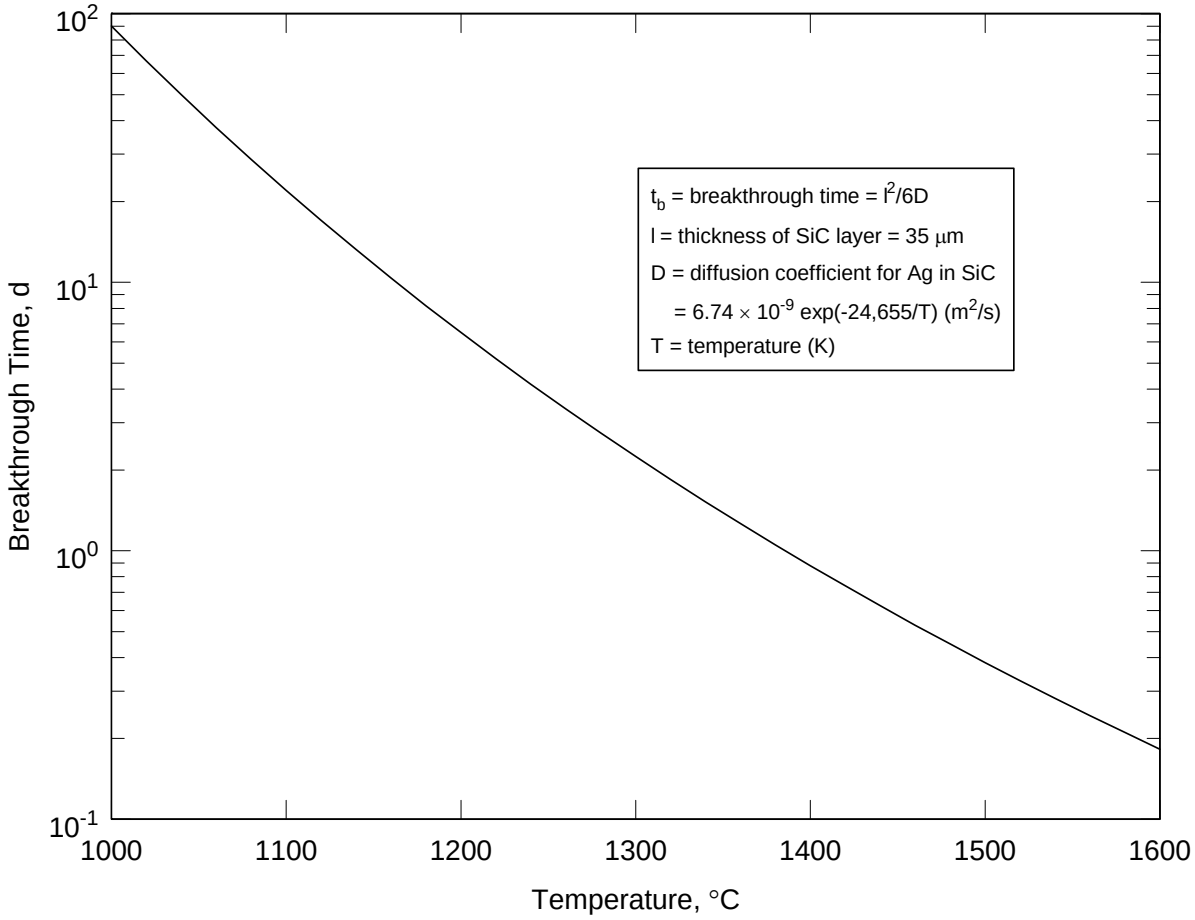

Figure 3-31. Breakthrough Time for Ag Diffusing Through a 35-μm SiC Layer.

3.1.7.3 Performance Capability of High-Quality TRISO Fuel

The Germans have manufactured high-quality, TRISO-coated fuels that have performed exceptionally well during irradiation and accident-condition testing. Table 3-11 provides a summary of performance data for high-quality German fuels with 10%-enriched UO_2 kernels and 20%-enriched UCO kernels. Figure 3-32 shows the irradiation temperatures and fuel burnups achieved during individual tests of German fuel with fuel-failure fractions < 10^{-5} at the end of irradiation. The Japanese have achieved a similar level of success with their low-enriched UO_2 fuel. The U.S. is developing UCO coated-particle fuel with similar requirements for as-manufactured quality and performance during normal operation and accident conditions [Petti, 2005].

Table 3-11. Summary of Performance Data for High-Quality TRISO Fuel Manufactured in Germany

	UO_2 Kernels[(a)]	UCO Kernels[(b)]
Fraction of particles with as-manufactured defective coating systems	$5 \times 10^{-5} – 1 \times 10^{-4}$	$< 10^{-4}$
Fuel burnup (% FIMA)	7 – 15	18.6 – 22.2
Fast neutron fluence (10^{25}/m^2)[(c)]	4 – 8	1.8 – 3.2
Fuel irradiation temperature (°C)[(d)]	700 – 1320	900 – 1350
Fractional release of Kr-85m at end of irradiation	~10^{-7} at 1100°C	~2×10^{-7} at 1100°C
Fractional release of Cs-137 at end of irradiation	$10^{-6} – 10^{-4}$	not measured
Fraction of coating systems that failed during accident-condition testing	• $< 10^{-5}$ when heated at 1600°C for up to 500 h. • $10^{-4} – 10^{-3}$ when heated at 1800°C for > 20 h.	not measured
Fractional release of Cs-137 during accident-condition testing	• $2 \times 10^{-5} – 8 \times 10^{-4}$ when heated at 1600°C for 500 h. • $10^{-6} – 5 \times 10^{-5}$ during loss-of-coolant simulation test with peak temperature of 1620°C. • $4 \times 10^{-4} – 6 \times 10^{-2}$ when heated at 1800°C for 20 to 200 h.	not measured
Fractional release of Ag-110m during accident-condition testing	• $9 \times 10^{-4} – 3 \times 10^{-2}$ when heated at 1600°C for 500 h. • $8 \times 10^{-4} – 8 \times 10^{-2}$ during loss-of-coolant simulation test with peak temperature of 1620°C. • $8 \times 10^{-2} – 0.81$ when heated at 1800°C for 20 to 200 h.	not measured

(a) Performance data were taken from [IAEA, 1997] and are from a series of irradiation and heating tests.
(b) Performance data were taken from [Borchardt, 1982] and are from a single irradiation test.
(c) Neutron energies greater than 0.1 MeV.
(d) In general, temperatures varied significantly with irradiation time and with location of the fuel within the irradiation-test capsule.

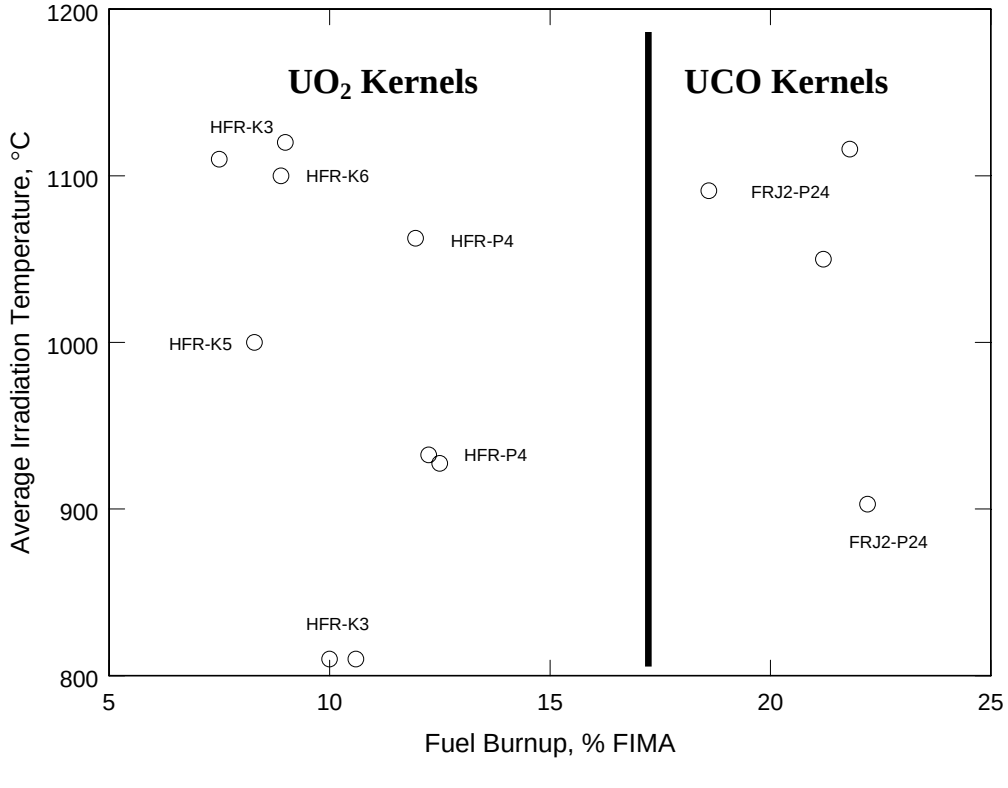

Figure 3-32. Irradiation Conditions During Testing of High-Quality German Fuel. The symbol labels identify the individual irradiation tests. In all cases, the fuel-failure fraction at the end of irradiation was $< 10^{-5}$.

Two advanced coated particle designs are being considered to provide additional performance margins at higher temperatures. These particle designs incorporate ZrC either as a replacement for the SiC layer or as an oxygen getter within the particle. These particle designs are discussed in more detail in Appendix A and have been included as part of the Advanced Gas Reactor development plan for advanced fuels [Hanson, 2004].

3.1.7.4 Radionuclide Transport Mechanisms

Radionuclide transport is modeled in the fuel kernel, the particle coatings, fuel-compact matrix, fuel-element graphite, primary coolant circuit, and reactor building. [IAEA, 1997] provides an excellent overview and an extensive bibliography of radionuclide transport mechanisms. The transport of radionuclides from the location of their birth through the various material regions of the core to their release into the helium coolant is a relatively complicated process. The principal steps and pathways are shown schematically in Fig. 3-33. Also for certain classes of radionuclides, some steps are eliminated (e.g., noble gases are not diffusively released from intact TRISO particles and are not significantly retarded by the compact matrix or fuel-element graphite).

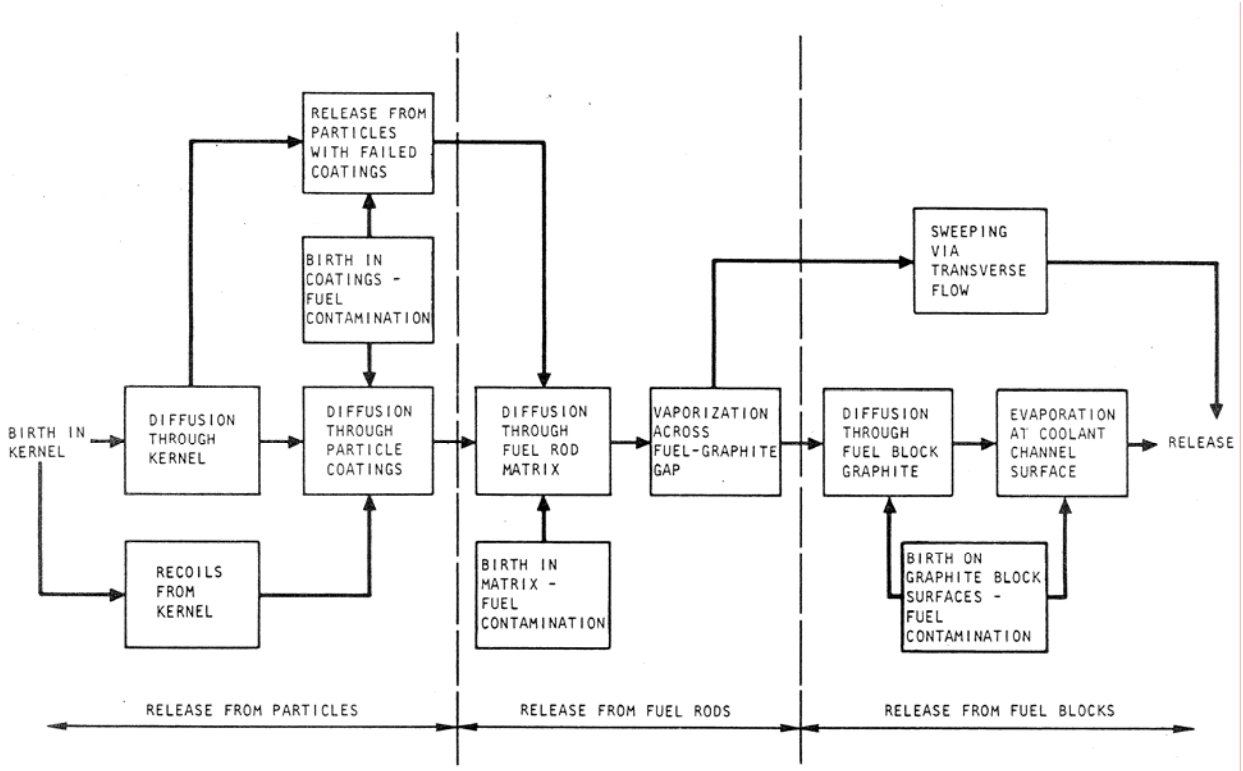

Figure 3-33. Principal Steps in Radionuclide Release from the H2-MHR Core

While the actual radionuclide transport phenomena in the core can be very complex, the basic approach for modeling these phenomena is to treat radionuclide transport as a solid-state diffusion problem with various modifications and/or additions to account for the effects of irradiation and heterogeneities in the core materials. The point of departure is typically Fick's second law of diffusion.

Under normal operating conditions, the fission gases, including iodines, are quantitatively retained by the coatings of an intact TRISO particle. The release of fission gases from HM contamination and failed fuel with exposed fuel kernels is expressed in terms of the release rate-to-birth rate ratio (R/B); at steady-state, R/B is numerically equal to the fractional release. Semi-empirical correlations for R/B have been derived from experimental data and are typically expressed as:

$$\left(R/B\right)_{ji} = 3\sqrt{\left(\frac{\xi_j}{\lambda_i}\right)} \bullet f(T) \bullet f(Bu) \ ,$$

where ξ_j = reduced diffusion coefficient for chemical species j, λ_i = decay constant for isotope i, f(T) = empirical function of temperature, and f(Bu) = empirical function of burnup. The square-root dependence of R/B on isotope half-life results from the analytical solution to the diffusion equation and has been confirmed by measurements of fission-gas release during irradiation testing of fuels and operation of earlier generation gas-cooled reactors, including Peach Bottom

and Ft. St. Vrain. For Kr-85m (half-life = 4.48 h), experimental data show the R/B for an exposed kernel to be in the range 0.005 to 0.01 at 1100°C.

The transport of the volatile fission metals, including Ag, Cs, Sr, and Eu, in the PyC and SiC coatings is modeled as a transient Fickian diffusion process. At sustained temperatures above approximately 1600°C, the SiC coating begins to degrade as a result of fission-product attack. Under these conditions, the fractional release of the Cs isotopes is taken as a measure of the rate of SiC degradation. Figure 3-34 which shows data obtained during postirradiation heating at 1700°C of Japanese low-enriched UO_2 fuel from capsule HRB-22. The release profiles indicate Ag is diffusively released from intact TRISO, Kr is retained by PyC coatings, and Cs is slowly released as the SiC degrades.

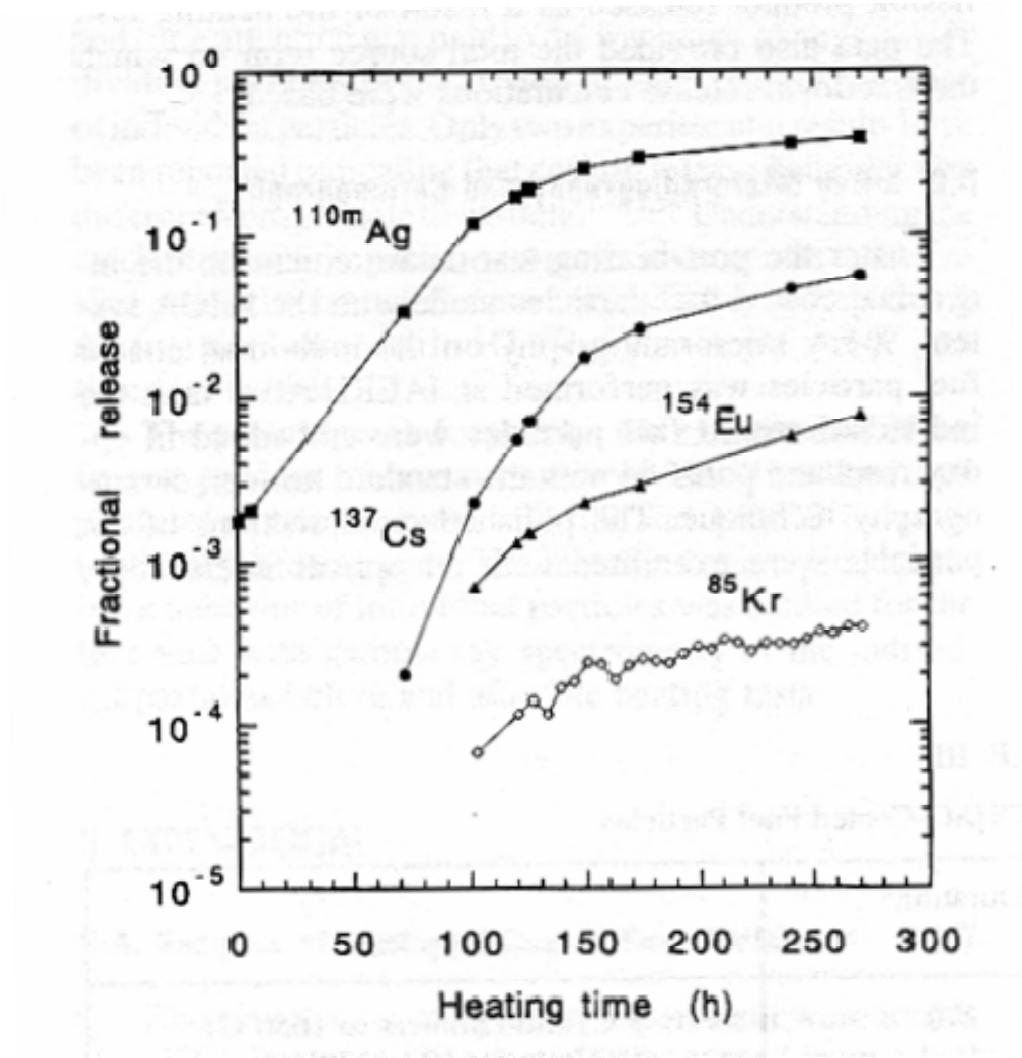

Figure 3-34. Postirradiation Heating of Japanese LEU UO_2 Fuel

The transport of volatile fission metals in fuel-compact matrix and graphite is also modeled as transient diffusion processes. It is assumed that sorption equilibrium prevails in the gap between the fuel compact and the fuel hole surface of the fuel block. At the coolant boundary,

the mass flux from the surface into the flowing coolant is given by the product of a convective mass transfer coefficient and the concentration gradient between the equilibrium desorption pressure and the mixed-mean concentration in the coolant. Diffusion coefficients and sorption isotherms have been determined experimentally for a number of nuclear graphites and matrix materials [IAEA, 1997].

The transport and deposition of condensable radionuclides from the flowing helium coolant to fixed surfaces in the primary coolant circuit is essentially a convective mass transfer problem. Usually, deposition is conceived as a two-step process: (1) gaseous diffusion to the wall and (2) a wall effect, typically an adsorption process. The latter step is necessary because numerous experiments have shown that, under certain circumstances, graphitic and metallic surfaces have a limited capacity to sorb certain radioactive species. The sorptivity of metals for volatile fission products is typically a function of surface oxidation state and temperature. The wall effect may be simply an adsorption process whereby the active sites are confined to the surface. Alternatively, there are some data suggesting that certain radionuclides, principally Ag isotopes, may penetrate into the bulk of metallic components.

The condensable radionuclides that are plated out in the primary circuit may be partially reentrained and released to the reactor building during rapid depressurization transients. A potentially significant removal mechanism, especially during rapid depressurizations, is mechanical reentrainment of deposited particulate matter contaminated by plateout and/or spallation of friable surface films; this mechanical reentrainment is traditionally referred to as "liftoff". Empirical liftoff models have been developed by correlating the fractional reentrainment of plated out fission products measured in blowdown tests with the shear ratio (the ratio of the wall shear during a depressurization transient to that during normal operation).

The VLPC of the H2-MHR is expected to be a significant barrier to the release of condensable radionuclides to the environment during accident conditions. Consequently, the natural removal mechanisms, including condensation, gravitational settling, and turbulent deposition are modeled.

3.1.7.5 Fuel Quality and Performance Requirements

For previous gas-cooled reactor designs, the requirements for as-manufactured quality and in-service performance of coated-particle fuel have been based on a two-tier set of radionuclide design criteria (allowable core release rates), referred to as the "Design" and "Maximum Expected" criteria. This approach has also been adopted for the H2-MHR fuel. The "Design" criteria represent upper limits for all normal operating conditions and any off-normal events that are expected to occur during operation of the plant.[5] These criteria are used when assessing the impact of plant operation on public safety, to size helium purification and radioactive waste systems, and to design plant hardware and shielding. The "Design Criteria" account for uncertainties in the design methods and supporting data, and represent a design margin over the "Maximum Expected" criteria, which are used for applications where "best-estimate" results are appropriate, including developing component removal and maintenance procedures. The fuel and reactor core are to be designed such that there is at least a 50% probability that the radionuclide releases will be less than the "Maximum Expected" criteria, and at least a 95% probability that the releases will be less than the "Design" criteria. The logic for deriving these

[5] These types of off-normal events are often referred to as Anticipated Operational Occurrences (AOOs).

fuel requirements is illustrated in Fig. 3-35. Top-level requirements for the H2-MHR are defined by both the regulators and the users. Lower-level requirements are then systematically derived using the systems-engineering approach described in Section 2.1. With this approach, the radionuclide control requirements for each of the release barriers can be defined. For example, starting with the allowable doses at the site boundary, limits on radionuclide releases from the VLPC, reactor vessel, and reactor core are successively derived. Fuel failure criteria are in turn derived from the allowable core release limits. Finally, the required as-manufactured fuel attributes are derived from the in-reactor fuel-failure criteria, with consideration of achievable values based on existing fuel manufacturing experience, thereby providing a logical basis for the fuel quality specifications.

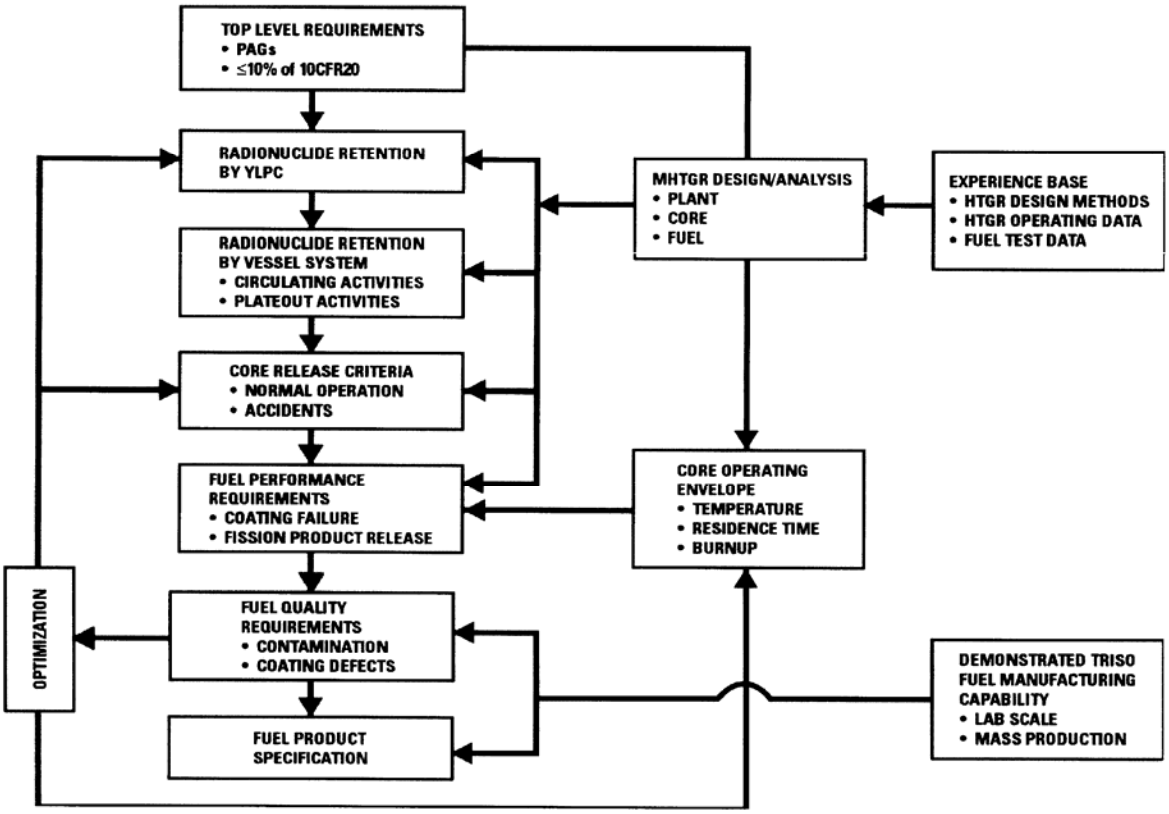

Figure 3-35. Logic for Derivation of Fuel Quality Requirements

As discussed in Section 3.1.4, optimization of the H2-MHR core nuclear and thermal hydraulic design should result in fuel service conditions that are not significantly different from those for the GT-MHR. As a result, the fuel quality and performance requirements for the H2-MHR are identical to those for the GT-MHR. The service conditions, as-manufactured quality requirements, and in-service performance requirements for the H2-MHR fuel are given in Tables 3-12 through 3-14. The requirements for in-service performance are specified on a core-average basis. The maximum allowable release fractions for 30.2-yr Cs-137 and 249.8-d Ag-110m are included in Table 3-14 because these nuclides are expected to be the strongest

contributors to worker dose, based on previous assessments of radionuclide plateout distributions and plant-maintenance requirements.

Table 3-12. Service Conditions for Fissile and Fertile Fuel

Parameter	Fissile Fuel		Fertile Fuel	
	Peak	Core Average	Peak	Core Average
Fuel temperature (normal operation), °C	1250	[850]	1250	[850]
Fuel temperature (accident conditions), °C	1600	—	1600	—
Fuel burnup, % FIMA	26	[15]	7	[4]
Fast fluence, 10^{25} n/m^2 (E > 0.18 MeV)	5	[3]	5	[3]
Core residence time, EFPD	850	850	850	850

Quantities in brackets indicate preliminary values.

Table 3-13. As-Manufactured Quality Requirements for Fissile and Fertile Fuel

Parameter	Fissile Fuel		Fertile Fuel	
	Maximum Expected	Design	Maximum Expected	Design
Missing or defective buffer	1.0×10^{-5}	2.0×10^{-5}	[1.0×10^{-5}]	[2.0×10^{-5}]
Defective SiC	5.0×10^{-5}	1.0×10^{-4}	[5.0×10^{-5}]	[1.0×10^{-4}]
HM contamination	1.0×10^{-5}	2.0×10^{-5}	[1.0×10^{-5}]	[5.0×10^{-5}]
HM contamination outside intact SiC	6.0×10^{-5}	1.2×10^{-4}	[6.0×10^{-5}]	[1.2×10^{-4}]

Quantities in brackets indicate preliminary values.

Table 3-14. In-Service Performance Requirements for Fissile and Fertile Fuel

Parameter	Fissile Fuel		Fertile Fuel	
	Maximum Expected	Design	Maximum Expected	Design
Allowable Fuel Failure Fraction (Normal Operation)	5.0×10^{-5}	2.0×10^{-4}	$[5.0 \times 10^{-5}]$	$[2.0 \times 10^{-4}]$
Allowable Fuel Failure Fraction (Accident Conditions)	$[1.5 \times 10^{-4}]$	$[6.0 \times 10^{-4}]$	$[1.5 \times 10^{-4}]$	$[6.0 \times 10^{-4}]$
Allowable Cs-137 Release Fraction (Normal Operation)	1.0×10^{-5}	1.0×10^{-4}	$[1.0 \times 10^{-5}]$	$[1.0 \times 10^{-4}]$
Allowable Cs-137 Release Fraction (Accident Conditions)	1.0×10^{-4}	$[1.0 \times 10^{-3}]$	$[1.0 \times 10^{-4}]$	$[1.0 \times 10^{-3}]$
Allowable Ag-110m Release Fraction (Normal Operation)	2.0×10^{-4}	2.0×10^{-3}	$[2.0 \times 10^{-4}]$	$[2.0 \times 10^{-3}]$
Allowable Ag-110m Release Fraction (Accident Conditions)	$[2.0 \times 10^{-3}]$	$[2.0 \times 10^{-2}]$	$[2.0 \times 10^{-3}]$	$[2.0 \times 10^{-2}]$

Quantities in brackets indicate preliminary values.

3.2 Heat Transport Systems

The Primary and Secondary Heat Transport Systems (HTS) are described in the following sections. The Primary HTS provides cooling for the MHR module and transfers its heat through the Intermediate Heat Exchanger (IHX) to the Secondary HTS. The Secondary HTS is included as part of the H2-MHR design to provide physical separation between the Reactor System and Hydrogen Production System. Pressurized helium is used as the heat transfer fluid for both the Primary HTS and Secondary HTS. The Secondary HTS transfers its heat to the H_2SO_4 decomposers and vaporizers in the Hydrogen Production System. The secondary helium coolant is maintained at a pressure slightly higher than both the primary helium coolant in the IHX and the $H_2O/H_2SO_4/SO_3/SO_2/O_2$ mixtures in the H_2SO_4 decomposers and vaporizers. If a drop in pressure is detected in the Secondary HTS, the Investment Protection System (IPS) automatically performs the following actions:

- Trips the reactor and primary and secondary coolant circulators.
- Closes the secondary loop isolation valves to isolate the system from both the IHX and the Hydrogen Production System in order to prevent chemical and/or radioactive contamination of the Secondary HTS. **[TBD]**

3.2.1 Primary Heat Transport System

The primary components of the Primary HTS are the IHX and the primary coolant circulator.

3.2.1.1 IHX Design

The IHX design is based on the Printed Circuit Heat Exchanger (PCHE) concept developed by Heatric (www.heatric.com), which consists of metal plates that are diffusion bonded to restore the properties of the base metal (see Fig. 3-36). Fluid-flow channels are chemically milled into the plates using a technique that is similar to that used for etching printed electrical circuits. The PCHE concept allows for simultaneous high-temperature and high-pressure operation with relatively thin wall thicknesses between the primary and secondary coolants. PCHEs are typically four to six times smaller than conventional shell-and-tube heat exchangers of equivalent heat duty. With this technique, the PCHE design can be optimized for specific applications. Designs have been developed with thermal effectiveness greater than 98%.

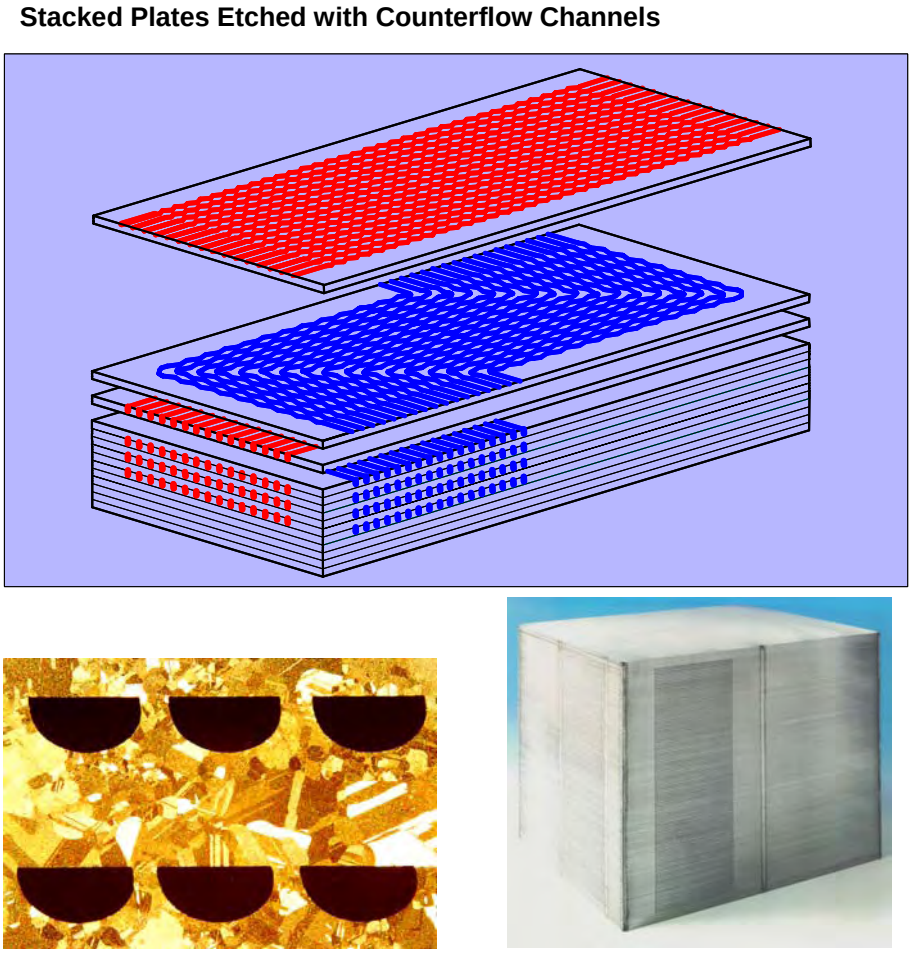

Figure 3-36. PCHE Design Technology (figure courtesy of HEATRIC Corporation)

This H2-MHR IHX design consists of 40 Heatric-type modules manufactured from a high-temperature alloy (Inconel 617 and Hastelloy-XR are candidate materials). Each module has a heat duty of approximately 15.5 MW(t), which provides about 20 MW(t) margin over the required heat duty of 600 MW(t). Each module weighs approximately 5 tonnes and has dimensions of 0.6 m × 0.65 m × 1.5 m. In order to minimize the size and weight of the IHX vessel, it is desirable to use a compact arrangement to house the PCHE modules within the vessel. However, sufficient room must be provided to accommodate differential thermal expansion (using expansion joints) and headers. Preliminary results indicate that it should be possible to design a 600-MW(t) IHX with a vessel that is of similar size as the reactor vessel. Within the IHX vessel, the modules are arranged in 8 axial layers, with 5 modules per layer. The IHX vessel is a pressure boundary for the secondary helium coolant and will be designed according to Section III of the ASME Code. The IHX vessel is manufactured using SA533 steel, and insulated with kaowool to maintain operating temperatures below 350°C and prevent creep damage. Design parameters for a 600-MW(t) IHX are given in Table 3-15. Figure 3-37 shows a preliminary IHX design concept.

Table 3-15. 600-MW(t) IHX Design Parameters

Total Number of Modules	40
Number of Axial Layers	8
Number of Modules Per Layer	5
Module Height (m)	1.5
Module Length (m)	0.65
Module Width (m)	0.6
IHX Wall Thickness (mm)	2
Total Heat Transfer Area (m^2)	9145
Primary Helium Flow Rate (kg/s)	320
Primary Helium Inlet Temperature (°C)	950
Primary Helium Outlet Temperature (°C)	590
Primary Helium Inlet Pressure (MPa)	7.0
Primary Helium Pressure Drop (MPa)	0.03
Secondary Helium Flow Rate (kg/s)	320
Secondary Helium Inlet Temperature (°C)	565
Secondary Helium Outlet Temperature (°C)	925
Secondary Helium Inlet Pressure (MPa)	7.1
Secondary Helium Pressure Drop (MPa)	0.03
Heat Exchanger Effectiveness (%)	93.5

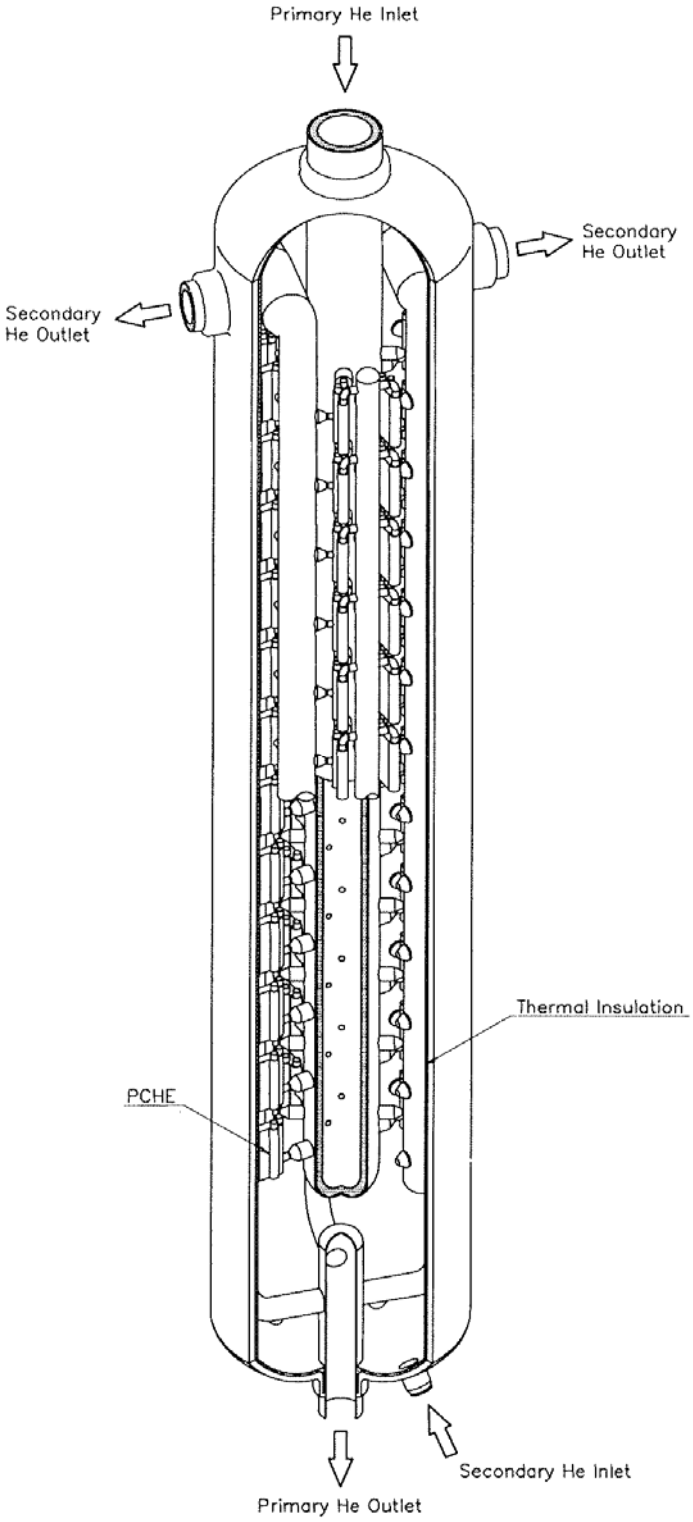

Figure 3-37. Preliminary IHX Design Concept. (Figure courtesy of Toshiba Corporation, Yokohama, Japan.)

3.2.1.2 Primary Coolant Circulator

The primary circulator is located on the cold leg of the primary circuit. For earlier gas-cooled reactor designs that used a steam cycle to generate electricity, the primary circulator was housed within the steam-generator vessel. A similar configuration is being considered for the H2-MHR, with the circulator housed within the IHX vessel. Alternatively, the circulator may be housed within a separate vessel. Figure 3-38 shows the primary circulator design concept. The circulator is a vertically-oriented, two-stage axial flow machine powered with a variable speed electric motor and is sized for a total pressure drop of 100 kPa. The corresponding pumping power is 8.2 MW and the required electrical power for the motor is 10.2 MW (assuming a circulator efficiency of 80%). During normal operation, the shaft is supported using magnetic bearings and mechanical catcher bearings are provided in the event of magnetic bearing failure. The catcher bearings also support the shaft when the machine is not running. The use of magnetic bearings eliminates the possibility of lubricant ingress, reduces the required maintenance, and simplifies operation and control. The motor is submerged to prevent shaft penetration of the primary pressure boundary and is an integral part of the compressor rotor. Clean helium purge flow from the helium purification system at a pressure slightly higher than the primary coolant pressure is used to prevent contamination of the motor. When the circulator is operating, two cooling fans mounted on the shaft generate helium flow through the motor, around the magnetic bearing windings, and through a helium-to-water heat exchanger, where the heat from electrical and rotor windage losses is dissipated. The design includes two, 100% capacity cooling systems. The helium pressure is higher than the water pressure. If a leak occurs in one of the heat exchangers (detected by an increase in water pressure), the circuit is isolated and heat is rejected by the redundant heat exchanger.

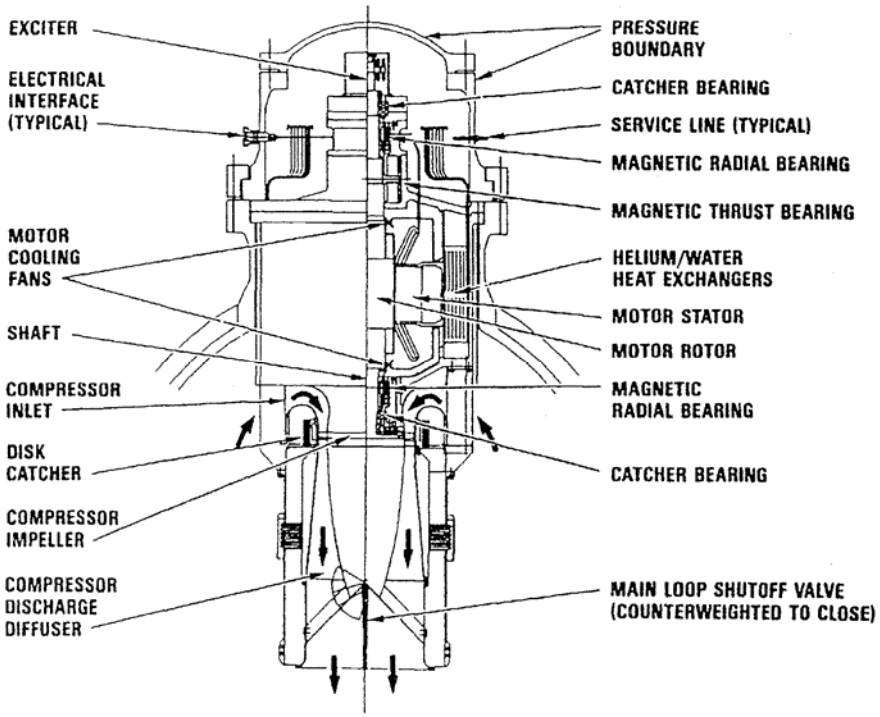

Figure 3-38. Primary Circulator Design Concept

3.2.2 Secondary Heat Transport System

The pre-conceptual design for the Secondary HTS was developed as part of a related NERI project sponsored by the DOE [Summers, 2006]. Key considerations for design of this system are (a) the heat transfer fluid, (b) the configuration and overall length of the piping system, (c) the system pressure drop and pumping requirements, (d) requirements for loop isolation. For the H2-MHR pre-conceptual design phase, pressurized helium was selected as the heat transfer fluid for the Secondary HTS. During the preliminary and final design phases, trade studies should be performed to evaluate alternative fluids (e.g., molten salts) for the Secondary HTS.

3.2.2.1 Piping Configuration

As shown in Fig. 3-39, both parallel and concentric piping configurations were evaluated. The concentric piping configuration is similar to the design of the cross vessel and hot duct assembly described in Section 3.1.2. Both configurations were designed according to the parameters and requirements given in Table 3-16. The allowable temperature drops on the hot and cold legs were set to 1°C in order to limit parasitic heat losses. [6] This design requirement was satisfied for both configurations by using ceramic insulating blankets.

A comparison of the two configurations is summarized in Table 3-17. In terms of overall performance, capital costs, and secondary coolant circulator requirements, the differences between the two configurations are small. For both configurations, the secondary coolant circulator is designed for a total secondary loop pressure drop of about 150 kPa, which is about 50% higher than that for the primary loop. The parallel-pipe configuration is a less complex design and is more amenable for interfacing with the secondary loop isolation valves (see Fig. 1-1). For these reasons, the parallel-pipe configuration has been selected as the baseline design for the H2-MHR Secondary HTS.

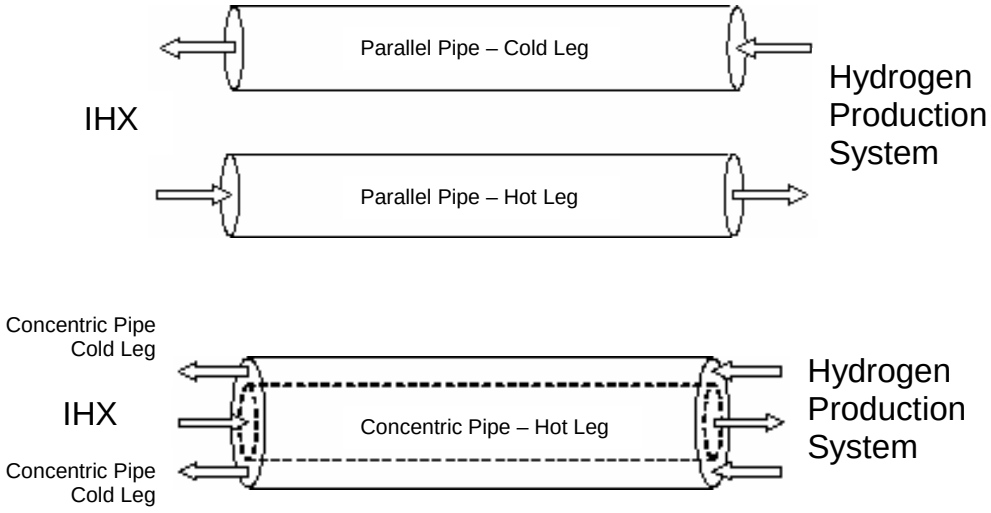

Figure 3-39. Parallel and Concentric Piping Concepts for Secondary HTS

[6] A 1°C temperature drop corresponds to a parasitic heat loss of 1.67 MW.

Table 3-16. Secondary Heat Transport System Design Parameters

Cold Leg Helium Temperature at IHX Inlet (°C)	565
Hot Leg Helium Temperature at IHX Outlet (°C)	925
Helium Flow Rate (kg/s)	321
Heat Transferred Through IHX (MW)	600
Helium Pressure at IHX Outlet (MPa)	7.07
Pressure Drop Associated with Hydrogen Production System (kPa)	100
Pressure Drop Associated with IHX (kPa)	30
Allowable Temperature Drop on Hot Leg from IHX to Hydrogen Production System (°C)	1
Allowable Temperature Drop on Cold Leg from Hydrogen Production System to IHX (°C)	1
Ambient Temperature (°C)	15
Pipe Length (m)	115

Table 3-17. Comparison of Parallel and Concentric Piping Configurations

Hot Leg Pipe/Duct	**Parallel Configuration**	**Concentric Configuration**
Material of Construction	Carbon Steel	High-Temperature Alloy
Operating Temperature (°C)	200	556
Pipe/Duct Inside Diameter (in.)	66	60
Pipe/Duct Wall Thickness (in.)	1.3	0.24
Inner Insulation Thickness (in.)	4.8	1.8
Outer Insulation Thickness (in.)	0.17	None
Pressure Drop (kPa)	11.1	11.0
Cold Leg Pipe		
Material of Construction	Carbon Steel	Carbon Steel
Operating Temperature (°C)	200	200
Pipe/Duct Inside Diameter (in.)	66	96
Pipe/Duct Wall Thickness (in.)	1.3	1.9
Inner Insulation Thickness (in.)	2.3	3.3
Outer Insulation Thickness (in.)	0.17	0.25
Pressure Drop (kPa)	5.2	6.6
Circulator Pumping Requirements		
Pressure Drop Associated with Piping (kPa)	16.3	17.6
Total Pressure Drop (kPa)	146.3	147.7
Required Pumping Power (MW)	11.6	11.7
Cost Assessment		
Piping Capital Cost ($M)	4.1	5.0
Circulator Capital Cost ($M)	17.2	17.3
Total Capital Cost ($M)	21.3	22.3

3.2.2.2 High-Temperature Isolation Valves

The Secondary HTS may require valves to isolate the Hydrogen Production Plant from the MHR System. Isolation valves on the hot leg would be exposed to helium with temperature in excess of 900°C, which requires a design that prevents thermal deformation of the valve seat at high temperatures. If isolation is a requirement, the high-temperature isolation valve (HTIV) design will based on the design being developed by the Japan Atomic Energy Agency (JAEA) for coupling the HTTR to an engineering-scale, SI-based hydrogen production plant [Ohashi, 2005]. This design concept is shown in Fig. 3-40 and consists of an angle valve with an inner thermal insulator (glass wool) and a flat valve seat. The valve body and seat are composed of Hastelloy-X and the valve seat is coated with a metal consisting of Stellite No. 6 with 30 wt. % Cr_3C_2. JAEA has performed tests on a scaled model of this HTIV concept. The measured helium leak rates at temperatures up to 900°C and differential pressures across the valve seat up to 4.1 MPa were less than 0.1 cm^3/s and well below the JAEA target value of 4.4 cm^3/s. However, the test also showed that durability of the valve seat may be an issue that requires further technology development. Another significant issue is scaling up the HTIV design for the large-diameter pipes that are required in order to use pressurized helium as the secondary coolant. These issues could have a significant impact on design of the Secondary HTS and should be included as part of trade studies performed during the conceptual, preliminary, and final design phases to evaluate alternative coolants for the secondary loop. In addition, detailed safety and investment risk assessments should be performed to determine if HTIVs are required for the H2-MHR design.

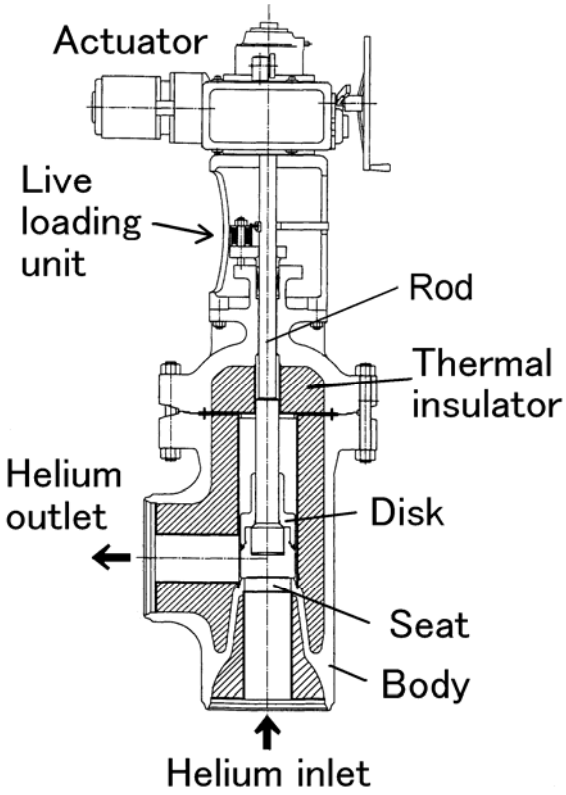

Figure 3-40. High-Temperature Isolation Valve Design Concept (figure courtesy of the Japan Atomic Energy Agency, Oarai, Japan)

3.2.3 Residual Heat Removal System

As shown in Fig. 1-2, the Residual Heat Removal System (RHRS) is installed as a parallel train on the Secondary HTS. The RHRS is sized to remove the same heat loads as the SCS; 40 MW(t) under pressurized conditions and 14.1 MW(t) under depressurized conditions. As is the case for the SCS, the residual heat removed by the RHRS is transferred to a cooling water system that rejects the heat to the atmosphere through an air-cooled heat exchanger. When the RHRS is operating, the secondary loop isolation valves on the hydrogen production side are shut. The RHRS is not a safety-related system. The design and physical location of the RHRS will be evaluated further during the conceptual, preliminary, and final design phases. Considerations include the physical space required for the system and the impact of the shutdown transient on IHX design and performance.

3.3 Helium Services Systems

Separate Helium Purification Systems (HPS) are provided for the primary and secondary coolants. These systems are used to maintain acceptable levels of chemical impurities and circulating radioactivity in the primary and secondary coolant systems. Each purification system interfaces with a Helium Transfer and Storage System.

3.3.1 Primary Coolant Helium Purification System

The Primary Coolant HPS processes a slipstream flow of the primary coolant to remove chemical and radioactive impurities (including tritium). The slipstream flow fraction is approximately 1% (or less) of the total primary coolant flow rate. The primary functions of the Primary Coolant HPS are:

- Remove chemical and radioactive impurities from the helium coolants.
- Pressurize, depressurize, and control the primary helium coolant inventory (in conjunction with Helium Transfer and Storage System).
- Provide purified helium for purges and buffers.
- Maintain the primary coolant system at slightly below atmospheric pressure during refueling/maintenance.
- Purify helium pumped to storage.

For the H2-MHR, another key function of the purification systems is to limit tritium and other radioactive contamination in the hydrogen product gas.

A helium purification train is provided for each reactor module and is located in the reactor building. The slipstream flow is extracted from the cold leg at the exit of the primary coolant circulator. Most of the purified helium is returned to the cold leg at the inlet of the primary coolant circulator. A portion of the purified helium is returned to other locations to purge vessel seals, shutdown circulator seals, and vessel relief piping. The purification train is shown in Fig.

3-41 and the components are described in Table 3-18. Spares are maintained for the helium compressors, filters, and adsorber beds in order to maintain high availability and reliability.

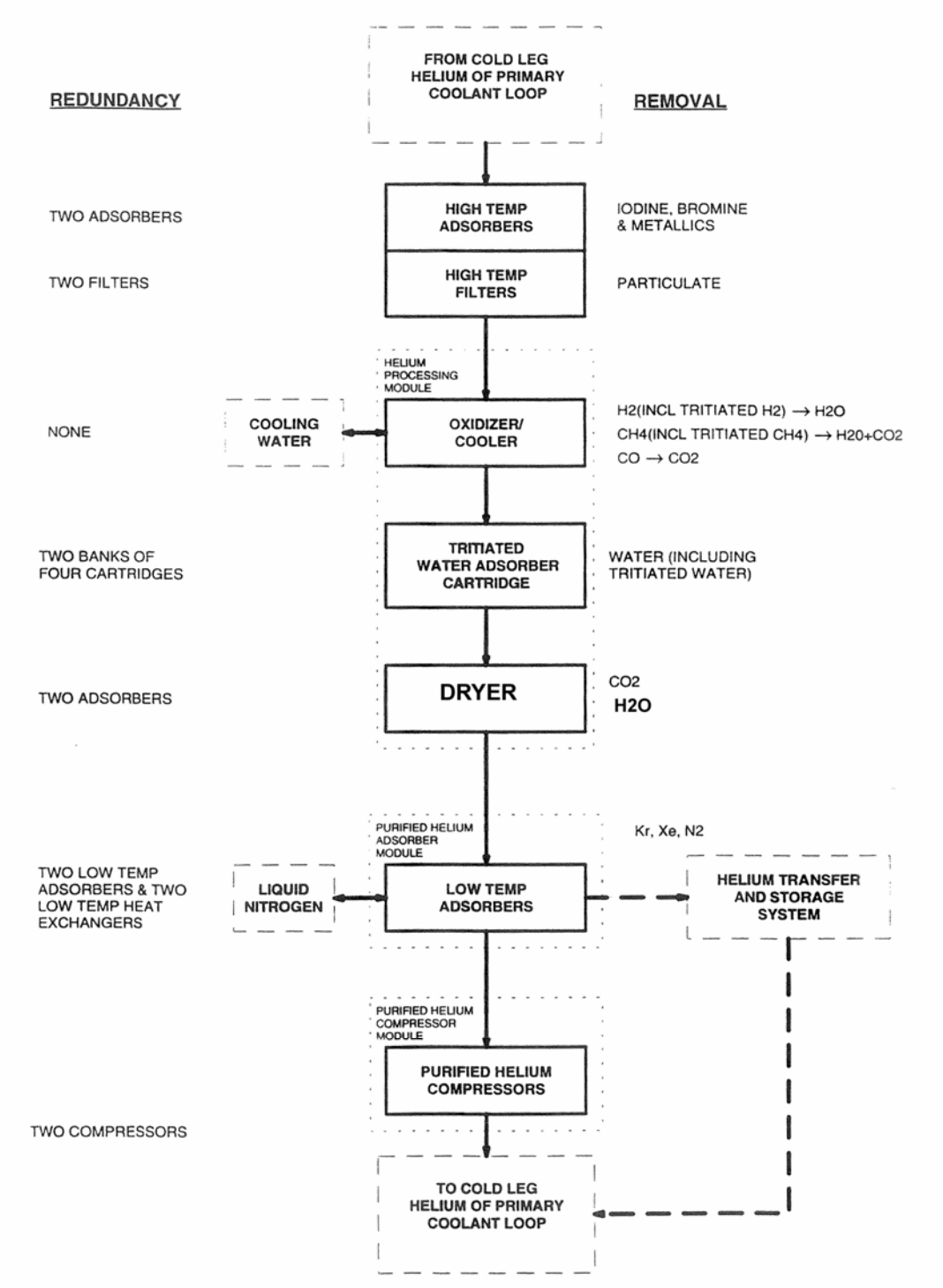

Figure 3-41. Helium Purification Train Block Diagram

Table 3-18. Primary Helium Purification System Description

Component	Function	Description
High Temperature Adsorber	Remove iodine, bromine, and metallic fission products.	Charcoal-filled cartridge within a flanged vessel
High Temperature Filter	Remove particulates	Filter cartridge housed within a flanged vessel. Filter specifications TBD.
Oxidizer	Oxidizes H_2 (including tritiated H_2) to H_2O. Oxidizes CH_4 to H_2O and CO_2. Oxidizes CO to CO_2.	Vessel filled with oxidizing agent (e.g., CuO). Continuous on-line analysis of the outlet gas determines whether oxidizing (O_2) or reducing (H_2) gases need to be added to the helium entering the vessel.
Cooler	Condense water vapor. Remove tritiated water.	Shell and tube heat exchanger with helium on the tube side and cooling water on the shell side. Drain tank with liquid level instrumentation is connected to the tube side. Water is pumped periodically from the drain tank to the Liquid Radioactive Waste System.
Dryer	Remove remaining H_2O (including tritiated H_2O) and CO_2.	Vessel filled with molecular sieve adsorbent.
Low Temperature Absorber	Remove noble-gas fission products (primarily Kr and Xe isotopes), N_2, and CH_4.	Charcoal-filled cylinder centrally positioned within a liquid nitrogen-filled shell. Counterflow of helium and low-pressure liquid nitrogen, with nitrogen vaporizing on the shell side. A downstream filter removes any charcoal debris resulting from erosion.
Compressor Module	Return the purified helium to the primary circuit.	Compressor, pulsation bottles to dampen flow oscillations, aftercooler to remove heat of compression (so that cool helium is available for purge applications), and appropriate valves, instrumentation, and controls.

3.3.2 Secondary Coolant Helium Purification System

The Secondary Helium Purification System is similar in design to the Primary Helium Purification System, except that the high and low temperature adsorbers are not required to remove fission products.

The slipstream flow fraction will be determined largely by the impurity specifications (including tritium) for the hydrogen product gas.

3.3.3 Helium Transfer and Storage Systems

Separate Helium Transfer and Storage Systems are provided for the primary and secondary coolants. The primary functions of these systems are given below:

- Provide storage capacity for helium during depressurizations for refueling and maintenance.
- Supply coolant system makeup helium during normal plant operation.
- Provide a source of high pressure helium for specific plant uses.
- Transfer and distribute helium among various plant users.
- Work in conjunction with the HPS to pressurize, depressurize, and control the primary and secondary coolant inventories.

As shown in Fig. 3-42, the Helium Transfer and Storage Systems consist of a high-pressure section and a low-pressure section. The high-pressure section supplies make-up helium to compensate for losses and helium for purge-flow requirements. The low-pressure section receives helium from the coolant system for inventory control. The system is equipped with compressors to transfer helium between the high- and low-pressure sections.

3.3.4 Tritium Control

A key requirement for the H2-MHR is to produce hydrogen gas that meets customer requirements for product quality. Tritium is produced in limited quantities in the MHR and it has the potential to migrate through the heat-transfer surfaces of the IHX and the high-temperature heat exchangers in the hydrogen production system. Sources of tritium include:

- Ternary fission (fission yield is ~10^{-4}).
- Neutron activation of He-3 (He-3 abundance is ~2×10^{-7}).
- Neutron reactions with trace levels of lithium present in graphite and fuel compact matrix material.
- Neutron reactions with B-10 present in control rods and burnable poison.

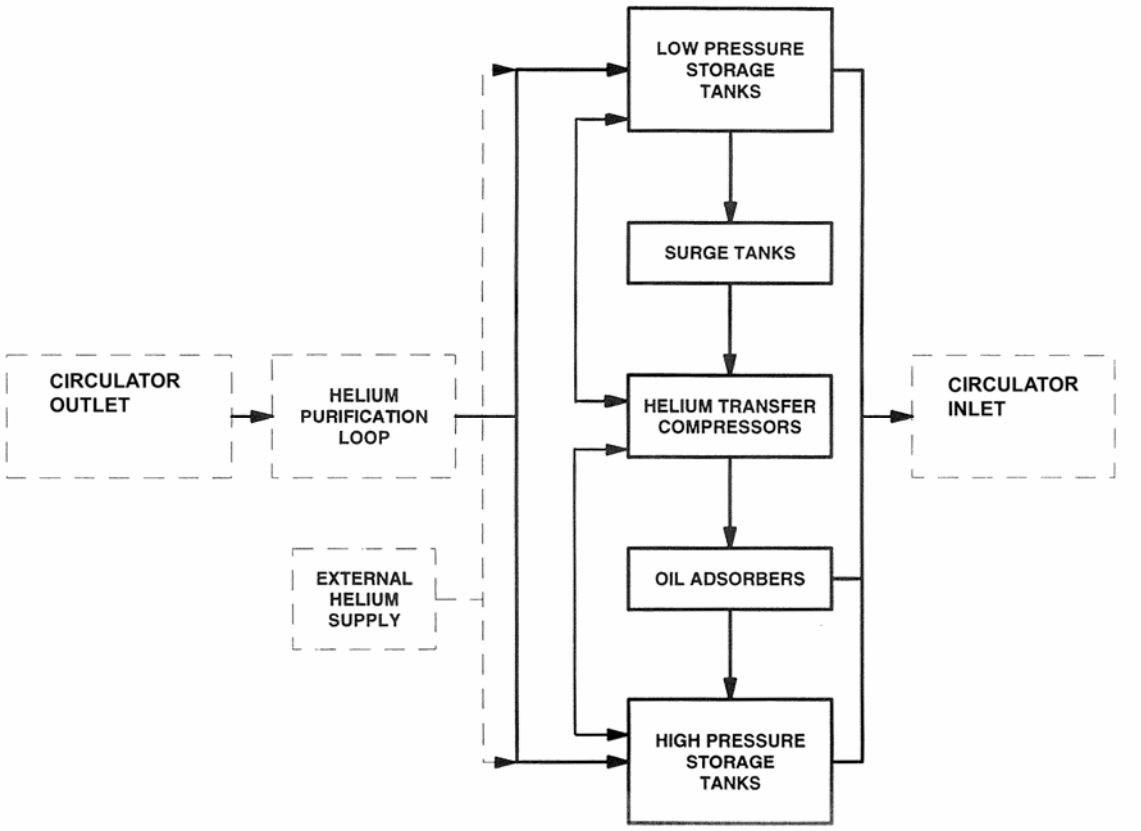

Figure 3-42. Helium Transfer and Storage System Block Diagram

Ternary fission typically contributes to about 60% of the total tritium source term. At sufficiently low temperatures, this source of tritium is retained effectively by the TRISO coating system. However, the H2-MHR core will include regions that operate at temperatures greater than 1000°C for significant periods of time. Figure 3-43 shows the expected fractional tritium release from TRISO-coated fuel particles as a function of time at temperature. If fuel is maintained at 1300°C for 100 days, the fractional tritium release is expected to be about 0.2. Activation of He-3 and neutron reactions with lithium and boron each contribute to about 20% of the total tritium source term.

The tritium concentration in the primary coolant is determined by a balance between production and removal. Removal mechanisms include radioactive decay, slipstream coolant purification (a titanium sponge or a CuO oxidation bed is typically used to remove tritium), and sorption onto graphite. A previous assessment of tritium behavior in the Fort St. Vrain reactor indicated that at high temperatures, the core graphite was very effective at removing tritium from the primary coolant. Figure 3-44 shows measured tritium concentrations in the Fort St. Vrain primary coolant. When the reactor was at full power, tritium concentrations generally remained below about 10^{-5} $\mu Ci/cm^3$.

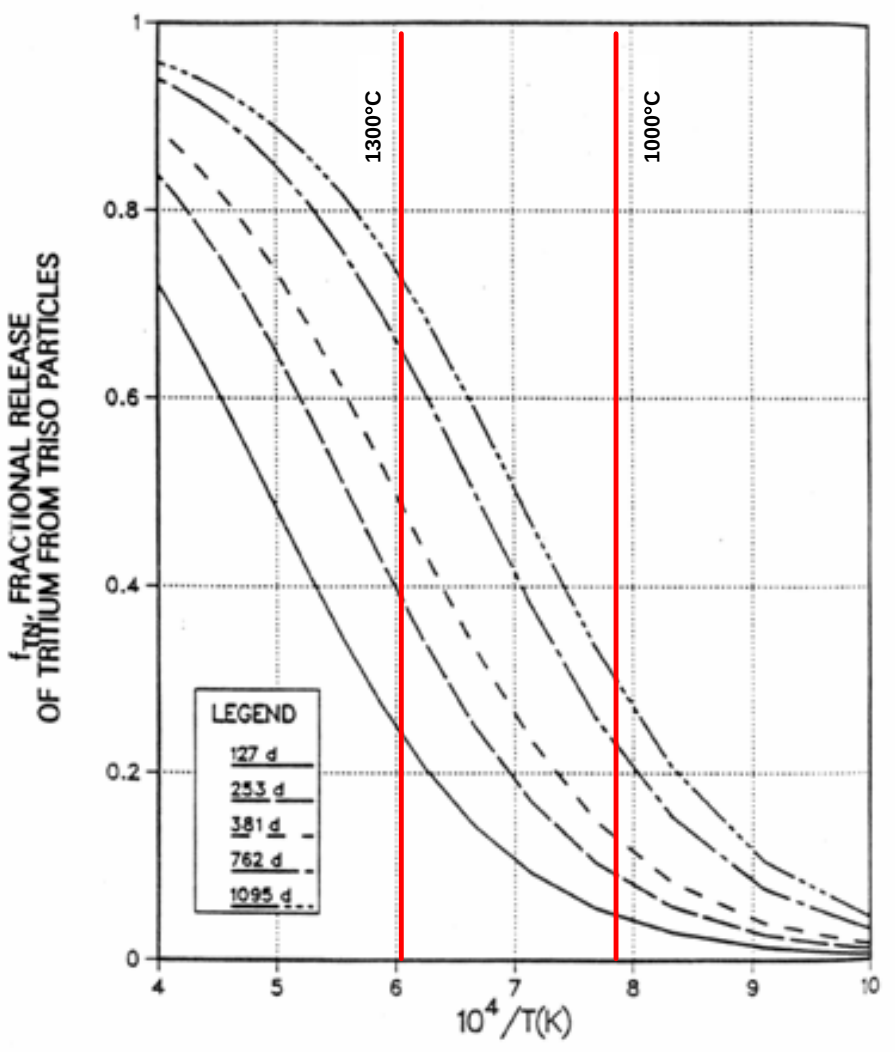

Figure 3-43. Tritium Release from TRISO-Coated Fuel Particles

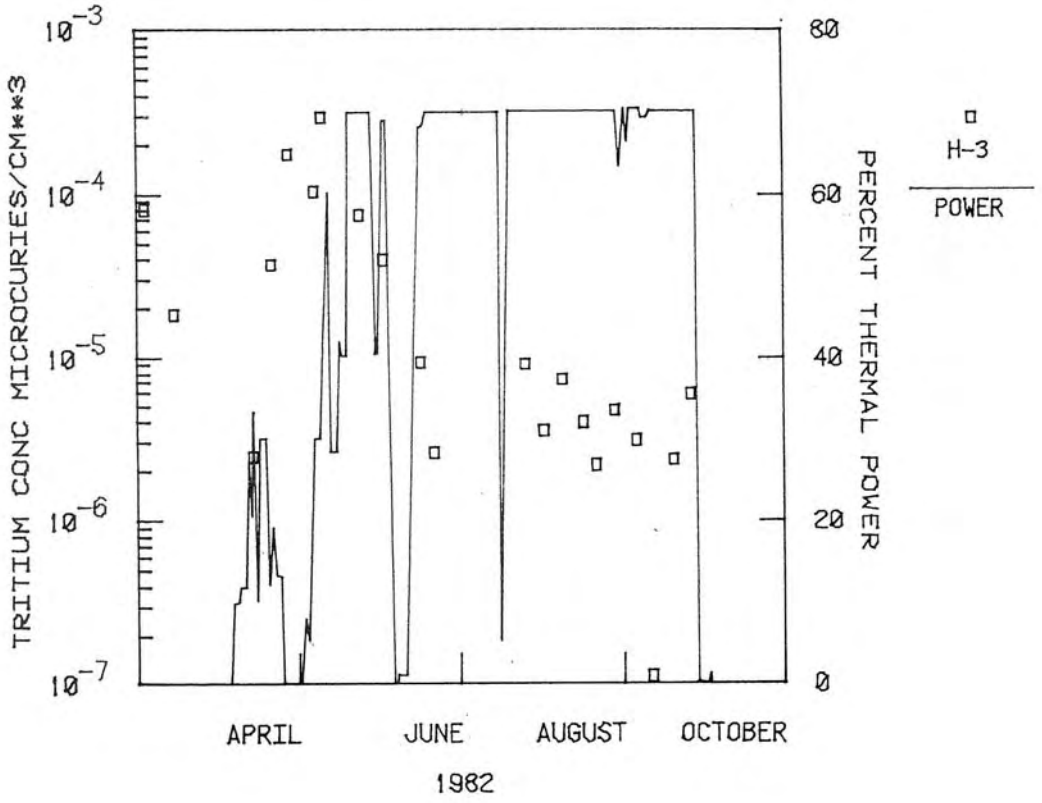

Figure 3-44. Measured Tritium Concentration in Fort St. Vrain Primary Coolant

Figure 3-45 shows conceptually how the tritium migrates through the Hydrogen Production System to the product gas. In order to asses the potential for tritium contamination in the hydrogen product gas, an assessment of tritium permeation through a Heatric-type IHX was performed. A semi-empirical correlation for Incoloy 800 was used to estimate the tritium flux from the primary-side helium to the secondary-side helium:

$$Flux = 61.02\ C_t \sqrt{P / C_{H_2}}\ \frac{\exp(-6250/T)}{t} \qquad (\mu Ci/m^2 - h),$$

where $C_t \equiv$ tritium concentration in the primary coolant, referenced to standard temperature and pressure ($\mu Ci/m^3$), $P \equiv$ total primary-side pressure (atm), $C_{H_2} \equiv$ hydrogen impurity concentration in the primary coolant (ppmv), T = IHX wall temperature (K), and t = IHX wall thickness (mm). The IHX design parameters were obtained from Table 3-14. The hydrogen impurity concentration was conservatively assumed to be at its lowest expected level of 0.2 ppmv. The IHX wall temperature was assumed to vary linearly from the primary coolant inlet value (950°C) to the outlet value (590°C). Based on the data shown on Fig. 3-44, the quantity C_t was assumed to be 10 $\mu Ci/m^3$. Using these assumptions, the tritium permeation rate to the secondary side was calculated to be approximately 40 $\mu Ci/s$. If the tritium is assumed to be in

the form HT, the mass permeation rate is approximately 5.5×10^{-12} kg/s. Assuming a helium purification flow fraction of 0.5% on the secondary loop, the tritium concentration in the secondary coolant is reduced to about 5×10^{-6} μCi/cm^3 at atmospheric pressure. Assuming the heat exchanger walls in the hydrogen production plant provide the same resistance as those of the IHX, the HT mass permeation rate to the product gas is reduced to 2.75×10^{-18} kg/s. For a hydrogen production rate of 3.5 kg/s, the HT concentration in the product gas is about 8×10^{-13} ppmw, which corresponds to about 1×10^{-12} μCi/cm^3 at standard temperature and pressure. This concentration is five orders of magnitude below the limit specified in 10CFR20 for the maximum allowable tritium concentration in an uncontrolled area.

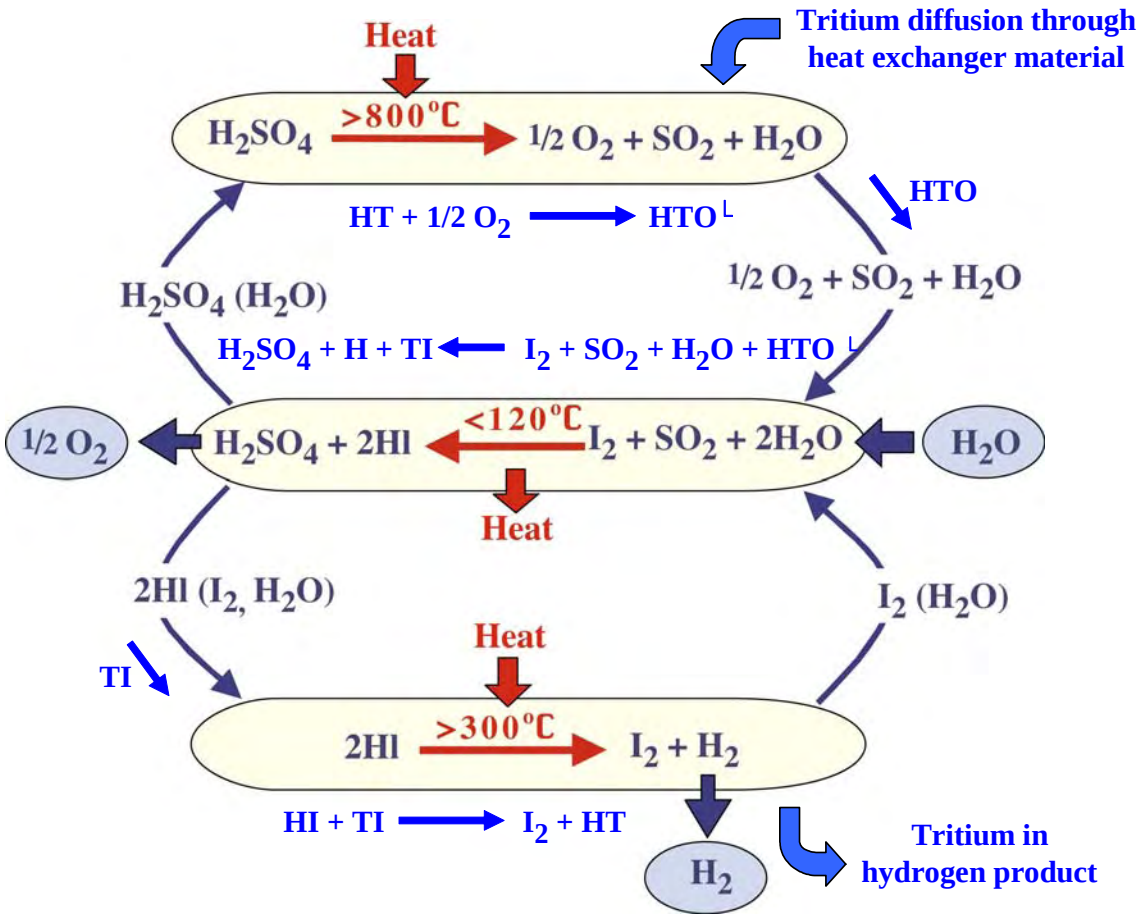

Figure 3-45. Tritium Migration Pathways in the SI Cycle

Based on this assessment, it should be possible to control tritium concentrations in the product gas to acceptable levels. More detailed assessments of tritium source terms, product gas contamination, and tritium release to the environment should be performed during the preliminary and final design stages. International standards should also be developed for hydrogen product gas produced using nuclear energy.

3.4 Hydrogen Production System

The Hydrogen Production System design is based on the design described in [Brown, 2003]. The current design reflects optimization of the flowsheets to increase the hydrogen production rate and improve efficiency.

3.4.1 Sulfur-Iodine Process Description

The S-I thermochemical cycle consists of three chemical reactions that result in dissociation of water into hydrogen at oxygen;

Bunsen Reaction: $I_2 + SO_2 + 2H_2O \rightarrow 2HI + H_2SO_4$ **(T ~ 120°C)**

H_2SO_4 Decomposition: $H_2SO_4 \rightarrow SO_2 + H_2O + {}^1/_2O_2$ **(T > 800°C)**

HI Decomposition: $2HI \rightarrow I_2 + H_2$ **(T > 350°C)**

$H_2O \rightarrow H_2 + {}^1/_2O_2$

All three reactions are all operated under conditions of chemical equilibrium. Energy inputs to the process are heat to the endothermic H_2SO_4 and HI decomposition reactions and electrical energy required for pumping process fluids. Heat at about 120°C is rejected from the exothermic Bunsen reaction. With the exception of water, all reactants are regenerated and recycled.

The Hydrogen Production System design is organized into subsystems according to these three chemical reactions. These subsystems are referred to as Sections 1, 2, and 3. Section 1 (Bunsen reaction) includes all the process equipment associated with production of the aqueous sulfuric acid phase and the $HI/I_2/H_2O$ phase. Section 1 also includes equipment to purify the oxygen before release. Section 2 concentrates the aqueous sulfuric acid phase and then decomposes the concentrated acid. The decomposition products and the water removed from concentrating the acid are returned to Section 1. Section 3 concentrates and decomposes hydrogen iodide. Section 3 also includes equipment to purify the product hydrogen gas.

The flowsheets for Sections 2 and 3 have been analyzed and optimized using AspenPlus process-simulation software.[7] Because there are still very limited thermophysical property data for the $HI/I_2/H_2O$ vapor equilibrium, the equilibrium conditions for Section 1 are based on previous calculations [Norman, 1982]. Approximately two-thirds of the fresh water required for hydrogen production is supplied to Section 3 and the remainder is supplied to Section 1. The product hydrogen gas is produced at a pressure of 4.0 MPa.

3.4.1.1 Section 1 (Bunsen Reaction)

The flowsheet for Section 1 is shown in Fig. 3-46 and Table 3-19 provides a description of the Section 1 process streams.[8] This flowsheet is essentially the same as that described in [Brown,

[7] A description of the AspenPlus software is available at http://www.aspentech.com/brochures/aspenplus.pdf.

[8] The stream flow rates correspond to process heat being supplied from a single, 600 MW(t) MHR module.

2003] and is based on experimental data obtained in the 1980s. A key component in Section 1 is the flow reactor R101, which functions as a heat exchanger. Because the kinetics of the Bunsen reaction are very fast, the rate of heat transfer controls the reaction rate. The mixture exiting R101 consists of three immiscible phases, of which two are liquid and one is gas. These phases are separated in component S101. Each of these phases then follows a different path through the other components. The lower phase, which consists of $HI/I_2/H_2O$ in the approximate molar ratios 2/8/10, is stripped of dissolved SO_2 and H_2SO_4 in the packed column C102. Prior to stripping, the pressure is first lowered in order to use a recycle O_2 stream as the stripping agent. The SO_2 is directly stripped by the O_2 stream. As the SO_2 is depleted, the reaction equilibrium shifts to produce more SO_2 from H_2SO_4 reacting with HI, which results in simultaneous removal of SO_2 and H_2SO_4. The stripped lower phase exits C102 and is transferred to Section 3, where it is processed to produce the hydrogen product gas. The upper phase exiting S101 (aqueous H_2SO_4) is transferred to boost reactor C103, which is also a packed column. A portion of the upper phase exiting C102 (O_2 and SO_2) is also transferred to C103. In this column, the sulfuric acid is concentrated by contacting it with I_2 and SO_2. The molar ratio of H_2SO_4 to H_2O entering C103 is about 1/6 and is increased to about 1/4 at the exit of C103.

The remaining equipment in Section 1 is associated with processing the O_2 stream. The SO_2 is scrubbed from the O_2 stream in packed column C101. A small amount of iodine is added to C101 in order to minimize the amount of water required to remove SO_2 via the Bunsen reaction. The water streams to C101 are supplied from Section 2 and are cooled prior to entering C101 in order to remove the heat of reaction and minimize the amount of heat that is removed by R103. The SO_2 remaining in the upper phase that exits boost reactor C103 is scrubbed from the oxygen in packed column C104. Because all of the SO_2 exiting C102 can not be used in boost reactor C103, a portion of this stream is transferred to packed column C105 to scrub the SO_2 from the oxygen. This SO_2 is then transferred to R101. Energy recovery turbines are used to recover the work available from the compressed gasses and to provide the O_2 stripping gas at an appropriate pressure.

Because the design point at the outlet of component R101 is essentially fixed in terms of temperature, compositions of both liquid phases, and the partial pressure of SO_2, the only free variable is the system pressure. The system pressure must be below the operating pressure of Section 2 so that the gases can flow from Section 2 without compression. The pressure must also be sufficiently high for efficient operation of the SO_2 stripping column. Operating R101 at higher pressures does provide the benefit of a lower SO_2 to O_2 ratio at the exit of this reactor, which leaves less SO_2 to be removed in the first oxygen scrubber (C101). The operating pressure for R101 has been set at 0.7 MPa.

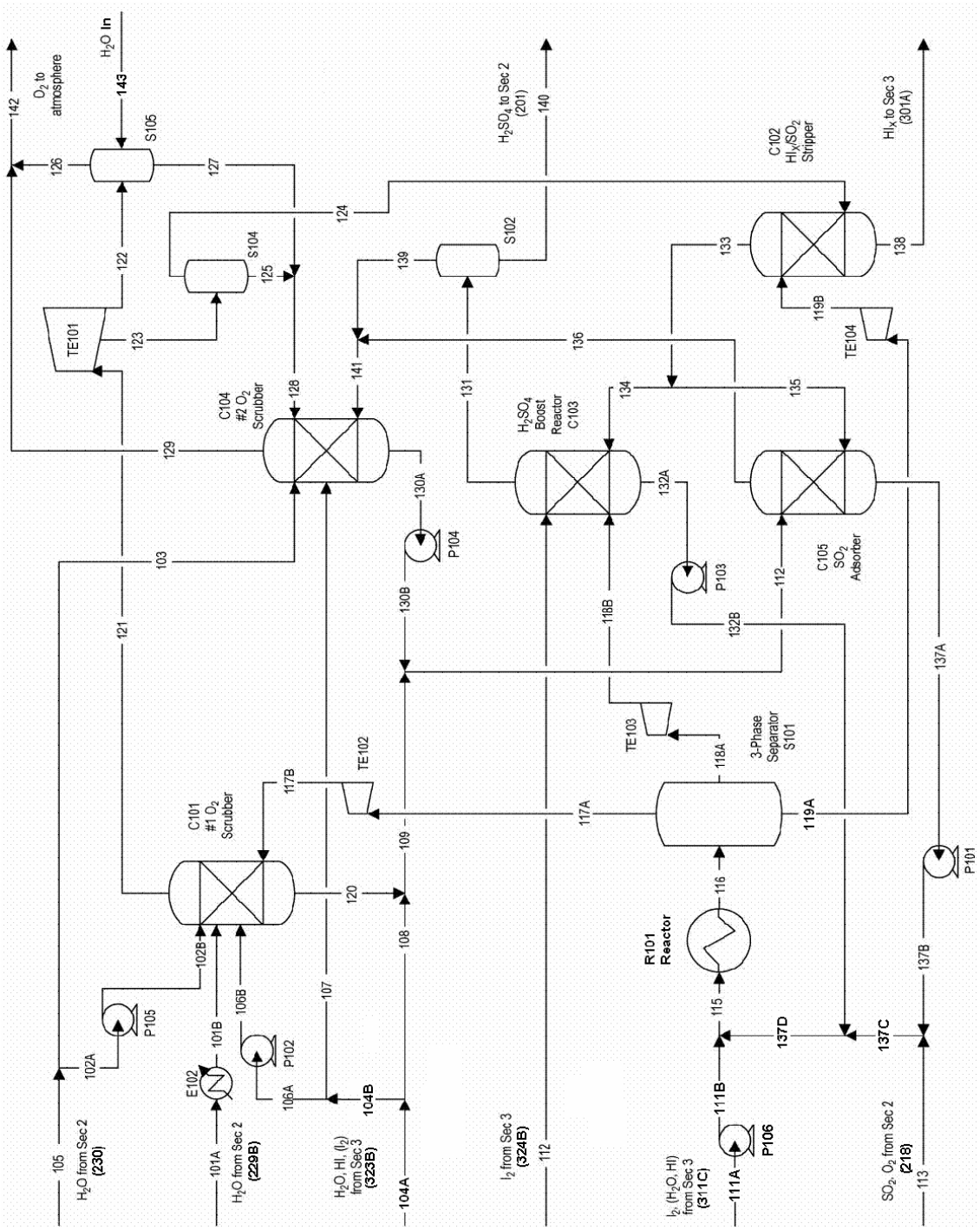

Figure 3-46. SI Process Section 1 Flowsheet

Table 3-19. SI Process Section 1 Flow Stream Description

Stream ID	Stream Flow Rates (moles/s)							Phase	Pressure (Bar)	Temp. (°C)
	H_2SO_4	HI	I_2	H_2O	SO_2	O_2	Total			
101A	8.05E+00	0.00E+00	0.00E+00	6.01E+03	1.61E+00	0.00E+00	6.02E+03	L	12.00	40.6
101B	8.05E+00	0.00E+00	0.00E+00	6.01E+03	1.61E+00	0.00E+00	6.02E+03	L	12.00	86.5
102A	1.13E+02	0.00E+00	0.00E+00	4.42E+02	2.01E+02	1.61E+00	7.58E+02	L	1.01	38.0
102B	1.13E+02	0.00E+00	0.00E+00	4.42E+02	2.01E+02	1.61E+00	7.58E+02	L	4.40	38.0
103	1.61E+00	0.00E+00	0.00E+00	2.07E+03	0.00E+00	0.00E+00	2.07E+03	L	1.01	38.0
104A	0.00E+00	6.58E+01	1.40E+02	6.39E+03	0.00E+00	0.00E+00	6.60E+03	L	7.00	120.4
104B	0.00E+00	1.32E+02	8.09E+01	1.04E+03	0.00E+00	0.00E+00	1.25E+03	L	7.00	120.4
105	1.14E+02	0.00E+00	0.00E+00	2.51E+03	2.01E+02	1.61E+00	2.83E+03	L	L	-272.1
106A	0.00E+00	1.98E+00	4.19E+00	1.92E+02	0.00E+00	0.00E+00	1.98E+02	L	7.00	120.4
106B	0.00E+00	1.98E+00	4.19E+00	1.92E+02	0.00E+00	0.00E+00	1.98E+02	L	12.00	120.4
107	0.00E+00	1.30E+02	7.67E+01	8.44E+02	0.00E+00	0.00E+00	1.05E+03	L	1.01	95.4
108	0.00E+00	0.00E+00	5.86E+01	5.35E+03	0.00E+00	0.00E+00	5.41E+03	L	4.20	95.4
109	2.25E+02	1.98E+00	7.49E+01	6.46E+03	6.32E+02	3.22E+00	7.40E+03	L	1.85	119.9
111A	0.00E+00	3.39E+03	2.40E+04	3.00E+04	0.00E+00	0.00E+00	5.74E+04	L	7.00	118.8
111B	0.00E+00	3.39E+03	2.40E+04	3.00E+04	0.00E+00	0.00E+00	5.74E+04	L	12.00	119.9
112	0.00E+00	3.87E-01	3.33E+03	6.71E+01	0.00E+00	0.00E+00	3.40E+03	L	7.00	115.6
113	0.00E+00	0.00E+00	0.00E+00	2.42E+01	1.41E+03	8.04E+02	2.24E+03	V	7.00	40.1
115	3.50E+02	1.77E+04	7.85E+04	1.17E+05	3.65E+03	8.05E+02	2.18E+05	V+L	7.00	115.6
116	1.54E+03	2.00E+04	7.73E+04	1.15E+05	2.46E+03	8.05E+02	2.17E+05	V+L	7.00	119.9
117A	0.00E+00	0.00E+00	1.21E+01	5.44E+01	2.29E+02	8.05E+02	1.10E+03	V	7.00	119.9
117B	0.00E+00	0.00E+00	1.21E+01	5.44E+01	2.29E+02	8.05E+02	1.10E+03	V	4.20	81.1
118A	1.54E+03	0.00E+00	0.00E+00	8.29E+03	2.48E+01	0.00E+00	9.85E+03	L	7.00	119.9
118B	1.54E+03	0.00E+00	0.00E+00	8.29E+03	2.48E+01	0.00E+00	9.85E+03	L	1.85	119.9
119A	0.00E+00	2.00E+04	7.73E+04	1.06E+05	2.21E+03	0.00E+00	2.06E+05	L	7.00	119.9
119B	0.00E+00	2.00E+04	7.73E+04	1.06E+05	2.21E+03	0.00E+00	2.06E+05	L	1.85	119.9
120	2.25E+02	1.98E+00	1.63E+01	1.11E+03	6.32E+02	3.22E+00	1.98E+03	L	4.20	111.3
121	0.00E+00	0.00E+00	0.00E+00	2.41E+01	0.00E+00	8.05E+02	8.29E+02	V	4.20	111.3
122	0.00E+00	0.00E+00	0.00E+00	1.53E+01	0.00E+00	5.11E+02	5.26E+02	L+V	1.01	111.3
123	0.00E+00	0.00E+00	0.00E+00	8.85E+00	0.00E+00	2.94E+02	3.02E+02	L+V	1.85	15.9
124	0.00E+00	0.00E+00	0.00E+00	4.34E+00	0.00E+00	2.94E+02	2.98E+02	V	1.85	15.9
125	0.00E+00	0.00E+00	0.00E+00	4.51E+00	0.00E+00	0.00E+00	4.51E+00	L	1.85	15.9
126	0.00E+00	0.00E+00	0.00E+00	8.21E+00	0.00E+00	5.11E+02	5.19E+02	V	1.01	15.9
127	0.00E+00	0.00E+00	0.00E+00	7.08E+00	0.00E+00	0.00E+00	7.08E+00	L	1.01	15.9
128	0.00E+00	0.00E+00	0.00E+00	1.16E+01	0.00E+00	0.00E+00	1.16E+01	L	1.01	15.9
129	0.00E+00	0.00E+00	0.00E+00	2.28E+01	0.00E+00	2.94E+02	3.16E+02	V	1.01	39.9
130A	7.19E+01	2.70E+02	3.65E+01	2.89E+03	0.00E+00	0.00E+00	3.27E+03	L	1.01	119.9
130B	7.19E+01	2.70E+02	3.65E+01	2.89E+03	0.00E+00	0.00E+00	3.27E+03	L	1.85	119.9
131	1.65E+03	0.00E+00	2.96E+01	6.66E+03	7.64E+01	2.49E+01	8.44E+03	L	1.85	111.4
132A	0.00E+00	2.23E+02	1.28E+03	1.49E+03	2.49E+01	0.00E+00	3.02E+03	L	1.85	111.4
132B	0.00E+00	2.23E+02	1.28E+03	1.49E+03	2.49E+01	0.00E+00	3.02E+03	L	7.00	111.4
133	0.00E+00	0.00E+00	4.36E+01	6.00E+02	2.21E+03	2.94E+02	3.14E+03	V	1.85	119.9
134	0.00E+00	0.00E+00	3.70E+00	5.10E+01	1.87E+02	2.49E+01	2.67E+02	V	1.85	119.9
135	0.00E+00	0.00E+00	3.99E+01	5.49E+02	2.02E+03	2.69E+02	2.88E+03	V	1.85	119.9
136	0.00E+00	0.00E+00	4.83E-01	5.79E+01	1.61E-01	2.69E+02	3.27E+02	V	1.85	96.5
137A	3.50E+02	1.61E+04	8.92E+03	1.09E+05	2.02E+03	0.00E+00	1.36E+05	L	1.85	96.5
137B	3.50E+02	1.61E+04	8.92E+03	1.09E+05	2.02E+03	0.00E+00	1.36E+05	L	7.00	96.5
137C	0.00E+00	2.00E+04	7.72E+04	1.06E+05	0.00E+00	0.00E+00	2.03E+05	L	1.85	119.9
137D	0.00E+00	0.00E+00	2.96E+01	6.98E+01	7.02E+01	2.49E+01	1.95E+02	V	1.85	111.4
140	1.65E+03	0.00E+00	0.00E+00	6.59E+03	6.28E+00	0.00E+00	8.24E+03	L	1.85	111.4
141	0.00E+00	0.00E+00	3.01E+01	1.28E+02	7.03E+01	2.94E+02	5.22E+02	V	1.85	102.0
142	0.00E+00	0.00E+00	0.00E+00	3.11E+01	0.00E+00	8.05E+02	8.36E+02	V	1.01	24.9
143	0.00E+00	0.00E+00	0.00E+00	5.88E+02	0.00E+00	0.00E+00	5.88E+02	L	1.01	24.9

3.4.1.2 Section 2 (Sulfuric Acid Decomposition)

The flowsheet for Section 2 is shown in Fig. 3-47 and Table 3-20 provides a description of the Section 2 process streams. Section 2 concentrates and decomposes the aqueous sulfuric acid phase that is transferred from Section 1. All of the heat from the Secondary HTS is transferred to Section 2. As discussed in Section 3.2, the sulfuric acid vaporizers and decomposers are operated at a pressure slightly lower than that of the secondary helium coolant in order to prevent chemical contamination of the Secondary HTS while minimizing pressure differentials across these components. For the current flowsheet, the sulfuric acid decomposers are assumed to operate at 7.05 MPa.

The Section 2 flowsheet previously incorporated a direct contact heat/mass transfer unit. In this unit the concentrated acid is counter-currently contacted with the exiting decomposition products. Undecomposed SO_3 in the gas phase is adsorbed into the liquid stream. The heat of SO_3 in the solution vaporizes additional water, which further concentrates the acid and improves the efficiency of the process. However, when sulfuric acid decomposition is performed at pressures above about 1.8 MPa, the direct contact heat/mass transfer unit is no longer very effective at its secondary function of adsorbing SO_3 and vaporizing water. At high pressures all the SO_3 condenses with water to form sulfuric acid prior to the contactor and water in the SO_2/O_2 stream is adsorbed in the acid and recycled back into the decomposer. For these reasons, the direct contact unit was replaced with a counter-current heat exchanger (component H206).

The H_2SO_4/H_2O stream from Section 1 (201) is concentrated in three successive vacuum flashes. The first flash (S201) is adiabatic but heat is added in the other two flashes. The first flash cools the stream significantly below the temperatures of Section 1 so that heat released in R103 can be used to evaporate water in the second flash (S202) of Section 2. The third vacuum flash (S203) uses heat recovered from Section 3. The vapors from the three flashes are cooled and the condensate returned to Section 1 (229B), as are the condensed vapors from the vacuum pump (228B). The concentrated acid is pumped from vacuum conditions to the pressure of the decomposition subsection using P201 and passed to the counter-current vapor-liquid recuperator (H206).

The hot liquid from the recuperator is heated and vaporized in three stages. The first two evaporators (H207 and H208A) are flow-through evaporators, with the stream progressively vaporized as it passes through the counter current heat exchangers. The condensate from the decomposer product is added between the first and second vaporizers. Any minerals that enter with the deionized water feed to the process and any mobile corrosion products from the entire system will eventually be deposited in the sulfuric acid decomposition process. If the final evaporation occurred while the stream was flowing through tubes, the minerals and corrosion products could deposit on the heat transfer surfaces and contribute to fouling or even plugging. For this reason, the third vaporizer (H208B) is a pool-type unit.

The sulfuric acid vapors are decomposed in two steps;

$$\mathbf{H_2SO_4 \leftrightarrow SO_3 + H_2O \quad (T > 450°C)}$$

$$\mathbf{SO_3 \rightarrow SO_2 + {}^1/_2O_2 \quad (T > 800°C)}$$

The first reaction is very fast and equilibrium is maintained, shifting to more complete decomposition as the temperature is raised or as SO_3 is removed by the second reaction. The first reaction begins to occur in the final vaporizer (H208B), but most of the vaporization occurs primarily in H209, which is a standard counter-current heat exchanger.

The second reaction requires a catalyst. The catalytic reaction occurs in two decomposers (H210A and H210B). Conceptually the decomposers are counter-current heat exchangers with catalyst on the heat transfer surfaces. The differences between the two decomposers are in how they are heated. H210B is heated with helium from the Secondary HTS (HE1). Decomposer H210A, which operates at slightly lower temperatures, is heated with both secondary helium (HE2) and the decomposer product (213A). In addition, both helium and decomposer product are used in parallel to heat the gas-gas recuperator (H209) and vaporizers 2 and 3 (H208A and H208B). Only the decomposer product is used to heat the first vaporizer (H207). Finally, the decomposer is used to provide the heat requirements for Section 3 (H213A). Some condensation occurs in this final heat exchanger. The product gases (215A) are separated (S207) from the condensate and pass to the gas-liquid recuperator (H206). The condensate (214) is recycled to the second vaporizer (H208A). The condenser (H213A) and separator (S207) are physically located above the vaporizers (H208A and H208B) such that the gravitational head exceeds the pressure drop through the decomposition system, which eliminates the need for a pump capable of operating at these extreme conditions.

The two-phase product from the decomposition system (215B) is separated and power is recovered separately from the two phases. Each phase is cooled to as low a temperature as practical before they are transferred to Section 1. Condensate from the cooling process is transferred separately to Section 1.

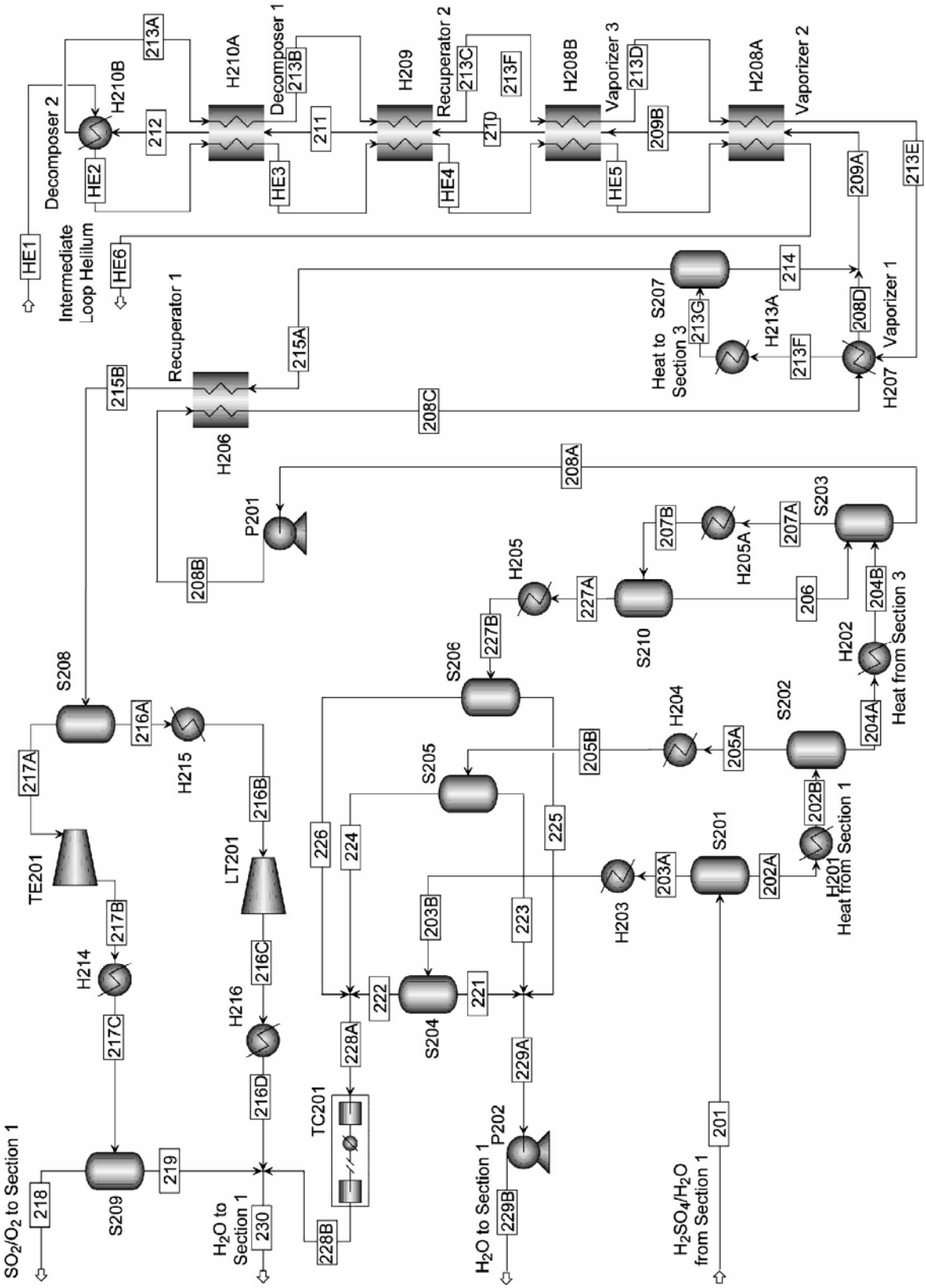

Figure 3-47. SI Process Section 2 Flowsheet

Table 3-20. SI Process Section 2 Flow Stream Description

Stream	Stream Flow Rates (moles/s)						Phase	Pressure (bar)	Temp. (°C)
	H_2O	H_2SO_4	SO_3	SO_2	O_2	Total			
201	6931.57	1732.89	0	6.44	0	8670.9	L	1.85	111.8
202A	6921.92	1732.89	0	1.61	0	8656.42	L	0.1	66.4
202B	6921.92	1732.89	0	1.61	0	8656.42	V+L	0.1	110
203A	9.65	0	0	4.83	0	14.48	V	0.1	66.4
203B	9.65	0	0	4.83	0	14.48	V	0.1	40
204A	3292.01	1732.89	0	0	0	5024.9	L	0.1	110
204B	3292.01	1732.89	0	0	0	5024.9	V+L	0.1	194.2
205A	3629.9	0	0	1.61	0	3631.51	V	0.1	110
205B	3629.9	0	0	1.61	0	3631.51	L	0.1	40
206	350.76	320.19	0	0	0	670.95	L	0.1	160
207A	2730.47	329.85	0	0	0	3060.32	V	0.1	189.9
207B	2730.47	329.85	0	0	0	3060.32	V+L	0.1	160
208A	912.3	1723.24	0	0	0	2635.54	L	0.1	189.9
208C	912.3	1723.24	0	0	0	2635.54	L	70.5	376.9
208D	912.3	1723.24	0	0	0	2635.54	L	70.5	401.9
209A	2278.34	3037.79	0	0	0	5316.13	L	70.5	403
209B	2921.94	2394.19	643.6	0	0	5959.73	V+L	70.5	563.9
210	4141.57	1174.57	1863.22	0	0	7179.36	V	70.5	626.9
213A	5256.6	61.14	1369.26	1609	804.5	9100.5	V	70.5	900
213G	3890.56	1427.18	3.22	1609	804.5	7734.46	V+L	70.5	401.9
214	1366.04	1314.55	0	0	0	2680.59	L	70.5	401.9
215A	2524.52	111.02	3.22	1609	804.5	5052.26	V	70.5	401.9
215B	2521.3	114.24	0	1609	804.5	5049.04	V+L	70.5	250.9
216A	806.11	114.24	0	85.28	1.61	1007.24	L	70.5	252.6
216B	806.11	114.24	0	85.28	1.61	1007.24	L	70.5	120
216C	806.11	114.24	0	85.28	1.61	1007.24	L	2	118.9
216D	806.11	114.24	0	85.28	1.61	1007.24	V+L	2	40
217A	1715.19	0	0	1523.72	802.89	4041.8	V	70.5	252.6
217B	1715.19	0	0	1523.72	802.89	4041.8	V+L	7	128.3
217C	1715.19	0	0	1523.72	802.89	4041.8	V+L	7	40
218	24.14	0	0	1411.09	802.89	2238.12	V	7	40
219	1691.06	0	0	111.02	0	1802.08	L	7	40
221	0	0	0	0	0	0	L	0.1	40
222	9.65	0	0	4.83	0	14.48	V	0.1	40
223	3628.3	0	0	1.61	0	3629.91	L	0.1	39.6
224	1.61	0	0	0	0	1.61	V	0.1	39.6
225	2379.71	8.05	0	0	0	2387.76	L	0.1	40
226	0	0	0	0	0	0	V+L	0.1	40
227A	2379.71	8.05	0	0	0	2387.76	V	0.1	160
227B	2379.71	8.05	0	0	0	2387.76	L	0.1	40
228A	9.65	0	0	4.83	0	14.48	V	0.1	40
228B	9.65	0	0	4.83	0	14.48	V+L	7	120
229	6008.01	8.05	0	1.61	0	6017.67	L	12	40.5
HE1	0	0	0	0	0	0	V	70.6	924
HE6	0	0	0	0	0	0	V	69.6	557.5

3.4.1.3 Section 3 (Hydrogen Iodide Decomposition)

Two different processes are being investigated for HI decomposition. One process, referred to as extractive distillation, uses phosphoric acid to strip HI from the HI-water-iodine mixture and to break the HI-water azeotrope. The other process is referred to as reactive distillation and involves reacting the HI-water-iodine mixture in a reactive bed to effect the separation process and produce hydrogen. Extractive distillation is a proven process, but requires significant amounts of energy and many components to perform the extraction, distillation, concentration, reaction, and separation steps of the process (see Fig. 3-48). The kinetics for reactive distillation are still relatively unknown, but the process can be performed in a single component without requiring concentration of the acid (see Fig. 3-49). For the n^{th}-of-a-kind SI-Based H2-MHR pre-conceptual design, the HI decomposition flowsheet is based on the reactive distillation process. One disadvantage of reactive distillation is that there is significant recycle of HI back to Section 1, which increases equipment sizes for Section 1.

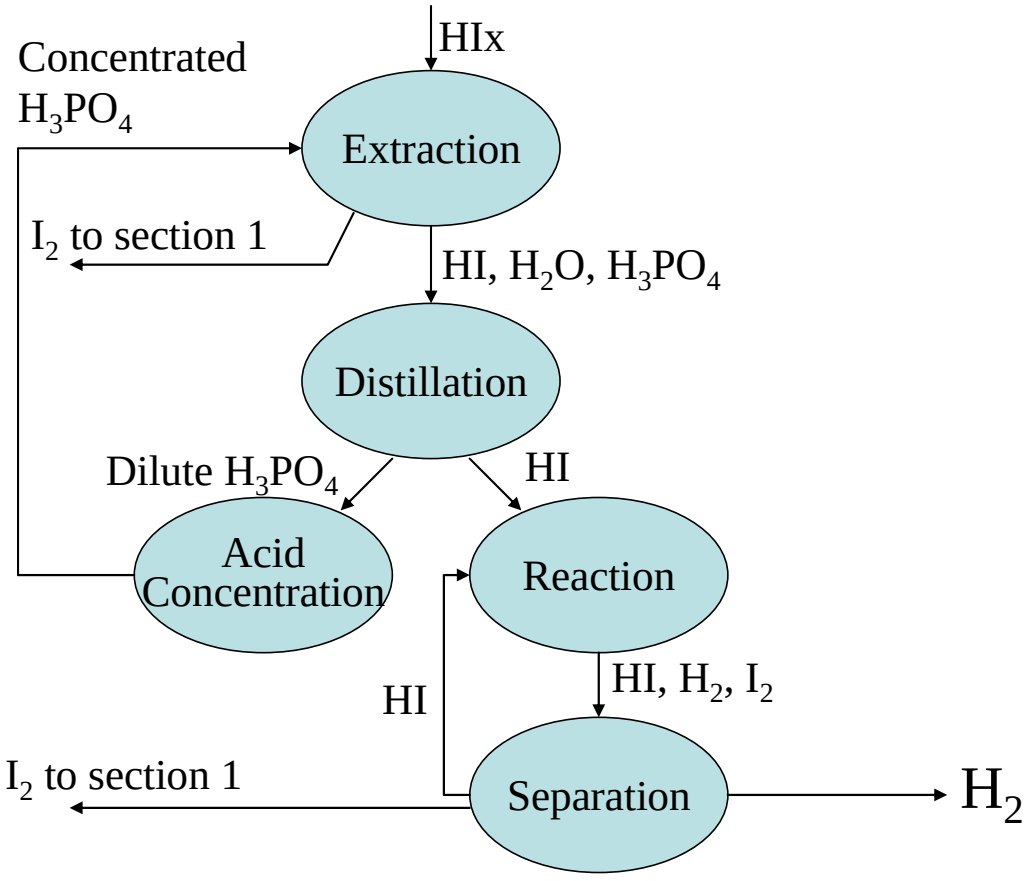

Figure 3-48. Extractive Distillation Process Schematic

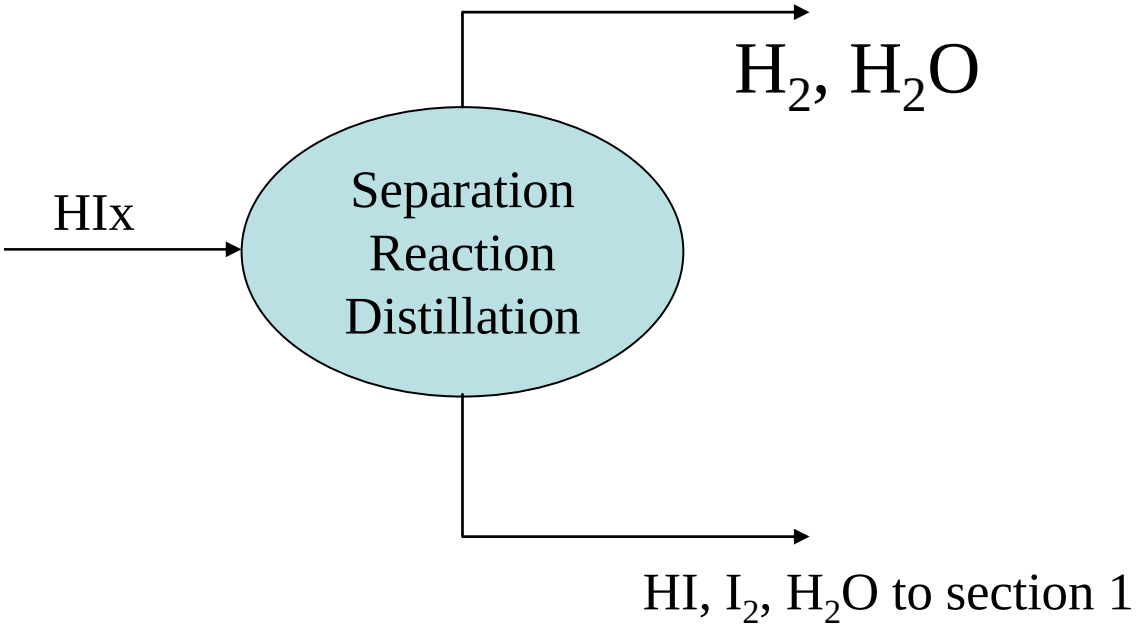

Figure 3-49. Reactive Distillation Process Schematic

The flowsheet for Section 3 is shown in Fig. 3-50 and Table 3-21 provides a description of the Section 2 process streams. The reactive distillation process is performed within a packed-bed distillation column using activated carbon as a catalyst. Significant quantities of heat are required for Section 3, but there are also significant quantities of heat available for recovery within Section 3. Because much of the heat available for recovery is at a temperature lower than required for process operations, heat pumps (using water as the working fluid) are used to transfer the heat from the lower temperature source to the higher temperature sink. The distillation column has a high heat duty in the reboiler and has heat available from the condenser. The first heat pump transfers heat from the condenser to the reboiler at the expense of externally supplied shaft work. Much of the heat is used to break the binding energy of the $HI/I_2/H_2O$ complex. For recycled HI, the heat of mixing is recovered and a second heat pump is used to raise the temperature of this stream to that required for heating the distillation column feed. The remaining heat duty of Section 3 is recovered from the decomposer products of Section 2.

The heat pumps consist of a multi-staged steam compressor, a hot heat exchanger complex that transfers heat to the process and condenses steam, an expansion valve in which the condensate is partially flashed and the pressure is lowered, and a cold heat exchanger in which the condensate is evaporated. Mechanical energy drives the compressor and much of this mechanical energy adds internal energy to the steam. The hot heat exchanger network includes the interstage coolers of the compressor as well as the subsequent condenser.

Recovery of the heat of mixing of the $HI/I_2/H_2O$ is necessary for process efficiency but does require additional process steps (described below) to produce a stream of pure I_2 that is required for operation of the H_2SO_4 boost reactor in Section 1. The HI_X from Section 1 (301A) is pumped up to the operating pressure of the reactive distillation column (C301) and heated to the required feed temperature in a series of heat exchangers (H301, H302, and H303). Most of the

required heat is recovered from cooling hot streams, but a portion of the heat is obtained from Heat Pump 2. The distillation column operates with a vapor product (305) consisting of $HI/H_2/H_2O$. The cold side reflux condenser on C301 is HP1-QH, which is the heat input to Heat Pump 1. The hot side of the reboiler on C301 is HP2-QC. The still also has an auxiliary reboiler (C301F3), and the hot side of this reboiler is H213 of Section 2. The auxiliary reboiler includes a three-phase flash drum that produces a vapor phase and two liquid phases. The vapor phase feeds back into the distillation. The heavier liquid phase is nearly pure iodine. This phase is cooled, washed with water in C303, and returned to Section 1 for use in the H_2SO_4 boost reactor. The lighter liquid phase is cooled to the same temperature as the column overhead and then combined with the column overhead (306) to recover the heat of solution from the undecomposed HI. This heat is removed in H304, which is the hot side of HP2-QC and the heat input to Heat Pump 2. HP2-QH, the heat output of Heat Pump 2, is the hot side of H303 and the final preheat of the still feed. The two-phase stream leaving H304 is separated in S301. The vapor phase contains the hydrogen product gas. This stream is cooled in H308 and the condensate is removed in S302. The hydrogen is then washed with water in C302 to yield the final hydrogen product. The condensate from S302 consists of two liquid phases. The heavier phase is primarily iodine and is washed in C303 for use in the H_2SO_4 boost reactor of Section 1. The lighter phase is mostly water and is combined with the lower phase from C302, which is also mostly water. These two streams function as the wash for C303.

Pure water is not very effective at washing iodine out of hydrogen, but iodine is very soluble in HI. For this reason, a small amount of the distillation overhead (313A) is split from the main flow (305), cooled, and then added back to the wash column (C301) at an intermediate stage.

The liquid phase from S301 is split for heat recovery. Part of the heat is recovered into the column feed and the remainder is cooled in H305, which is the hot side of H202 in Section 2.

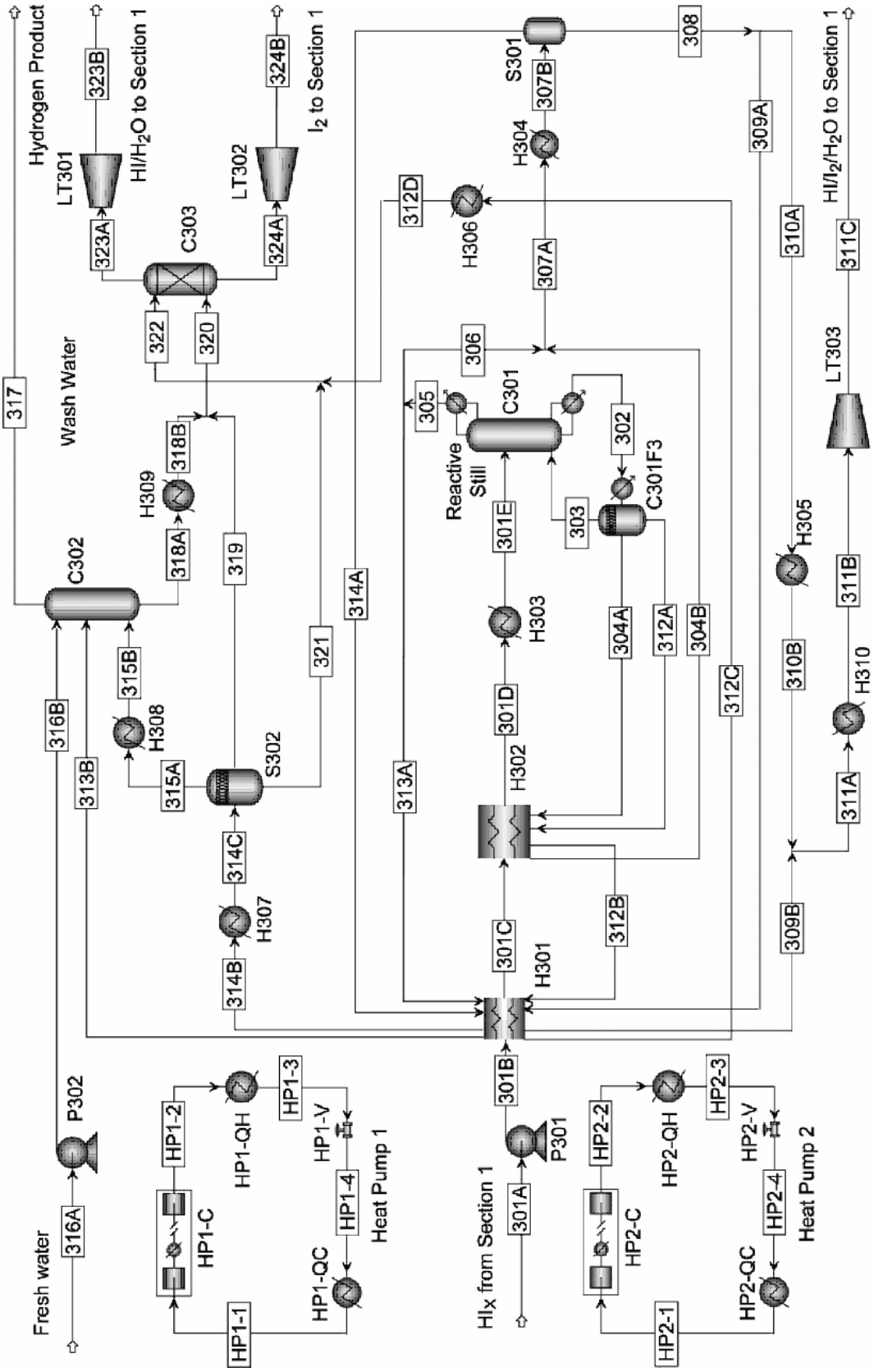

Figure 3-50. SI Process Section 3 Flowsheet

Table 3-21. SI Process Section 3 Flow Stream Description

Stream	Stream Flow Rates (moles/s)					Phase	Pressure (bar)	Temp. (°C)
	H_2O	I_2	HI	H_2	Total			
301A	35359.8	25838.61	6705.71	0	67904.07	L	1.85	119.85
301B	35359.8	25838.61	6705.71	0	67904.07	L	40.00	123.07
301C	35359.8	25838.61	6705.71	0	67904.07	L	40.00	247.17
301D	35359.8	25838.61	6705.71	0	67904.07	L	40.00	269.87
301E	35359.8	25838.61	6705.71	0	67904.07	V + L	40.00	282.46
302	28364.1	31351.82	4598.21	0.03	64314.16	L	40.00	289.69
303	11305.8	3891.17	1846.26	0.03	17043.26	V	40.00	289.06
304A	16789.9	25042.22	2715.56	0	44547.65	L	40.00	289.06
304B	16789.9	25042.22	2715.56	0	44547.65	L	40.00	257.17
305	18301.5	3.01	703.63	1625.06	20633.16	V	40.00	262.17
306	18027	2.96	693.08	1600.69	20323.68	V	40.00	262.17
307A	34816.8	25045.18	3408.64	1600.69	64871.32	V + L	40.00	271.06
307B	34816.8	25045.18	3408.64	1600.69	64871.32	V + L	40.00	257.17
308	29973.6	23996.51	3389.36	11.85	57371.36	L	40.00	257.17
309A	21714	17383.96	2455.38	8.58	41561.95	L	40.00	257.17
309B	21714	17383.96	2455.38	8.58	41561.95	L	40.00	139.01
310A	8259.62	6612.54	933.98	3.26	15809.4	L	40.00	257.17
310B	8259.62	6612.54	933.98	3.26	15809.4	L	40.00	139.01
311A	29973.6	23996.51	3389.36	11.85	57371.36	L	40.00	139.01
311B	29973.6	23996.51	3389.36	11.85	57371.36	L	40.00	120
311C	29973.6	23996.51	3389.36	11.85	57371.36	L	7.00	118.78
312A	268.43	2418.44	36.39	0	2723.26	L	40.00	289.06
312B	268.43	2418.44	36.39	0	2723.26	L	40.00	257.17
312C	268.43	2418.44	36.39	0	2723.26	L	40.00	139.01
313A	274.52	0.05	10.55	24.38	309.5	V	40.00	262.17
313B	274.52	0.05	10.55	24.38	309.5	V + L	40.00	139.01
314A	4843.16	1048.67	19.28	1588.84	7499.95	V	40.00	257.17
314B	4843.16	1048.67	19.28	1588.84	7499.95	V + L	40.00	139.01
314C	4843.16	1048.67	19.28	1588.84	7499.95	V + L	40.00	120
315A	88.31	7.67	0	1585.46	1681.44	V	40.00	120
315B	88.31	7.67	0	1585.46	1681.44	V + L	40.00	40
316A	1072.72	0	0	0	1072.72	L	1.01	25
316B	1072.72	0	0	0	1072.72	L	40.00	27.26
317	1.76	0	0	1609	1610.76	V	40.00	28.82
318A	1433.79	7.72	10.55	0.84	1452.9	L	40.00	42.97
318B	1433.79	7.72	10.55	0.84	1452.9	V + L	40.00	110
319	4733.41	25.3	19.13	2.74	4780.58	L	40.00	120
320	6167.2	33.02	29.69	3.58	6233.49	V + L	40.00	117.69
321	21.45	1015.7	0.14	0.64	1037.93	L	40.00	120
322	289.87	3434.14	36.54	0.64	3761.19	L	40.00	118.27
322D	268.43	2418.44	36.39	0	2723.26	L	40.00	120
323A	6390	139.55	65.84	2.38	6597.77	L	40.00	120.55
323B	6390	139.55	65.84	2.38	6597.77	L	7.00	120.39
324A	67.07	3327.61	0.39	1.84	3396.91	L	40.00	118.04
324B	67.07	3327.61	0.39	1.84	3396.91	L	7.00	115.57
HP1-1	55382.4	0	0	0	55382.39	V	44.77	257.12
HP1-2	55382.4	0	0	0	55382.39	V	71.60	288.46
HP1-3	55382.4	0	0	0	55382.39	L	71.60	287.4
HP1-4	55382.4	0	0	0	55382.39	V + L	44.77	257.12
HP2-1	11999.6	0	0	0	11999.57	V	41.21	252.13
HP2-2	11999.6	0	0	0	11999.57	V	79.50	295.69
HP2-3	11999.6	0	0	0	11999.57	L	79.50	294.6
HP2-4	11999.6	0	0	0	11999.57	V + L	41.21	252.13

3.4.2 Major Equipment Description

The major equipment for the Hydrogen Production System includes pumps, compressors, flow reactors, packed columns, phase separators, liquid/vapor expanders, and energy-recovery turbines. The major pieces of equipment for each section (and the associated capital costs discussed in Section 4.4) are based on scaling the designs described in [Brown, 2003] and are described in Tables 3-22 through 3-24. Components that operate at higher temperatures are typically manufactured from nickel alloys. More detailed equipment specifications and cost estimates will be performed during the preliminary and final design phases. The materials for vessels and piping are typically carbon steel with fluorocarbon linings.

Table 3-22. Description of Major Equipment – Section 1

Flowsheet ID	Description	Parallel Units	Materials of Construction
C-101	Primary O_2 scrubber, vertical vessel	2	Carbon Steel
C-102	Lower phase SO_2 scrubber, vertical vessel	2	Carbon Steel
C-103	H_2SO_4 boost reactor, Vertical Vessel	2	Carbon Steel
C-104	Secondary O_2 scrubber, vertical vessel	2	Carbon Steel
C-105	SO_2 absorber, vertical vessel	2	Carbon Steel
S-101	3-phase cyclonic Knockout drum, vertical vessel	2	Carbon Steel
S-102	Flash drum, vertical vessel	2	Carbon Steel
S-104	Primary O2 water knockout drum, carbon steel	2	Carbon Steel
S-105	Secondary O2 water knockout drum, carbon steel, horizontal vessel	2	Carbon Steel
R-101	Flow reactor with integral shell-and-tube heat exchanger	2	Carbon Steel
E-102	Shell-and-tube heat exchanger to cool water supplied to C101	1	Carbon Steel
P-101	Flourocarbon-lined centrifugal pump	3	Stainless Steel
P-102	Flourocarbon-lined centrifugal pump	3	Ni Alloy
P-103	Flourocarbon-lined centrifugal pump	3	Ni Alloy
P-104	Flourocarbon-lined centrifugal pump	3	Ni Alloy
P-105	Flourocarbon-lined centrifugal pump	3	Carbon Steel
P-106	Flourocarbon-lined centrifugal pump	3	Ni Alloy
TE-101	O_2 Axial Gas Turbine	1	Ni Alloy
TE-102	S-101 Overhead Liquid Expander	2	Ni Alloy
TE-103	S-101 SideLiquid Expander	2	Ni Alloy
TE-104	S-101 Bottoms Liquid Expander	2	Ni Alloy

Table 3-23. Description of Major Equipment – Section 2

Flowsheet ID	Description	Parallel Units	Materials of Construction
H210A	Helium-side exchanger vessel for Decomposer 1	1	Carbon Steel
H210A	Process-side exchanger vessel for Decomposer 1	1	Carbon Steel
H210B	Helium exchanger vessel for Decomposer 2	1	Carbon Steel
S201	Section feed flash drum	1	Carbon Steel
S202	Section feed bottoms flash drum	1	Carbon Steel
S203	S202 bottoms flash drum	1	Carbon Steel
S204	S201 overhead product flash vessel	1	Carbon Steel
S205	S202 overhead product flash vessel	1	Carbon Steel
S206	S210 overhead product flash vessel	1	Carbon Steel
S207	Decomposer loop flash vessel	1	Carbon Steel
S208	Decomposer loop vapor product flash vessel	1	Carbon Steel
S209	Decomposer loop vapor product flash vessel	1	Carbon Steel
S210	S203 overhead product flash vessel	1	Carbon Steel
H203	H203 to cooling water, shell and tube heat exchanger	1	Carbon Steel/Ni
H204	H204 to cooling water, shell and tube heat exchanger	1	Carbon Steel/Ni
H205	H205 to cooling water, shell and tube heat exchanger	1	Carbon Steel/Ni
H205A	H205A to cooling water, shell and tube heat exchanger	1	Carbon Steel/Ni
H214	H214 to cooling water, shell and tube heat exchanger	1	Carbon Steel/Ni
H215	H215 to cooling water, shell and tube heat exchanger	1	Carbon Steel/Ni
H216	H216 to cooling water, shell and tube heat exchanger	1	Carbon Steel/Ni
H206	Decomposer loop pre-heat exchanger, shell and tube heat exchanger	1	Ni/Ni
H207	Flow Vaporizor 1, shell and tube heat exchanger	1	Ni/Ni
H208A	Flow Vaporizor 2, shell and tube heat exchanger	1	Ni/Ni
H208B	Pool Boiler	1	Ni/Ni
H209	Decomposer Preheat, shell and tube heat exchanger	1	Carbon Steel / SiC
P-201	Decomposer loop centrifugal pump	2	Stainless Steel
P-202	Water return to Section 1, centrifugal pump	2	Carbon Steel
TC201	H_2O/SO_2 compressor	1	Ni Alloy
TE201	SO_2/O_2 expander, axial gas turbine	1	Ni Alloy
LT201	H_2O/H_2SO_4 liquid expander	1	Ni Alloy

Note: H201, H202, H213A interface with Section 3 (referred to as H312, H313, and H305 in Section 3).

Table 3-24. Description of Major Equipment – Section 3

Item	Description	Parallel Units	Materials of Construction
H-301	Shell and tube heat exchanger	10	Carbon Steel
H-302	Shell and tube heat exchanger	10	Carbon Steel
H-303	Shell and tube heat exchanger, receives some heat from HP1-QH	10	Carbon Steel
H-304	Shell and tube heat exchanger, receives some heat from HP2-QH	10	Carbon Steel
H-305	Shell and tube heat exchanger, receives heat from HP1-QH, HP2-QH, and stream 213F in Section 2	10	Carbon Steel
H-306	Shell and tube heat exchanger, provides heat to HP1-QC	10	Carbon Steel
H-307	Shell and tube heat exchanger, provides heats to HP2-QC	10	Carbon Steel
H-308	Shell and tube heat exchanger, rejects heat to cooling water	1	Carbon Steel
H-309	Shell and tube heat exchanger, receives some heat from H307	1	Carbon Steel
H-310	Shell and tube heat exchanger, rejects heat to cooling water	1	Carbon Steel
H-311	Dumps H306 to Cooling Water	1	Carbon Steel
H-312	Shell and tube heat exchanger, receives some heat from H305 and transfers heat stream 204A in Section 2	1	Carbon Steel
H-313	Shell and tube heat exchanger, receives heat from H305, H310, and Section 1	1	Carbon Steel
S-301	Flash drum, vertical vessel	10	Carbon Steel
S-302	Flash drum, vertical vessel	10	Carbon Steel
C301F3	Flash drum, vertical vessel	10	Carbon Steel
C-301	Reactive still, vertical vessel	10	Carbon Steel
C-301i	C301 Internals, vessel trays and sieves	10	Monel
C-302	H_2 product scrubber, vertical vessel	10	Carbon Steel
C-303	I_2 scrubber for Section 1 boost reactor (C103)	10	Carbon Steel
P-301	Feed pump to reactive column (C301)	11	Stainless Steel
P-302	Fresh water feed pump	11	Carbon Steel
HP1-C	Axial Compressor for Heat Pump 1	10	Nickel alloy
HP2-C	Axial compressor for Heat Pump 2	10	Nickel alloy
LT301	Liquid expander, 40 bar to 7 bar	10	Carbon Steel
LT302	Liquid expander, 40 bar to 7 bar	10	Carbon Steel
LT303	Liquid expander, 40 bar to 7 bar (incorrectly shown as compressor on Fig. 3-50)	10	Carbon Steel

3.4.3 Overall Plant Efficiency

The hydrogen production rate for the 4-module plant is 6436 moles/s = 12.97 kg/s. The corresponding heat rate is 1840.44 MW(t), using the higher heating value of hydrogen (141.9 MJ/kg). The MHR modules produces 2400 MW(t). Shaft work associated with the primary and secondary coolant circulators produces 96 MW(t). Shaft work associated with the Hydrogen Production System produces 684 MW(t). The Hydrogen Production System is assumed to produce 15 MW(e) through energy-recovery turbines and house loads are assumed to be 6 MW(e). Assuming pump motor efficiencies of 95% and electricity produced at 48% thermal efficiency using GT-MHRs, the net electricity required by the plant is 812 MW(e). The overall plant efficiency is then estimated to be:

$$\eta_{plant} = 100 \times \frac{1841.15}{2400 + 812/0.48} = 45.0\%$$

3.5 Plant Protection and Monitoring Systems

3.5.1 Reactor Protection System

The design of the Reactor Protection System (RPS) is similar to that for the GT-MHR [Shenoy, 1996]. The RPS provides an integrated response to initiating events (e.g., loss of offsite power) in order to ensure safe shutdown of the reactor. Each MHR module has an independent RPS, and the RPS is independent of other control systems, including the Investment Protection System (IPS). The RPS monitors plant parameters, including neutron flux, primary and secondary coolant flow rates, primary and secondary coolant pressures, primary coolant inlet and outlet temperatures, primary coolant moisture concentration, and secondary coolant radioactivity. If the plant parameters are not within their allowable ranges, the RPS performs its safety-related function to trip the reactor using the control rods or the independent reserve shutdown system. The RPS uses two-out-of-four coincidence logic to satisfy safety and availability requirements. For the H2-MHR, the trip setpoints will be established during the preliminary and final design stages.

3.5.2 Investment Protection System

The design of the IPS is similar to that of the GT-MHR. The IPS does not perform any safety-related functions. Each MHR module has an independent IPS, and the IPS is independent of other control systems, including the RPS. The IPS monitors plant parameters, including primary and secondary coolant flow rates, primary and secondary coolant pressures, primary coolant inlet and outlet temperatures, secondary coolant radioactivity, and SCS cooling water radioactivity. If the plant parameters are not within their allowable ranges, the IPS performs its investment-protection functions, which include:

- Secondary HTS isolation **[TBD]**
- Hydrogen Production Plant isolation **[TBD]**
- SCS cooling water isolation

- Primary and secondary coolant circulator trip
- RHRS startup
- SCS startup

For the H2-MHR, the setpoints for these functions and functions associated specifically with the Hydrogen Production Plant will be established during the conceptual, preliminary, and final design stages.

3.5.3 Plant Monitoring System

The plant monitoring system includes instrumentation to monitor (1) the primary coolant, (2) radioactive effluents, (3) non-radioactive effluents, (4) meteorological conditions, and (5) seismic events.

The Primary Coolant Monitoring System monitors the chemical and radiological impurities in the primary coolant and helium purification systems during all modes of plant operation. The important impurities that are monitored include:

Non-Condensable Gases: CO, CO_2, H_2, CH_4, N_2, O_2, H_2O, Ar, Ne, Xe, Kr, and tritium.

Condensable Gases: fission products (I, Cs, and Te), sulfur gases (H_2S, S_2, and SO_2), chlorine gases (HCl and Cl_2), and oil vapor.

Dust/Aerosol Particles: graphite/carbon and metal oxides.

In-situ probes are used to monitor plateout of radionuclides in the primary coolant circuit.

The Radiation Monitoring System monitors all effluents from the plant, monitors plant radiation areas, provides health-physics data, and provides early warning of plant equipment malfunctions that may result in radioactivity release. Airborne radiation monitors survey airborne particulate and noble-gas radioactivity discharged from the plant to the environment. Area radiation monitors measure radiation levels in designated plant areas to detect any abnormal migration of radioactivity.

The Environmental Monitoring System monitors the chemistry and non-radiological physical parameters of liquid and gaseous effluents that are discharged from the plant. The Meteorological Monitoring System includes one or more meteorological towers and instrumentation to measure temperature, barometric pressure, humidity, wind velocity and direction, and atmospheric stability. The Seismic Monitoring System includes sensors and instrumentation to detect and record the seismic motions experienced by structures and equipment in the event of an earthquake.

3.6 Balance of Plant and Auxiliary Systems

The balance of plant and auxiliary systems for the H2-MHR are very similar in design to those for the GT-MHR. Brief descriptions of key systems are given in the sections below. More detailed descriptions are available in [Shenoy, 1996].

3.6.1 Fuel Handling and Storage System

The Fuel Handling and Storage System (FHSS) design is the same as that for the GT-MHR. The FHSS is used for (1) receiving and inspecting new fuel elements, (2) transporting fuel elements to local storage facilities, (3) extracting irradiated fuel assemblies out of the MHR modules and transporting them to local storage facilities, (4) installing new fuel elements in the MHR core, (5) transporting spent fuel elements from the local storage facilities to the packaging and shipping facility, and (6) packaging the spent fuel elements for shipping. The FHSS is also used to retrieve and replace spent reflector elements and to manipulate special tools for in-service inspection of reactor components. Figure 3-51 shows the layout of the FHSS.

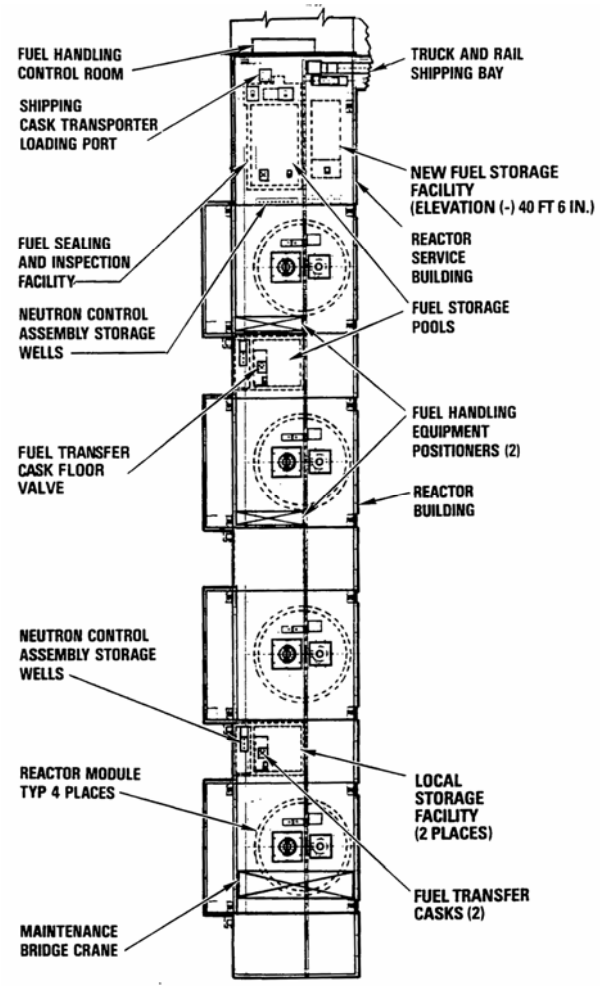

Figure 3-51. Fuel Handling and Storage System Layout

In-core handling of fuel elements is performed by joint operation of the fuel handling machine and fuel transfer cask. As shown in Fig. 3-52, these components are mounted on the fuel handling equipment support structure which is located above the reactor vessel. The fuel handling machine grapples each fuel element, one at a time, and deposits them on the fuel transfer cask guide sleeve. The fuel transfer cask grapples the elements, raises then out of the core, and deposits them onto internal sliding storage tables. After the transfer cask is filled (9 elements), it is transported to the local storage facility adjacent to the MHR module being serviced, where the elements are unloaded. During the unloading process, a second fuel transfer cask is placed over the reactor to receive a load of fuel elements. When the second cask is filled, it is transported to a second location at the local storage facility and unloaded. This cycle of alternating fuel transfer cask operations is repeated until a complete core sector has been emptied. The sequence is reversed to load the core sector with both fresh fuel elements and the elements from that sector that have been irradiated for one cycle. This process is repeated for the remaining core sectors. During a refueling outage, one-half of the 1020 fuel elements and an average of one-fourth of the replaceable reflector elements are replaced, and the estimated refueling time is 20.7 days.

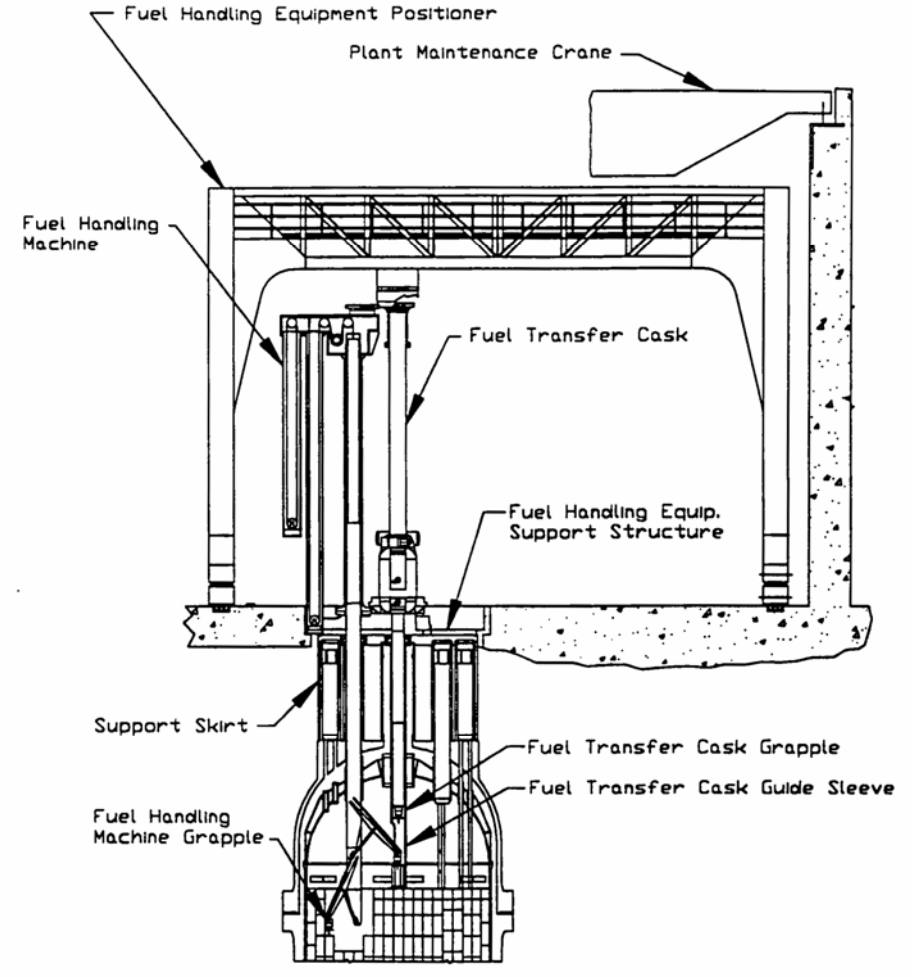

Figure 3-52. Fuel Handling Equipment Arrangement

3.6.2 Spent Fuel Storage System

The Spent Fuel Storage System (SFSS) consists of dry storage wells immersed in a pool of water. There are two spent fuel storage pools with independent cooling systems. Decay heat is transferred to circulating cooling water in the storage pool and rejected to the atmosphere using an air-cooled heat exchanger. Each storage pool contains 350 dry storage wells and each well stores eight spent fuel elements. Two 100% capacity pumps and one 100% capacity heat exchanger are provided for each pool.

3.6.3 Radioactive Waste Management and Decontamination System

The Radioactive Waste Management and Decontamination System design is the same as that for the GT-MHR and consists of separate systems to process liquid, gaseous, and solid radioactive waste. This system is located in the Radioactive Waste Management Building and also includes decontamination equipment to decontaminate components such as valves and small pumps prior to maintenance.

The Liquid Radioactive Waste Management System uses filtration and mixed-bed demineralization to treat the liquid waste. Treated and purified liquid wastes are reused in the plant. Spent resins are transferred to the solid radioactive waste management system. The total amount of liquid radioactive waste processed by this system is approximately 10 m^3 per module per year.

The Gaseous Radioactive Waste Management System processes radioactive waste gas to reduce the radioactivity to levels that are acceptable for discharge to the atmosphere. Most of the gas processed by the system requires only filtration and monitoring before release. However, waste gas from the primary Helium Purification System requires holdup to allow decay of short-lived radionuclides before release. The total amount of gaseous radioactive waste processed by this system is approximately 3500 m^3 per module per year.

The Solid Radioactive Waste Management System collects and solidifies radioactive waste (including spent resins). The solid waste is packaged into drums that are shipped offsite for disposal. The total amount of solid radioactive waste processed by this system is approximately 70 m^3 per module per year.

3.6.4 Heating, Ventilation, and Air Conditioning Systems

The Heating, Ventilation, and Air Conditioning (HVAC) Systems designs are similar to those for the GT-MHR. For the H2-MHR, the Control Building HVAC system is designed to protect the reactor operators from airborne radioactivity and from toxic material concentrations resulting from chemical spills or accidents associated with the Hydrogen Production System.

3.6.5 Hydrogen Production Water Supply System

The H2-MHR Hydrogen Production Water Supply System consists of a storage tank that receives tap water, a centrifugal feedwater pump, a water purification system, and an instrumentation system for measuring water-quality parameters. The water purification system is designed to maintain water chemistry to minimize corrosion and fouling of heat-exchanger surfaces in the Hydrogen Production System. Water coolant chemistry requirements include

maintaining resistivity >1.0 megaohm-cm, maintaining total dissolved solids < 0.05 kg/m3, and maintaining the dissolved oxygen concentration below 10 ppb. The water purification system design includes the following components:

1. A 2-micron cartridge-type prefilter with sintered stainless steel media to control the size and concentration of suspended solids.

2. A cation exchange unit to remove dissolved cations and to adsorb colloidal-sized particles.

3. A mixed bed ion exchange unit to remove dissolved anions and any remaining dissolved cations.

4. A vacuum deaerator or membrane degasifier to remove dissolved oxygen.

5. A 2-micron cartridge-type postfilter with sintered stainless steel media to protect the Hydrogen Production Water Supply System from particles generated in the water purification train (e.g., from breakdown of resins or degasifier membranes).

3.6.6 Waste Heat Rejection System

For the SI-Based H2-MHR plant, waste heat is rejected primarily from Section 1 of the Hydrogen Production System. The total heat rejection rate is 336 MW(t). The design of the Waste Heat Rejection System is similar to that for the GT-MHR, with wet mechanical draft cooling towers rejecting heat to the atmosphere. The system is sized to reject 386 MW(t), which provides a margin of 15% above the expected maximum heat duty. Three one-half capacity pumps are provided to circulate the water between the Hydrogen Production System and the Waste Heat Rejection System.

The majority of the heat is transferred through evaporation of a small fraction of the circulating water. A makeup water system replenishes water lost to evaporation and is also used to control the water chemistry in the circulating water. Excess makeup water is blown down from the cooling tower basin to the receiving water body. The water released from evaporation and blow down are potential sources of tritium release to the environment and these sources are factored into the design of the Helium Purification Systems.

3.7 Buildings and Structures

The overall plant arrangement is described in Section 2.3. The following sections describe the Reactor Building and other major building are described in the following sections.

3.7.1 Reactor Building and Vented Low-Pressure Containment

The Reactor Building is a multi-celled, embedded structure constructed of cast-in-place reinforced concrete. The degree of embedment was selected to serve a number of objectives, including reduced cost and complexity of construction, ease of operation, minimization of shielding, and good seismic performance. The operating floor of the power plant is set at site grade, with a common maintenance enclosure covering the operating area traversed by shared refueling equipment. There are two floors below grade with a rectangular footprint which are

used to house mechanical, electrical, and instrumentation systems dedicated to each reactor. A number of additional mechanical and electrical systems which do not require radiation shielding or protection from external hazards are designed to be delivered to the site as prefabricated modules and located at grade outside the maintenance enclosure. The Reactor Building below elevation -30 ft. is configured as a cylinder to enable it to resist soil and groundwater pressure. The reactor and IHX vessels are located within this space. Access to and from the cylindrical portion of the building for piping, electrical services, personnel, and the concentric RCCS ducting is made from the rectangular portion of the building between elevations -30 ft. and grade. Access for refueling and for major maintenance activities is from the operating floor. There are two extensions of the reinforced concrete Reactor Building above grade. On the east side of the Reactor Building, the reinforced concrete portion of the building extends to elevation +95 ft. 6 in. to serve as the Reactor Cavity Cooling System elevated inlet-outlet structure.

The Reactor Building has been divided into two distinct zones for purposes of the HVAC design. The cells containing the primary HPS components, the vent path sections above grade west of the maintenance enclosure, and most of the cells in the cylindrical portion of the building have been designed to form a closed, interconnected space which is normally isolated from the environment. Air is recirculated internally and heat is removed by chilled water-cooled air handling units. The balance of the rectangular portion of the building, the personnel access stairways, the personnel elevator shaft into the silo portion of the building, and the space below the reactor vessel have been designed to be conditioned by a once-through flow of heated or cooled air. The RCCS panels, where they enter the closed portion of the Reactor Building, are regarded as part of the vented low pressure containment boundary. In essence, air flowing inside the RCCS ducts and panels is outside the Reactor Building. The walls, doors, plugs, and other barriers which separate the closed, recirculated portion of the building from the once-through cooled portion of the building or from the outside environment (including the RCCS panels and ducts) constitute the fourth containment barrier. Leakage from within this portion of the Reactor Building to the other part of the Reactor Building or to the environment has the potential to transport fission products from the containment to the environment. This space is also the portion of the Reactor Building which is affected by the specified building leak rate. The net free volume within this space is approximately 260,000 ft^3. This space is designed to have a leak rate of no greater than 1 volume per day at an internal pressurization of 1 psid, and to vent whenever the internal pressure exceeds 1 psid. It is expected that essentially none of the leakage which occurs will be from the surfaces of the building which are in contact with the soil, and that the specified leak rate represents an upper bound on the exchange which could occur between the building interior and the environment, since the pressure and therefore the leakage will normally decrease over the course of an accident. Architectural features such as doors, gaskets around floor plugs, and penetrations are important to establishing the building leak rate but can be modified to achieve the specified value.

In the event of a large primary coolant leak within the closed portion of the Reactor Building, the internal pressure will exceed 1 psid. Gases are able to flow from any compartment through the building and out the vent path relief valves or dampers to the atmosphere. The vent dampers are maintained in a closed position by gravity, and the weight of the damper determines the relief setpoint pressure, which is the internal pressure needed to open the damper. This design must be considered preliminary. The relief setpoint pressure affects both the nominal reactor building leak rate and the building pressure transients following a large primary coolant leak. The building relief setpoint pressure and vent opening area can both be adjusted if needed to

obtain satisfactory performance during a pressure transient. The reinforced concrete building and RCCS panels have been designed to withstand pressure transient loadings of 10 psid.

3.7.2 Other Major Buildings

The Reactor Service Building is a multilevel reinforced concrete structure located at grade level next to the Reactor Building. This building is subdivided into several compartments to house equipment common to all four modules. The fuel handling area is located within the Reactor Service Building. This area contains facilities for introducing new fuel, for loading and shipping spent fuel casks, for storing new fuel, and for inspecting new and spent fuel. The Hot Service Facility is located inside a shielded vault in the Reactor Service Building adjacent to the fuel sealing and inspection facility. The Hot Service Facility provides the capability for inspection, maintenance, and repair of reactor service equipment and tools. The facility includes viewing windows, operating galleries outside the vault, manipulators to perform the inspection, maintenance, and repair services, as well as portable decontamination equipment. The Personnel Service Building is a grade-level structure, located next to the Reactor Service Building, which houses facilities for monitoring, controlling, and minimizing human exposure to radioactivity. In addition to the hot chemistry laboratory and radiation decontamination facilities, the building also houses locker rooms, a cold (nonradioactive) chemistry laboratory, and a supervisor's office. A fuel handling control station for monitoring and controlling fuel handling activities is located in the Personnel Service Building.

The Radioactive Waste Management Building, is located next to the Reactor Service Building, and houses the solid radioactive waste train, liquid radioactive waste train, and gaseous radioactive waste train. Tanks, pumps, and filters which handle radioactive materials are housed in concrete cubicles to provide radiation shielding and protection for the environment. The Radioactive Waste Management Building is a reinforced concrete and steel structure.

4. Plant Assessments

As part of this pre-conceptual design study, assessments of the H2-MHR plant were performed in the areas of safety, availability, licensing, and economics.

4.1 Safety Assessment

The following sections describe the safety features of the H2-MHR and assessments of bounding accidents involving loss of flow and loss of coolant.

4.1.1 Passive Safety Features

Passive safety features of the H2-MHR include the (1) ceramic, coated-particle fuel that maintains its integrity at high temperatures during normal operation and LOCAs; (2) an annular graphite core with high heat capacity that limits the temperature rise during a LOCA; (3) a relatively low power density that helps to maintain acceptable temperatures during normal operation and accidents; (4) an inert helium coolant, which reduces circulating and plateout activity; and (5) a negative temperature coefficient of reactivity that ensures control of the reactor for all credible reactivity insertion events. Also, as discussed in Section 3.1.7, the fuel, the graphite, the primary coolant pressure boundary, and the low-pressure vented containment building provide multiple barriers to the release of fission products.

4.1.2 Safety-Related Systems, Structures, and Components

Based on preliminary safety assessments, the following systems, structures, and components (SSCs) are classified as safety-related:

- MHR System, including neutron control assemblies, ex-vessel neutron detectors, reactor internals, reactor core, and fuel.
- Reactor Vessel and Cross Vessel.
- Reactor Cavity Cooling System.
- Reactor Protection System, including all sensors, control logic, and housings that support safety-related reactor trips.
- Fuel storage pools and wells, which are part of the Reactor service Building.
- Essential AC and DC Electrical Systems.

4.1.3 Accident Analysis

In terms of safety consequences, the bounding accidents for the H2-MHR are a loss of flow leading to a high pressure conduction cooldown (HPCC) and loss of coolant leading to a low pressure conduction cooldown (LPCC). The HPCC event is typically initiated by trip of the primary and/or secondary helium circulators. The RPS automatically initiates a reactor trip on low flow or loss of power to the circulators. The system pressure equilibrates at about 5 MPa after about 50 hours following initiation of the event. Because the system remains at high

pressure, the decay heat is more uniformly distributed within the core and vessel than during a LPCC event. The LPCC event is typically initiated by a small primary coolant leak, causing the system to depressurize to atmospheric pressure. The Reactor Protection System automatically initiates a reactor trip on low coolant pressure. For both events, the SCS fails to start and decay heat is removed by thermal radiation and natural convection from the reactor vessel to the RCCS (see Fig. 4-1).

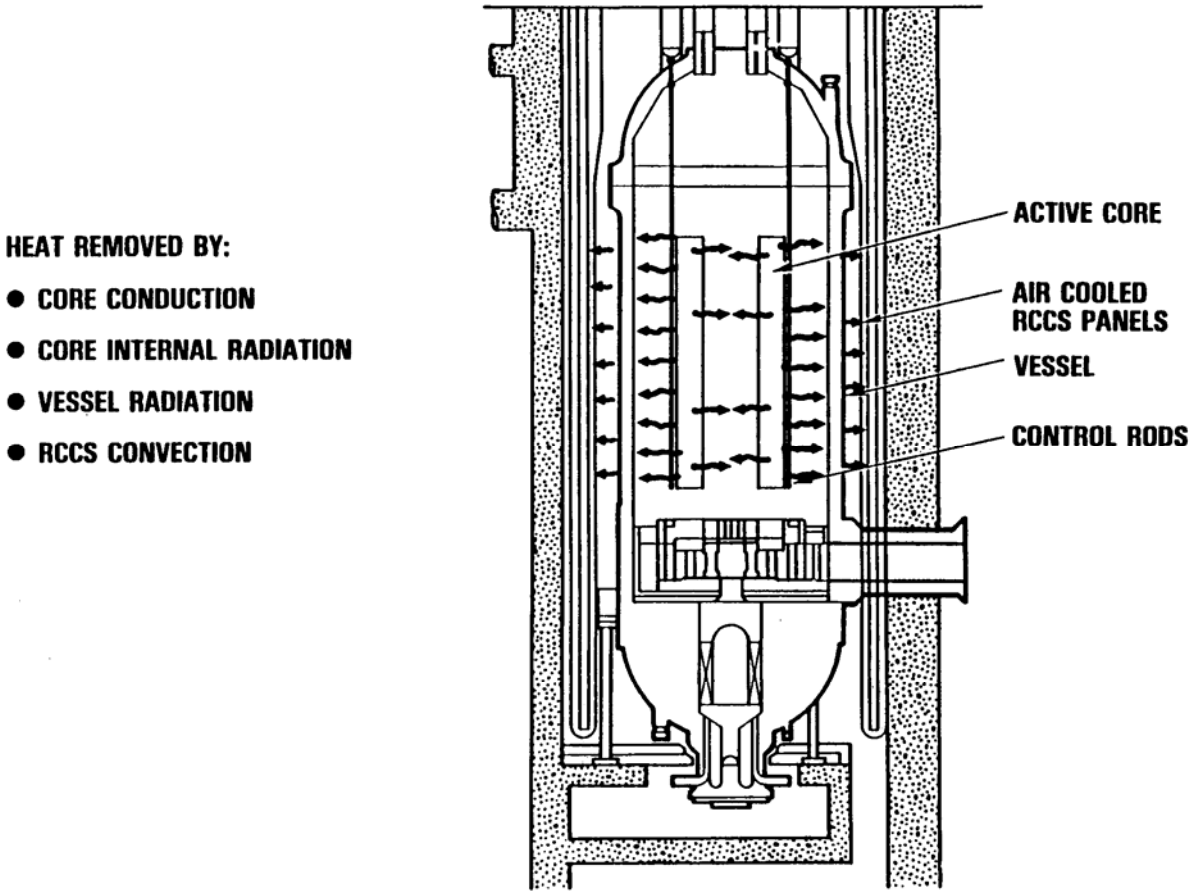

Figure 4-1. Passive Heat Removal to the RCCS During HPCC and LPCC Events

These events have been analyzed in detail for the GT-MHR, and the results have shown that peak fuel temperatures remain below the design goal of 1600°C, and the temperatures for the vessel and other safety-related SSCs also remain below acceptable limits. Using the ATHENA model described in Section 3.1.4, these events were re-analyzed using the H2-MHR initial conditions. Figure 4-2 shows the calculated peak fuel temperatures for the HPCC and LPCC events. For the LPCC event, the peak fuel temperature is 1525°C and occurs about 60 hours following initiation of the event. For the HPCC event, the peak fuel temperature is 1349°C and occurs about 50 hours following initiation of the event. As shown in Fig. 4-3, the calculated peak vessel temperatures for the HPCC and LPCC events were approximately 478°C and 517°C, respectively. For both events, the peak vessel temperatures occurred about 72 hours following initiation of the event.

These results are consistent with previous results for the GT-MHR and show that the H2-MHR should retain the passive safety characteristics of the GT-MHR.

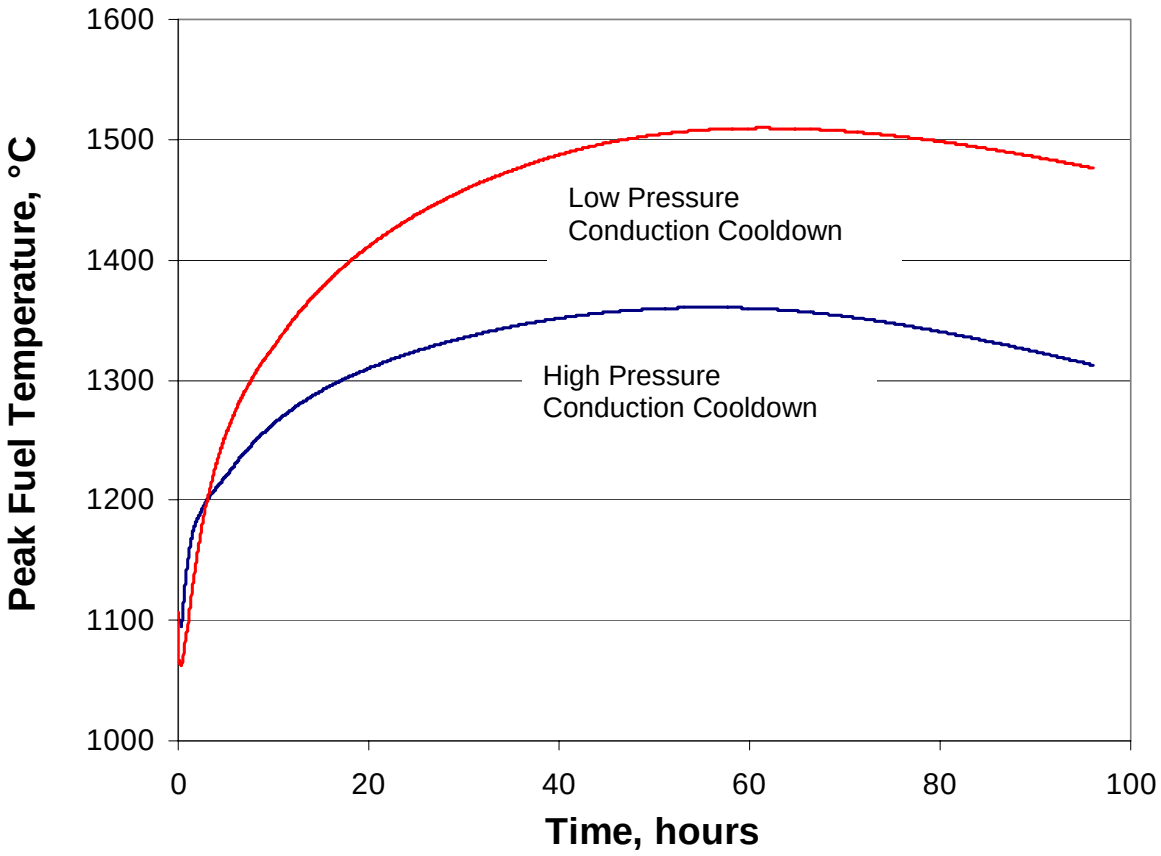

Figure 4-2. Peak Fuel Temperatures During HPCC and LPCC Events

4.2 Availability Assessment

The availability assessment accounts for scheduled outages and forced outages associated with the MHR nuclear island and the hydrogen production plant. Scheduled outages account for 526 hours per year. Forced outages account for 630 to 764 hours per year, depending on the level of redundancy for some of the dynamic components in the hydrogen production plant. These outages correspond to plant availability factors ranging from 0.85 to 0.87. The bases for these availability assessments are described in more detail in the following sections.

For large-scale deployment of nuclear hydrogen production, hydrogen storage systems could be used to meet peak demand requirements. Except during outages, the H2-MHR plants would be operated at their rated capacity. When demand is lower, some of the hydrogen would be diverted to a storage system for later use when demand is higher. For example, if hydrogen is used primarily for the transportation sector, stored hydrogen would be recovered primarily during peak driving periods (e.g., summer months).

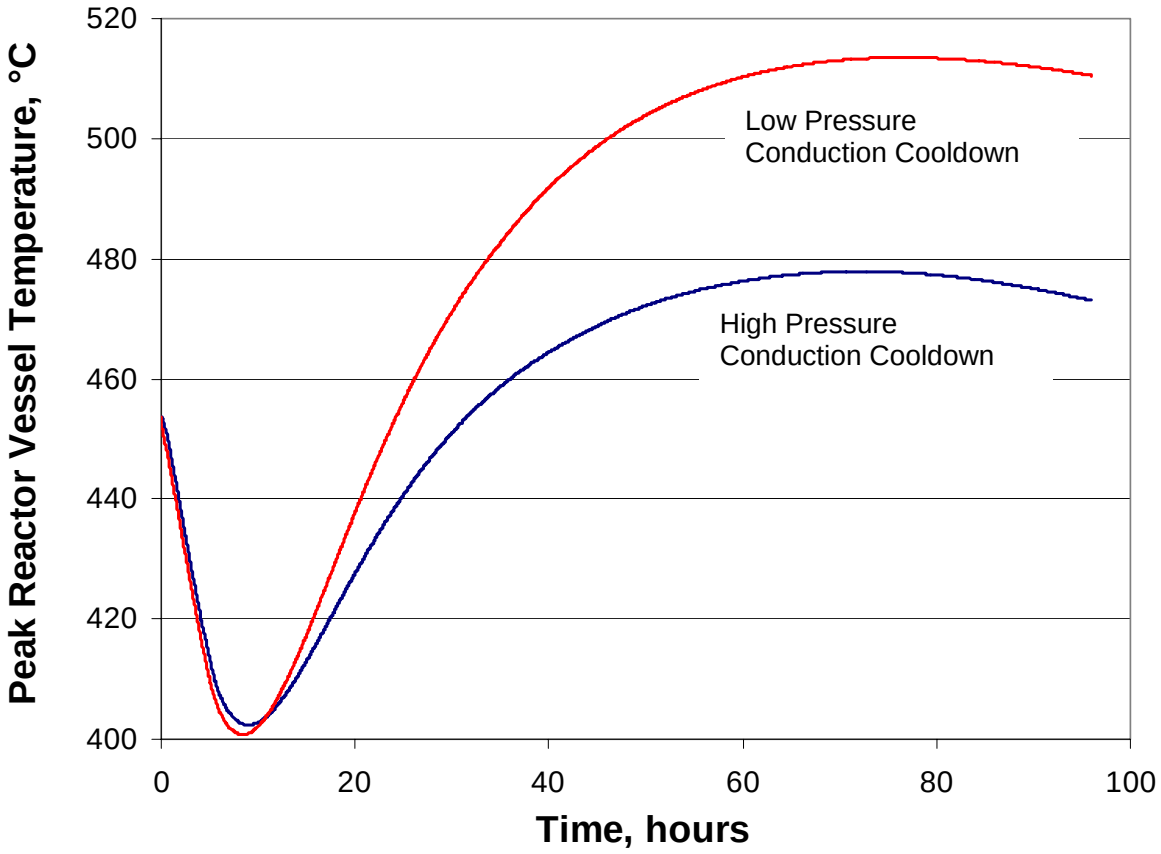

Figure 4-3. Peak Vessel Temperatures During HPCC and LPCC Events

4.2.1 Scheduled Outages

The scheduled outage assessment is based on previous studies performed for the GT-MHR and earlier MHR concepts that used a steam cycle for power conversion (Ref. 1). These studies showed that scheduled outages associated with the PCS for the GT-MHR or the circulator and steam generator associated with the steam-cycle plants could be performed simultaneously with other scheduled maintenance activities that require reactor shutdown and depressurization (e.g., refueling). This conclusion also applies to the circulators and IHX associated with the SI-based H2-MHR. A detailed scheduled outage assessment has not been performed for the hydrogen production plant, but it is expected these maintenance activities could also be performed during scheduled reactor shutdowns and hence should have no impact on the overall unavailability associated with scheduled outages. Hence, the SI-based H2-MHR scheduled outage rate is assumed to be the same as that for the GT-MHR, which was estimated to be 526 hours per year.

4.2.2 Forced Outages – MHR Nuclear Island

The MHR nuclear island forced outage assessment is also based on previous studies performed for the GT-MHR and earlier MHR concepts that used a steam cycle for power

conversion [Shenoy, 1996]. Forced outages are expressed in terms of equivalent forced outage hours (EFOH) at full power. The EFOH as a function of the major systems associated with the MHR nuclear island are given in Table 4-1. The total EFOH is 566.9.

Table 4-1. EFOH for MHR Nuclear Island System

System	EFOH
Reactor System	30.8
Vessel System	108.2
Primary Heat Transport System	112.9
Secondary Heat Transport System	112.9
Shutdown Cooling System	6.8
Helium Purification Systems	24.7
Plant Control, Data, and Instrumentation Systems	100.9
Balance of Plant and Auxiliary Systems	69.7
Total	566.9

4.2.3 Forced Outages – Hydrogen Production Plant

Forced outage assessments for the SI-based hydrogen production plant were performed using the SAPHIRE (Systems Analysis Programs for Hands-on Integrated Reliability Evaluations) code [INL, 1998]. The SAPHIRE code evolved from the Integrated Reliability and Risk Analysis System (IRRAS) code, which is a state-of-the-art, microcomputer-based probabilistic risk assessment model development and analysis tool.

Figure 4-4 shows the master fault tree for the SI-based hydrogen production process. There are three transfer gates in the master fault tree that link to the individual fault trees for each of the chemical reaction sections in the SI process (i.e., the Bunsen reaction section, the H_2SO_4 decomposition section, and the HI decomposition section). The master fault tree, when linked to the individual fault trees for each of the three separate chemical reactions, provides the basis for evaluating and improving overall plant reliability, and assessing plant availability based on component failure rates and mission times. The fault tree model has the capability to analyze the integrated process or each of the sections in the process flow sheet separately.

The SAPHIRE model assumes separate hydrogen production trains for each of the four MHR modules and consists of 27 fault trees, 115 sub-trees and 274 basic events. Several data bases were used to determine component failure rates. The Process Equipment Reliability Data by the Center for Chemical Process Safety (CCPS) of the American Institute of Chemical Engineers includes accumulated and aggregated data from nuclear power plants, chemical process industries, offshore petroleum platforms, etc. The Offshore Reliability Data (OREDA) covers reliability data from a wide range of equipment used in oil and natural gas exploration and production industries, as well as some onshore equipment. The European Industry Reliability Data Bank (EIReDA) is the reliability database for the probabilistic safety assessment of nuclear power plants in France.

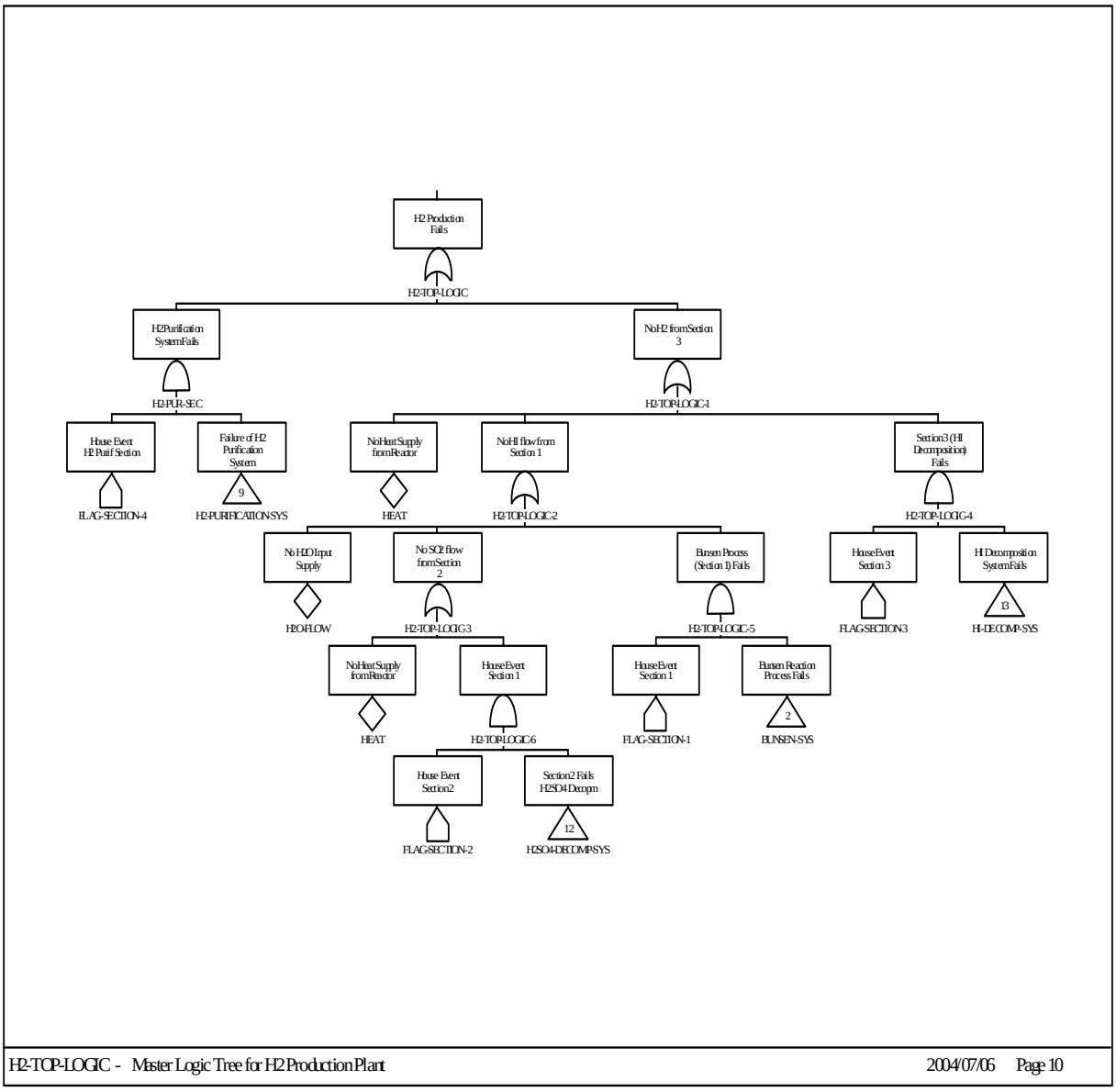

Figure 4-4. Master Fault Tree model for Hydrogen Production Process

The overall plant availability accounts for down time based on component failure probabilities and the mean repair time for failed components when no component redundancies are included. Assuming no redundancies, SAPHIRE results indicate approximately 194 EFOH, or 8 days per year. As expected, results show that single failures of dynamic components (i.e., turbines, pumps, etc.) are the biggest contributors to the system unavailability. If redundancy is included for the eleven components with highest failure probability, SAPHIRE results show that the EFOH can be reduced to about 60. For comparison, the EFOH associated with the PCS and related systems for the GT-MHR are approximately 175 [Shenoy, 1996].

4.3 Licensing Assessment

The licensability of the GT-MHR and earlier steam-cycle MHR concepts is discussed in [Shenoy, 1996]. Based on the licensing history and safety performance of HTGRs in the United States and NRC review of earlier steam-cycle MHR concepts, it is expected the GT-MHR will be licensable in the current commercial nuclear regulatory environment.

The H2-MHR is not expected to present any significant licensing challenges relative to the GT-MHR or other reactor concepts. However, a key consideration for safety and licensing of the H2-MHR is co-location of the MHR modules with a hydrogen production plant. As illustrated in Fig. 4-5, it is proposed to locate the two facilities as close as possible (within 100 m or less) in order to minimize the distance over which high-temperature heat is transferred. INL has recently performed an engineering evaluation for these separation requirements and has concluded separation distances in the range of 60 m to 120 m should be adequate in terms of safety [Smith, 2005]. Other recommendations from the INL study include a 100 kg on-site limit for hydrogen storage, use of double-walled pipes for hydrogen transport, and location of the nuclear plant control room outside of the dispersion zone for chemical release. The below-grade installation of the MHR modules, combined with an earthen berm for defense-in-depth, provide additional safety margin for co-location of the two facilities. Detailed safety assessments should be performed in the preliminary and final design phases to better define the risk envelope associated with co-location of the MHR modules and hydrogen production plant.

JAEA has performed computational fluid dynamics simulations of transport and detonation of a hydrogen cloud resulting from an accident in the hydrogen production plant. JAEA has also concluded that relatively short separation distances between the nuclear reactor and hydrogen production plant should not compromise overall plant safety, especially if an earthen berm or other barrier is placed between the nuclear reactor and hydrogen production plant [Nishihara, 2005].

4.4 Economic Assessment

The economic assessment was performed for an n^{th}-of-a-kind plant consisting of four, 600-MW(t) MHR modules coupled to a hydrogen production plant. The instantaneous hydrogen production rate is 12.97 kg/s, which corresponds to a plant hydrogen production rate of 368,300 tonnes per year at a plant capacity factor of 0.9. The baseline estimate was based on the following assumptions:

Construction time period:	36 months
Annual interest rate:	7%, compounded monthly
Fixed charge rate:	12.6% (regulated utility)
MHR plant indirect costs:	35% of direct costs
SI plant indirect costs:	20% of direct costs
MHR plant contingency costs:	5% of total (direct + indirect) construction costs
SI plant contingency costs:	10% of total (direct + indirect) construction costs

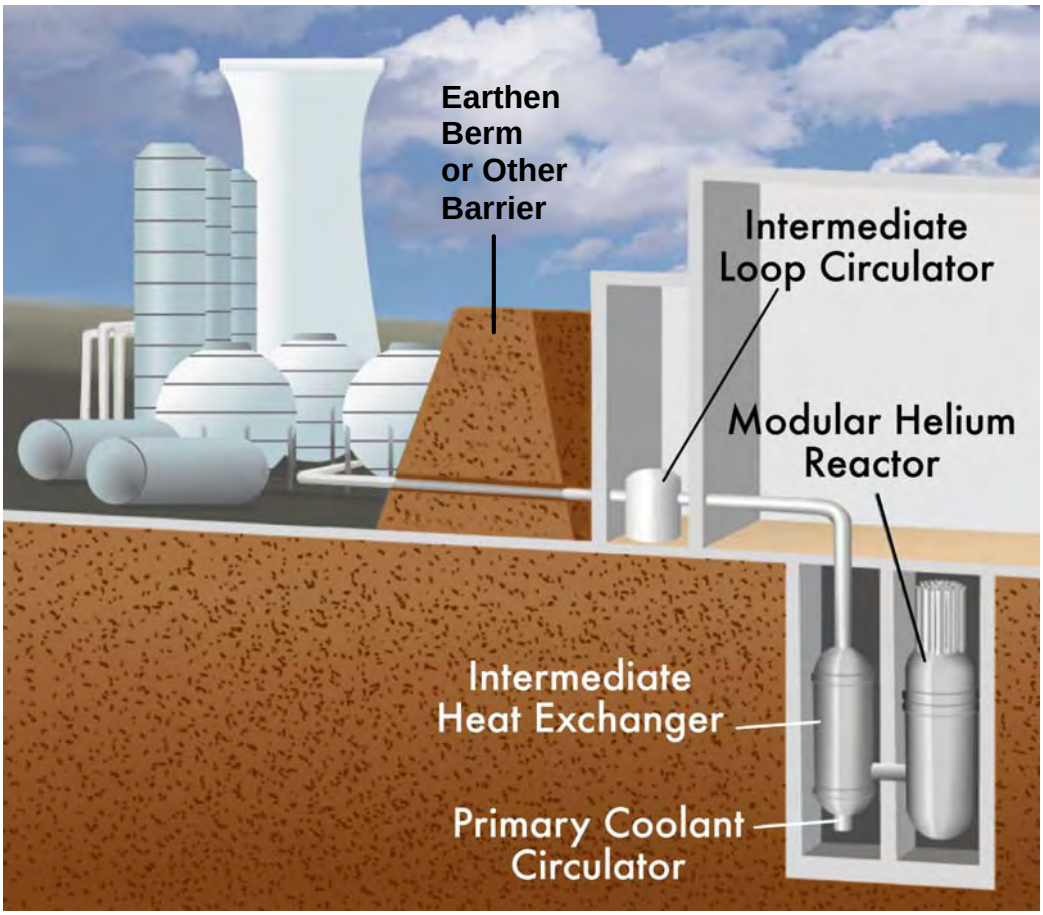

Figure 4-5. Concept for Co-Location of the MHR with Hydrogen Production

4.4.1 Capital Costs

Capital costs are summarized in Table 4-2. The total plant capital cost is estimated to be $2.51 billion, with the MHR plant accounting for $1.44 billion and the SI-based hydrogen production plant accounting for $1.07 billion. The cost per kW of hydrogen (assuming a HHV of 141.9 MJ/kg) is approximately $1,360. The MHR equipment costs are based on scaling previous estimates for the GT-MHR, removing costs associated with the PCU, and increasing costs of some reactor internal equipment to account for the use of higher-temperature materials and thermal hydraulic design optimization [Summers, 2004]. Capital costs for the Primary and Secondary HTS were developed independently. Capital costs for the SI plant equipment are based on scaling previous estimates [(Brown, 2003), (Summers, 2004)], accounting for flow sheet modifications, an increase in the hydrogen production rate, and equipment scale up to reduce the number of parallel trains and associated capital costs. Capital costs were also escalated to 2005 dollars. The indirect costs account for construction services, home office engineering and services, field office engineering and services, and owner's costs. The owner's costs also include the costs associated with licensing the nuclear facility.

Table 4-2. Summary of SI-Based H2-MHR Plant Capital Costs

Account Description	**Costs, $M**
MHR System Capital Costs	
Structures and Improvements	142.1
MHR Equipment	319.5
Electrical Equipment	44.7
Miscellaneous Plant Equipment	30.1
Heat Rejection System	38.5
Primary HTS Capital Costs	
Primary Coolant Circulator	60.0
IHX	100.0
IHX Vessel	40.0
Primary Helium Services System	5.0
Secondary HTS Capital Costs	
Secondary Coolant Circulator	70.0
Secondary HTS Piping	25.0
Secondary Helium Services System	4.0
Secondary HTS Isolation Valves	20.0
Residual Heat Removal System	16.0
Total MHR Plant Direct Costs	914.9
Total MHR Plant Indirect Costs	320.2
Total MHR Plant Base Construction Costs	1,235.1
Contingency	61.8
Overnight MHR Plant Construction Costs	1,296.9
Interest During Construction	141.6
Total MHR Plant Capital Investment	1,434.4
SI Plant Capital Costs	
Section 1 (Bunsen Reaction)	35.0
Section 2 (H_2SO_4 Decomposition)	59.2
Section 3 (HI Decomposition)	243.8
Vapor Recompression Equipment	312.0
Auxiliary Equipment	25.0
Iodine Inventory	58.2
Total SI Direct Costs	733.2
Total SI Indirect Costs	146.6
Total SI Plant Base Construction Costs	897.8
Contingency	88.0
Overnight SI Plant Construction Costs	967.8
Interest During Construction	105.7
Total SI Plant Capital Investment	1,073.5
Total Plant Capital Investment	2,450.2
	$ per kW of H_2 based on HHV
Installed Capital Cost	1,364.3

4.4.2 Operations and Maintenance Costs

Operations and maintenance (O&M) costs are summarized in Table 4-3. With the exception of electricity costs, the O&M costs given in Table 4-3 are based assumptions used for previous estimates [(Brown, 2003), (Summers, 2004)]. As discussed in Section 3.4.3, the plant requires 812 MW(e) of electricity, mostly for shaft work associated with the SI process. The cost of this electricity accounts for approximately 66% of the plant O&M costs. For the baseline estimate, it is assumed the H2-MHR plant is part of an energy park that includes electricity-producing GT-MHRs, and the electricity is supplied at a busbar cost of $ 0.035/kW(e)-hr.

Table 4-3. Summary of SI-Based H2-MHR Plant O&M Costs

Account Description	Costs, $M/yr
MHR O&M Costs	
Reactor Operations	31.4
Decommissioning	6.0
Total MHR O&M Costs	37.4
SI Plant O&M Costs	
Water Supply	3.7
Operating Labor	5.1
Supervisory and Clerical Labor	0.8
Maintenance and Repairs	44.0
Operating Supplies	6.0
Laboratory Charges	0.8
Taxes	14.7
Administrative Costs	1.0
Total SI Plant O&M Costs	76.6
Nuclear Fuel Costs	71.2
Electricity Costs	224.1
Total Plant O&M Costs	338.1

4.4.3 Hydrogen Production Costs

The hydrogen production costs are summarized in Table 4-4 and Fig. 4-6. The fixed-charge rate was assumed to be 12.6%, which corresponds to a regulated utility [Summers, 2004]. The baseline hydrogen production cost is estimated to be $1.97/kg. The cost of electricity accounts for approximately 30% of the hydrogen production cost.

Table 4-4. Summary of SI-Based H2-MHR Plant Hydrogen Production Costs

Account	Cost ($M/yr)	Percent of Total
MHR Plant Capital Charges	181.2	24.9
SI Plant Capital Charges	135.3	18.6
MHR Plant O&M Costs	37.4	5.2
SI Plant O&M Costs	76.6	10.6
Nuclear Fuel Costs	71.2	9.8
Electricity Costs	224.1	30.9
Total Annual Costs	725.8	
	kg/yr	
Hydrogen Produced	3.68×10^8	
	$/kg	
Hydrogen Production Cost	1.97	

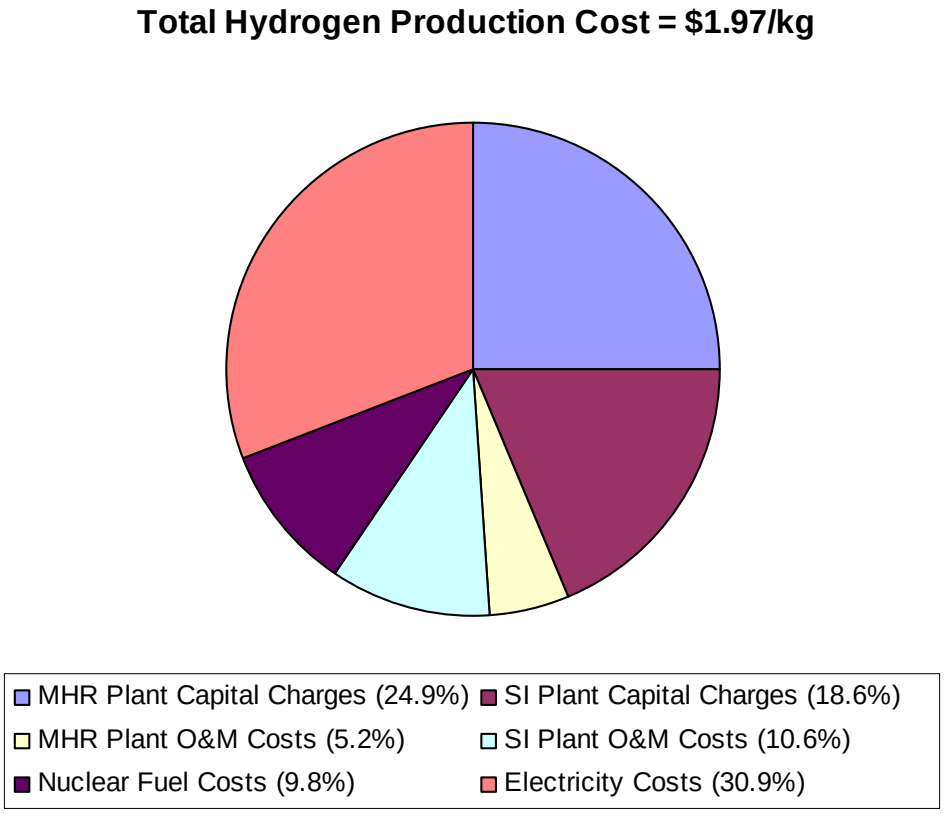

Figure 4-6. SI-Based H2-MHR Plant Hydrogen Production Costs (Baseline Estimate)

4.4.4 Parametric Studies

Parametric studies were performed to determine the sensitivity of the hydrogen production costs and efficiency to (1) the shaft worked required for the SI process, (2) the thermal efficiency to produce electricity, (3) construction time, (4) fixed charged rate, and (5) external electricity cost. As shown in Table 4-5, the shaft work required by the SI process has a significant influence on both hydrogen production efficiency and cost. A 25% reduction in the required shaft work reduces the hydrogen production cost by about $0.17/kg. The cost reductions result from both a reduced cost of electricity and lower capital costs for vapor recompression equipment. If the required shaft work could be reduced by 50%, the hydrogen production cost would drop from the baseline estimate of $1.97/kg to $1.62/kg. If electricity were supplied by conventional LWRs operating with 32% thermal efficiency, the overall plant efficiency drops from 45.0% to 37.3% because of the additional heat required to produce the electricity at lower efficiency. Assuming that LWRs and GT-MHRs provide electricity at the same cost, the thermal efficiency for producing electricity has no impact on hydrogen production and plant capital costs. Increasing the construction time from 36 to 60 months results in higher interest charges, but the increase in hydrogen production cost is only $0.07/kg. Increasing the fixed charge rate from 12.6% to 16.6 % (which is representative of an unregulated utility) results in an increase in hydrogen production cost of $0.27/kg. Increasing the cost of external electricity from $0.035/kW(e)-hr to $0.05/kW(e)-hr (which is representative of costs for a large-scale industrial user) increases the hydrogen production cost by $0.26/kg.

Table 4-5. Results of H2-MHR Plant Economic Parametric Studies

Parameters		Overall Hydrogen Production Efficiency (%)	Capital Cost $/kW-$H_2$ (HHV)	Hydrogen Production Cost ($/kg)
Shaft work required for SI process, MW(t)	684	45.0	1364.3	1.97
	513	49.5	1325.0	1.80
	342	55.1	1279.9	1.62
Thermal efficiency to produce external electricity, MW(e)/MW(t)	0.48	45.0	1364.3	1.97
	0.32	37.3	1364.3	1.97
Construction time, months	36	45.0	1364.3	1.97
	48	45.0	1414.8	2.00
	60	45.0	1467.3	2.04
Fixed charge rate, %	12.6	45.0	1364.3	1.97
	16.6	45.0	1330.8	2.24
External electricity costs, $/kW(e)-hr	0.035	45.0	1364.3	1.97
	0.05	45.0	1364.3	2.23

Note: Shaded rows indicate parameters and results for the baseline estimate.

4.4.5 Comparison with Steam-Methane Reforming

Figure 4-7 shows a comparison of nuclear hydrogen production costs with the costs for producing hydrogen using steam-methane reforming (SMR). The overall reaction for steam-methane reforming produces 1 mole of CO_2 for every 4 moles of H_2 produced:

$$CH_4 + 2H_2O \rightarrow 4H_2 + CO_2$$

Because of environmental concerns associated with CO_2 emissions, future SMR plants may be required to sequester and dispose of CO_2. The cost of CO_2 sequestration and disposal is uncertain. For this comparison, sequestration/disposal costs of $30 and $50 per tonne of CO_2 were assumed, which is consistent with a previous study performed by the Electric Power Research Institute [EPRI, 2003].[9] These costs correspond to additions of $0.16 and $0.27 per kg of H_2 produced. For hydrogen produced using nuclear energy, oxygen is a byproduct that potentially could produce additional revenue. For this comparison, an oxygen credit of $20 per tonne of O_2 was assumed, which is also consistent with the previous EPRI study [EPRI, 2003]. This credit corresponds to $0.16 per kg of H_2 produced.

In December 2005 the wellhead price for natural gas was $10.02 per 1000 cubic feet, which corresponds to $9.72/MMBtu.[10] At this price, nuclear hydrogen production is economically competitive with SMR. If a CO_2 sequestration/disposal cost and an O_2 credit are assumed, nuclear hydrogen production is economically competitive with SMR for natural gas prices in the range $6 to $8/MMBtu.

[9] For most SMR plants, approximately 25% of the CH_4 feedstock is burned to provide the heat required for hydrogen production, which increases the CO_2 production rate by about 25%. However, it is not practical to separate CO_2 from atmospheric nitrogen in the burner flue gas. For this study, additional costs associated with CO_2 emissions taxes were not considered.

[10] Natural gas prices are available from the U.S. DOE Energy Information Administration website (http://www.eia.doe.gov/). The unit MMBtu is a “thousand thousand” Btu, or one million Btu.

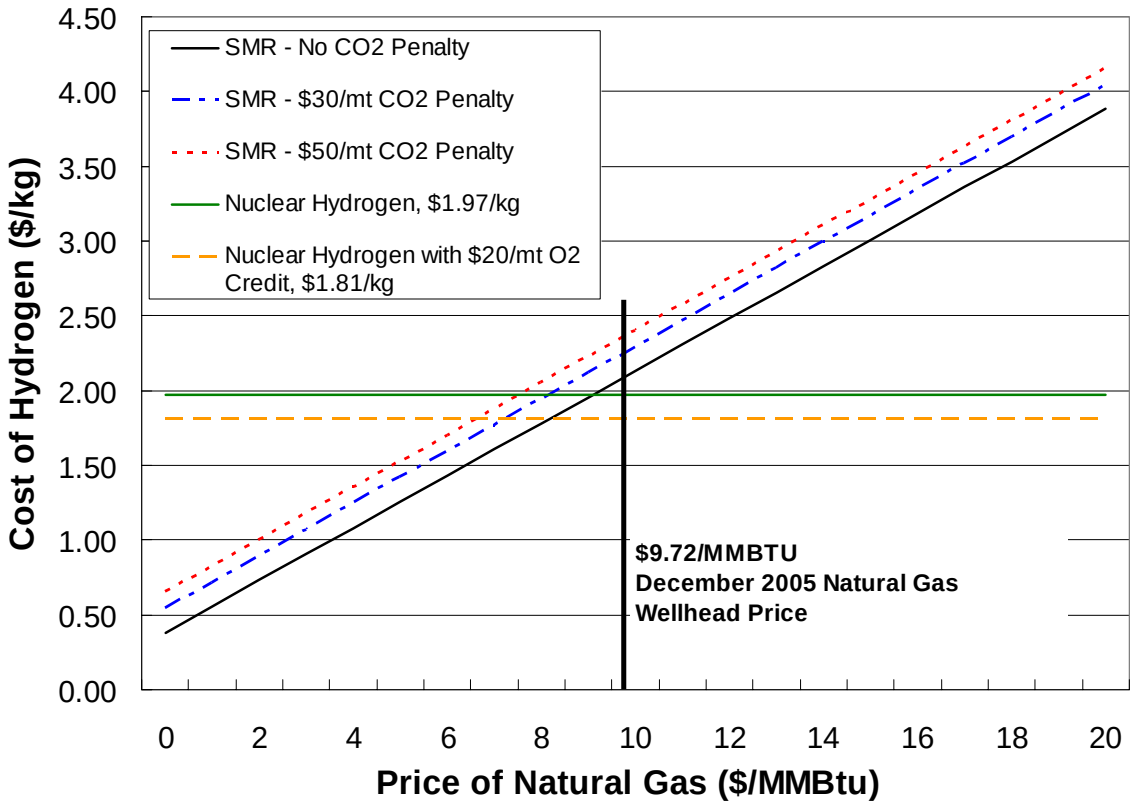

Figure 4-7. Comparison of Nuclear and SMR Hydrogen Production Costs

5. Technology Development and Risk Reduction

Based on this pre-conceptual design study, the H2-MHR is capable of producing hydrogen economically, safely, and with minimal environmental impact. It is recommended that the H2-MHR design development be continued through the conceptual, preliminary, and final design phases. Also, it is recommended that future H2-MHR design work be closely coupled with ongoing and planned technology-development programs, in order to ensure that the data obtained by these programs satisfies specific needs of the H2-MHR design. Key areas for technology development include:

- Pilot-scale demonstration and control of the SI process at high efficiency.
- SI process materials development.
- SI process heat exchangers and reaction vessels.
- Development of high-temperature reactor-internal components, including control rods with C-C composite cladding and bypass flow sealing keys.
- IHX demonstration.
- Fuel development and qualification.
- High-temperature circulator demonstration.
- HTIV demonstration.

Many of these areas are being addressed by ongoing technology-development programs in the U.S. ([Schultz, 2004], [DOE, 2005], and [Petti, 2005]), Japan, and other countries. Unfortunately, these programs are not integrated and are not driven by the Design Data Needs (DDNs) to support a specific design. As a result, some of the data obtained by these programs may not ultimately be useful for supporting the design of a practical nuclear hydrogen production plant.

The model illustrated in Fig. 5-1 is recommended for integration of design with technology development in order to maximize the benefit of the technology-development programs in terms of supporting a plant design and minimizing the technical risk of the design. This model is based on successful Engineering Development and Demonstration (ED&D) programs conducted and managed by General Atomics for DOE projects, including Accelerator Production of Tritium, the Salt Waste Processing Facility, the commercial GT-MHR, and the New Production Reactor.

As shown in Fig. 5-1, the process begins by evaluating design requirements and reviewing existing design data from a variety of sources. Design assessments and trade studies are performed, eventually leading to key design selections and a technical baseline that meets all design requirements. As indicated on Fig. 5-1, it may be reasonable to revise one or more design requirements during the process if the overall impact is small. At this point, a design has been developed that meets all requirements, but requires some technology development to confirm assumptions upon which the design is based. Also, if necessary, the process allows for an early testing path to provide early confirmation of basic assumptions. The technology development process begins with the design organization preparing DDNs, which are formal project documents that include fallback positions in the event the testing programs do not produce acceptable results or the test could not be performed for budget or other reasons. The DDNs provide a concise statement of the required data and the associated schedule, quality, and accuracy requirements. In addition to preparing DDNs, the design organization also prepares a Test Specification that defines the data requirements in more detail. The technology

organization is responsible for developing Technology Developing Plans and Test Plans for specific tests. As indicated on Fig. 5-1, the design and technology organizations work together during preparation of the DDNs, Test Specifications, Technology Development Plans, and specific Test Plans. The technology organization then conducts the technology development programs and generates the design data. If feasible, the technology organization may integrate their activities with other (e.g., international) programs in order to minimize costs. After the design data are obtained, the design and technology organizations work together to determine if the DDNs are satisfied. If the DDNs are satisfied, the key design selections and technical baseline are finalized and the design is completed. If a DDN is not satisfied, the most likely path forward is to adopt the fallback position, which could mean additional margin is added to a certain area of plant design in order to reduce technical risk. However, depending on the results of a specific test program, a more reasonable path forward may be to re-evaluate a key design selection and return to the design process. As indicated on Fig. 5-1, an Independent Review and Verification organization is established at the start of the process to provide oversight of both the design and technology development processes.

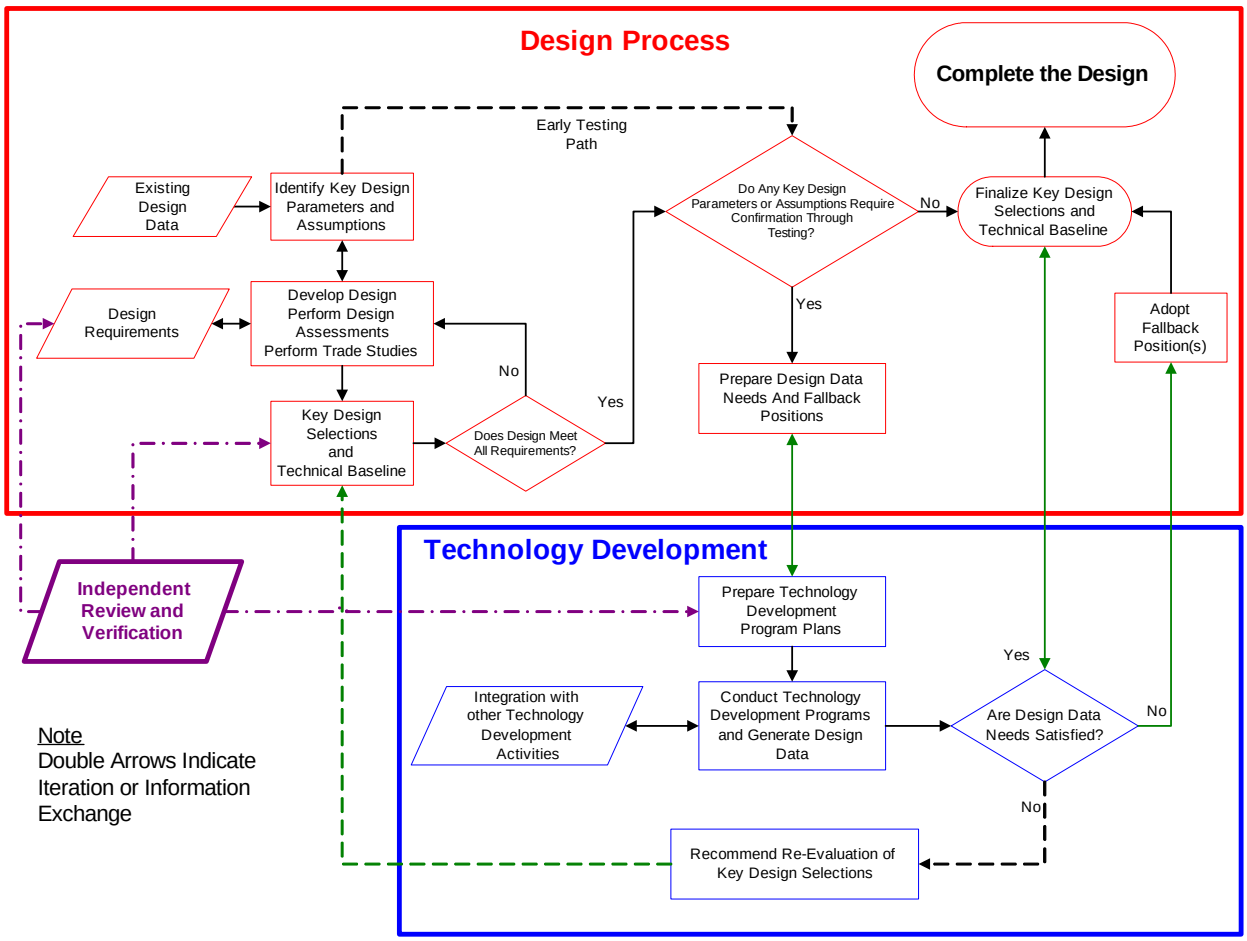

Figure 5-1. Integration of Design with Technology Development

6. References

Baxter, 2005 — Baxter, A., et al., "MHR Fuel Cycle Options for the Future Sustainability of Nuclear Power," *Proceedings of Global 2005*, October 9-13, 2005, Tsukuba, Japan, Paper 314.

Borchardt, 1982 — Borchardt, G., et al., "Experiment FRJ2-P24 Bestrahlungsbericht," Interner Bericht KFA-ZBB-IB-19/82, Kernforschungsanlage Jülich GmbH, Jülich, Federal Republic of Germany, August 1982.

Bullock, 1983 — Bullock, R.E. and J.L. Kaae, "Performance of Coated UO_2 Particles Gettered with ZrC," *J. Nuc. Mat.*, **115**, 69 (1983).

Bullock, 1984 — Bullock, R.E., "Fission-Product Release During Post irradiation Annealing of Several Types of Coated Fuel Particles," *J. Nuc. Mat*, **125**, 304 (1984).

Brown, 2003 — Brown, L.C., et al., High Efficiency Generation of Hydrogen Fuels Using Nuclear Power, GA-A24285, Rev. 1, General Atomics, San Diego, CA, December 2003.

Carlson, 1986 — Carlson, K., P. A. Roth, and V. H. Ransom, ATHENA Code Manual Volume I: Code Structure, System Models, and Solution Methods, EGG-RTH-7397, Idaho National Engineering Laboratory, Idaho Falls, ID, 1986.

DOE, 2005 — Nuclear Hydrogen Initiative Ten Year Program Plan, Department of Energy, Office of Advanced Nuclear Research, March 2005. http://neri.inel.gov/program_plans/pdfs/nhi_plan.pdf

EPRI, 2003 — High-Temperature Gas-Cooled Reactors for the Production of Hydrogen: An Assessment in Support of the Hydrogen Economy," EPRI Report 1007802, Electric Power Research Institute, Palo Alto, CA, April 2003.

Hanson, 2004 — Hanson, D. and J. Saurwein, Development Plan for Advanced High Temperature Coated-Particle Fuels, PC-000513, Rev. 0, General Atomics, San Diego, CA, 2004.

IAEA, 1997 — Fuel Performance and Fission Product Behavior in Gas Cooled Reactors, IAEA-TECDOC-978, International Atomic Energy Agency, Vienna, Austria, November 1997.

Inaba, 2005 — Inaba, Y., et al., "Study on Control Characteristics for HTTR Hydrogen Production System with Mock-up Test Facility. System Controllability Test for Fluctuation of Chemical Reaction," *Nuclear Engineering and Design*," **235**, pp, 111-121, 2005.

INL, 1998 — Systems Analysis Program for Hands on Integrated Reliability Evaluation (SAPHIRE) Version 6.0, NUREG-6116, Idaho National Laboratory, Idaho Falls, ID,1998.

Iyoku, 2005 — Iyoku, T., et al., "HTTR Test Program Towards Coupling with the SI Process," Third Information Exchange Meeting on the Nuclear Production of Hydrogen and Second HTTR Workshop on Hydrogen Production Technologies, Japan Atomic Energy Agency, Oarai, Japan, October 5-7, 2005, OECD Nuclear Energy Agency, Paris, France.

Kubo, 2005 — Kubo, S., et al., "A Bench-Scale Hydrogen Production Test by the Thermochemical Water-Splitting Iodine-Sulfur Process," *Proceedings of Global 2005*, October 9-13, 2005, Tsukuba, Japan, Paper 474.

LaBar, 2003 — LaBar, M., et al., "The Gas Turbine Modular Helium Reactor," *Nuclear News*, **Vol. 46**, *No. 11*, p. 28 (2003).

Maruyama, 1994 — Maruyama, S. et al., "Evaluation of Core Thermal and Hydraulic Characteristics of HTTR," *Nucl. Eng. Des.*, **Vol. 152**, pp. 183-196, 1994.

Minato, 1995 — MINATO, K., et al., "Review of Experimental Studies of Zirconium Carbide Coated Fuel Particles for High Temperature Gas-Cooled Reactors," *JAERI-Review-95-004*, Japan Atomic Energy Research Institute, Oarai, Japan (1995).

Myers, 1987 — Myers, B., Fuel Design Data Manual, MAN-910866, Issue F, General Atomics, San Diego, CA, August 1987.

Nishihara, 2005 — Nishihara, T., et al., "Analytical Study on Hydrogen Dispersion in the HTGR Hydrogen Production System," Proceedings of Global 2005, Tsukuba, Japan, October 9-13, 2005, Paper No. 284.

Norman, 1982 — Norman, J., et al., Thermochemical Water-Splitting Cycle, Bench-Scale Investigations and Process Engineering, Final Report for the Period February 1977 through December 31, 1981, GA-A16713, General Atomics, San Diego, CA, 1982.

Ohashi, 2005 — Ohashi, H., et al., "Current Status of Research and Development on System Integration Technology for Connection between HTGR and Hydrogen Production System at JAEA," Third Information Exchange Meeting on the Nuclear Production of Hydrogen and Second HTTR Workshop on Hydrogen Production Technologies, Japan Atomic Energy Agency, Oarai, Japan, October 5-7, 2005, OECD Nuclear Energy Agency, Paris, France.

Petti, 2005 — Petti, D., et al., Technical Program Plan for the Advanced Gas Reactor Fuel Development and Qualification Program, INL/EXT-05-00465, Rev. 1, Idaho National Laboratory, Idaho Falls, ID, August 2005.

Richards, 2004 — Richards, M., et al., "Thermal Hydraulic Design of a Modular Helium Reactor Core Operating at 1000°C Coolant Outlet Temperature," *Proceedings of the 6th International Conference on Nuclear Thermal Hydraulics, Operations and Safety (NUTHOS-6)*, October 4-8, 2004, Nara, Japan, Atomic Energy Society of Japan, Tokyo, Japan, 2004.

Schultz, 2004 — Schultz, R., et al., Next Generation Nuclear Plant – Design Methods Development and Validation Research and Development Program Plan, INEEL/EXT-04-02293, Idaho National Engineering and Environmental Laboratory, Idaho Falls, ID, September 2004.

Shenoy, 1996 — Shenoy, A.S., GT-MHR Conceptual Design Description Report, RGE-910720, Rev. 1, General Atomics, San Diego, CA, July 1996.

Smith, 2005 — Smith, C., et al., An Engineering Analysis for Separation Requirements of a Hydrogen Production Plant and High-Temperature Nuclear Reactor, INL/EXT-05-00317, Rev. 0, Idaho National Laboratory, Idaho Falls, ID, USA, March 2005.

Summers, 2004 — Summers, W., et al., Centralized Hydrogen Production from Nuclear Power: Infrastructure Analysis and Test-Case Design Study, Interim Project Report, Phase A Infrastructure Analysis, NERI Project 02-160, WSRC-TR-2004-00318, Rev. 0, Westinghouse Savannah River Company, Savannah River National Laboratory, Aiken, SC, July 2004.

Summers, 2006 — Summers, W., et al., Centralized Hydrogen Production from Nuclear Power: Infrastructure Analysis and Test-Case Design Study, Final Project Report, Phase B Test-Case Preconceptual Design, NERI Project 02-160, WSRC-MS-2005-00693, Rev. 0, Westinghouse Savannah River Company, Savannah River National Laboratory, Aiken, SC, February 2006.

Terada, 2005 — Terada, A., et al., “Development of Hydrogen Production Technology by Thermo-Chemical Water Splitting Process – Pilot Test Plan,” *Proceedings of Global 2005*, October 9-13, 2005, Tsukuba, Japan, Paper 427.

Appendix A
Advanced Fuels

ZrC-TRISO Fuel

The conventional TRISO coating consists of four layers and three materials; a low-density pyrolytic carbon layer (buffer), an inner high-density pyrolytic carbon layer (IPyC), an SiC layer, and an outer high-density pyrolytic carbon layer (OPyC). Based on the data obtained from a limited number of irradiation tests, there is some evidence that ZrC may be a more effective than SiC as a barrier to fission product release at high temperatures [Minato, 1995]. For this reason, ZrC-TRISO fuel was evaluated as a potential option for the H2-MHR. As indicated in Fig. A-1, use of ZrC will have a negative impact on the neutron economy because of its higher absorption cross section in the 10^2 to 10^5 eV neutron energy range. To quantify this effect, a the MHR core physics design was analyzed using ZrC-TRISO fuel in place of the reference SiC-TRISO fuel. The results showed Zr behaves like a nonburnable poison, and its effects can be compensated for by reducing the amount of B_4C fixed burnable poison that is normally loaded into the core for reactivity control and power shaping. Figure A-2 shows reactivity (k-effective) as a function of irradiation time for cores fueled with SiC-TRISO- and ZrC-TRISO-coated particles. For the ZrC-TRISO fueled core, the reactivity associated with lumped burnable poison was reduced by 14% to compensate for the additional poisoning caused by Zr. Based on this assessment, ZrC-TRISO fuel remains a viable option to achieve higher operating temperatures for the H2-MHR core.

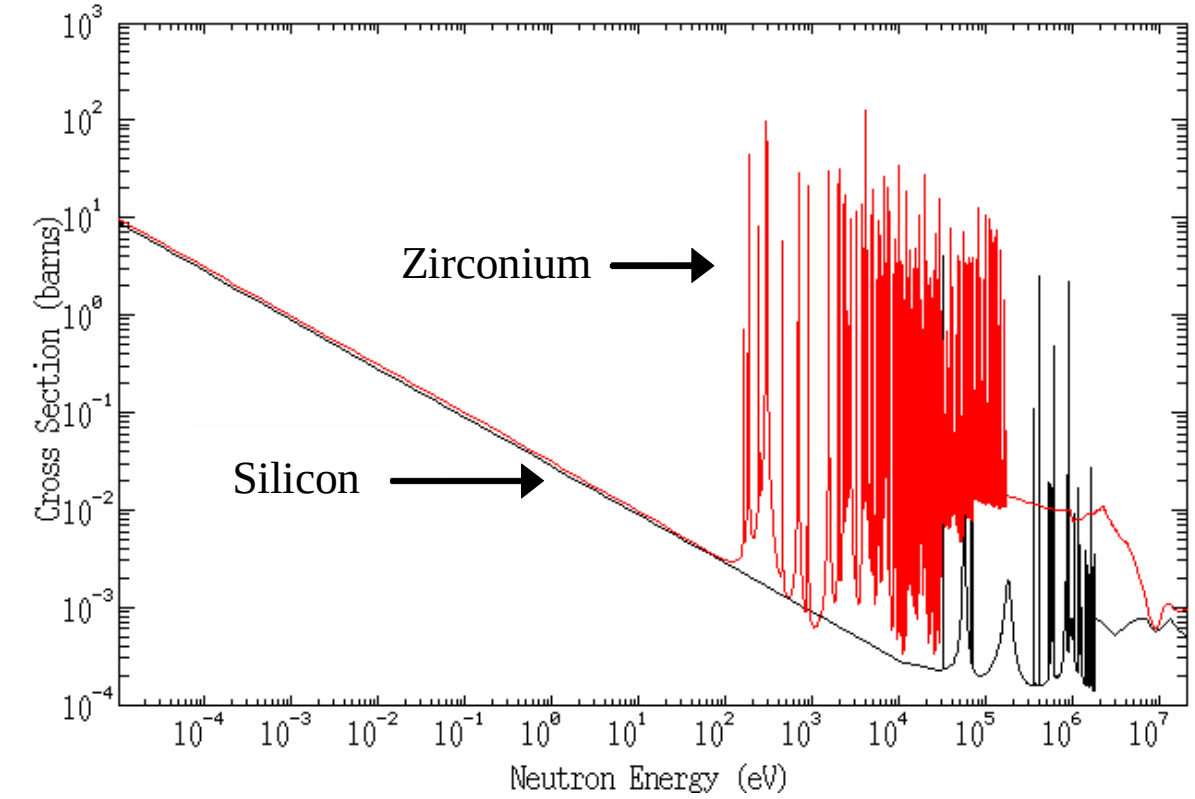

Figure A-1. Neutron Total Absorption Cross Sections for Silicon and Zirconium

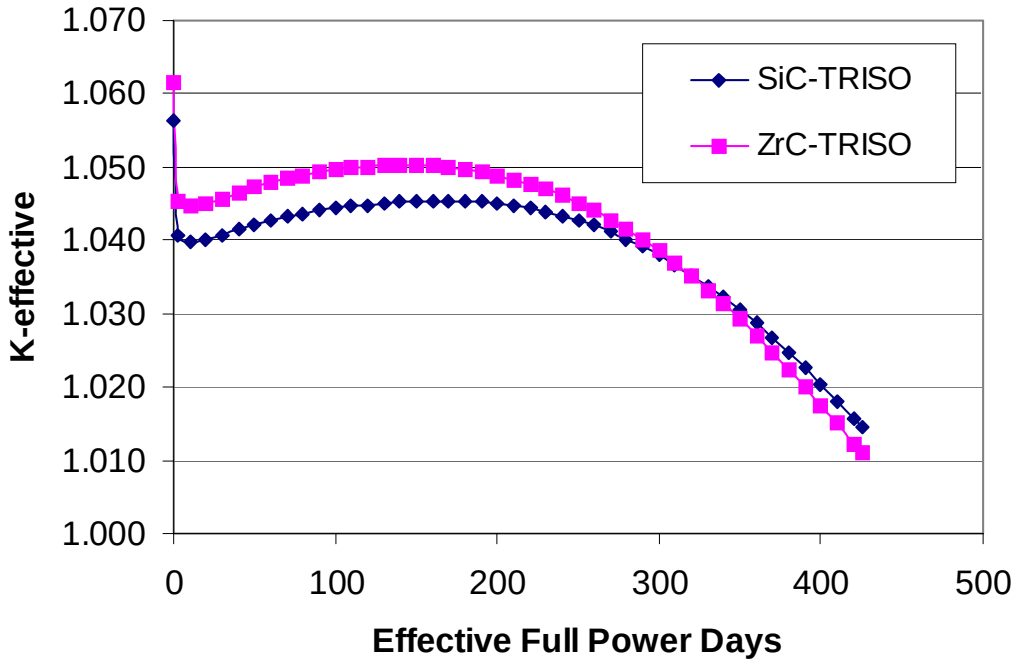

Figure A-2. Core Reactivity as a Function of Irradiation Time

ZrC-Gettered, TRISO Fuel

In the U.S., the use of ZrC as an oxygen getter was investigated during irradiation testing of SiC-TRISO particles with UO_2 kernels [Bullock, 1983]. Two types of ZrC-gettered fuel were tested; one with ZrC dispersed in the buffer and one with a thin (~10 µm) ZrC layer deposited outside the kernel. For both designs, a pyrocarbon seal coat was first deposited directly over the kernel to protect it from chemical attack by chlorine compounds that are generated during deposition of ZrC. For the latter design, an additional function of the ZrC was to suppress kernel swelling during irradiation. The particles were irradiated in both loose-particle and compact form at temperatures in the range 900°C – 1200°C, out to burnups in the range 21 – 27% FIMA and fast neutron fluences in the range 3.4×10^{25} – 6.6×10^{25} n/m^2. Irradiation times were approximately 170 d. Results are summarized below.

- For both particle designs, overall performance was good, with no evidence of kernel migration or pressure-vessel failure, indicating the ZrC was an effective oxygen getter.

- Growth features, consisting primarily of carbon, were observed in the kernel, but they did not affect performance.

- For a majority of the particles, the thin ZrC layer surprisingly remained intact. Failure of this layer was not observed in particles irradiated at ~900°C. For particles irradiated above ~1100°C , the fraction of particles with failed ZrC layers was ~25%. Kernel expansion was suppressed for particles with intact ZrC layers, and the kernels remained dense at high burnup.

- Particles with thin ZrC layers were analyzed for gamma spectra and showed excellent retention of fission products. There was some limited evidence that Ag-110m was effectively retained at high irradiation temperatures.

Figure A-3 shows the typical postirradiation appearance of a particle with a thin ZrC layer surrounding the kernel.

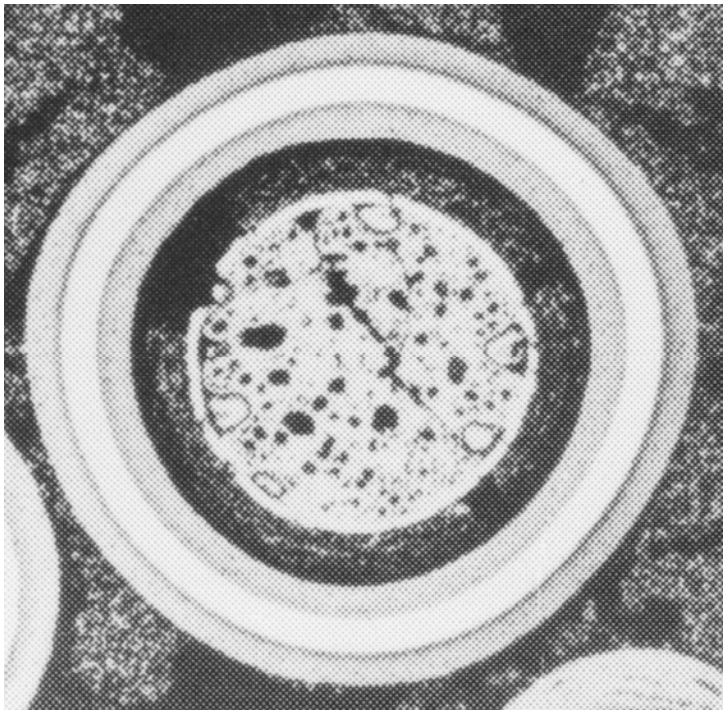

Figure A-3. Cross Section of an Irradiated ZrC-gettered, SiC-TRISO Particle. The irradiation conditions were 1020°C, 20% FIMA, and fast neutron fluence of 3.7×10^{25} n/m^2. The ZrC was deposited as a thin layer surrounding the kernel.

To further investigate the possibility that ZrC can effectively retain Ag, a test was performed in which particles previously irradiated at ~900°C were heated at 1500°C for 10,000 h [Bullock, 1984]. In addition to both ZrC-gettered designs, SiC-TRISO fuels with UC_2, UO_2, and UCO kernels were tested for comparison. Ten particles of each type were tested. Release of Eu-154, Ag-110m, Cs-134, and Ce-144 was measured at various times during the heating test. The particles with the thin ZrC layer were the only ones to be completely retentive of all nuclides. The other fuel types all released Ag-110m and Eu-154 at significant levels. Particles with UC_2 kernels released Cs-134 and Ce-144 at significant levels, and particles with UO_2 kernels released Cs-134 at significant levels. The superior performance of the particles with thin ZrC layers is not completely understood. One explanation is the ZrC layer remained intact and was an effective barrier to release, possibly because of its higher density relative to SiC (6.7 vs. 3.2 g/cm^3). Another possibility is that because the kernel remains dense when constrained by an intact ZrC layer, the fission products are effectively trapped within the kernel.

Appendix B
Publications

The following publications were prepared during the course of this NERI project:

1. M.B. Richards, A.S. Shenoy, F. Venneri, M.P. LaBar, K.R. Schultz, and L.C. Brown, “The Modular Helium Reactor for Future Energy Needs,” submitted to ICAPP ’06, Reno, NV, June 4-8, 2006, Paper 6154.

2. S.M.M. Reza, E.A. Harvego, M. Richards, and K.L. Peddicord, “Design of an Alternative Inlet Flow Configuration for the Modular Helium Reactor,” submitted to ICAPP ’06, Reno, NV, June 4-8, 2006, Paper 6338.

3. E.A. Harvego, S.M.M. Reza, M. Richards, and A. Shenoy, “An Evaluation of Reactor Cooling and Coupled Hydrogen Production Processes Using the Modular Helium Reactor,” accepted for publication in *Nuclear Engineering and Design*.

4. M. Richards, A. Shenoy, K. Schultz, L. Brown, E. Harvego, M. McKellar, F. Okamoto, N. Handa, J. Coupey, and S. Reza, “Conceptual Designs for MHR-Based Hydrogen Production Systems,” Proceedings of Global 2005, Tsukuba, Japan, Oct. 9-13, 2005, paper 190.

5. M. Richards, A. Shenoy, K. Schultz, L. Brown, E. Harvego, M. McKellar, J. Coupey, S. Reza, F. Okamoto, and N. Handa, “H2-MHR Conceptual Designs Based on the SI Process and HTE,” Proceedings of the NEA-OECD Third Information Exchange Meeting on Nuclear Production of Hydrogen and Second HTTR Workshop on Hydrogen Production Technologies, Japan Atomic Energy Agency, Oarai, Japan, October 5-7, 2005. Accepted for publication in *International Journal of Nuclear Hydrogen Production and Applications*.

6. M.B. Richards, A. Shenoy, and E. Harvego, "Conceptual Design of an MHR Plant Used to Produce Hydrogen," *ANS Transactions*, Vol. 92, pp. 104-105, 2005.

7. M. Richards, A. Shenoy, K. Schultz, L. Brown, F. Okamoto, Y. Kiso, N. Handa, and R. Kato, “The H2-MHR: Nuclear Hydrogen Production Using the Modular Helium Reactor,” Proceedings of ICAPP ’05, Seoul, Korea, May 15-19, 2005.

8. E. Harvego, S. Reza, M. Richards, and A. Shenoy, “Hydrogen Production Using the Modular Helium Reactor,” proceedings of ICONE-13, Beijing, China, May 16-20,2005, paper ICONE13-50281.

9. M. Richards, A. Shenoy, Y. Kiso, N. Tsuji, N. Kodochigov, and S. Shepelev, “Thermal Hydraulic Design of a Modular Helium Reactor Core Operating at 1000°C Coolant Outlet Temperature,” *Proceedings of the 6th International Conference on Nuclear Thermal Hydraulics, Operations and Safety (NUTHOS-6)*, October 4-8, 2004, Nara, Japan, Atomic Energy Society of Japan, Tokyo, Japan (2004).

10. M. Richards, A. Shenoy, K. Schultz, L. Brown, G. Besenbruch, N. Handa, and J. Das, “Assessment of MHR-Based Hydrogen Energy Systems,” proceedings of the 15th World Hydrogen Energy Conference, Yokohama, Japan, June 27 – July 2, 2004.

11. M. Richards, A. Shenoy, and K. Schultz, “MHR-Based Hydrogen Production Systems,” Proceedings of ICAPP ’04, Pittsburgh, PA, June 13-17, 2004, paper 4312.

12. M. Richards and A. Shenoy, “Hydrogen Generation Using the Modular Helium Reactor,” Proceedings of ICONE12, Arlington, VA, April 25-29, 2004, paper ICONE12-49228.

13. M. Richards and A. Shenoy, “Hydrogen Production Plant Using the Modular Helium Reactor,” Proceedings of the AIChE 2003 Spring National Meeting, New Orleans, LA, April 2003.

Part 2

H2-MHR Pre-Conceptual Design Report: HTE-Based Plant, General Atomics Report GA-A25402, April 2006.

H2-MHR

GA-A25402

Hydrogen
Production
Modular Helium
Reactor

H2-MHR Pre-Conceptual Design Report: HTE-Based Plant

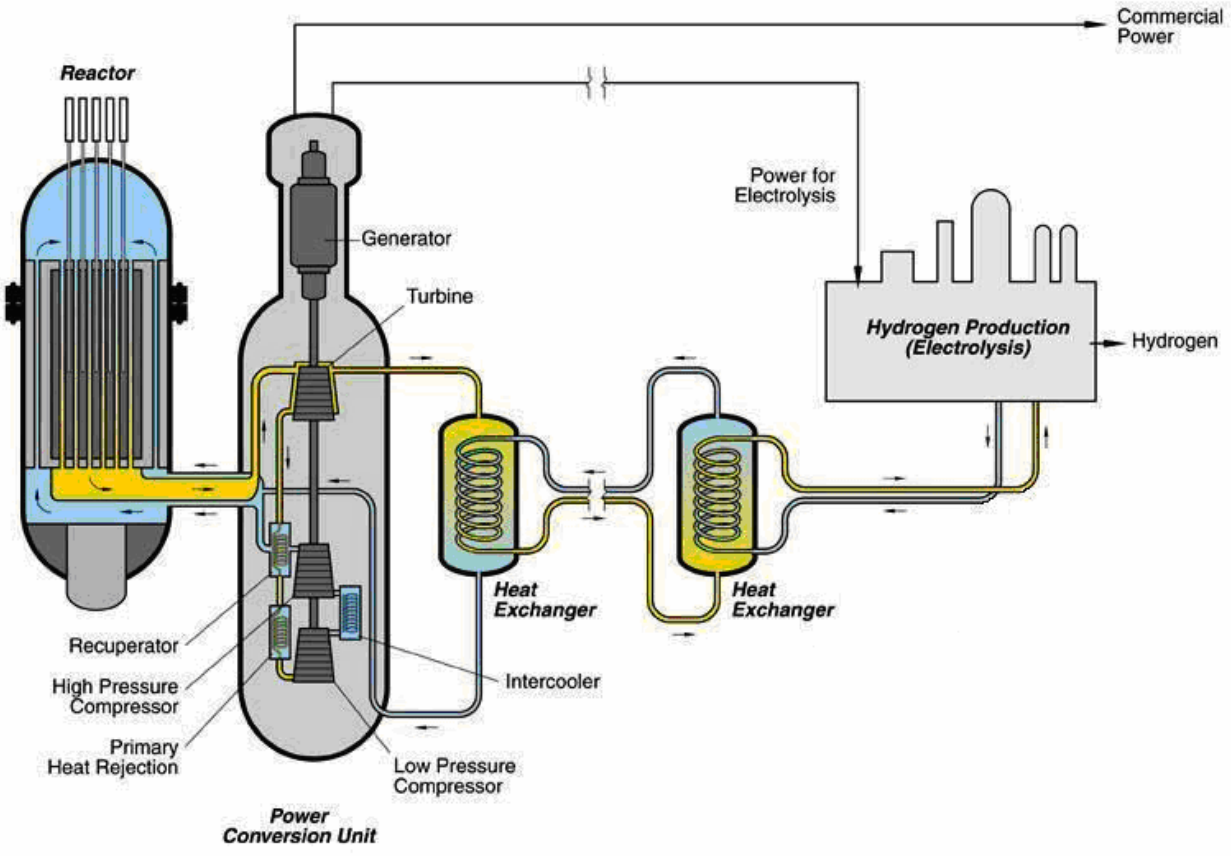

GENERAL ATOMICS

Idaho National Laboratory
Texas A&M University

US DOE Contract No. DE-FG03-02SF22609/A000
Nuclear Energy Research Initiative

April 2006

DISCLAIMER

H2-MHR PRE-CONCEPTUAL DESIGN REPORT: HTE-BASED PLANT

FINAL TECHNICAL REPORT FOR THE PERIOD SEPTEMBER 2002 THROUGH SEPTEMBER 2005

by

M.B. Richards, A.S. Shenoy, E.A. Harvego,[†]
M.G. McKellar,[†] K.L. Peddicord,[‡]
S.M.M. Reza,[‡] and J.P. Coupey[‡]

[†]Idaho National Laboratory, Idaho Falls, ID
[‡]Texas A&M University, College Station, TX

US DOE Contract No. DE-FG03-02SF22609/A000
Nuclear Energy Research Initiative
Project 2002-196

General Atomics Project 30165

GA-A25402

April 2006

GENERAL ATOMICS

EXECUTIVE SUMMARY

Hydrogen and electricity are expected to dominate the world energy system in the long term. The world currently consumes about 50 million metric tons of hydrogen per year, with the bulk of it being consumed by the chemical and refining industries. The demand for hydrogen is expected to increase, especially if the U.S. and other countries shift their energy usage towards a hydrogen economy, with hydrogen consumed as an energy commodity by the transportation, residential, and commercial sectors. However, there is strong motivation to not use fossil fuels in the future as a feedstock for hydrogen production, because the greenhouse gas carbon dioxide is a byproduct and fossil fuel prices are expected to increase significantly.

For electricity and hydrogen production, an advanced reactor technology receiving considerable international interest is a modular, passively-safe version of the high-temperature, gas-cooled reactor (HTGR), known in the U.S. as the Modular Helium Reactor (MHR), which operates at a power level of 600 MW(t). For electricity production, the MHR operates with an outlet helium temperature of 850°C to drive a direct, Brayton-cycle power-conversion system (PCS) with a thermal-to-electrical conversion efficiency of 48 percent. This concept is referred to as the Gas Turbine MHR (GT-MHR). For hydrogen production, both electricity and process heat from the MHR are used to produce hydrogen. This concept is referred to as the H2-MHR.

The growing international interest in the MHR concept is the direct result of MHR design features, which include:

(1) Passive Safety, Competitive Economics, and Siting Flexibility. The MHR does not require active safety systems to ensure public and worker safety. The high-energy conversion efficiency of the MHR, combined with the elimination of active safety systems, result in a design that is passively safe and economically competitive with other non-passively safe reactor concepts. Because of its high efficiency, the MHR rejects less waste heat than other reactor concepts. This design feature, combined with passive safety, allows for more flexible siting options for the MHR.

(2) High Temperature Capability and Flexible Energy Outputs. The MHR is capable of producing process-heat temperatures of 950°C and higher. This high-temperature capability translates into a high-energy conversion efficiency for a variety of energy outputs, including electricity, hydrogen production, and synthetic fuel production.

(3) Flexible Fuel Cycles. The MHR can operate efficiently and economically with several different fuel cycles. MHR designs have been developed utilizing low-enriched (LEU) uranium fuels, high-enriched uranium (HEU) fuels, mixed uranium/thorium and plutonium/thorium fuels, and surplus weapons-grade plutonium fuels. The thermal neutron spectrum of the MHR, combined with robust, ceramic-coated particle fuel, allow for very high burnup in a single pass through the reactor. More recently, an MHR design has been developed to deeply burn plutonium and other transuranic (TRU) actinides recovered from light-water reactor (LWR) spent fuel. The flexible fuel cycle capability of the MHR, combined with its flexible energy output capability (see Fig. E-1), result in a design concept that is very well suited for a wide variety of energy-growth scenarios.

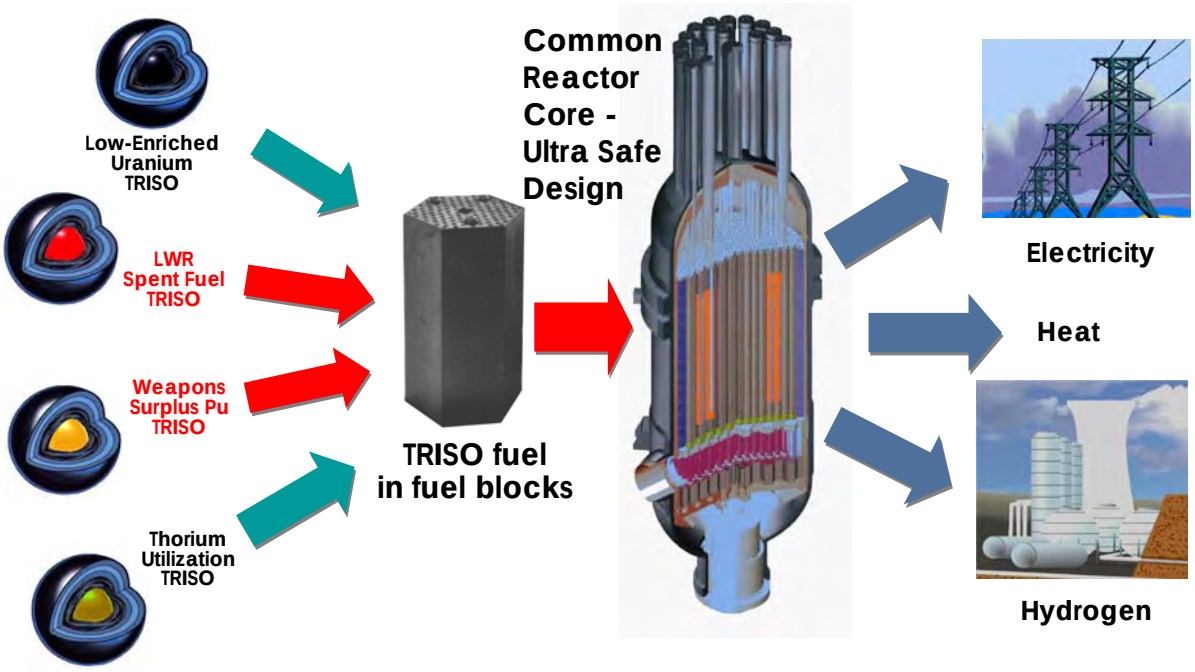

Fig. E-1. MHR Fuel Cycle and Energy Output Options

Nuclear Hydrogen Production

In principle, nuclear electricity can be used to split water using conventional low-temperature electrolyzers. For a conventional LWR that produces electricity with approximately 33% thermal efficiency and current generation electrolyzers operating with an efficiency of about 75% to convert electricity to high-pressure hydrogen, the overall efficiency for hydrogen production is approximately 25%. If a GT-MHR is used to produce the electricity with 48% thermal efficiency, the overall efficiency for hydrogen production improves to 36%. However, even with high-efficiency electricity production, economic evaluations of coupling nuclear energy to low-temperature electrolysis have generally not been favorable when compared to steam-methane reforming (SMR). For these reasons, two concepts that make direct use of the MHR high-temperature process heat are being investigated in order to improve the efficiency and economics of hydrogen production. The first concept involves coupling the MHR to the Sulfur-Iodine (SI) thermochemical water splitting process and is referred to as the SI-Based H2-MHR. The second concept involves coupling the MHR to high-temperature electrolysis (HTE) and is referred to as the HTE-Based H2-MHR. Both processes have the potential to produce hydrogen with high efficiency and have been proven to work at the laboratory scale. This report provides a pre-conceptual design description of a full-scale, n^{th}-of-a-kind HTE-Based H2-MHR plant, as illustrated in Fig. E-2. The SI-Based H2-MHR is described in a separate report.

Overall Plant Design

As shown in Fig. E-3, Modular Helium Reactors (MHRs) supply both the heat to generate steam and the electricity to split the steam into hydrogen and oxygen. Electricity is generated using a direct, Brayton-cycle power-conversion system (PCS). Approximately 90% of the heat generated by the MHR modules is used to produce electricity. The remainder of the heat is transferred though an intermediate heat exchanger (IHX) to produce steam. As indicated in

Fig. E-3, steam is supplied to both the anode and cathodes sides of the electrolyzers. The steam supplied to the cathode side is split into hydrogen and oxygen. The oxygen is transferred through the electrolyte to the anode side. The steam supplied to the anode side is used to sweep the oxygen from electrolyzer modules. The steam supplied to the cathode side is first mixed with a small portion of the hydrogen stream in order to ensure reducing conditions and prevent oxidation of the electrodes. Heat is recuperated from both the hydrogen/steam and oxygen/steam streams exiting the electrolyzer. A small quantity of electricity is generated from the oxygen/steam stream to provide power for plant house loads. The full-scale plant includes four, 600-MW(t) MHR modules. The reactor design and PCS are essentially the same as that for the GT-MHR, but with some minor modifications to allow operation with a higher coolant-outlet temperature of 950°C in order to increase hydrogen-production efficiency. Nominal plant design parameters are given in Table E-1. At a 90% capacity factor, the plant produces 2.68 × 10^5 metric tons of hydrogen per year at an efficiency of 55.8% (based on the higher heating value of hydrogen) with a product gas pressure of 4.95 MPa.

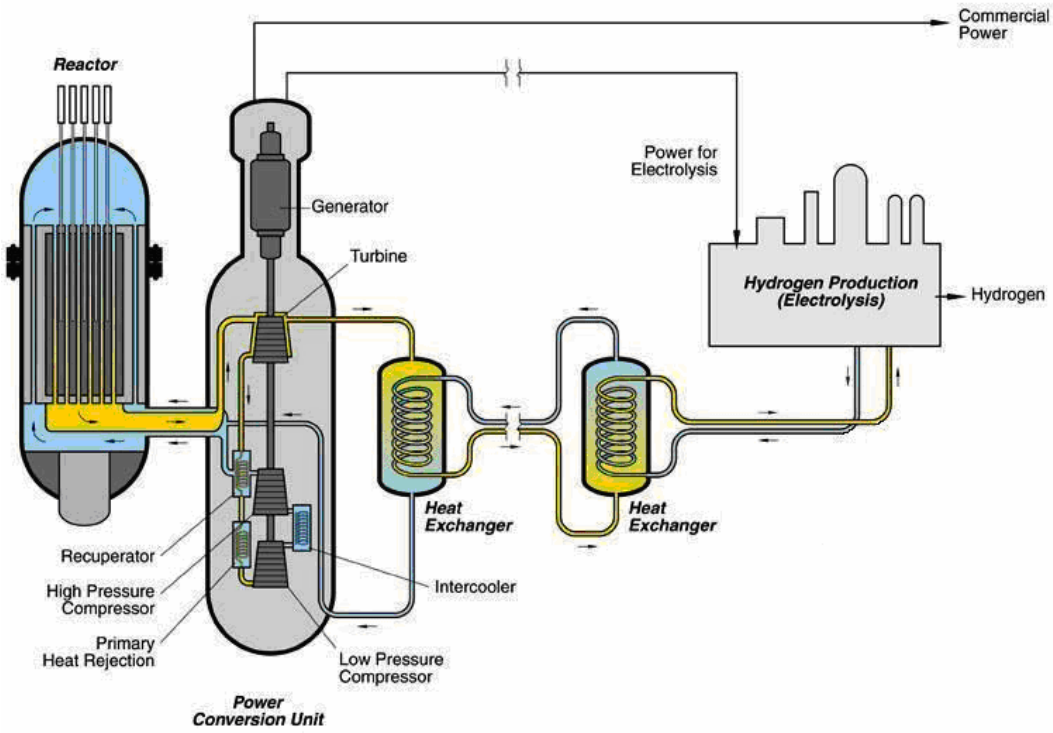

Figure E-2. HTE-Based H2-MHR Concept

Electrolysis is performed at high temperatures using solid oxide electrolyzer (SOE) modules. The module design is based on the planar cell technology (see Fig. E-4) being developed as part of a collaborative project between Idaho National Laboratory (INL) and Ceramatec of Salt Lake City, UT. Stacked assemblies of 100-mm × 100-mm cells have been tested successfully at INL and design parameters have been developed for a 12.5 kW(e), 500-cell stack. An SOE module would contain 40 500-cell stacks and consume 500 kW(e). Eight modules could be installed within a structure that is similar in size to the trailer portion of a typical tractor-trailer. Approximately 292 of these 8-module units would be required for a full-scale plant with four 600-MW(t) MHR modules. Figure E-5 illustrates this SOE module concept.

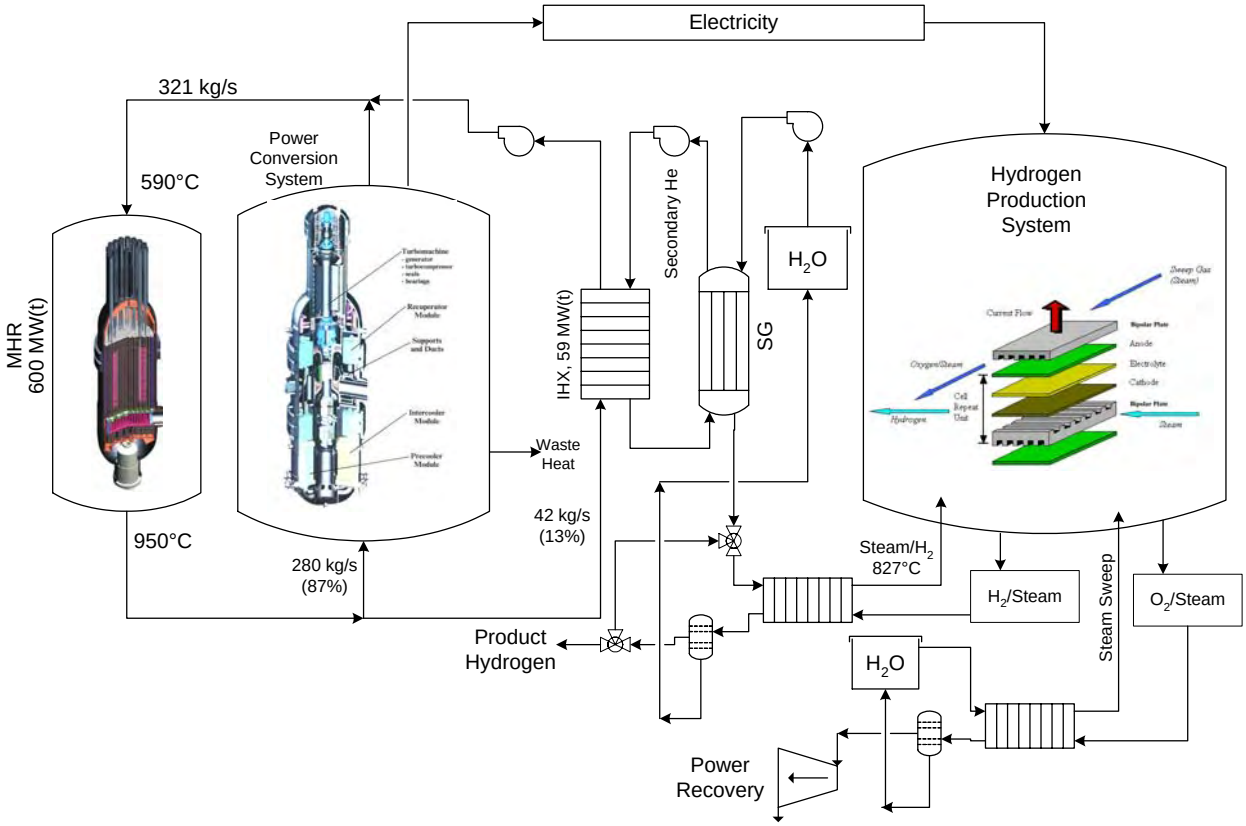

Figure E-3. HTE-Based H2-MHR Process Schematic

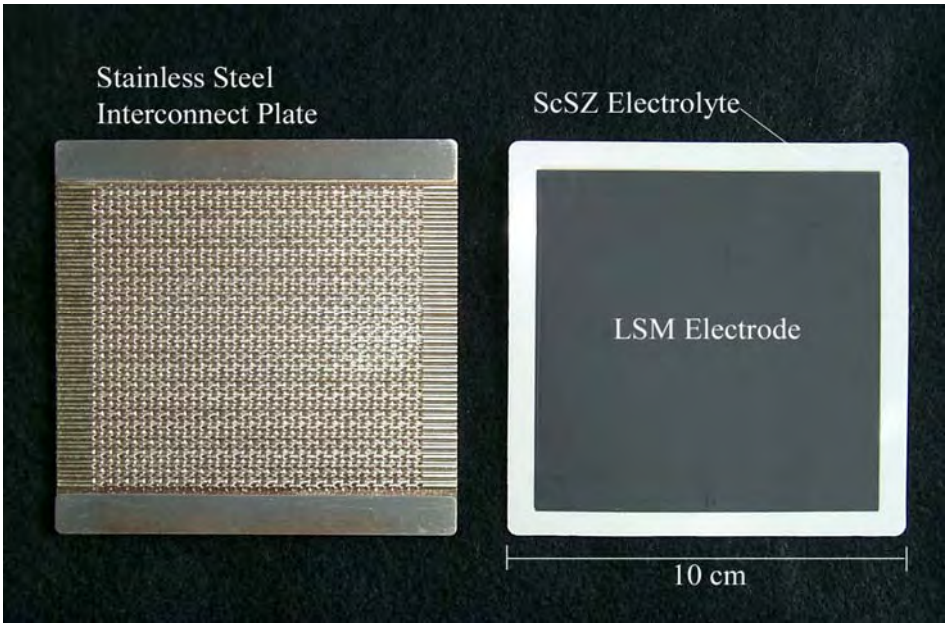

Figure E-4. Interconnect Plate and Single SOE Cell

Table E-1. H2-MHR Nominal Plant Design Parameters

MHR System	
Number of modules	4
Module power rating	600 MW(t)
Core inlet/outlet temperatures	590°C / 950°C
Peak fuel temperature – normal operation	1250°C - 1350°C
Peak fuel temperature – accident conditions	< 1600°C
Helium mass flow rate	321 kg/s
Total MHR System pressure drop	80 kPa
Power Conversion System	
Mass flow rate	280 kg/s
Heat supplied from MHR System	542 MW(t)
Turbine inlet/outlet temperatures	950°C / 600°C
Turbine inlet/outlet pressures	7.0 MPa / 2.8 MPa
Generator efficiency	98 %
Electricity generated	292 MW(e)
Electricity generation efficiency*	53.9%
Heat Transport and Recovery System	
Primary helium flow rate	42 kg/s
Secondary helium flow rate	18.1 kg/s
IHX heat duty	59 MW(t)
IHX primary side inlet/outlet temperatures	950°C / 679°C
IHX secondary side inlet/outlet temperatures	292°C / 917°C
Steam production rate	23.6 kg/s
Mass flow rate of hydrogen added to steam	0.3 kg/s
Temperature of steam/hydrogen supplied to SOE	827°C
Hydrogen Production System	
Peak SOE temperature	862°C
Peak SOE pressure	5.0 MPa
Product hydrogen pressure	4.95 MPa
Annual hydrogen production**	2.68×10^5 metric tons
Plant hydrogen production efficiency*, ***	55.8%

* Neglects parasitic heat losses from the Reactor Cavity Cooling System and Shutdown Cooling System.
** Based on a 4-module plant and an overall plant capacity factor of 90%.
*** Based on the higher heating value of hydrogen (141.9 MJ/kg).

GT-MHR Design and Passive Safety Features

The GT-MHR design is shown in Fig. E-6. Passive safety features of the MHR include the (1) ceramic, coated-particle fuel that maintains its integrity at high temperatures during normal operation and loss of coolant accidents (LOCAs); (2) an annular graphite core with high heat capacity that limits the temperature rise during a LOCA; (3) a relatively low power density that

helps to maintain acceptable temperatures during normal operation and accidents; (4) an inert helium coolant, which reduces circulating and plateout activity; and (5) a negative temperature coefficient of reactivity that ensures control of the reactor for all credible reactivity insertion events. The fuel, the graphite, the primary coolant pressure boundary, and the low-pressure vented containment building provide multiple barriers to the release of fission products.

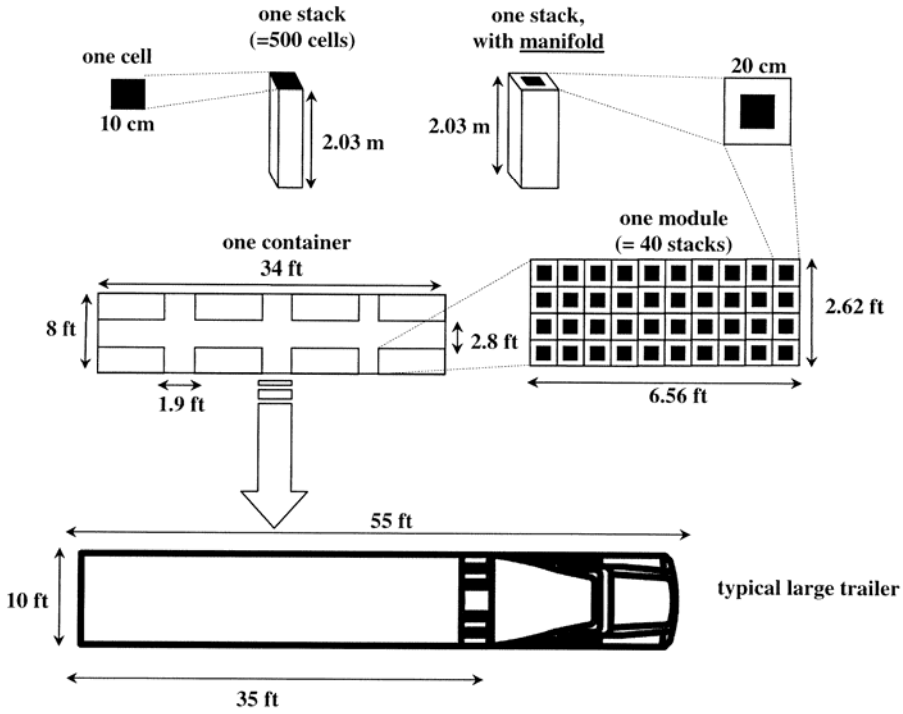

Figure E-5. SOE Module Concept

The MHR fuel element and its components are shown in Fig. E-7. The fuel for the H2-MHR consists of microspheres of uranium oxycarbide that are coated with multiple layers of pyrocarbon and silicon carbide. The H2-MHR core is designed to use a blend of two different particle types; a fissile particle that is enriched to 19.8% U-235 and fertile particle with natural uranium (0.7% U-235). The fissile/fertile loading ratio is varied with location in the core, in order to optimize reactivity control, minimize power peaking, and maximize fuel cycle length. The buffer, inner pyrolytic carbon (IPyC), silicon carbide (SiC), and outer pyrolytic carbon (OPyC) layers are referred to collectively as a TRISO coating. The coating system can be viewed as a miniature pressure vessel that provides containment of radionuclides and gases. This coating system is also an excellent engineered barrier for long-term retention of radionuclides in a repository environment.

The H2-MHR is not expected to present any significant licensing challenges relative to the GT-MHR or other reactor concepts. However, a key consideration for safety and licensing of the H2-MHR is co-location of the MHR modules with a hydrogen production plant. It is proposed to locate the two facilities as close as possible (within 100 m or less) in order to minimize the distance over which high-temperature heat is transferred. Idaho National Laboratory (INL) has recently performed an engineering evaluation for these separation

requirements and has concluded separation distances in the range of 60 m to 120 m should be adequate in terms of safety.

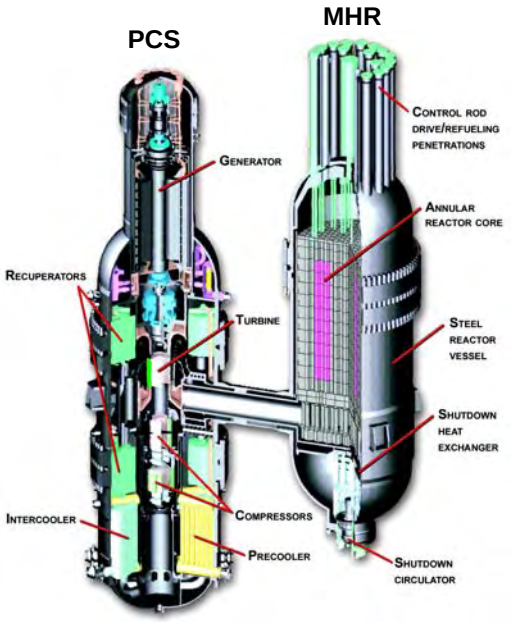

Figure E-6. GT-MHR Design

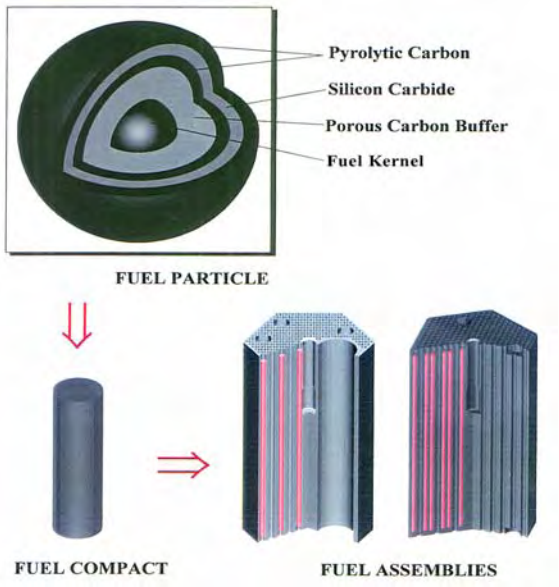

Figure E-7. MHR Fuel Element Components

Economic Evaluation

An economic evaluation was performed assuming the plant could be constructed in 36 months with an annual interest rate of 7% and a fixed charge rate of 12.6% (corresponding to a regulated utility). The capital costs of the GT-MHR Plant and Hydrogen Production Plant were estimated to be $1.42 billion and $1.16 billion, respectively, for a total H2-MHR plant capital cost of $2.58 billion. The SOE module cost was assumed to be $500/kW(e). The installed capital cost is approximately $1,920/kW-$H_2$ using the higher heating value of hydrogen (141.9 MJ/kg). The total operations and maintenance (O&M) costs are estimated to be about $119 million per year. The hydrogen production cost is estimated to be $1.92/kg. As shown in Fig. E-8, Hydrogen Production Plant capital costs contribute to about 28% of the hydrogen production cost. If the SOE module cost is increased to $1,000/kW(e), the installed capital cost and hydrogen production cost increase to $2,560/kW-$H_2$ and $2.55/kg, respectively.

Figure E-9 shows a comparison of nuclear hydrogen production costs with the costs for producing hydrogen using SMR. In December 2005 the wellhead price for natural gas was $10.02 per 1000 cubic feet, which corresponds to $9.72/MMBtu. At this price, nuclear hydrogen production is economically competitive with SMR. Nuclear hydrogen production is economically competitive with SMR for natural gas prices in the range $6 to $8/MMBtu, if a CO_2 sequestration/disposal cost for SMR and an O_2 credit for nuclear hydrogen production are assumed.

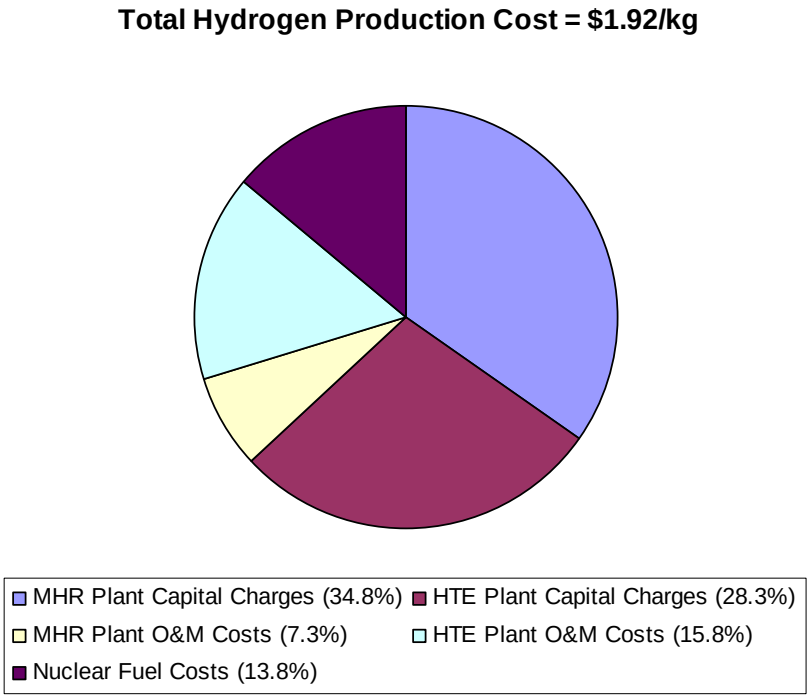

Figure E-8. Hydrogen Production Costs (Baseline Estimate)

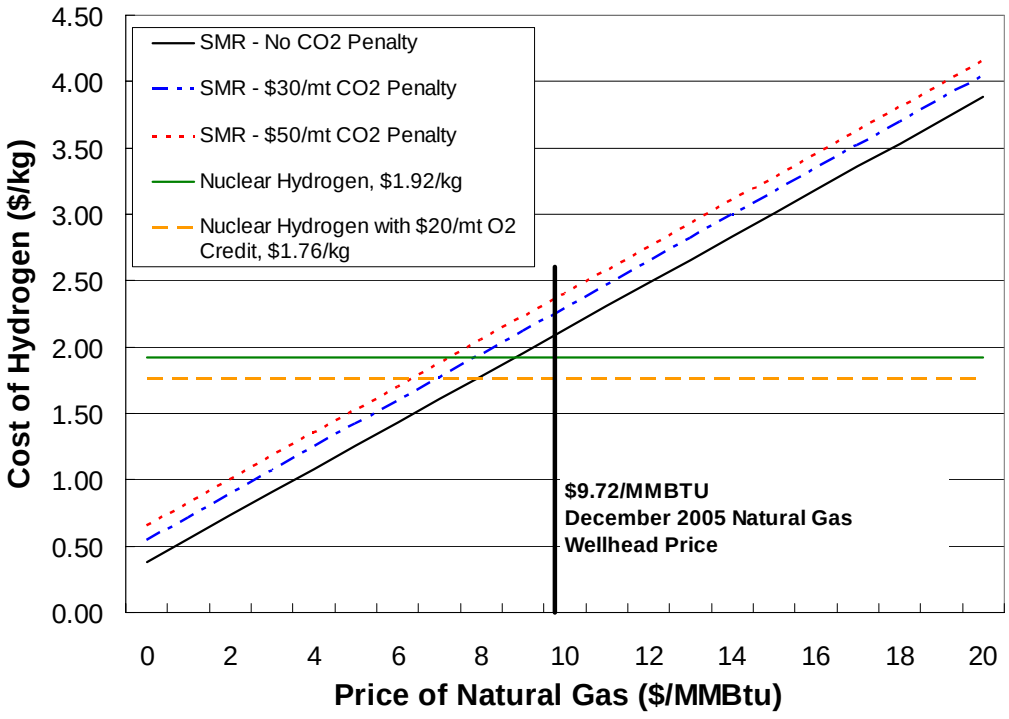

Figure E-9. Comparison of Nuclear and SMR Hydrogen Production Costs

Recommendations

Based on this pre-conceptual design study, the H2-MHR is capable of producing hydrogen economically, safely, and with minimal environmental impact. It is recommended that the H2-MHR design development be continued through the conceptual, preliminary, and final design phases. Also, it is recommended that future H2-MHR design work be closely coupled with ongoing and planned technology-development programs, in order to ensure that the data obtained by these programs satisfies specific needs of the H2-MHR design. This model for integration of design with technology development is illustrated in Fig. E-10 and is based on successful Engineering Development and Demonstration (ED&D) programs conducted and managed by General Atomics for Department of Energy projects, including Accelerator Production of Tritium, the Salt Waste Processing Facility, the commercial GT-MHR, and the New Production Reactor.

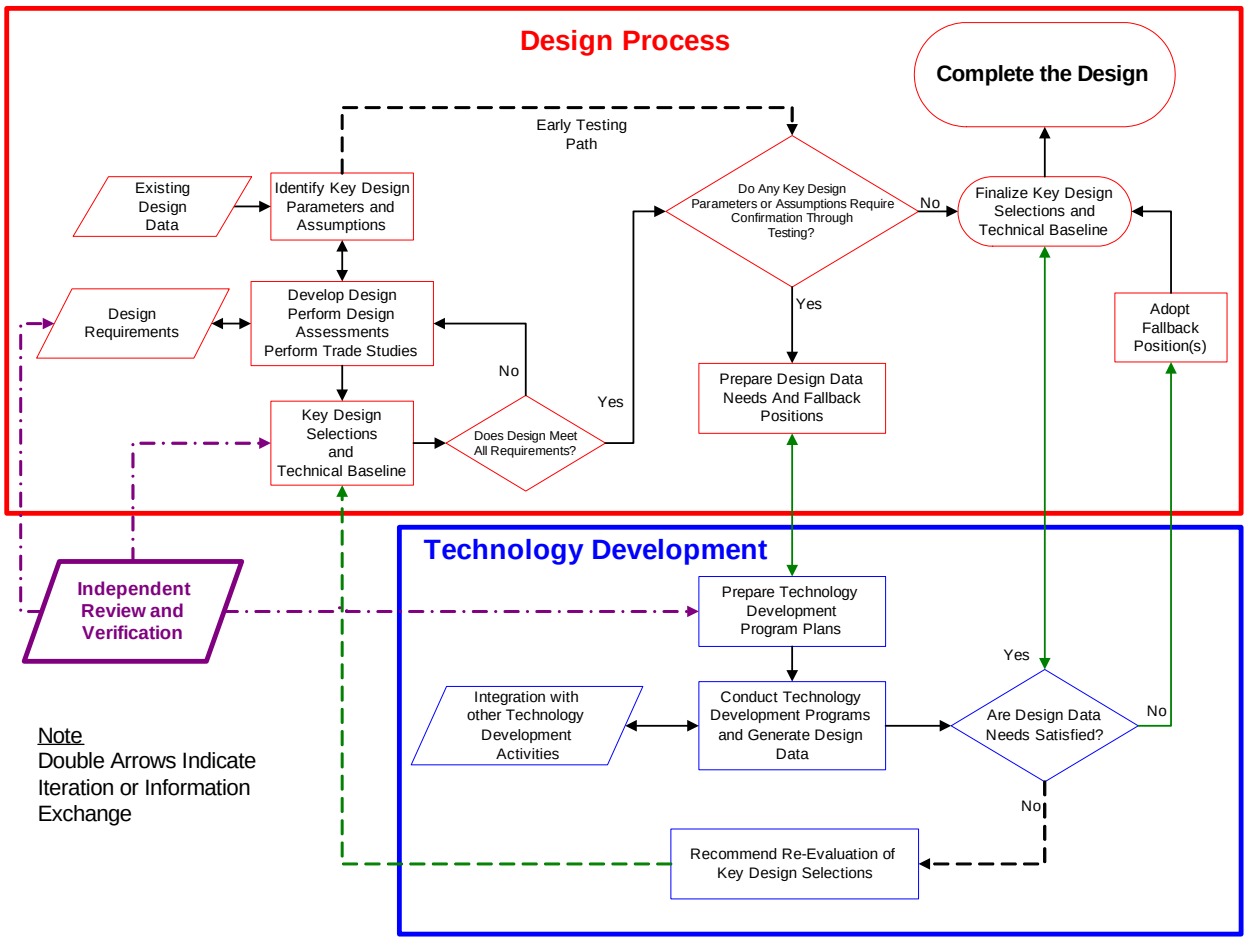

Figure E-10. Integration of Design with Technology Development

ACKNOWLEDGEMENTS

This work was funded by the U.S. Department of Energy Nuclear Energy Research Initiative (NERI), under grant DE-FG03-02SF22609/A000.

The authors would also like to acknowledge the contributions and assistance provided by Toshiba Corporation of Yokohama, Japan, Fuji Electric Systems of Kawasaki city, Japan, and the Japan Atomic Energy Agency (JAEA) of Oarai, Japan. From Toshiba Corporation, thanks are extended to Norihiko Handa and Masaru Fukuie for discussions regarding integrating the Modular Helium Reactor with High Temperature Electrolysis (HTE). From Fuji Electric Systems, thanks are extended to Futoshi Okamoto, Yoshihiro Kiso, and Nobumasa Tsuji for their help with optimizing the Modular Helium Reactor thermal hydraulic design for higher temperature operation. In 2004 and 2005, JAEA conducted very successful and very informative workshops on nuclear hydrogen production, which provided information that was very useful for this NERI project. The primary author would especially like to thank Dr. Kazuhiko Kunitomi and Dr. Tetsuaki Takeda of JAEA for their assistance and hospitality.

The HTE technology described in this report is based on the concepts being developed and tested as part of a collaborative project between Ceramatec Advanced Materials & Electrochemical Technologies of Salt Lake City, UT and Idaho National Laboratory (INL). Special thanks are extended to Dr. Ashok Joshi of Ceramatec for hosting a very informative meeting on HTE technology in December 2004 and to Dr. Steve Herring of INL.

TABLE OF CONTENTS

Executive Summary iii
Acronyms and Abbreviations xviii

1. Introduction and Background 1-1
1.1 Modular Helium Reactor Design Status 1-2
1.2 Hydrogen Production Using High-Temperature Electrolysis 1-4
2. Overall Plant Description 2-1
2.1 Plant Level Functions and Performance Requirements 2-1
2.2 Work Breakdown Structure and Responsibility Assignment Matrix 2-5
2.3 Overall Plant Arrangement 2-7
2.4 Nominal Plant Design Parameters 2-7
2.5 Plant Operation 2-7
3. Plant Technical Description 3-1
3.1 MHR System Design 3-1
3.1.1 Reactor System 3-1
3.1.1.1 Fuel Design 3-3
3.1.1.2 Reactor Core and Internals 3-9
3.1.1.3 Neutron Control System 3-11
3.1.2 Cross Vessel and Hot Duct Assembly 3-15
3.1.3 Reactor Vessel 3-15
3.1.4 Design Modifications for Higher Temperature Operation 3-18
3.1.4.1 Inlet Flow Configuration Modifications 3-18
3.1.4.2 Vessel Cooling 3-24
3.1.4.3 Power and Flow Distribution Optimization 3-25
3.1.5 Shutdown Cooling System 3-29
3.1.6 Reactor Cavity Cooling System 3-33
3.1.6.1 RCCS Cooling Panels 3-34
3.1.6.2 RCCS Operation 3-35
3.1.7 Fuel Performance and Radionuclide Control 3-36
3.1.7.1 Radionuclide Containment System 3-37
3.1.7.2 Fuel Failure Mechanisms 3-39
3.1.7.3 Performance Capability of High-Quality TRISO Fuel 3-45
3.1.7.4 Radionuclide Transport Mechanisms 3-47
3.1.7.5 Fuel Quality and Performance Requirements 3-50
3.2 Power Conversion System 3-53
3.3 Heat Transport and Recovery System 3-56
3.3.1 Heat Exchangers 3-56
3.3.2 Circulators 3-59
3.3.3 High-Temperature Isolation Valves 3-59
3.4 Helium Services Systems 3-59
3.4.1 Primary Coolant Helium Purification System 3-60
3.4.2 Secondary Coolant Helium Purification System 3-63

3.4.3 Helium Transfer and Storage Systems 3-63
3.4.4 Tritium Control....3-63
3.5 Hydrogen Production System....3-67
3.5.1 Process Flow Stream Description 3-69
3.5.2 Solid Oxide Electrolyzer Modules....3-69
3.5.3 Power Recovery System....3-69
3.6 Plant Protection and Monitoring Systems....3-72
3.6.1 Reactor Protection System....3-72
3.6.2 Investment Protection System....3-73
3.6.3 Plant Monitoring System 3-74
3.7 Balance of Plant and Auxiliary Systems....3-74
3.7.1 Fuel Handling and Storage System....3-75
3.7.2 Spent Fuel Storage System 3-77
3.7.3 Radioactive Waste Management and Decontamination System 3-77
3.7.4 Heating, Ventilation, and Air Conditioning Systems....3-77
3.7.5 Hydrogen Production Water Supply System....3-77
3.7.6 Waste Heat Rejection System....3-78
3.8 Buildings and Structures 3-78
3.8.1 Reactor Building and Vented Low-Pressure Containment....3-78
3.8.2 Other Major Buildings....3-80
4. Plant Assessments 4-1
4.1 Safety Assessment 4-1
4.1.1 Passive Safety Features 4-1
4.1.2 Safety-Related Systems, Structures, and Components....4-1
4.1.3 Accident Analysis 4-1
4.2 Availability Assessment....4-3
4.2.1 Scheduled Outages....4-4
4.2.2 Forced Outages – MHR Nuclear Island 4-4
4.2.3 Forced Outages – Hydrogen Production Plant....4-5
4.3 Licensing Assessment....4-6
4.4 Economic Assessment....4-7
4.4.1 Capital Costs....4-8
4.4.2 Operations and Maintenance Costs....4-10
4.4.3 Hydrogen Production Costs 4-10
4.4.4 Parametric Studies....4-12
4.4.5 Comparison with Steam-Methane Reforming 4-13
5. Technology Development and Risk Reduction....5-1
6. References....6-1
Appendix A – Advanced Fuels A-1
Appendix B – Publications.... B-1

List of Figures

Figure 1-1. HTE-Based H2-MHR Concept 1-1
Figure 1-2. HTE-Based H2-MHR Process Schematic 1-2
Figure 1-3. The Gas-Turbine Modular Helium Reactor 1-3
Figure 1-4. Interconnect Plate and Single SOE Cell 1-4
Figure 1-5. SOE Stacked Cell Assembly 1-5
Figure 2-1. H2-MHR High-Level Function Flow Block Diagram 2-2
Figure 2-2. H2-MHR Plant Arrangement 2-9
Figure 3-1. Modular Helium Reactor System 3-1
Figure 3-2. MHR Fuel Element Components 3-3
Figure 3-3. MHR Standard Fuel Element 3-7
Figure 3-4. MHR Core Design 3-10
Figure 3-5. MHR Core Arrangement 3-11
Figure 3-6. Outer Neutron Control Assembly Design 3-12
Figure 3-7. Neutron Control Assembly Installation 3-13
Figure 3-8. Control Rod Design 3-14
Figure 3-9. Hot Duct Assembly 3-16
Figure 3-10. Reactor Vessel 3-17
Figure 3-11. GT-MHR Cross Section at Vessel Midplane 3-19
Figure 3-12. Reactor Vessel Configured with Alternative Inlet Flow Paths 3-20
Figure 3-13. MHR Configured with PSR Inlet Flow 3-21
Figure 3-14. ATHENA Model for the MHR Vessel and Internals 3-22
Figure 3-15. ATHENA Model for the RCCS 3-23
Figure 3-16. Predicted Failure of the SiC Layer by Fission Product Corrosion 3-26
Figure 3-17. Axial Temperature Distribution in the H2-MHR Hot Coolant Channel 3-26
Figure 3-18. Column-Average Power Factors 3-27
Figure 3-19. MHR FLOWNET Coolant Flow Distribution Model 3-28
Figure 3-20. Shutdown Cooling System General Arrangement 3-29
Figure 3-21. SCS Circulator and Heat Exchanger 3-31
Figure 3-22. SCS Circulator Sectional View 3-32
Figure 3-23. Passive Air-Cooled RCCS 3-33
Figure 3-24. RCCS Panel Layout 3-35
Figure 3-25. H2-MHR Radionuclide Containment System 3-37
Figure 3-26. TRISO Particle Failure Mechanisms 3-39
Figure 3-27. Calculated Tangential Stresses at the Middle of the SiC Layer 3-41
Figure 3-28. Irradiation-Induced Strain in Pyrocarbon as a Function of BAF 3-42
Figure 3-29. OPyC Performance Predictions 3-42
Figure 3-30. Localized Fission-Product Attack of the SiC Layer 3-44
Figure 3-31. Breakthrough Time for Ag Diffusing Through a 35-μm SiC Layer 3-45
Figure 3-32. Irradiation Conditions During Testing of High-Quality German Fuel 3-47
Figure 3-33. Principal Steps in Radionuclide Release from the H2-MHR Core 3-48
Figure 3-34. Postirradiation Heating of Japanese LEU UO_2 Fuel 3-49
Figure 3-35. Logic for Derivation of Fuel Quality Requirements 3-51
Figure 3-36. Power Conversion System Design Concept 3-54
Figure 3-37. PCS Design Parameters 3-55
Figure 3-38. PCHE Design Technology 3-58
Figure 3-39. High-Temperature Isolation Valve Design Concept 3-60
Figure 3-40. Helium Purification Train Block Diagram 3-61

Figure 3-41. Helium Transfer and Storage System Block Diagram 3-64
Figure 3-42. Tritium Release from TRISO-Coated Fuel Particles 3-65
Figure 3-43. Measured Tritium Concentration in Fort St. Vrain Primary Coolant 3-66
Figure 3-44. HTE Process Flowsheet 3-68
Figure 3-45. HYSYS Implementation of HTE Process Flowsheet 3-70
Figure 3-46. SOE Module Concept 3-73
Figure 3-47. Fuel Handling and Storage System Layout 3-75
Figure 3-48. Fuel Handling Equipment Arrangement 3-76
Figure 4-1. Passive Heat Removal to the RCCS During HPCC and LPCC Events 4-2
Figure 4-1. Peak Fuel Temperatures During HPCC and LPCC Events 4-3
Figure 4-3. Peak Vessel Temperatures During HPCC and LPCC Events 4-4
Figure 4-4. Master Fault Tree Model for Hydrogen Production Processes 4-6
Figure 4-5. Concept for Co-Location of the MHR with Hydrogen Production 4-8
Figure 4-6. HTE-Based H2-MHR Plant Hydrogen Production Costs (Baseline Estimate) 4-11
Figure 4-7. Comparison of Nuclear and SMR Hydrogen Production Costs 4-14
Figure 5-1. Integration of Design Process with Technology Development 5-2
Figure A-1. Neutron Total Absorption Cross Sections for Silicon and Zirconium A-1
Figure A-2. Core Reactivity as a Function of Irradiation Time A-2
Figure A-3. Cross Section of an Irradiated ZrC-gettered, SiC-TRISO Particle A-3

List of Tables

Table 2-1. Work Breakdown Structure and Responsibility Assignment Matrix 2-7
Table 2-2. H2-MHR Nominal Plant Design Parameters 2-9
Table 3-1. H2-MHR Core Design Parameters 3-2
Table 3-2. Coated Particle Design Parameters 3-4
Table 3-3. Fuel Compact Design Parameters 3-6
Table 3-4. H2-MHR Standard Fuel Element Design Parameters 3-8
Table 3-5. Reactor Vessel Design Parameters 3-18
Table 3-6. Impact of Higher Coolant Temperatures 3-23
Table 3-7. Optimized PSR Inlet Flow Configuration 3-24
Table 3-8. Reactor Vessel and Fuel Temperatures as a Function of Vessel Cooling Flow Rate 3-25
Table 3-9. Shutdown Cooling System Design Parameters 3-30
Table 3-10. RCCS Steady State Performance at 100% Reactor Power 3-36
Table 3-11. Summary of Performance Data for High-Quality TRISO Fuel Manufactured in Germany 3-46
Table 3-12. Service Conditions for Fissile and Fertile Fuel 3-52
Table 3-13. As-Manufactured Quality Requirements for Fissile and Fertile Fuel 3-52
Table 3-14. In-Service Performance Requirements for Fissile and Fertile Fuel 3-53
Table 3-15. PCS Thermodynamic and Performance Parameters 3-56
Table 3-16. HTRS Heat Exchanger Design Conditions 3-57
Table 3-17. HTRS Circulator Design Conditions 3-59
Table 3-18. Primary Helium Purification System Description 3-62
Table 3-19. HTE Process Flow Stream Description 3-71
Table 3-20. Design Parameters for a 500-Cell SOE Stack 3-72
Table 4-1. EFOH for MHR Nuclear Island System 4-5
Table 4-2. Summary of HTE-Based H2-MHR Capital Costs 4-9

Table 4-3. Summary of HTE-Based H2-MHR O&M Costs....4-10
Table 4-4. Summary of HTE-Based H2-MHR Plant Hydrogen Production Costs....4-11
Table 4-5. Results of H2-MHR Plant Economic Parametric Studies....4-12

Acronyms and Abbreviations

AOO	Anticipated Operational Occurrence
ASME	American Society of Mechanical Engineers
ATHENA	Advanced Thermal Energy Network Analysis
BAF	Bacon Anisotropy Factor
CAA	Clean Air Act
C-C	Carbon-Fiber Reinforced Carbon
CCPS	Center for Chemical Process Safety
CFR	Code of Federal Regulations
CWA	Clean Water Act
DDN	Design Data Need
EAB	Exclusion Area Boundary
ED&D	Engineering Development and Demonstration
EFOH	Effective Forced Outage Hours
EFPD	Effective Full Power Days
EIReDA	European Industry Reliability Data Bank
EPRI	Electric Power Research Institute
ESH&Q	Environmental, Safety, Health, and Quality
FDDM	Fuel Design Data Manual
FHSS	Fuel Handling and Storage System
FIMA	Fissions per Initial Metal Atom
FFBD	Function Flow Block Diagram
GA	General Atomics
GT-MHR	Gas Turbine MHR
H2-MHR	Hydrogen Production MHR
HEU	High-Enriched Uranium
HM	Heavy Metal
HPCC	High Pressure Conduction Cooldown
HPS	Helium Purification System
HTE	High Temperature Electrolysis
HTGR	High Temperature Gas-Cooled Reactor

Acronyms and Abbreviations

HTIV	High Temperature Isolation Valve
HTS	Heat Transport System
HTTR	High Temperature Test Reactor
HVAC	Heating, Ventilation, and Air Conditioning
IAEA	International Atomic Energy Agency
IHX	Intermediate Heat Exchanger
INL	Idaho National Laboratory
IPS	Investment Protection System
IPyC	Inner Pyrocarbon
JAEA	Japan Atomic Energy Agency
LBP	Lumped Burnable Poison
LMTD	Log Mean Temperature Difference
LOCA	Loss of Coolant Accident
LPCC	Low Pressure Conduction Cooldown
LEU	Low-Enriched Uranium
LWR	Light Water Reactor
MHR	Modular Helium Reactor
MMBtu	million (thousand-thousand) Btu
NERI	Nuclear Energy Research Initiative
NESHAP	National Emissions Standards for Hazardous Air Pollutants
O&M	Operations & Maintenance
OSHA	Occupational, Safety, and Health Administration
OPyC	Outer Pyrocarbon
OREDA	Offshore Reliability Data
PCS	Power Conversion System
PSR	Permanent Side Reflector
PyC	Pyrocarbon
R/B	Release Rate to Birth Rate
RHRS	Residual Heat Removal System
RSC	Reserve Shutdown Control
RCCS	Reactor Cavity Cooling System

Acronyms and Abbreviations

RPS	Reactor Protection System
SAPHIRE	Systems Analysis Programs for Hands-on Integrated Reliability Evaluations
SI	Sulfur-Iodine
SiC	Silicon Carbide
SCS	Shutdown Cooling System
SFSS	Spent Fuel Storage System
SNL	Sandia National Laboratories
SMR	Steam-Methane Reforming
SOE	Solid Oxide Electrolyzer
SSC	Systems, Structures, and Components
TBD	To Be Determined
TRISO	TRI-material, ISOtropic
TRU	Transuranic
UA	Product of Overall Heat Transfer Coefficient and Heat Transfer Area
VLPC	Vented Low Pressure Containment
WBS	Work Breakdown Structure

1. Introduction and Background

This report provides a pre-conceptual design description of a full-scale, nth-of-a-kind nuclear hydrogen production plant that is based on coupling the Modular Helium Reactor (MHR) to High-Temperature Electrolysis (HTE). This concept is referred to as the HTE-based H2-MHR and is illustrated in Fig. 1-1. The full-scale plant includes four, 600-MW(t) MHR modules. As shown in Fig. 1-2, Modular Helium Reactors (MHRs) supply both the heat to generate steam and the electricity to split the steam into hydrogen and oxygen. Electricity is generated using a direct, Brayton-cycle power-conversion system (PCS). Approximately 90% of the heat generated by the MHR modules is used to produce electricity. The remainder of the heat is transferred though an intermediate heat exchanger (IHX) to produce steam. As indicated in Fig. 1-2, steam is supplied to both the anode and cathodes sides of the electrolyzers. The steam supplied to the cathode side is split into hydrogen and oxygen. The oxygen is transferred through the electrolyte to the anode side. The steam supplied to the anode side is used to sweep the oxygen from electrolyzer modules. The steam supplied to the cathode side is first mixed with a small portion of the hydrogen stream in order to ensure reducing conditions and prevent oxidation of the electrodes. Heat is recuperated from both the hydrogen/steam and oxygen/steam streams exiting the electrolyzer. A small quantity of electricity is generated from the oxygen/steam stream to provide power for plant house loads.

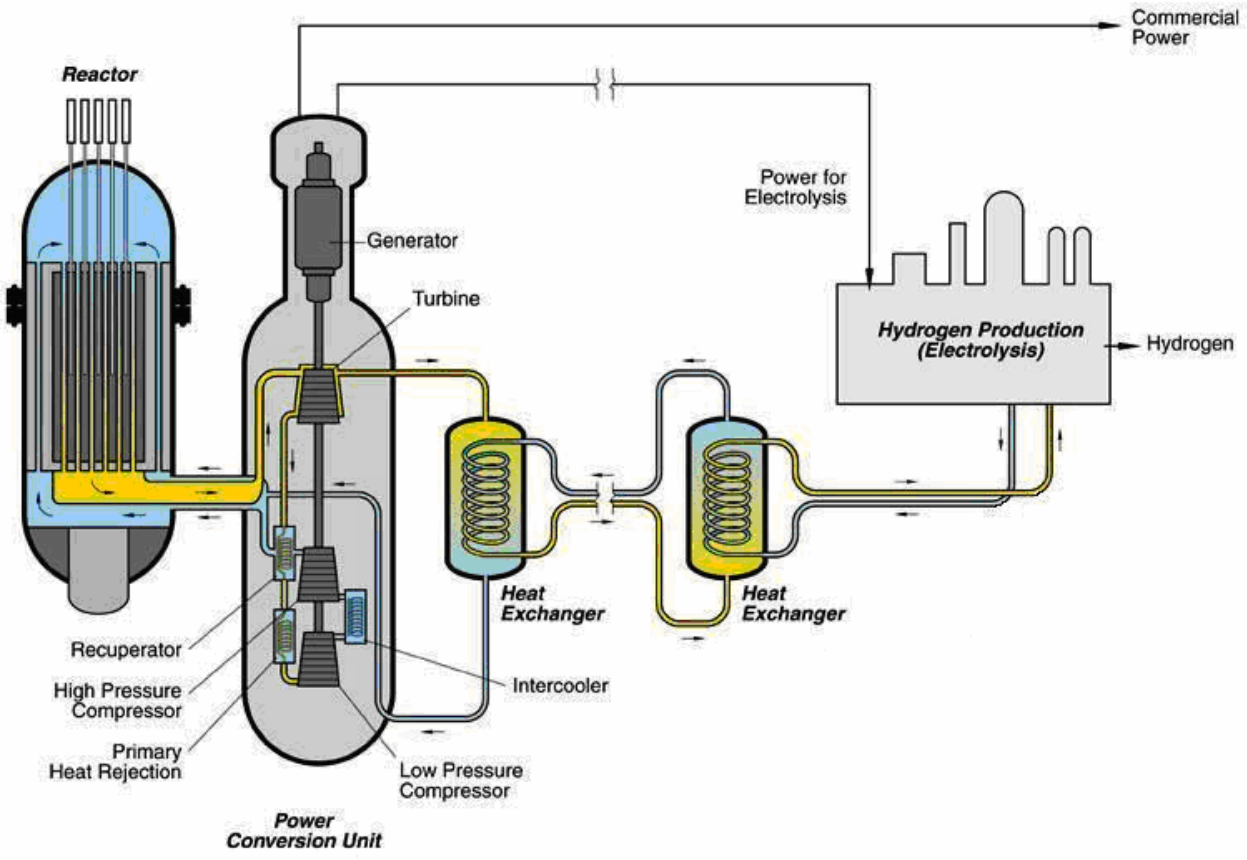

Figure 1-1. HTE-Based H2-MHR Concept

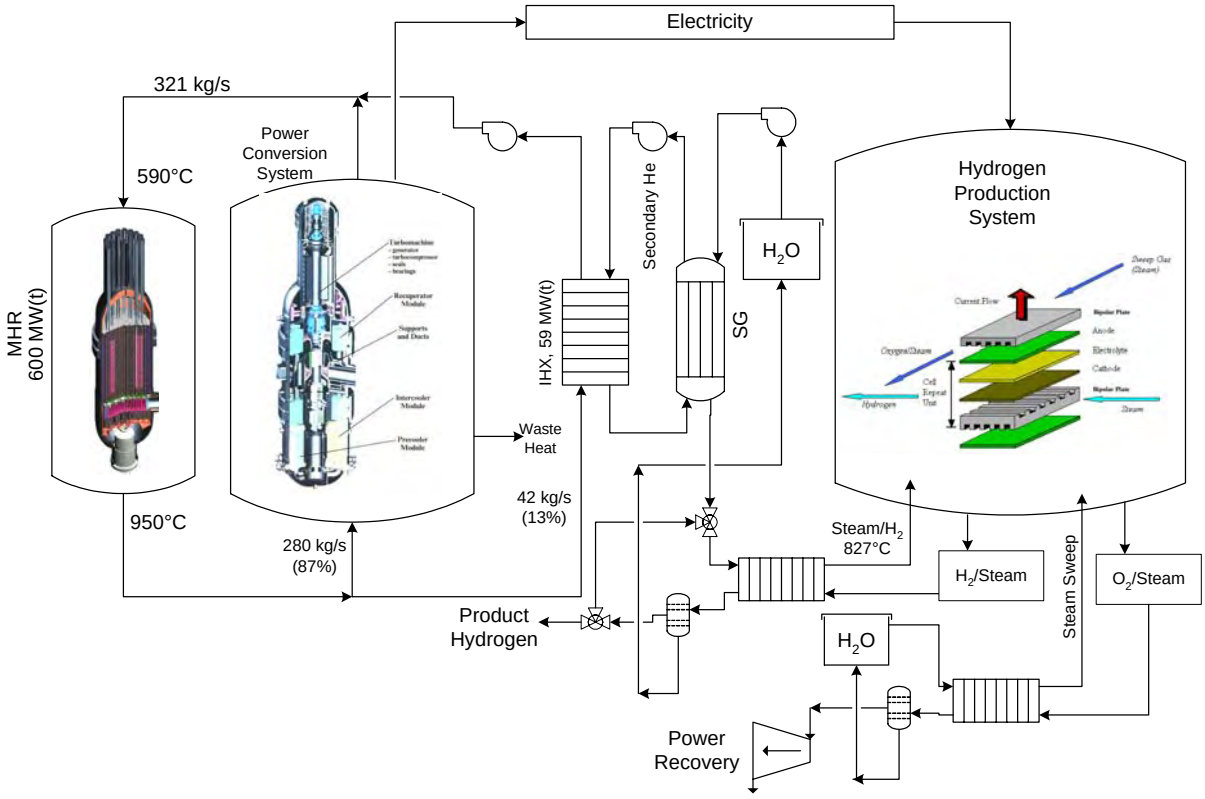

Figure 1-2. HTE-Based H2-MHR Process Schematic

1.1 Modular Helium Reactor Design Status

The Modular Helium Reactor Design is based on high-temperature, gas-cooled reactor technology that has been under development since the middle 1960s for electricity production and a variety of process-heat applications, including the production of hydrogen. In more recent years, General Atomics (GA) has been developing a passively safe, modular-sized design referred to as the Modular Helium Reactor (MHR). For electricity production, this concept operates with a thermal power level of 600 MW and an outlet helium temperature of 850°C to drive a direct, Brayton cycle PCS with a thermal-to-electrical conversion efficiency of 48 percent (see Fig. 1-3). This concept is referred to as the Gas Turbine MHR (GT-MHR) and is described in [Shenoy, 1996].

Development of the GT-MHR has continued under the International GT-MHR Project, which was started in 1995 by GA and Minatom (currently Rosatom) of Russia for the mission of disposition of surplus weapons-grade plutonium. The project is currently being funded on a parity basis by the U.S. and Russian governments under the "Agreement Between the Government of the United States of America and the Government of the Russian Federation on Scientific and Technical Cooperation in the Management of Plutonium that has Been Withdrawn from Nuclear Military Programs". Some funding for development of the PCS was obtained from the Electric Power Research Institute (EPRI) in the U.S. and from the European Union and Japan through their membership in the International Science and Technology Center. Under

this project the bulk of the design work and technology development is performed in Russia. United States organizations, including GA and Oak Ridge National Laboratory, have assisted the project through oversight and sharing experiences in design and operation of gas-cooled reactors and transferring technologies and computer codes used for design.

The GT-MHR Conceptual Design for plutonium disposition was completed in 1997 and was independently reviewed by a panel of experts representing the U.S., Russia, Japan, Germany and France. The review confirmed the capability of the GT-MHR to deeply burn weapons-grade plutonium in a once-through fuel cycle. The panel concluded the GT-MHR was a viable design that merited further development and there were no insurmountable obstacles to prevent construction of a GT-MHR on a reasonable schedule. The Preliminary Design Phase was completed in 2002 and reviewed by Minatom. The GT-MHR was approved in Russia as an innovative, next-generation concept for generation of electricity and process heat. Work is currently focused on areas related to technical risks, including coated particle fuel development, demonstration of the PCS with electromagnetic bearings, and verification/validation of computer codes for core design, including core physics, thermal hydraulics, fuel performance, and fission product transport. [LaBar, 2003] provides additional information on the GT-MHR design and its technology background. For hydrogen production, the reactor design and PCS are essentially the same as that for the GT-MHR, but with some minor modifications to allow operation with a higher coolant-outlet temperature of 950°C in order to increase hydrogen-production efficiency.

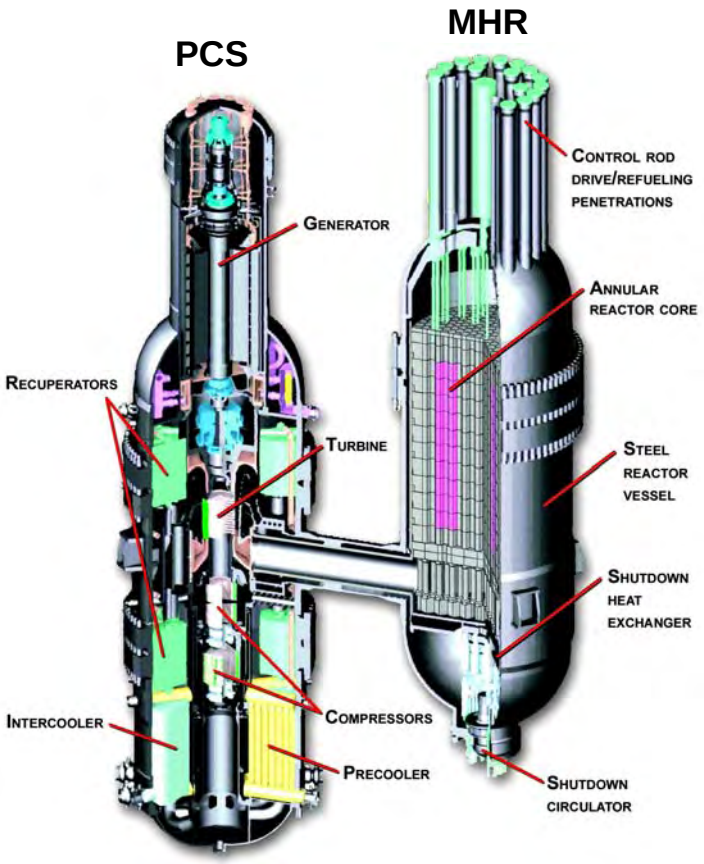

Figure 1-3. The Gas-Turbine Modular Helium Reactor

1.2 Hydrogen Production Using High-Temperature Electrolysis

In principle, nuclear electricity can be used to split water using conventional low-temperature electrolyzers. For a conventional LWR that produces electricity with approximately 33% thermal efficiency and current generation electrolyzers operating with an efficiency of about 75% to convert electricity to high-pressure hydrogen, the overall efficiency for hydrogen production is approximately 25%. If a GT-MHR is used to produce the electricity with 48% thermal efficiency, the overall efficiency for hydrogen production improves to 36%. However, even with high-efficiency electricity production, economic evaluations of coupling nuclear energy to low-temperature electrolysis have generally not been favorable when compared to steam-methane reforming (SMR). Because the electrical energy required to split the water molecule decreases with increasing temperature, the efficiency of electrolysis can be improved if it is performed at higher temperatures, especially if process heat is used directly to convert water into steam.

High-temperature electrolysis can be performed using solid oxide electrolyzers (SOEs). For the HTE-Based H2-MHR, the SOE modules are based on the planar cell technology (see Fig. 1-4) that has recently been successfully tested as part of a collaborative project between Idaho National Laboratory (INL) and Ceramatec [Herring, 2005]. Stacked assemblies of 100-mm × 100-mm cells have been tested successfully at INL (see Fig. 1-5).

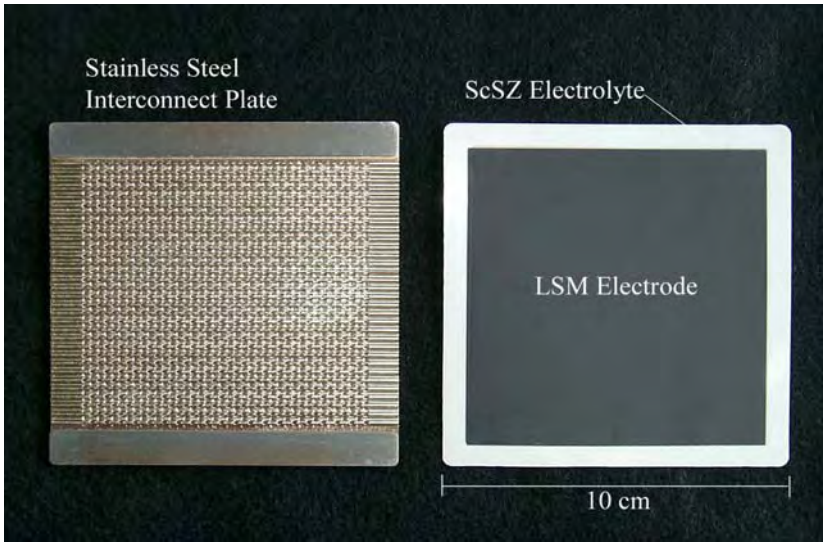

Figure 1-4. Interconnect Plate and Single SOE Cell

Figure 1-6 shows a schematic diagram of a unit cell. The electrolysis stack for the HTE-based H2-MHR will be operated at or near the thermal-neutral voltage (1.288 V at 850°C). At this voltage, the endothermic heat of reaction is balanced by ohmic heating in the stack, such that no additional heat is required for the stack to maintain high temperature. The stack consists of individual cells with 100 mm x 100 mm active area. The cell electrolyte is fabricated from either yttria- or scandia-stabilized zirconia. A 1.5 mm cathode plate made of nickel cermet material is bonded to one side of the electrolyte. A 0.05 mm anode plate is bonded to the other side of the electrolyte. The anode is composed of a mixed (i.e., both electronic and ionic) conducting

perovskite, lanthanum manganate ($LaMnO_3$) material. Bipolar plates with a doped lanthanum chromite (e.g.,, $La_{0.8}Ca_{0.2}CrO_3$) are attached to the outside of the anode and cathode, and join the anode and cathode of adjacent units to form the stack. The bipolar plates also provide flow passages between each of the units in the stack for the steam-hydrogen mixture and separate passages for the steam/oxygen sweep gas. The relatively small active area of the individual cells is determined by the thermal expansion compatibility between the electrolyte and the electrodes.

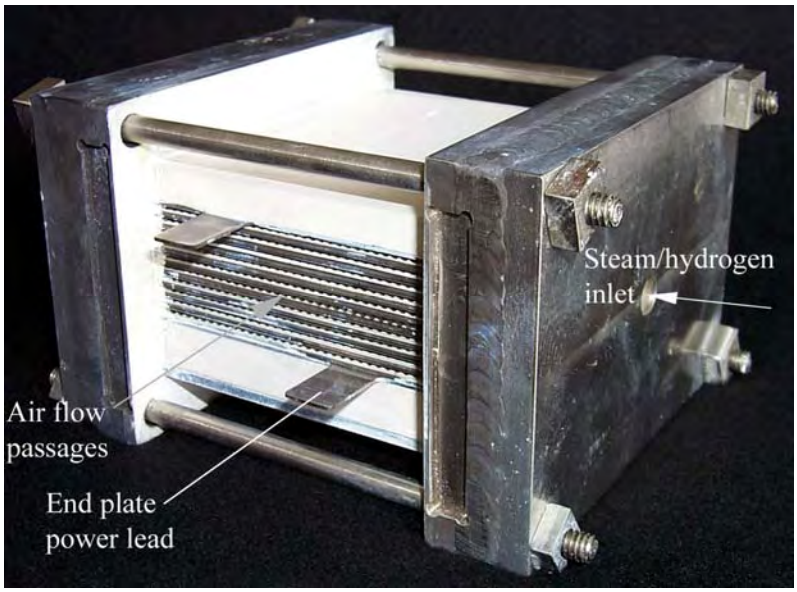

Figure 1-5. SOE Stacked Cell Assembly

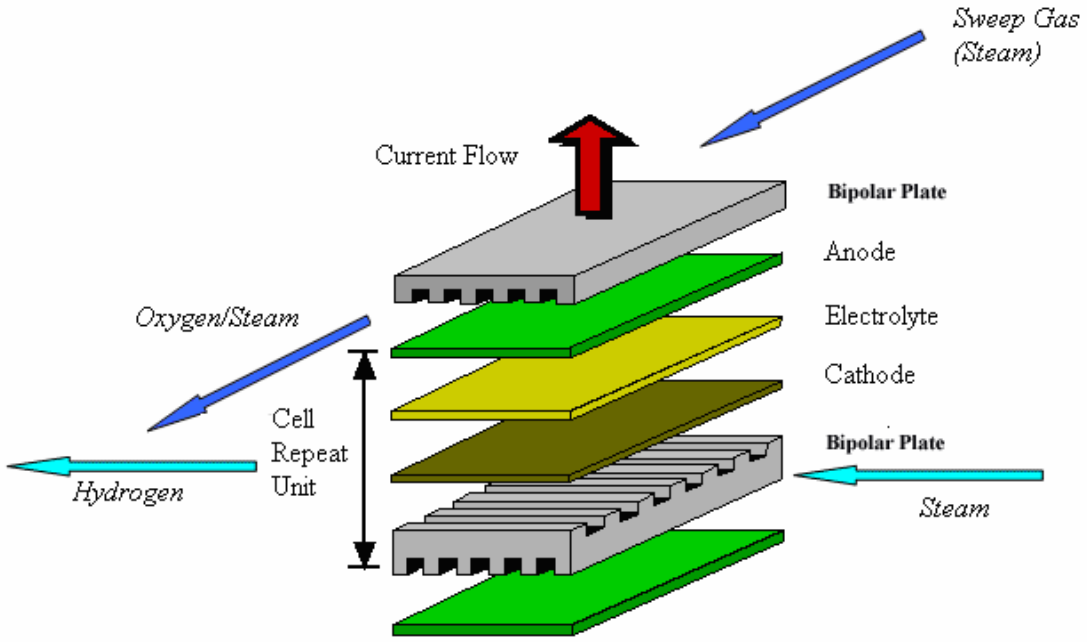

Figure 1-6. SOE Unit Cell Schematic

2. Overall Plant Description

2.1 Plant Level Functions and Performance Requirements

As part of this pre-conceptual design study, a systems-engineering approach has been used to develop functions and performance requirements for the H2-MHR at the plant/major system level. A function is a succinct statement that describes the purpose of the plant/system. Each function must have at least one performance requirement. A performance requirement quantifies how well its associated function must be performed. Brackets **[ ]** are used to identify information that is preliminary in nature, results from a design uncertainty, originates from insufficient documentation, or needs verification. **TBD** (To Be Determined) is used when numeric values or descriptive information is not yet available.

The following numbering convention is used to identify functions: F-P-XXXX, where F stands for Function, P stands for Plant/Major System level, and XXXX is a 4-digit number. Similarly, performance requirements are identified according to PR-P-XXXX, where PR stands for Requirement.

The primary function of the H2-MHR is to supply hydrogen gas to end users. This is accomplished using HTE with the heat and electricity supplied from MHRs. As shown in Fig. 2-1, the functional decomposition has been developed using a Function Flow Block Diagram (FFBD). When viewed from left-to-right, the functions flow from higher level to lower level. The lower-level functions describe how higher level functions are performed. Preliminary performance requirements have been prepared for the higher-level functions and are given below.

F-P-0010 Supply Hydrogen Gas

The Performance Requirement(s) associated with this function are:

PR-P-0010 The availability of hydrogen gas supplied from the H2-MHR plant shall be **[**99%**]**.

PR-P-0020 The H2-MHR plant shall supply **[**2.68×10^5**]** mt of hydrogen per year.

PR-P-0020 Chemical impurities in the product hydrogen gas shall be less than **[**0.2**]** %.

PR-P-0025 The moisture content of the product hydrogen gas shall not exceed **TBD** ppm

PR-P-0030 The tritium content in the product hydrogen gas shall not exceed **TBD** picocuries per liter.

PR-P-0040 The concentration of total radioactivity in the hydrogen gas shall not exceed **TBD** Ci/m^3.

PR-P-0050 Hydrogen gas shall be supplied at a pressure of **[**4.95**]** MPa.

PR-P-0060 Hydrogen gas shall be supplied at a temperature of **[**27**]** °C.

PR-P-0070 The H2-MHR plant shall have a hydrogen storage capacity of **TBD** mt.

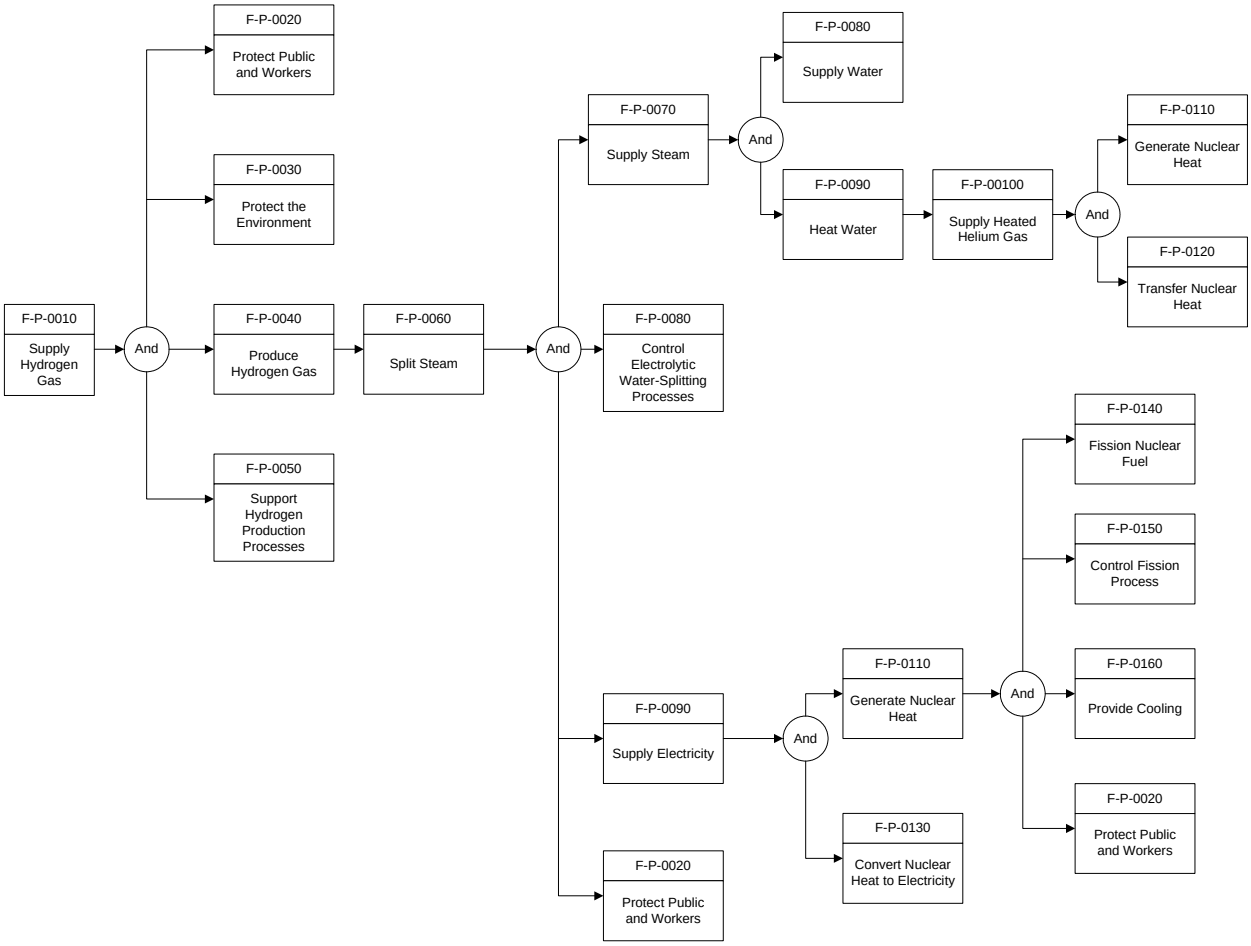

Figure 2-1. H2-MHR High-Level Function Flow Block Diagram

F-P-0020 Protect Public and Workers

The Performance Requirement(s) associated with this function are:

PR-P-0080 Occupational radiation exposures shall be no greater than 10% of the limits specified in 10 CFR 20.

PR-P-0090 During design-basis accidents, offsite radiation doses to the public shall be less than the limits specified in 10 CFR 100.

PR-P-0100 During design-basis accidents, offsite doses at the site Exclusion Area Boundary (EAB) shall be less than those specified in the Manual of Protective

Action Guides and Protective Actions for Nuclear Incidents (EPA-520/1-75-001) for sheltering and evacuation.

PR-P-0110 During normal operation, offsite radiation doses to the public shall be less than the limits specified in Appendix I of 10 CFR 50 and 40 CFR 190.

PR-P-0120 The individual acute and latent fatality risks shall be less than the limits specified on 51 FR 130.

PR-P-0130 The H2-MHR plant shall comply with all applicable OSHA General Industry Standards, including 29 CFR 1910.132 - 133 and 135 - 136, Personal Protective Equipment (including general requirements, eye and face protection) and 29 CFR1910.134, Respiratory Protection for all applicable hazardous chemicals.

PR-P-0140 Exposures to any given hazardous chemical shall not exceed the maximum acceptable levels found in OSHA 29 CFR1910.1000, Subpart Z; and other OSHA substance-specific standards.

PR-P-0160 The H2-MHR plant shall comply with OSHA requirements contained in 29 CFR 1910.119 for preventing or minimizing the consequences of catastrophic releases of toxic, reactive, flammable, or explosive chemicals.

F-P-0030 Protect the Environment

The Performance Requirement(s) associated with this function are:

PR-P-0170 Emissions from the H2-MHR plant shall not exceed established EPA limits on the amount hazardous air pollutants and all other applicable requirements of the Clean Air Act/Air Programs (CAA), 40 CFR 50-99, and all state and local requirements.

PR-P-0180 Emissions from the H2-MHR plant will comply with all applicable requirements of the Clean Water Act/Water Programs (CWA), 40 CFR 100-149, and all state and local requirements.

PR-P-0190 Emissions from the H2-MHR plant shall comply with the requirements of 40 CFR 61, National Emissions Standards for Hazardous Air Pollutants (NESHAP) and all applicable state and local air permit requirements.

PR-P-0200 The release of gaseous, liquid, and solid radioactive materials to the environment shall not exceed applicable federal, state, and local environmental protection requirements.

F-P-0040 Produce Hydrogen Gas

The Performance Requirement(s) associated with this function are:

PR-P-0210 The overall efficiency for hydrogen production shall be **[**>40%**]**.

F-P-0050 Support Hydrogen Production Processes

The Performance Requirement(s) associated with this function are:

PR-P-0220 **TBD** MW of electricity shall be supplied to the H2-MHR plant.

PR-P-0230 **TBD** MW of electricity shall be available to the H2-MHR plant from a backup power source.

PR-P-0240 A nominal **[**246.5**]** MW of waste heat shall be removed from the H2-MHR plant systems when all 4 modules are operating at 100% capacity under the following ambient conditions: **[**35.5**]**°C dry-bulb temperature, **[**25**]**°C wet-bulb temperature.

PR-P-0250 Systems and components shall be protected from the effects of the environment, including natural phenomena hazards.

2.2 Work Breakdown Structure and Responsibility Assignment Matrix

A level 2 Work Breakdown Structure (WBS) has been developed for the H2-MHR project and is shown in Table 2-1, along with the Responsibility Assignment Matrix for the Design Organization, Technology Organization, and Owner/Operator. It is expected the Design Organization would be a consortium of companies with experience in designing and building commercial-scale nuclear reactors and large-scale chemical plants. The Technology Organization would include U.S. national laboratories and other organizations qualified to perform the required technology development activities. The Owner/Operator could be a commercial utility, an energy company, the U.S. Department or Energy, or a consortium of these organizations. The H2-MHR project could also include international collaboration in the Design, Technology, and Owner/Operator areas.

Table 2-1. Work Breakdown Structure and Responsibility Assignment Matrix

WBS	Title	Design Organization	Technology Organization	Owner / Operator
1.0	Plant Definition			
1.1	Systems Identification	X		
1.2	Plant and Systems Functions	X		X
1.3	Performance Requirements	X		X
1.4	Design Requirements	X		X
1.5	ESH&Q* Requirements	X		X
1.6	Interface Requirements	X		X
2.0	MHR System Design			
2.1	Core Nuclear / Thermal Hydraulic Design	X		
2.2	Fuel Design	X		
2.3	Reactor Internals Design	X		
2.5	Shutdown Cooling System Design	X		
2.4	RCCS Design	X		
2.5	Fuel Performance / Radionuclide Transport	X		
3.0	MHR System Technology Development			
3.1	Fuel	X	X	
3.2	Graphite	X	X	
3.3	Metals	X	X	
3.4	Radionuclide Transport	X	X	
4.0	Power Conversion System (PCS) Design			
4.1	Turbomachine	X		
4.2	Recuperator	X		
4.3	Precooler and Intercooler	X		
4.4	PCS Component Supports and Ducts	X		
4.5	Removal and Replacement of PCS Components	X		
5.0	PCS Technology Development	X	X	
6.0	Heat Transport and Recovery			

Table 2-1. Work Breakdown Structure and Responsibility Assignment Matrix

WBS	Title	Design Organization	Technology Organization	Owner / Operator
	System (HTRS) Design			
6.1	IHX Design	X		
6.2	Primary and Secondary Coolant Circulators	X		
6.3	Steam Generator / Superheater	X		
6.4	Other Heat Exchangers	X		
6.0	HTRS Technology Development		X	
6.1	Heat Exchangers	X	X	
6.2	High Temperature Helium Circulators	X	X	
7.0	Water Supply System			
7.1	Feedwater and Condensate Pump			
7.2	Water Purification System			
8.0	H_2 Production System Design			
8.1	Electrolyzer Modules	X		
8.2	Heat / Mass Balances	X		
8.3	Power Supply System	X		
8.4	Power Recovery System	X		
8.5	H_2 Startup System	X		
8.6	Facility Layout	X		
9.0	H_2 Production System Technology Development			
9.1	Pilot-Scale Demonstration	X	X	
9.2	SOE Materials/Technology	X	X	
10.0	Plant Level Systems Design			
10.1	Plant Site / Arrangement	X		X
10.2	BOP and Auxiliary Systems	X		
10.3	Plant Integration	X		X
10.4	Design Review / Customer Requirements			X
11.0	Plant Assessments			
11.1	Trade Studies and Sensitivity Analysis	X		
11.2	Safety Assessment	X		
11.3	Availability Assessment	X		
11.4	Licensing Assessment	X		X
11.5	Economic Assessment	X		X
11.6	Nominal Plant Performance / Operation	X		
11.7	Transient Operation and Control	X		
11.8	Identification of Design Data Needs	X		
12.0	Project Management			
12.1	Project Planning and Coordination	X		
12.2	Project Monitoring	X		
12.3	Project Review	X	X	X
12.4	Annual / Final Reports	X	X	X

* ESH&Q = Environmental, Safety, Health, and Quality

2.3 Overall Plant Arrangement

The plot plan for the H2-MHR plant is shown on Fig. 2-2. The layout is very similar to the layout for a 4-unit GT-MHR plant [Shenoy, 1996], with the addition of the electrolyzer units and other equipment for Hydrogen Production Plant. The plant occupies a footprint of approximately 690 m × 503 m. The Hydrogen Production Plant is located outside of the nuclear plant boundary and is classified as a non-nuclear system.

2.4 Nominal Plant Design Parameters

The nominal plant design parameters are given in Table 2-2. On an annual basis, the HTE-based H2-MHR plant produces 2.68×10^5 metric tons at a plant capacity factor of 90%. The overall plant efficiency for hydrogen production is 55.8%.

2.5 Plant Operation

The H2-MHR is intended to operate at full, base-load power excect during planned outages for refueling and other maintenance. Planned outages for the MHR System will be staggered from module to module to minimize the overall impact on availability. Also, the H2-MHR plant will be part of a network of plants that includes a hydrogen storage system in order to ensure overall hydrogen availability of 99% or greater to the end user. When hydrogen demand is lower, the H2-MHR plants will continue to operate at their base-load capacity, but divert some of the hydrogen to the storage facility for later use when demand is higher. For example, if hydrogen is used primarily by the transportation sector, stored hydrogen would be recovered primarily during peak driving periods.

Procedures for startup/shutdown of the plant and overall plant control will be developed during the preliminary and final design phases. A potential issue is propagation of thermal disturbances in the Hydrogen Production System (e.g., from failure of a pump motor) that impact the MHR primary coolant inlet/outlet temperatures beyond the scram setpoints. As discussed in [Inaba, 2005], the propagation of thermal disturbances in the Hydrogen Production System can be mitigated by ensuring there is sufficient water in the Hydrogen Production System that undergoes phase change at constant temperature.

Table 2-2. H2-MHR Nominal Plant Design Parameters

MHR System	
Number of modules	4
Module power rating	600 MW(t)
Core inlet/outlet temperatures	590°C / 950°C
Peak fuel temperature – normal operation	1250°C - 1350°C
Peak fuel temperature – accident conditions	< 1600°C
Helium mass flow rate	321 kg/s
Total MHR System pressure drop	80 kPa
Power Conversion System	
Mass flow rate	280 kg/s
Heat supplied from MHR System	542 MW(t)
Turbine inlet/outlet temperatures	950°C / 600°C
Turbine inlet/outlet pressures	7.0 MPa / 2.8 MPa
Generator efficiency	98 %
Electricity generated	292 MW(e)
Electricity generation efficiency*	53.9%
Heat Transport and Recovery System	
Primary helium flow rate	42 kg/s
Secondary helium flow rate	18.1 kg/s
IHX heat duty	58 MW(t)
IHX primary side inlet/outlet temperatures	950°C / 679°C
IHX secondary side inlet/outlet temperatures	292°C / 917°C
Steam production rate	23.6 kg/s
Mass flow rate of hydrogen added to steam	0.3 kg/s
Temperature of steam/hydrogen supplied to SOE	827°C
Hydrogen Production System	
Peak SOE temperature	862°C
Peak SOE pressure	5.0 MPa
Product hydrogen pressure	4.95 MPa
Annual hydrogen production**	2.68×10^5 metric tons
Plant hydrogen production efficiency*, ***	55.8%

* Neglects parasitic heat losses from the Reactor Cavity Cooling System and Shutdown Cooling System.

** Based on a 4-module plant and an overall plant capacity factor of 90%.

*** Based on the higher heating value of hydrogen (141.9 MJ/kg).

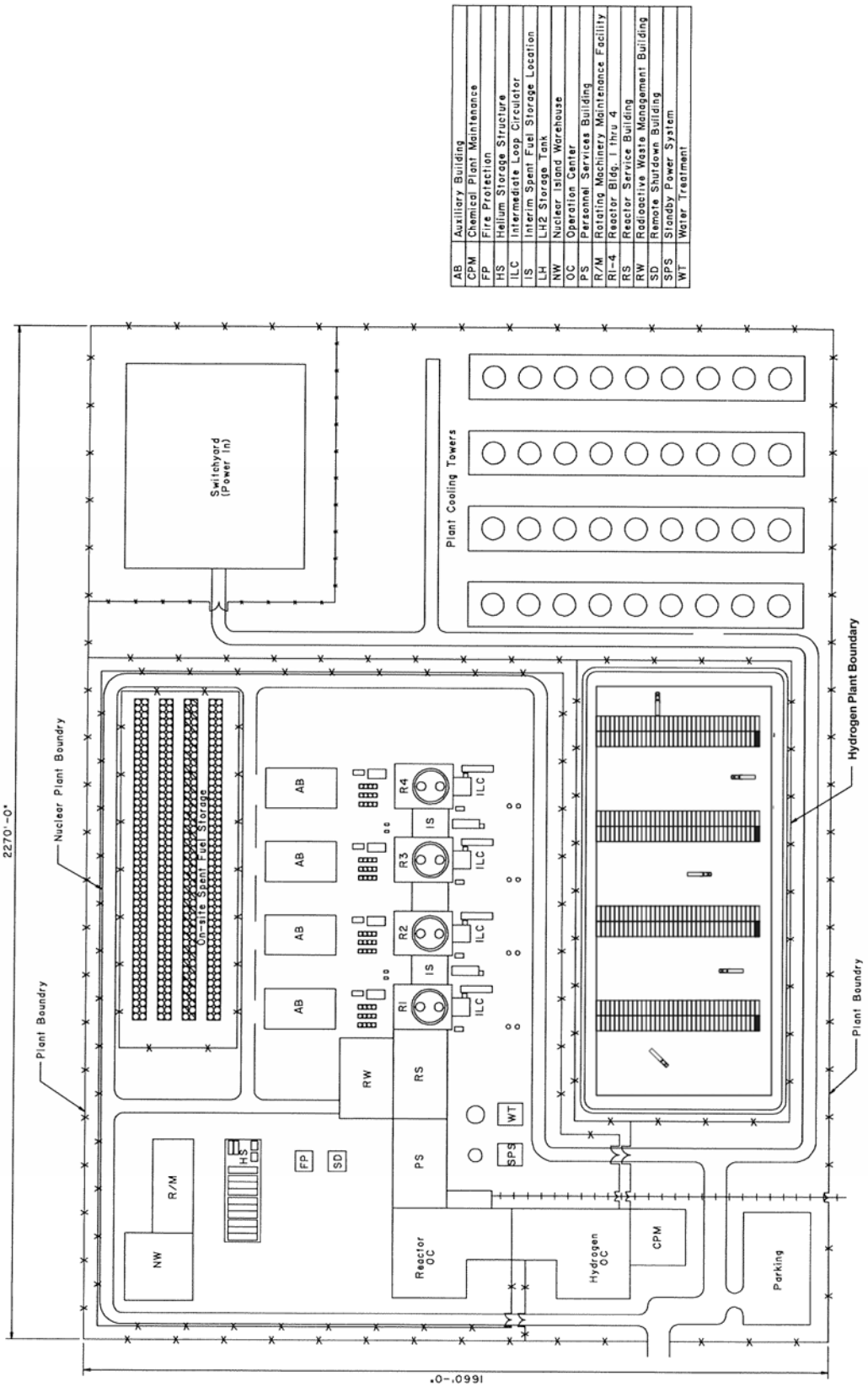

Figure 2-2. H2-MHR Plant Arrangement

3. Plant Technical Description

3.1 MHR System Design

The MHR system design includes the Reactor System, Cross Vessel and Hot Duct Assembly, Reactor Vessel, Shutdown Cooling System (SCS), and Reactor Cavity Cooling System (RCCS). These systems and design modifications for higher temperature operation are described in the following sections. The MHR design features for fuel performance and radionuclide control are described in Section 3.1.7.

3.1.1 Reactor System

Figure 3-1 shows a cross-sectional view of the Reactor System, which includes the reactor core, the Neutron Control System, and other equipment within the reactor vessel. The H2-MHR core design parameters are summarized in Table 3-1.

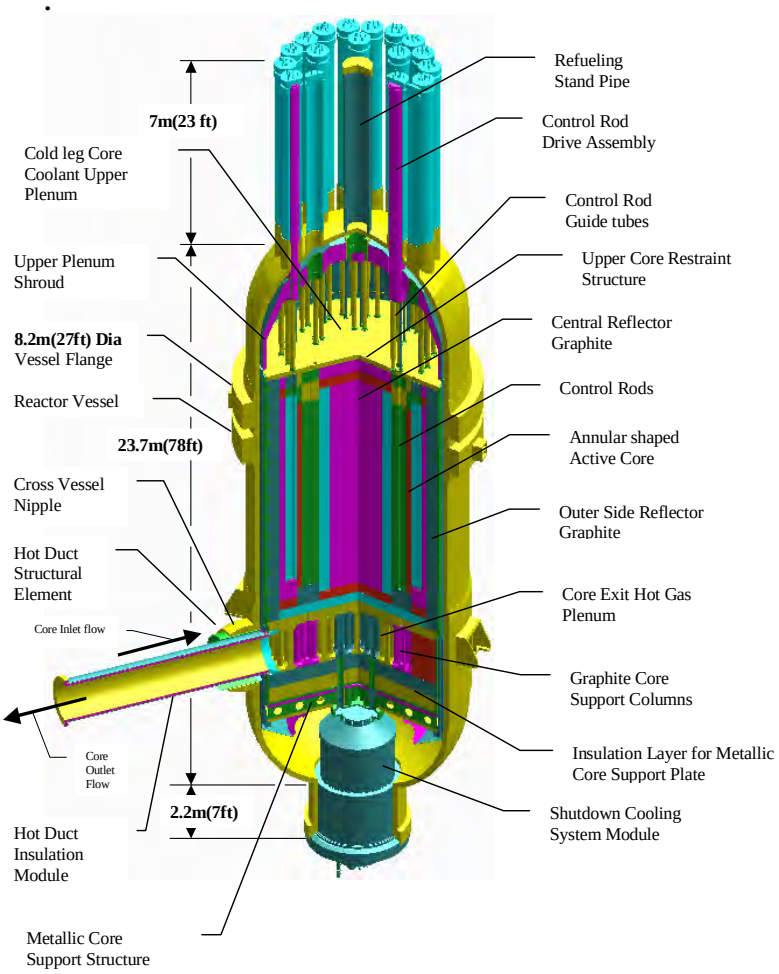

Figure 3-1. Modular Helium Reactor System

Table 3-1. H2-MHR Core Design Parameters

Core thermal power (MW)	600
Number of fuel columns	102
Number of fuel blocks per column	10
Thermal power density (MW/m^3)	6.6
Effective inner diameter of active core (m)	2.96
Effective outer diameter of active core (m)	4.83
Active core height (m)	7.93
Fissile fuel (19.8% enriched in U-235)	$UC_{0.5}O_{1.5}$
Fertile Fuel (natural U)	$UC_{0.5}O_{1.5}$
Equilibrium fuel cycle length (full-power days)	425
Number of columns per refueling segment	51
Mass of heavy metal per refueling segment (kg)	1748 (fissile fuel)
	514 (fertile fuel)
Core inlet temperature (°C)	590
Core outlet temperature (°C)	950
Core upper plenum inlet pressure (MPa)	7.1
Core pressure drop (MPa)	0.058
Coolant flow rate (kg/s)	322

3.1.1.1 Fuel Design

The H2-MHR fuel element and its components are shown in Fig. 3-2. The fuel for the H2-MHR consists of microspheres of uranium oxycarbide that are coated with multiple layers of pyrocarbon and silicon carbide. The H2-MHR core is designed to use a blend of two different particle types; a fissile particle that is enriched to 19.8% U-235 and fertile particle with natural uranium (0.7% U-235). The fissile/fertile loading ratio is varied with location in the core, in order to optimize reactivity control, minimize power peaking, and maximize fuel cycle length. The buffer, inner pyrolytic carbon (IPyC), silicon carbide (SiC), and outer pyrolytic carbon (OPyC) layers are referred to collectively as a TRISO[1] coating. The coating system can be viewed as a miniature pressure vessel that provides containment of radionuclides and gases. This coating system is also an excellent engineered barrier for long-term retention of radionuclides in a repository environment. Coated particle design parameters are given in Table 3-2. The functions of the fuel kernel and coating layers during operation of the H2-MHR are described below.

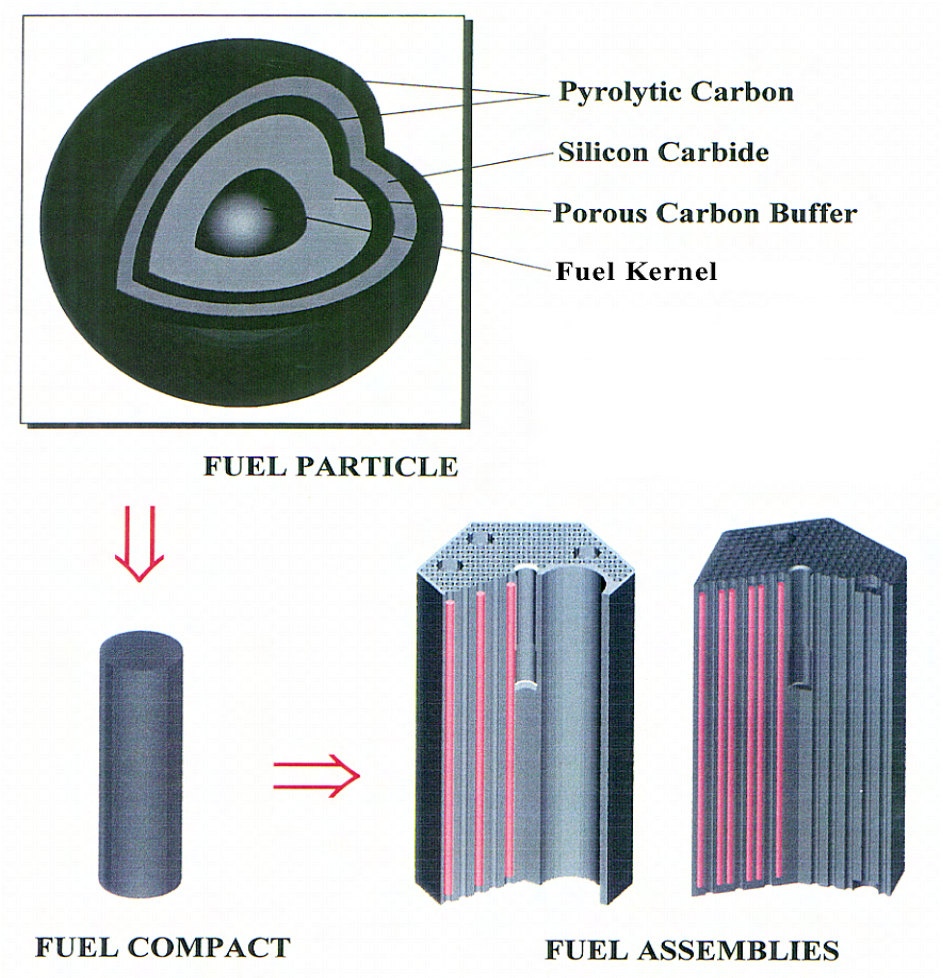

Figure 3-2. MHR Fuel Element Components

[1] TRISO is an acronym for TRI-material, ISOtropic, with the materials being low-density pyrolytic carbon (buffer), high density pyrolytic carbon (IPyC and OPyC), and SiC.

Table 3-2. Coated Particle Design Parameters

	Fissile Particle	Fertile Particle
Composition	$UC_{0.5}O_{1.5}$	$UC_{0.5}O_{1.5}$
Uranium enrichment, %	19.8	0.7 (Natural Uranium)
Dimensions (µm)		
Kernel Diameter	350	500
Buffer thickness	100	65
IPyC thickness	35	35
SiC thickness	35	35
OPyC thickness	40	40
Particle diameter	770	850
Material Densities (g/cm^3)		
Kernel	10.5	10.5
Buffer	1.0	1.0
IPyC	1.87	1.87
SiC	3.2	3.2
OPyC	1.83	1.83
Elemental Content Per Particle (µg)		
Carbon	305.7	379.9
Oxygen	25.7	61.6
Silicon	104.5	133.2
Uranium	254.1	610.2
Total particle mass (µg)	690.0	1184.9
Design burnup (% FIMA)[a]	26	7

Note
a. FIMA is an acronym for Fissions per Initial Metal Atom.

Fuel Kernel

The oxycarbide kernel composition was selected for the H2-MHR primarily because of its ability to perform well at relatively high burnup. The carbide component of the kernel undergoes oxidation to getter excess oxygen released during fission. If the carbide component were not present, excess oxygen would react with carbon in the buffer to form carbon monoxide. High levels of carbon monoxide can lead to failure of the coating system by overpressurization and kernel migration (see Section 3.1.7.2). The oxide component of the kernel is highly effective at retaining many radionuclides that can chemically attack or diffuse through the coating layers (e.g., lanthanides and strontium, respectively).

Buffer

The buffer is deposited over the kernel and consists of low-density, porous pyrocarbon. The buffer attenuates fission fragments that recoil from the kernel and provides sufficient void space to accommodate gases, including gaseous fission products and CO. The buffer also acts as a sacrificial layer to accommodate potential kernel migration and swelling and isolates the kernel from load-bearing layers of the coating system.

IPyC Layer

The high-density IPyC layer serves to protect the kernel and buffer from chemical attack by chlorine compounds, which are generated as byproducts during deposition of the SiC layer. The IPyC layer also provides a smooth surface for deposition of the SiC layer and delays transport of radionuclides to the SiC layer. The IPyC layer shrinks with the accumulation of fast neutron fluence, which helps to maintain the SiC layer in compression, provided the bond between the IPyC and SiC layers remains strong and continuous during irradiation (see Section 3.1.7.2).

SiC Layer

The SiC layer is deposited under conditions to produce a high-density, high-strength coating with a fine-grain microstructure. This layer provides the primary structural support to accommodate stresses generated by internal gas pressure and irradiation-induced dimensional changes of the pyrocarbon layers. The SiC layer provides an impermeable barrier to gaseous, volatile, and most metallic fission products during normal operation and hypothetical accidents. Dimensional changes of the SiC are very small during irradiation, and it is considered to be dimensionally stable.

OPyC Layer

The high-density OPyC layer protects the SiC layer from mechanical damage that may occur during fabrication of fuel compacts and fuel elements, and provides a bonding surface for the compact matrix. The OPyC layer also shrinks during irradiation, which helps to maintain the SiC layer in compression. The OPyC layer prevents the release of gaseous fission products, if both the IPyC and SiC layers are defective or fail in service.

Fuel Compacts

Each fuel compact is a mixture of fissile, fertile, and graphite shim particles bonded together with a carbonaceous matrix into a rod-shaped compact with dimensions 12.45 mm (0.49 in.) in diameter and 49.3 mm (1.94 in.) in length. The fuel compacts are stacked in the blind fuel holes of the graphite fuel element. Graphite plugs are cemented into the tops of the fuel holes to enclose the stacked compacts. Because of sorption mechanisms, the fuel compacts can provide an additional barrier to the release of metallic fission products. Fuel compact design parameters are given in Table 3-3.

Graphite Fuel Element Blocks

The standard GT-MHR fuel-element graphite block and the arrangement of fuel holes, coolant holes, and lumped burnable poison[2] (LBP) holes is shown in Figure 3-3. The graphite blocks are fabricated from high-purity, nuclear-grade graphite. Each block is a right hexagonal prism with dimensions 794 mm (31.2 in.) in length and 360 mm (14.2 in.) across the flats of the hexagonal cross section. Fuel and coolant holes run parallel through the length of the block in a regular triangular pattern of nominally two fuel holes per coolant hole. The pitch of the coolant and fuel-hole array is 18.8 mm (0.74 in.). The minimum web thickness between a coolant hole

[2] B_4C is used as lumped (or fixed) burnable poison to control reactivity. Compacts containing coated B_4C and graphite shim granules are inserted into holes designated for lumped burnable poison, which are located near the corners of the block.

and fuel hole is 4.5 mm (0.18 in.). This web provides an additional barrier to release of metallic fission products. Design parameters for the standard fuel element are given in Table 3-4. A standard fuel element has 210 blind fuel holes, 108 coolant holes, and contains 3126 fuel compacts. In addition to standard fuel elements, the GT-MHR active core contains fuel elements with a single, larger diameter channel (3.75 to 4.0 in.) to allow insertion of additional poison for reserve shutdown capability.

Table 3-3. Fuel Compact Design Parameters

Diameter, mm	12.45
Length, mm	49.3
Volume, cm^3	6.0
Shim particle composition	H-451 or TS-1240 graphite
Shim particle size	99 wt % < 1.19 mm
	95 wt % < 0.59 mm
Shim particle density (g/cm^3)	1.74
Binder type	Petroleum pitch
Filler	Petroleum derived graphite flour
Matrix density (g/cm^3)	0.8 to 1.2
Volume fraction occupied by matrix	0.39
Volume fraction occupied by shim particles in an average compact[a]	0.41
Volume fraction occupied by fissile particles in an average compact[a]	0.17
Volume fraction occupied by fertile particles in an average compact[a]	0.03
Number of fissile particles in an average compact[a]	4310
Number of fertile particles in an average compact[a]	520
Mass of carbon in an average compact,[a,b] g	6.62

Notes
a. Values for an average compact are determined by assuming heavy metal (uranium) is distributed uniformly in the reactor core.
b. This value excludes carbon in the layers of the coated particles. For an average compact, there is an additional 1.32 g of carbon associated with fissile particles and an additional 0.20 g of carbon associated with fertile particles.

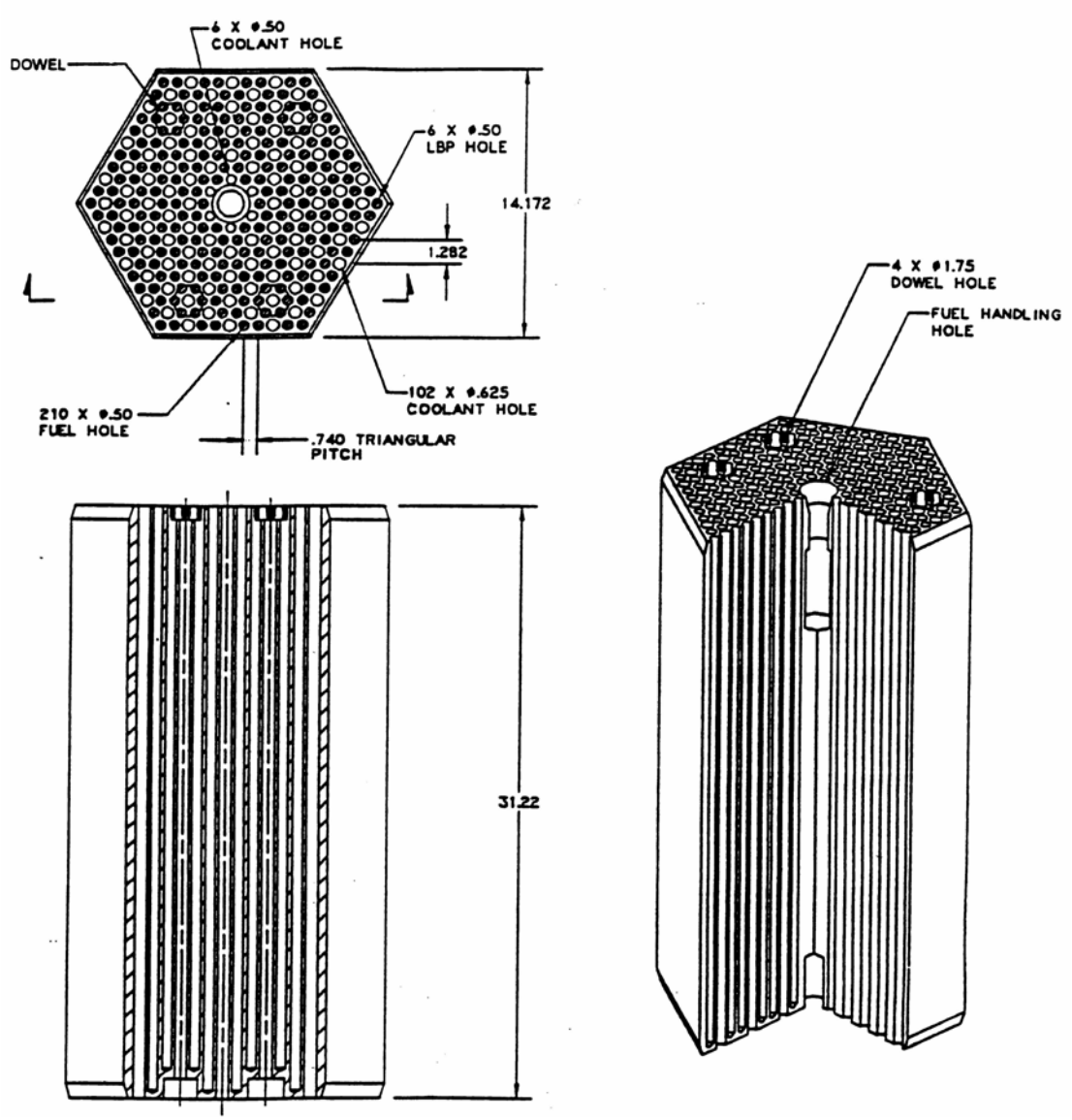

Figure 3-3. MHR Standard Fuel Element (dimensions shown are in inches)

Table 3-4. H2-MHR Standard Fuel Element Design Parameters

Shape	Hexagonal Prism
Type of graphite	Nuclear Grade H-451 or Equivalent
Mass of graphite per element	90 kg
Dimensions	794 mm (31.2 in.) in length
	360 mm (14.2 in.) across flats of hexagon
Volume[a]	0.0889 m^3
Total number of fuel holes	210
Number of fuel holes under dowels	24
Fuel hole diameter	12.7 mm (0.5 in.)
Fuel hole length	752.6 mm (29.63 in.) under dowels
	781.5 mm (30.77 in.) not under dowels
Number of fuel compacts per fuel hole	14 for holes under dowels
	15 for holes not under dowels
Number of fuel compacts per element	3126
LBP holes per element	6
LBP hole diameter	12.7 mm (0.5 in.)
LBP hole length	781.5 mm (30.77 in.)
Total number of coolant holes	108
Coolant hole diameter	15.88 mm (0.625 in.) for larger holes
	12.7 mm (0.5 in.) for the 6 smaller holes near the center of the block
Pitch of coolant/fuel-hole array	18.8 mm (0.74 in.)
Total mass of an average fuel element[b,c]	122 kg
Mass of carbon in an average fuel element[b,d]	110.7 kg
Mass of low-enriched uranium fuel in an average fresh fuel element[b]	3.43 kg
Mass of natural uranium fuel in an average fresh fuel element[b]	0.995 kg
Number of fissile particles in an average fuel element[b]	1.35×10^7
Number of fertile particles in an average fuel element[b]	1.63×10^6
Electrical energy generated by an average fuel element at discharge[b]	0.637 MW_e-yr

Notes
a. Calculated assuming a solid hexagonal prism with all fuel and coolant holes filled, i.e., this is the physical volume a fuel element would occupy.
b. Values for an average fuel element are determined by assuming heavy metal (uranium) is distributed uniformly in the reactor core.
c. This value includes graphite and fuel compacts, but excludes lumped burnable poison.
d. This value excludes carbon in the layers of the coated particles. For an average fuel element, there is an additional 4.13 kg of carbon associated with fissile particles and an additional 0.62 kg of carbon associated with fertile particles.

3.1.1.2 Reactor Core and Internals

Figure 3-4 shows the MHR core design. The MHR active core consists of 102 fuel columns in three annular rings with 10 fuel blocks per fuel column, for a total of 1020 fuel blocks in the active core. As shown in Fig. 3-5, the core is designed with 120-degree symmetry and the control rods are also operated symmetrically. The outer reflector contains 36 control rods, arranged as 12 groups with 3 rods per group. There are 4 control-rod groups in the active core, again with 3 rods per group. The core also contains 18 channels for insertion of reserve shutdown control (RSC) material (in the form of boronated pellets), in the event the control rods become inoperable. During operation, control rods in the active core are completely withdrawn, and only the control rods in the outer reflector are used for control. This control method precludes damage to the in-core control rods during loss-of-coolant accidents. A control rod design using a carbon-carbon composite for the cladding material is being evaluated that would allow the in-core rods (or control rods located in the inner reflector) to be used during normal operation, which will provide greater flexibility for flattening the radial power distribution and provide some additional margin for maintaining fuel temperatures and fuel performance within acceptable limits.

For the equilibrium fuel cycle, one-half of the core (510 fuel elements) is reloaded every 425 full-power days, corresponding to an equilibrium residence time of 850 effective full-power days (EFPD) for each fuel element. Each reload segment contains 1746 kg of low-enriched uranium and 507 kg of natural uranium.

In addition to the fuel elements, other graphite reactor internal components include the side, central, top, and bottom graphite reflector elements and the graphite core support assembly. Fuel and reflector elements are aligned using four dowel/socket connections at each axial element-to-element interface. Metallic reactor internal components include the metallic core support, the upper core restraint, and the upper plenum shroud. These metallic components are manufactured from high-temperature alloys (e.g., Incoloy 800H, Hastelloy-X, or Inconel 617).

From top to bottom, the graphite core support assembly consists of two layers of hexagonal elements, support pedestals for the fuel and reflector columns that form the lower plenum, and the lower plenum floor, which consists of a layer of graphite elements and two layers of ceramic elements that insulate the metallic core support from the hot helium in the lower plenum. The upper core restraint elements have the same hexagonal cross sections as the graphite elements below them and are one-half the height of a standard fuel element. Dowel/socket connections are used to align the core-restraint elements with the graphite blocks. The core restraint elements are also keyed to each other and to the core barrel. The upper core restrain blocks provide stability during refueling and maintain relatively uniform and small gaps between columns during operation. The metallic core support surrounds the core and includes a floor section and a core barrel that are welded together. The metallic core support is supported both vertically and laterally by the reactor vessel. The upper plenum shroud is a welded, continuous dome that rests on top of the core barrel to form the upper plenum. The upper plenum shroud includes penetrations for inserting control rods and reserve shutdown material, for refueling, and for core component replacement.

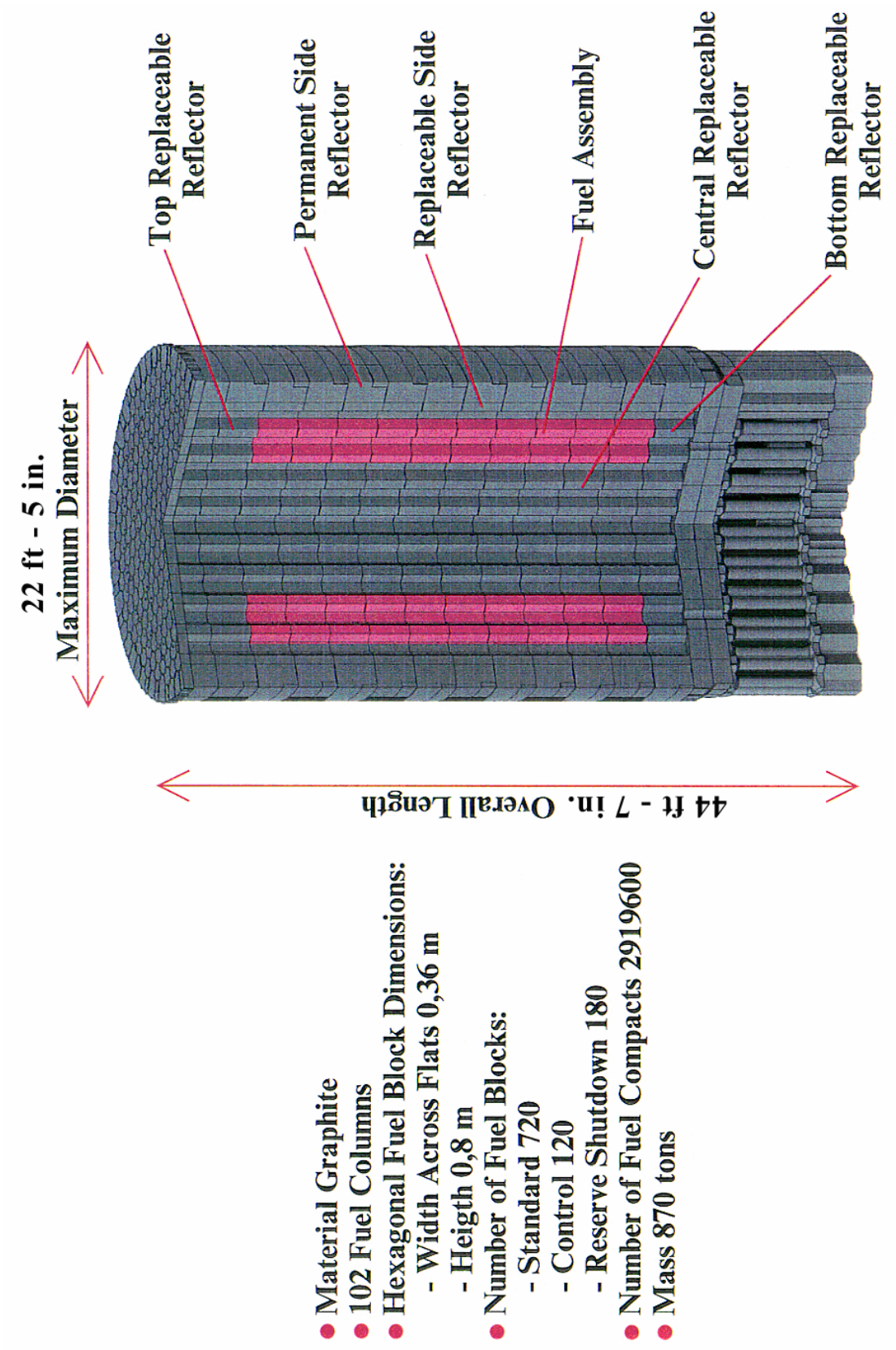

Figure 3-4. MHR Core Design

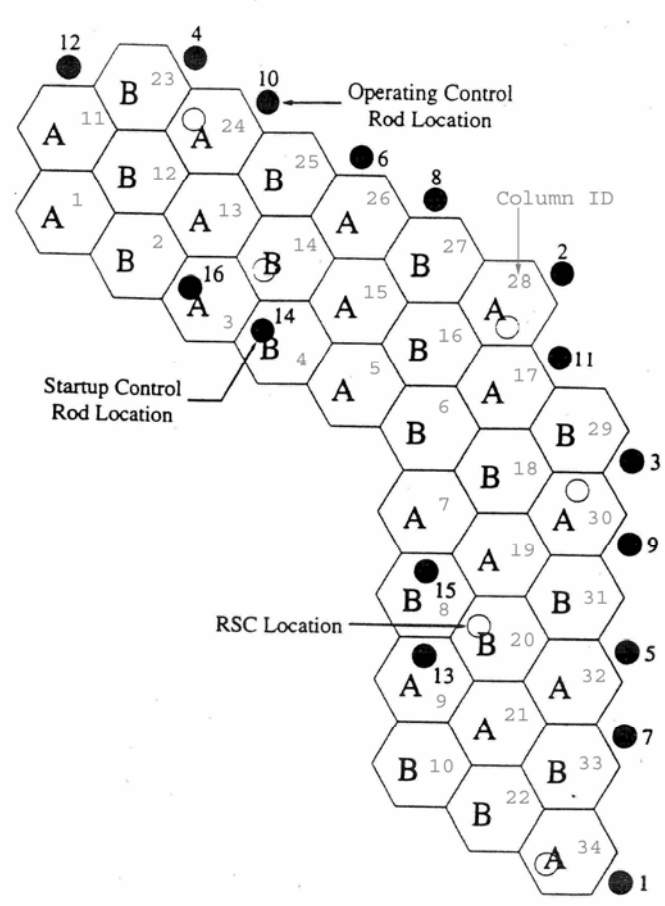

Figure 3-5. MHR Core Arrangement. The letters A and B identify the two fuel segments. The numbered, filled circles identify locations of the control-rod groups. The open circles identify the locations of RSC channels.

3.1.1.3 Neutron Control System

The neutron control system design is the same as that for the GT-MHR (Ref. 1). The system components consist of inner and outer neutron control assemblies, source-range detector assemblies, ex-vessel neutron detector assemblies, and the in-core flux mapping system. The locations of neutron control assemblies and RSC channels are shown in Fig. 3-5.

Figure 3-6 shows the design of an outer neutron control assembly and Fig. 3-7 shows installation of the neutron control assemblies in the top head of the reactor vessel. The structural equipment consists of an upper structural frame, gamma shielding, neutron shielding, thermal barrier, upper and lower guide tubes, and seals. The gamma shielding is a corrosion-resistant plug that protects maintenance crew against gamma radiation from the core and activated control rods. The neutron shielding consists of boronated graphite elements that

prevent activation of the upper portion of the vessel. The control rod guide tubes extend from the gamma shielding downward through the top head of the reactor vessel and upper plenum shroud to the upper core restraint elements. The guide tubes provide a clear passage for the control rods as they are inserted into and withdrawn from the core.

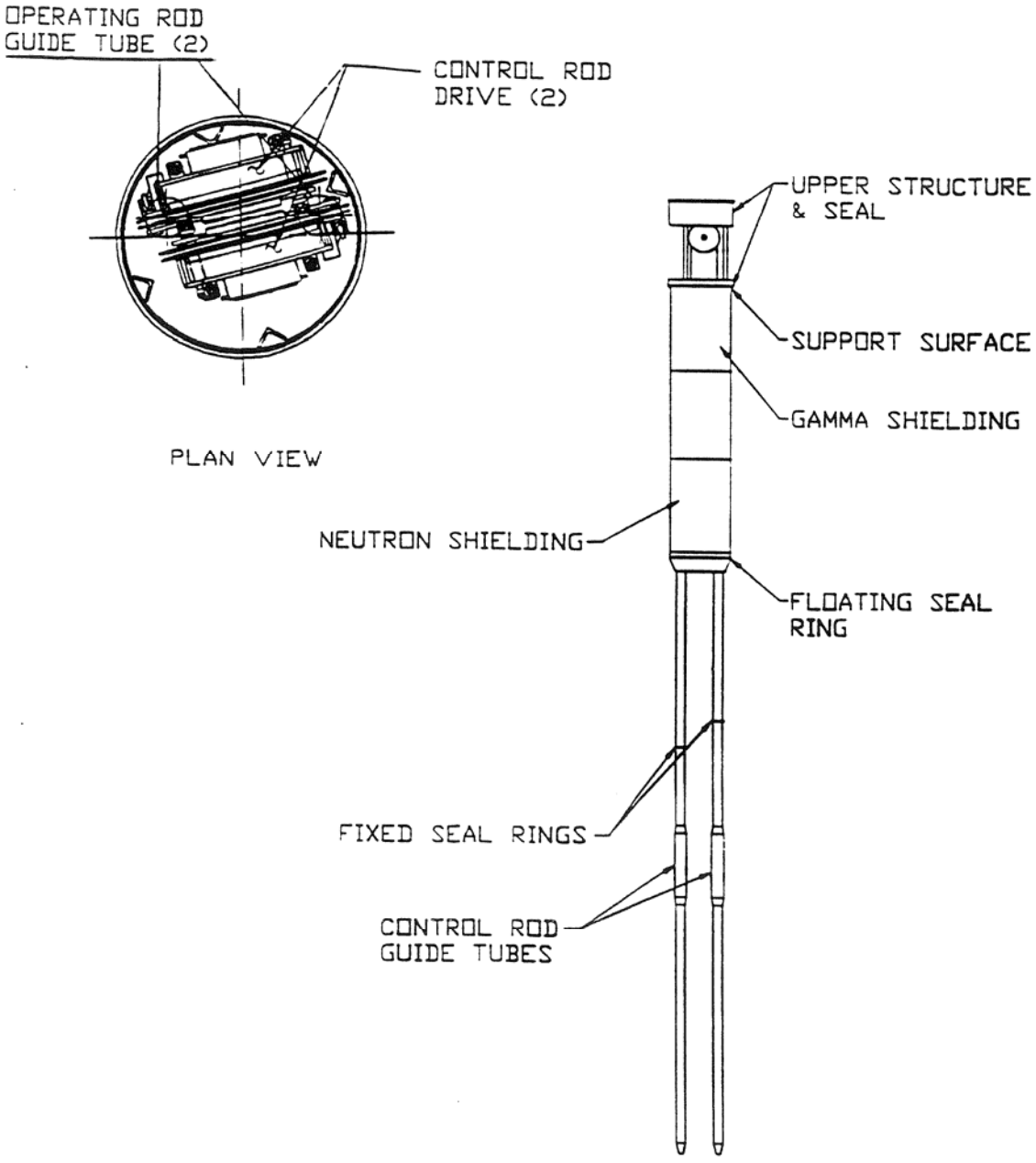

Figure 3-6. Outer Neutron Control Assembly Design

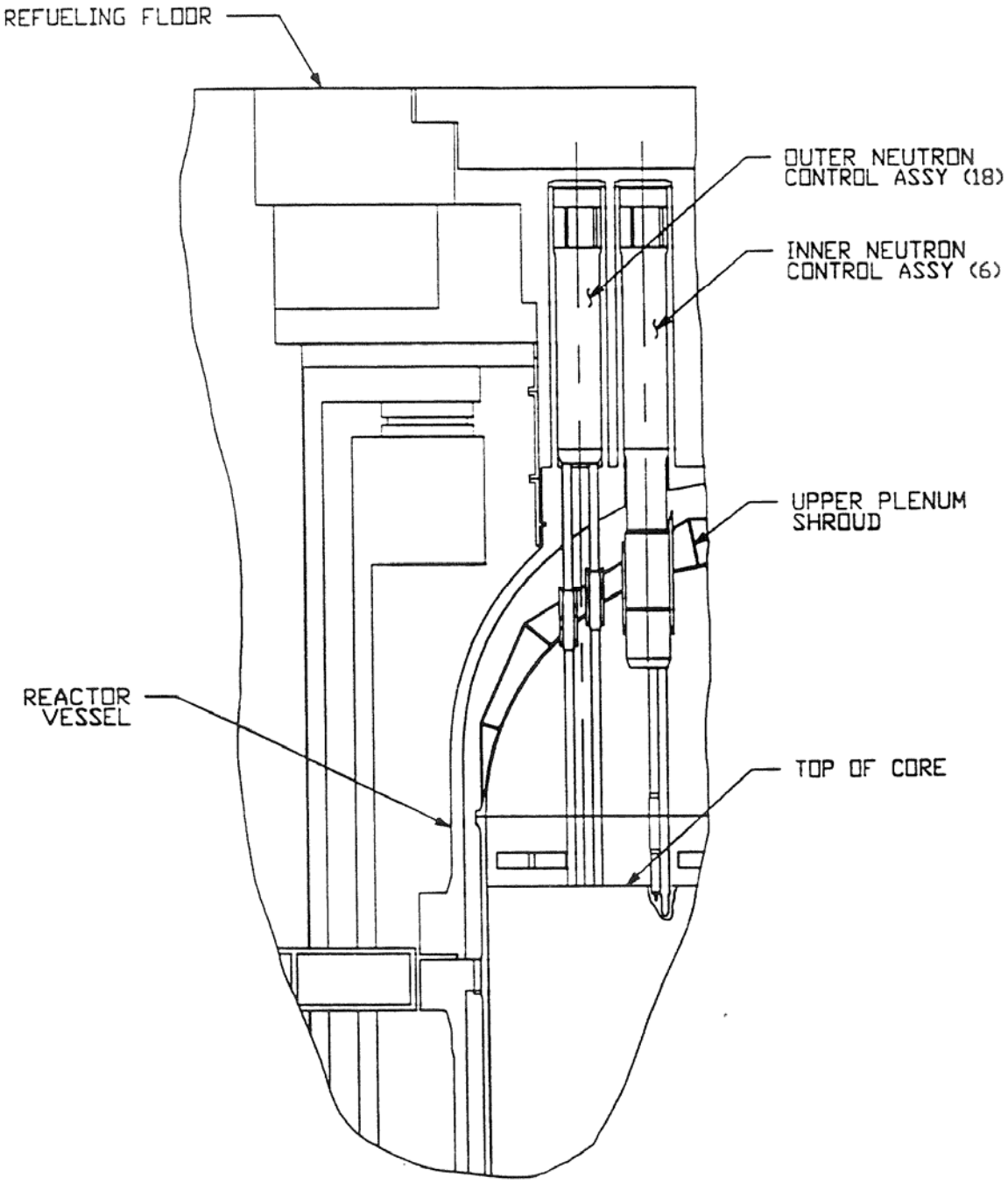

Figure 3-7. Neutron Control Assembly Installation

All neutron control assemblies are equipped with two independent control rod drive units. The control rod drive equipment is located in the upper part of the neutron control assembly. The equipment consists of a DC torque motor, a 60:1 speed reducer, and a cable storage drum, all of which are mounted on a metal frame. The control rod is lowered and raised with a flexible high-nickel alloy cable.

Figure 3-8 shows the control rod design. The neutron absorber material consists of B_4C granules uniformly dispersed in a graphite matrix and formed into annular compacts. The boron is enriched to 90 weight percent B-10 and the compacts contain 40 weight percent B_4C. The compacts have an inner diameter of 52.8 mm and an outer diameter of 82.6 diameter, and are enclosed in Incoloy 800H canisters for structural support. Alternatively, carbon-fiber reinforced carbon (C-C) composite canisters may be used for structural support. The control rod consists of a string of 18 canisters with sufficient mechanical flexibility to accommodate any postulated offset between elements, even during a seismic event.

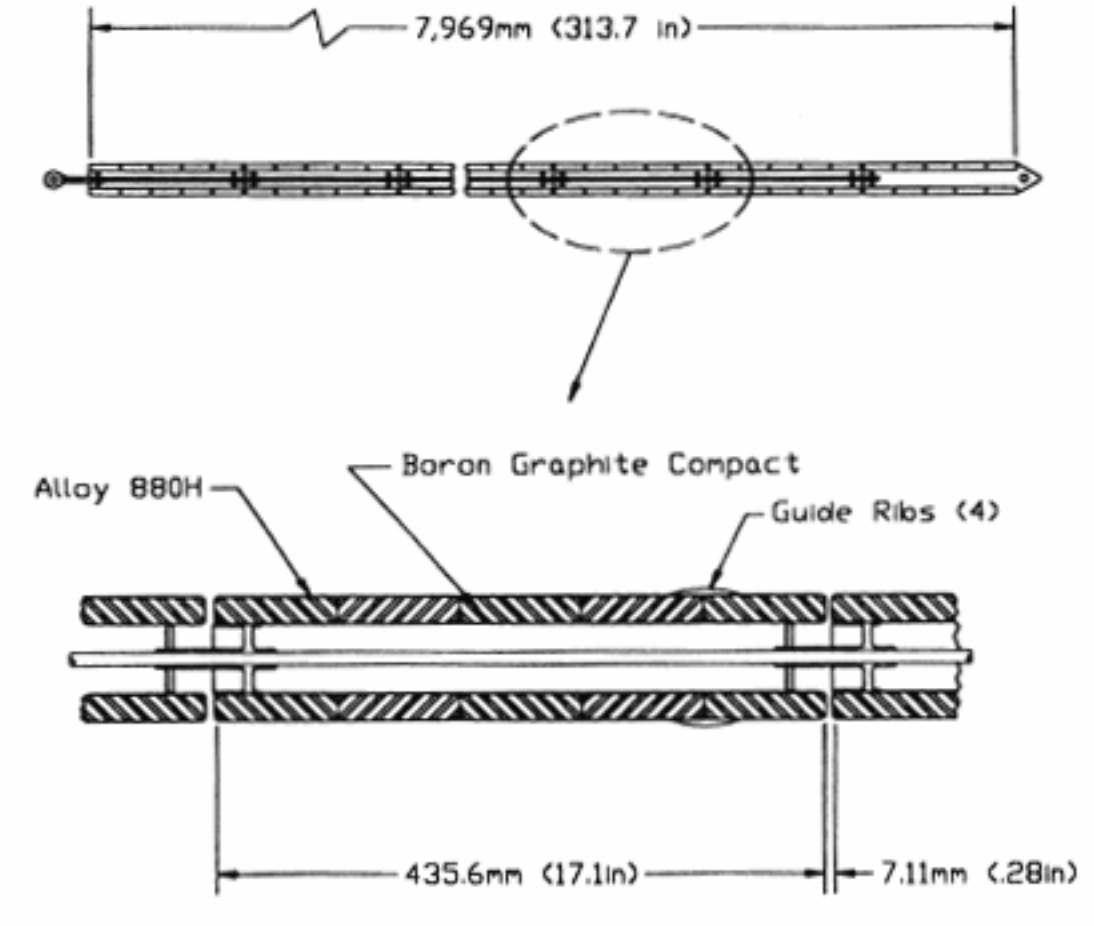

Figure 3-8. Control Rod Design

The reserve shutdown control material is of the same composition as that for the control rods, except the B_4C granules and graphite matrix are formed into cylindrical pellets with rounded ends and a diameter of 14 mm. The B_4C granules are coated with dense PyC to prevent oxidation during off-normal events. The pellets are stored in hoppers located above the reactor core in both the both the inner and outer neutron control assemblies.

During normal operation, the neutron flux levels are monitored by 6, symmetrically-spaced ex-vessel fission chamber thermal neutron detectors. The signals from these detectors interface with the automatic control and protection systems to operate the control rod drives or the

reserve shutdown control equipment. Three fission chamber source-range detectors are used to monitor neutron flux during startup and shutdown. These detectors are symmetrically spaced in reentrant penetrations located in the bottom head of the reactor vessel. These penetrations extend into vertical channels in the reflector elements near the bottom of the core. The in-core flux mapping system consists of movable detectors in the central column of the inner reflector and in the outer permanent reflectors. The system enters from a housing located above the reactor vessel and vertically traverses down through the core to the bottom reflectors. The system contains two independent fission chambers and a single thermocouple.

3.1.2 Cross Vessel and Hot Duct Assembly

As shown in Fig. 3-9, the hot duct is concentrically located within the cross vessel. The hot duct provides the hot-leg primary coolant flow path from the reactor vessel to the IHX vessel. The annular space between the hot duct assembly and cross vessel provides the cold-leg primary coolant flow path from the IHX vessel to the reactor vessel. The hot duct assembly includes a ceramic fiber insulation layer to minimize heat transfer between the hot-leg and cold-leg flow paths. The hot duct material is a high-temperature alloy (e.g., Incoloy 800H, Hastelloy-X, or Inconel 617).

The cross vessel is a one-piece forged cylinder that is designed and fabricated according to Section III of the ASME Code. The cross vessel has an inner diameter of 2.29 m, a wall thickness of 7.62 cm, and is approximately 2.86 m in length. The reference material for the cross vessel is 9Cr-1Mo-V steel. Other candidate materials are 2¼Cr-1Mo steel and 15Cr-2Mo-V steel. As discussed in Section 3.1.4, a design alternative is being considered to incorporate cooling of the reactor vessel, such that proven light water reactor vessel materials (e.g., SA533 steel) could be used for the reactor vessel without causing creep damage. If this alternative is selected, the cross vessel would also likely be manufactured using the same material, which would require using internal insulation to protect the cross vessel from creep damage.

3.1.3 Reactor Vessel

The H2-MHR reactor vessel design is nearly identical to that for the GT-MHR. Modifications to the H2-MHR reactor vessel design for higher temperature operation are described in Section 3.1.4.

As shown in Fig. 3-10, the reactor vessel is composed of a main cylindrical section with hemispherical upper and lower heads. The upper head is bolted to the cylindrical section and includes penetration housings for the neutron control assemblies and the in-vessel flux monitoring unit. These housings are sealed with a blind flange. The lower head is welded to the cylindrical section and includes penetrations for the Shutdown Cooling System (SCS), in-service inspection access, and source-range neutron detectors. The upper portion of the lower head incorporates a ring forging that provides support to the core through the core support structure. Lateral seismic restraint is provided to the core by six lugs welded to the interior surface of the vessel, near the top of the cylindrical section. The cylindrical section also includes a nozzle forging for attachment of the cross vessel, reactor vessel support lugs, and lateral restraint keys. The reference material for the reactor vessel is 9Cr-1Mo-V steel. Other candidate materials are 2¼Cr-1Mo steel and 15Cr-2Mo-V steel. The reactor vessel design parameters are given in Table 3-5.

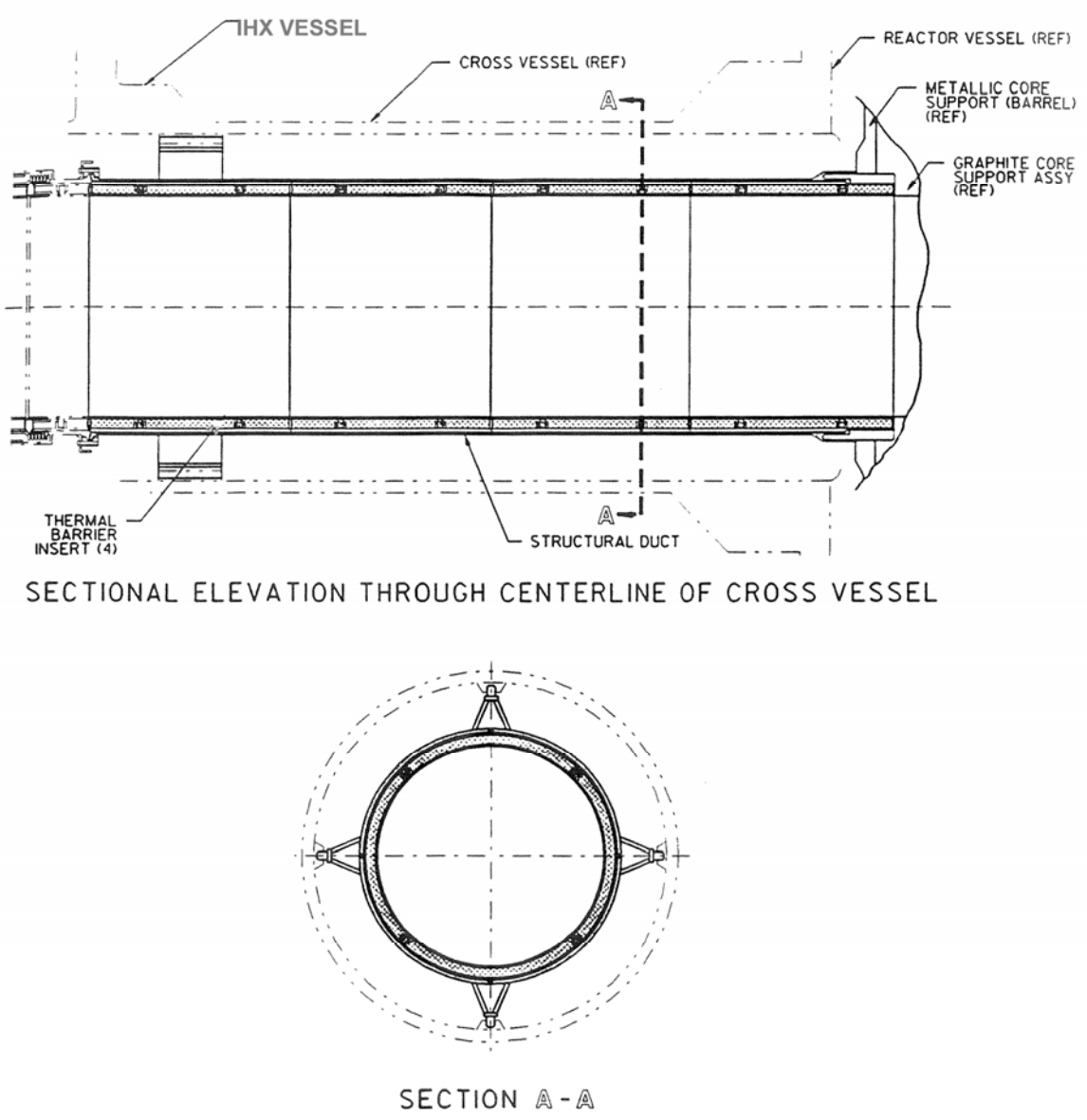

Figure 3-9. Hot Duct Assembly

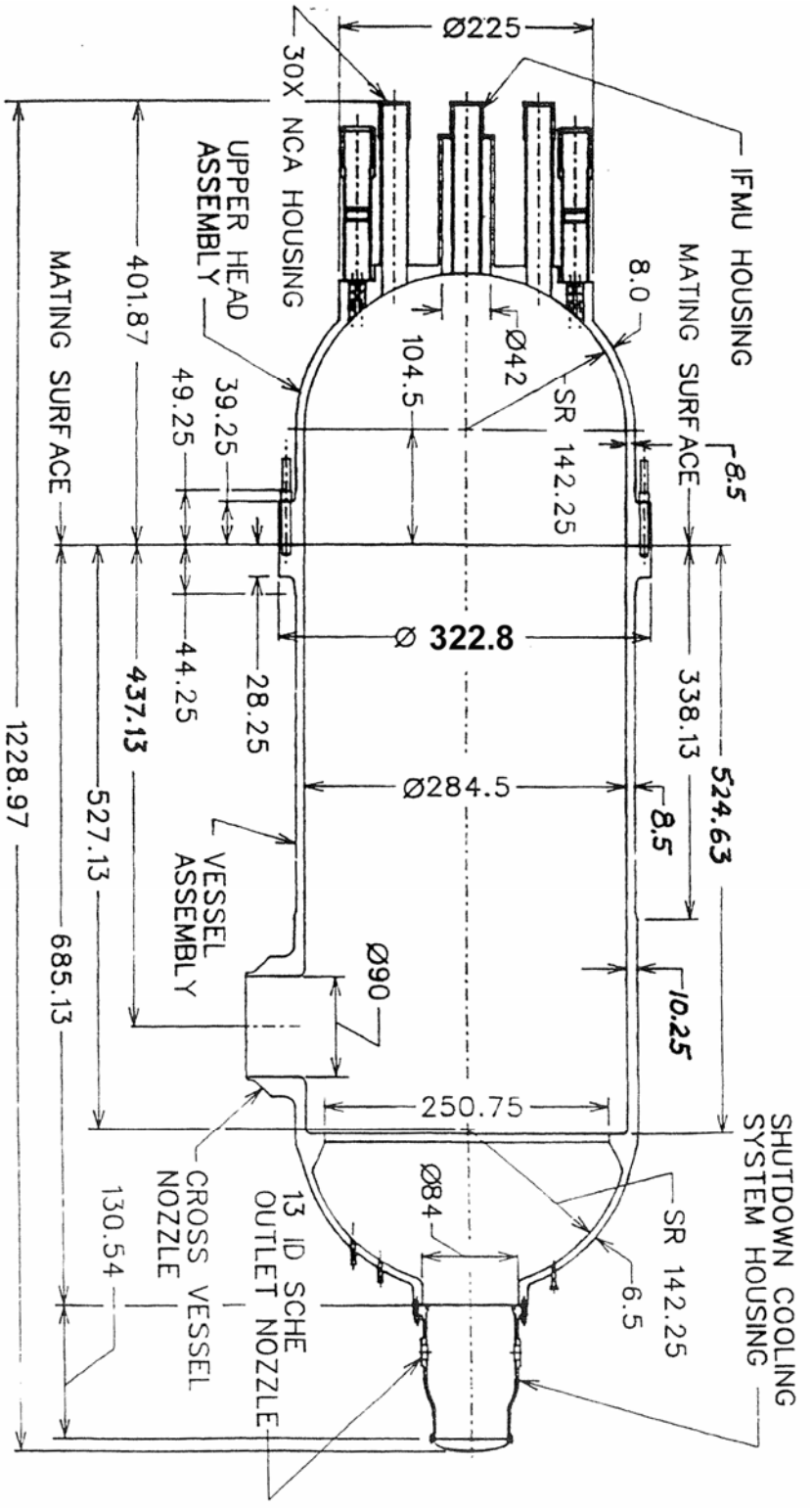

Figure 3-10. Reactor Vessel (dimensions are in Inches)

Table 3-5. Reactor Vessel Design Parameters

Reference Material	9Cr-1Mo-V steel
Height	31.0 m
Vessel Inner Diameter	7.2 m
Vessel Outer Diameter	8.2 m (at flange)
Wall Thicknesses	
Top Head	0.203 m
Shell	0.216 m
Thickened Ring	0.261 m
Bottom Head	0.165 m
Total Vessel Assembly Weight	838 mt
Upper Head Weight	490 mt
Design Lifetime	60 y
Design Temperature	495°C

3.1.4 Design Modifications for Higher Temperature Operation

Modifications to the MHR design for higher temperature operation include routing the inlet flow through holes in the Permanent Side Reflector (PSR) to lower vessel temperatures, optimization of the fuel block loading during refueling to reduce peak power factors, and minor changes to the reactor internal design to reduce bypass flow. An additional modification under consideration is using a slipstream flow of lower temperature helium to provide vessel cooling, such that proven light water vessel materials could be used for the MHR vessel.

3.1.4.1 Inlet Flow Configuration Modifications

The GT-MHR was designed to operate with coolant inlet and outlet helium temperatures of 490°C and 850°C, respectively. For the GT-MHR, the inlet coolant flow is routed through riser channel boxes between the core barrel and vessel (see Fig. 3-11). With this configuration, the design of the reactor vessel (including wall thickness and materials selection) is driven in large measure by the design point selected for the coolant inlet temperature. For the GT-MHR, the inlet temperature also has a significant impact on performance of the PCS. The design point of 490°C ensures high-efficiency operation of the PCS and acceptable operating conditions for a reactor vessel manufactured from a Cr-Mo steel (e.g., 2¼Cr-1Mo, 9Cr-1Mo-V, and 15Cr-2Mo-V). The design point of 850°C for the outlet temperature eliminates the need for turbine blade cooling and ensures acceptable performance of the ceramic coated-particle fuel during normal operation.

For the H2-MHR, it is desirable to increase the coolant outlet temperature in order to improve the efficiency and economics of hydrogen production, and a design point of 950°C has been selected. Scoping calculations have shown a point design with coolant inlet and outlet temperatures of 490°C and 1000°C, respectively may be feasible in terms of acceptable fuel temperatures during normal operation if the coolant flow distribution is optimized to divert more flow to the hotter columns using fixed orifices in the upper and/or lower reflectors of the cooler columns [Richards 2004]. However, confirmation of this design option will require a significant level of design work, including developing a fuel cycle that ensures relatively stable power

distributions over the entire fuel cycle and for all anticipated operating conditions. Also, operating with an outlet temperature above 950°C will have a significant impact on the IHX design and may require a ceramic or super-alloy IHX, which could involve a significant period of development and testing before it is qualified as a nuclear reactor primary coolant boundary.

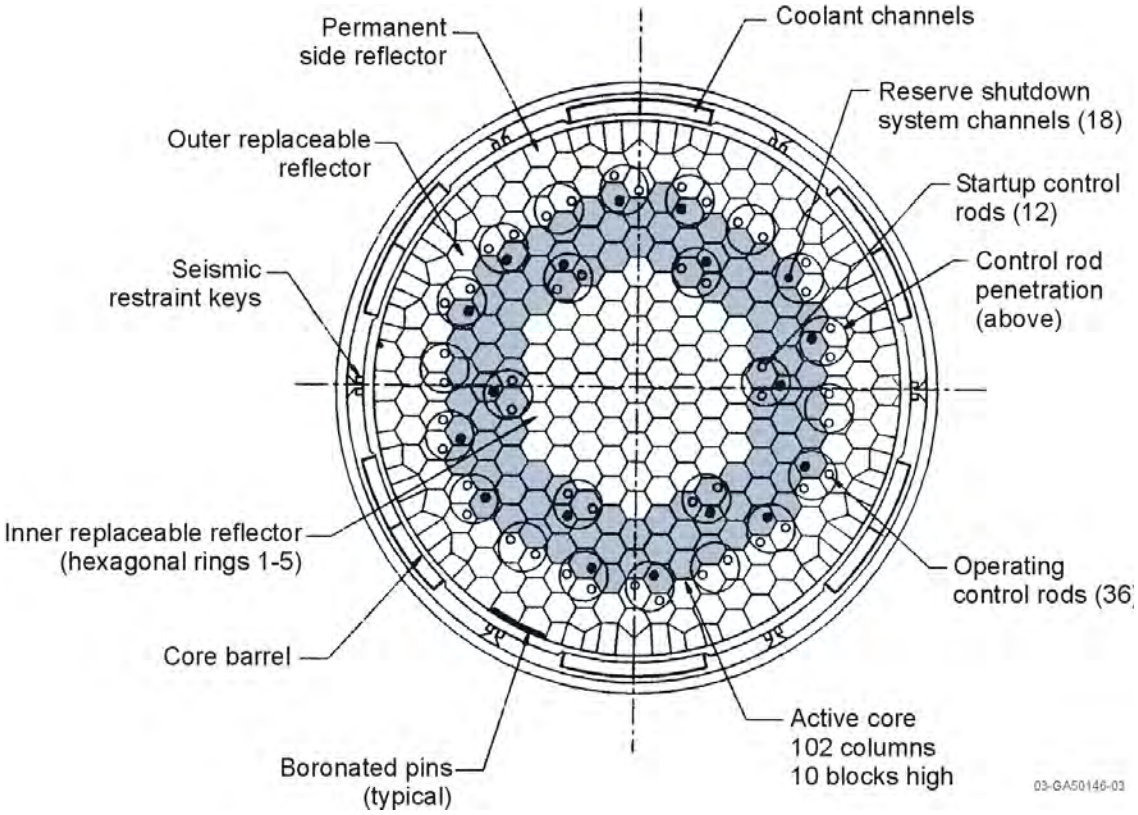

Figure 3-11. GT-MHR Cross Section at Vessel Midplane. Inlet flow is routed through the channel boxes located between the core barrel and reactor vessel.

The coolant inlet temperature was also increased by 100°C to 590°C to provide a sufficiently high coolant flow and convective heat-transfer rate within the MHR core that ensures acceptable fuel performance and limits release of Ag-110m and other noble-metal fission products that can diffuse through intact SiC coatings at high temperatures. However, this higher coolant-inlet temperature will result in reactor vessel temperatures that could exceed the limits for Cr-Mo steels if the current GT-MHR flow configuration was used. Higher vessel temperatures will also result in higher parasitic heat losses to the RCCS during normal operation.

The Advanced Thermal Energy Network Analysis (ATHENA) code [Carlson, 1986] was used to assess the impact of higher coolant temperatures on steady-state vessel temperatures, parasitic RCCS heat losses, and fuel temperatures during normal operation and accident conditions. Both the reference GT-MHR inlet flow configuration and two alternative inlet flow configurations were evaluated. These alternative configurations route the flow through either holes in the inner

reflector [see Fig. 3-12(a)] or holes in the PSR [see Fig. 3-12(b)], in order to increase the thermal resistance between the inlet flow path and the vessel. Preliminary evaluations showed that both configurations had nearly the same effect in terms of reducing vessel temperatures and parasitic heat losses to the RCCS. However, routing the inlet flow through the inner reflector resulted in a greater loss of heat capacity (from removal of graphite to provide the flow paths), which caused peak fuel temperatures to increase by about 40°C during a depressurized loss-of-coolant accident (LOCA). For these reasons, the PSR inlet flow configuration was adopted for the H2-MHR. Figure 3-13 shows a cross-sectional view of the revised configuration with inlet coolant holes in the PSR.

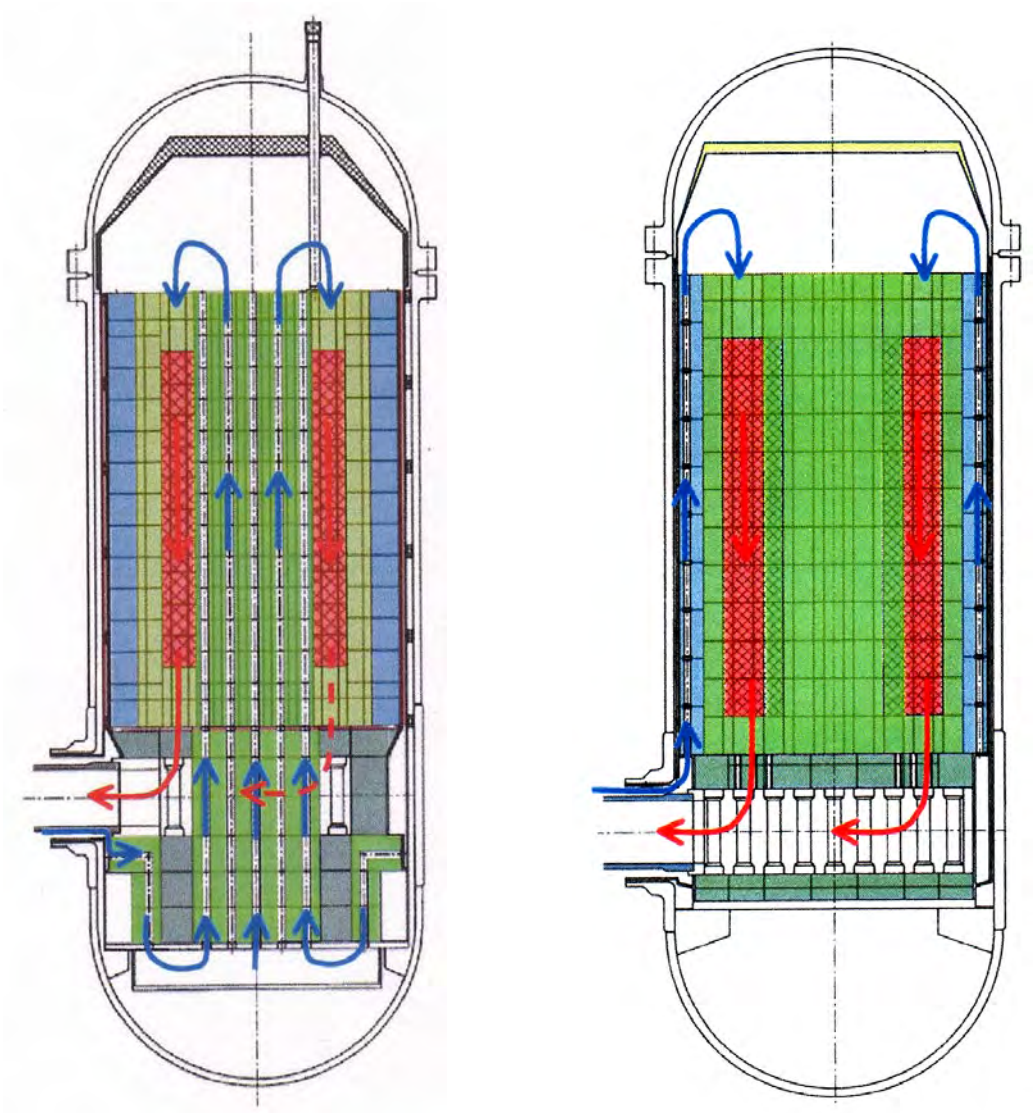

Figure 3-12. Reactor Vessel Configured with Alternative Inlet Flow Paths. (a) Flow routed through inner reflector. (b) Flow routed through PSR. (Figure courtesy of Fuji Electric Systems, Kawasaki-city, Japan)

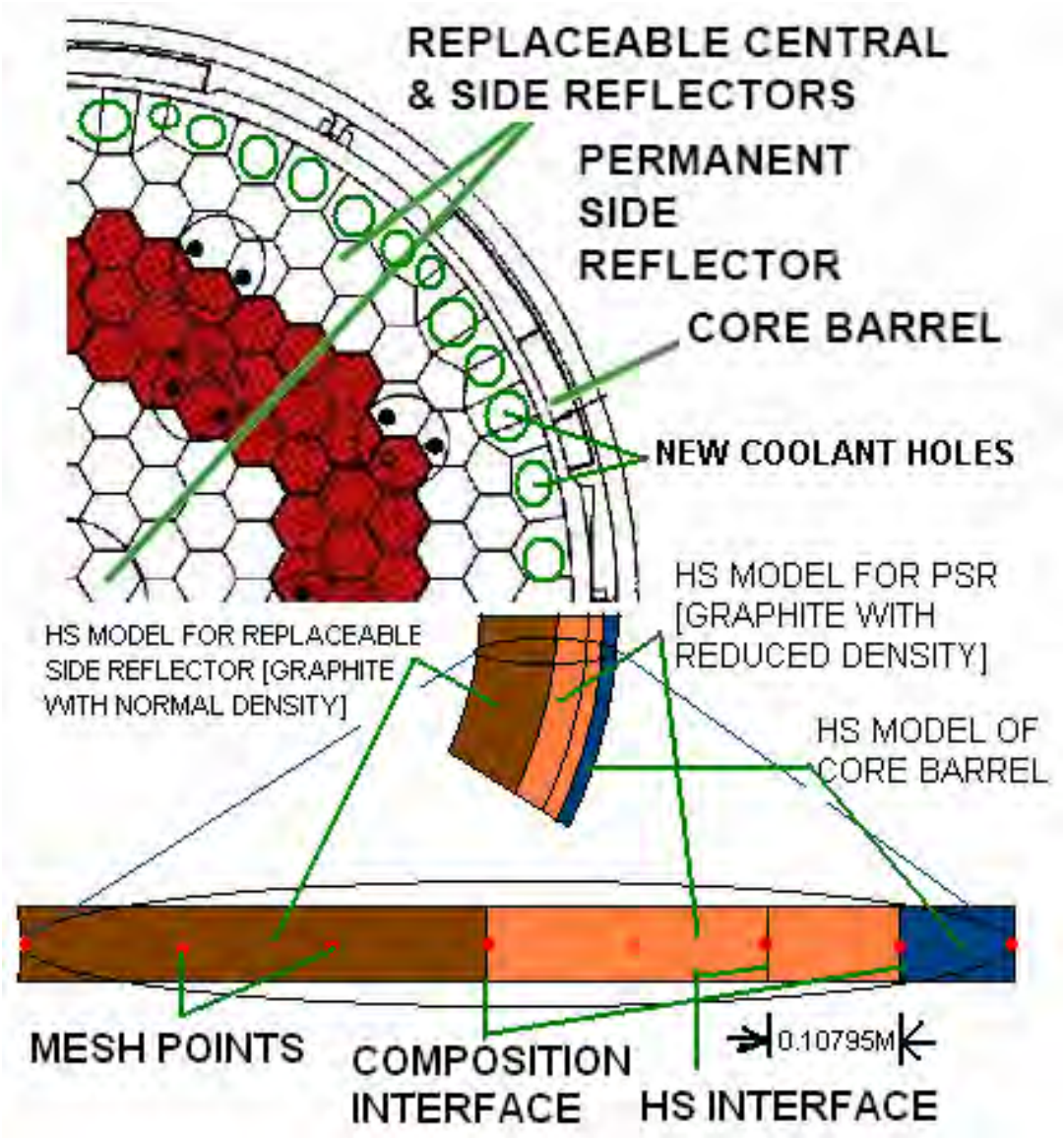

Figure 3-13. MHR Configured with PSR Inlet Flow (HS = ATHENA Heat Structure)

Figure 3-14 shows the ATHENA thermal hydraulic model for the MHR vessel and internals. The active core is modeled as three annular rings with an axial node for each of the ten fuel blocks in the active core. Flow from the upper plenum to the outer plenum is modeled using five parallel channels. Three of these channels provide cooling for the active core (one channel for each fuel ring) and two channels are used to represent bypass flow. Radial and axial conduction are modeled in active core and reflectors, and radiative heat transfer is modeled between the core barrel and reactor vessel. Heat is conducted through the reactor vessel and radiative heat transfer is modeled between the reactor vessel and RCCS. Figure 3-15 shows the ATHENA thermal hydraulic model for the RCCS. ATHENA heat structures are used to model the RCCS risers and downcomers.

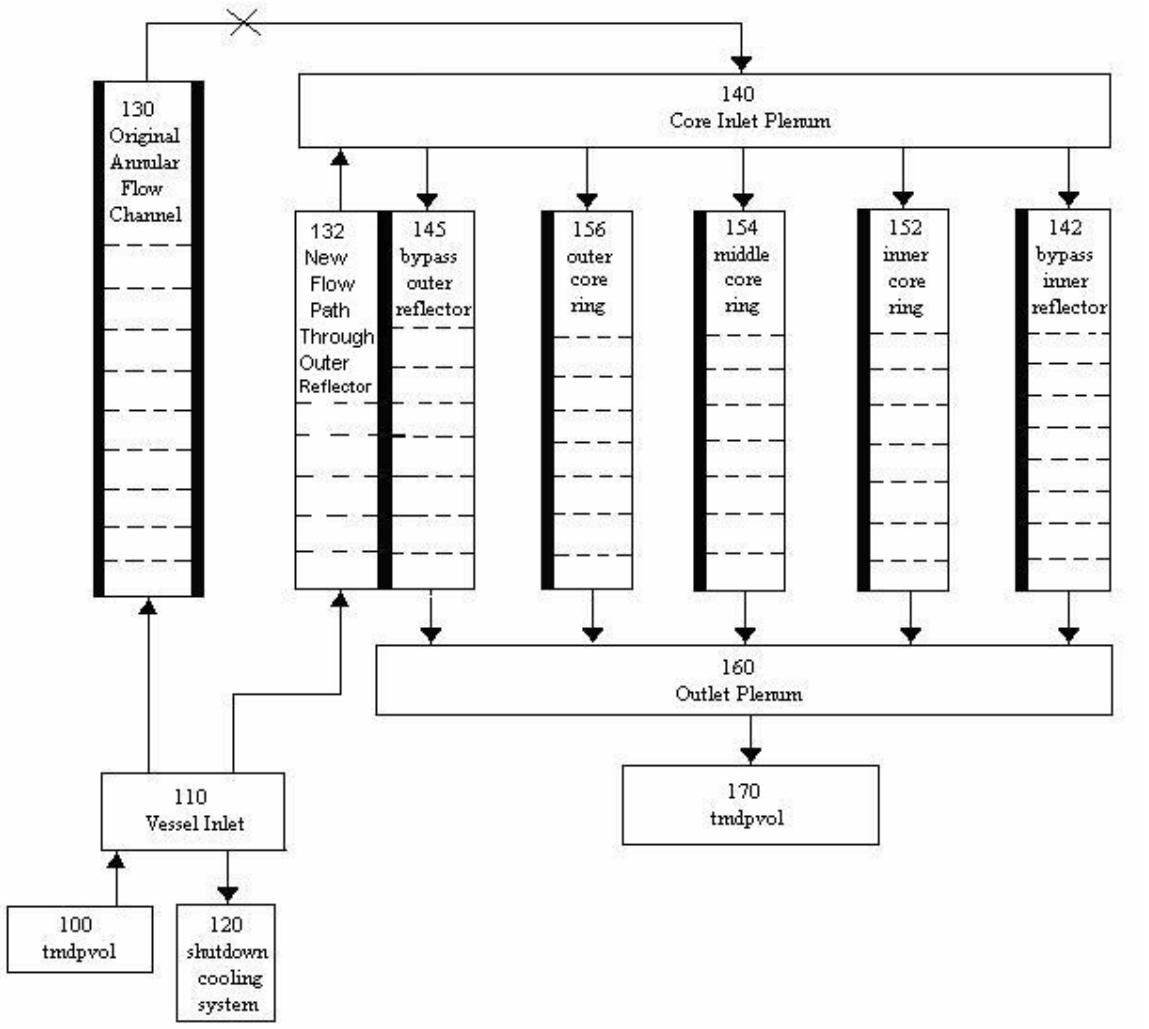

Figure 3-14. ATHENA Model for the MHR Vessel and Internals

Calculations performed using the current GT-MHR flow configuration are given in Table 3-5. Increasing the coolant inlet temperature from 490°C to 590°C causes the peak vessel temperature to increase from 453°C to 541°C, which exceeds the design limit of 495°C specified for 9Cr-1Mo-V steel (see Table 3-6). The parasitic heat loss to the RCCS increases from 3.3 MW to 4.5 MW and the core pressure drop increases by about 10% because of the increase in helium viscosity with temperature.

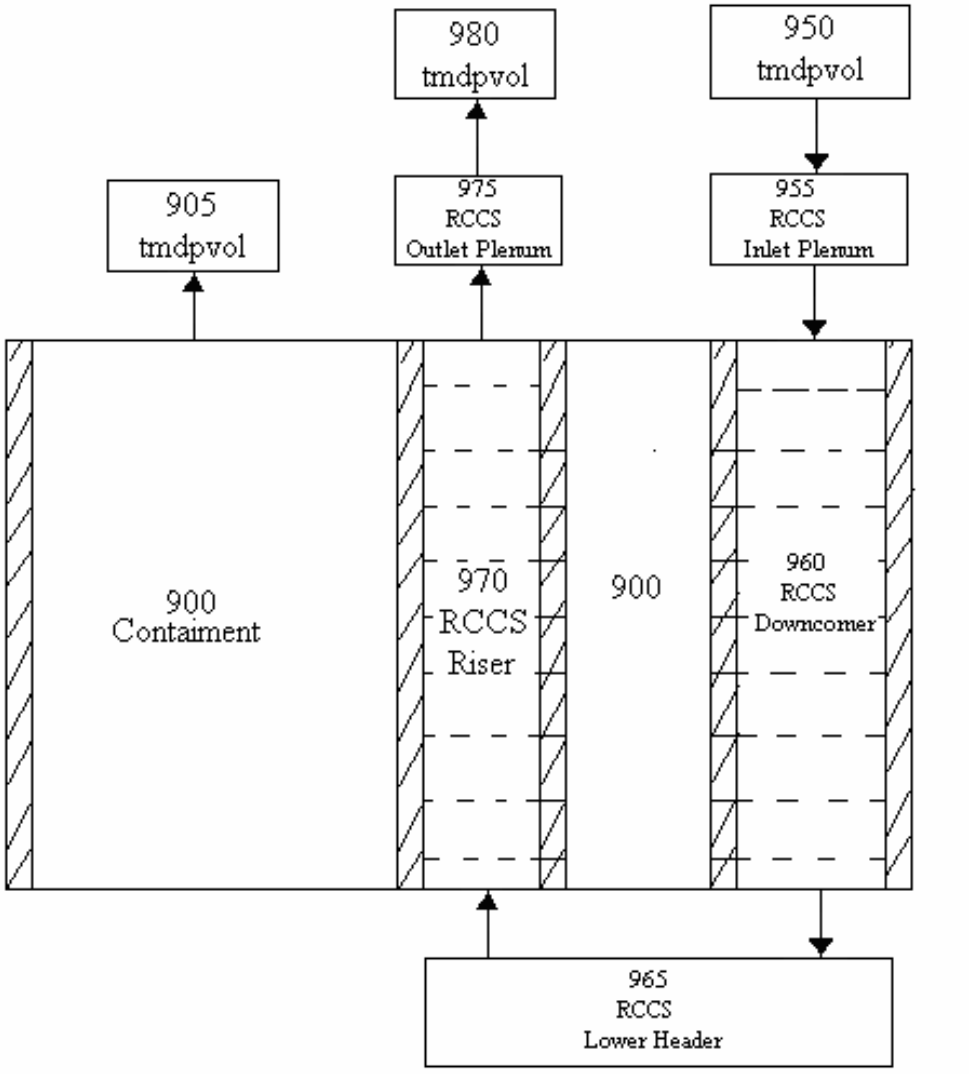

Figure 3-15. ATHENA Model for the RCCS

Table 3-6. Impact of Higher Coolant Temperatures (Reference GT-MHR Flow Configuration)

	Coolant Inlet/Outlet Temperature (°C)	
	490/850	**590/950**
Maximum Vessel Temperature (°C)	453	541
Parasitic Heat Loss to RCCS (MW)	3.3	4.5
Total Core Pressure Drop (kPa)	51	56

Calculations were performed with the ATHENA model to optimize the PSR inlet flow configuration. Considerations included the quantity of graphite (and associated heat capacity) removed to form the coolant holes, total pressure drop through the vessel and its impact on pumping power requirements, and coolant inlet velocity. Inlet coolant hole diameters of 4, 6, and 8 inches were used, depending on the cross-sectional area and shape of the PSR columns. The reconfigured PSR blocks should provide sufficient wall thicknesses to accommodate stresses and, if necessary, provide space to include boronated rods to reduce the accumulated fast neutron fluence to the reactor vessel. Parameters for the optimized PSR inlet flow configuration are given in Table 3-7. The maximum steady-state fuel temperature was predicted to be 1106°C. These calculations were performed using centrally-peaked axial power profiles. The maximum fuel temperature will be approximately 100°C higher under conditions of partial control rod insertion, which shifts the peak axial power factor towards the bottom of the core where coolant temperatures are higher. However, the fuel temperatures should be well within the margins of acceptable performance for SiC-TRISO fuel under all anticipated conditions for normal operation. The maximum steady-state vessel temperature was predicted to be 420°C, which is well within the margin for acceptable performance of 9Cr-1Mo-V steel. Additional analyses are needed to determine the impact on vessel temperatures of any leakage flow from the PSR inlet flow path to the annular space between the core barrel and reactor vessel.

Table 3-7. Optimized PSR Inlet Flow Configuration

PSR Total Inlet Coolant Flow Area	1.64 m^2
Total Graphite Removed from Outer Reflector	10%
Number of Coolant Holes	
4 in.	18
6 in.	18
18 in.	36
Total Vessel Pressure Drop	80 kPa
Maximum Steady State Fuel Temperature	1106°C
Maximum Steady State Vessel Temperature	420°C
Parasitic Heat Loss to RCCS	2.1 MW
Maximum Coolant Velocity in Core	53.2 m/s
Maximum Inlet Coolant Velocity in PSR	45.5 m/s

The primary impact of the PSR inlet flow configuration is an increase in total vessel pressure drop of about 25 kPa, primarily because the inlet flow area is reduced from 4.62 m^2 for the original channel-box flow configuration to 1.64 m^2 for the PSR flow configuration. As shown in Section 4.1, the PSR inlet flow configuration has little impact on fuel and vessel temperatures during accident conditions.

3.1.4.2 Vessel Cooling

Although 2¼Cr-1Mo steel was used to manufacture the reactor vessel for the JAEA 30-MW(t) High Temperature Test Reactor, there is limited experience with using this material, and no

large nuclear reactor vessels have been manufactured using this material or 9Cr-1Mo-V steel. For this reason, it is of interest to pursue design options that would lower the vessel temperature, such that proven light water reactor vessel materials (e.g., SA533 steel) could be used for the MHR vessel. JAEA has adopted a configuration for the GTHTR300 design (which is similar to the GT-MHR) that routes a small fraction of the 140°C flow from the high-pressure compressor to a path between the core barrel and reactor vessel in order to keep the SA533 vessel temperature below the creep-damage limit. For H2-MHR, a potential source of cold helium is the return path from the slipstream flow that is routed through the helium purification system to control chemical impurities and circulating radioactivity (see Section 3.3.1). Table 3-8 shows preliminary ATHENA results for peak fuel and vessel temperatures as a function of the cold helium flow rate used to provide vessel cooling. These results are consistent with the JAEA results, and show that vessel cooling may be a viable design option. However, additional analyses are required, particularly in terms of the impact of this configuration on passive safety and investment protection. If steel with higher-temperature capability is required for the reactor vessel, a viable option is 15Cr-2Mo-V, which has been used in Russia for nuclear pressure vessels.

Table 3-8. Reactor Vessel and Fuel Temperatures as a Function of Vessel Cooling Flow Rate

Vessel cooling flow rate (kg/s)	0	9.6	12.8	16.0
Vessel cooling inlet temperature (°C)	—	140	140	140
Coolant inlet temperature (°C)	590	590	590	590
Peak fuel temperature (°C)	1168	1172	1174	1176
Maximum wall-averaged vessel temperature (°C)	480	378	356	338

3.1.4.3 Power and Flow Distribution Optimization

At sufficiently high temperatures, failure of the SiC layer of the TRISO coating can occur as the result of corrosion by fission products (mainly Pd). Figure 3-16 shows an estimate (using GA design correlations) of the SiC layer failure probability as a function of time and temperature. Based on these calculations, temperatures in the range 1250°C to 1350°C have generally been adopted as a “rule of thumb” peak temperature limit for SiC-TRISO fuel during normal operation. Because the coolant flows downward through the MHR core, the peak fuel temperatures tend to occur toward the bottom of the core (see Fig. 3-17), and an increase in coolant-outlet temperature generally results in a near proportional increase in fuel temperature. However, the increase in coolant outlet temperature can be compensated for by optimizing the core power and flow distributions.

The baseline refueling scheme for the GT-MHR is to replace entire columns, such that at the beginning of an equilibrium cycle one-half of the core consists of fuel columns that contain fresh (“new”) fuel and the other half of the core consists of columns that contain “old” fuel that has been irradiated for one 425-EFPD cycle. Previous studies have shown that power distributions can be flattened if a concept referred to as fuel placement is used. With this concept, each column contains both new and old fuel in alternating layers at the beginning of an equilibrium cycle. In effect, fuel placement reduces the “age” component of power peaking. As shown in Fig. 3-18, the fuel-placement refueling scheme can reduce the peak column-averaged power factor by about 6%. Also, the use of high-temperature, composite-clad control rods will allow the use of control rods in the inner reflector, which could further reduce power peaking factors.

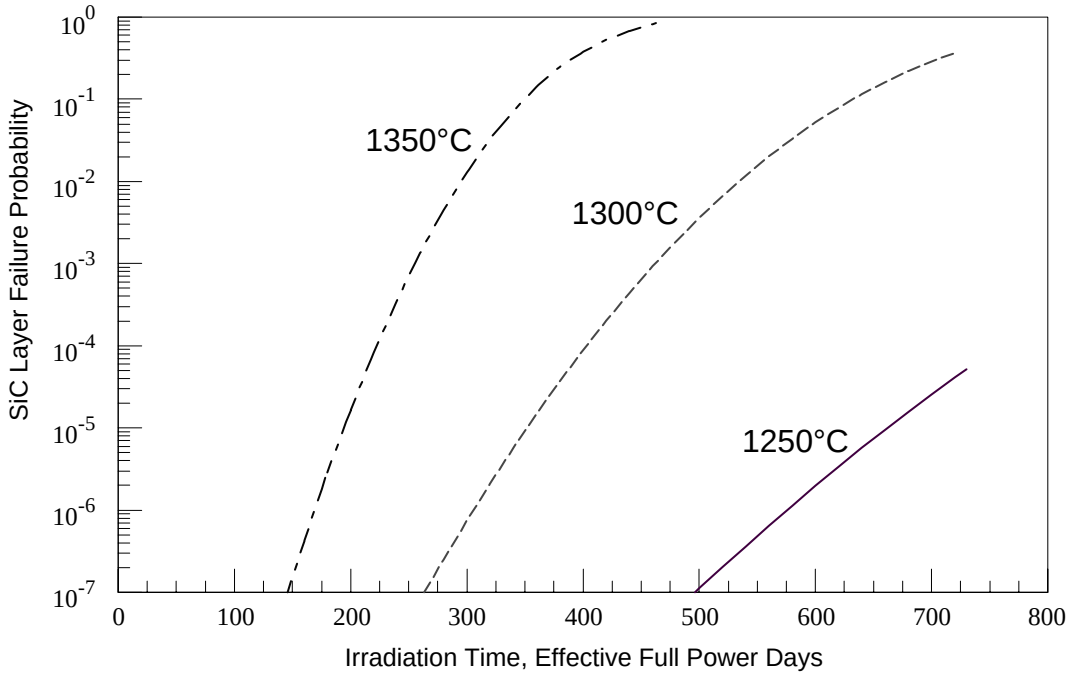

Figure 3-16. Predicted Failure of the SiC Layer by Fission Product Corrosion

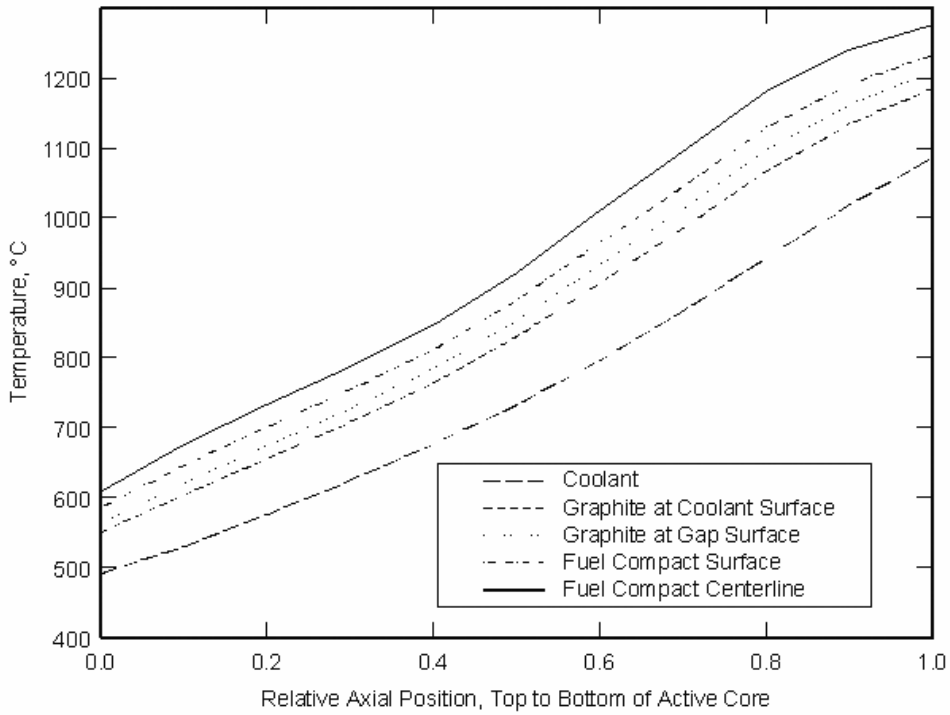

Figure 3-17. Axial Temperature Distribution in the H2-MHR Hot Coolant Channel

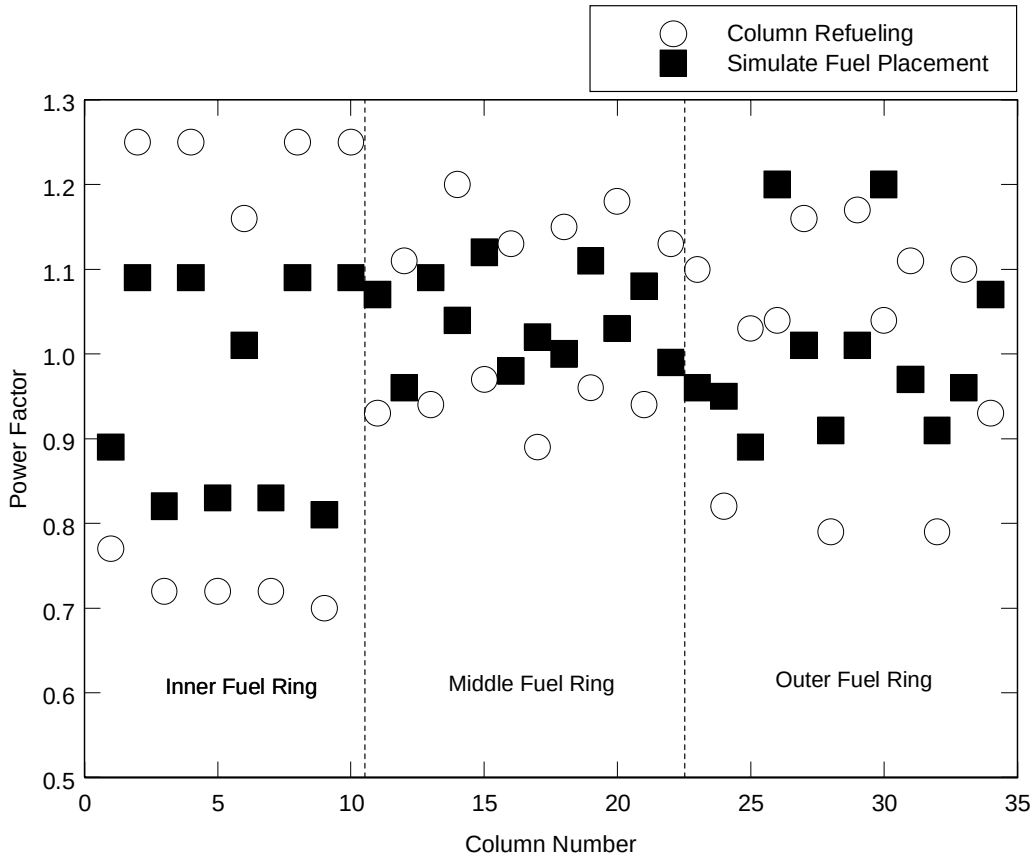

Figure 3-18. Column-Average Power Factors

Fuel temperatures can also be reduced by reducing bypass flow. For the reference GT-MHR core design, a portion of the coolant (~20%) bypasses the coolant holes and flows into gaps between the blocks and into control-rod channels. The control-rod channels have orifices to minimize bypass flow while also maintaining adequate cooling for the control rods. Approximately 3% of the coolant flows into control-rod channels. Composite-clad control rods require little or no cooling, which helps reduce the bypass flow fraction. Bypass flow can also be reduced by using additional lateral restraints and graphite sealing keys below the active core. Figure 3-19 shows a FLOWNET [Maruyama, 1994] model used to estimate the coolant flow distribution in the MHR core. Parametric studies performed with this model show that bypass flow near the bottom of the core (where temperatures are the highest) can be reduced to about 10% of the total flow [Richards, 2004].

Preliminary calculations have shown these measures to optimize the core nuclear and thermal hydraulic design should effectively compensate for the increase in the inlet and outlet coolant temperature design points, in terms of maintaining acceptable fuel temperatures during normal operation. If necessary, using fixed orifices on selected fuel columns can be used as an option to provide additional margin for fuel temperatures.

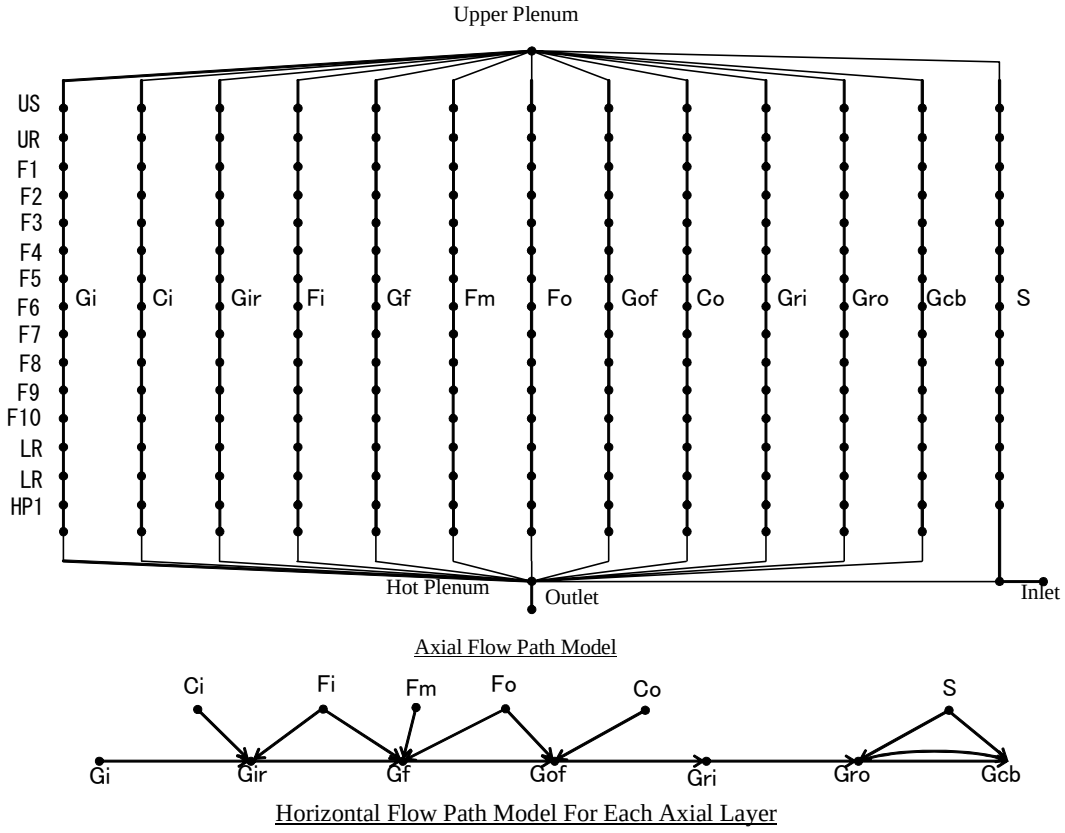

Ci:	Control rod hole in fuel region
Co:	Control rod hole in outer reflector
Fi:	Coolant channel of inner layer fuel column
Fm:	Coolant channel of central layer fuel column
Fo:	Coolant channel of outer layer fuel column
Gi:	Gap flow path in inner reflector region
Gri:	Gap flow path between inner reflector and fuel region
Gf:	Gap flow path in fuel region
Gof:	Gap flow path between fuel and outer reflector column
Gri:	Gap flow path among outer replaceable reflector
Gro:	Gap flow path between outer replaceable reflector and permanent reflector
Gcb:	Gap flow path between permanent reflector and core barrel
S:	Inlet flow path

Figure 3-19. MHR FLOWNET Coolant Flow Distribution Model (Figure courtesy of Fuji Electric Systems, Kawasaki-city, Japan)

3.1.5 Shutdown Cooling System

The Shutdown Cooling System (SCS) provides decay heat removal when the Heat Transport System (HTS) is off line. The SCS consists of a circulator with shutoff valve, a heat exchanger, a control system, a shutdown cooling water system, and equipment for servicing the circulator and heat exchanger. The SCS design is the same as that for the GT-MHR [Shenoy, 1996]. Figure 3-20 shows the SCS cooling loop and the location of the shutdown heat exchanger and shutdown circulator in the reactor vessel.

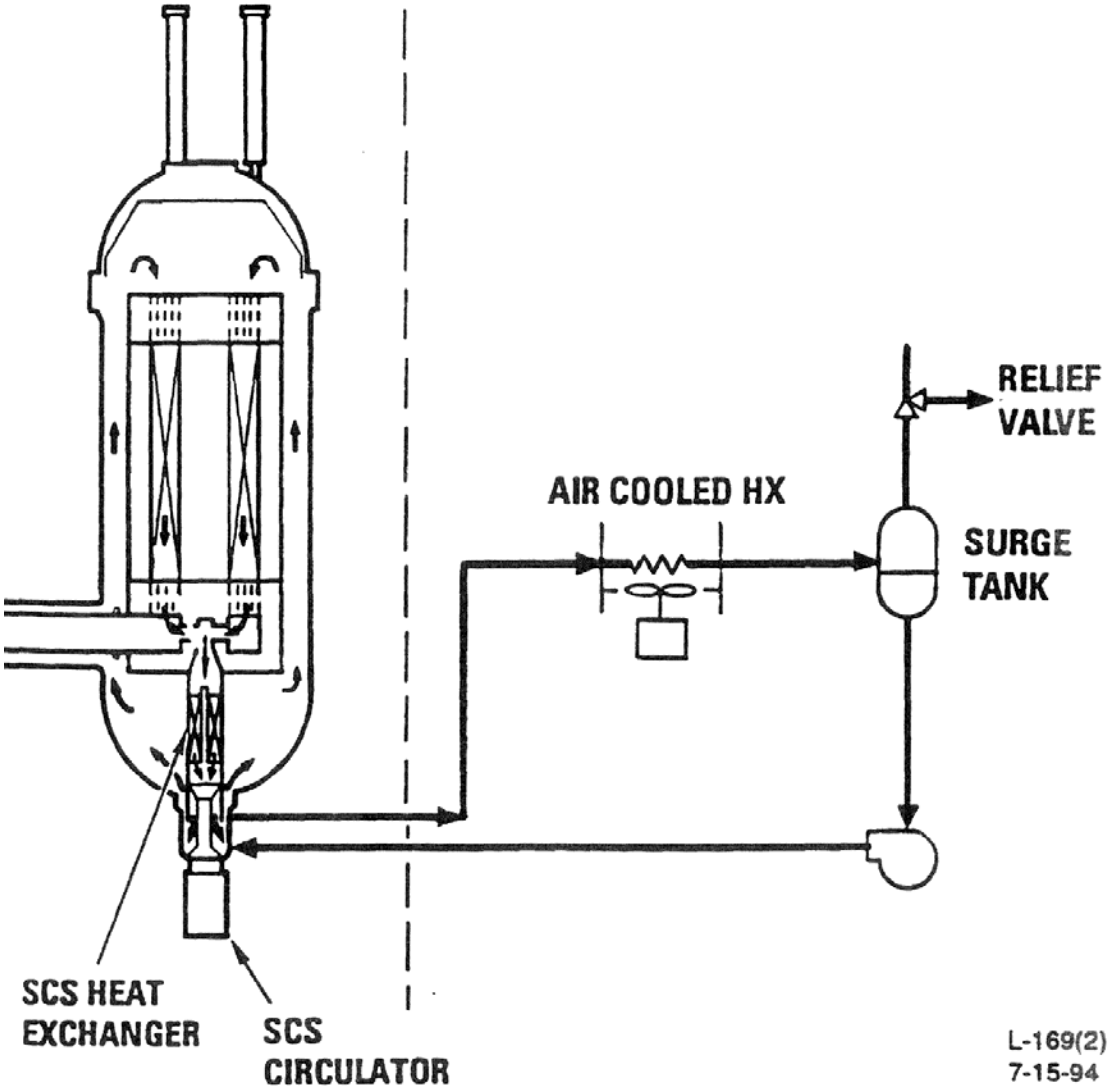

Figure 3-20. Shutdown Cooling System General Arrangement

The SCS consists of a single loop (one per reactor module) with the heat exchanger in series with the circulator and loop shutoff valve assembly. These components are located at the bottom of the reactor vessel. Hot helium from the core outlet plenum flows through multiple

parallel openings (pipes) in the center of the core support structure and into the heat exchanger. Once cooled, the helium continues downward through the loop shutoff valve to the circulator where it is compressed and discharged into the reactor vessel bottom head cavity. The cool helium then flows through the internal passage formed by the core support structure, up through the flow channels in the PSR, and into the core inlet plenum. The loop is completed as the helium flows down through the reactor core. The heat is transferred to a cooling water system that rejects the heat to the atmosphere through an air-cooled heat exchanger.

Because of the pressure drop associated with the IHX and other primary HTS components, there will be some back flow of helium through the IHX vessel. This backflow is factored into the SCS design in order to prevent local flow reversals and ensure adequate core cooling.

The SCS is sized to remove decay heat under both pressurized and depressurized conditions. Under pressurized conditions the SCS is sized to remove up to 40 MW(t) per module. When the reactor system is shutdown and depressurized for maintenance or refueling, the SCS is sized to remove up to 14.1 MW(t). [Typically, maintenance activities are performed at least 24 hr after reactor shutdown, which corresponds to a decay heat load of about 5.8 MW(t).] To ensure high reliability, the SCS can draw electrical power from either normal or standby systems. Table 3-9 provides the design parameters for the SCS heat exchanger and circulator, which are shown in Fig 3-21. Figure 3-22 shows a sectional view of the SCS circulator.

Table 3-9. Shutdown Cooling System Design Parameters

Shutdown Heat Exchanger	**Depressurized**	**Pressurized**
Design Heat duty, MW(t)	14.1	40
Helium inlet temperature, °C (°F)	1032 (1890)	807 (1485)
Helium outlet temperature, °C (°F)	179 (355)	341 (645
Helium flow, kg/sec (lb/hr)	3.21 (25,438)	14.51 (115,200)
Water flow, kg/sec (lb/hr)	57.19 (454,000)	57.19 (454,000)
Water inlet temperature, °C (°F)	60 (140)	60 (140)
Shutdown Circulator		
Motor power, kW (hp)	323 (433)	TBD
Speed, rpm	6000	TBD
Exit pressure, kPa (psia)	84.1 (12.2)	TBD
Inlet temperature, °C (°F)	179 (355)	341 (645)
Helium pressure rise, kPa (psid)	6.14 (0.89)	TBD
Helium flow, kg/sec (lb/hr)	3.21 (25,438)	14.51 (115,200)

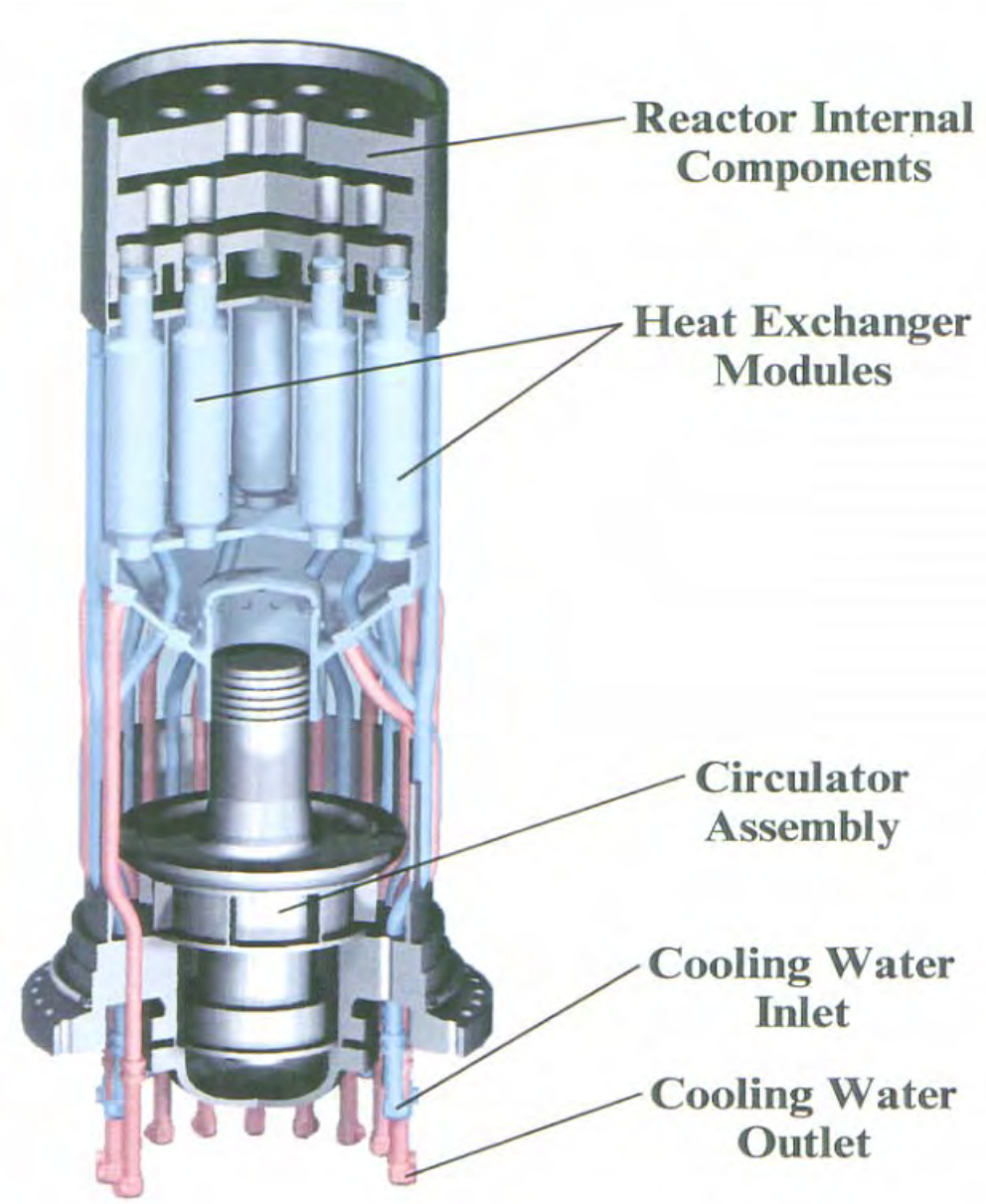

Figure 3-21. SCS Circulator and Heat Exchanger

During normal operation of the reactor system, the SCS operates in a standby mode. During this mode, a small amount of cold leg helium leaks (back flows) through the closed shutdown valve and flows opposite the normal flow direction through the SCS circulator and over the SCS heat exchanger tubes. In this mode the circulator is not operating, but the SCS cooling water system supplies a small amount of water flow to the heat exchanger. This water flow prevents thermal shock when the SCS switches to an active cooling mode, but also results in a parasitic heat loss of up to 1.3 MW(t) during normal operation. Therefore, the standby-mode water flow must be set as low as possible without resulting in one or both of the following adverse conditions: (a) boiling and/or (b) static instability due to the large hydrostatic head in the heat exchanger. During standby mode, the primary coolant helium pressure is higher than the SCS

water pressure, in order to prevent water ingress into the reactor system during normal operation. The SCS is manually switched from standby mode to an active cooling mode at the discretion of an operator.

The SCS control system includes protection features to actuate isolation valves and shutdown the circulator if the following events are detected: heat exchanger leaks, circulator overspeed, low cooling water flow, loss of net positive suction head, and high heat exchanger temperatures.

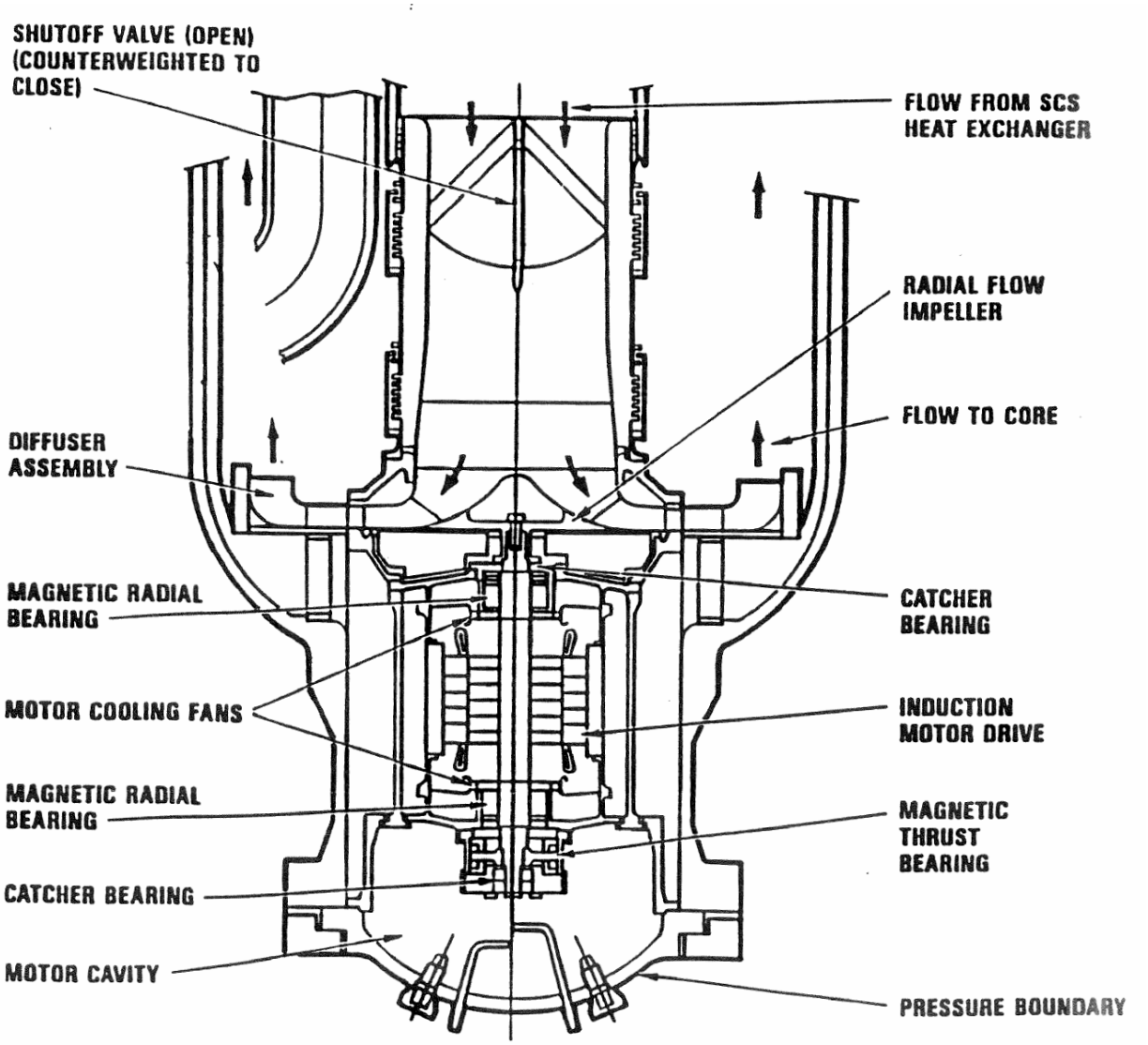

Figure 3-22. SCS Circulator Sectional View

3.1.6 Reactor Cavity Cooling System

The Reactor Cavity Cooling System (RCCS) is a Safety-Related system that provides a passive means of removing core residual heat during accident conditions when neither the HTS nor the SCS is available. The RCCS design is the same as that for the GT-MHR (GA 1996). Shown schematically in Fig. 3-23, the RCCS is a completely passive design that has no pumps, circulators, valves, or other active components. The RCCS receives heat transferred from the uninsulated reactor vessel by thermal radiation and natural convection. RCCS components include cooling panels that surround the reactor vessel, inlet/outlet structures that are located above grade on top of the reactor building, and a concentric duct system with the annular, outer flow path acting as the cold leg and the inner flow path acting as the hot leg. Through a balance of buoyancy and gravitational forces, natural convection airflow is established through the RCCS circuit.

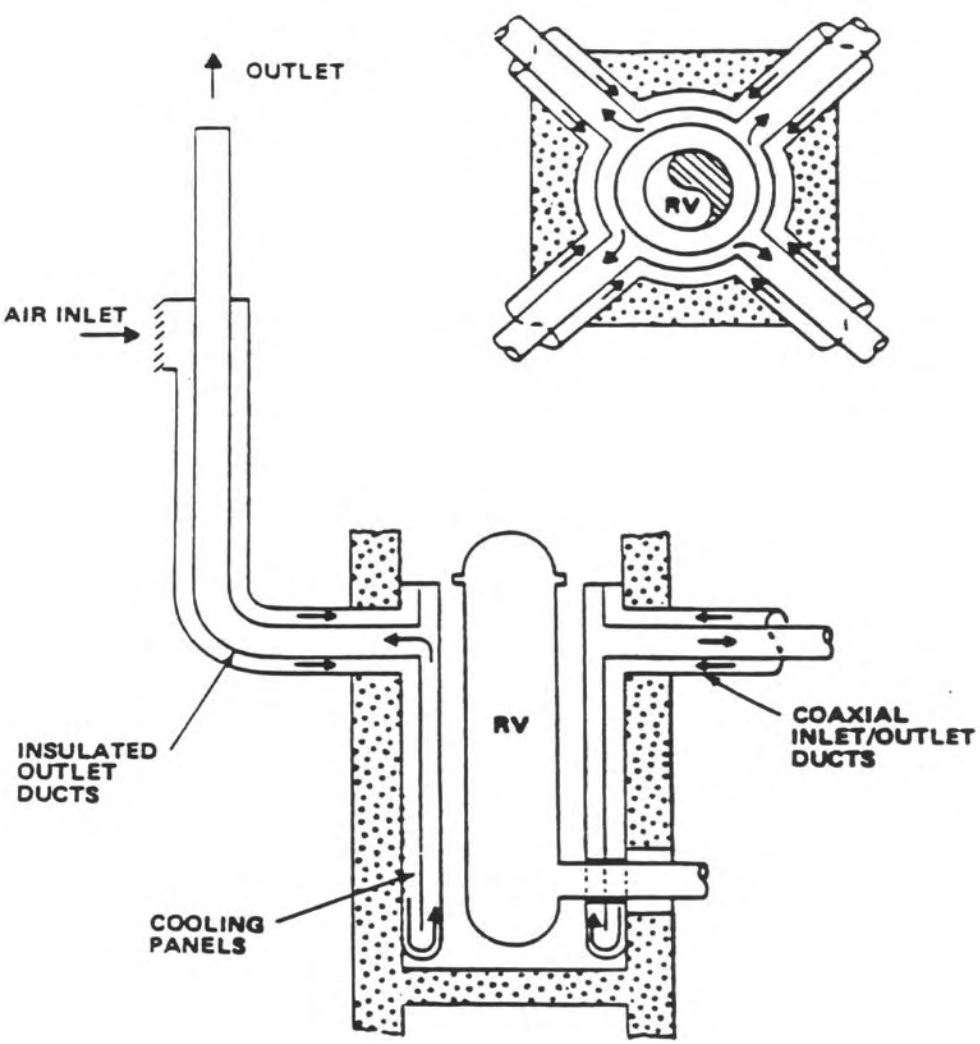

Figure 3-23. Passive Air-Cooled RCCS

The RCCS has multiple inlet/outlet ports and interconnected parallel flow paths to ensure cooling in the event of blockage of any single duct or opening, and is robustly designed to survive all credible accidents scenarios. Nevertheless, if the RCCS were to fail, the MHR is designed to allow heat transfer from the core to the surrounding ground. Under these beyond-design basis accident conditions, damage to the reactor vessel and silo concrete may occur, but peak fuel temperatures remain below 1600°C and 10CFR100 offsite dose limits are not exceeded.

The system is required to operate continuously in all modes of plant operation to support normal operation, and, if forced cooling is lost, it functions to remove decay heat to ensure investment and safety protection. The RCCS consists of a cooling panel which includes cold downcomers and hot risers and is located inside the reactor cavity surrounding the reactor vessel. Connected to the cooling panel are the concentric hot and cold ducts which connect the panel to the inlet/outlet structure.

3.1.6.1 RCCS Cooling Panels

As shown in Fig. 3-24, the RCCS panels follow the internal contour of the reactor cavity and surround the reactor vessel over its full circumference and length. The cold sides of the RCCS panels consists of four parts: upper cold plenum, downcomer, bottom cold plenum, and drain arrangement. The upper cold plenum receives cold air from the ductwork and distributes the cold air over the full circumference and directs the airflow to the downcomers. It also protects the concrete portion of the cavity ceiling from reactor vessel heat and serves as a quiescent/damping chamber which attenuates the effects of any atmospheric disturbance in the incoming cold air.

A reflective surface/insulation with a metal cover is provided as a part of the downcomer. This surface is attached to the inner plate and faces the reactor vessel. It serves to reflect the reactor vessel heat back to the cavity, and also protects the cold incoming air from being prematurely heated as it flows through the downcomer.

The bottom cold plenum, located at the bottom end of the downcomer, is essentially a box-shaped continuous ring header around the reactor vessel along the cavity wall. It permits change in airflow direction with minimal flow resistance and facilitates proper distribution of airflow to the riser part of the cooling panel. Any atmospheric disturbance and maldistribution that may have propagated down to the bottom of the cooling panel is suppressed in the bottom plenum and proper airflow distribution is restored.

Several drain connections are provided in the bottom cold plenum to drain any water that may be collected from the incoming air. Although the input/output structure is designed to prevent rain water from entering the RCCS, potential sources of water are mist entrained in the air, or some condensation on the cooler surfaces. The drain lines do not have any valves or pumps, and the cooling panels drain to the sump by gravity. The drain lines are oversized to provide flow in the event they become partially obstructed.

The hot side of the RCCS cooling panel consists of two parts: the riser and the hot plenum. The riser part consists of vertical rectangular structural steel tubes arranged around the reactor vessel. The tubes rise from the bottom cold plenum and connect to the hot plenum located at the top of the reactor cavity. The hot riser tubes are supported on the bottom plenum which

enables the tubes and the hot plenum to expand as they are heated. The design and configuration of the lateral support plates also accommodate thermal expansion of the tubes. The entire RCCS cooling panel assembly is a stable rigid structure which is designed for all required thermal, seismic, and pressure loading (due to tornado or pipe rupture).

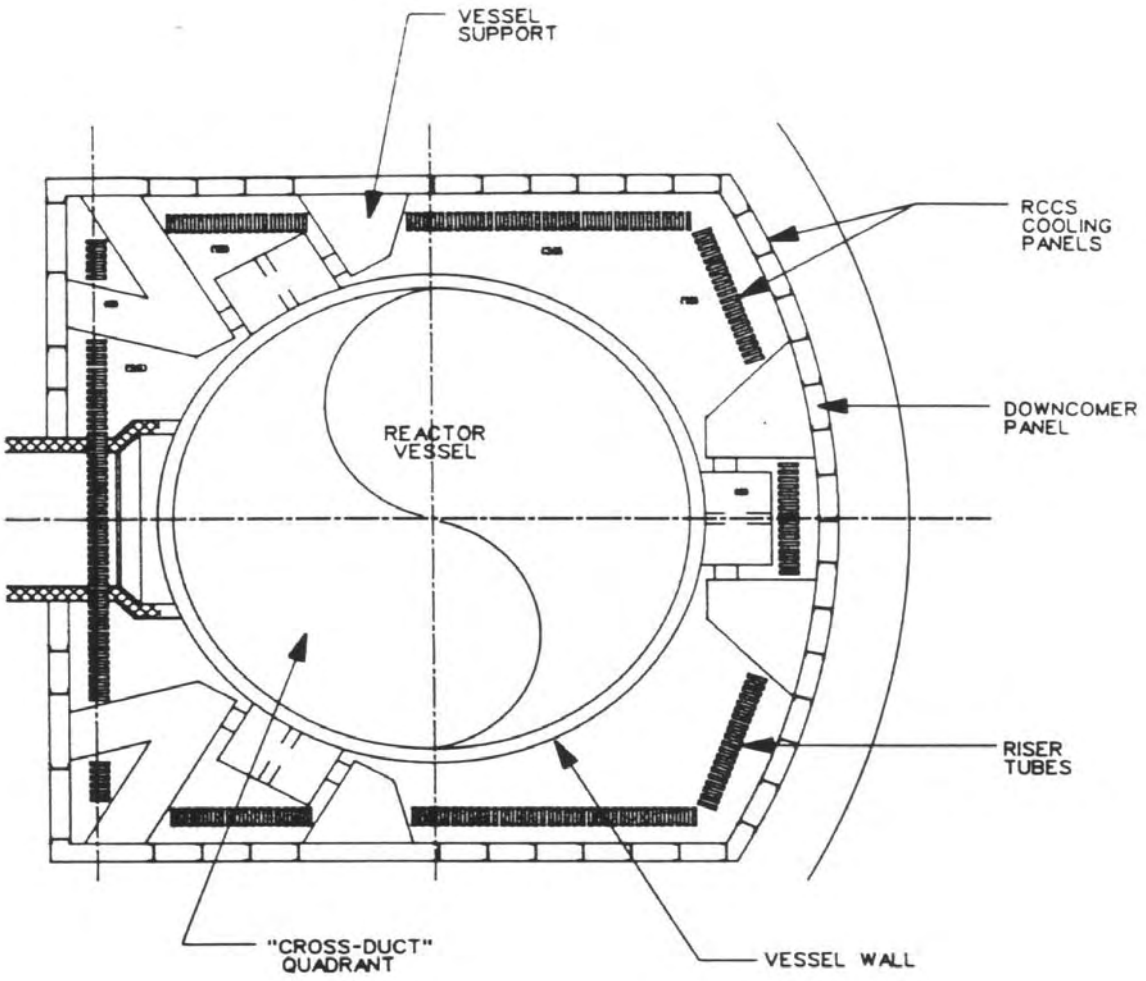

Figure 3-24. RCCS Panel Layout

3.1.6.2 RCCS Operation

The RCCS is designed to remove ~4 MW when the primary cooling circuit is either pressurized or depressurized. The RCCS is not required to remove decay heat during normal operation. However, since the system is passive, the system removes some parasitic heat during normal power operation, and removes some decay heat during normal shutdown because of the difference in the reactor vessel temperature and the outside air temperature.

During normal power operation, forced circulation of the primary coolant results in a near-uniform vessel temperature. The RCCS is designed to accommodate outside air temperatures

over a range of -42°C (-45°F) to 43°C (110°F). The performance of the RCCS at 100% reactor power with 43°C ambient air temperature is summarized in Table 3-10. The H2-MHR is designed to operate with coolant inlet and outlet temperatures that are 100°C than those for the GT-MHR. However, as discussed in Section 3.1.4, design modifications for higher-temperature operation of the H2-MHR should result in vessel temperatures and parasitic heat losses to the RCCS that are within the envelope of the GT-MHR RCCS design.

Table 3-10. RCCS Steady State Performance at 100% Reactor Power

Reactor Vessel	
Heat loss to RCCS, kW	3300
Inside wall temperature, °C (°F)	485 (905)
Average outside wall temperature, °C (°F) (not including flange)	446 (835)
Maximum outside wall temperature, °C (°F)	474 (886)
Cooling Panel (Front)	
Average temperature, °C (°F)	267 (513)
Maximum temperature, °C (°F)	323 (613)
Air inlet temperature, °C (°F)	43 (110)
Air outlet temperature, °C (°F)	274 (515)
Airflow kg/sec (lbm/hr)	14.3 (113,500)
Maximum velocity, m/sec (ft/sec) at exit from panel	11.5 (37.7)
Structure	
Concrete surface temperature, °C (°F)	49 (120)

3.1.7 Fuel Performance and Radionuclide Control

For modular gas-cooled reactor designs, a hallmark philosophy has been adopted since the early 1980s to design the plant such that radionuclides would be retained in the core during normal operation and postulated accidents. The key to achieving this safety goal is the reliance upon ceramic-coated fuel particles for primary fission product containment at their source, along with passive cooling to assure that the integrity of the coated particles is maintained even if the normal active cooling systems were permanently disrupted. This design philosophy has been carried forward for all subsequent MHR designs, including the H2-MHR. Fuel performance and radionuclide control in gas-cooled reactors is discussed in detail in numerous publications, including IAEA 1997, Hanson 2002, and Hanson 2003.

3.1.7.1 Radionuclide Containment System

The radionuclide containment system for the MHR, which reflects a defense-in-depth philosophy, is comprised of multiple barriers to limit radionuclide release from the core to the environment to insignificant levels during normal operation and postulated accidents. As shown schematically in Fig. 3-25, the five principal release barriers are: (1) the fuel kernel; (2) the particle coatings (particularly the SiC coating); (3) the fuel element structural graphite; (4) the primary coolant pressure boundary; and (5) the reactor building/containment structure. The effectiveness of each individual barrier for containing radionuclides depends upon a number of fundamental factors including the chemistry and half-lives of the various radionuclides, the service conditions in terms of burnup, fluence, temperature, and time at temperature, and the specific conditions associated with accident scenarios.

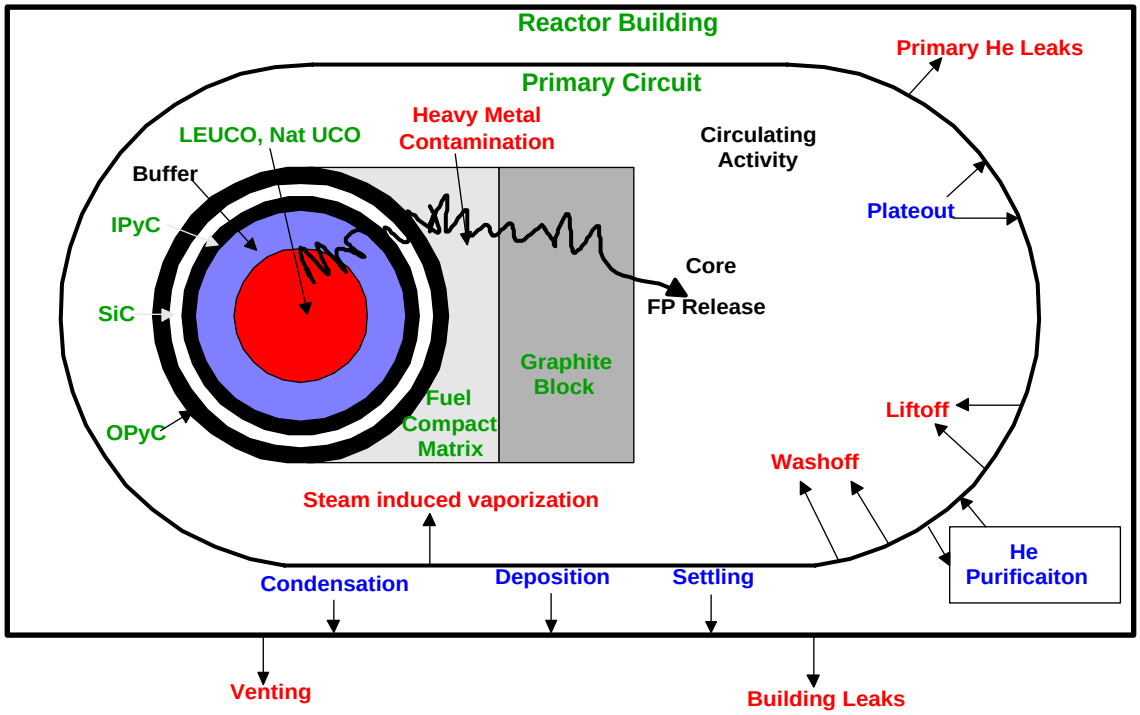

Figure 3-25. H2-MHR Radionuclide Containment System

The first barrier to fission product release is the fuel kernel itself. Under normal operating conditions, the kernel retains >95% of the radiologically important, short-lived fission gases such as Kr-88 and I-131. However, the effectiveness of a UCO kernel for retaining gases can be reduced at elevated temperatures or if an exposed kernel is hydrolyzed by reaction with trace amounts of water vapor which may be present in the helium coolant. The retentiveness of oxidic fuel kernels for long-lived, volatile fission metals such as Cs, Ag, and Sr is strongly dependent upon temperature and burnup.

The second, and most important, barrier to fission product release from the core is the silicon carbide and pyrocarbon coatings of each fuel particle. Both the SiC and PyC coatings provide a barrier to the release of fission gases. The SiC coating acts as the primary barrier to the

release of metallic fission products because of the low solubilities and diffusion coefficients of fission metals in SiC; the PyC coatings are partially retentive of Cs at lower temperatures but provide little holdup of Ag and Sr.

The fuel-compact matrix and the graphite fuel block collectively are the third release barrier. The compact matrix is relatively porous and provides little holdup of the fission gases which are released from the fuel particles. However, the matrix is a composite material which has a high content of amorphous carbon, and this constituent of the matrix is highly sorptive of metallic fission products, especially Sr. While the matrix is highly sorptive of metals, it provides little diffusive resistance to the release of fission metals because of its high interconnected porosity.

The fuel-element graphite, which is denser and has a more ordered structure than the fuel-compact matrix, is somewhat less sorptive of the fission metals than the matrix, but it is much more effective as a diffusion barrier than the latter. The effectiveness of the graphite as a release barrier decreases as the temperature increases. Under typical core conditions, the fuel element graphite attenuates the release of Cs from the core by an order of magnitude, and the Sr is essentially completely retained.

Typically, the two dominant sources of fission product release from the core are as-manufactured, heavy-metal (HM) contamination (i.e., heavy metal outside the coated particles) and particles whose coatings are defective or fail in service. In addition, volatile fission metals (e.g., Cs, Ag, Sr) can diffuse through intact SiC coatings if the fuel is maintained at high temperatures for sufficiently long time periods. However, for the H2-MHR core design, this mechanism should not be a significant contributor to fission-product release during normal operation, except possibly for Ag-110m and other isotopes of Ag.

The fourth release barrier is the primary coolant pressure boundary. Once the fission products have been released from the core into the coolant, they are transported throughout the primary circuit by the helium coolant. The helium purification system (HPS) efficiently removes both gaseous and metallic fission products from the primary coolant at a rate determined by the slipstream flow rate through the purification system. However, for the condensable fission products, the dominant removal mechanism is deposition (“plateout”) on the various helium-wetted surfaces in the primary circuit (i.e., the deposition rate greatly exceeds the purification rate). The plateout rate is determined by the mass transfer rates from the coolant to the fixed surfaces and by the sorptivities of the various materials of construction for the volatile fission products and by their service temperatures. Condensable radionuclides may also be transported throughout the primary circuit sorbed on particulates (“dust”) which may be present in the primary coolant; the plateout distribution of these contaminated particulates may be considerably different than the distribution of radionuclides transported as atomic species.

The circulating and plateout activities in the primary coolant circuit are potential sources of environmental release in the event of primary coolant leaks or as a result of the venting of primary coolant in response to over pressurization of the primary circuit. The fraction of the circulating activity lost during such events is essentially the same as the fraction of the primary coolant that is released, although the radionuclide release can be mitigated by pump down through the HPS if the leak rate is sufficiently slow. A small fraction of the plateout may also be reentrained, or “lifted off,” if the rate of depressurization is sufficiently rapid. The amount of fission product liftoff is expected to be strongly influenced by the amount of dust in the primary

circuit as well as by the presence of friable surface films on primary circuit components which could possibly spall off during a rapid depressurization.

The reactor building/containment structure is the fifth barrier to the release of radionuclides to the environment. Its effectiveness as a release barrier is highly event-specific. The vented low pressure containment (VLPC) may be of limited value as a release barrier during rapid depressurization events; however, it is of major importance during longer-term events during which forced cooling is unavailable. Under such conditions, the natural removal mechanisms occurring in the VLPC, including condensation, fallout, and plateout, serve to attenuate the release of condensable radionuclides, including radiologically important iodines, by at least an order of magnitude.

3.1.7.2 Fuel Failure Mechanisms

A number of failure mechanisms have been observed during irradiation testing and post-irradiation heating of coated-particle fuels, including pressure-vessel failure, kernel migration, and corrosion of the SiC layer by fission products. These failure mechanisms are illustrated in Fig. 3-26 and may be categorized as structural/mechanical or thermochemical in nature. Failure mechanisms in both categories can be affected by the release of excess oxygen during fission and subsequent formation of carbon monoxide. [IAEA, 1997] provides an excellent overview of these mechanisms and an extensive bibliography.

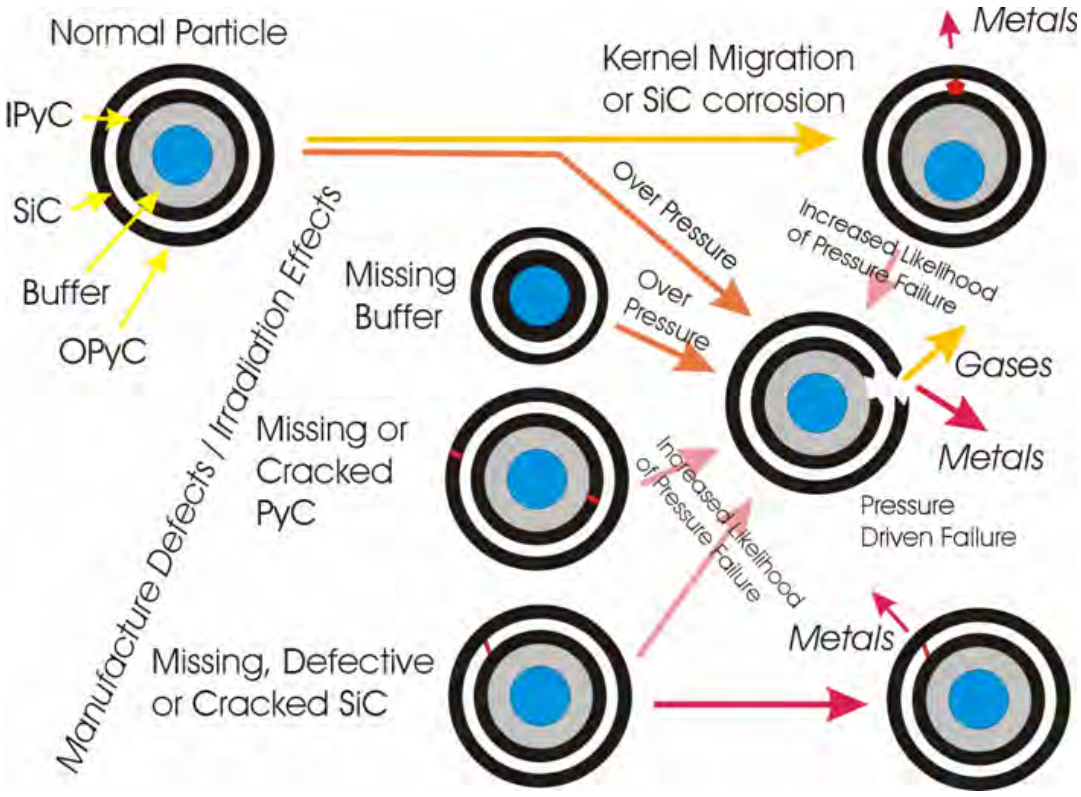

Figure 3-26. TRISO Particle Failure Mechanism

Carbon Monoxide Formation

For a substoichiometric metal oxide kernel (MO_{2-x}) or an oxycarbide (MC_xO_{2-x}), a mass balance for the excess oxygen generated as a function of burnup is given by

$$N_O / N_M = [2 - N_B] [FIMA - x/2] - (N_B) (x/2) \quad ,$$

where N_O = number of excess oxygen atoms, N_M = number of initial heavy metal atoms, and N_B = number of oxygen atoms bound per fission.[3] The burnup $FIMA_{CO}$ at which CO formation begins is given by

$$FIMA_{CO} = x/(2 - N_B) \quad .$$

For uranium fuels at moderate burnups, a reasonable lower bound for N_B is approximately 1.5. For x in the range 0.2 to 0.5, the quantity $FIMA_{CO}$ = 0.4 to 1.0 (40% to 100%), which virtually precludes CO formation during irradiation of H2-MHR fuel.

Structural/Mechanical Mechanisms

During irradiation, long-lived and stable fission gases are released from the kernel into the buffer, which increases the internal gas pressure. For some particle designs, carbon monoxide can also be generated during irradiation, which further increases the gas pressure. Because the SiC layer has a much higher elastic modulus than the pyrocarbon layers,[4] it bears most of the internal pressure force, which produces a tensile stress. However, the pyrocarbon layers undergo shrinkage during irradiation, which produces compressive forces in the SiC layer. As shown in Fig. 3-27, the compressive forces from pyrocarbon shrinkage more than compensate for the tensile stresses from internal pressure, such that the SiC remains in compression provided at least one of the pyrocarbon layers remains intact. From a structural / mechanical perspective, the SiC layer will remain intact provided (a) it remains in compression or (b) the tensile stress in the SiC layer does not exceed its strength.

As discussed above, shrinkage of the pyrocarbon layers during irradiation is a favorable attribute, in terms of the compressive forces applied to the SiC layer. However, pyrocarbon shrinkage produces tensile stresses in the pyrocarbon layers themselves, which can lead to failure of these layers. The strains and stresses generated in the pyrocarbon layers are complex functions of fast neutron fluence, irradiation temperature, and coating material properties. A property that greatly affects pyrocarbon performance is anisotropy, which can be quantified using X-ray or optical diffraction techniques. Anisotropy is usually expressed in terms of the Bacon Anisotropy Factor (BAF). For a perfectly isotropic material, BAF = 1, and for a perfectly oriented medium, BAF = ∞. Figure 3-28 shows irradiation-induced strains of pyrocarbon in the tangential direction for BAF values ranging from 1.02 to 1.05. Pyrocarbon layers are able to perform well out to high fast neutron fluences because the irradiation-induced strains and stresses are relaxed to some extent by irradiation-induced creep. Unfortunately, the

[3] Oxygen atoms are released during the fission process. The parameter N_B is the number of oxygen atoms per fission that are bound as stable oxides. These bound oxygen atoms are not available to react with carbon in the buffer layer to form CO.

[4] In other words, SiC is much stiffer than pyrocarbon. Because of this property, it is reasonable to assume the IPyC and OPyC are isolated from each other when evaluating performance of these layers and overall performance of the TRISO coating system.

measured data for pyrocarbon creep coefficients is widely scattered. Figure 3-29 shows calculations of OPyC performance for a range of creep coefficients (denoted by K_S on Fig. 3-29) that are well within the measured data base. At an irradiation temperature of 1200°C and a fast neutron fluence of 8×10^{25} n/m^2, the predicted OPyC failure fraction can range from 1.0 (K_S = 1.0) to < 2×10^{-3} (K_S = 2.5). Also shown on Fig. 3-29 is the model taken from the General Atomics Fuel Design Data Manual (FDDM) [Myers, 1987]. Although the FDDM model is very simplistic, it is representative of the data base for pyrocarbons that perform well under irradiation.

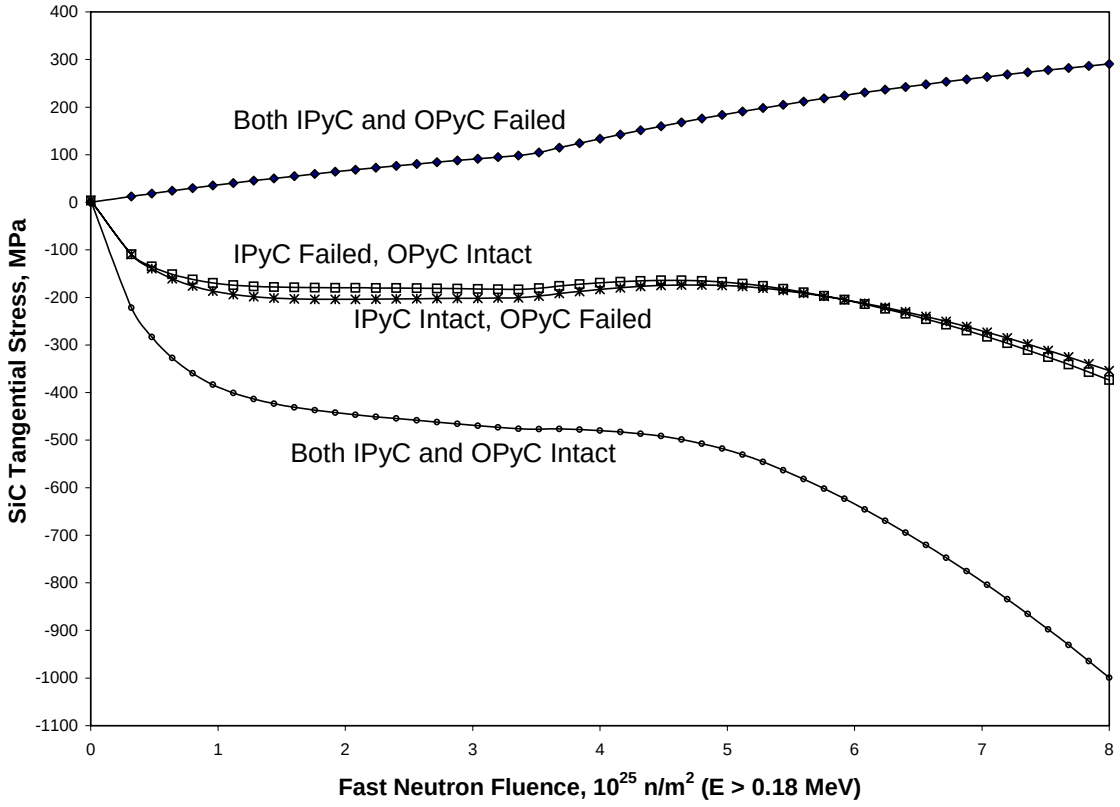

Figure 3-27. Calculated Tangential Stresses at the Middle of the SiC Layer. As indicated in the figure, the SiC layer remains in compression if one or both pyrocarbon layers remains intact.

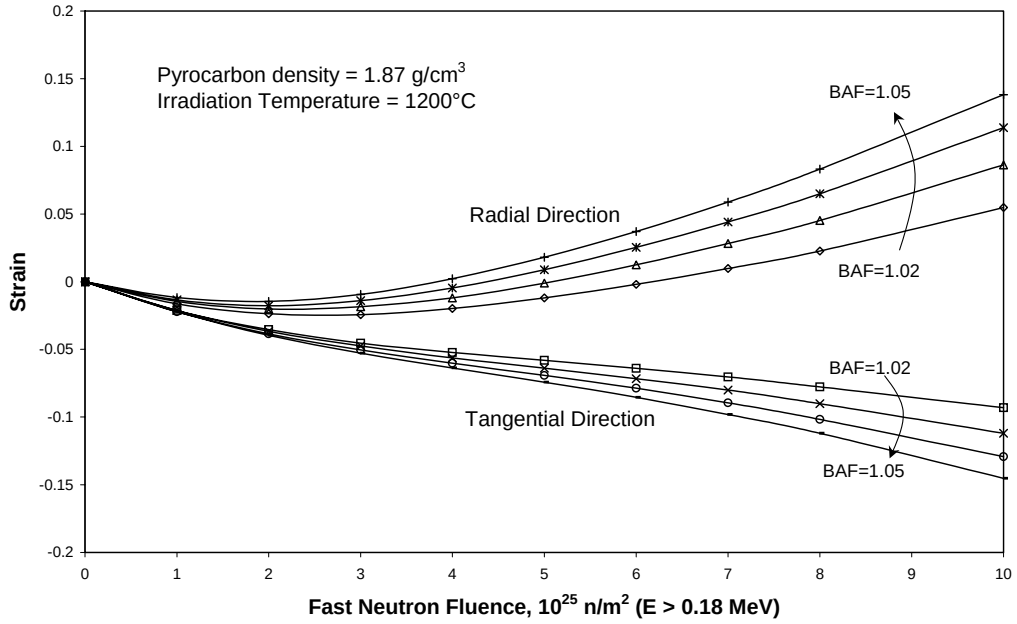

Figure 3-28. Irradiation-Induced Strain in Pyrocarbon as a Function of BAF

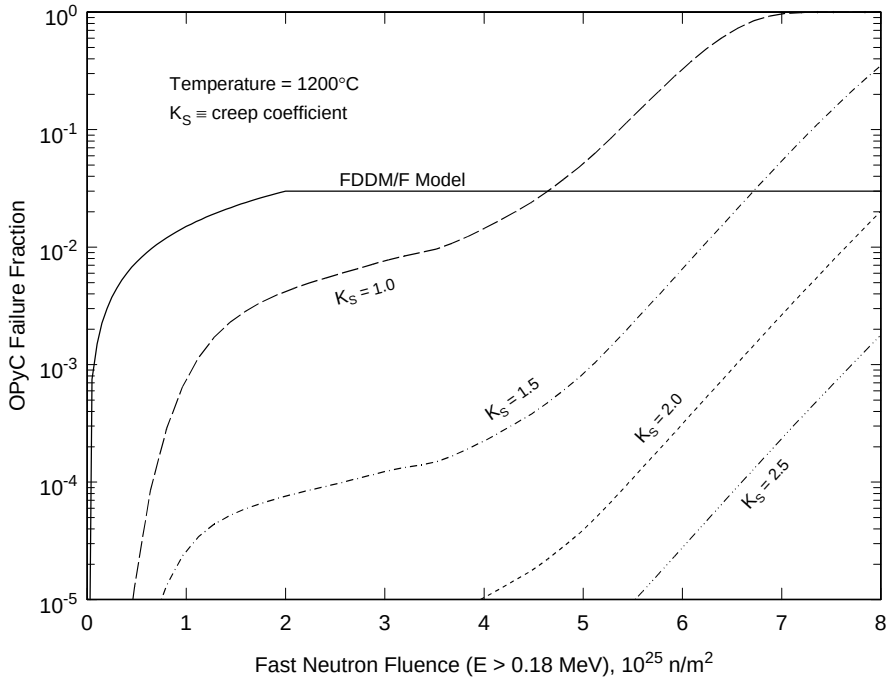

Figure 3-29. OPyC Performance Predictions. Calculations were performed for creep coefficients ranging from 1.0 to 2.5.

In the absence of compressive forces from the pyrocarbon layers, the tensile stress σ_{SiC} in the SiC layer may be calculated with reasonable accuracy using the thin-shell approximation:

$$\sigma_{SiC} = \frac{P r_{SiC}}{2 t_{SiC}} \quad ,$$

where P ≡ internal pressure inside the particle, r_{SiC} ≡ radius to the middle of the SiC layer, and t_{SiC} ≡ thickness of the SiC layer. Pressure vessel failure occurs when σ_{SiC} exceeds the strength of the SiC layer. The SiC layer failure fraction (f_{SiC}) is calculated using a Weibull distribution for the strength of the SiC layer. Assuming volume flaws and a uniform stress distribution in the SiC layer, the quantity failure probability f_{SiC} is determined from:

$$f_{SiC} = 1 - \exp\left[-\left(\frac{\sigma_{SiC}}{\sigma_o} \right)^m V_{SiC} \right] \quad ,$$

where σ_o ≡ Weibull characteristic strength, m ≡ Weibull modulus, and V_{SiC} ≡ volume of the SiC layer. The parameters σ_o and m are derived from experimental data. For the H2-MHR fissile and fertile particle designs, the internal pressure results almost entirely from the release of stable fission gases, because the carbide phase of the kernel getters excess oxygen and precludes formation of CO (see discussion above). For these particle designs, pressure vessel failure occurs only in the small fraction of particles with defective (missing or undersized) buffer layers that do not provide sufficient void space for gas accumulation.

Thermochemical Mechanisms

Under conditions of high temperature and high thermal gradient, oxide and carbide fuel kernels can migrate up the thermal gradient. This phenomenon is often referred to as the “amoeba effect” and can lead to complete failure of the coating system. For carbide kernels, migration is caused by solid-state diffusion of carbon to the cooler side of the kernel. For oxide kernels, migration may be caused by carbon diffusion or gas-phase diffusion of CO or other gaseous carbon compounds. As discussed above, CO generation should be negligible for H2-MHR fuel, and kernel migration should be a negligible contributor to fuel failure.

Noble metals (e.g., Ru, Rh, Pd, and Ag) are produced with relatively high yield during fission of uranium and plutonium fuels. During irradiation, the thermochemical conditions are not conducive for these elements to form stable oxides, and they can readily migrate out of the fuel kernel, regardless of its composition. Reactions of SiC with Pd have been observed during post-irradiation examinations of TRISO fuel. Although the quantity of Pd is small compared with the mass of the SiC layer, the reaction is highly localized, and complete penetration of the SiC layer can occur if high temperatures are maintained for long periods of time (see Fig. 3-30). As discussed in Section 3.1.4.3, corrosion of the SiC layer by fission products is a key factor for determining limitations on fuel temperatures.

At very high temperatures (above about 1800°C for extended periods of time), SiC will decompose into its constituent elements. The silicon vaporizes, leaving a porous carbon structure. For the H2-MHR, this failure mechanism should be a negligible contributor to fuel failure during normal operation and accident conditions.

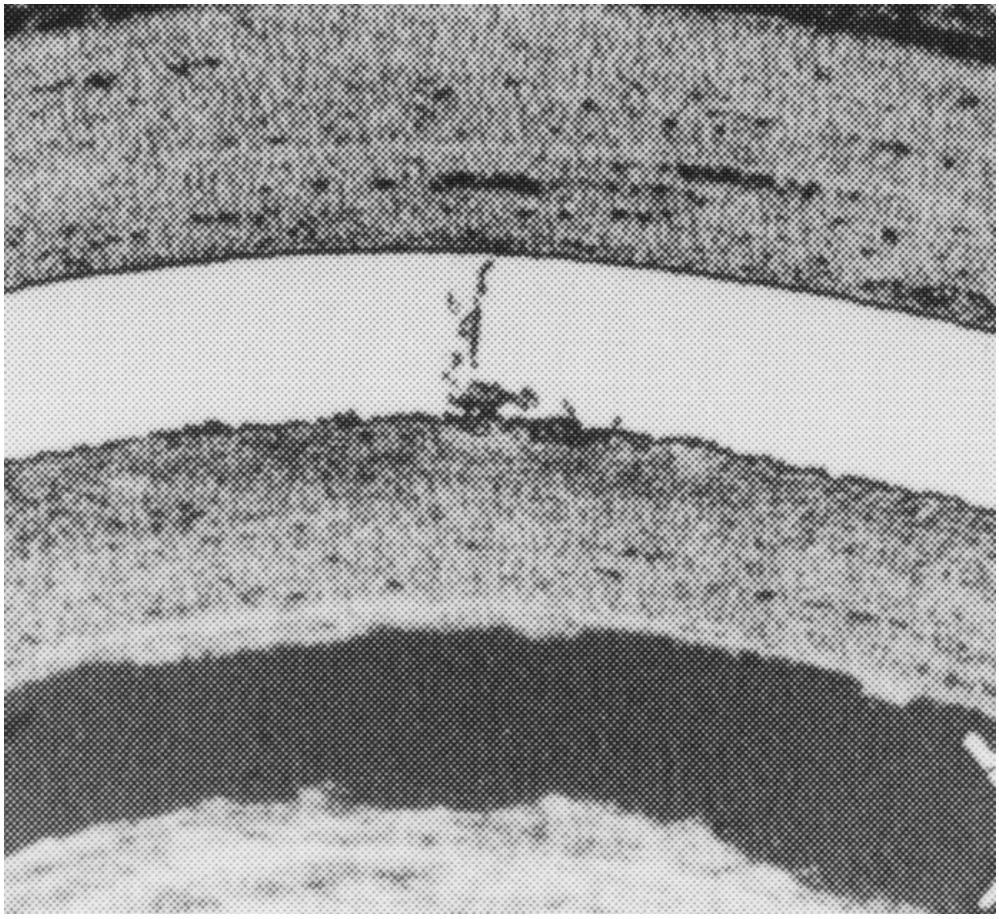

Figure 3-30. Localized Fission-Product Attack of the SiC Layer.

Diffusive Release Through Intact Coatings

Based on previous irradiation testing and post-irradiation heating, SiC is not very retentive of Ag (and possibly other noble metals) at high temperatures. The Ag-110m transports through the primary cooling circuit and deposits on the cooler wetted surfaces, which could impact operations and maintenance activities. The plateout activity is also a potential source of radioactivity release during hypothetical accidents involving a rapid loss of coolant, when the shear forces during depressurization are sufficiently high to remove some of the deposited activity. Figure 3-31 shows the breakthrough time as a function of temperature for Ag diffusing through a 35-µm SiC layer. For temperatures above 1000°C, the breakthrough time is less than 100 days, which is well below the fuel residence time of 850 days. As discussed in Section 3.1.4, limiting the release of Ag to acceptable levels is largely accomplished through optimization of the nuclear and thermal hydraulic design of the reactor core.

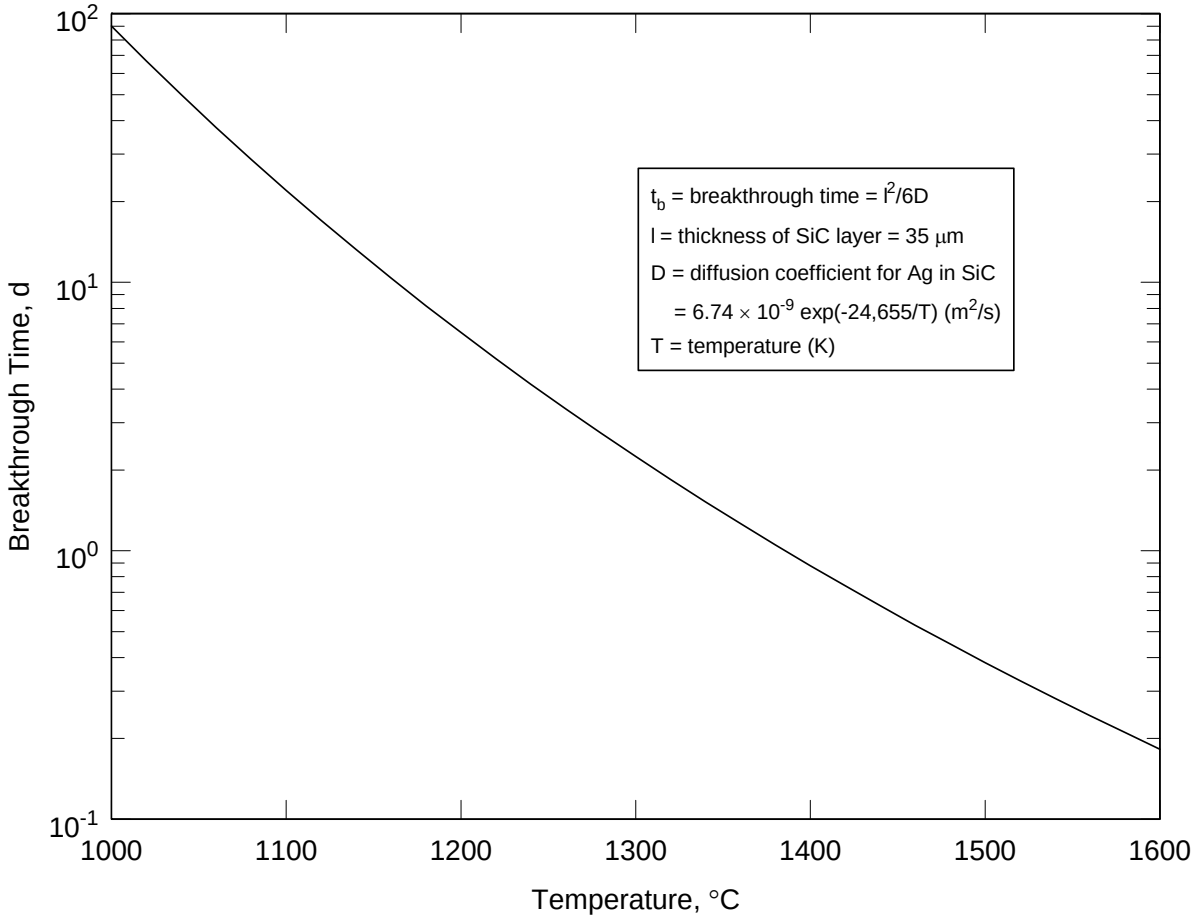

Figure 3-31. Breakthrough Time for Ag Diffusing Through a 35-μm SiC Layer.

3.1.7.3 Performance Capability of High-Quality TRISO Fuel

The Germans have manufactured high-quality, TRISO-coated fuels that have performed exceptionally well during irradiation and accident-condition testing. Table 3-11 provides a summary of performance data for high-quality German fuels with 10%-enriched UO_2 kernels and 20%-enriched UCO kernels. Figure 3-32 shows the irradiation temperatures and fuel burnups achieved during individual tests of German fuel with fuel-failure fractions < 10^{-5} at the end of irradiation. The Japanese have achieved a similar level of success with their low-enriched UO_2 fuel. The U.S. is developing UCO coated-particle fuel with similar requirements for as-manufactured quality and performance during normal operation and accident conditions [Petti, 2005].

Table 3-11. Summary of Performance Data for High-Quality TRISO Fuel Manufactured in Germany

	UO_2 Kernels[a]	UCO Kernels[b]
Fraction of particles with as-manufactured defective coating systems	$5 \times 10^{-5} – 1 \times 10^{-4}$	$< 10^{-4}$
Fuel burnup (% FIMA)	7 – 15	18.6 – 22.2
Fast neutron fluence (10^{25}/m^2)[c]	4 – 8	1.8 – 3.2
Fuel irradiation temperature (°C)[d]	700 – 1320	900 – 1350
Fractional release of Kr-85m at end of irradiation	~10^{-7} at 1100°C	~2×10^{-7} at 1100°C
Fractional release of Cs-137 at end of irradiation	$10^{-6} – 10^{-4}$	not measured
Fraction of coating systems that failed during accident-condition testing	• $< 10^{-5}$ when heated at 1600°C for up to 500 h. • $10^{-4} – 10^{-3}$ when heated at 1800°C for > 20 h.	not measured
Fractional release of Cs-137 during accident-condition testing	• $2 \times 10^{-5} – 8 \times 10^{-4}$ when heated at 1600°C for 500 h. • $10^{-6} – 5 \times 10^{-5}$ during loss-of-coolant simulation test with peak temperature of 1620°C. • $4 \times 10^{-4} – 6 \times 10^{-2}$ when heated at 1800°C for 20 to 200 h.	not measured
Fractional release of Ag-110m during accident-condition testing	• $9 \times 10^{-4} – 3 \times 10^{-2}$ when heated at 1600°C for 500 h. • $8 \times 10^{-4} – 8 \times 10^{-2}$ during loss-of-coolant simulation test with peak temperature of 1620°C. • $8 \times 10^{-2} – 0.81$ when heated at 1800°C for 20 to 200 h.	not measured

[a] Performance data were taken from [IAEA, 1997] and are from a series of irradiation and heating tests.
[b] Performance data were taken from [Borchardt, 1982] and are from a single irradiation test.
[c] Neutron energies greater than 0.1 MeV.
[d] In general, temperatures varied significantly with irradiation time and with location of the fuel within the irradiation-test capsule.

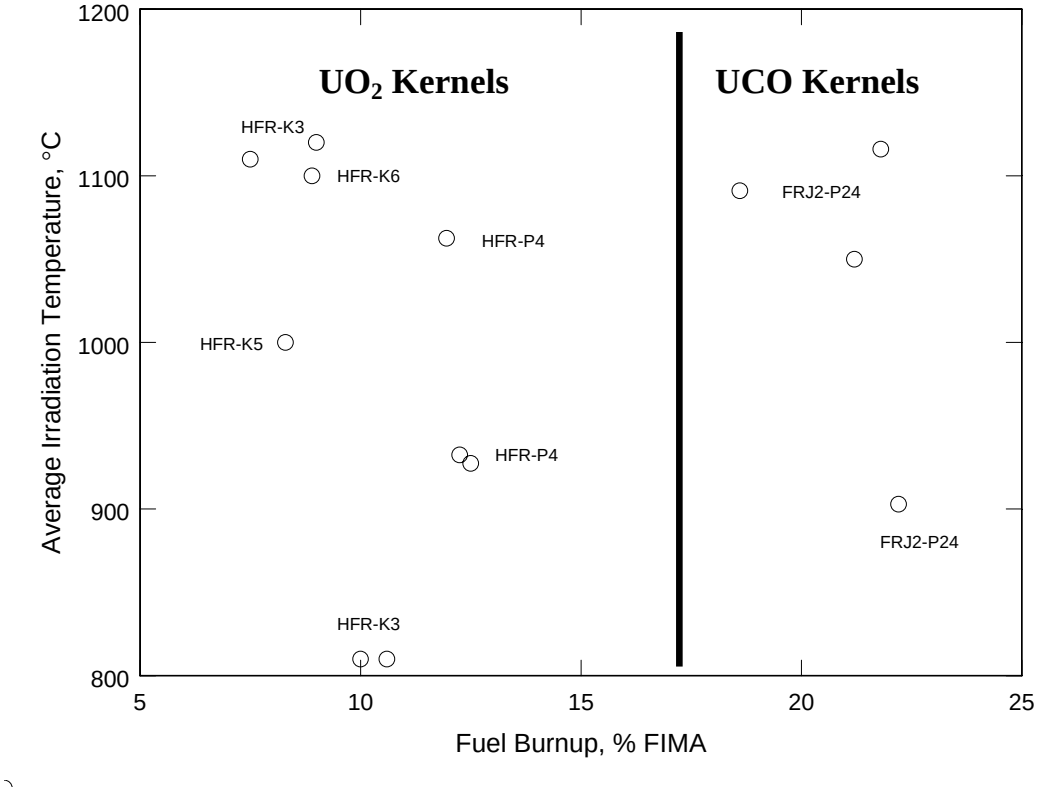

Figure 3-32. Irradiation Conditions During Testing of High-Quality German Fuel. The symbol labels identify the individual irradiation tests. In all cases, the fuel-failure fraction at the end of irradiation was $< 10^{-5}$.

Two advanced coated particle designs are being considered to provide additional performance margins at higher temperatures. These particle designs incorporate ZrC either as a replacement for the SiC layer or as an oxygen getter within the particle. These particle designs are discussed in more detail in Appendix A and have been included as part of the Advanced Gas Reactor development plan for advanced fuels [Hanson, 2004].

3.1.7.4 Radionuclide Transport Mechanisms

Radionuclide transport is modeled in the fuel kernel, the particle coatings, fuel-compact matrix, fuel-element graphite, primary coolant circuit, and reactor building. [IAEA, 1997] provides an excellent overview and an extensive bibliography of radionuclide transport mechanisms. The transport of radionuclides from the location of their birth through the various material regions of the core to their release into the helium coolant is a relatively complicated process. The principal steps and pathways are shown schematically in Fig. 3-33. Also for certain classes of radionuclides, some steps are eliminated (e.g., noble gases are not diffusively released from intact TRISO particles and are not significantly retarded by the compact matrix or fuel-element graphite).

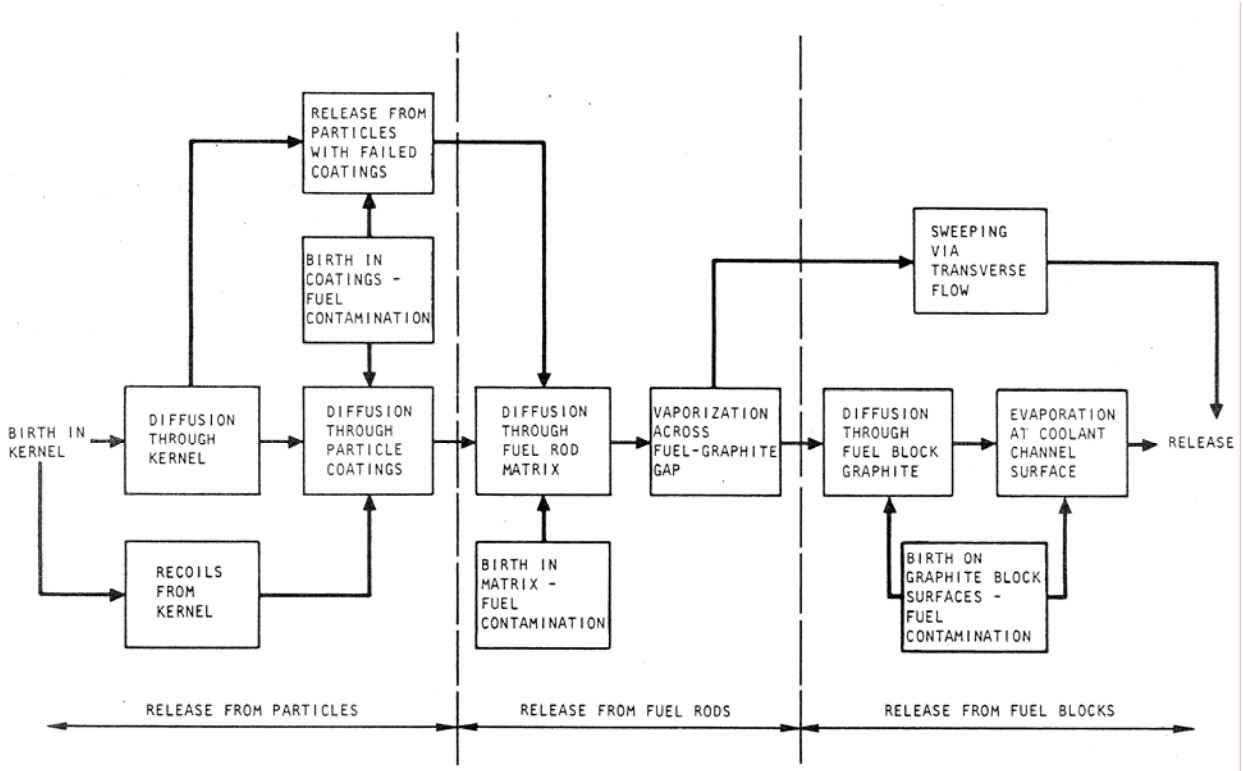

Figure 3-33. Principal Steps in Radionuclide Release from the H2-MHR Core

While the actual radionuclide transport phenomena in the core can be very complex, the basic approach for modeling these phenomena is to treat radionuclide transport as a solid-state diffusion problem with various modifications and/or additions to account for the effects of irradiation and heterogeneities in the core materials. The point of departure is typically Fick's second law of diffusion.

Under normal operating conditions, the fission gases, including iodines, are quantitatively retained by the coatings of an intact TRISO particle. The release of fission gases from HM contamination and failed fuel with exposed fuel kernels is expressed in terms of the release rate-to-birth rate ratio (R/B); at steady-state, R/B is numerically equal to the fractional release. Semi-empirical correlations for R/B have been derived from experimental data and are typically expressed as:

$$\left(R/B\right)_{ji} = 3\sqrt{\left(\frac{\xi_j}{\lambda_i}\right)} \bullet f(T) \bullet f(Bu) \ ,$$

where ξ_j = reduced diffusion coefficient for chemical species j, λ_i = decay constant for isotope i, f(T) = empirical function of temperature, and f(Bu) = empirical function of burnup. The square-root dependence of R/B on isotope half-life results from the analytical solution to the diffusion equation and has been confirmed by measurements of fission-gas release during irradiation testing of fuels and operation of earlier generation gas-cooled reactors, including Peach Bottom

and Ft. St. Vrain. For Kr-85m (half-life = 4.48 h), experimental data show the R/B for an exposed kernel to be in the range 0.005 to 0.01 at 1100°C.

The transport of the volatile fission metals, including Ag, Cs, Sr, and Eu, in the PyC and SiC coatings is modeled as a transient Fickian diffusion process. At sustained temperatures above approximately 1600°C, the SiC coating begins to degrade as a result of fission-product attack. Under these conditions, the fractional release of the Cs isotopes is taken as a measure of the rate of SiC degradation. Figure 3-34 which shows data obtained during postirradiation heating at 1700°C of Japanese low-enriched UO_2 fuel from capsule HRB-22. The release profiles indicate Ag is diffusively released from intact TRISO, Kr is retained by PyC coatings, and Cs is slowly released as the SiC degrades.

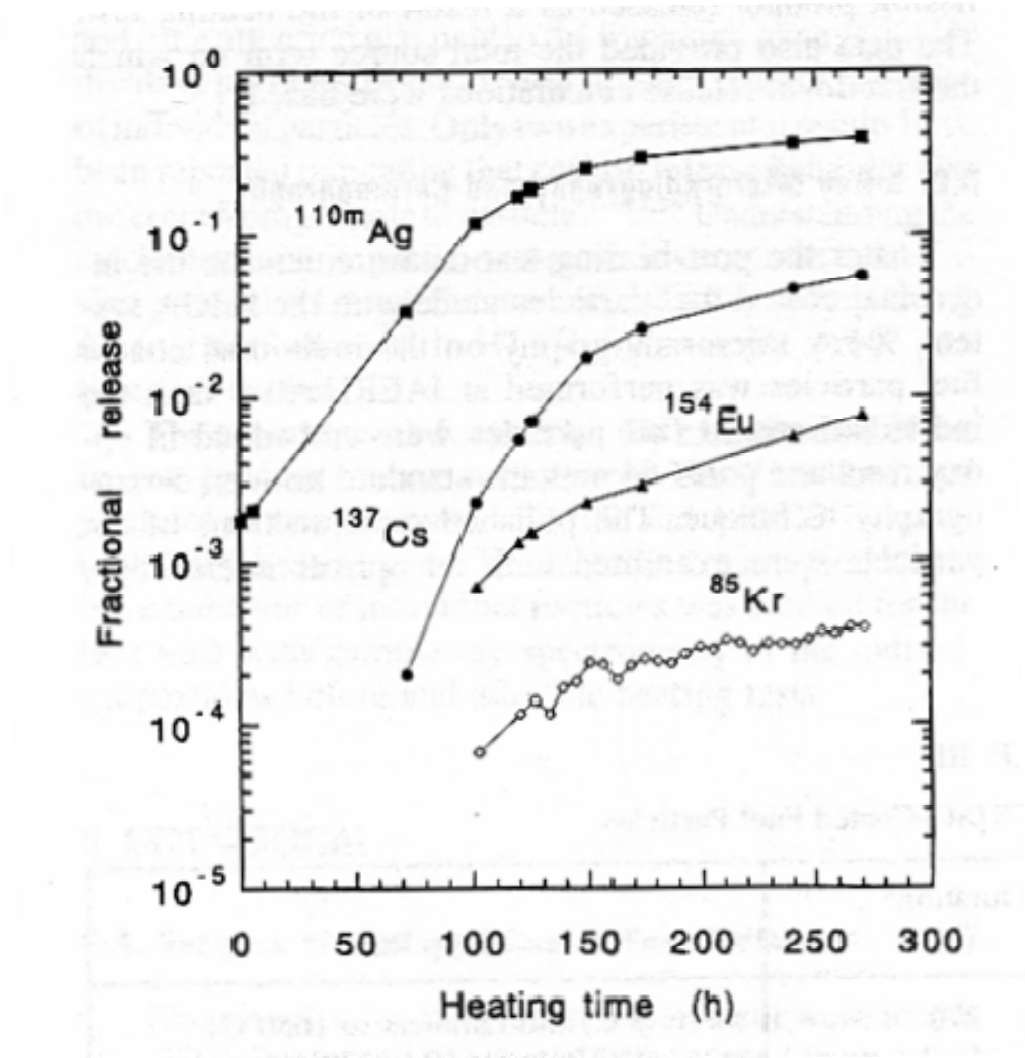

Figure 3-34. Postirradiation Heating of Japanese LEU UO_2 Fuel

The transport of volatile fission metals in fuel-compact matrix and graphite is also modeled as transient diffusion processes. It is assumed that sorption equilibrium prevails in the gap between the fuel compact and the fuel hole surface of the fuel block. At the coolant boundary,

the mass flux from the surface into the flowing coolant is given by the product of a convective mass transfer coefficient and the concentration gradient between the equilibrium desorption pressure and the mixed-mean concentration in the coolant. Diffusion coefficients and sorption isotherms have been determined experimentally for a number of nuclear graphites and matrix materials [IAEA, 1997].

The transport and deposition of condensable radionuclides from the flowing helium coolant to fixed surfaces in the primary coolant circuit is essentially a convective mass transfer problem. Usually, deposition is conceived as a two-step process: (1) gaseous diffusion to the wall and (2) a wall effect, typically an adsorption process. The latter step is necessary because numerous experiments have shown that, under certain circumstances, graphitic and metallic surfaces have a limited capacity to sorb certain radioactive species. The sorptivity of metals for volatile fission products is typically a function of surface oxidation state and temperature. The wall effect may be simply an adsorption process whereby the active sites are confined to the surface. Alternatively, there are some data suggesting that certain radionuclides, principally Ag isotopes, may penetrate into the bulk of metallic components.

The condensable radionuclides that are plated out in the primary circuit may be partially reentrained and released to the reactor building during rapid depressurization transients. A potentially significant removal mechanism, especially during rapid depressurizations, is mechanical reentrainment of deposited particulate matter contaminated by plateout and/or spallation of friable surface films; this mechanical reentrainment is traditionally referred to as "liftoff". Empirical liftoff models have been developed by correlating the fractional reentrainment of plated out fission products measured in blowdown tests with the shear ratio (the ratio of the wall shear during a depressurization transient to that during normal operation).

The VLPC of the H2-MHR is expected to be a significant barrier to the release of condensable radionuclides to the environment during accident conditions. Consequently, the natural removal mechanisms, including condensation, gravitational settling, and turbulent deposition are modeled.

3.1.7.5 Fuel Quality and Performance Requirements

For previous gas-cooled reactor designs, the requirements for as-manufactured quality and in-service performance of coated-particle fuel have been based on a two-tier set of radionuclide design criteria (allowable core release rates), referred to as the "Design" and "Maximum Expected" criteria. This approach has also been adopted for the H2-MHR fuel. The "Design" criteria represent upper limits for all normal operating conditions and any off-normal events that are expected to occur during operation of the plant.[5] These criteria are used when assessing the impact of plant operation on public safety, to size helium purification and radioactive waste systems, and to design plant hardware and shielding. The "Design Criteria" account for uncertainties in the design methods and supporting data, and represent a design margin over the "Maximum Expected" criteria, which are used for applications where "best-estimate" results are appropriate, including developing component removal and maintenance procedures. The fuel and reactor core are to be designed such that there is at least a 50% probability that the radionuclide releases will be less than the "Maximum Expected" criteria, and at least a 95% probability that the releases will be less than the "Design" criteria. The logic for deriving these

[5] These types of off-normal events are often referred to as Anticipated Operational Occurrences (AOOs).

fuel requirements is illustrated in Fig. 3-35. Top-level requirements for the H2-MHR are defined by both the regulators and the users. Lower-level requirements are then systematically derived using the systems-engineering approach described in Section 2.1. With this approach, the radionuclide control requirements for each of the release barriers can be defined. For example, starting with the allowable doses at the site boundary, limits on radionuclide releases from the VLPC, reactor vessel, and reactor core are successively derived. Fuel failure criteria are in turn derived from the allowable core release limits. Finally, the required as-manufactured fuel attributes are derived from the in-reactor fuel-failure criteria, with consideration of achievable values based on existing fuel manufacturing experience, thereby providing a logical basis for the fuel quality specifications.

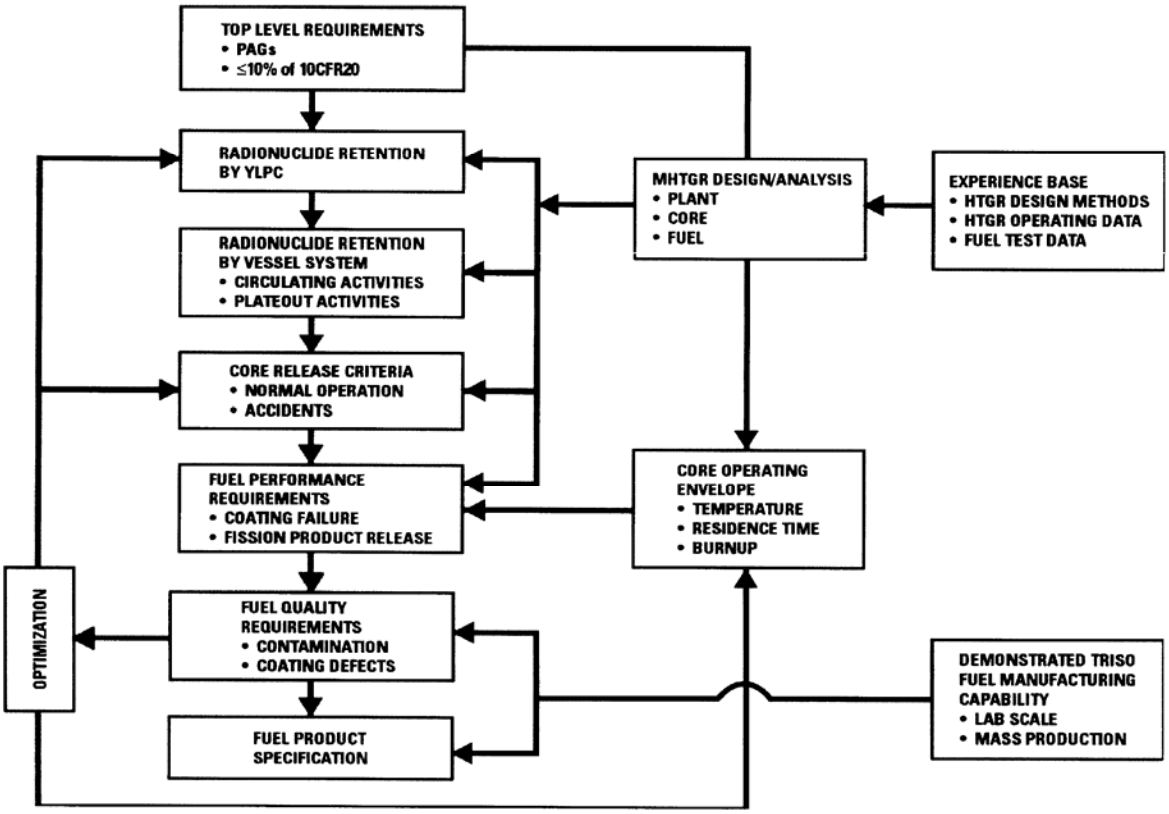

Figure 3-35. Logic for Derivation of Fuel Quality Requirements

As discussed in Section 3.1.4, optimization of the H2-MHR core nuclear and thermal hydraulic design should result in fuel service conditions that are not significantly different from those for the GT-MHR. As a result, the fuel quality and performance requirements for the H2-MHR are identical to those for the GT-MHR. The service conditions, as-manufactured quality requirements, and in-service performance requirements for the H2-MHR fuel are given in Tables 3-12 through 3-14. The requirements for in-service performance are specified on a core-average basis. The maximum allowable release fractions for 30.2-yr Cs-137 and 249.8-d Ag-110m are included in Table 3-14 because these nuclides are expected to be the strongest

contributors to worker dose, based on previous assessments of radionuclide plateout distributions and plant-maintenance requirements.

Table 3-12. Service Conditions for Fissile and Fertile Fuel

Parameter	Fissile Fuel		Fertile Fuel	
	Peak	Core Average	Peak	Core Average
Fuel temperature (normal operation), °C	1250	[850]	1250	[850]
Fuel temperature (accident conditions), °C	1600	—	1600	—
Fuel burnup, % FIMA	26	[15]	7	[4]
Fast fluence, 10^{25} n/m^2 (E > 0.18 MeV)	5	[3]	5	[3]
Core residence time, EFPD	850	850	850	850

Quantities in brackets indicate preliminary values.

Table 3-13. As-Manufactured Quality Requirements for Fissile and Fertile Fuel

Parameter	Fissile Fuel		Fertile Fuel	
	Maximum Expected	Design	Maximum Expected	Design
Missing or defective buffer	1.0×10^{-5}	2.0×10^{-5}	[1.0×10^{-5}]	[2.0×10^{-5}]
Defective SiC	5.0×10^{-5}	1.0×10^{-4}	[5.0×10^{-5}]	[1.0×10^{-4}]
HM contamination	1.0×10^{-5}	2.0×10^{-5}	[1.0×10^{-5}]	[5.0×10^{-5}]
HM contamination outside intact SiC	6.0×10^{-5}	1.2×10^{-4}	[6.0×10^{-5}]	[1.2×10^{-4}]

Quantities in brackets indicate preliminary values.

Table 3-14. In-Service Performance Requirements for Fissile and Fertile Fuel

Parameter	Fissile Fuel		Fertile Fuel	
	Maximum Expected	Design	Maximum Expected	Design
Allowable Fuel Failure Fraction (Normal Operation)	5.0×10^{-5}	2.0×10^{-4}	[5.0×10^{-5}]	[2.0×10^{-4}]
Allowable Fuel Failure Fraction (Accident Conditions)	[1.5×10^{-4}]	[6.0×10^{-4}]	[1.5×10^{-4}]	[6.0×10^{-4}]
Allowable Cs-137 Release Fraction (Normal Operation)	1.0×10^{-5}	1.0×10^{-4}	[1.0×10^{-5}]	[1.0×10^{-4}]
Allowable Cs-137 Release Fraction (Accident Conditions)	1.0×10^{-4}	[1.0×10^{-3}]	[1.0×10^{-4}]	[1.0×10^{-3}]
Allowable Ag-110m Release Fraction (Normal Operation)	2.0×10^{-4}	2.0×10^{-3}	[2.0×10^{-4}]	[2.0×10^{-3}]
Allowable Ag-110m Release Fraction (Accident Conditions)	[2.0×10^{-3}]	[2.0×10^{-2}]	[2.0×10^{-3}]	[2.0×10^{-2}]

Quantities in brackets indicate preliminary values.

3.2 Power Conversion System

The PCS design concept is shown in Fig. 3-36 and the design is based on the GT-MHR [Shenoy, 1996]. Design features of the PCS include (1) a direct Brayton cycle that improves efficiency and economics; (2) a vertical shaft that minimizes blade/stator clearances to reduce bypass flows, reduces plant footprint and associated capital costs, allows vertical lifts for maintenance, and the use of gravity to offset turbine thrust; (3) electromagnetic bearings that reduce energy losses and eliminate the possibility of lubricant ingress into the primary circuit; (4) a single stage of intercooling that improves thermal efficiency by about 2%; and (5) a submerged generator that eliminates a rotating seal[6] in the primary pressure boundary and reduces leakage of primary helium coolant.

For the HTE-based H2-MHR, approximately 90% of the heat generated by the MHR is used to make the electricity supplied to the SOE modules, and the remaining heat is used to generate the steam that is supplied to the SOE modules. The PCS thermodynamic model was included as part of an overall process simulation model for the HTE-based H2-MHR using HYSYS process simulation software.[7] The PCS thermodynamic and performance parameters are shown on Fig. 3-37 and given in Table 3-15.

[6] Dry seal technology development is being performed in Russia as part of a program sponsored by the International Science and Technology Center. If this technology development is successful, it would allow locating the generator outside of the primary pressure boundary.
[7] A description for HYSYS software is available at http://www.aspentech.com/product.cfm?ProductID=274.

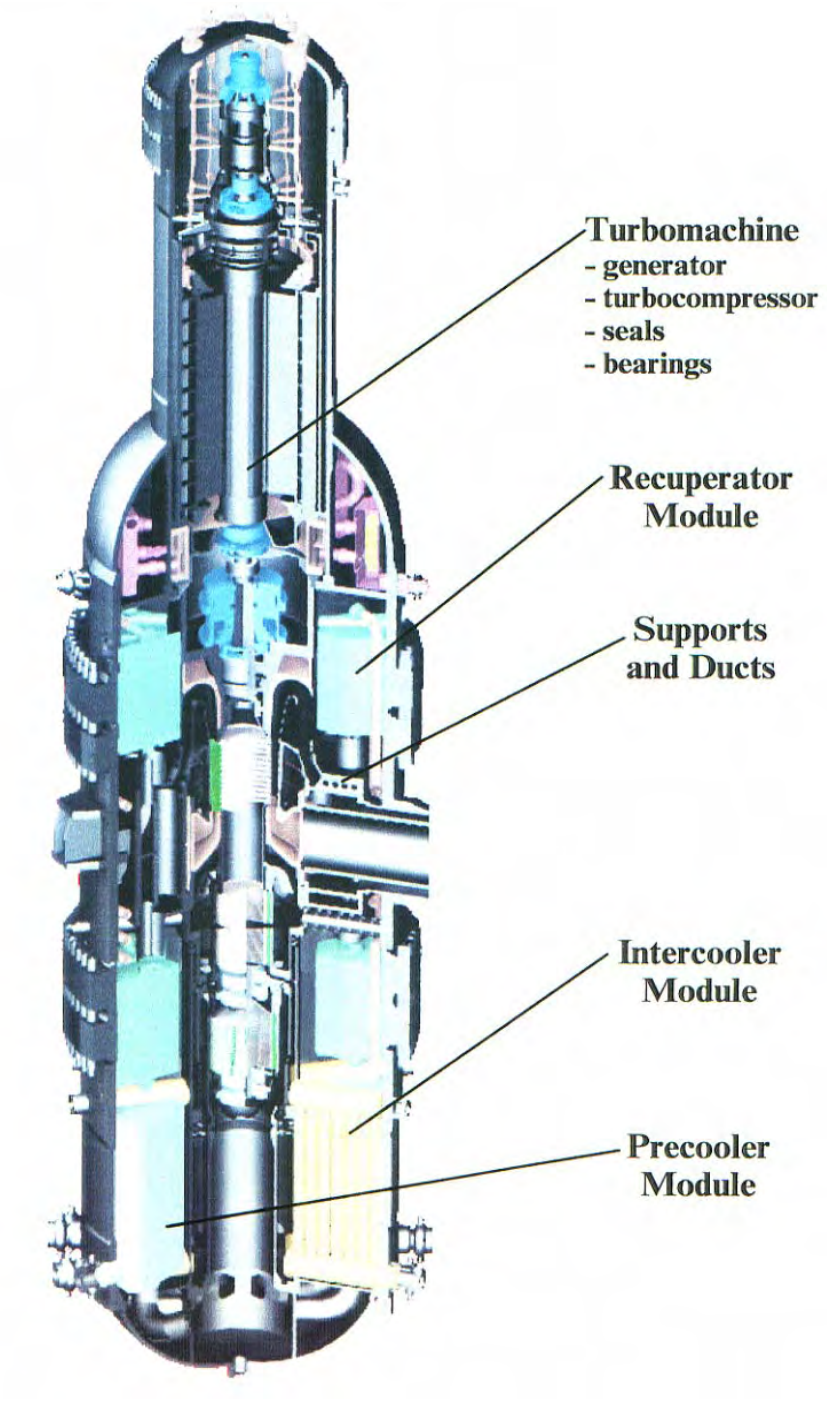

Figure 3-36. Power Conversion System Design Concept

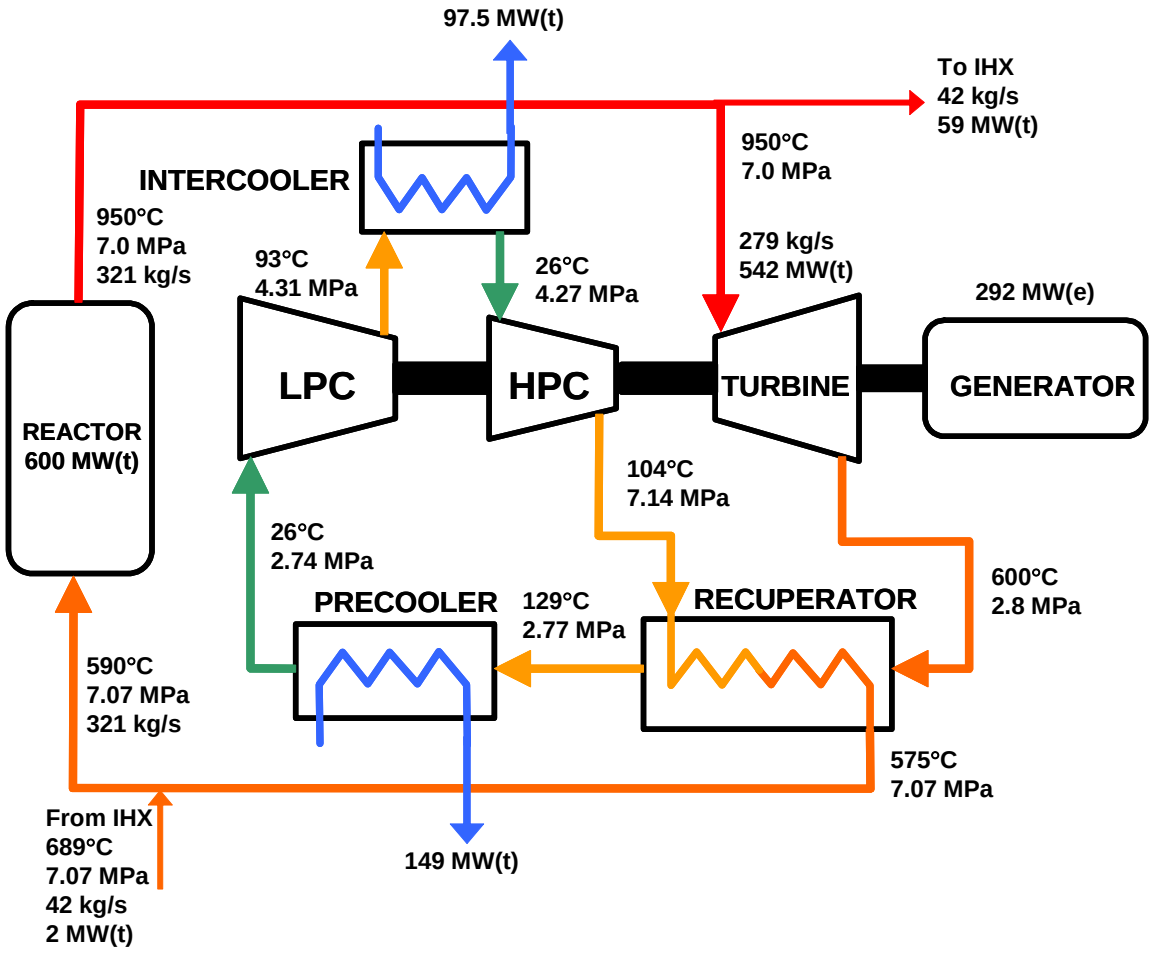

Figure 3-37. PCS Design Parameters

Table 3-15. PCS Thermodynamic and Performance Parameters

Mass flow rate, kg/s	280
Heat supplied from MHR System, MW(t)	542
Turbine inlet/outlet temperatures, °C	950 / 600
Turbine inlet/outlet pressures, MPa	7.0 / 2.8
Recuperator low pressure side inlet/outlet temperatures, °C	600 / 129
Recuperator low pressure side inlet/outlet pressures, MPa	2.8 / 2.77
Precooler inlet/outlet temperatures, °C	129 / 26
Precooler inlet/outlet pressures, MPa	2.77 / 2.74
Precooler heat rejection rate, MW(t)	149
Low pressure compressor inlet/outlet temperatures, °C	26 / 93
Low pressure compressor inlet/outlet pressures, MPa	2.74 / 4.3
Intercooler inlet/outlet temperatures, °C	93 / 26
Intercooler inlet/outlet pressures, MPa	4.31 / 4.27
Intercooler heat rejection rate, MW(t)	97.5
High pressure compressor inlet/outlet temperatures, °C	26 / 104
High pressure compressor inlet/outlet pressures, MPa	4.27 / 7.14
Recuperator high pressure side inlet/outlet temperatures, °C	104 / 575
Recuperator high pressure side inlet/outlet pressures, MPa	7.14 / 7.07
Generator efficiency, %	98
Electricity generated, MW(e)	292
Electricity generation efficiency*, %	53.9

* Neglects parasitic heat losses from the RCCS and SCS.

3.3 Heat Transport and Recovery System

The Heat Transport and Recovery System (HTRS) transfers approximately 58 MW(t) from each MHR module to generate the high-temperature steam that is supplied to the SOE modules. The system was designed based on interfacing with a single, 600-MW(t) MHR module and is replicated for each of the four MHR modules.

3.3.1 Heat Exchangers

The HTRS includes the following heat exchangers: (1) an IHX to transfer heat from the primary to the secondary helium circuit; (2) a Steam Generator / Superheater to generate superheated steam; (3) a High Temperature Heater to further superheat the steam; (4) a Hydrogen Recuperator to recover heat from the hydrogen/steam mixture exiting the SOE modules and transfer that heat to the feedwater; (5) an Oxygen Recuperator to recover the heat from the steam/oxygen stream exiting the SOE modules and use that heat to generate superheated sweep steam; and (6) a Sweep Heater to further superheat the sweep steam. The design conditions for these heat exchangers are given in Table 3-16 and were determined using the HYSYS process simulation model.

Table 3-16. HTRS Heat Exchanger Design Conditions

Parameter	IHX	Steam Generator	Superheater	High Temperature Heater	Hydrogen Recuperator	Oxygen Recuperator	Sweep Heater
Heat Duty, MW(t)	58.7	23.5	30.4	3.35	43.4	37.3	5.97
UA*, 10^5 W/°C	4.09	2.81	1.94	N/A	7.85	6.16	0.37
LMTD, °C**	143.5	83.6	157.1	N/A	55.3	60.5	162.4
Primary Side Fluid	Helium	Helium	Helium	Steam/ Hydrogen	Hydrogen/ Steam	Water/ Steam	Helium
Primary Side Flow Rate, kg/s	41.7	18.1	18.1	23.9	5.3	10.5	18.1
Primary Side Inlet/Outlet Temperature, °C	950/679	530/280	854/530	772/827	862/27	22/586	917/854
Primary Side Inlet/Outlet Pressure, MPa	7.0/6.93	5.82/5.76	5.88/5.82	5.05/5.0	5.0/4.95	5.1/5.05	5.94/5.88
Secondary Side Fluid	Helium	Water/ Steam	Steam/ Hydrogen	Electric Heat	Water/ Steam	Oxygen/ Steam	Steam
Secondary Side Flow Rate, kg/s	18.1	23.6	23.9	N/A	23.6	29.1	10.5
Secondary Side Inlet/Outlet Temperature, °C	292/917	267/281	258/772	N/A	22/267	862/202	586/827
Secondary Side Inlet/Outlet Pressure, MPa	6.0/5.94	5.15/5.10	5.10/5.05	N/A	5.20/5.15	5.0/4.95	5.05/5.0

* UA = product of overall heat transfer coefficient and heat transfer area,
** LMTD = log mean temperature difference.

Detailed designs for these heat exchangers will be developed during the conceptual, preliminary, and final design phases. The pre-conceptual Steam Generator/Superheater design is based on similar helical-coil concepts for MHR plant designs that used a steam cycle to produce electricity. For the HTE-based H2-MHR plant, Inconel 617 has been selected as the material for the helical coil in order to accommodate the higher temperatures. An option for the IHX and other heat exchanger designs is the Printed Circuit Heat Exchanger (PCHE) concept developed by Heatric (www.heatric.com), which consists of metal plates that are diffusion bonded to restore the properties of the base metal (see Fig. 3-38). Fluid-flow channels are chemically milled into the plates using a technique that is similar to that used for etching printed electrical circuits. The PCHE concept allows for simultaneous high-temperature and high-pressure operation with relatively thin wall thicknesses between the primary and secondary coolants. PCHEs are typically four to six times smaller than conventional shell-and-tube heat exchangers of equivalent heat duty. With this technique, the PCHE design can be optimized for specific applications. Designs have been developed with thermal effectiveness greater than 98%. The Oxygen Recuperator design will require a material that can withstand a very high temperature, oxidizing environment. Possible materials for this application include Inconel alloys with dispersed aluminum and niobium-55 / titanium alloys.

The IHX vessel is a pressure boundary for the secondary helium coolant and will be designed according to Section III of the ASME Code. The IHX vessel is manufactured using SA533 steel, and insulated with kaowool to maintain operating temperatures below 350°C and prevent creep damage.

Stacked Plates Etched with Counterflow Channels

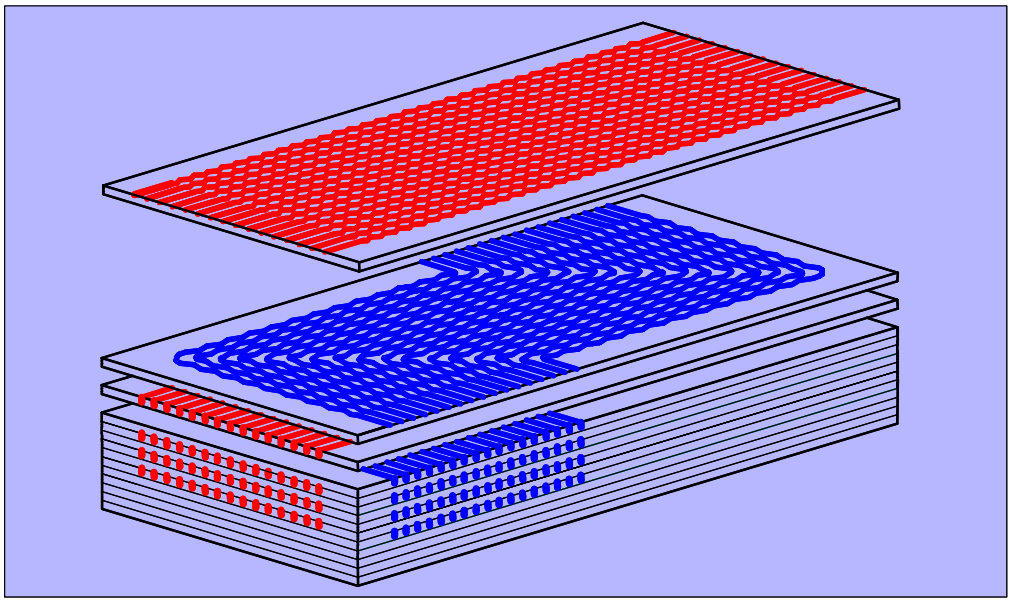

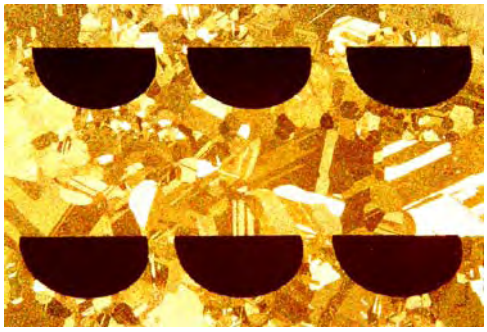

Diffusion-Bonded Microstructure

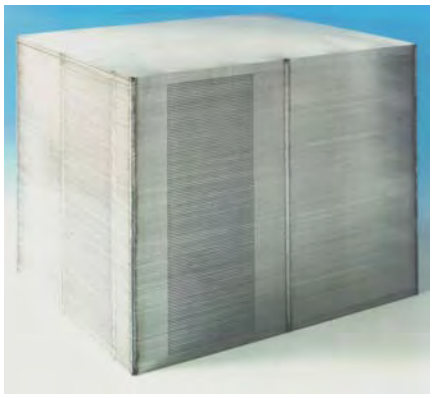

Diffusion-Bonded Plate Assembly

Figure 3-38. PCHE Design Technology (figure courtesy of HEATRIC Corporation)

3.3.2 Circulators

The primary and secondary helium circulators are included as part of the HTRS design. Both circulators are located on the cold legs of their circuits. Detailed designs for these circulators will be developed during the conceptual, preliminary, and final design phases. The design conditions for these circulators are given in Table 3-17 and were determined using the HYSYS process simulation model.

Table 3-17. HTRS Circulator Design Conditions

Parameter	Primary Helium Circulator	Secondary Helium Circulator
Flow Rate, kg/s	41.7	18.1
Inlet/Outlet Pressure, MPa	6.93/7.07	5.76/6.0
Inlet/Outlet Temperature, °C	679/689	280/292
Shaft Work, MW	2.22	1.15

3.3.3 High-Temperature Isolation Valves

At this stage of the HTE-based H2-MHR design, it has not been determined if high-temperature isolation valves (HTIVs) will be required for the HTRS. If HTIVs are required on the hot leg, the design will based on the HTIV design being developed by the Japan Atomic Energy Agency (JAEA) for coupling the HTTR to an engineering-scale, hydrogen production plant based on the Sulfur-Iodine thermochemical water-splitting process [Ohashi, 2005]. This design concept is shown in Fig. 3-39 and consists of an angle valve with an inner thermal insulator (glass wool) and a flat valve seat. The valve body and seat are composed of Hastelloy-X and the valve seat is coated with a metal consisting of Stellite No. 6 with 30 wt. % Cr_3C_2. JAEA has performed tests on a scaled model of this HTIV concept. The measured helium leak rates at temperatures up to 900°C and differential pressures across the valve seat up to 4.1 MPa were less than 0.1 cm^3/s and well below the JAEA target value of 4.4 cm^3/s. However, the test also showed that durability of the valve seat may be an issue that requires further technology development.

3.4 Helium Services Systems

Separate Helium Purification Systems (HPS) are provided for the primary and secondary coolants. These systems are used to maintain acceptable levels of chemical impurities and circulating radioactivity in the primary and secondary coolant systems. Each purification system interfaces with a Helium Transfer and Storage System.

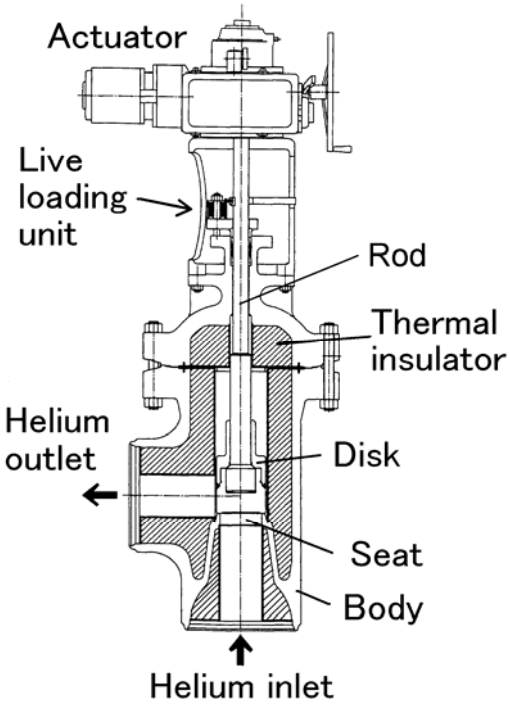

Figure 3-39. High-Temperature Isolation Valve Design Concept (figure courtesy of the Japan Atomic Energy Agency, Oarai, Japan)

3.4.1 Primary Coolant Helium Purification System

The Primary Coolant HPS processes a slipstream flow of the primary coolant to remove chemical and radioactive impurities (including tritium). The slipstream flow fraction is approximately 1% (or less) of the total primary coolant flow rate. The primary functions of the Primary Coolant HPS are:

- Remove chemical and radioactive impurities from the helium coolants.
- Pressurize, depressurize, and control the primary helium coolant inventory (in conjunction with Helium Transfer and Storage System).
- Provide purified helium for purges and buffers.
- Maintain the primary coolant system at slightly below atmospheric pressure during refueling/maintenance.
- Purify helium pumped to storage.

For the H2-MHR, another key function of the purification systems is to limit tritium and other radioactive contamination in the hydrogen product gas.

A helium purification train is provided for each reactor module and is located in the reactor building. The slipstream flow is extracted from the cold leg at the exit of the primary coolant circulator. Most of the purified helium is returned to the cold leg at the inlet of the primary coolant circulator. A portion of the purified helium is returned to other locations to purge vessel seals, shutdown circulator seals, and vessel relief piping. The purification train is shown in Fig. 3-40 and the components are described in Table 3-18. Spares are maintained for the helium compressors, filters, and adsorber beds in order to maintain high availability and reliability.

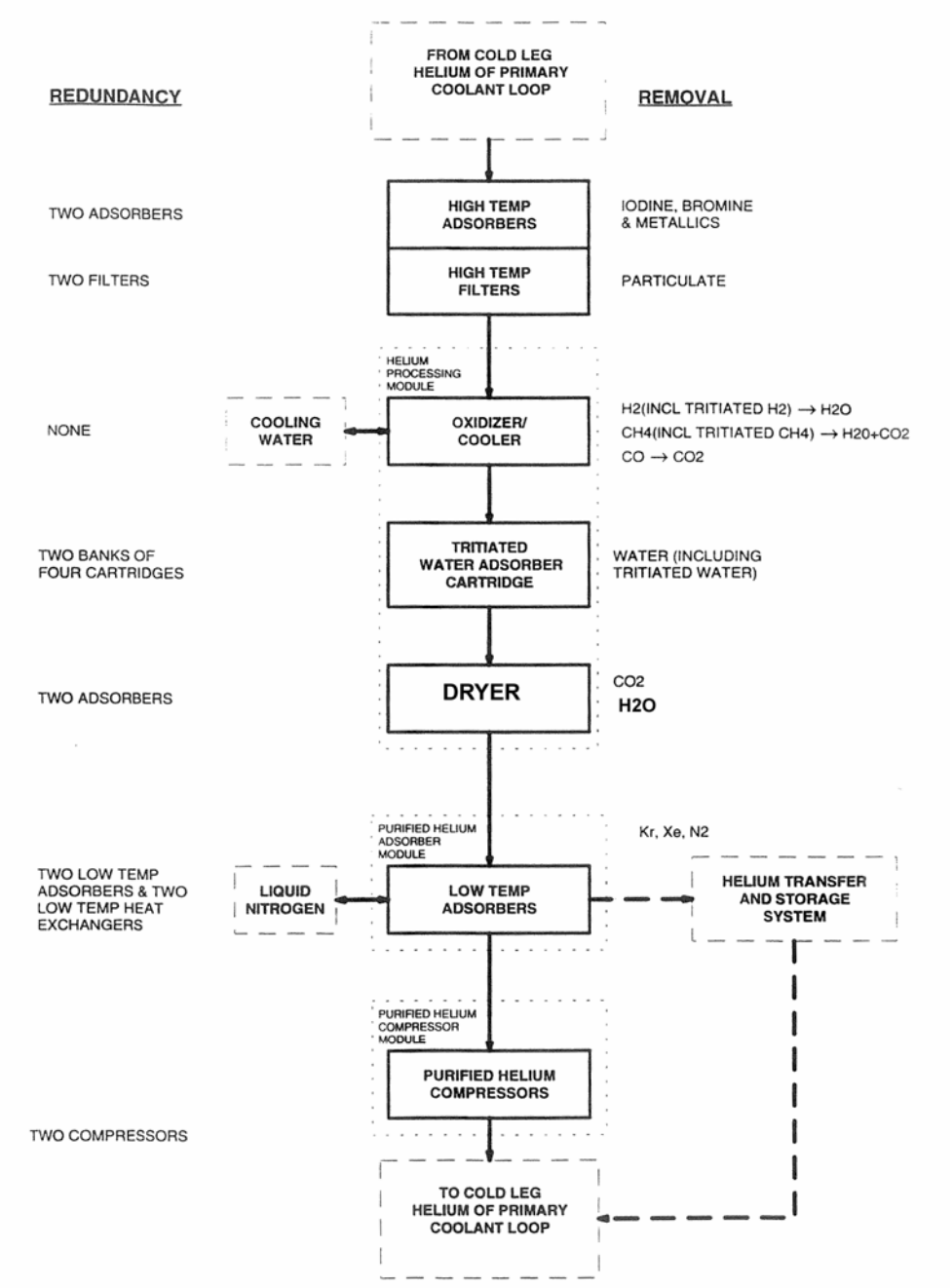

Figure 3-40. Helium Purification Train Block Diagram

Table 3-18. Primary Helium Purification System Description

Component	Function	Description
High Temperature Adsorber	Remove iodine, bromine, and metallic fission products.	Charcoal-filled cartridge within a flanged vessel
High Temperature Filter	Remove particulates	Filter cartridge housed within a flanged vessel. Filter specifications TBD.
Oxidizer	Oxidizes H_2 (including tritiated H_2) to H_2O. Oxidizes CH_4 to H_2O and CO_2. Oxidizes CO to CO_2.	Vessel filled with oxidizing agent (e.g., CuO). Continuous on-line analysis of the outlet gas determines whether oxidizing (O_2) or reducing (H_2) gases need to be added to the helium entering the vessel.
Cooler	Condense water vapor. Remove tritiated water.	Shell and tube heat exchanger with helium on the tube side and cooling water on the shell side. Drain tank with liquid level instrumentation is connected to the tube side. Water is pumped periodically from the drain tank to the Liquid Radioactive Waste System.
Dryer	Remove remaining H_2O (including tritiated H_2O) and CO_2.	Vessel filled with molecular sieve adsorbent.
Low Temperature Absorber	Remove noble-gas fission products (primarily Kr and Xe isotopes), N_2, and CH_4.	Charcoal-filled cylinder centrally positioned within a liquid nitrogen-filled shell. Counterflow of helium and low-pressure liquid nitrogen, with nitrogen vaporizing on the shell side. A downstream filter removes any charcoal debris resulting from erosion.
Compressor Module	Return the purified helium to the primary circuit.	Compressor, pulsation bottles to dampen flow oscillations, aftercooler to remove heat of compression (so that cool helium is available for purge applications), and appropriate valves, instrumentation, and controls.

3.4.2 Secondary Coolant Helium Purification System

The Secondary HPS is similar in design to the Primary HPS, except that the equipment sizes are much smaller than those for the Primary HPS because of the much smaller secondary coolant flow rate. In addition, high and low temperature adsorbers (to remove fission products) may not be required for the Secondary HPS.

The slipstream flow fraction will be determined largely by the impurity specifications (including tritium) for the hydrogen product gas.

3.4.3 Helium Transfer and Storage Systems

Separate Helium Transfer and Storage Systems are provided for the primary and secondary coolants. The primary functions of these systems are given below:

- Provide storage capacity for helium during depressurizations for refueling and maintenance.
- Supply coolant system makeup helium during normal plant operation.
- Provide a source of high pressure helium for specific plant uses.
- Transfer and distribute helium among various plant users.
- Work in conjunction with the HPS to pressurize, depressurize, and control the primary and secondary coolant inventories.

As shown in Fig. 3-41, the Helium Transfer and Storage Systems consist of a high-pressure section and a low-pressure section. The high-pressure section supplies make-up helium to compensate for losses and helium for purge-flow requirements. The low-pressure section receives helium from the coolant system for inventory control. The system is equipped with compressors to transfer helium between the high- and low-pressure sections.

3.4.4 Tritium Control

A key requirement for the H2-MHR is to produce hydrogen gas that meets customer requirements for product quality. Tritium is produced in limited quantities in the MHR and it has the potential to migrate through the heat-transfer surfaces of the IHX and the high-temperature heat exchangers in the hydrogen production system. Sources of tritium include:

- Ternary fission (fission yield is ~10^{-4}).
- Neutron activation of He-3 (He-3 abundance is ~2×10^{-7}).
- Neutron reactions with trace levels of lithium present in graphite and fuel compact matrix material.
- Neutron reactions with B-10 present in control rods and burnable poison.

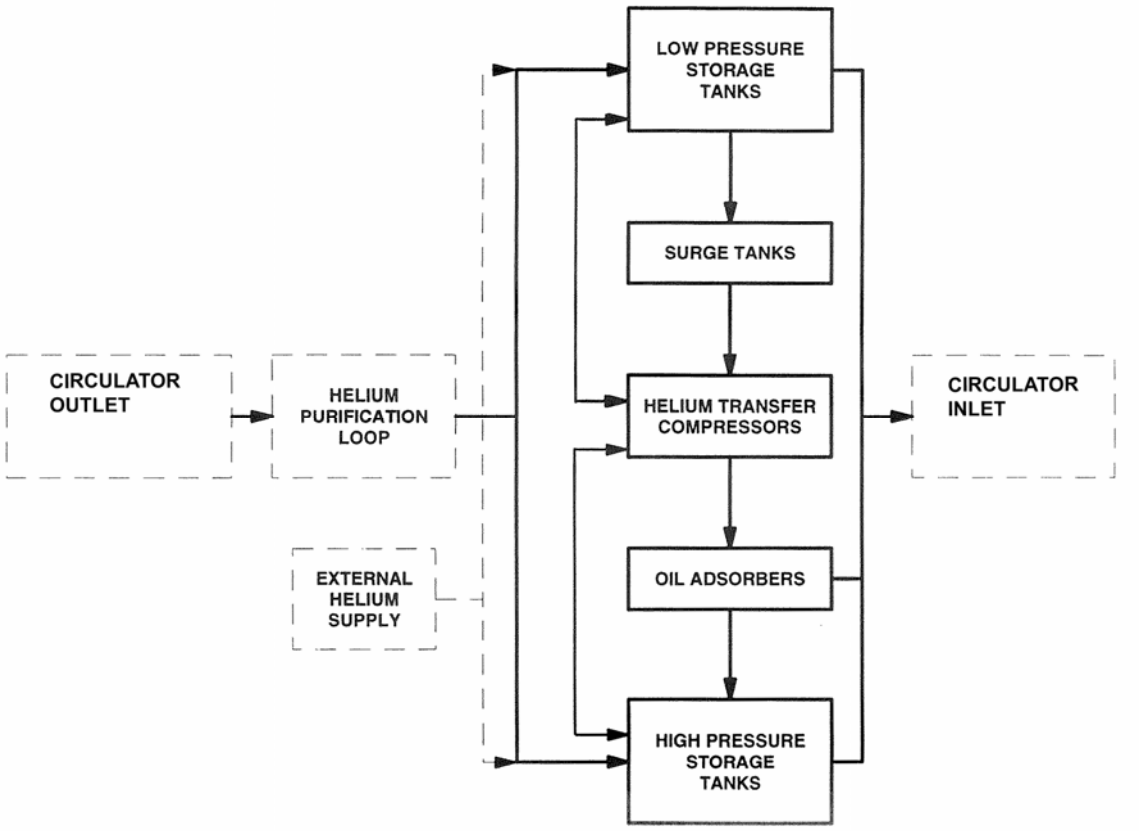

Figure 3-41. Helium Transfer and Storage System Block Diagram

Ternary fission typically contributes to about 60% of the total tritium source term. At sufficiently low temperatures, this source of tritium is retained effectively by the TRISO coating system. However, the H2-MHR core will include regions that operate at temperatures greater than 1000°C for significant periods of time. Figure 3-42 shows the expected fractional tritium release from TRISO-coated fuel particles as a function of time at temperature. If fuel is maintained at 1300°C for 100 days, the fractional tritium release is expected to be about 0.2. Activation of He-3 and neutron reactions with lithium and boron each contribute to about 20% of the total tritium source term.

The tritium concentration in the primary coolant is determined by a balance between production and removal. Removal mechanisms include radioactive decay, slipstream coolant purification (a titanium sponge or a CuO oxidation bed is typically used to remove tritium), and sorption onto graphite. A previous assessment of tritium behavior in the Fort St. Vrain reactor indicated that at high temperatures, the core graphite was very effective at removing tritium from the primary coolant. Figure 3-43 shows measured tritium concentrations in the Fort St. Vrain primary coolant. When the reactor was at full power, tritium concentrations generally remained below about 10^{-5} $\mu Ci/cm^3$.

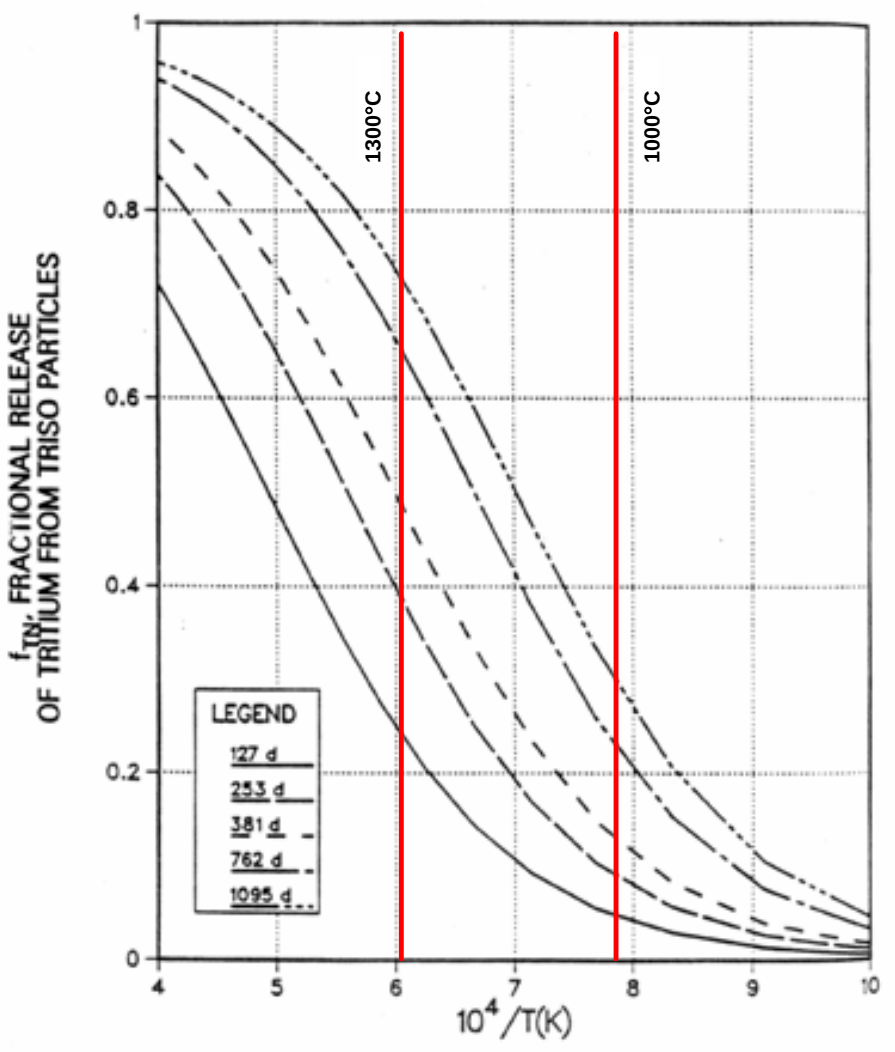

Figure 3-42. Tritium Release from TRISO-Coated Fuel Particles

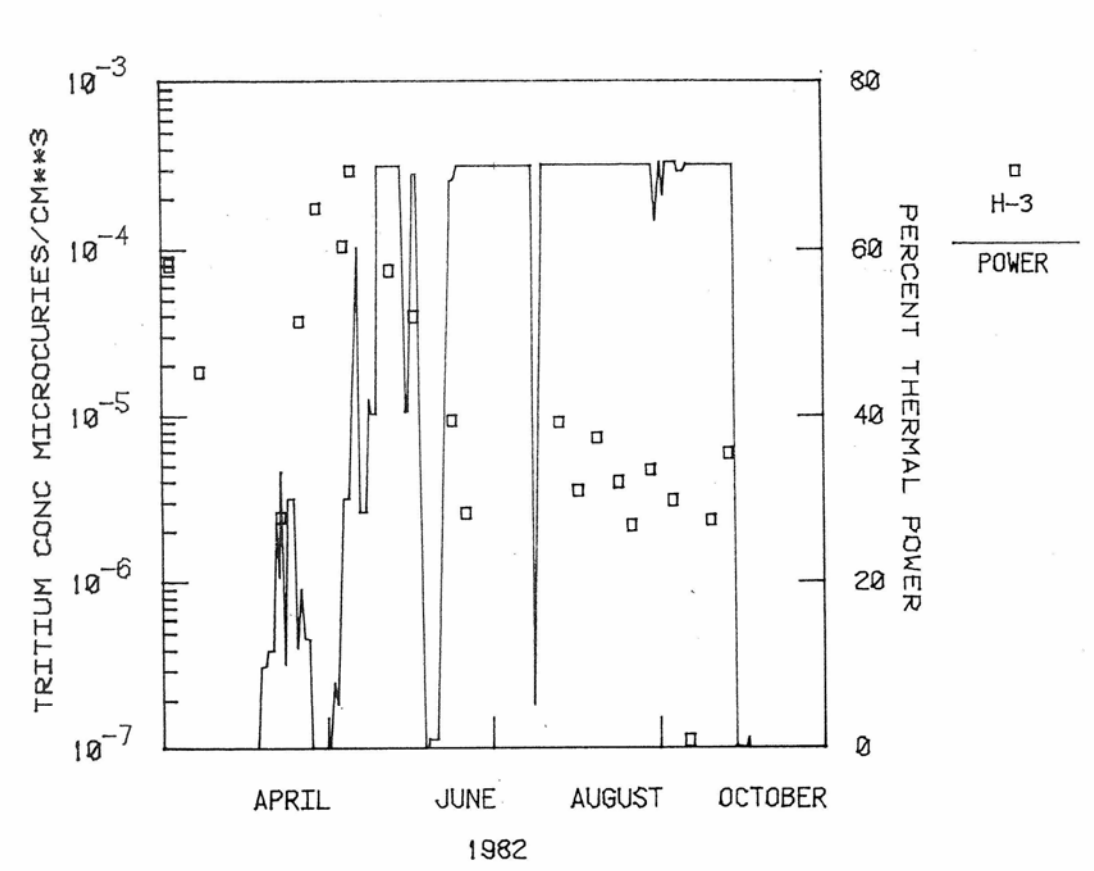

Figure 3-43. Measured Tritium Concentration in Fort St. Vrain Primary Coolant

In order to asses the potential for tritium contamination in the hydrogen product gas, an assessment of tritium permeation through a Heatric-type IHX (with an assumed heat transfer surface area of 1200 m^2) was performed. A semi-empirical correlation for Incoloy 800 was used to estimate the tritium flux from the primary-side helium to the secondary-side helium:

$$Flux = 61.02\ C_t \sqrt{P / C_{H_2}}\ \frac{\exp(-6250/T)}{t} \qquad (\mu Ci/m^2 - h),$$

where $C_t \equiv$ tritium concentration in the primary coolant, referenced to standard temperature and pressure ($\mu Ci/m^3$), $P \equiv$ total primary-side pressure (atm), $C_{H_2} \equiv$ hydrogen impurity concentration in the primary coolant (ppmv), T = IHX wall temperature (K), and t = IHX wall thickness (mm). The hydrogen impurity concentration was conservatively assumed to be at its lowest expected level of 0.2 ppmv. The IHX wall temperature was assumed to vary linearly from the primary coolant inlet value (950°C) to the outlet value (679°C). Based on the data shown on Fig. 3-43, the quantity C_t was assumed to be 10 $\mu Ci/m^3$. Using these assumptions, the tritium permeation rate to the secondary side was calculated to be approximately 6 $\mu Ci/s$. If the tritium is assumed to be in the form HT, the mass permeation rate is approximately 8.8×10^{-13} kg/s. Assuming a helium purification flow fraction of 0.5% on the secondary loop, the tritium concentration in the

secondary coolant is reduced to about 6×10^{-7} μCi/cm^3 at atmospheric pressure. Assuming the heat exchanger walls in the hydrogen production plant provide the same resistance as those of the IHX, the HT mass permeation rate to the product gas is reduced to 5×10^{-20} kg/s. For a hydrogen production rate of 2.36 kg/s, the HT concentration in the product gas is about 2×10^{-14} ppmw, which corresponds to about 2.5×10^{-14} μCi/cm^3 at standard temperature and pressure. This concentration is more than six orders of magnitude below the limit specified in 10CFR20 for the maximum allowable tritium concentration in an uncontrolled area.

Based on this assessment, it should be possible to control tritium concentrations in the product gas to acceptable levels. More detailed assessments of tritium source terms, product gas contamination, and tritium release to the environment should be performed during the preliminary and final design stages. International standards should also be developed for hydrogen product gas produced using nuclear energy.

3.5 Hydrogen Production System

The Hydrogen Production System is based on coupling the MHR to SOE modules. As shown in Fig. 3-44, Modular Helium Reactors (MHRs) supply both the heat to generate steam and the electricity to split the steam into hydrogen and oxygen. Electricity is generated using a direct, Brayton power-conversion system (PCS). Approximately 90% of the heat generated by the MHRs is used to produce electricity. The remainder of the heat is transferred though an intermediate heat exchanger (IHX) to produce steam. As indicated in Fig. 3-44, steam is supplied to both the anode and cathodes sides of the electrolyzers. The steam supplied to the cathode side is split into hydrogen and oxygen. The oxygen is transferred through the electrolyte to the anode side. The steam supplied to the anode side is used to sweep the oxygen from electrolyzer modules. The steam supplied to the cathode side is first mixed with a small portion of the hydrogen stream in order to endure reducing conditions and prevent oxidation of the electrodes. Heat is recuperated from both the hydrogen/steam and oxygen/steam streams exiting the electrolyzer. A small quantity of electricity is generated from the oxygen stream to provide power for plant house loads.

The hydrogen production rate per MHR module is 2.36 kg/s and 9.44 kg/s for a 4-module plant. The corresponding heat rate is 1339.5 MW(t), using the higher heating value of hydrogen (141.9 MJ/kg). The MHR modules produces 2400 MW(t). The overall plant efficiency is then estimated to be:

$$\eta_{plant} = 100 \times \frac{1339.5}{2400} = 55.8\%$$

At a 90% plant capacity factor, the plant produces 2.68×10^5 metric tons of hydrogen per year at a product gas pressure of 4.95 MPa. The MHR System, PCS, and HTRS are described in Sections 3.1 through 3.3. The Hydrogen Production System, including the SOE modules and Power Recovery System are described in the following sections. The Water Supply System is described in Section 3.7.5. Other miscellaneous plant equipment includes a hydrogen storage tank for startup, a small hydrogen re-circulator, valves, piping, and instrumentation.

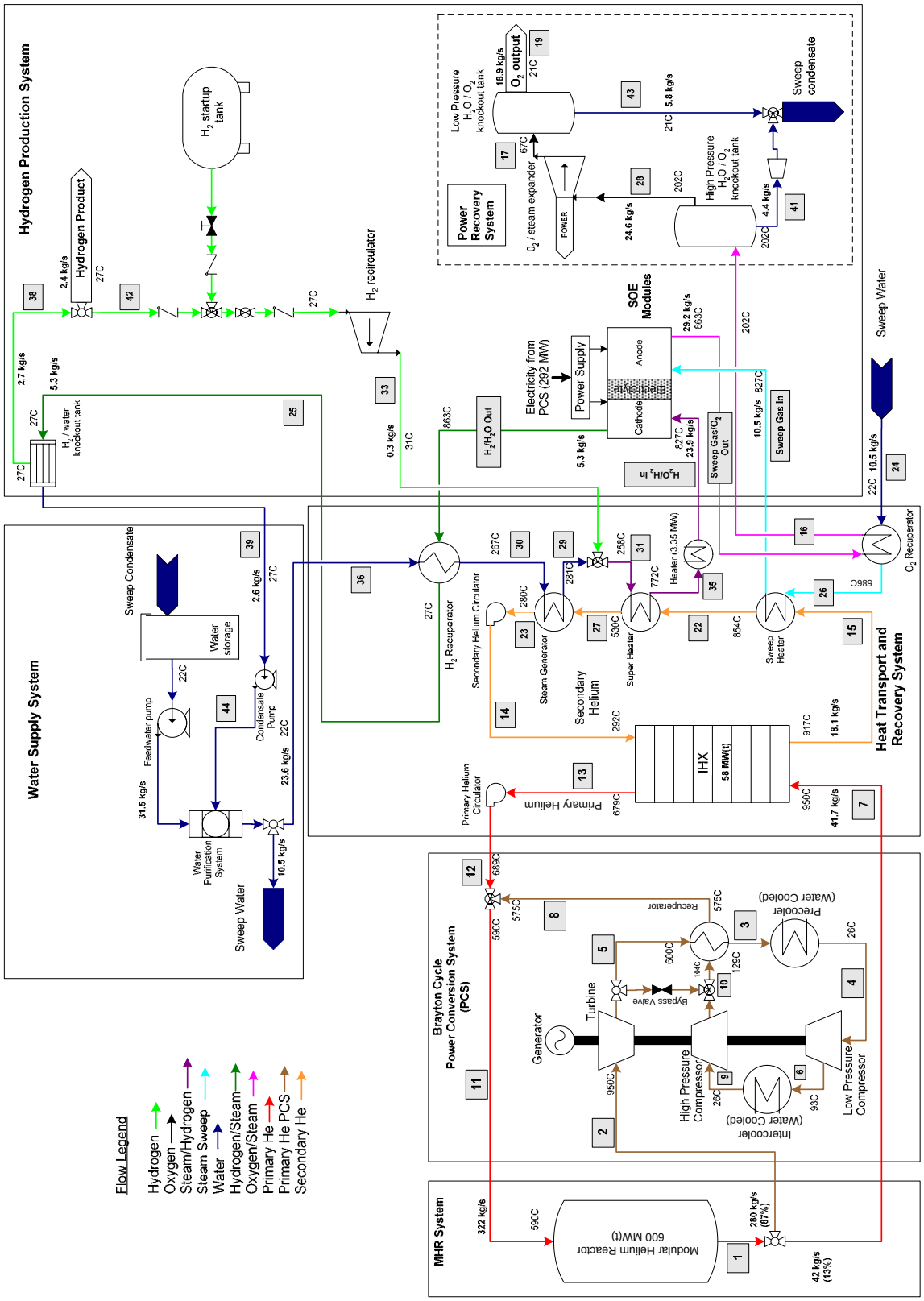

Figure 3-44. HTE Process Flowsheet

3.5.1 Process Flow Stream Description

The process flow streams are identified by the gray boxes shown on Fig. 3-44. As discussed previously, the entire process shown on Fig. 3-44 was simulated using HYSYS process-simulation software. The HYSYS implementation of the flowsheet is shown in Fig. 3-45. For this particular application, INL developed an SOE electrochemical process model that was incorporated into HYSYS. Table 3-19 provides a description of composition, vapor fraction, flow rate, temperature, and pressure of each flow stream.

3.5.2 Solid Oxide Electrolyzer Modules

The SOE modules are based on the planar cell technology described in Section 1.2. Design parameters for a 12.5 kW(e), 500-cell stack are given in Table 3-20. For the HTE-based H2-MHR, it is anticipated that a module would contain 40 stacks and consume 500 kW(e). A module would occupy approximately 4.2 m^2 of floor space, which includes space allocated for internal manifolding, piping, etc. Eight modules could be installed within a structure that is similar in size to the trailer portion of a typical tractor-trailer. Approximately 292 of these 8-module units would be required for a full-scale plant with four 600-MW(t) MHR modules. Figure 3-46 illustrates this SOE module concept.

3.5.3 Power Recovery System

As shown on Fig. 3-44, the HTE process flowsheet includes a Power Recovery System to generate power from the oxygen/steam stream exiting the SOE modules. This system includes a turbine and high and low pressure drums to remove water. The water is recycled back to the Water Supply System. The turbine operates with adiabatic and polytropic efficiencies of 80% and 77%, respectively, and produces approximately 8.3 MW(e). This electricity is used for house plant loads, including power required for the High Temperature Heater.

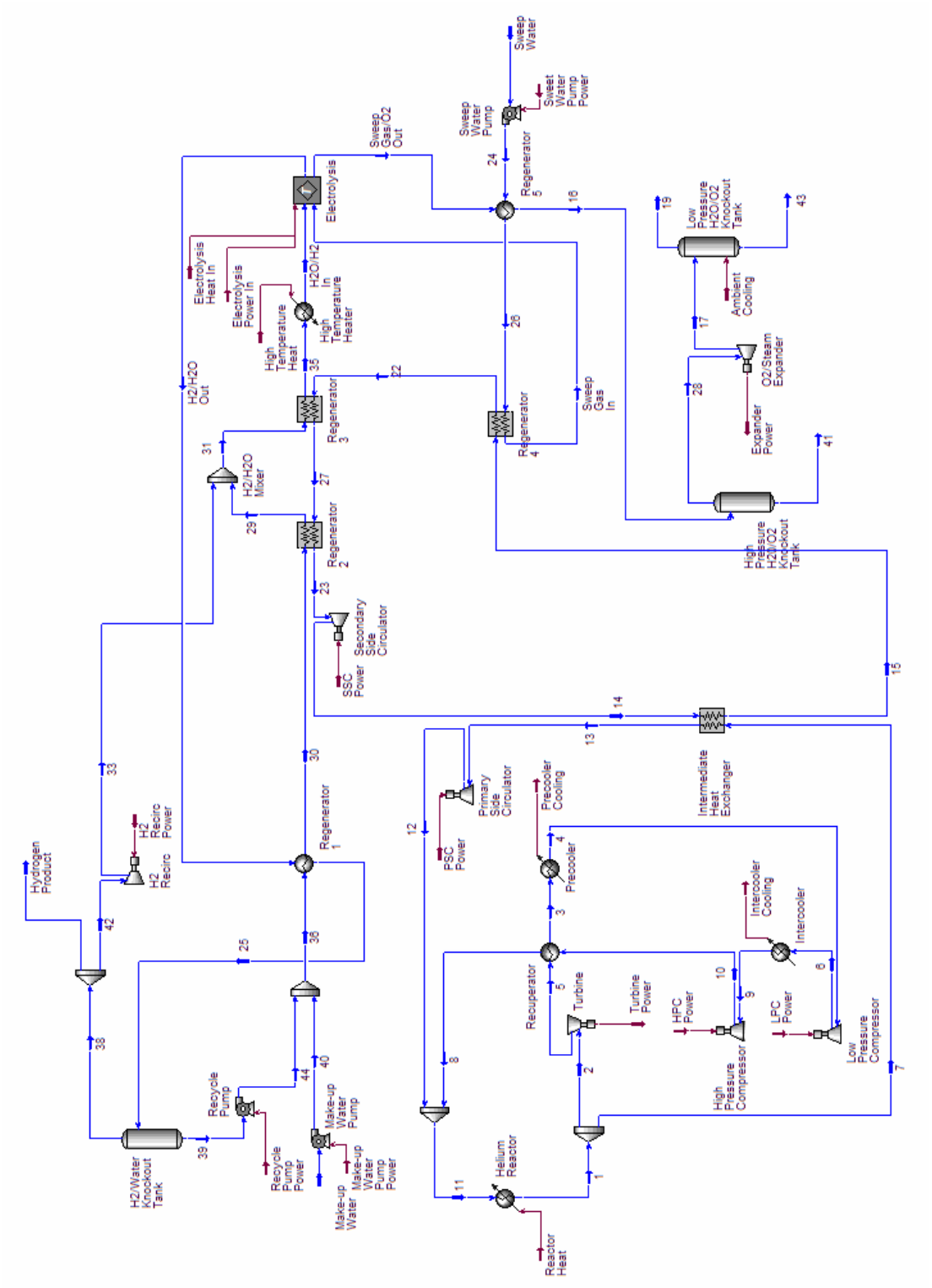

Figure 3-45. HYSYS Implementation of HTE Process Flowsheet

Table 3-19. HTE Process Flow Stream Description

Stream	Stream Composition (mole fraction)				Vapor Fraction	Flow Rate (kg/s)	Temp. (°C)	Press. (MPa)
	H_2	H_2O	O_2	He				
1	0	0	0	1.0	1.0	322.2	950	7.00
2	0	0	0	1.0	1.0	280.6	950	7.00
3	0	0	0	1.0	1.0	280.6	129	2.77
4	0	0	0	1.0	1.0	280.6	26	2.74
5	0	0	0	1.0	1.0	280.6	600	2.80
6	0	0	0	1.0	1.0	280.6	93	4.31
7	0	0	0	1.0	1.0	41.7	950	7.00
8	0	0	0	1.0	1.0	280.6	575	7.07
9	0	0	0	1.0	1.0	280.6	26	4.27
10	0	0	0	1.0	1.0	280.6	104	7.14
11	0	0	0	1.0	1.0	322.2	590	7.07
12	0	0	0	1.0	1.0	41.7	689	7.07
13	0	0	0	1.0	1.0	41.7	679	6.93
14	0	0	0	1.0	1.0	18.1	292	6.00
15	0	0	0	1.0	1.0	18.1	917	5.94
16	0	0.5	0.5	0	0.788	29.2	202	4.95
17	0	0.3658	0.6342	0	0.870	24.6	67	1.01
19	0	0.0244	0.9756	0	1.0	18.9	21	1.01
22	0	0	0	1.0	1.0	18.1	854	5.88
23	0	0	0	1.0	1.0	18.1	280	5.76
24	0	1.0	0	0	0.0	10.5	22	5.10
25	0.9	0.1	0	0	0.9008	5.25	27	4.95
26	0	1.0	0	0	1.0	10.5	586	5.05
27	0	0	0	1.0	1.0	18.1	530	5.82
28	0	0.3658	0.6342	0	1.0	24.6	202	4.95
29	0	1.0	0	0	1.0	23.6	281	5.10
30	0	1.0	0	0	0.4202	23.6	267	5.15
31	0.1	0.9	0	0	1.0	23.9	258	5.10
33	0.9991	0.0009	0	0	1.0	0.30	31	5.10
35	0.1	0.9	0	0	1.0	23.9	772	5.05
36	0	1.0	0	0	0.0	23.6	22	5.20
38	0.9991	0.0009	0	0	1.0	2.66	27	4.95
39	0.0001	0.9999	0	0	0.0	2.60	27	4.95
41	0	0.9983	0.0017	0	0.0	4.44	202	4.95
42	0.9991	0.0009	0	0	1.0	0.30	27	4.95
43	0	1.0	0	0	0.0	5.78	21	1.01
44	0.0001	0.9999	0	0	0.0	2.60	27	5.20
Sweep Gas In	0	1.0	0	0	1.0	10.5	827	5.00
H_2O/H_2 In	0.1	0.9	0	0	1.0	23.9	827	5.00
Sweep Gas/O_2 Out	0	0.5	0.5	0	1.0	29.2	863	5.00
H_2/H_2O Out	0.9	0.1	0	0	1.0	5.25	863	5.00
Hydrogen Product	0.9991	0.0009	0	0	1.0	2.36	27	4.95

Table 3-20. Design Parameters for a 500-Cell SOE Stack

Cell Area	
Individual Cell Width	10 cm
Individual Cell Active Area	100 cm^2
Total Number of Cells	12 x 10^6
Total Active Cell Area	120,000 m^2
Cell Thickness	
Electrolyte	10 µm (ScSZ - Scandia Stabilized Zirconia)
Anode	1500 µm (LSM - Strontium Doped Lathanum Manganite)
Cathode	50 µm (Nickel Zirconia Cermet)
Bipolar Plate	2.5 mm (Stainless Steel)
Total Cell Thickness	4.06 mm
Stack Dimensions	
Cells per Stack	500
Stack Height	2.03 m
Stack Volume	0.0203 m^3
Stack Volume with Manifold	0.0812 m^3

3.6 Plant Protection and Monitoring Systems

3.6.1 Reactor Protection System

The design of the Reactor Protection System (RPS) is similar to that for the GT-MHR [Shenoy, 1996]. The RPS provides an integrated response to initiating events (e.g., loss of offsite power) in order to ensure safe shutdown of the reactor. Each MHR module has an independent RPS, and the RPS is independent of other control systems, including the Investment Protection System (IPS). The RPS monitors plant parameters, including neutron flux, primary and secondary coolant flow rates, primary and secondary coolant pressures, primary coolant inlet and outlet temperatures, primary coolant moisture concentration, and secondary coolant radioactivity. If the plant parameters are not within their allowable ranges, the RPS performs its safety-related function to trip the reactor using the control rods or the independent reserve shutdown system. The RPS uses two-out-of-four coincidence logic to satisfy safety and availability requirements. For the H2-MHR, the trip setpoints will be established during the preliminary and final design stages.

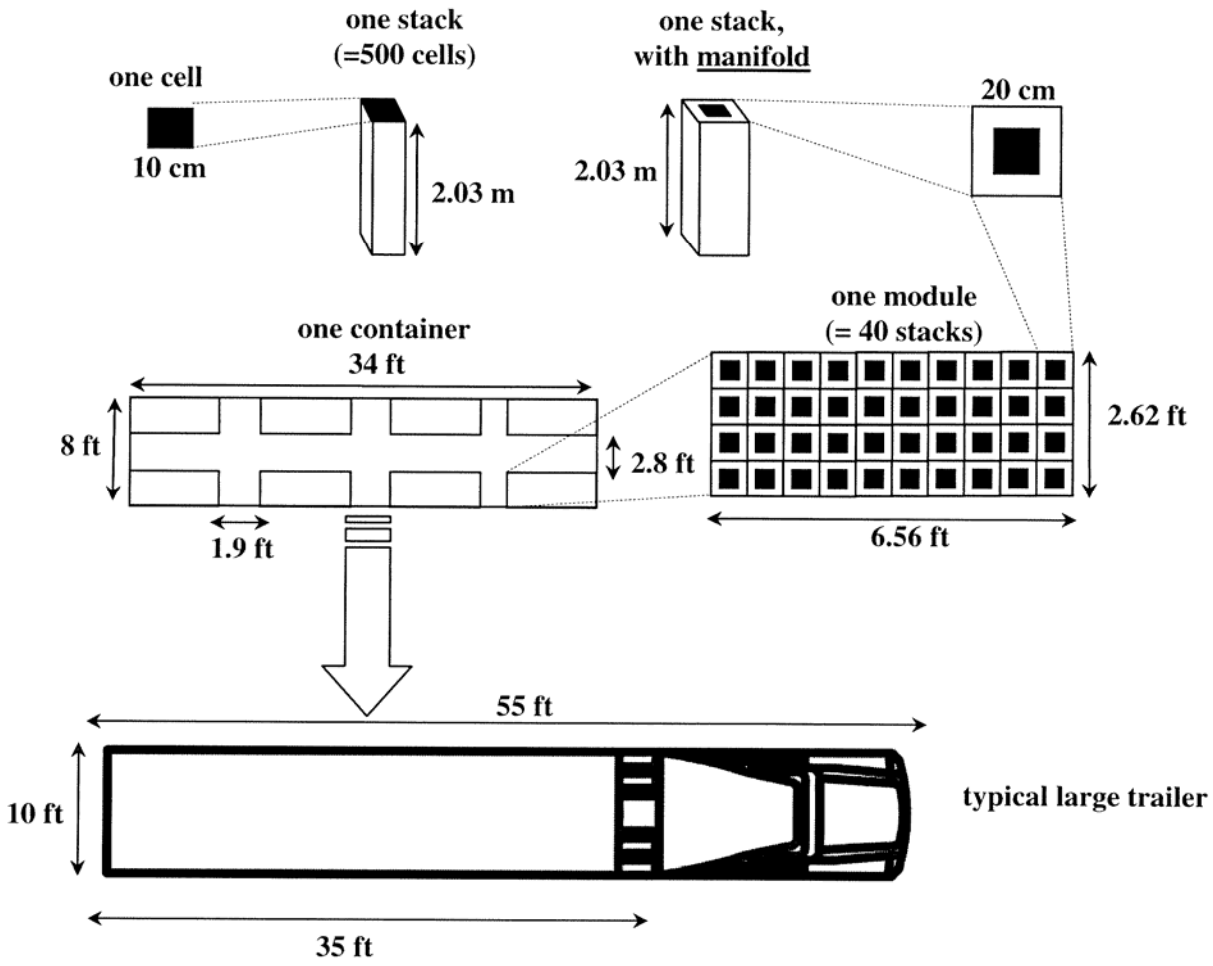

Figure 3-46. SOE Module Concept

3.6.2 Investment Protection System

The design of the IPS is similar to that of the GT-MHR. The IPS does not perform any safety-related functions. Each MHR module has an independent IPS, and the IPS is independent of other control systems, including the RPS. The IPS monitors plant parameters, including primary and secondary coolant flow rates, primary and secondary coolant pressures, primary coolant inlet and outlet temperatures, secondary coolant radioactivity, and SCS cooling water radioactivity. If the plant parameters are not within their allowable ranges, the IPS performs its investment-protection functions, which include:

- Secondary HTS isolation
- Hydrogen Production Plant isolation
- SCS cooling water isolation

- Primary and secondary coolant circulator trip
- RHRS startup
- SCS startup

For the H2-MHR, the setpoints for these functions and functions associated specifically with the Hydrogen Production Plant will be established during the preliminary and final design stages.

3.6.3 Plant Monitoring System

The plant monitoring system includes instrumentation to monitor (1) the primary coolant, (2) radioactive effluents, (3) non-radioactive effluents, (4) meteorological conditions, and (5) seismic events.

The Primary Coolant Monitoring System monitors the chemical and radiological impurities in the primary coolant and helium purification systems during all modes of plant operation. The important impurities that are monitored include:

Non-Condensable Gases: CO, CO_2, H_2, CH_4, N_2, O_2, H_2O, Ar, Ne, Xe, Kr, and tritium.

Condensable Gases: fission products (I, Cs, and Te), sulfur gases (H_2S, S_2, and SO_2), chlorine gases (HCl and Cl_2), and oil vapor.

Dust/Aerosol Particles: graphite/carbon and metal oxides.

In-situ probes are used to monitor plateout of radionuclides in the primary coolant circuit.

The Radiation Monitoring System monitors all effluents from the plant, monitors plant radiation areas, provides health-physics data, and provides early warning of plant equipment malfunctions that may result in radioactivity release. Airborne radiation monitors survey airborne particulate and noble-gas radioactivity discharged from the plant to the environment. Area radiation monitors measure radiation levels in designated plant areas to detect any abnormal migration of radioactivity.

The Environmental Monitoring System monitors the chemistry and non-radiological physical parameters of liquid and gaseous effluents that are discharged from the plant. The Meteorological Monitoring System includes one or more meteorological towers and instrumentation to measure temperature, barometric pressure, humidity, wind velocity and direction, and atmospheric stability. The Seismic Monitoring System includes sensors and instrumentation to detect and record the seismic motions experience by structures and equipment in the event of an earthquake.

3.7 Balance of Plant and Auxiliary Systems

The balance of plant and auxiliary systems for the H2-MHR are very similar in design to those for the GT-MHR. Brief descriptions of key systems are given in the sections below. More detailed descriptions are available in [Shenoy, 1996].

3.7.1 Fuel Handling and Storage System

The Fuel Handling and Storage System (FHSS) design is the same as that for the GT-MHR. The FHSS is used for (1) receiving and inspecting new fuel elements, (2) transporting fuel elements to local storage facilities, (3) extracting irradiated fuel assemblies out of the MHR modules and transporting them to local storage facilities, (4) installing new fuel elements in the MHR core, (5) transporting spent fuel elements from the local storage facilities to the packaging and shipping facility, and (6) packaging the spent fuel elements for shipping. The FHSS is also used to retrieve and replace spent reflector elements and to manipulate special tools for in-service inspection of reactor components. Figure 3-47 shows the layout of the FHSS.

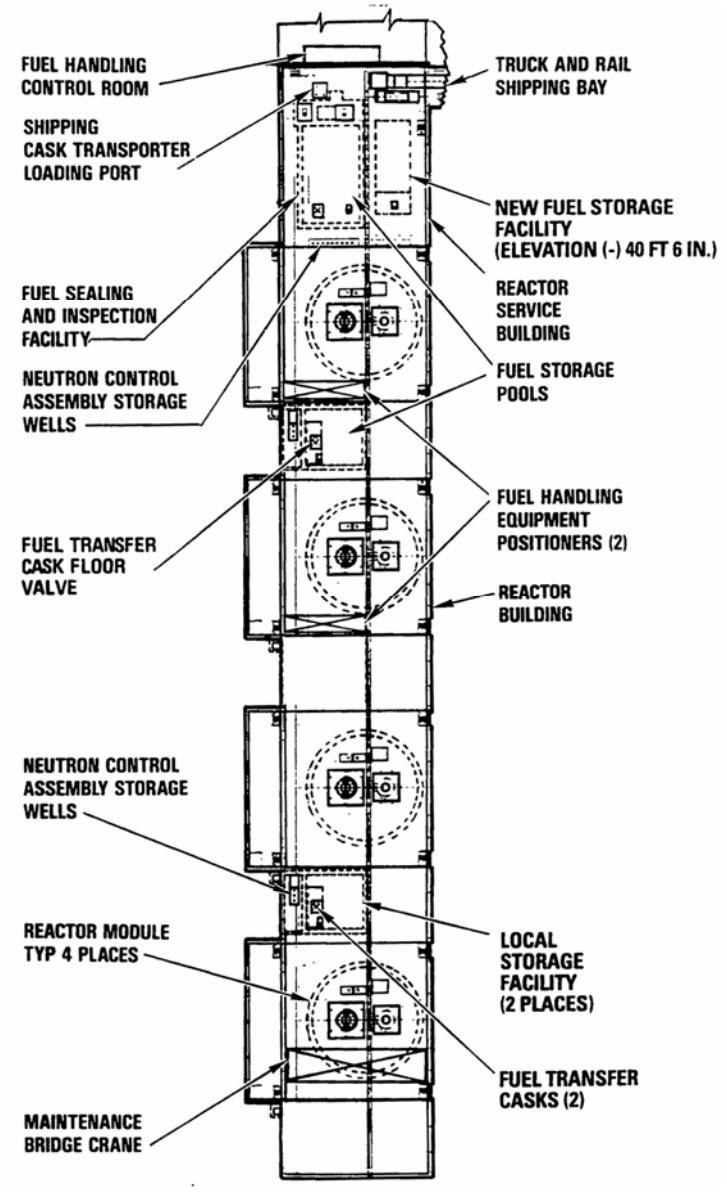

Figure 3-47. Fuel Handling and Storage System Layout

In-core handling of fuel elements is performed by joint operation of the fuel handling machine and fuel transfer cask. As shown in Fig. 3-48, these components are mounted on the fuel handling equipment support structure which is located above the reactor vessel. The fuel handling machine grapples each fuel element, one at a time, and deposits them on the fuel transfer cask guide sleeve. The fuel transfer cask grapples the elements, raises then out of the core, and deposits them onto internal sliding storage tables. After the transfer cask is filled (9 elements), it is transported to the local storage facility adjacent to the MHR module being serviced, where the elements are unloaded. During the unloading process, a second fuel transfer cask is placed over the reactor to receive a load of fuel elements. When the second cask is filled, it is transported to a second location at the local storage facility and unloaded. This cycle of alternating fuel transfer cask operations is repeated until a complete core sector has been emptied. The sequence is reversed to load the core sector with both fresh fuel elements and the elements from that sector that have been irradiated for one cycle. This process is repeated for the remaining core sectors. During a refueling outage, one-half of the 1020 fuel elements and an average of one-fourth of the replaceable reflector elements are replaced, and the estimated refueling time is 20.7 days.

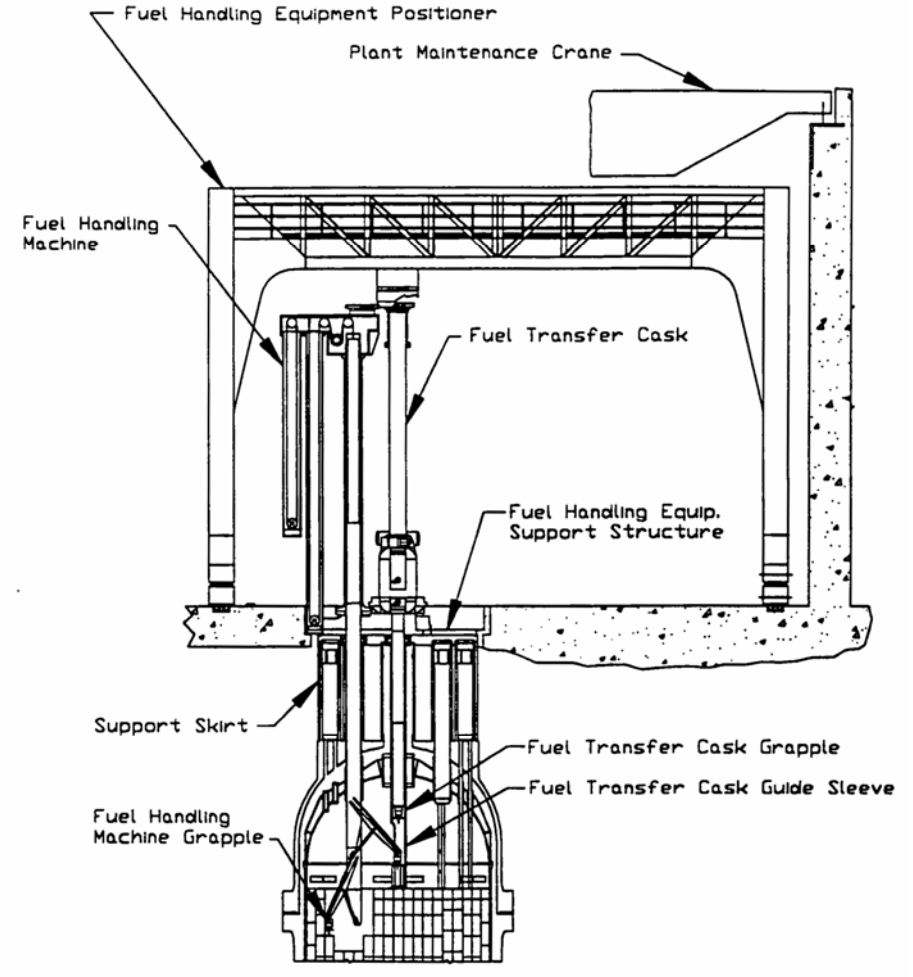

Figure 3-48. Fuel Handling Equipment Arrangement

3.7.2 Spent Fuel Storage System

The Spent Fuel Storage System (SFSS) consists of dry storage wells immersed in a pool of water. There are two spent fuel storage pools with independent cooling systems. Decay heat is transferred to circulating cooling water in the storage pool and rejected to the atmosphere using an air-cooled heat exchanger. Each storage pool contains 350 dry storage wells and each well stores eight spent fuel elements. Two 100% capacity pumps and one 100% capacity heat exchanger are provided for each pool.

3.7.3 Radioactive Waste Management and Decontamination System

The Radioactive Waste Management and Decontamination System design is the same as that for the GT-MHR and consists of separate systems to process liquid, gaseous, and solid radioactive waste. This system is located in the Radioactive Waste Management Building and also includes decontamination equipment to decontaminate components such as valves and small pumps prior to maintenance.

The Liquid Radioactive Waste Management System uses filtration and mixed-bed demineralization to treat the liquid waste. Treated and purified liquid wastes are reused in the plant. Spent resins are transferred to the solid radioactive waste management system. The total amount of liquid radioactive waste processed by this system is approximately 10 m^3 per module per year.

The Gaseous Radioactive Waste Management System processes radioactive waste gas to reduce the radioactivity to levels that are acceptable for discharge to the atmosphere. Most of the gas processed by the system requires only filtration and monitoring before release. However, waste gas from the primary Helium Purification System requires holdup to allow decay of short-lived radionuclides before release. The total amount of gaseous radioactive waste processed by this system is approximately 3500 m^3 per module per year.

The Solid Radioactive Waste Management System collects and solidifies radioactive waste (including spent resins). The solid waste is packaged into drums that are shipped offsite for disposal. The total amount of solid radioactive waste processed by this system is approximately 70 m^3 per module per year.

3.7.4 Heating, Ventilation, and Air Conditioning Systems

The Heating, Ventilation, and Air Conditioning (HVAC) Systems designs are similar to those for the GT-MHR. For the H2-MHR, the Control Building HVAC system is designed to protect the reactor operators from airborne radioactivity and from toxic material concentrations resulting from chemical spills or accidents associated with the Hydrogen Production System.

3.7.5 Hydrogen Production Water Supply System

The H2-MHR Hydrogen Production Water Supply System consists of a storage tank that receives tap water, centrifugal feedwater and condensate pumps, a water purification system, and an instrumentation system for measuring water-quality parameters. The water purification system is designed to maintain water chemistry to minimize corrosion and fouling of heat-exchanger surfaces in the Hydrogen Production System. Water coolant chemistry requirements

include maintaining resistivity >1.0 megaohm-cm, maintaining total dissolved solids < 0.05 kg/m3, and maintaining the dissolved oxygen concentration below 10 ppb. The water purification system design includes the following components:

1. A 2-micron cartridge-type prefilter with sintered stainless steel media to control the size and concentration of suspended solids.

2. A cation exchange unit to remove dissolved cations and to adsorb colloidal-sized particles.

3. A mixed bed ion exchange unit to remove dissolved anions and any remaining dissolved cations.

4. A vacuum deaerator or membrane degasifier to remove dissolved oxygen.

5. A 2-micron cartridge-type postfilter with sintered stainless steel media to protect the Hydrogen Production Water Supply System from particles generated in the water purification train (e.g., from breakdown of resins or degasifier membranes).

3.7.6 Waste Heat Rejection System

As indicated in Table 3-15, 246.5 MW(t) of waste heat is rejected from the precooler and intercooler modules of the PCS. The design of the Waste Heat Rejection System is similar to that for the GT-MHR, with wet mechanical draft cooling towers rejecting heat to the atmosphere. The system is sized to reject 284 MW(t), which provides a margin of 15% above the expected maximum heat duty. Three one-half capacity pumps are provided to circulate the water between the Hydrogen Production System and the Waste Heat Rejection System.

The majority of the heat is transferred through evaporation of a small fraction of the circulating water. A makeup water system replenishes water lost to evaporation and is also used to control the water chemistry in the circulating water. Excess makeup water is blown down from the cooling tower basin to the receiving water body. The water released from evaporation and blow down are potential sources of tritium release to the environment and these sources are factored into the design of the Helium Purification Systems.

3.8 Buildings and Structures

The overall plant arrangement is described in Section 2.3. The following sections describe the Reactor Building and other major building are described in the following sections.

3.8.1 Reactor Building and Vented Low-Pressure Containment

The Reactor Building is a multi-celled, embedded structure constructed of cast-in-place reinforced concrete. The degree of embedment was selected to serve a number of objectives, including reduced cost and complexity of construction, ease of operation, minimization of shielding, and good seismic performance. The operating floor of the power plant is set at site grade, with a common maintenance enclosure covering the operating area traversed by shared refueling equipment. There are two floors below grade with a rectangular footprint which are used to house mechanical, electrical, and instrumentation systems dedicated to each reactor. A

number of additional mechanical and electrical systems which do not require radiation shielding or protection from external hazards are designed to be delivered to the site as prefabricated modules and located at grade outside the maintenance enclosure. The Reactor Building below elevation -30 ft. is configured as a cylinder to enable it to resist soil and groundwater pressure. The reactor and IHX vessels are located within this space. Access to and from the cylindrical portion of the building for piping, electrical services, personnel, and the concentric RCCS ducting is made from the rectangular portion of the building between elevations -30 ft. and grade. Access for refueling and for major maintenance activities is from the operating floor. There are two extensions of the reinforced concrete Reactor Building above grade. On the east side of the Reactor Building, the reinforced concrete portion of the building extends to elevation +95 ft. 6 in. to serve as the Reactor Cavity Cooling System elevated inlet-outlet structure.

The Reactor Building has been divided into two distinct zones for purposes of the HVAC design. The cells containing the primary HPS components, the vent path sections above grade west of the maintenance enclosure, and most of the cells in the cylindrical portion of the building have been designed to form a closed, interconnected space which is normally isolated from the environment. Air is recirculated internally and heat is removed by chilled water-cooled air handling units. The balance of the rectangular portion of the building, the personnel access stairways, the personnel elevator shaft into the silo portion of the building, and the space below the reactor vessel have been designed to be conditioned by a once-through flow of heated or cooled air. The RCCS panels, where they enter the closed portion of the Reactor Building, are regarded as part of the vented low pressure containment boundary. In essence, air flowing inside the RCCS ducts and panels is outside the Reactor Building. The walls, doors, plugs, and other barriers which separate the closed, recirculated portion of the building from the once-through cooled portion of the building or from the outside environment (including the RCCS panels and ducts) constitute the fourth containment barrier. Leakage from within this portion of the Reactor Building to the other part of the Reactor Building or to the environment has the potential to transport fission products from the containment to the environment. This space is also the portion of the Reactor Building which is affected by the specified building leak rate. The net free volume within this space is approximately 260,000 ft^3. This space is designed to have a leak rate of no greater than 1 volume per day at an internal pressurization of 1 psid, and to vent whenever the internal pressure exceeds 1 psid. It is expected that essentially none of the leakage which occurs will be from the surfaces of the building which are in contact with the soil, and that the specified leak rate represents an upper bound on the exchange which could occur between the building interior and the environment, since the pressure and therefore the leakage will normally decrease over the course of an accident. Architectural features such as doors, gaskets around floor plugs, and penetrations are important to establishing the building leak rate but can be modified to achieve the specified value.

In the event of a large primary coolant leak within the closed portion of the Reactor Building, the internal pressure will exceed 1 psid. Gases are able to flow from any compartment through the building and out the vent path relief valves or dampers to the atmosphere. The vent dampers are maintained in a closed position by gravity, and the weight of the damper determines the relief setpoint pressure, which is the internal pressure needed to open the damper. This design must be considered preliminary. The relief setpoint pressure affects both the nominal reactor building leak rate and the building pressure transients following a large primary coolant leak. The building relief setpoint pressure and vent opening area can both be adjusted if needed to obtain satisfactory performance during a pressure transient. The reinforced concrete building and RCCS panels have been designed to withstand pressure transient loadings of 10 psid.

3.8.2 Other Major Buildings

The Reactor Service Building is a multilevel reinforced concrete structure located at grade level next to the Reactor Building. This building is subdivided into several compartments to house equipment common to all four modules. The fuel handling area is located within the Reactor Service Building. This area contains facilities for introducing new fuel, for loading and shipping spent fuel casks, for storing new fuel, and for inspecting new and spent fuel. The Hot Service Facility is located inside a shielded vault in the Reactor Service Building adjacent to the fuel sealing and inspection facility. The Hot Service Facility provides the capability for inspection, maintenance, and repair of reactor service equipment and tools. The facility includes viewing windows, operating galleries outside the vault, manipulators to perform the inspection, maintenance, and repair services, as well as portable decontamination equipment. The Personnel Service Building is a grade-level structure, located next to the Reactor Service Building, which houses facilities for monitoring, controlling, and minimizing human exposure to radioactivity. In addition to the hot chemistry laboratory and radiation decontamination facilities, the building also houses locker rooms, a cold (nonradioactive) chemistry laboratory, and a supervisor's office. A fuel handling control station for monitoring and controlling fuel handling activities is located in the Personnel Service Building.

The Radioactive Waste Management Building, is located next to the Reactor Service Building, and houses the solid radioactive waste train, liquid radioactive waste train, and gaseous radioactive waste train. Tanks, pumps, and filters which handle radioactive materials are housed in concrete cubicles to provide radiation shielding and protection for the environment. The Radioactive Waste Management Building is a reinforced concrete and steel structure.

4. Plant Assessments

As part of this pre-conceptual design study, assessments of the H2-MHR plant were performed in the areas of safety, availability, licensing, and economics.

4.1 Safety Assessment

The following sections describe the safety features of the H2-MHR and assessments of bounding accidents involving loss of flow and loss of coolant.

4.1.1 Passive Safety Features

Passive safety features of the H2-MHR include the (1) ceramic, coated-particle fuel that maintains its integrity at high temperatures during normal operation and LOCAs; (2) an annular graphite core with high heat capacity that limits the temperature rise during a LOCA; (3) a relatively low power density that helps to maintain acceptable temperatures during normal operation and accidents; (4) an inert helium coolant, which reduces circulating and plateout activity; and (5) a negative temperature coefficient of reactivity that ensures control of the reactor for all credible reactivity insertion events. Also, as discussed in Section 3.1.7, the fuel, the graphite, the primary coolant pressure boundary, and the low-pressure vented containment building provide multiple barriers to the release of fission products.

4.1.2 Safety-Related Systems, Structures, and Components

Based on preliminary safety assessments, the following systems, structures, and components (SSCs) are classified as safety-related:

- MHR System, including neutron control assemblies, ex-vessel neutron detectors, reactor internals, reactor core, and fuel.
- Reactor Vessel and Cross Vessel.
- Reactor Cavity Cooling System.
- Reactor Protection System, including all sensors, control logic, and housings that support safety-related reactor trips.
- Fuel storage pools and wells, which are part of the Reactor Service Building.
- Essential AC and DC Electrical Systems.

4.1.3 Accident Analysis

In terms of safety consequences, the bounding accidents for the H2-MHR are a loss of flow leading to a high pressure conduction cooldown (HPCC) and loss of coolant leading to a low pressure conduction cooldown (LPCC). The HPCC event is typically initiated by trip of the primary and/or secondary helium circulators. The RPS automatically initiates a reactor trip on low flow or loss of power to the circulators. The system pressure equilibrates at about 5 MPa after about 50 hours following initiation of the event. Because the system remains at high

pressure, the decay heat is more uniformly distributed within the core and vessel than during a LPCC event. The LPCC event is typically initiated by a small primary coolant leak, causing the system to depressurize to atmospheric pressure. The Reactor Protection System automatically initiates a reactor trip on low coolant pressure. For both events, the SCS fails to start and decay heat is removed by thermal radiation and natural convection from the reactor vessel to the RCCS (see Fig. 4-1).

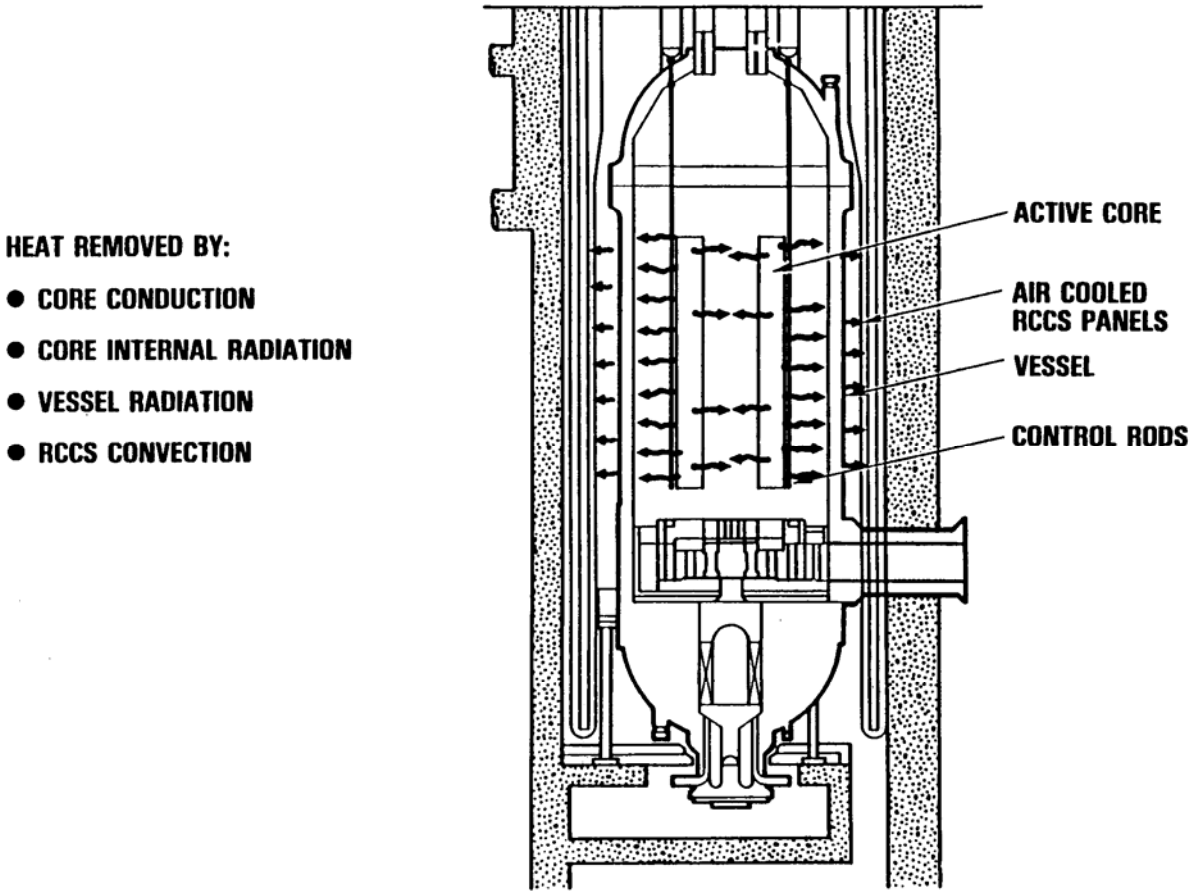

Figure 4-1. Passive Heat Removal to the RCCS During HPCC and LPCC Events

These events have been analyzed in detail for the GT-MHR, and the results have shown that peak fuel temperatures remain below the design goal of 1600°C, and the temperatures for the vessel and other safety-related SSCs also remain below acceptable limits. Using the ATHENA model described in Section 3.1.4, these events were re-analyzed using the H2-MHR initial conditions. Figure 4-2 shows the calculated peak fuel temperatures for the HPCC and LPCC events. For the LPCC event, the peak fuel temperature is 1525°C and occurs about 60 hours following initiation of the event. For the HPCC event, the peak fuel temperature is 1349°C and occurs about 50 hours following initiation of the event. As shown in Fig. 4-3, the calculated peak vessel temperatures for the HPCC and LPCC events were approximately 478°C and 517°C, respectively. For both events, the peak vessel temperatures occurred about 72 hours following initiation of the event.

These results are consistent with previous results for the GT-MHR and show that the H2-MHR should retain the passive safety characteristics of the GT-MHR.

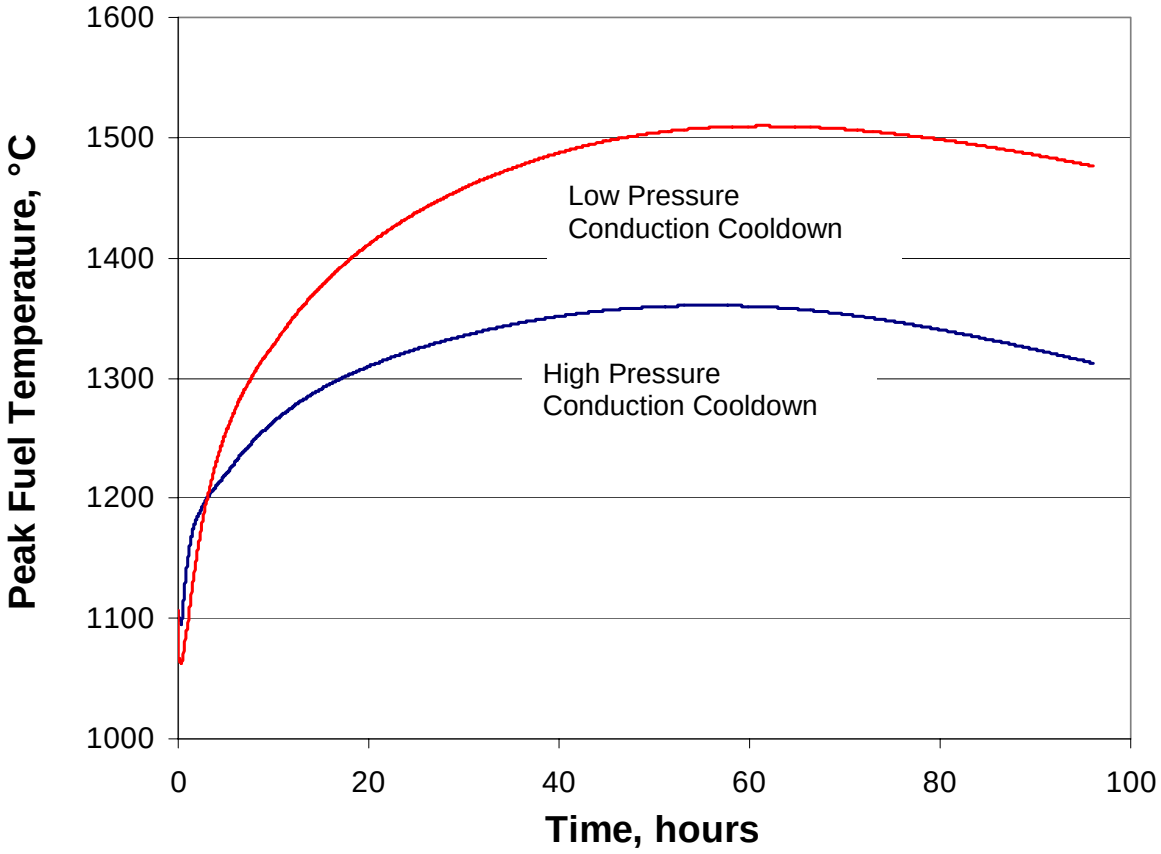

Figure 4-2. Peak Fuel Temperatures During HPCC and LPCC Events

4.2 Availability Assessment

The availability assessment accounts for scheduled outages and forced outages associated with the MHR nuclear island and the hydrogen production plant. Scheduled outages account for 526 hours per year. Forced outages account for 543 to 617 hours per year, depending on the level of redundancy for some of the dynamic components in the hydrogen production plant. These outages correspond to plant availability factors of 0.87 and 0.88, respectively. The bases for these availability assessments are described in more detail in the following sections.

For large-scale deployment of nuclear hydrogen production, hydrogen storage systems could be used to meet peak demand requirements. Except during outages, the H2-MHR plants would be operated at their rated capacity. When demand is lower, some of the hydrogen would be diverted to a storage system for later use when demand is higher. For example, if hydrogen is used primarily for the transportation sector, stored hydrogen would be recovered primarily during peak driving periods (e.g., summer months).

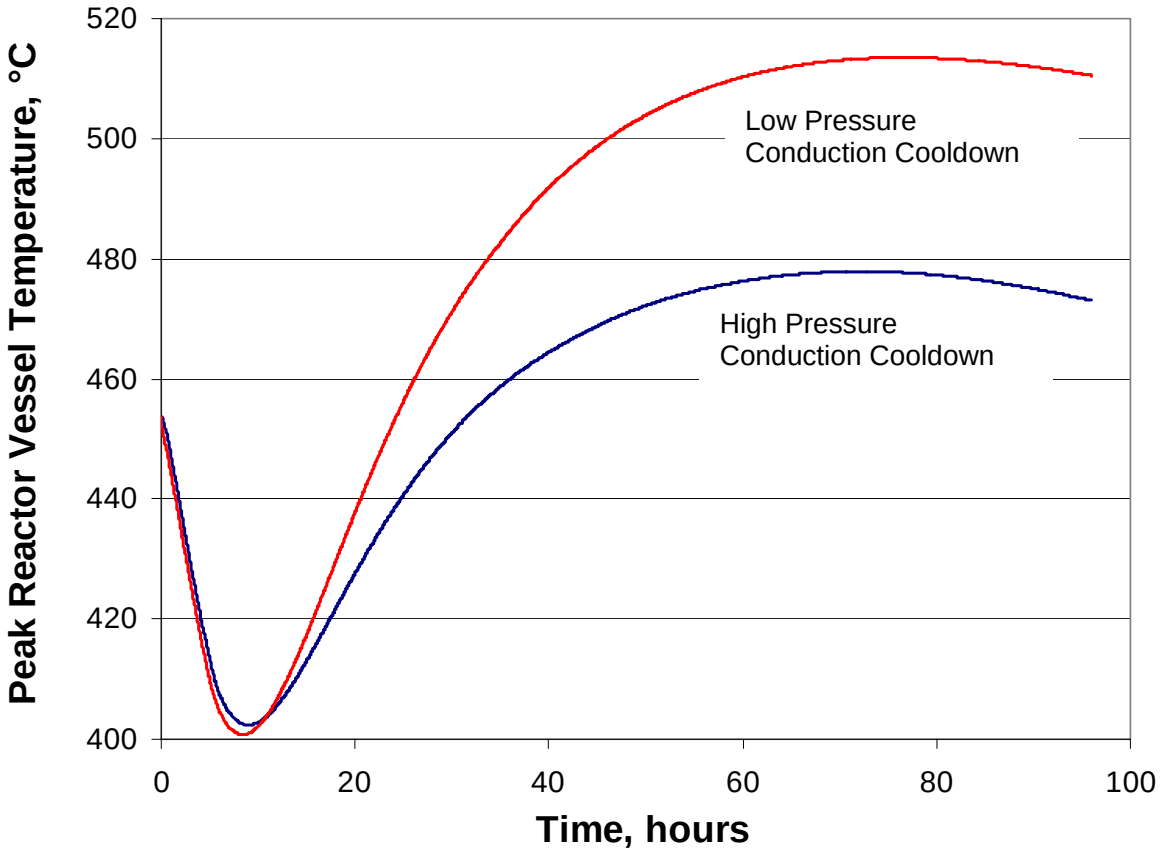

Figure 4-3. Peak Vessel Temperatures During HPCC and LPCC Events

4.2.1 Scheduled Outages

The scheduled outage assessment is based on previous studies performed for the GT-MHR and earlier MHR concepts that used a steam cycle for power conversion (Ref. 1). These studies showed that scheduled outages associated with the PCS for the GT-MHR or the circulator and steam generator associated with the steam-cycle plants could be performed simultaneously with other scheduled maintenance activities that require reactor shutdown and depressurization (e.g., refueling). This conclusion also applies to the heat exchangers and other mechanical equipment associated with the HTE-based H2-MHR. A detailed scheduled outage assessment has not been performed for the hydrogen production plant, but it is expected these maintenance activities could also be performed during scheduled reactor shutdowns and hence should have no impact on the overall unavailability associated with scheduled outages. Hence, the HTE-based H2-MHR scheduled outage rate is assumed to be the same as that for the GT-MHR, which was estimated to be 526 hours per year.

4.2.2 Forced Outages – MHR Nuclear Island

The MHR nuclear island forced outage assessment is also based on previous studies performed for the GT-MHR and earlier MHR concepts that used a steam cycle for power

conversion [Shenoy, 1996]. Forced outages are expressed in terms of equivalent forced outage hours (EFOH) at full power. The EFOH as a function of the major systems associated with the MHR nuclear island are given in Table 4-1. The total EFOH is 517.5.

Table 4-1. EFOH for MHR Nuclear Island System

System	EFOH
Reactor System	30.8
Vessel System	108.2
PCS/Turbomachinery	229.4
Shutdown Cooling System	6.8
Helium Purification Systems	24.7
Plant Control, Data, and Instrumentation Systems	100.9
Balance of Plant and Auxiliary Systems	69.7
Total	570.5

4.2.3 Forced Outages – Hydrogen Production Plant

Forced outage assessments for the HTE-based hydrogen production plant were performed using the SAPHIRE (Systems Analysis Programs for Hands-on Integrated Reliability Evaluations) code [INL, 1998]. The SAPHIRE code evolved from the Integrated Reliability and Risk Analysis System (IRRAS) code, which is a state-of-the-art, microcomputer-based probabilistic risk assessment model development and analysis tool.

Figure 4-4 shows the master fault tree for the HTE-based hydrogen production process. The SAPHIRE model assumes separate hydrogen production trains for each of the four MHR modules. Several data bases were used to determine component failure rates. The Process Equipment Reliability Data by the Center for Chemical Process Safety (CCPS) of the American Institute of Chemical Engineers includes accumulated and aggregated data from nuclear power plants, chemical process industries, offshore petroleum platforms, etc. The Offshore Reliability Data (OREDA) covers reliability data from a wide range of equipment used in oil and natural gas exploration and production industries, as well as some onshore equipment. The European Industry Reliability Data Bank (EIReDA) is the reliability database for the probabilistic safety assessment of nuclear power plants in France.

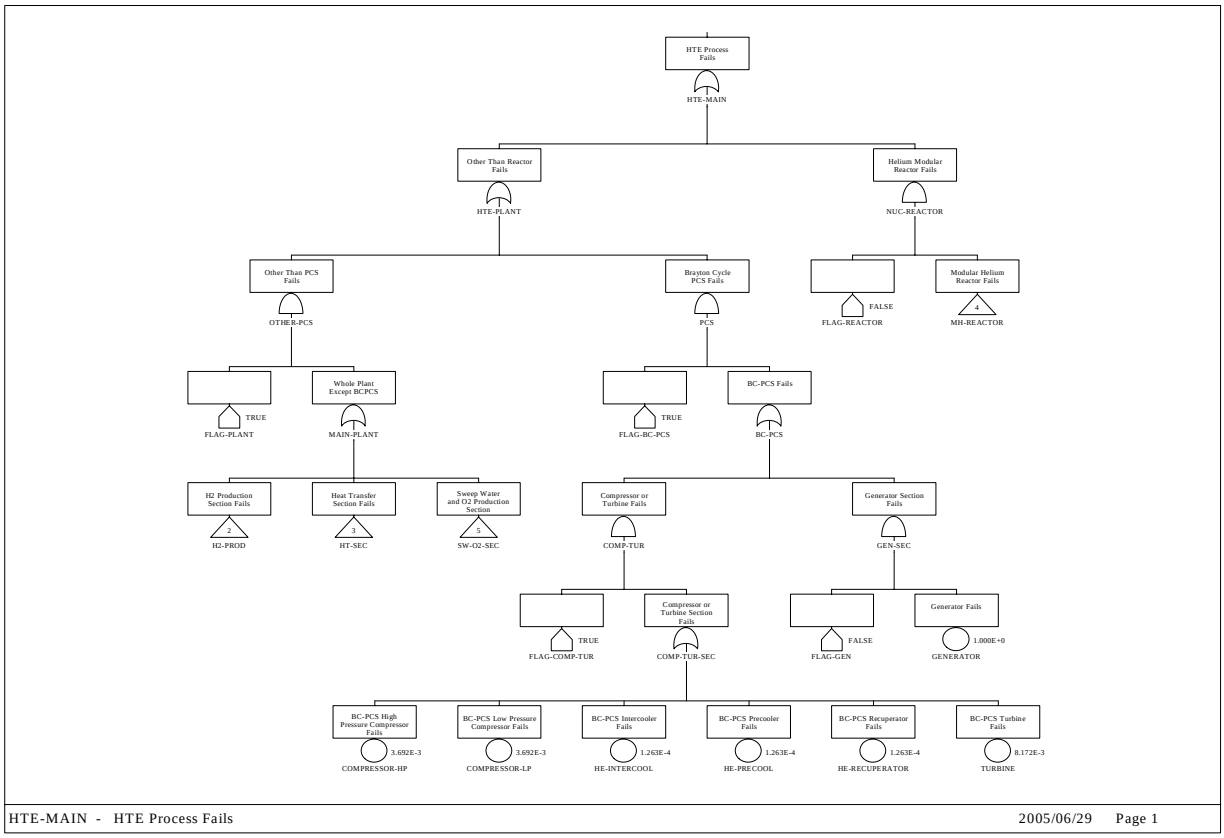

Figure 4-4. Master Fault Tree model for Hydrogen Production Process

The overall plant availability accounts for down time based on component failure probabilities and the mean repair time for failed components when no component redundancies are included. Assuming no redundancies, SAPHIRE results indicate approximately 96 EFOH, or 4 days per year. As expected, results show that single failures of dynamic components (i.e., turbines, pumps, etc.) are the biggest contributors to the system unavailability. If redundancy is included for the three components with highest failure probability (the H_2 recirculator and the primary and secondary side helium circulators), SAPHIRE results show that the EFOH can be reduced to about 35.

4.3 Licensing Assessment

The licensability of the GT-MHR and earlier steam-cycle MHR concepts is discussed in [Shenoy, 1996]. Based on the licensing history and safety performance of HTGRs in the United States and NRC review of earlier steam-cycle MHR concepts, it is expected the GT-MHR will be licensable in the current commercial nuclear regulatory environment.

The H2-MHR is not expected to present any significant licensing challenges relative to the GT-MHR or other reactor concepts. However, a key consideration for safety and licensing of the H2-MHR is co-location of the MHR modules with a hydrogen production plant. As illustrated in

Fig. 4-5, it is proposed to locate the two facilities as close as possible (within 100 m or less) in order to minimize the distance over which high-temperature heat is transferred. INL has recently performed an engineering evaluation for these separation requirements and has concluded separation distances in the range of 60 m to 120 m should be adequate in terms of safety [Smith, 2005]. Other recommendations from the INL study include a 100 kg on-site limit for hydrogen storage, use of double-walled pipes for hydrogen transport, and location of the nuclear plant control room outside of the dispersion zone for chemical release. The below-grade installation of the MHR modules, combined with an earthen berm for defense-in-depth, provide additional safety margin for co-location of the two facilities. Detailed safety assessments should be performed in the preliminary and final design phases to better define the risk envelope associated with co-location of the MHR modules and hydrogen production plant.

JAEA has performed computational fluid dynamics simulations of transport and detonation of a hydrogen cloud resulting from an accident in the hydrogen production plant. JAEA has also concluded that relatively short separation distances between the nuclear reactor and hydrogen production plant should not compromise overall plant safety, especially if an earthen berm or other barrier is placed between the nuclear reactor and hydrogen production plant [Nishihara, 2005].

4.4 Economic Assessment

The economic assessment was performed for an n^{th}-of-a-kind plant consisting of four, 600-MW(t) MHR modules coupled to a hydrogen production plant. The instantaneous hydrogen production rate is 9.59 kg/s, which corresponds to a plant hydrogen production rate of 268,000 tonnes per year at a plant capacity factor of 0.9. The baseline estimate was based on the following assumptions:

Construction time period:	36 months
Annual interest rate:	7%, compounded monthly
Fixed charge rate:	12.6% (regulated utility)
MHR plant indirect costs:	35% of direct costs
HTE plant indirect costs:	20% of direct costs
MHR plant contingency costs:	5% of total (direct + indirect) construction costs
HTE plant contingency costs:	10% of total (direct + indirect) construction costs

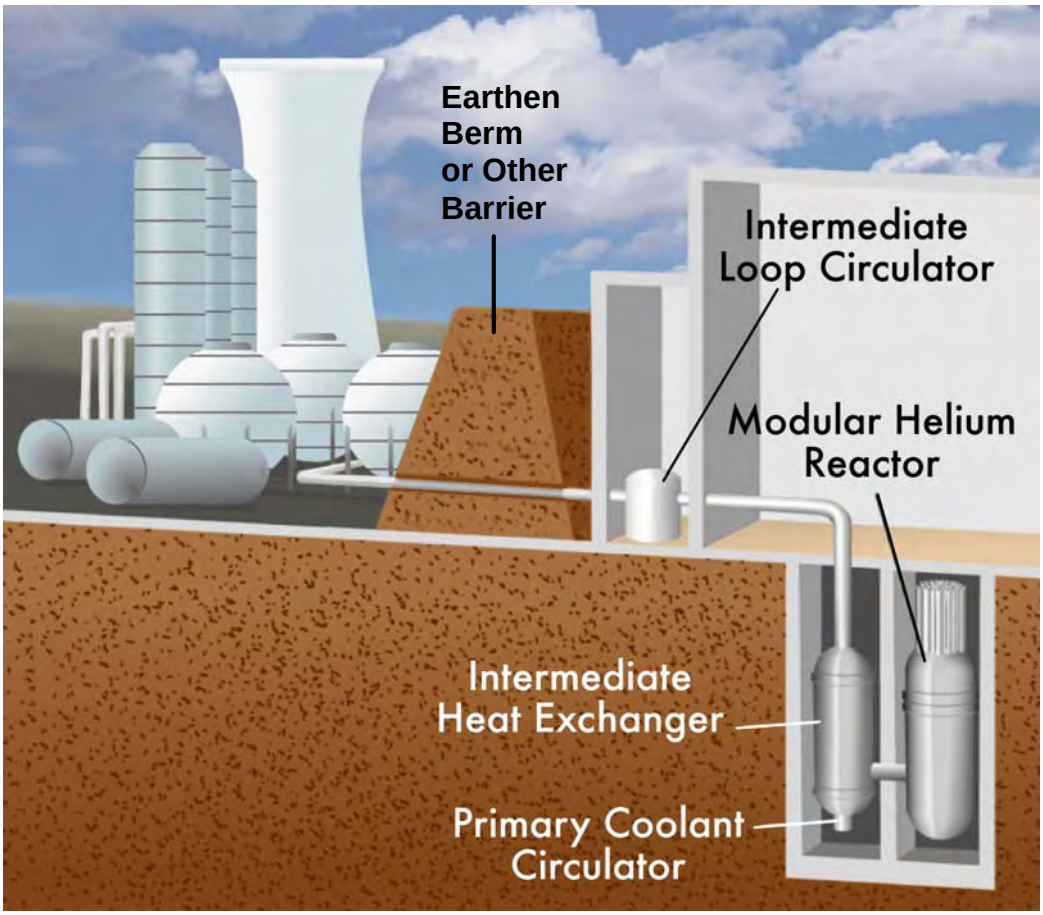

Figure 4-5. Concept for Co-Location of the MHR with Hydrogen Production

4.4.1 Capital Costs

Capital costs are summarized in Table 4-2. The total plant capital cost is estimated to be $2.58 billion, with the MHR plant accounting for $1.42 billion and the HTE-based hydrogen production plant accounting for $1.16 billion. The cost per kW of hydrogen (assuming a HHV of 141.9 MJ/kg) is approximately $1,920. The MHR plant equipment includes the MHR system and the PCS, and capital costs are based on scaling previous estimates for the GT-MHR and increasing costs of some reactor internal equipment to account for the use of higher-temperature materials and thermal hydraulic design optimization [Summers, 2004]. The hydrogen production plant includes the SOE modules, the HTRS, the Power Recovery System, the Water Supply System, and other miscellaneous equipment. The capital cost for the SOE modules is based on a unit cost of $500 per kW(e) supplied to the modules. Capital costs for pumps, circulators, and heat exchangers were based on scaling previous estimates for similar equipment. Capital costs were also escalated to 2005 dollars. The indirect costs account for construction services, home office engineering and services, field office engineering and services, and owner's costs. The owner's costs also include the costs associated with licensing the nuclear facility.

Table 4-2. Summary of HTE-Based H2-MHR Plant Capital Costs

Account Description	**Costs, $M**
MHR Plant Capital Costs	
Structures and Improvements	142.4
MHR Equipment	517.9
PCS Equipment	111.1
Electrical Equipment	66.2
Miscellaneous Plant Equipment	30.1
Heat Rejection System	35.1
Total MHR Plant Direct Costs	902.8
Total MHR Plant Indirect Costs	316.0
Total MHR Plant Base Construction Costs	1,218.8
Contingency	60.9
Overnight MHR Plant Construction Costs	1,279.7
Interest During Construction	139.7
Total MHR Plant Capital Investment	1,419.4
HTE Plant Capital Costs	
Primary Coolant Circulator	17.6
Secondary Coolant Circulator	10.7
IHX	29.4
IHX Vessel	11.8
Primary Helium Services System	4.6
HTE Piping	5.0
Secondary Helium Services System	0.8
HTRS Isolation Valves	4.7
Steam Generator / Superheater	27.9
Oxygen Recuperator	22.4
Hydrogen Recuperator	24.5
Sweep Heater	7.5
High Temperature Heater	5.3
Power Recovery System	20.0
Water Supply System	4.0
Miscellaneous Plant Equipment	10.0
SOE Modules	584.0
Total HTE Plant Direct Costs	790.2
Total HTE Plant Indirect Costs	158.0
Total HTE Plant Base Construction Costs	948.3
Contingency	94.8
Overnight HTE Plant Construction Costs	1,043.1
Interest During Construction	113.9
Total HTE Plant Capital Investment	1,156.9
Total Plant Capital Investment	2,576.4
	$ per kW of H_2 based on HHV
Installed Capital Cost	1,923.3

4.4.2 Operations and Maintenance Costs

Operations and maintenance (O&M) costs are summarized in Table 4-3. The O&M costs given in Table 4-3 are based on assumptions used for previous estimates [(Brown, 2003), (Summers, 2004)]. For the HTE plant, a key parameter is the maintenance and repair costs associated with the SOE modules. For the baseline estimate, the maintenance and repair costs for the HTE plant are assumed to be 6% of the direct costs.

Table 4-3. Summary of HTE-Based H2-MHR Plant O&M Costs

Account Description	Costs, $M/yr
MHR O&M Costs	
Reactor Operations	31.8
Decommissioning	6.0
Total MHR O&M Costs	37.8
HTE Plant O&M Costs	
Water Supply	3.1
Operating Labor	5.1
Supervisory and Clerical Labor	0.8
Maintenance and Repairs	47.4
Operating Supplies	7.1
Laboratory Charges	0.8
Taxes	15.8
Administrative Costs	1.0
Total HTE Plant O&M Costs	81.1
Nuclear Fuel Costs	71.2
Total Plant O&M Costs	118.9

4.4.3 Hydrogen Production Costs

The hydrogen production costs are summarized in Table 4-4 and Fig. 4-6. The fixed-charge rate was assumed to be 12.6%, which corresponds to a regulated utility [Summers, 2004]. The baseline hydrogen production cost is estimated to be $1.92/kg.

Table 4-4. Summary of HTE-Based H2-MHR Plant Hydrogen Production Costs

Account	Cost ($M/yr)	Percent of Total
MHR Plant Capital Charges	178.8	34.8
HTE Plant Capital Charges	145.8	28.3
MHR Plant O&M Costs	37.8	7.3
HTE Plant O&M Costs	81.1	15.8
Nuclear Fuel Costs	71.2	13.8
Total Annual Costs	514.7	
	kg/yr	
Hydrogen Produced	2.68×10^8	
	$/kg	
Hydrogen Production Cost	1.92	

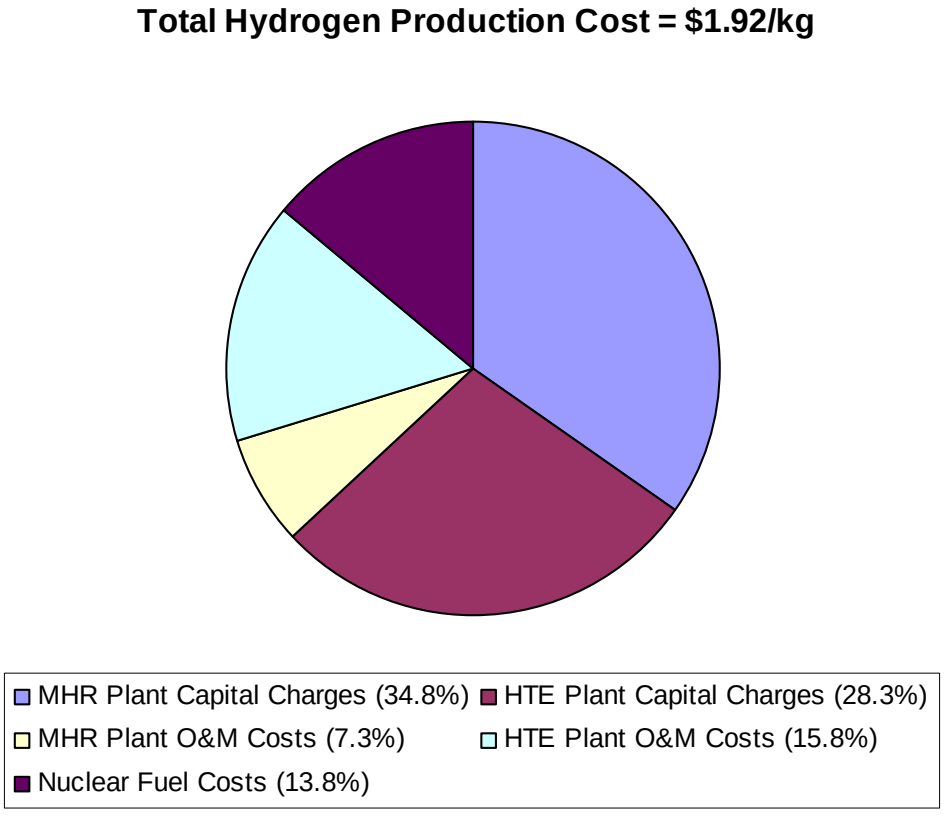

Figure 4-6. HTE-Based H2-MHR Plant Hydrogen Production Costs (Baseline Estimate)

4.4.4 Parametric Studies

Parametric studies were performed to determine the sensitivity of the hydrogen production cost to (1) SOE module unit cost, (2) SOE module maintenance and repair cost, (3) construction time, and (4) fixed charged rate. As shown in Table 4-5, the SOE module unit cost has a significant influence on both the capital and hydrogen production costs. A 50% increase in the SOE module unit cost increases the hydrogen production cost by about $0.30/kg. If the SOE module unit cost is increased from $500/kW(e) to $1000/kW(e), the hydrogen production cost increases from $1.92/kg to $2.52/kg. If the SOE module maintenance and repair cost is increased from 6% to 12% of direct costs, the hydrogen production cost increases by $0.15/kg. Increasing the construction time from 36 to 60 months results in higher interest charges, which increases the hydrogen production cost by $0.09/kg. Increasing the fixed charge rate from 12.6% to 16.6 % (which is representative of an unregulated utility) results in an increase in hydrogen production cost of $0.39/kg.

Table 4-5. Results of H2-MHR Plant Economic Parametric Studies

Parameters		Capital Cost $/kW-$H_2$ (HHV)	Hydrogen Production Cost ($/kg)
SOE Module Unit Costs, $/kW(e)	500	1923.3	1.92
	750	2242.5	2.22
	1000	2561.6	2.52
SOE Module Maintenance and Repair Costs, % of direct costs	6.0	1923.3	1.92
	12.0	1923.3	2.07
Construction time, months	36	1923.3	1.92
	48	1994.5	1.97
	60	2069.1	2.01
Fixed charge rate, %	12.6	1923.3	1.92
	16.6	1923.3	2.31

Note: Shaded rows indicate parameters and results for the baseline estimate.

4.4.5 Comparison with Steam-Methane Reforming

Figure 4-7 shows a comparison of nuclear hydrogen production costs with the costs for producing hydrogen using steam-methane reforming (SMR). The overall reaction for steam-methane reforming produces 1 mole of CO_2 for every 4 moles of H_2 produced:

$$CH_4 + 2H_2O \rightarrow 4H_2 + CO_2$$

Because of environmental concerns associated with CO_2 emissions, future SMR plants may be required to sequester and dispose of CO_2. The cost of CO_2 sequestration and disposal is uncertain. For this comparison, sequestration/disposal costs of $30 and $50 per tonne of CO_2 were assumed, which is consistent with a previous study performed by the Electric Power Research Institute [EPRI, 2003].[8] These costs correspond to additions of $0.16 and $0.27 per kg of H_2 produced. For hydrogen produced using nuclear energy, oxygen is a byproduct that potentially could produce additional revenue. For this comparison, an oxygen credit of $20 per tonne of O_2 was assumed, which is also consistent with the previous EPRI study [EPRI, 2003]. This credit corresponds to $0.16 per kg of H_2 produced.

In December 2005 the wellhead price for natural gas was $10.02 per 1000 cubic feet, which corresponds to $9.72/MMBtu.[9] At this price, nuclear hydrogen production is economically competitive with SMR. If a CO_2 sequestration/disposal cost and an O_2 credit are assumed, nuclear hydrogen production is economically competitive with SMR for natural gas prices in the range $6 to $8/MMBtu.

[8] For most SMR plants, approximately 25% of the CH_4 feedstock is burned to provide the heat required for hydrogen production, which increases the CO_2 production rate by about 25%. However, it is not practical to separate CO_2 from atmospheric nitrogen in the burner flue gas. For this study, additional costs associated with CO_2 emissions taxes were not considered.

[9] Natural gas prices are available from the U.S. DOE Energy Information Administration website (http://www.eia.doe.gov/). The unit MMBtu is a “thousand thousand” Btu, or one million Btu.

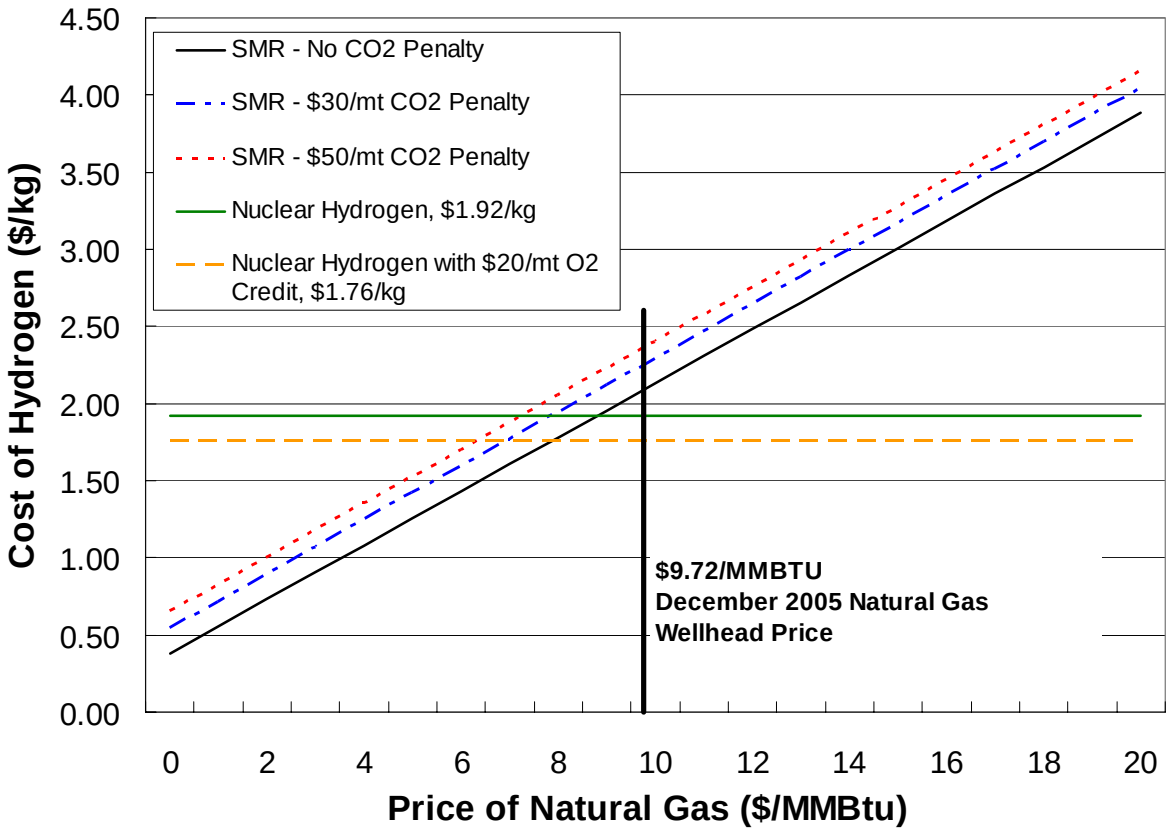

Figure 4-7. Comparison of Nuclear and SMR Hydrogen Production Costs

5. Technology Development and Risk Reduction

Based on this pre-conceptual design study, the H2-MHR is capable of producing hydrogen economically, safely, and with minimal environmental impact. It is recommended that the H2-MHR design development be continued through the conceptual, preliminary, and final design phases. Also, it is recommended that future H2-MHR design work be closely coupled with ongoing and planned technology-development programs, in order to ensure that the data obtained by these programs satisfies specific needs of the H2-MHR design. Key areas for technology development include:

- Pilot-scale demonstration and control of the HTE process at high efficiency.
- HTE materials development.
- Development of high-temperature reactor-internal components, including control rods with C-C composite cladding and bypass flow sealing keys.
- IHX and other high-temperature heat exchanger development.
- Fuel development and qualification.
- High-temperature circulator demonstration.

Many of these areas are being addressed by ongoing technology-development programs in the U.S. ([Schultz, 2004], [DOE, 2005], and [Petti, 2005]), Japan, and other countries. Unfortunately, these programs are not integrated and are not driven by the Design Data Needs (DDNs) to support a specific design. As a result, some of the data obtained by these programs may not ultimately be useful for supporting the design of a practical nuclear hydrogen production plant.

The model illustrated in Fig. 5-1 is recommended for integration of design with technology development in order to maximize the benefit of the technology-development programs in terms of supporting a plant design and minimizing the technical risk of the design. This model is based on successful Engineering Development and Demonstration (ED&D) programs conducted and managed by General Atomics for DOE projects, including Accelerator Production of Tritium, the Salt Waste Processing Facility, the commercial GT-MHR, and the New Production Reactor.

As shown in Fig. 5-1, the process begins by evaluating design requirements and reviewing existing design data from a variety of sources. Design assessments and trade studies are performed, eventually leading to key design selections and a technical baseline that meets all design requirements. As indicated on Fig. 5-1, it may be reasonable to revise one or more design requirements during the process if the overall impact is small. At this point, a design has been developed that meets all requirements, but requires some technology development to confirm assumptions upon which the design is based. Also, if necessary, the process allows for an early testing path to provide early confirmation of basic assumptions. The technology development process begins with the design organization preparing DDNs, which are formal project documents that include fallback positions in the event the testing programs do not produce acceptable results or the test could not be performed for budget or other reasons. The DDNs provide a concise statement of the required data and the associated schedule, quality, and accuracy requirements. In addition to preparing DDNs, the design organization also prepares a Test Specification that defines the data requirements in more detail. The technology organization is responsible for developing Technology Developing Plans and Test Plans for specific tests. As indicated on Fig. 5-1, the design and technology organizations work together

during preparation of the DDNs, Test Specifications, Technology Development Plans, and specific Test Plans. The technology organization then conducts the technology development programs and generates the design data. If feasible, the technology organization may integrate their activities with other (e.g., international) programs in order to minimize costs. After the design data are obtained, the design and technology organizations work together to determine if the DDNs are satisfied. If the DDNs are satisfied, the key design selections and technical baseline are finalized and the design is completed. If a DDN is not satisfied, the most likely path forward is to adopt the fallback position, which could mean additional margin is added to a certain area of plant design in order to reduce technical risk. However, depending on the results of a specific test program, a more reasonable path forward may be to re-evaluate a key design selection and return to the design process. As indicated on Fig. 5-1, an Independent Review and Verification organization is established at the start of the process to provide oversight of both the design and technology development processes.

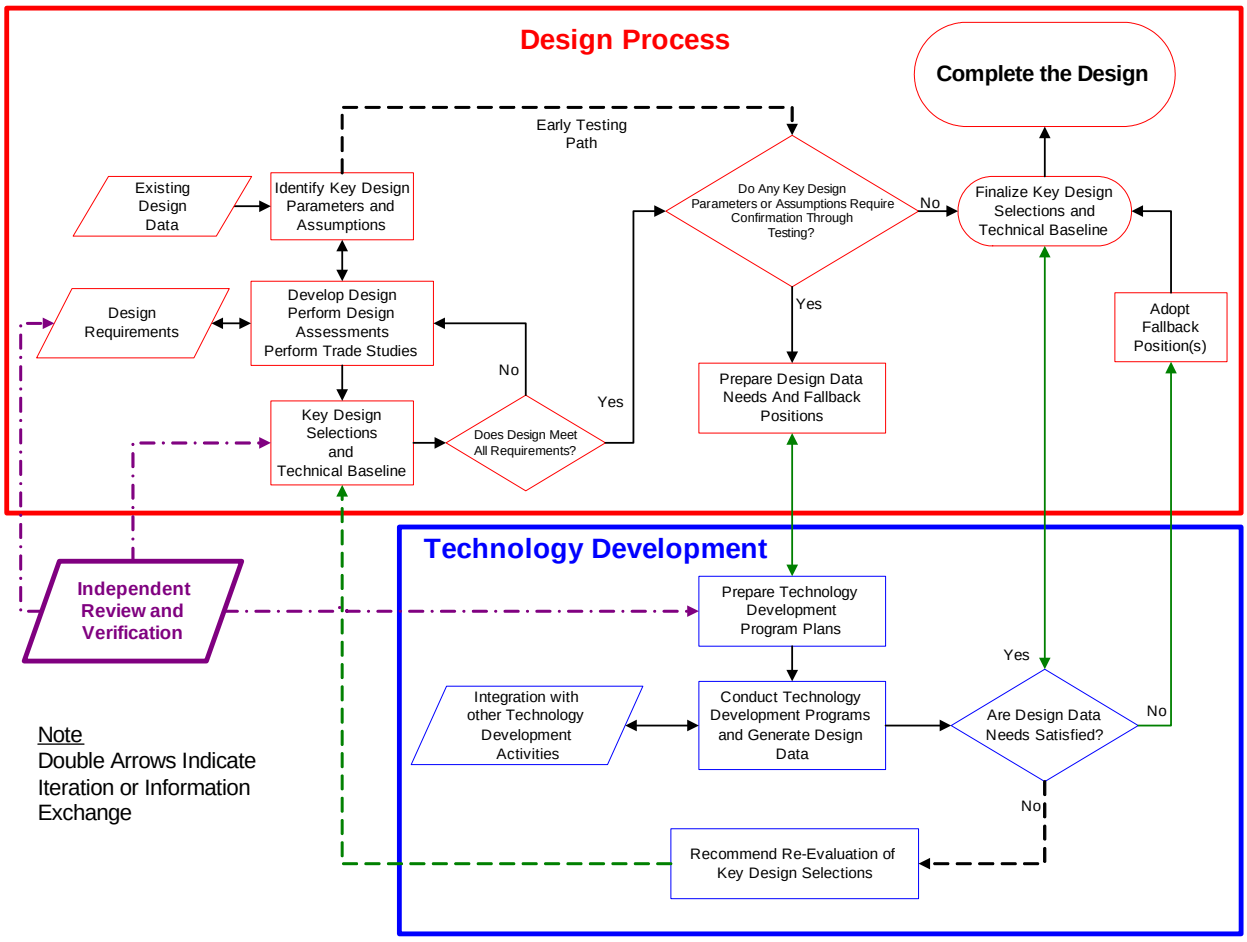

Figure 5-1. Integration of Design with Technology Development

6. References

Baxter, 2005 — Baxter, A., et al., "MHR Fuel Cycle Options for the Future Sustainability of Nuclear Power," *Proceedings of Global 2005*, October 9-13, 2005, Tsukuba, Japan, Paper 314.

Borchardt, 1982 — Borchardt, G., et al., "Experiment FRJ2-P24 Bestrahlungsbericht," Interner Bericht KFA-ZBB-IB-19/82, Kernforschungsanlage Jülich GmbH, Jülich, Federal Republic of Germany, August 1982.

Bullock, 1983 — Bullock, R.E. and J.L. Kaae, "Performance of Coated UO_2 Particles Gettered with ZrC," *J. Nuc. Mat.*, **115**, 69 (1983).

Bullock, 1984 — Bullock, R.E., "Fission-Product Release During Post irradiation Annealing of Several Types of Coated Fuel Particles," *J. Nuc. Mat*, **125**, 304 (1984).

Brown, 2003 — Brown, L.C., et al., High Efficiency Generation of Hydrogen Fuels Using Nuclear Power, GA-A24285, Rev. 1, General Atomics, San Diego, CA, December 2003.

Carlson, 1986 — Carlson, K., P. A. Roth, and V. H. Ransom, ATHENA Code Manual Volume I: Code Structure, System Models, and Solution Methods, EGG-RTH-7397, Idaho National Engineering Laboratory, Idaho Falls, ID, 1986.

DOE, 2005 — Nuclear Hydrogen Initiative Ten Year Program Plan, Department of Energy, Office of Advanced Nuclear Research, March 2005. http://neri.inel.gov/program_plans/pdfs/nhi_plan.pdf

EPRI, 2003 — High-Temperature Gas-Cooled Reactors for the Production of Hydrogen: An Assessment in Support of the Hydrogen Economy," EPRI Report 1007802, Electric Power Research Institute, Palo Alto, CA, April 2003.

Hanson, 2004 — Hanson, D. and J. Saurwein, Development Plan for Advanced High Temperature Coated-Particle Fuels, PC-000513, Rev. 0, General Atomics, San Diego, CA, 2004.

Herring, 2005 — Herring, J.S., et al., "Progress in High-Temperature Electrolysis for Hydrogen Production Using Planar SOFC Technology," Proceedings of the 2005 AIChE Spring National Meeting, Atlanta, GA, April 10-14, 2005, Paper 74f.

IAEA, 1997 — Fuel Performance and Fission Product Behavior in Gas Cooled Reactors, IAEA-TECDOC-978, International Atomic Energy Agency, Vienna, Austria, November 1997.

Inaba, 2005 — Inaba, Y., et al., "Study on Control Characteristics for HTTR Hydrogen Production System with Mock-up Test Facility. System Controllability Test for Fluctuation of Chemical Reaction," *Nuclear Engineering and Design*," **235**, pp, 111-121, 2005.

INL, 1998 — Systems Analysis Program for Hands on Integrated Reliability Evaluation (SAPHIRE) Version 6.0, NUREG-6116, Idaho National Laboratory, Idaho Falls, ID,1998.

Iyoku, 2005 — Iyoku, T., et al., "HTTR Test Program Towards Coupling with the SI Process," Third Information Exchange Meeting on the Nuclear Production of Hydrogen and Second HTTR Workshop on Hydrogen Production Technologies, Japan Atomic Energy Agency, Oarai, Japan, October 5-7, 2005, OECD Nuclear Energy Agency, Paris, France.

Kubo, 2005 — Kubo, S., et al., "A Bench-Scale Hydrogen Production Test by the Thermochemical Water-Splitting Iodine-Sulfur Process," *Proceedings of Global 2005*, October 9-13, 2005, Tsukuba, Japan, Paper 474.

LaBar, 2003 — LaBar, M., et al., "The Gas Turbine Modular Helium Reactor," *Nuclear News*, **Vol. 46**, *No. 11*, p. 28 (2003).

Maruyama, 1994 — Maruyama, S. et al., "Evaluation of Core Thermal and Hydraulic Characteristics of HTTR," *Nucl. Eng. Des.*, **Vol. 152**, pp. 183-196, 1994.

Minato, 1995 — MINATO, K., et al., "Review of Experimental Studies of Zirconium Carbide Coated Fuel Particles for High Temperature Gas-Cooled Reactors," *JAERI-Review-95-004*, Japan Atomic Energy Research Institute, Oarai, Japan (1995).

Myers, 1987 — Myers, B., Fuel Design Data Manual, MAN-910866, Issue F, General Atomics, San Diego, CA, August 1987.

Nishihara, 2005 — Nishihara, T., et al., "Analytical Study on Hydrogen Dispersion in the HTGR Hydrogen Production System," Proceedings of Global 2005, Tsukuba, Japan, October 9-13, 2005, Paper No. 284.

Ohashi, 2005 — Ohashi, H., et al., "Current Status of Research and Development on System Integration Technology for Connection between HTGR and Hydrogen Production System at JAEA," Third Information Exchange Meeting on the Nuclear Production of Hydrogen and Second HTTR Workshop on Hydrogen Production Technologies, Japan Atomic Energy Agency, Oarai, Japan, October 5-7, 2005, OECD Nuclear Energy Agency, Paris, France.

Petti, 2005 — Petti, D., et al., Technical Program Plan for the Advanced Gas Reactor Fuel Development and Qualification Program, INL/EXT-05-00465, Rev. 1, Idaho National Laboratory, Idaho Falls, ID, August 2005.

Richards, 2004 — Richards, M., et al., "Thermal Hydraulic Design of a Modular Helium Reactor Core Operating at 1000°C Coolant Outlet Temperature," *Proceedings of the 6th International Conference on Nuclear Thermal Hydraulics, Operations and Safety (NUTHOS-6)*, October 4-8, 2004, Nara, Japan, Atomic Energy Society of Japan, Tokyo, Japan, 2004.

Schultz, 2004 — Schultz, R., et al., Next Generation Nuclear Plant – Design Methods Development and Validation Research and Development Program Plan, INEEL/EXT-04-02293, Idaho National Engineering and Environmental Laboratory, Idaho Falls, ID, September 2004.

Shenoy, 1996 — Shenoy, A.S., GT-MHR Conceptual Design Description Report, RGE-910720, Rev. 1, General Atomics, San Diego, CA, July 1996.

Smith, 2005 — Smith, C., et al., An Engineering Analysis for Separation Requirements of a Hydrogen Production Plant and High-Temperature Nuclear Reactor, INL/EXT-05-00317, Rev. 0, Idaho National Laboratory, Idaho Falls, ID, USA, March 2005.

Summers, 2004 — Summers, W., et al., Centralized Hydrogen Production from Nuclear Power: Infrastructure Analysis and Test-Case Design Study, Interim Project Report, Phase A Infrastructure Analysis, NERI Project 02-160, WSRC-TR-2004-00318, Rev. 0, Westinghouse Savannah River Company, Savannah River National Laboratory, Aiken, SC, July 2004.

Terada, 2005 — Terada, A., et al., "Development of Hydrogen Production Technology by Thermo-Chemical Water Splitting Process – Pilot Test Plan," *Proceedings of Global 2005*, October 9-13, 2005, Tsukuba, Japan, Paper 427.

Appendix A
Advanced Fuels

ZrC-TRISO Fuel

The conventional TRISO coating consists of four layers and three materials; a low-density pyrolytic carbon layer (buffer), an inner high-density pyrolytic carbon layer (IPyC), an SiC layer, and an outer high-density pyrolytic carbon layer (OPyC). Based on the data obtained from a limited number of irradiation tests, there is some evidence that ZrC may be a more effective than SiC as a barrier to fission product release at high temperatures [Minato, 1995]. For this reason, ZrC-TRISO fuel was evaluated as a potential option for the H2-MHR. As indicated in Fig. A-1, use of ZrC will have a negative impact on the neutron economy because of its higher absorption cross section in the 10^2 to 10^5 eV neutron energy range. To quantify this effect, a the MHR core physics design was analyzed using ZrC-TRISO fuel in place of the reference SiC-TRISO fuel. The results showed Zr behaves like a nonburnable poison, and its effects can be compensated for by reducing the amount of B_4C fixed burnable poison that is normally loaded into the core for reactivity control and power shaping. Figure A-2 shows reactivity (k-effective) as a function of irradiation time for cores fueled with SiC-TRISO- and ZrC-TRISO-coated particles. For the ZrC-TRISO fueled core, the reactivity associated with lumped burnable poison was reduced by 14% to compensate for the additional poisoning caused by Zr. Based on this assessment, ZrC-TRISO fuel remains a viable option to achieve higher operating temperatures for the H2-MHR core.

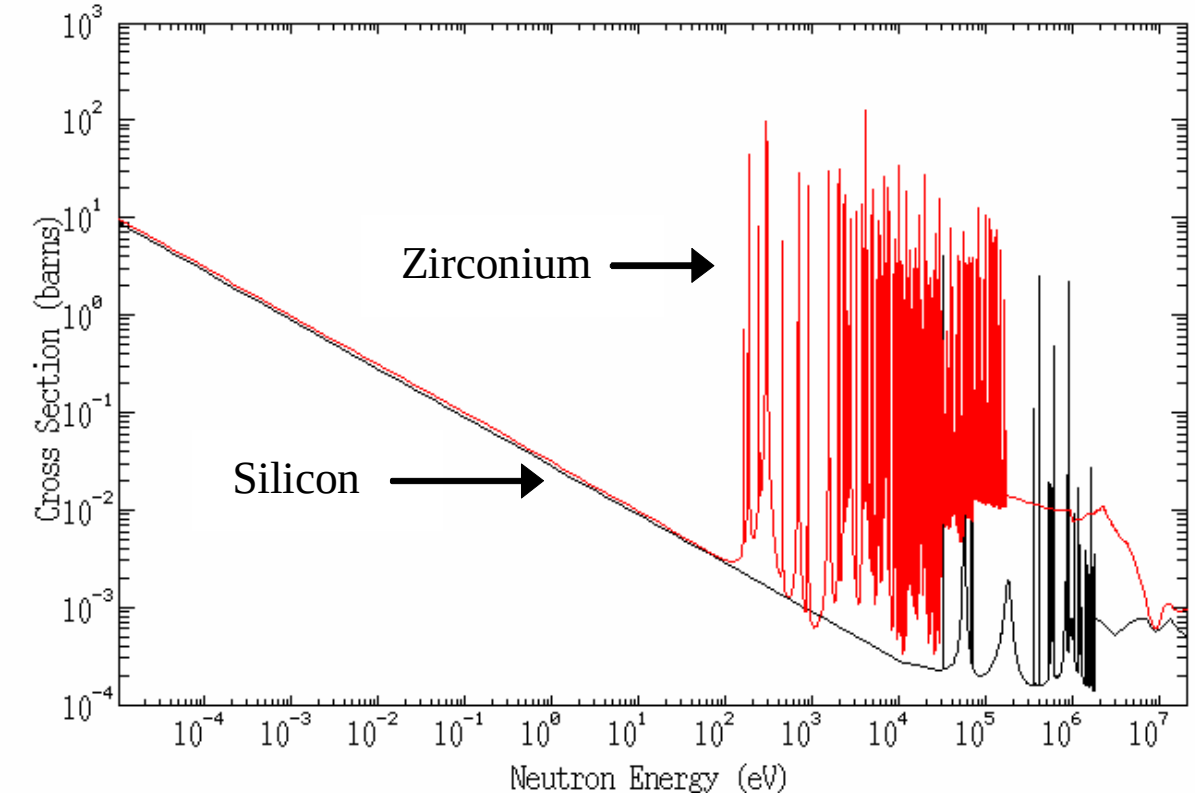

Figure A-1. Neutron Total Absorption Cross Sections for Silicon and Zirconium

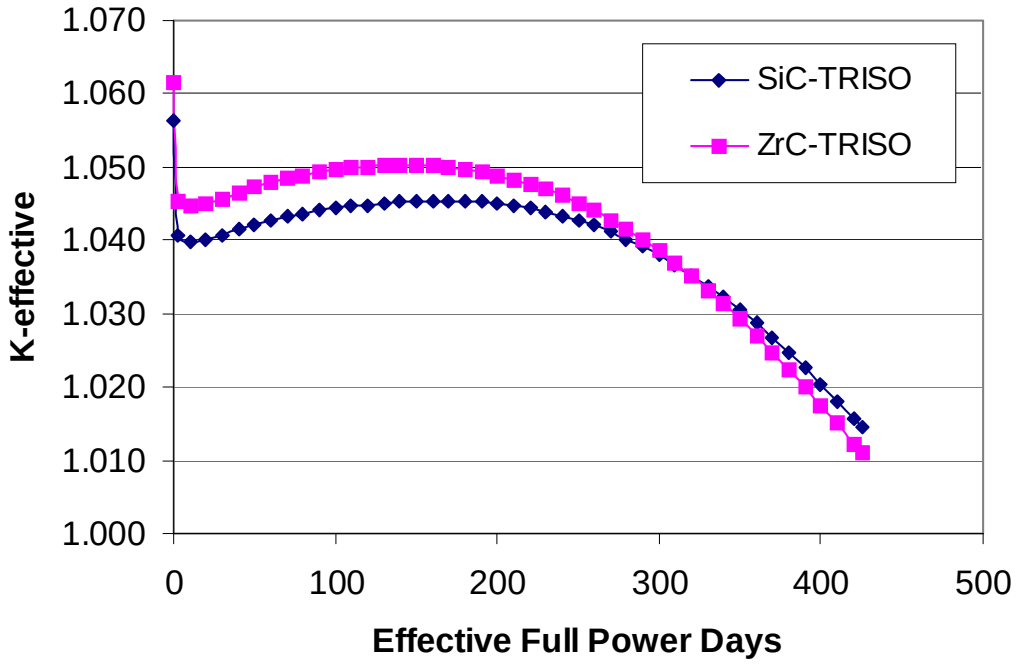

Figure A-2. Core Reactivity as a Function of Irradiation Time

ZrC-Gettered, TRISO Fuel

In the U.S., the use of ZrC as an oxygen getter was investigated during irradiation testing of SiC-TRISO particles with UO_2 kernels [Bullock, 1983]. Two types of ZrC-gettered fuel were tested; one with ZrC dispersed in the buffer and one with a thin (~10 µm) ZrC layer deposited outside the kernel. For both designs, a pyrocarbon seal coat was first deposited directly over the kernel to protect it from chemical attack by chlorine compounds that are generated during deposition of ZrC. For the latter design, an additional function of the ZrC was to suppress kernel swelling during irradiation. The particles were irradiated in both loose-particle and compact form at temperatures in the range 900°C – 1200°C, out to burnups in the range 21 – 27% FIMA and fast neutron fluences in the range 3.4×10^{25} – 6.6×10^{25} n/m^2. Irradiation times were approximately 170 d. Results are summarized below.

- For both particle designs, overall performance was good, with no evidence of kernel migration or pressure-vessel failure, indicating the ZrC was an effective oxygen getter.

- Growth features, consisting primarily of carbon, were observed in the kernel, but they did not affect performance.

- For a majority of the particles, the thin ZrC layer surprisingly remained intact. Failure of this layer was not observed in particles irradiated at ~900°C. For particles irradiated above ~1100°C , the fraction of particles with failed ZrC layers was ~25%. Kernel expansion was suppressed for particles with intact ZrC layers, and the kernels remained dense at high burnup.

- Particles with thin ZrC layers were analyzed for gamma spectra and showed excellent retention of fission products. There was some limited evidence that Ag-110m was effectively retained at high irradiation temperatures.

Figure A-3 shows the typical postirradiation appearance of a particle with a thin ZrC layer surrounding the kernel.

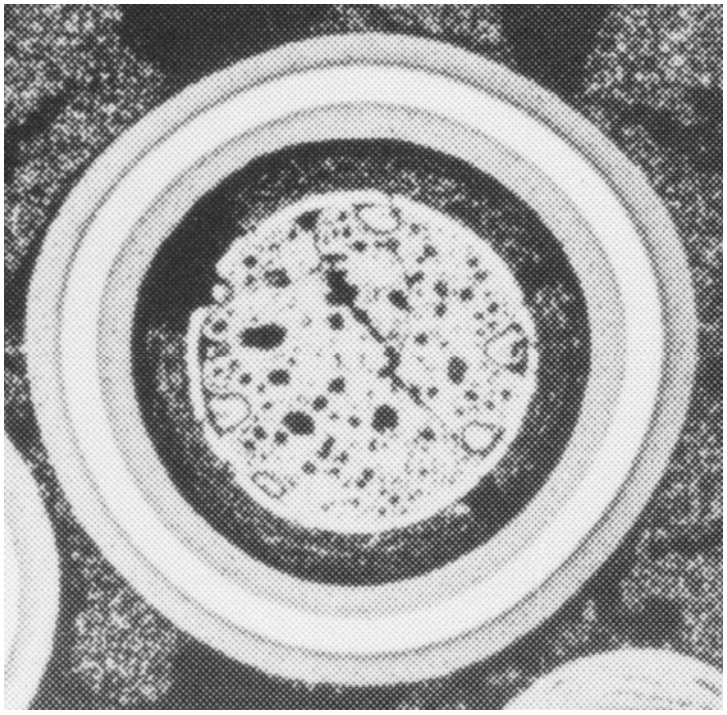

Figure A-3. Cross Section of an Irradiated ZrC-gettered, SiC-TRISO Particle. The irradiation conditions were 1020°C, 20% FIMA, and fast neutron fluence of 3.7×10^{25} n/m^2. The ZrC was deposited as a thin layer surrounding the kernel.

To further investigate the possibility that ZrC can effectively retain Ag, a test was performed in which particles previously irradiated at ~900°C were heated at 1500°C for 10,000 h [Bullock, 1984]. In addition to both ZrC-gettered designs, SiC-TRISO fuels with UC_2, UO_2, and UCO kernels were tested for comparison. Ten particles of each type were tested. Release of Eu-154, Ag-110m, Cs-134, and Ce-144 was measured at various times during the heating test. The particles with the thin ZrC layer were the only ones to be completely retentive of all nuclides. The other fuel types all released Ag-110m and Eu-154 at significant levels. Particles with UC_2 kernels released Cs-134 and Ce-144 at significant levels, and particles with UO_2 kernels released Cs-134 at significant levels. The superior performance of the particles with thin ZrC layers is not completely understood. One explanation is the ZrC layer remained intact and was an effective barrier to release, possibly because of its higher density relative to SiC (6.7 vs. 3.2 g/cm^3). Another possibility is that because the kernel remains dense when constrained by an intact ZrC layer, the fission products are effectively trapped within the kernel.

Appendix B
Publications

The following publications were prepared during the course of this NERI project:

1. M.B. Richards, A.S. Shenoy, F. Venneri, M.P. LaBar, K.R. Schultz, and L.C. Brown, "The Modular Helium Reactor for Future Energy Needs," submitted to ICAPP '06, Reno, NV, June 4-8, 2006, Paper 6154.

2. S.M.M. Reza, E.A. Harvego, M. Richards, and K.L. Peddicord, "Design of an Alternative Inlet Flow Configuration for the Modular Helium Reactor," submitted to ICAPP '06, Reno, NV, June 4-8, 2006, Paper 6338.

3. E.A. Harvego, S.M.M. Reza, M. Richards, and A. Shenoy, "An Evaluation of Reactor Cooling and Coupled Hydrogen Production Processes Using the Modular Helium Reactor," accepted for publication in *Nuclear Engineering and Design*.

4. M. Richards, A. Shenoy, K. Schultz, L. Brown, E. Harvego, M. McKellar, F. Okamoto, N. Handa, J. Coupey, and S. Reza, "Conceptual Designs for MHR-Based Hydrogen Production Systems," Proceedings of Global 2005, Tsukuba, Japan, Oct. 9-13, 2005, paper 190.

5. M. Richards, A. Shenoy, K. Schultz, L. Brown, E. Harvego, M. McKellar, J. Coupey, S. Reza, F. Okamoto, and N. Handa, "H2-MHR Conceptual Designs Based on the SI Process and HTE," Proceedings of the NEA-OECD Third Information Exchange Meeting on Nuclear Production of Hydrogen and Second HTTR Workshop on Hydrogen Production Technologies, Japan Atomic Energy Agency, Oarai, Japan, October 5-7, 2005. Accepted for publication in *International Journal of Nuclear Hydrogen Production and Applications*.

6. M.B. Richards, A. Shenoy, and E. Harvego, "Conceptual Design of an MHR Plant Used to Produce Hydrogen," *ANS Transactions*, Vol. 92, pp. 104-105, 2005.

7. M. Richards, A. Shenoy, K. Schultz, L. Brown, F. Okamoto, Y. Kiso, N. Handa, and R. Kato, "The H2-MHR: Nuclear Hydrogen Production Using the Modular Helium Reactor," Proceedings of ICAPP '05, Seoul, Korea, May 15-19, 2005.

8. E. Harvego, S. Reza, M. Richards, and A. Shenoy, "Hydrogen Production Using the Modular Helium Reactor," proceedings of ICONE-13, Beijing, China, May 16-20,2005, paper ICONE13-50281.

9. M. Richards, A. Shenoy, Y. Kiso, N. Tsuji, N. Kodochigov, and S. Shepelev, "Thermal Hydraulic Design of a Modular Helium Reactor Core Operating at 1000°C Coolant Outlet Temperature," *Proceedings of the 6th International Conference on Nuclear Thermal Hydraulics, Operations and Safety (NUTHOS-6)*, October 4-8, 2004, Nara, Japan, Atomic Energy Society of Japan, Tokyo, Japan (2004).

10. M. Richards, A. Shenoy, K. Schultz, L. Brown, G. Besenbruch, N. Handa, and J. Das, "Assessment of MHR-Based Hydrogen Energy Systems," proceedings of the 15th World Hydrogen Energy Conference, Yokohama, Japan, June 27 – July 2, 2004.

11. M. Richards, A. Shenoy, and K. Schultz, “MHR-Based Hydrogen Production Systems,” Proceedings of ICAPP ’04, Pittsburgh, PA, June 13-17, 2004, paper 4312.

12. M. Richards and A. Shenoy, “Hydrogen Generation Using the Modular Helium Reactor,” Proceedings of ICONE12, Arlington, VA, April 25-29, 2004, paper ICONE12-49228.

13. M. Richards and A. Shenoy, “Hydrogen Production Plant Using the Modular Helium Reactor,” Proceedings of the AIChE 2003 Spring National Meeting, New Orleans, LA, April 2003.

Part 3

Milestone Status and Budget Summary

Addendum
NERI Project 2002-196
Milestone Status and Budget Summary

Status Summary of NERI Tasks – Year 1

Milestone	Description	Planned Completion Date	Actual Completion Date	Percent Complete
A1	Plant Functions and Requirements Report	3/28/03	4/18/03	100
B1	Status Report – IHX Design	7/31/03	7/31/03	100
C1	Status Report – Fuel Element Design / Fuel Performance Impacts	9/26/03	9/26/03	100
D1	Status Report – Tritium Transport	9/26/03	9/26/03	100
E1	Submit Technical Paper to Conference	1/13/03	1/13/03	100
F1	SI Process Development and Flowsheet - 900°C	8/29/03	8/29/03	100
G1	Equipment Sizing – Facility Layout Drawing	4/30/03	5/14/03	100
H1	Letter Report – H2-MHR ESH&Q Requirements	3/28/03	3/28/03	100
I1	Letter Report – H2-MHR RELAP Model Development / Analysis	9/26/03	9/26/03	100
K1	Letter Report – Core Physics Design	8/29/03	9/26/03	100
L1	Letter Report – Core Thermal Hydraulic Design	8/29/03	9/26/03	100
N1	First Quarter Report	1/31/03	1/31/03	100
N2	Second Quarter Report	4/30/03	4/30/03	100
N3	Third Quarter Report	7/31/03	7/31/03	100
N4	Annual Report	10/31/03	10/31/03	100

Addendum
NERI Project 2002-196
Milestone Status and Budget Summary

Status Summary of NERI Tasks – Year 2

Milestone	Description	Planned Completion Date	Actual Completion Date	Percent Complete
A1	Update Plant Functions and Requirements Report	9/24/04	9/24/04	100
B1	Report – Core Nuclear / Thermal Hydraulic Design	9/24/04	9/24/04	100
C1	Report – Fuel Performance	9/24/04	9/24/04	100
D1	Report – H2-MHR Plant Configurations	9/24/04	9/24/04	100
E1	Prepare Technical Papers	4/30/04	6/30/04	100
F1	SI Process Flow Sheet	5/28/04	9/24/04	100
G1	Equipment Sizing – P&IDs	9/24/04*	deferred	20
H1	Report – Availability Assessment	9/24/04	9/24/04	100
I1	Report – H2-MHR RELAP Model Development / Analysis	9/24/04	9/24/04	100
K1	Report – Core Physics Design	5/28/04	9/24/04	100
L1	Report – Core Thermal Hydraulic Design	5/28/04	9/24/04	100
N1	First Quarter Report	1/30/04	1/30/04	100
N2	Second Quarter Report	4/30/04	4/30/04	100
N3	Third Quarter Report	7/30/04	7/30/04	100
N4	Annual Report	10/29/04	10/29/04	100

* The completion of this task is deferred to the third year of the project.

Addendum
NERI Project 2002-196
Milestone Status and Budget Summary

Status Summary of NERI Tasks – Year 3

Milestone	Description	Planned Completion Date	Actual Completion Date	Percent Complete
A1	Complete Reactor System Design	5/27/05	6/24/05	100
B1	Complete Conceptual Design Report – SI-Based Plant	9/30/05	3/30/06	100
C1	Complete Conceptual Design Report – HTE-Based Plant	9/30/05	3/30/06	100
D1	Report – Economic Evaluations (SI and HTE)	8/26/05	2/25/06	100
E1	Prepare Technical Papers	9/30/05	12/30/06	100
F1	Report – Process Flow Sheet – Equipment Lists	6/24/05	11/30/06	100
G1	Report – Cost Estimate Update	7/29/05	2/25/06	100
H1	Report – Availability Assessments (SI and HTE)	9/30/05	9/30/05	100
I1	Report – Safety Assessments	9/30/05	9/30/05	100
J1	Report – HTE Plant Conceptual Design	9/30/05	9/30/05	100
L1	Report – Availability Assessments (TAMU)	9/30/05	9/30/05	100
M1	Report – HTE Conceptual Design (TAMU)	9/30/05	9/30/05	100
O1	First Quarter Report	1/28/05	1/28/05	100
O2	Second Quarter Report	4/29/05	4/29/05	100
O3	Third Quarter Report	7/29/05	7/29/05	100
O4	Project Final Report	12/30/05	3/30/06	100

Addendum
NERI Project 2002-196
Milestone Status and Budget Summary

Budget Data (as of 3/30/06)
($K)

Phase / Budget Period			Approved Spending Plan	Actual Spent to Date
	From	To	Total	Total
Year 1	9/1/02	9/30/03	252	219
Year 2	10/1/03	9/30/04	486	491
Year 3	10/1/04	3/30/06	472	500
		Totals	1210	1210

The project was scheduled to end on 9/30/05 with the final project report due on 12/31/05. However, the project received a no-cost extension through 3/30/06. As shown below, the project expenditures were slightly below the spending plan for the first two years of the project. The remaining project funds were expended during the final project year and the extension period.